Carbamoyl Fluorides: Scalable Synthesis and Applications in Suzuki Cross-Coupling Reactions

Jesse LeBlanc

A Dissertation submitted to the Faculty of Graduate studies in partial fulfillment of the requirements for the degree of Doctor of Philosophy

Graduate Program in Chemistry

York University

Toronto, Ontario

September 2026

© Jesse LeBlanc, 2026

Abstract

Amides are highly prevalent in the pharmaceutical, agrochemical and material industries. Typically, amides are prepared through C–N bond-forming reactions between amines and carboxylic acids or activated carboxylic acid derivatives. This dissertation describes an improved, scalable synthesis of carbamoyl fluorides and their use as competent electrophiles in metal-catalyzed Suzuki cross-coupling reactions to prepare amides through C–C bond formation.

The synthesis of carbamoyl fluorides previously reported by our group, involving the reaction of secondary amines with 4-methylpyridine *N*-oxide and (triphenylphosphonio)difluoroacetate, was modified for larger-scale preparation of carbamoyl fluorides. Systematic evaluations of reaction safety, work-up, purification, and scale-up provided a practical procedure for preparing a diverse range of carbamoyl fluorides up to the decagram scale.

Carbamoyl fluorides were then evaluated as electrophiles in palladium- and nickel-catalyzed Suzuki cross-coupling reactions. A general nickel-catalyzed cross-coupling was developed and optimized. The resulting reaction conditions were successfully applied for the preparation of a diverse range of more than 45 amides, in high yields.

Detailed mechanistic studies accompanied the development of the nickel-catalyzed Suzuki cross-coupling of carbamoyl fluorides with alkyl boranes. Several nickel complexes associated with catalyst activation and proposed catalytic intermediates were isolated, structurally characterized, and evaluated for catalytic activity.

Overall, this work establishes a simple, robust, and accessible procedure for the multigram-scale preparation of carbamoyl fluorides and demonstrates their value as stable, modular starting

materials for the synthesis of amides through C–C bond formation. The palladium- and nickel-catalyzed Suzuki cross-coupling reactions described expand the range of amides that can be prepared from carbamoyl halides and provide a foundation for their continued development in cross-coupling chemistry.

Acknowledgments

First, I would like to thank my supervisor, Prof. Christine Le, for giving me the opportunity to work in her group. It has been an extraordinary privilege to grow and expand my knowledge, both as a chemist and as a person. I am incredibly grateful for your seemingly infinite patience, guidance, mentorship, and wisdom; without you, I would never have become the chemist I am today. Despite the hardships I have faced along the way, I would not change any of it. I am proud to call you my supervisor and mentor, and I will forever look up to you as a role model.

I would also like to thank the members of my internal supervisory committee, Prof. Thomas Baumgartner and Prof. Ryan Hili, as well as the members of my external committee, Prof. Sophie Rousseaux and Prof. Paul O'Brien. I greatly appreciate the time and effort you have provided. I am also grateful to Prof. Arturo Orellana, Prof. Christopher Caputo, Prof. Gino Lavoie, Prof. Thomas Baumgartner, and Prof. Pierre Potvin for their help and guidance throughout my time as a graduate student.

Additionally, a special thank-you to the past and present technical staff at York, particularly Michelle Barton-Marsh and Mr. Woo, for helping me operate equipment and for lending or donating an incredible amount of glassware and equipment to our lab. Without your help, much of the work described in this dissertation would not have been possible.

Dr. Howard Hunter and Dmitry Pichugin, you have both taught me so much about NMR spectroscopy and generously shared your knowledge and wisdom with me. Throughout my time at York, you have been lifelines for the chemistry department and truly the heart of its synthetic groups. I have deeply enjoyed all of our conversations, whether about research, vacations, or life in general. It has been an honor and a pleasure to get to know you both throughout my time at York!

The people I've worked with throughout my time as a graduate student have made this journey truly amazing. Victor Flores Romero—you were the first friend I made in grad school and became my honorary work husband. It has been a pleasure to work alongside you for so many years, I've had so much fun on all the adventures we shared. Dusty Cadwallader, Maryam Jabbarpoor, and Kate Skinner, it has been so much fun getting to know all of you and watching us grow as people over the years. You have become family to me. I truly have enjoyed sharing this journey with you, whether on an average Tuesday in the lab or over frosty drinks on someone's birthday. You have made this journey so enjoyable.

Zichuan Chen, Samantha Galea, Emily Woo, and Justin Laurie, it has been a pleasure to mentor each of you and watch you grow into amazing chemists and people. Samantha, I am so sorry that I put you through the beginning of the work described in Chapter 4 of this dissertation. I don't think anyone will ever fully understand the range of emotions we experienced during that part of the project. Thank you so much for your patience and persistence throughout one of the most challenging parts of my PhD. You are an amazing chemist and person—never stop believing in yourself!

To my partner, Monica Blake, you mean so much more to me than I could express. You have been nothing but supportive throughout my entire time at York, and it has meant the world to me. You have been there on my darkest and most devastating days to support me and lift my spirits, and you have also been there to celebrate every success and triumph alongside me. I cannot imagine having gone through this journey with anyone else. My mother, Debbie LeBlanc, and my sister, Sally LeBlanc, also have my deepest thanks for all of their support, I love you both dearly.

Finally, my deepest thanks go out to those who were there in the beginning of my journey but are sadly no longer with us to see its conclusion. To my grandparents, Lloyd Hicks and Yvonne

LeBlanc; none of this would have been possible without either of you and I would not be the person I am today without you.

To my high school science teacher, Trevor Nason: your enthusiasm, passion and love for science inspired me to make something of my life and taught me that it was okay to be curious and ask questions. I have never stopped thinking about you or your infectious curiosity, I have carried that part of you with me ever since we met. I would have never even considered going to postsecondary, let alone graduate studies, had I not met you. Thank you so much. You will never be forgotten.

Table of Contents

Abstract ii
Acknowledgments iv
Table of Contents vii
List of Figures x
List of Schemes xv
List of Tables xix
List of Abbreviations xxii
Chapter 1: Introduction 1
1.1. Synthesis of Amides 1
1.1.1. Traditional Methods 2
1.2. Carbamoyl Halides 5
1.2.1. Carbamoyl Chlorides 6
1.2.2. Carbamoyl Fluorides 9
1.3. Transition-Metal-Catalyzed Amide Synthesis Using Carbamoyl Halides 15
1.3.1. Carbamoyl Chlorides 18
1.3.2. Carbamoyl Fluorides 22
1.4. Conclusion and Research Prelude 25
1.5. References 28
Chapter 2: Scalable Synthesis of Carbamoyl Fluorides 34
2.1. Author contributions 34
2.2. Motivation and Research Plans 35
2.3. Results and Discussion 38
2.3.1. Evaluation of Reaction and Reagent Safety 38
2.3.2. Work-up Optimization 43
2.3.3. Scaled up Substrate Scope 47
2.3.4. Alternative Reaction Conditions for Further Scale Up 52
2.4. References 56
2.5. Chapter 2 Appendix 58
Chapter 3: Palladium Catalyzed Cross-Coupling of Carbamoyl Fluorides 81

3.1. Author contributions 81
3.2. Motivation and Research Plans 82
3.3. Introduction 84
3.3.1. Directing Groups for C–F bond activation 84
3.4. Results and Discussion 87
3.4.1. Reaction Optimization and Scope 87
3.4.2. Mechanistic Studies 88
3.4.2.1. Role of TPPO 88
3.4.2.2. Synthesis and Evaluation of Proposed Catalytic Intermediates 95
3.5. Conclusion and Future Work 108
3.6. References 109
3.7. Chapter 3 Appendix 113
Chapter 4: Nickel Catalyzed Cross-Coupling of Carbamoyl Fluorides 117
4.1. Author contributions 117
4.2. Motivation and Research Plans 118
4.3. Introduction 119
4.3.1. Carbamoyl Fluorides in Metal-Catalyzed Cross-Coupling Reactions 119
4.4. Results and Discussion 121
4.4.1. Reaction Discovery 121
4.4.2. Reaction Optimization 129
4.4.2.1. Ligand Screen 129
4.4.2.2. Alkene to H-9BBN Ratio Screen 132
4.4.2.3. Base and Water Cross-Screen 134
4.4.2.4. Base-Solvent Cross-Screen 138
4.4.2.5. Borane Nucleophile Screen 142
4.4.2.6. Concentration and Catalyst Loading Screen 143
4.4.2.7. Reaction Temperature Screen 144
4.4.2.8. Reaction Time Screen 145
4.4.2.9. Equivalents of Alkylborane Screen 146
4.4.2.10. Premixing of Pre-catalyst and Alkylborane 147
4.4.2.11. Pre-catalyst Screen 149

4.4.2.12. Summary of Reaction Optimization Studies 151
4.4.3. Substrate Purification 152
4.4.4. Substrate Scope 159
4.4.5. Mechanistic Studies 169
4.4.5.1. Pre-mixing Investigation 169
4.4.5.2. Synthesis of Catalytically Relevant Ni(I) Complexes 174
4.4.5.3. Synthesis of Catalytically Relevant Ni(II) Complexes 200
4.4.5.4. Reaction Monitoring 211
4.4.5.5. Assessment of Catalytically Relevant Complexes 216
4.4.5.6. Miscellaneous Mechanistic Studies 236
4.4.5.7. Mechanistic Summary 247
4.5. Conclusion and Future Work 251
4.6. References 253
4.7. Chapter 4 Appendix 259
Appendix 301
Complete List of References 416
Chapter 1 416
Chapter 2 422
Chapter 3 425
Chapter 4 429

List of Figures

Figure 1.1: Various applications of amides. 1
Figure 1.2: Resonance structures of amides. 2
Figure 1.3: Synthesis of amides through direct condensation. 3
Figure 1.4: Representative amide coupling reaction facilitated by stoichiometric coupling reagent. 4
Figure 1.5: Representative preparation of amides by carboxylic acid activation with oxalyl chloride 5
Figure 1.6: (Top) Comparison of carbamoyl halides to amides and acyl halides. (Bottom) Depiction of resonance stabilization of carbamoyl halides. 6
Figure 1.7: Conventional preparation of CMFs using halide exchange. 9
Figure 1.8: CMF stability in various solvent systems over 24 hours. 12
Figure 1.9: Solid-state structure of carbamoylated Ser94 residue using the indicated CMF. Structure accessed from the Protein Data Bank: pdb_00009nix. 14
Figure 1.10: General Suzuki cross-coupling reaction mechanism. 16
Figure 1.11: General Ni(I)/Ni(III) Suzuki cross-coupling reaction mechanism. 16
Figure 1.12: Revised Ni(0)/Ni(II) catalytic cycle, with consideration for the role of base and water. 17
Figure 2.1: Typical methods of preparing CMFs. 36
Figure 2.2: Graphs of reaction temperature and pressure of standard CMF synthesis with and without a pressure relief check valve. 39
Figure 2.3: Standard reaction apparatus with pressure relief valve and bubbler. 40
Figure 2.3: Standard reaction apparatus with pressure relief valve and bubbler.Pressure-relief valve 40
Figure 3.1: Representative examples of APIs containing 2-pyridyl amides. 82
Figure 3.2: Example illustrating how a directing group can position a target bond in close proximity to a metal center, facilitating bond activation. 86
Figure 3.3: Formation of a highly strained four-member palladacycle upon decarbonylation. 86
Figure 3.4: Boronic acid - boroxine equilibrium. 92
Figure 3.5: Solid state structure of boronic acid dimer stabilized by hydrogen bonding with TPPO. Crystallographic data obtained from CCDC reference number: 861749. Select hydrogen atoms have been omitted for clarity. ORTEP drawn at 50% probability. .. 93
Figure 3.6: ^{1}H NMR spectra of commercial 4-methylphenylboronic acid with varying amounts of TPPO. Spectra were acquired in $CDCl_3$ 94
Figure 3.7: Series of ^{1}H NMR spectra from heating reaction mixture described in Scheme 3.4 A after various amounts of time at the indicated temperatures. For clarity aromatic resonances between approximately 7.8 to 6.5 ppm have been omitted from the spectra. 97
Figure 3.8: Solid state structure of $Pd(PPh_3)_3$ isolated from reaction outlined in Scheme 3.4 98

Figure 3.9: Solid-state structure of complex 3.5. Hydrogen atoms have been omitted for clarity. ORTEP drawn at 50% probability. 99
Figure 3.10: Solid state structure of complex 3.10. Hydrogen atoms have been omitted for clarity. ORTEP drawn at 50% probability. 102
Figure 3.11: ^{1}H NMR spectra of 3.7 showing incomplete methylation of precursor 3.6. 102
Figure 3.12: Solid-state structure of complex 3.11. Hydrogen atoms have been omitted for clarity. ORTEP drawn at 50% probability. 103
Figure 3.13: Solid state structure of complex 3.4. Hydrogen atoms have been omitted for clarity. ORTEP drawn at 50% probability. 104
Figure 4.1: Solid state structure of oxidative addition complex 4.6 (ORTEP drawn at 50% probability, hydrogen atoms have been omitted for clarity) 123
Figure 4.2: Solid state structure of oxidative addition complex 4.8. ORTEP drawn at 50% probability, hydrogen atoms have been omitted for clarity. 125
Figure 4.3: List of ligands with abbreviations and ligand codes used in Table 4.3. 132
Figure 4.4: Visual cue observed during premixing. 147
Figure 4.5: Appearance of reactions solutions after 22 hours with varying premixing times. ... 149
Figure 4.6: ^{1}H NMR spectra of crude cross-coupling reaction mixture. (A) Spectra acquired in $CDCl_3$. (B) ^{1}H NMR spectra acquired after extensive mixing of biphasic crude mixture of $CDCl_3/D_2O$, followed by centrifugation. 152
Figure 4.7: Representative example of a typical TLC plate from a crude reaction mixture once stained in PMA. Spots circled in red indicate all spots visible under UV light. 153
Figure 4.8: General oxidation and radical generation pathways of alkyl-9-BBN. 154
Figure 4.9: ^{1}H NMR spectra of crude cross-coupling reaction mixture. (A) NMR sample prepared in a nitrogen filled glovebox, spectra acquired in $CDCl_3$. (B) NMR sample prepared in a nitrogen filled glovebox and NMR tube cap removed for 30 seconds, recapped, and vigorously shaken for 1-2 minutes, spectra acquired in $CDCl_3$..... 155
Figure 4.10: Formation of TEMPO adduct 4.9 under aerobic conditions. 155
Figure 4.11: TLC experiments used to evaluated effectiveness of various alkyl-9-BBN quenching experiments. Lanes titled Amide are of shown as a reference representing the desired products R_f. 156
Figure 4.12: General reaction scheme for the oxidation of alkyl-9-BBNs with NMO..... 157
Figure 4.13: TLC plate illustrating the ability of NMO to quench residual alkyl-9-BBN in crude a reaction mixture. 157
Figure 4.14: Proposed comproportionation mechanism for reduction of $(dppf)Ni^{II}Cl_2$. 170
Figure 4.15: Proposed mechanism for a Ni(0)/Ni(II) Suzuki cross-coupling. 171
Figure 4.16: Proposed mechanism for a Ni(I)/Ni(III) Suzuki cross-coupling. 172
Figure 4.17: Proposed mechanism for direct Ni(I) Suzuki cross-coupling. 173
Figure 4.18: Proposed disproportionation mechanism of Alkyl-Ni(I). 174
Figure 4.19: Solid-state structures of 4.15 (A) and 4.14 (B). ORTEP drawn at 50% probability, hydrogen atoms have been omitted for clarity. 175

Figure 4.20: ^{31}P {^{1}H} NMR spectrum of crude reaction mixture using 4.12 and BnMgCl, spectra acquired in C_6D_6..... 175
Figure 4.21: Solid state structure of complex 4.16. ORTEP drawn at 50% probability, hydrogen atoms have been omitted for clarity. 176
Figure 4.22: ^{31}P {^{1}H} NMR spectrum of crude reaction mixture using 4.12 and *n*-BuLi, spectra acquired in C_6D_6..... 177
Figure 4.23: Solid state structure of complex 4.17. ORTEP drawn at 50% probability, select hydrogen atoms and solvent molecules have been omitted for clarity, and hydrogen atoms shown were located with residual electron density. 178
Figure 4.24: Solid state structure of complex 4.18. ORTEP drawn at 50% probability, select hydrogen atoms and solvent molecules have been omitted for clarity. Hydrogen atoms shown were located with residual electron density. Only one independent molecule per unit cell is drawn 181
Figure 4.25: Proposed mechanism for the formation of complex 4.17 181
Figure 4.26: Proposed mechanism for a Ni(I)/Ni(III) Suzuki cross-coupling. 183
Figure 4.27: Proposed mechanism for transmetalation in a Ni(I)/Ni(III) catalytic cycle. 184
Figure 4.28: Solid-state structures of 4.22 (A) and 4.26 (B). ORTEP drawn at 50% probability, select hydrogen atoms have been omitted for clarity. Hydrogen atoms shown were successfully located in the residual electron density map..... 186
Figure 4.29: Solid-state structures of 4.29. ORTEP drawn at 50% probability. Due to poor data quality and significant disorder, solid-state structure shown only for structural connectivity. 190
Figure 4.30: Solid-state structures of complex 4.31. ORTEP drawn at 50% probability, select hydrogen atoms have been omitted for clarity. Hydrogen atoms shown were located from the residual electron density map. 192
Figure 4.31: Proposed mechanism for the formation of complex V from IV-C. 193
Figure 4.32: ^{11}B {^{1}H} NMR spectra of complex 4.31 heated at 70 ℃ overtime. Spectra acquired in C_6D_6. 194
Figure 4.33: Proposed mechanism for a Ni(I)/Ni(III) Suzuki cross-coupling. 195
Figure 4.34: Solid state structure of complex 4.35. ORTEP drawn at 50% probability, select hydrogen atoms have been omitted for clarity, and hydrogen atoms shown were located with residual electron density. 198
Figure 4.35: Solid state structure of complex 4.36. ORTEP drawn at 50% probability, select hydrogen atoms have been omitted for clarity, and hydrogen atoms shown were located with residual electron density. 199
Figure 4.36: ^{19}F {^{1}H} and ^{31}P {^{1}H} NMR spectra of complex 4.37 acquired in THF-H_8. 201
Figure 4.37: High-spin to low-spin equilibrium for an ideal trigonal bipyramidal complex. 201
Figure 4.38: Solid state structure of complex 4.37. ORTEP drawn at 50% probability, hydrogen atoms have been omitted for clarity. (Bottom) Select atoms have been removed for clarity..... 202

Figure 4.40: Solid-state structure of complex 4.39. ORTEP drawn at 50% probability, hydrogen atoms have been omitted for clarity. 204
Figure 4.39: ^{19}F {^{1}H} and ^{31}P {^{1}H} NMR spectra of reaction described in Scheme 4.37, all spectra were acquired in Tol-d_8. 204
Figure 4.41: Anticipated crystal field diagram of oxidative addition complex 4.40. 205
Figure 4.42: Solid-state structure of 4.41. ORTEP drawn at 50% probability, hydrogen atoms have been omitted for clarity. 205
Figure 4.43: ^{31}P {^{1}H} NMR spectra of the crude reaction mixture described in Scheme 4.38, all spectra were acquired in C_6D_6. 206
Figure 4.44: Crude ^{31}P {^{1}H} NMR spectrum of reaction described in Scheme 4.39, spectrum was acquired in C_6D_6. 206
Figure 4.45: ^{19}F {^{1}H} NMR spectrum from the attempted synthesis of 4.42 spectrum was acquired in C_6D_6. 207
Figure 4.46: ^{31}P {^{1}H} NMR spectra of the crude reaction mixture described in Scheme 4.41, all spectra were acquired in Tol-H_8. 209
Figure 4.47: ^{19}F {^{1}H} NMR showing the gradual generation of complex 4.45 after various amounts of time, all spectra were acquired in Tol-H_8. 210
Figure 4.48: Apparatus designed and fabricated to allow for efficient mixing of NMR tube contents at elevated temperatures. Files are available upon request. 212
Figure 4.49: ^{11}B {^{1}H} NMR spectra of the crude reaction mixture described in Scheme 4.42 after the indicated period of time, all spectra were acquired in THF-H_8. 213
Figure 4.50: ^{19}F {^{1}H} NMR spectra of the crude reaction mixture described in Scheme 4.42 after the indicated period of time, all spectra were acquired in THF-H_8. Spectra region between -30 ppm and -145 ppm has been omitted for clarity. Conversion was determined by quantitative NMR with Trifluorotoluene used as an internal standard. 214
Figure 4.51: ^{31}P {^{1}H} NMR spectra of the crude reaction mixture described in Scheme 4.42 after the indicated period of time, all spectra were acquired in THF-H_8. Spectra region between 35 ppm and 80 ppm has been omitted for clarity. 215
Figure 4.52: Complexes prepared to be evaluated for catalytic performance. 216
Figure 4.53: ^{19}F {^{1}H} NMR spectrum of complex 4.37 before and after addition of hydroxoborate 4.25. Spectrum was acquired in THF-H_8 220
Figure 4.54: ^{31}P {^{1}H} NMR spectra of reaction of 4.12 and 4.24 after the indicated period of time, all spectra were acquired in C_6D_6. 230
Figure 4.55: ^{31}P {^{1}H} NMR spectra of reaction between 4.15 and 2.2a after the indicated period of time at 80 °C, all spectra were acquired in Tol-d_8. 232
Figure 4.56: ^{1}H NMR spectra of reaction between 4.15 and 2.2a after the indicated period of time at 80 °C, all spectra were acquired in Tol-d_8. 233
Figure 4.57: ^{19}F {^{1}H} NMR spectra of reaction between 4.15 and 2.2a after the indicated period of time at 80 °C, all spectra were acquired in Tol-d_8. Spectrum region between -25

and -275 ppm have been omitted for clarity. Spectrum region between -275 and -320 ppm (right) has been significantly magnified relative to spectrum region between 5 and -25 ppm (left) for clarity. 234
Figure 4.58: Proposed catalytic pathways in which HDX can occur. 238
Figure 4.59: Crude ^{1}H NMR spectra of the standard cross-coupling reaction with H_2O (A) or D_2O (B), signals shown and integrated are of the benzylic and carbamoyl hydrogen atoms. All spectra were acquired in $CDCl_3$. Spectra region between -7.7 and 5.5 ppm have been omitted for clarity. GC-MS mass spectrum with retention time of 11.0 min (Right) from reaction employing D_2O. 240
Figure 4.60: Proposed mechanism for how formamide may be generated in the catalytic cycle. 241
Figure 4.61: Solid-state structure of complex 4.48. ORTEP drawn at 50% probability, hydrogen atoms have been omitted for clarity. 243
Figure 4.62: Complete proposed catalytic-cycle including mechanisms for by-product formation. 248

List of Schemes

Scheme 1.1: Representative example for the preparation of CMCls, and the proposed mechanism in which phosgene is generated from triphosgene and pyridine. 7
Scheme 1.2: General hydrolysis of CMCls. 8
Scheme 1.3: Reaction employing CMCls to prepare Rivastigmine. 8
Scheme 1.4: General scheme for the synthesis of CMFs using DAST and DMAP. 10
Scheme 1.5: General scheme for the synthesis of CMFs using DNTFB. 10
Scheme 1.6: Proposed mechanism for the synthesis of CMFs using PDFA. 11
Scheme 1.7: Representative reactions exploiting the unique properties CMFs beyond simply acting as a leaving group. 13
Scheme 1.8: Palladium catalyzed stereoselective intramolecular cyclization of CMCls. 20
Scheme 1.9: Early examples of cross-coupling reactions between CMCls and organoboron reagents. 21
Scheme 1.10: Suzuki cross-coupling of CMCls with alkyl-9-BBN derivatives. 21
Scheme 1.11: Representative reaction scheme for the carbamoyl fluoride-enabled enantioselective Ni-catalyzed carbocarbamoylation of unactivated alkenes. 23
Scheme 1.12: Representative reaction scheme for the nickel-catalyzed alkynylation of *N*-CF_3 CMFs. 23
Scheme 1.13: Representative example of the 1,4-arylcarbamoylation of 1,3-diene-tethered CMFs with arylboronic acids. 24
Scheme 2.1: Proposed mechanism for the synthesis of CMFs. 37
Scheme 2.2: Standard reaction conditions used to evaluate reaction pressure and heat generation. 39
Scheme 2.3: Synthetic route to prepare PDFA. 41
Scheme 2.4: Reaction schemes for the oxidation of PPh_3. 44
Scheme 2.5: Reaction conditions implemented including post-reaction modifications with S_8 to oxidize phosphine byproduct. 45
Scheme 2.6: Reaction conditions implemented including post-reaction modifications with H_2O_2 to oxidize phosphine byproduct. 45
Scheme 2.7: Substrate scope of *N*-phenylbenzylamine derivatives. ORTEP drawn at 50% probability, select hydrogen atoms have been omitted for clarity. 48
Scheme 2.8: Substrate scope of various cyclic CMFs. ORTEP drawn at 50% probability, hydrogen atoms have been omitted for clarity. [a]: Yield determined by quantitative NMR with trimethoxybenzene as internal standard. 49
Scheme 2.9: Substrate scope of miscellaneous and drug related CMFs. ORTEP drawn at 50% probability, select hydrogen atoms have been omitted for clarity. [a]: Yield determined by quantitative ^{1}H NMR spectroscopy with 1,3,5-trimethoxybenzene as internal standard. 51

Scheme 2.10: Improved reaction conditions for the synthesis of CMFs with KCO_2CF_2Br and DMSO in place of PDFA and 4-methylpyridine *N*-oxide. 53
Scheme 2.11: Reaction conditions and yields on 3.5 mmol scale using KCO_2CF_2Br and DMSO. [a]: Yield determined by quantitative NMR with trimethoxybenzene as internal standard. 54
Scheme 2.12: CMF substrate scope using modified reaction conditions, done by undergraduate student Emily Woo. [a]: Yields obtained when using previously established reaction conditions using PDFA and 4-methylpyridine *N*-oxide. 55
Scheme 3.1: Representative examples of the synthesis of 2-pyridyl amides. 82
Scheme 3.2: Reaction conditions used to carry out mercury drop test. 92
Scheme 3.3: Proposed catalytic cycle for the Suzuki cross-coupling of CMFs with boronic acids. 96
Scheme 3.4: Reaction scheme used to attempt the synthesis of complex 3.4. 97
Scheme 3.6: (A) Catalytic reaction conditions used to evaluate complex 3.5 as a potential on-cycle catalytic intermediate. (B) Catalytic reaction conditions evaluating $Pd[P(o\text{-}tol)_3]_2$ as a pre-catalyst. (B) Reaction performed by Maryam Jabbarpoor.**B** 100
Scheme 3.6: (A) Catalytic reaction conditions used to evaluate complex 3.5 as a potential on-cycle catalytic intermediate. (B) Catalytic reaction conditions evaluating $Pd[P(o\text{-}tol)_3]_2$ as a pre-catalyst. (B) Reaction performed by Maryam Jabbarpoor. 100
Scheme 3.7: Reaction scheme for the synthesis of complex 3.8. 101
Scheme 3.8: Synthetic conditions for the attempted synthesis of complex 3.4. Hydrogen atoms have been omitted for clarity. ORTEP drawn at 50% probability. 101
Scheme 3.9: Modified reaction scheme for the synthesis of precursor complex 3.8. 103
Scheme 3.10: Reaction scheme for the successful synthesis of 3.4. 104
Scheme 3.11: Reaction conditions for the synthesis of complex 3.10. 105
Scheme 3.12: Attempted synthetic methods for preparing 3.4 from 3.10 via halide exchange. . 105
Scheme 3.13: Synthetic conditions used to prepare complex 3.4. 106
Scheme 3.14: (A) Stoichiometric reaction conditions used to evaluate complex 3.4 as a potential on-cycle catalytic intermediate. (B) Catalytic reaction conditions used to evaluate complex 3.4 as a potential on-cycle catalytic intermediate. Both reactions were performed by Maryam Jabbarpoor. 107
Scheme 4.1: General reaction scheme for the cross-coupling conditions developed by Tlili and co-workers. 120
Scheme 4.2: Reaction conditions developed by Takemoto and co-workers. 121
Scheme 4.3: Reaction conditions used in attempted cross-coupling reaction. 122
Scheme 4.4: Synthesis of complexes 4.4 and 4.6 (ORTEP drawn at 50% probability, hydrogen atoms have been omitted for clarity) 123
Scheme 4.5: Reaction conditions used in cross-coupling of 2.2o and phenyl boronic acid. 124
Scheme 4.6: (A) Reaction conditions used to synthesize complex 4.7. (B) Reaction conditions used to synthesize complex 4.8. 125

Scheme 4.7: (A) Conditions for the stoichiometric reaction of 4.7 with 4-methoxyphenylboronic acid. (B) Conditions used in the attempted cross-coupling of CMF 2.2a and various borane nucleophiles. 126
Scheme 4.8: Reaction conditions used for replicate runs in Table 4.5. 135
Scheme 4.9: Reaction scheme of the optimized reaction conditions established in Section 4.4.2. 151
Scheme 4.10: Alkylborane substrate scope. Isolated yields are reported (ORTEP drawn at 50% probability, hydrogen atoms have been omitted for clarity)..... 161
Scheme 4.11: Carbamoyl fluoride substrate scope. Isolated yields are reported..... 164
Scheme 4.12: Unsuccessful or inconclusive substrates attempted during scope..... 167
Scheme 4.13: Substrate scope of aryl halide containing CMFs..... 168
Scheme 4.14: Generation of 4.12 during reaction premixing step. ORTEP drawn at 50% probability, hydrogen atoms have been omitted for clarity. 169
Scheme 4.15: Selective reduction of 4.10 to 4.12 with H-9BBN. 170
Scheme 4.16: Attempted synthesis of an alkyl-Ni(I) complex using Grignard reagents. 175
Scheme 4.17: Attempted synthesis of alkyl-Ni(I) complexes using organolithium reagents. 176
Scheme 4.18: Attempted synthesis of an alkyl-Ni(I) complex using $AlMe_3$. 177
Scheme 4.19: Attempted synthesis of alkyl-Ni(I) complexes using excess $AlMe_3$. 180
Scheme 4.20: Attempted synthesis of alkyl-Ni(I) complexes using TIBA..... 182
Scheme 4.21: Scope of synthesized alkyl-9-BBN and hydroxoborate salts. Reported are isolated yields..... 185
Scheme 4.22: Accidental synthesis of boroxane 4.27 due to the presence of excess H-9BBN and hydroxide when attempting to synthesize hydroxoborate salt 4.26. ORTEP drawn at 50% probability, hydrogen atoms have been omitted for clarity. 187
Scheme 4.23: Reaction conditions used to attempt the synthesis of hydroxoborate-Ni(I) complexes. 188
Scheme 4.24: Synthesis of 4.28 from 4.12 with excess TMS-OTf..... 189
Scheme 4.25: Reaction conditions to prepare complex 4.29. 189
Scheme 4.26: Reaction conditions to prepare complex 4.30. 190
Scheme 4.27: Reaction conditions to prepare complex 4.31. 191
Scheme 4.28: Synthetic conditions for the preparation of complex 4.15. 194
Scheme 4.29: Conditions used to synthesize complex 4.14. 195
Scheme 4.30: Reaction conditions used to attempt the synthesis of complex 4.32..... 196
Scheme 4.31: Attempted synthesis of complex 4.32 from 4.28..... 196
Scheme 4.32: Synthetic conditions used in the attempted synthesis of complex 4.33. 197
Scheme 4.33: Attempted synthesis of $(TMEDA)NiF_2$ and $(dppf)NiF_2$. 198
Scheme 4.34: Reaction conditions for the formation of complex 4.36. 199
Scheme 4.35: Synthetic conditions for the preparation of complex 4.37. 200

Scheme 4.36: Reaction conditions employed for the attempted synthesis of various oxidative addition complexes. ORTEP drawn at 50% probability, hydrogen atoms have been omitted for clarity. 203
Scheme 4.37: Reaction conditions employed for the attempted synthesis of an oxidative addition complex. 203
Scheme 4.38: Reaction conditions employed for the attempted synthesis of an oxidative addition complex. 205
Scheme 4.39: Reaction conditions employed for the attempted synthesis of an oxidative addition complex containing CMF 2.2x. 206
Scheme 4.40: Reaction conditions employed in the attempted synthesis of complex 4.42..... 207
Scheme 4.41: Reaction conditions employed for the formation of complex 4.45..... 208
Scheme 4.42: Reaction conditions employed for reaction monitoring experiments. 211
Scheme 4.43: Stoichiometric reaction condition used to evaluate complex 4.37 as a competent catalytic species. 219
Scheme 4.44: Stoichiometric reaction condition used to evaluate complex 4.37 as a competent catalytic species. 219
Scheme 4.45: Reaction conditions employed for evaluation of catalytic reactivity of complex 4.30. Conversions and yields acquired by ^{1}H NMR with 1,3,5 trimethoxybenzene as an internal standard..... 221
Scheme 4.46: Reaction conditions employed for evaluation of catalytic reactivity of complex 4.37. Conversions and yields acquired by ^{1}H NMR with 1,3,5 trimethoxybenzene as an internal standard..... 223
Scheme 4.47: Stoichiometric reaction condition used to evaluate reactivity between complex 4.15 and CMF 2.2a. 232
Scheme 4.48: Reaction conditions employed to synthesized Ni–TEMPO adduct 4.48. 243

List of Tables

Table 3.1: Catalyst screening for Suzuki-type cross-coupling of CMF 2.2o conducted by Maryam Jabbarpoor. [a]: Conversions and yields acquired by ^{1}H NMR with 1,3,5 trimethoxybenzene as an internal standard. [d]: Batch stored in Argon-filled glovebox at -35 °C. [e]: Batch stored under N_2 at 4 °C. Hydrogen atoms have been omitted for clarity. ORTEP drawn at 50% probability. 88
Table 3.2: The effect of TPPO with various boronic acid substrates. Reactions reported were conducted by Maryam Jabbarpoor. [a]: Conversions and yields acquired by ^{1}H NMR with 1,3,5 trimethoxybenzene as an internal standard. 89
Table 3.3: Phosphine oxide screening. [a]: Conversions and yields acquired by ^{1}H NMR with 1,3,5 trimethoxybenzene as an internal standard. Reactions performed by Maryam Jabbarpoor. 90
Table 3.4: Quantification of the influence of TPPO on the boronic acid–boroxine equilibrium. The relative mol% of boronic acid and boroxine were determined based on the total number of boron atoms present in solution. Accordingly, one equivalent of boroxine was counted as three boron equivalents. 94
Table 4.1: Reaction conditions used to evaluate various pre-catalysts for the cross-coupling of CMF 2.2o with an alkyl-9-BBN coupling partner. Conversions and yields acquired by quantitative ^{1}H NMR with 1,3,5 trimethoxybenzene as an internal standard. 127
Table 4.2: Reaction conditions used to evaluate pre-catalysts for the cross-coupling of CMF 2.2a with an alkyl-9-BBN coupling partner. Conversions and yields acquired by quantitative ^{1}H NMR with 1,3,5 trimethoxybenzene as an internal standard. 128
Table 4.3: Ligand screen, conversions and yields acquired by quantitative ^{1}H NMR with 1,3,5 trimethoxybenzene as an internal standard. 131
Table 4.4: Optimization of alkene and H-9BBN ratio for the Ni-catalyzed cross-coupling reaction. Conversions and yields acquired by ^{1}H NMR spectroscopy using 1,3,5 trimethoxybenzene as an internal standard. 134
Table 4.5: Yields for replicate runs using reaction conditions outlined in Scheme 4.8. Conversions and yields acquired by ^{1}H NMR spectroscopy using 1,3,5 trimethoxybenzene as an internal standard. 135
Table 4.6: Base and water cross-optimization. Conversions and yields acquired by ^{1}H NMR spectroscopy with 1,3,5 trimethoxybenzene as an internal standard. 137
Table 4.7: Carbonate and phosphate bases evaluated in THF, 1,4-dioxane, and toluene in the base-solvent cross-optimization. Conversions and yields acquired by ^{1}H NMR with 1,3,5 trimethoxybenzene as an internal standard. 139
Table 4.8: Fluoride and miscellaneous bases evaluated in THF, 1,4-dioxane, and toluene in the base-solvent cross-optimization. Conversions and yields acquired by ^{1}H NMR with 1,3,5 trimethoxybenzene as an internal standard. 141

Table 4.9: Borane nucleophile screening. Conversions and yields acquired by ^{1}H NMR spectroscopy using 1,3,5 trimethoxybenzene as an internal standard. 142
Table 4.10: Optimization table screening reaction concentrations and catalyst loadings. Conversions and yields acquired by ^{1}H NMR spectroscopy using 1,3,5 trimethoxybenzene as an internal standard. 143
Table 4.11: Reaction temperature screening, conversions and yields acquired by ^{1}H NMR with 1,3,5 trimethoxybenzene as an internal standard. 144
Table 4.12: Evaluation of optimal reaction time. Conversions and yields acquired by ^{1}H NMR spectroscopy using 1,3,5 trimethoxybenzene as an internal standard. 146
Table 4.13: Optimization of equivalents of alkylborane. Conversions and yields acquired by ^{1}H NMR with 1,3,5 trimethoxybenzene as an internal standard. 147
Table 4.14: Optimization of premixing times. Conversions and yields acquired by ^{1}H NMR spectroscopy using 1,3,5 trimethoxybenzene as an internal standard. 148
Table 4.15: Pre-catalyst screening. Conversions and yields acquired by ^{1}H NMR spectroscopy using 1,3,5 trimethoxybenzene as an internal standard. 150
Table 4.16: Evaluation of the stoichiometric reactivity of various Ni^{I}-Borate complexes. Conversions and yields acquired by ^{1}H NMR with 1,3,5 trimethoxybenzene as an internal standard. 217
Table 4.17: Evaluation of other catalytically related complexes. Entry 3 was conducted with a catalyst loading of 5 mol%. Conversions and yields acquired by ^{1}H NMR with 1,3,5 trimethoxybenzene as an internal standard. 225
Table 4.18: Reaction screening with various catalyst loadings of $(dppf)_2Ni^0$. Conversions and yields acquired by ^{1}H NMR with 1,3,5 trimethoxybenzene as an internal standard. 226
Table 4.19: Reaction screening at reduced temperatures with $(dppf)_2Ni^0$ as the pre-catalyst. Conversions and yields acquired by ^{1}H NMR with 1,3,5 trimethoxybenzene as an internal standard. 227
Table 4.20: Reaction screening with various pre-catalysts with no pre-mixing. Conversions and yields acquired by ^{1}H NMR with 1,3,5 trimethoxybenzene as an internal standard. 228
Table 4.21: Evaluation of deviations from optimized reaction conditions. Conversions and yields acquired by ^{1}H NMR with 1,3,5 trimethoxybenzene as an internal standard. 237
Table 4.22: Evaluation of specified deviations from optimized reaction conditions. Conversions and yields acquired by ^{1}H NMR with 1,3,5 trimethoxybenzene as an internal standard. 239
Table 4.23: Evaluation of specified deviations from optimized reaction conditions. Conversions and yields acquired by ^{1}H NMR with 1,3,5 trimethoxybenzene as an internal standard. 244

Table 4.24: Evaluation of specified deviations from optimized reaction conditions. Conversions and yields acquired by ^{1}H NMR with 1,3,5 trimethoxybenzene as an internal standard. 245

List of Abbreviations

2-MeTHF	2-methyltetrahydrofuran
$AlMe_3$	Trimethylaluminum
API	Active pharmaceutical ingredient
BF_3	Boron trifluoride
BF_3K	Potassium organotrifluoroborate
BINAP	2,2′-bis(diphenylphosphino)-1,1′-binaphthyl
Bn	Benzyl
BNeo	Boronic acid neopentylglycol ester
BnMgCl	Benzylmagnesium chloride
Bpin	Boronic acid pinacol ester
℃	Degree Celsius
CMCl	Carbamoyl Chloride
CMF	Carbamoyl Fluoride
CO	Carbon monoxide
CO_2	Carbon dioxide
$COCl_2$	Phosgene
COClF	Carbonyl chlorofluoride
COD	1,5-Cyclooctadiene
COF_2	Carbonyl fluoride
Com	Comproportionation
Cs	Caesium
Cu	Copper
Cy	Cyclohexyl
DAST	Diethylaminosulfur trifluoride
dba	Dibenzylideneacetone
DCC	Dicyclohexylcarbodiimide
DCM	Dichloromethane
DCU	Dicyclohexylurea
DFC	Difluorocarbene
DIPEA	Diisopropylethylamine
DMAc	Dimethylacetamide
DMAP	4-dimethylaminopyridine
DME	Dimethoxyethane
DMS	Dimethyl sulfide
DMSO	Dimethyl sulfoxide
DNTFB	2,4-dinitro-1-(trifluoromethoxy)benzene

dppf	1,1'-Bis(diphenylphosphino)ferrocene
DSC	Differential scanning calorimetry
equiv	Equivalents
Et	Ethyl
EtOAc	Ethylacetate
F_2-9-BBN	9,9-difluoro-9-borabicyclo-[3.3.1]-nonanate
Fc	Ferrocenyl
GC-MS	Gas chromatography-mass spectrometry
h	Hours
H_2	Molecular hydrogen
H_2O	Water
H_2O_2	Hydrogen peroxide
H-9BBN	9-borabicyclo[3.3.1]nonane
HCl	Hydrochloric acid
HDX	Hydrogen-deuterium exchange
HF	Hydrofluoric acid
Hg	Mercury
HO-9-BBN	9-bora-bicyclo[3.3.1]nonan-9-ol
Hz	Hertz
IC_{50}	Inhibitory concentration 50
IPA	Isopropanol
i-PrMgBr	Isopropylmagnesium bromide
K	Potassium
KIE	Kinetic isotope effect
KOH	Potassium hydroxide
KOtBu	Potassium tert-butoxide
LC_{50}	Lethal concentration 50
LG	Leaving Group
M	Molar
Me	Methyl
MeCN	Acetonitrile
MeLi	Methyllithium
MHz	Megahertz
MI	Migratory insertion
min	Minutes
mTorr	Millitorr
Na	Sodium
NaOH	Sodium Hydroxide

n-BuLi	*n*-butyllithium
NHBoc	*tert*-butyl carbamate
Ni	Nickel
NMO	*N*-methylmorpholine *N*-oxide
NMR	Nuclear magnetic resonance
OA	Oxidative addition
OAc	Acetate
Oct	Octyl
OTBS	*tert*-butyldimethylsilyl ether
OTf	Triflate
PCy_3	Tricyclohexylphosphine
Pd	Palladium
PDFA	(triphenylphosphonio)difluoroacetate
Ph	Phenyl
phen	1,10-phenanthroline
PMA	Phosphomolybdic acid
PMB	*p*-methoxybenzyl
PPh_3	Triphenylphosphine
ppm	Parts per million
PSI	Pounds per square inch
qNMR	Quantitative nuclear magnetic resonance
RE	Reductive elimination
RPM	Revolutions per minute
rt	Room temperature
S_8	Elemental Sulfur
SC-XRD	Single-crystal X-ray diffraction
TBAF	Tetra-n-butylammonium fluoride
TEMPO	(2,2,6,6-tetramethylpiperidin-1-yl)oxyl
THF	Tetrahydrofuran
TIBA	Triisobutylaluminum
Tl	Thallium
TLC	Thin layer chromatography
TLS	Turnover-limiting step
TM	Transmetalation
TMEDA	Tetramethylethylenediamine
TMS	Trimethylsilane
TMSCl	Trimethylsilyl chloride
TMSOTf	Trimethylsilyl trifluoromethanesulfonate

Tol	Toluene
TPPO	Triphenylphosphine oxide
TPPS	Triphenylphosphine sulfide
Zn	Zinc
β-H elim.	β-hydride elimination

Chapter 1: Introduction

1.1. Synthesis of Amides

Amides are among the most prevalent and important functional groups in chemistry. They are particularly significant in biological systems, where amide linkages constitute the peptide bonds that connect amino acids and define the primary structure of proteins. Amides are also widely encountered in natural products, pharmaceuticals, agrochemicals and synthetic materials including polyamides such as nylon, and industrial solvents such as dimethylacetamide (DMAc) (Figure 1.1).[1–8] The widespread use of amides arises from their distinctive combination of polarity, structural rigidity, hydrogen-bonding capability and chemical stability.

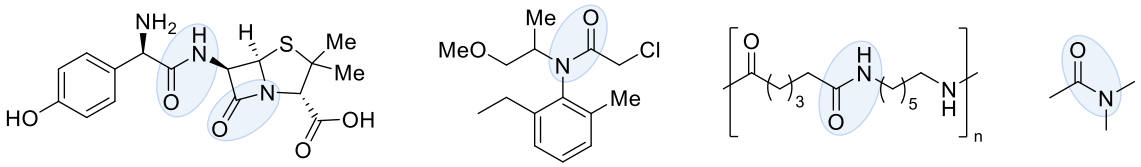

Figure 1.1: Various applications of amides.

These properties originate primarily from delocalization of the nitrogen lone pair into the adjacent carbonyl group (Figure 1.2 **A**). The resulting resonance stabilization imparts partial double bond character to the amide C–N bond, favoring a nearly planar geometry and restricting rotation about the bond (Figure 1.2 **B**).[9] This delocalization decreases the basicity and nucleophilicity of the nitrogen atom while simultaneously reducing the electrophilicity of the carbonyl carbon, making amides comparatively resistant to hydrolysis under neutral conditions. Nevertheless, amides are strongly polarized, with the carbonyl oxygen acting as a hydrogen-bond acceptor, while primary and secondary amides can additionally function as hydrogen-bond donors through their N–H bonds. These interactions influence molecular recognition, conformational

organization, and physical properties, all of which contribute to the stability of protein secondary structures and the mechanical properties of polyamide materials.[5,6,9]

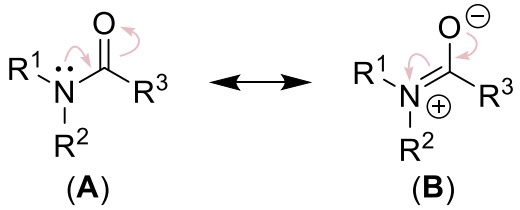

Figure 1.2: Resonance structures of amides.

Importantly, the inherent stability of amides does not preclude their use in subsequent transformations. Their stability allows them to persist through multistep synthetic sequences, while their controlled reactivity allows them to also function as versatile synthetic intermediates under appropriate activation conditions. Depending on their substituents, amides can undergo hydrolysis, reduction, dehydration, functionalization adjacent to the carbonyl group, or transition-metal-catalyzed activation of the normally unreactive amide C–N bond.[3,4,6,10] Consequently, methods that provide efficient access to structurally diverse amides are valuable for both preparing important end products and for enabling subsequent synthetic transformations. Although a comprehensive discussion of amide functionalization is beyond the scope of this dissertation, their widespread occurrence, desirable properties and synthetic versatility highlight the continued importance of developing efficient and selective methods for their formation.

1.1.1. Traditional Methods

The conceptually simplest route to an amide is the direct condensation of a carboxylic acid and amine, producing water as the sole stoichiometric byproduct (Figure 1.3). Under additive-free conditions, reaction of the carboxylic acid and amine forms an ammonium carboxylate salt, thereby decreasing the nucleophilicity of the amine.[11] Productive amidation is further impeded by the poor leaving-group ability of the carboxylic acid hydroxyl group and the reversibility of the

condensation. Consequently, direct amidation typically requires high temperatures, pressure, and/or continuous removal of water generated to drive the equilibrium toward product formation.[12,13] These forcing conditions can promote decomposition of thermally sensitive or structurally complex substrates, thereby limiting the general applicability of this approach. Nevertheless, direct amidation remains practical for sufficiently robust bulk chemicals and polymers, including nylon-6,6 and DMAc (Figure 1.3).[14–18]

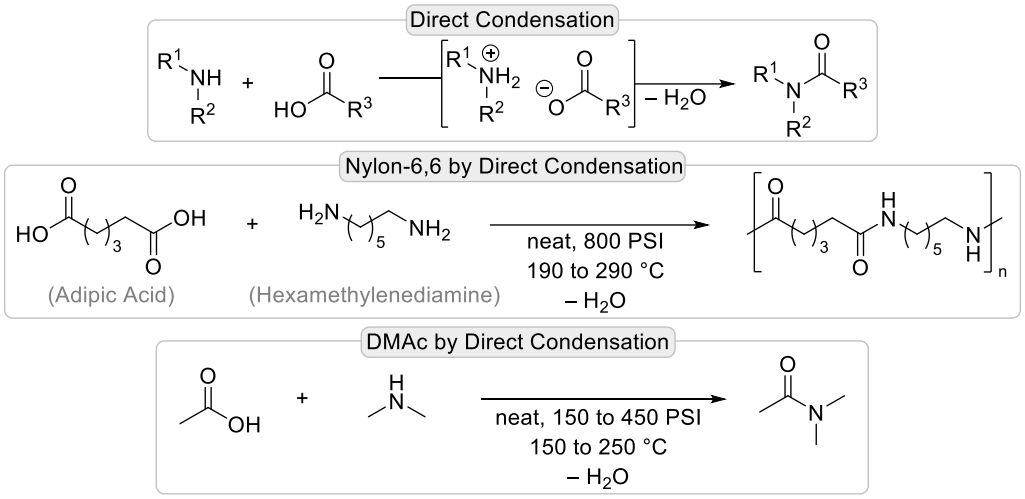

Figure 1.3: Synthesis of amides through direct condensation.

For the preparation of more structurally complex amides, industrial and laboratory methods generally rely on activation of the carboxylic acid. This may be achieved in situ using stoichiometric coupling reagents, including carbodiimides such as dicyclohexylcarbodiimide (DCC), or through prior activation of the carboxylic acid into a more reactive derivative. For example, treatment with oxalyl chloride generates the corresponding acyl chloride which reacts rapidly with the amine in a subsequent step. Although both approaches rely on the stoichiometric activation of carboxylic acid, they present different practical advantages and limitations.

Carbodiimides such as DCC allow activation and amide formation to be performed in a single reaction vessel under relatively mild conditions. Upon deprotonation of the carboxylic acid by DCC, reaction of the carboxylate with the protonated coupling reagent leads to the formation of an *O*-acylisourea. This intermediate is now sufficiently electrophilic to undergo nucleophilic attack by the amine, producing the desired amide and dicyclohexylurea (DCU) as a stoichiometric by-product (Figure 1.4). Competing rearrangement of the *O*-acylisourea to a stable *N*-acylurea can reduce the yield of the desired amide. DCC couplings additionally produce a significant amount of relatively high-molecular-weight waste. Although most DCU can often be removed by filtration, residual DCU can be difficult to completely separate from the amide product using purification techniques such silica gel chromatography.[19–21]

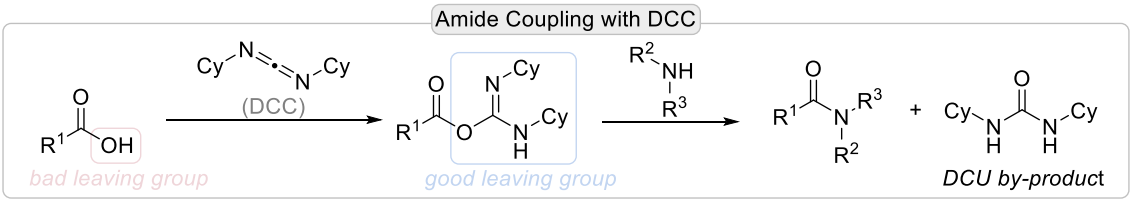

Figure 1.4: Representative amide coupling reaction facilitated by stoichiometric coupling reagent.

In contrast, prior conversion of a carboxylic acid to the corresponding acyl halide, often performed in situ using an appropriate halogenating reagent, generates a highly electrophilic intermediate that typically undergoes rapid aminolysis. This reaction affords the corresponding amide and one equivalent of acid (HX), which is generally neutralized using an additional equivalent of amine or an added base (Figure 1.5).[19,22,23] However, this same reactivity can result in competing acylation of other nucleophilic functional groups. In the case of acyl chlorides, moisture is generally excluded during their preparation and handling to minimize hydrolysis.[19,23,24] Depending on the choice of halogenating reagent and substrate, the conditions required for acyl halide formation may also be incompatible with acid-sensitive or nucleophilic functional groups. For example, formation of an acyl chloride using oxalyl chloride generates CO, CO_2, and HCl as

volatile by-products, simplifying their removal but requiring appropriate control of gas evolution and corrosive emissions.[19,22] Compared with DCC coupling, the absence of a high-molecular-weight DCU by-product can simplify purification, as excess base and the resulting ammonium halide salts can often be removed by aqueous work-up. Nevertheless, both activation strategies avoid forcing conditions associated with direct amidation but do so at the cost of additional stoichiometric reagent consumption and stoichiometric waste.[20,25]

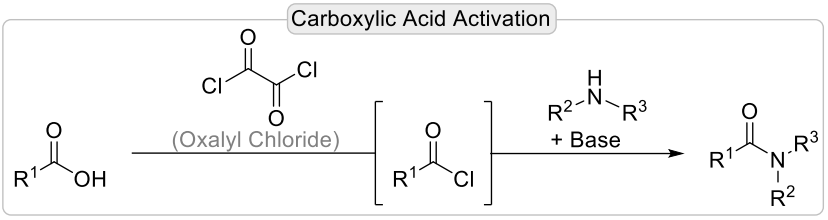

Figure 1.5: Representative preparation of amides by carboxylic acid activation with oxalyl chloride.

One particularly relevant class of activated carbonyl compounds is carbamoyl halides. These electrophilic precursors already contain the N–C(O) linkage of the target amide, enabling the remaining carbon substituent to be introduced through C–C bond formation at the carbonyl carbon rather than through conventional C–N bond formation. The following section discusses the synthesis, stability, and synthetic applications of these reagents.

1.2. Carbamoyl Halides

Carbamoyl halides are derivatives of carbamic acids that structurally combine the resonance-stabilized N–C(O) motif of an amide with the carbonyl-bound halide of an acid halide (Figure 1.6). With the general structure of R_2N–C(O)X, where X is either chlorine or fluorine (i.e., other halogenated derivatives are not typically accessible synthetically due to their instability). As with amides, carbamoyl halides are stabilized through delocalization of the nitrogen lone pair into the adjacent carbonyl group. This interaction imparts partial double-bond character to the N–C(O)

bond and decreases the electrophilicity of the carbonyl carbon relative to conventional acyl halides (Figure 1.6).[26–29] Nevertheless, the halide can serve as a leaving group during nucleophilic acyl substitution, while the C–X bond can also undergo transition-metal-mediated activation. Accordingly, reaction with oxygen-, nitrogen-, or sulfur-based nucleophiles affords carbamates, ureas, or thiocarbamates, respectively, whereas carbon-based nucleophiles or coupling partners can afford amides though C–C bond formation at the carbonyl carbon.[26–29] The identity of the halogen can strongly influence the stability and reactivity of these compounds.[27,30] The following sections discuss carbamoyl chlorides (CMCls) and carbamoyl fluorides (CMFs), which have received the greatest attention in synthesis.

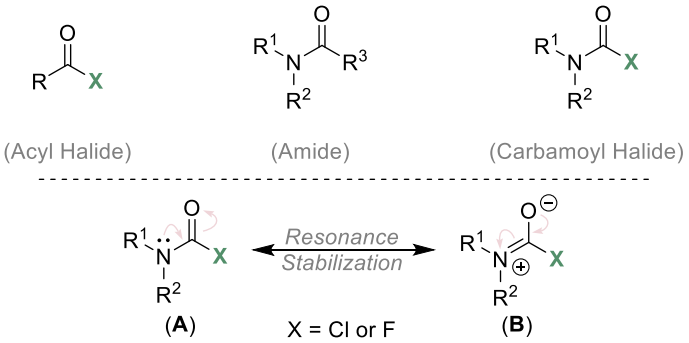

Figure 1.6: (Top) Comparison of carbamoyl halides to amides and acyl halides. (Bottom) Depiction of resonance stabilization of carbamoyl halides.

1.2.1. Carbamoyl Chlorides

Of the synthetically accessible carbamoyl halides, the chlorides are the most well studied. They are conventionally prepared by treating secondary amines with highly toxic phosgene ($COCl_2$) or a phosgene surrogate.[31,32] Triphosgene is frequently employed as a crystalline phosgene surrogate.[33,34] Although the crystalline nature of triphosgene can make it more convenient to measure and handle on the benchtop, this reagent should not be regarded as inherently safe or benign.[28,32] The typical method of generating CMCls is by initial treatment of triphosgene typically with an excess amount pyridine, followed by addition of the corresponding amine which generates

the corresponding CMCl (Scheme 1.1).[31] One potential side reaction during its preparation is the reaction of the newly formed CMCl with unconsumed secondary amine, resulting in the corresponding urea. Consequently, reagent stoichiometry, order of addition, neutralization of the generated HCl, and quenching of residual toxic phosgene must be carefully controlled.[32,35] The process-scale relevance of this approach has also been demonstrated in patents describing the direct phosgenation of secondary amines and subsequent purification of the CMCls by vacuum distillation. For example, a process patent filed by the Hoechst company reported isolated >90% yields for several CMCls derived from several α-branched secondary aliphatic amines.[35]

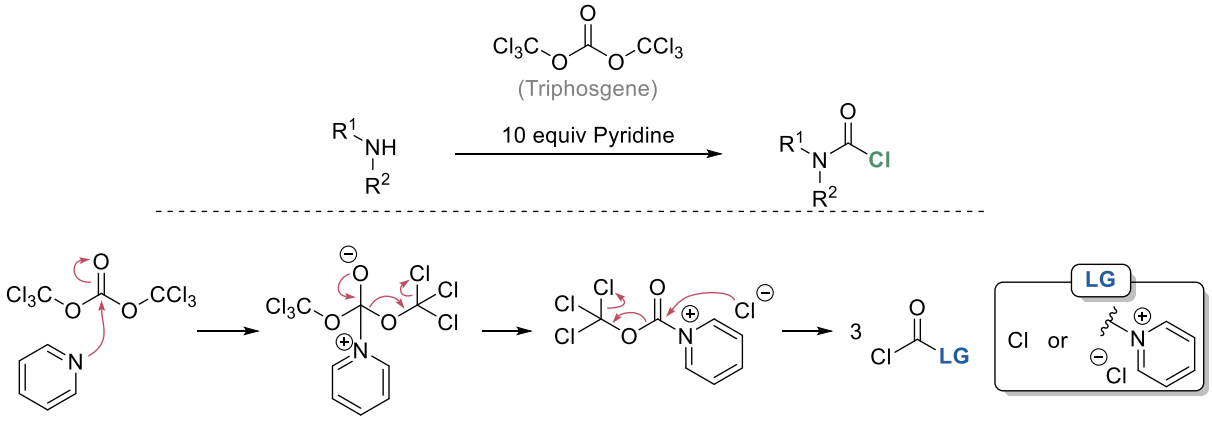

Scheme 1.1: Representative example for the preparation of CMCls, and the proposed mechanism in which phosgene is generated from triphosgene and pyridine.

The resonance stabilization caused by the nitrogen atom attenuates the electrophilicity of CMCls relative to acyl chlorides. This enables the isolation and purification of CMCls using conventional approaches like silica gel chromatography. However, this stabilization does not render them indefinitely stable or inert to hydrolysis. While many examples demonstrate a mild tolerance to intermittent contact with water, they are still typically susceptible to hydrolysis, resulting in the formation of secondary amine, CO_2, and HCl (Scheme 1.2).[36] Their reactivity and stability is largely dependent on the nitrogen substituents. For example, *N*,*N*-dimethylcarbamoyl chloride undergoes rapid hydrolysis under aqueous work-up conditions. Additionally, when one of

the nitrogen substituents is hydrogen, the resulting CMCl is generally unstable and readily eliminated HCl to form the corresponding isocyanate.[37] Consequently, CMCls are generally prepared and stored under dry conditions or are generated and consumed in situ.

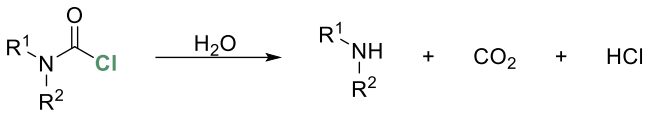

Scheme 1.2: General hydrolysis of CMCls.

Outside transition-metal catalysis, typical applications of CMCls involve their use as electrophiles in nucleophilic acyl substitution reactions. Typical nucleophiles include, alcohols, amines, or thiols affords carbamates, ureas, and thiocarbamates, respectively.[38–42] Notably, *N*-ethyl-*N*-methylcarbamoyl chloride has been employed for the carbamoylation of phenolic precursors in the synthesis of the acetylcholinesterase inhibitor *Rivastigmine* (Scheme 1.3).[43,44] With a patent describing this synthesis on a kilogram scale, demonstrating process-scale applicability of CMCls for installing substituted carbamate groups.[44]

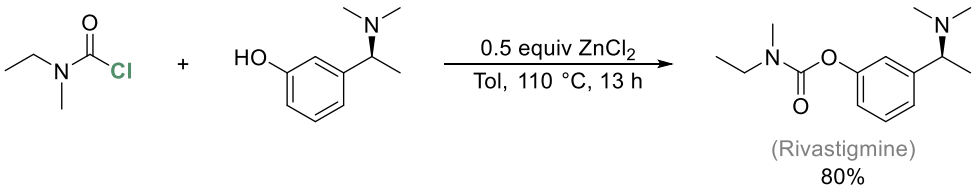

Scheme 1.3: Reaction employing CMCls to prepare Rivastigmine.

CMCls can also react with carbon-based nucleophiles to form amides through C–C bond formation at the carbonyl carbon. An early example was reported by Cuevas, Patil, and Snieckus, who trapped an *ortho*-lithiated α',α'-disilylated tertiary benzamide with *N*,*N*-diethylcarbamoyl chloride, thereby installing a tertiary amide substituent through C–C bond formation.[45,46] Comins and Hong subsequently used *N*,*N*-dimethylcarbamoyl chloride to trap the enolate of a cyclic ketone, affording a β-ketoamide that served as a key intermediate in the synthesis of (+)-elaeokanines A and C.[47,48] Although these reactions establish CMCls as versatile electrophilic

precursors to amides, their reliance on strongly basic and highly nucleophilic organometallic reagents can restrict functional-group compatibility. Overall, these established methods provide an important point of comparison for CMFs, whose preparation, stability, and synthetic applications are discussed in the following sections.

1.2.2. Carbamoyl Fluorides

Carbamoyl fluorides (CMFs) are the fluorinated analogues of CMCls and have historically received considerably less attention than their chloride counterparts. However, CMFs have gained increasing attention because of their distinctive balance of stability and reactivity. The discussion herein is limited to *N*,*N*-disubstituted CMFs derived from secondary amines. Despite their early discovery, the broader investigation of CMFs had been hindered by the limited availability of practical and general methods for their preparation. Traditionally, CMFs were prepared through halide exchange between the corresponding CMCl and a nucleophilic fluoride source, commonly potassium fluoride (Figure 1.7).[27,45,49] Although this approach is generally reliable, it requires prior preparation of the CMCl, thereby retaining the need for phosgene or a phosgene surrogate. Large excesses of the fluoride source and extended reaction times may also be required.[27,45,49] Alternatively, CMFs have also been prepared by treating secondary amines directly with carbonyl fluoride (COF_2) or carbonyl chlorofluoride (COClF)–the former will be referred to as difluorophosgene for the rest of this dissertation. However, the toxicity and gaseous nature of these reagents significantly limits the practicality of this approach, particularly in a conventional laboratory setting.[27,49]

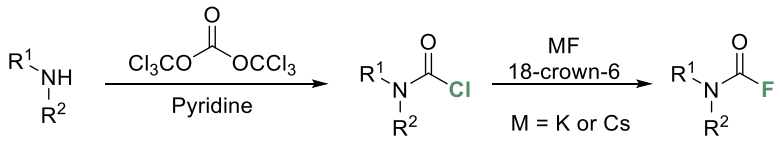

Figure 1.7: Conventional preparation of CMFs using halide exchange.

More recent methods have sought to prepare CMFs directly from secondary amines while avoiding the isolation or direct handling of difluorophosgene. In 2019, Onida and Tlili reported the direct synthesis of CMFs from secondary amines and carbon dioxide using diethylaminosulfur trifluoride (DAST) and 4-dimethylaminopyridine (DMAP) (Scheme 1.4).[50] This method employs carbon dioxide as the carbonyl source and avoids the preformation of CMCl, However, the relatively high cost, thermal instability, and potentially energetic decomposition of DAST presents important financial and safety concerns, particularly during reaction scale-up.



Scheme 1.4: General scheme for the synthesis of CMFs using DAST and DMAP.

Toulgoat, Billard and co-workers subsequently developed an alternative method based on the in situ formation of difluorophosgene.[51] Treatment of 2,4-dinitro-1-(trifluoromethoxy)benzene (DNTFB) with DMAP produced a solution containing a stable trifluoromethoxide salt, which decomposes upon addition of a hydrogen-bond donor to generate difluorophosgene in situ. Addition of secondary amine and diisopropylethylamine (DIPEA) afforded a range of CMFs (Scheme 1.5). However, the procedure also requires a separate reagent-preformation step and stoichiometric quantities of DNTFB, DMAP, and DIPEA, resulting in poor atom economy and the generation of substantial amounts of waste.

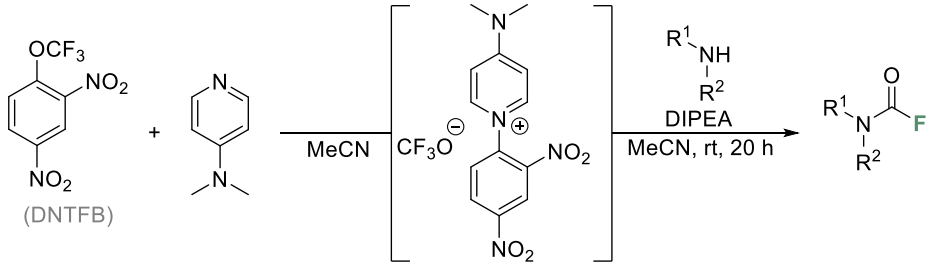

Scheme 1.5: General scheme for the synthesis of CMFs using DNTFB.

In 2022 our group reported a complementary synthesis of CMFs from secondary amines using bench-stable and readily handled reagents.[52] The proposed reaction mechanism proceeds through the thermally induced decarboxylation of (triphenylphosphonio)difluoroacetate (PDFA) to give phosphonium ylide **A**, which exists in equilibrium with free difluorocarbene (DFC) (**B**). Nucleophilic attack of DFC by 4-methylpyridine *N*-oxide forms zwitterion **C**, which subsequently collapses to generate COF_2 and one equivalent of 4-methylpyridine. Difluorophosgene then undergoes a typical nucleophilic acyl substitution reaction with the secondary amine, forming the desired CMF and one equivalent of HF, which is quenched in situ by the 4-methylpyridine byproduct (Scheme 1.6). The method was compatible with numerous secondary amines containing heterocycles, alkenes, alkynes, and other synthetically useful functional groups, with examples reported up to a one-gram scale. The work described in Chapter 2 extends this approach to the decagram scale preparation of CMFs, with particular emphasis on developing a practical reaction, work-up, and purification procedures suitable for large-scale synthesis. Section 2.5 discusses the hazards associated with difluorophosgene.

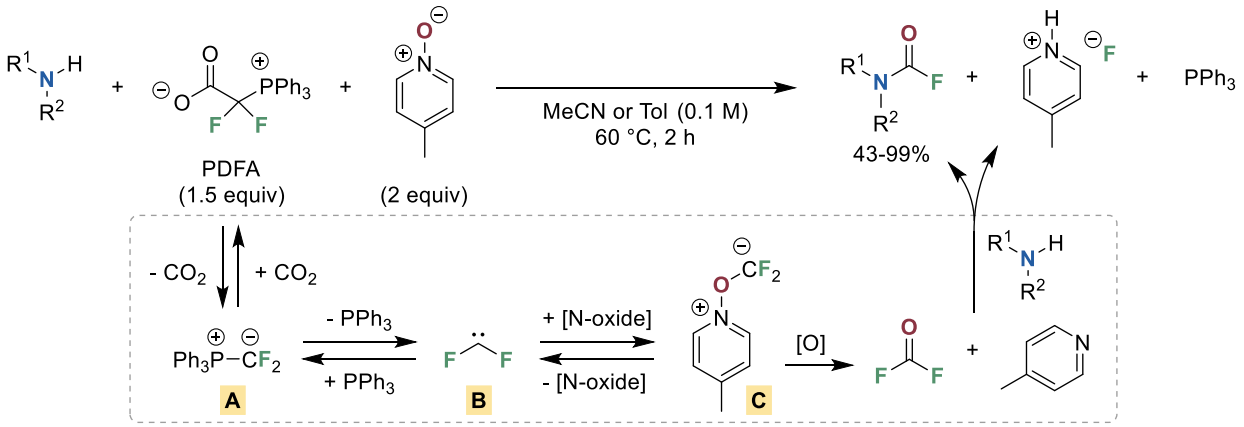

Scheme 1.6: Proposed mechanism for the synthesis of CMFs using PDFA.

Toulgoat, Billard and co-workers evaluated the stability of a representative CMF in several organic and aqueous media.[30] They were found to be stable at room temperature in dimethyl sulfoxide (DMSO), acetonitrile (MeCN), water, saline, and phosphate-buffered saline at pH 7.4.

Studies of the *N*-methyl-*N*-phenyl derivative demonstrated that more than 80% CMF remained after incubation in phosphate-buffered saline at 37 °C for 100 h and exhibited excellent compatibility with several nucleophilic amino acids. However, hydrolysis became more significant under basic conditions, with increased reaction rates in 1 M aqueous sodium hydroxide (Figure 1.8). These results demonstrate that some CMFs possess sufficient stability for aqueous manipulation and possible biological applications. Nevertheless, their relative stability is highly dependent on the nitrogen bound substituents of the CMF. For example, *N*-benzyl-*N*-2-pyridyl CMFs examined in this dissertation tolerate conventional aqueous work-up conditions but undergo hydrolysis following prolonged contact with water of the periods of days to weeks. By contrast, the analogous *N*-benzyl-*N*-phenyl CMF showed no detectable decomposition after one year immersed in water. It is therefore more accurate to describe CMFs as exhibiting enhanced but substrate-dependent stability relative to CMCls.

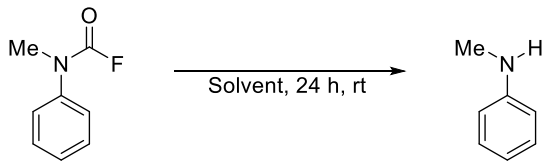

		%CMF Remaining
Solvents:	MeCN =	> 95%
	DMSO =	> 95%
	H_2O =	> 95%
	Saline =	> 95%
	HCl (1M) =	> 95%
	pH 4 =	> 95%
	pH 7 =	> 95%
	pH 10 =	~ 50%
	NaOH (1M) =	0%

Figure 1.8: CMF stability in various solvent systems over 24 hours.

Despite their increased stability, CMFs remain useful electrophilic intermediates and can be used as more stable alternatives to CMCls in select applications. An early synthetic application was reported by Hatch, who employed CMFs as intermediates in the preparation of insecticidal *N*-sulfenyl carbamates.[53] More recently, our group reported the fluoride-catalyzed coupling of CMFs with alkynylsilanes to produce alkynamides.[54] In this reaction, tetrabutylammonium fluoride (TBAF) activates the alkynylsilane, while formation of a strong Si–F bond provides a thermodynamic driving force for product formation (Scheme 1.7 **A**). Our group also demonstrated

that BF_3 can catalyze the intramolecular fluorocarbamoylation of alkynes, formally adding the carbamoyl and fluoride components across the alkyne in an atom-economical fashion (Scheme 1.7 **B**).[55] These transformations illustrate that fluorine can function not only as a leaving group but also as a component of catalytic activation and recycling pathways.

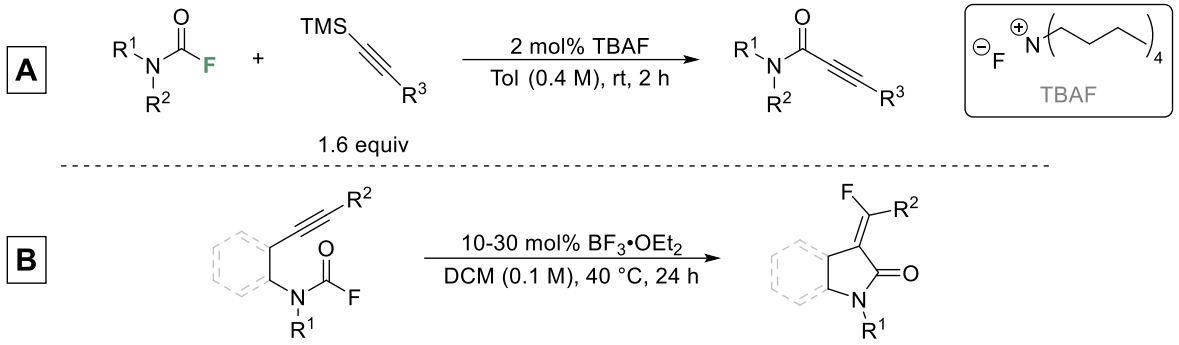

Scheme 1.7: Representative reactions exploiting the unique properties CMFs beyond simply acting as a leaving group.

The combination of enhanced aqueous stability and controlled electrophilicity has also prompted investigation of CMFs in chemical biology. Recently, Gobec, Knez and co-workers investigated CMFs as covalent inhibitors of Fphl, a serine hydrolase from *staphylococcus aureus*.[58] A focused library of 52 fragment-sized CMFs were evaluated, of which 51 inhibited Fphl during the initial screen. Two compounds displayed apparent nanomolar half maximal inhibitory concentration (IC_{50}) values following a one-hour incubation. Time-dependent inhibition, intact-protein mass spectrometry, and single-crystal X-ray crystallography (SC-XRD) supported covalent carbamoylation of the Ser94 residue (Figure 1.9). Although the tested compounds generally lacked substantial whole-cell antibacterial activity, the study establishes CMFs as tunable covalent warheads of serine hydrolase inhibition and provides a recent example of their potential application in chemical biology.

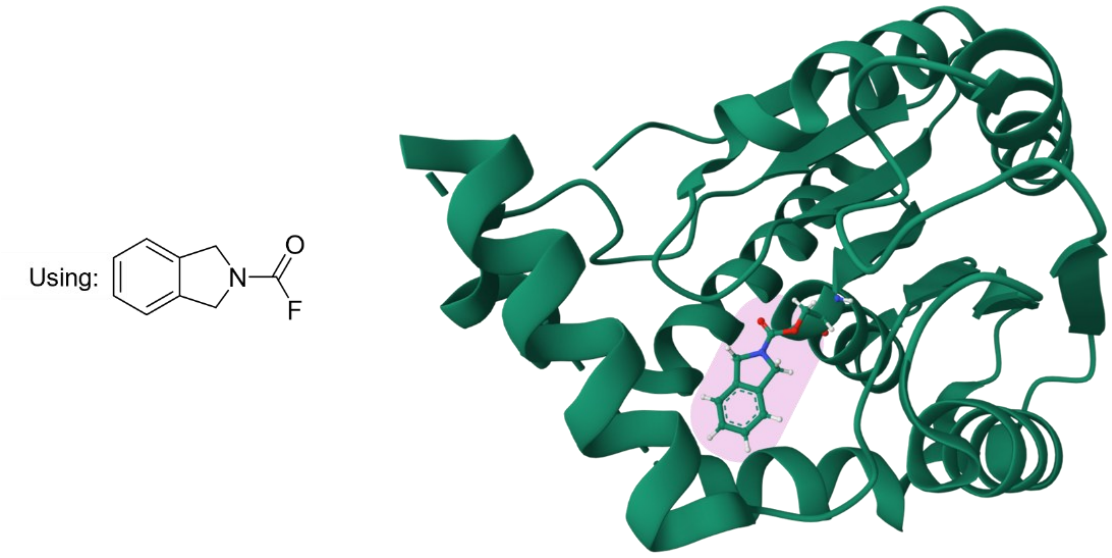

Figure 1.9: Solid-state structure of carbamoylated Ser94 residue using the indicated CMF. Structure accessed from the Protein Data Bank: pdb_00009nix.

Overall, CMFs occupy a useful intermediate position between the high reactivity of CMCls and the stability of conventional amides. Their enhanced stability typically allows for their isolation and purification, while the C–F bond retains latent reactivity that can be activated using nucleophilic, Lewis acidic, or transition metal catalysis. This combination of bench stability and tunable reactivity makes CMFs attractive electrophilic precursors for C–C bond formation and supports their emerging applications in organic synthesis, radiochemistry, and chemical biology. In particular, transition-metal catalysis provides an opportunity to selectively engage the carbamoyl C–F bond and further expand the used of CMFs in amide synthesis, as discussed in the following section.

1.3. Transition-Metal-Catalyzed Amide Synthesis Using Carbamoyl Halides

Transition-metal catalysis provides a complementary strategy for preparing amides from carbamoyl halides. Unlike conventional amidation methods, which are generally constructed through C–N bond formation, carbamoyl halides already contain the N–C(O) linkage present in the final product. Activation of the carbamoyl C–X bond by a transition-metal catalyst instead enables formation of a new C–C bond at the carbonyl carbon.

Among these transformations, the Suzuki-Miyaura cross-coupling is particularly attractive as many organoboron reagents are widely accessible, comparatively stable, and compatible with a broad range of functional groups.[59,60] Additionally, in surveys of pharmaceutical discovery chemistry, Suzuki cross-coupling reactions were among the most frequently employed transformations and represented one of the largest single class of C–C bond formation reactions.[61,62] Its practical utility has also led to widespread implementation in large-scale pharmaceutical manufacturing.[63] Despite this broad adoption, Suzuki cross-coupling reactions that directly afford amides through C–C bond formation of the carbamoyl carbon remain comparatively underdeveloped, with only a limited number of examples reported.[64–68] Accordingly, carbamoyl halides are promising electrophiles for expanding Suzuki-type amide synthesis and extend a well established, industrially relevant cross-coupling platform to this comparatively underdeveloped transformation.

In a general simplified Suzuki cross-coupling, the catalytic cycle begins with oxidative addition of the C–X bond of an organic electrophile to a low valent metal complex M(0) **I**, typically Pd(0) or Ni(0), generating the intermediate M(II) complex **II** bearing both the organic fragment

(R) and halide as ligands (Figure 1.10). Transmetalation subsequently transfers a second organic group (R'), from the organoboron reagent to the metal center forming intermediate **III**. Reductive elimination then forms a new C–C bond, releasing the cross-coupled product and regenerating the low-valent M(0) catalyst **I** (Figure 1.10).

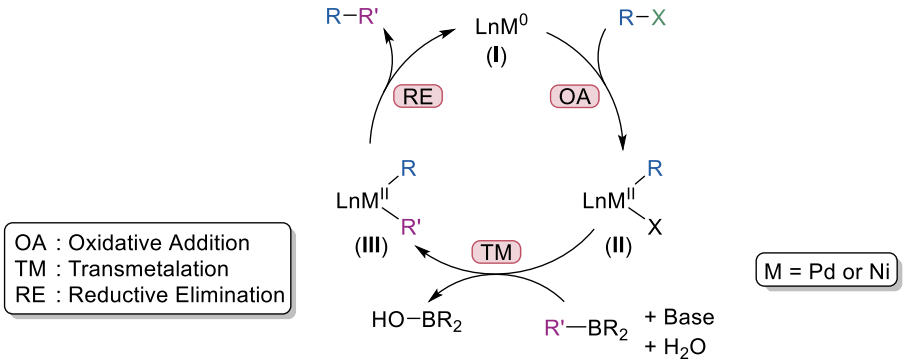

Figure 1.10: General Suzuki cross-coupling reaction mechanism.

Although this catalytic-cycle illustrates the principal bond-forming steps, the oxidation state and structure of catalytic intermediates, as well as the order in which they form, can depend on the metal-ligand combination employed. In particular, nickel-catalyzed Suzuki cross-coupling reactions can proceed though an alternative Ni(I)/Ni(III) pathway, where instead transmetalation occurs first with Ni(I) **IV**, forming the organonickel(I) intermediate **V**. Oxidative addition then forms a Ni(III) complex **VI** that reductively eliminates to afford the cross-coupled product and regenerate the Ni(I) catalyst **IV** (Figure 1.11).

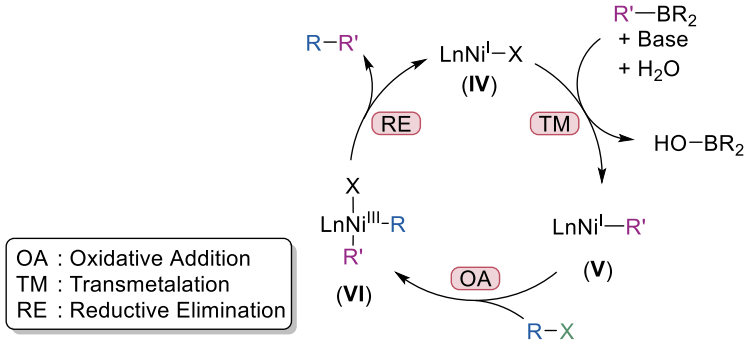

Figure 1.11: General Ni(I)/Ni(III) Suzuki cross-coupling reaction mechanism.

It is important to note that the base employed in Suzuki cross-coupling reactions can have a pronounced influence on transmetalation step through its effects on both the metal catalyst and organoboron reagent.[69–71] Water can play several roles, including solubilization of inorganic base and generation of hydroxide in situ which can facilitate activation of the organoboron reagent and the subsequent boron-to-metal transmetalation. Base may also promote ligand exchange of a metal halide with hydroxide, generating the corresponding metal-hydroxo complex (**II-A**) capable of transmetalating with a neutral organoboron reagent (Figure 1.12). Alternatively, reaction of hydroxide with the Lewis acidic organoboron may generate the tetra-coordinate boronate species that can undergo transmetalation with oxidative addition complex **II**. These pathways are not mutually exclusive, and their relative importance depends on the metal, ligand, base, solvent, and organoboron employed.[69–71] Water can additionally influence ion pairing and the hydrolysis and aggregation of organoboron reagents. Consequently, the effects of water and base cannot necessarily be considered independent.

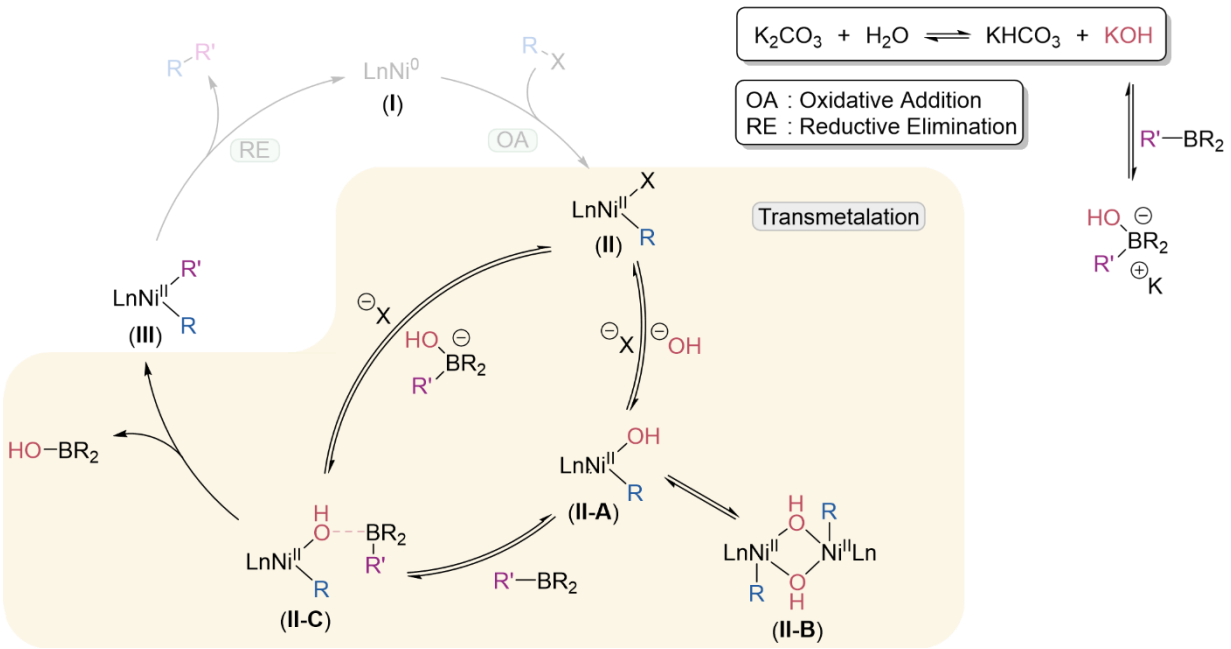

Figure 1.12: Revised Ni(0)/Ni(II) catalytic cycle, with consideration for the role of base and water.

The sensitivity of these equilibria can be particularly pronounced in nickel-catalyzed Suzuki cross-coupling reactions. Grimaud and co-workers found that dinuclear μ-hydroxo-bridged nickel complexes can function as a catalyst resting state (**II-B**), with their concentration controlled largely by the relative amount of base and boronic acid present.[71] Thus, although hydroxide can facilitate the formation of transmetalation-competent nickel species, excessive hydroxide may, in some catalytic systems sequester Ni(II) intermediates as μ-hydroxo-bridged dimers and decrease the concentration of reactive mononuclear species. The precise balance between water and base can therefore be an important determinant of nickel-catalyzed Suzuki cross-coupling reactions.

Accordingly, insufficient water or base can limit both the solubilization of the inorganic base and the formation of transmetalation-competent species. Whereas excessive water or hydroxide can alter nickel speciation and promote decomposition of the organoboron reagent. In reactions employing carbamoyl halides, hydrolysis of the electrophile under aqueous basic conditions introduces an additional competing pathway for substrate consumption. The optimal conditions therefore depend not only on the identities of the base and solvent but also their relative quantities and the amount of water present. This balance proved especially relevant to the nickel-catalyzed Suzuki cross-coupling of CMFs described in Chapter 4, for which control of the water-to-base ratio was critical to productive catalysis. The following sections examine the transition-metal-catalyzed reactions of CMCls and CMFs, beginning with the more extensively studied chloride derivatives.

1.3.1. Carbamoyl Chlorides

Carbamoyl chlorides have been extensively employed as electrophiles in transition-metal-catalyzed reactions. In many palladium- and nickel-catalyzed transformations, oxidative addition of the carbamoyl C–Cl bond to a low-valent metal center generates a metal-carbamoyl intermediate

that can participate in catalytic transformation such as migratory insertion, transmetalation, C–H functionalization, decarbonylation, or reductive elimination. Although, palladium catalysis has been studied most extensively, transformations involving nickel, copper, and iridium have also been reported.[72] Given the scope of this chemistry, a comprehensive review of transition-metal-catalyzed reactions of CMCls is beyond the scope of this dissertation. Accordingly, the following discussion focuses on representative intramolecular examples and the comparatively limited number of intermolecular cross-coupling reactions most relevant to the development of the CMF cross-coupling reactions discussed in Chapters 3 and 4.

The majority of transition-metal-catalyzed reactions of CMCls involve intramolecular reactions of substrates containing tethered alkenes, alkynes, or arenes.[72–75] These transformations take advantage of the proximity of the reacting groups to intercept the metal-carbamoyl intermediates and provide efficient access to lactams, oxindoles, and related nitrogen-containing heterocycles. Notably, Lautens, and co-workers reported a Pd(0)-catalyzed, exclusively trans-selective chlorocarbamoylation of alkyne-tethered aryl CMCls using a phosphaadamantane ligand, affording chloromethylene oxindoles in high yields and with excellent stereoselectivities (Scheme 1.8 **A**).[75] Mechanistic studies indicated that oxidative addition of the carbamoyl C–Cl bond occurs readily, whereas subsequent insertion of the tethered alkyne into the Pd-carbamoyl bond was turnover-limiting. The unusual *trans*-addition selectivity was attributed to rapid isomerization of the resulting alkenylpalladium intermediate before reductive elimination.[74,75] A mechanistically distinct Pd(II) catalyzed reaction was subsequently developed for the stereoselective synthesis of methylene oxindoles and was proposed to proceed through a Pd(II)/Pd(IV) catalytic cycle (Scheme 1.8 **B**).[73] These studies demonstrate that both Pd(0)- and Pd(II)-catalyzed pathways can add the carbamoyl and chloride fragments of a CMCl across a tethered alkyne, affording stereodefined

oxindoles. Nevertheless, both methods require an intramolecular substrate design and therefore do not address intermolecular amide formation.

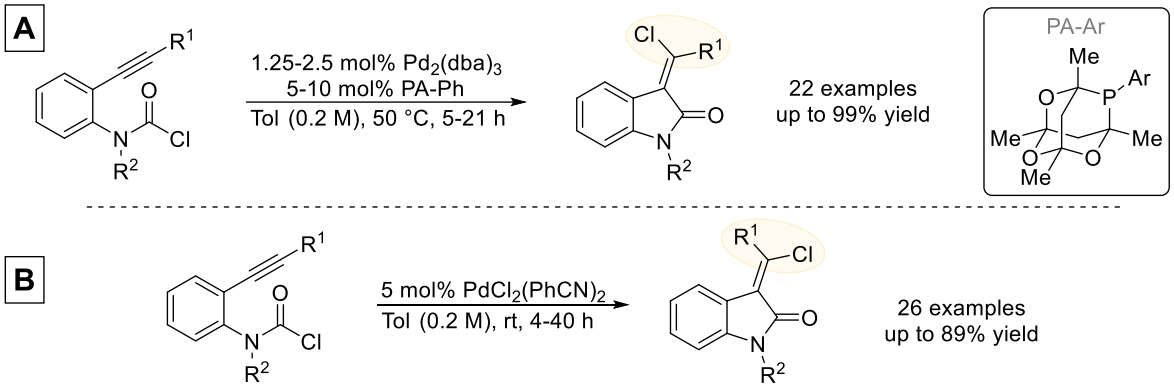

Scheme 1.8: Palladium catalyzed stereoselective intramolecular cyclization of CMCls.

Intermolecular cross-coupling reactions of CMCls are considerably less common. In 1991, Balas, Jousseaume, and co-workers reported the palladium catalyzed coupling of CMCls with aryl- and vinylstannanes. This method afforded a transition-metal-catalyzed route to tertiary amides through intermolecular C–C bond formation using CMCls.[76] Lemoucheux and co-workers subsequently demonstrated that nickel catalysts promote the coupling of *N*,*N*-dialkyl CMCls with alkyl- and aryl- Grignards.[77] Although these studies established the feasibility of intermolecular CMCl cross-coupling, the toxicity and persistence of organotin by-products and the nucleophilicity of Grignard reagents limit the practicality and functional-group compatibility of the respective methods.

Organoboron reagents are a comparatively stable and functional-group tolerant alternative for the intermolecular cross-coupling of CMCls. In 2005, Lysén and co-workers reported the palladium-catalyzed cross-coupling of *ortho*-substituted arylboronic esters with CMCls to afford tertiary benzamides (Scheme 1.9 **A**).[78] During the same year, Duan and Deng described the cross-coupling of arylboronic acids with *N*,*N*-dibutylcarbamoyl chlorides using $Pd(PPh_3)_4$ with Cu_2O as

a cocatalyst (Scheme 1.9 **B**).[64] Although several arylboronic acids were examined, the CMCl scope was limited to only *N*,*N*-dibutylcarbamoyl chloride.

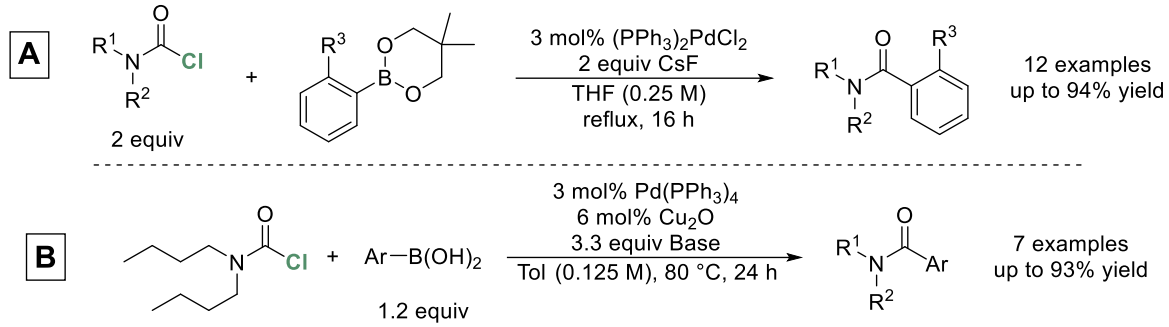

Scheme 1.9: Early examples of cross-coupling reactions between CMCls and organoboron reagents.

Takemoto and co-workers subsequently reported a one-pot amidation of alkenes through hydroboration and subsequent palladium-catalyzed cross-coupling with CMCls (Scheme 1.10).[68] Hydroboration of alkenes with 9-borabicyclo[3.3.1]nonane (denoted as H-9BBN throughout this dissertation to distinguish the B–H reagent from other B-substituted 9BBN species) generated the corresponding alkyl-9-BBN coupling partner, which was used as the nucleophile in the cross-coupling with CMCls. This transformation afforded tertiary amides through construction of a C(O)–C(sp^3) bond and represents and an important precedent for the cross-coupling of carbamoyl halides with alkylboranes.

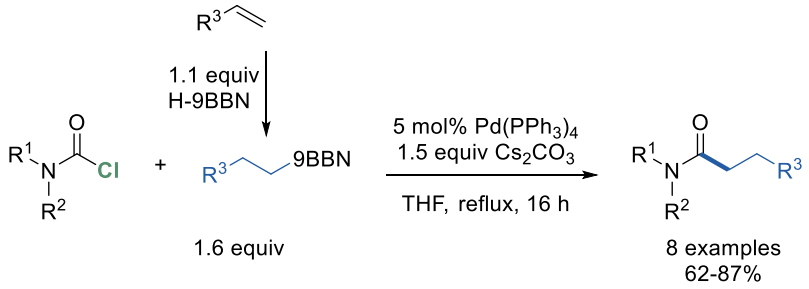

Scheme 1.10: Suzuki cross-coupling of CMCls with alkyl-9-BBN derivatives.

Collectively, these studies demonstrate that CMCls can participate in intermolecular Suzuki cross-coupling reactions with both C(sp^2)- and C(sp^3)-hybridized organoboron reagents. Nevertheless, the number of reported methods remain small relative to the extensive

intramolecular examples, with most studies examining a limited range of CMCl electrophiles. Furthermore, hydrolysis of CMCls can compete with productive cross-coupling under the aqueous basic conditions commonly employed in Suzuki cross-coupling reactions. The generally enhanced stability of CMFs therefore makes them an attractive alternative for transition-metal-mediated C–C bond formation. However, activation of the carbamoyl C–F bond introduces a distinct catalytic challenge, as discussed in the following section.

1.3.2. Carbamoyl Fluorides

Due to their decreased reactivity relative to CMCls, CMFs have been investigated considerably less in transition-metal-catalyzed transformations.[27] Prior to our work on the intermolecular cross-coupling reactions (described in Chapters 3 and 4 of this dissertation), only three transition-metal-catalyzed transformations of CMFs had been reported.[79–81] Two of these methods relied on intramolecular cyclization to intercept a metal-carbamoyl intermediate, whereas the only intermolecular example employed highly activated *N*–CF_3 substituted CMFs. Consequently, the ability of conventional unactivated CMFs to participate in direct intermolecular cross-coupling reactions remained largely unexplored.

In 2020 Ye, Luan, and co-workers reported the first nickel-catalyzed enantioselective carbocarbamoylation of unactivated alkenes using CMFs (Scheme 1.11).[81] Alkene-tethered CMFs were coupled with arylboronic acids to afford chiral γ-lactams bearing an all-carbon quaternary center. The proposed catalytic cycle proceeds through initial oxidative addition of the C–F bond to Ni(0), followed by intramolecular insertion of the tethered alkene into the Ni–carbamoyl bond. Subsequent transmetalation with the arylboronic acid and reductive elimination afforded the γ-lactam product. This report established that CMFs could undergo productive C–F bond activation

by nickel. However, coupling relied on intramolecular interception of the Ni–carbamoyl intermediate by the tethered alkene.

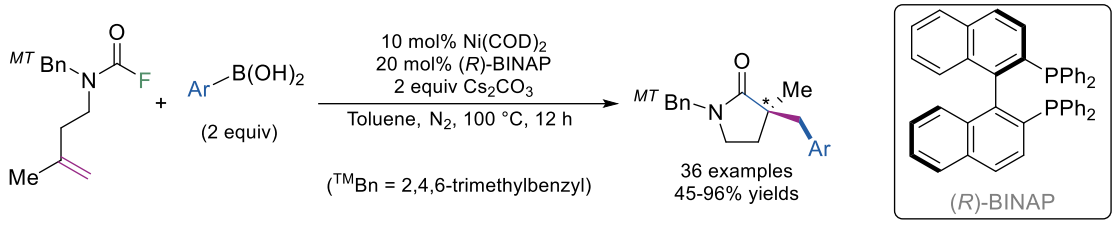

Scheme 1.11: Representative reaction scheme for the carbamoyl fluoride-enabled enantioselective Ni-catalyzed carbocarbamoylation of unactivated alkenes.

Schoenebeck and co-workers subsequently reported the nickel-catalyzed coupling of *N*–CF_3 CMFs with alkynylsilanes, providing the first synthetic access to *N*–CF_3 alkynamides (Scheme 1.12).[80] Importantly, this represented the only intermolecular transition-metal-catalyzed transformation of CMFs reported prior to the work described in this dissertation. The CMFs employed contained a strongly withdrawing *N*–CF_3 substituent, which rendered these CMFs significantly more electrophilic and activated relative to conventional *N*,*N*-disubstituted derivatives. Additionally, because of this increased electrophilicity, purification of the *N*–CF_3 CMFs was generally not possible, and most were employed as crude mixtures directly from the previous step. Although the resulting *N*–CF_3 alkynamides were reported to be robust, the specialized and highly activated nature of the starting CMFs limited the extent to which their reactivity could be considered representative of conventional CMFs. Nevertheless, this work demonstrated that intermolecular cross-coupling of CMFs was possible.

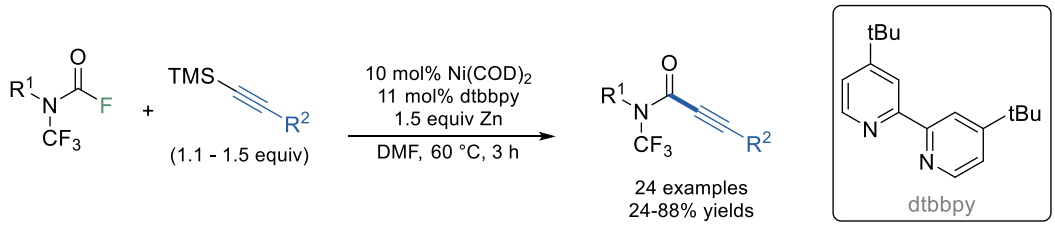

Scheme 1.12: Representative reaction scheme for the nickel-catalyzed alkynylation of *N*-CF_3 CMFs.

In the third and final example, Chen and co-workers developed a nickel-catalyzed enantioselective 1,4-arylcarbamoylation of 1,3-diene-tethered CMFs with arylboronic acids (Scheme 1.13).[79] This transformation afforded α-alkenylated γ-lactams proceeding through a similar mechanism analogous to that proposed by Ye and Luan. The reaction expanded CMF-enabled carbocarbamoylation to 1,3-dienes and provided access to a distinct class of stereodefined γ-lactams. As in the earlier report by Ye and Luan, productive coupling depended on intramolecular cyclization and did not provide a direct intermolecular route to acyclic amides.

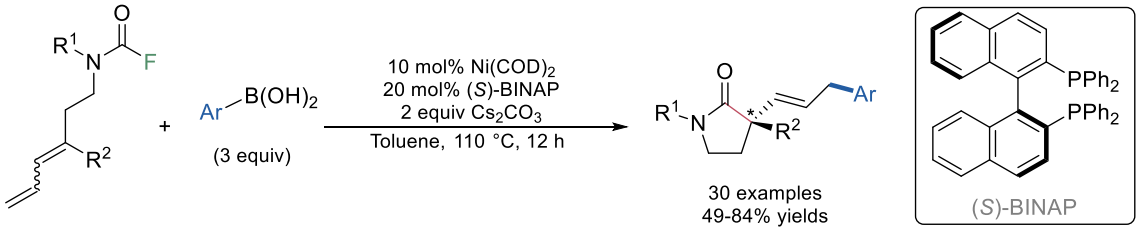

Scheme 1.13: Representative example of the 1,4-arylcarbamoylation of 1,3-diene-tethered CMFs with arylboronic acids.

Collectively, these studies established that nickel catalysts can activate CMFs and use the resulting metal-carbamoyl intermediates in C–C bond formation. Nevertheless, two methods relied on tethered unsaturated groups to promote intramolecular cyclization, whereas the sole intermolecular example employed strongly activated *N*–CF_3 CMFs. Accordingly, no general intermolecular metal-catalyzed cross-coupling of conventional *N*,*N*-disubstituted CMFs had been demonstrated.

However, during the work described in Chapter 4, Amgoune, Tlili, and co-workers reported the nickel-catalyzed Suzuki cross-coupling of conventional CMFs with aryl boronic acids.[82] Because this work appeared during our studies, its relationship to the work described in this dissertation is examined in the introduction of Chapter 4. The work presented in Chapter 4 investigates a complementary method involving intermolecular nickel-catalyzed cross-coupling of CMFs with alkylboranes, extending CMF cross-coupling to the formation of C(O)–C(sp^3) bonds.

1.4. Conclusion and Research Prelude

Amides are prevalent structural motifs in biological systems, pharmaceuticals, agrochemicals, polymers, and commodity chemicals, making their efficient preparation an important objective in synthetic organic chemistry. Conventional amidation methods generally construct the amide C–N bond through reactions between amines and carboxylic acids or activated carboxylic acid derivatives. Carbamoyl halides provide a complementary alternative approach, as the N–C(O) motif of the final amide is already incorporated into the starting material. The remaining carbon substituent can therefore be introduced using well-established methods for C–C bond formation to furnish the corresponding amides. Together, these retrosynthetic disconnections will be complementary, allowing for a broader scope of amide derivatives to be accessed.

CMCls have been used extensively in substitution, cyclization, and transition-metal-catalyzed reactions, but their susceptibility to hydrolysis can complicate their isolation, long-term storage, and use under aqueous or basic reaction conditions. In contrast, CMFs exhibit improved stability and resistance to hydrolysis but are considerably less established as competent electrophiles, particularly in intermolecular transition-metal-catalyzed reactions. Their reduced reactivity and strong carbamoyl C–F bond can present a substantial challenge for catalytic activation. Consequently, the broader objective of this dissertation is to establish CMFs as practical, bench-stable, and isolable electrophiles for the synthesis of amides through C–C bond formation. Achieving this objective requires practical and scalable methods for preparing CMFs and catalytic systems capable of activating the carbamoyl C–F bond, while promoting productive reactivity with carbon-based coupling partners.

Chapter 2 further builds on our group's previously developed synthesis of CMFs directly from secondary amines and adapts the method for practical, scalable preparation. Particular attention is given to evaluating reaction and reagent safety, optimizing work-up and purification procedures, and translating the modified methods from small-scale reactions to decagram-scale preparation. Together, these advances improve the accessibility of structurally diverse CMFs and facilitates their use as isolable synthetic compounds. This work also provides a foundation for further scale-up, with the longer-term goal of supporting the broader adoption of CMFs routinely used synthetic species in industrial-scale chemistry. (J. LeBlanc, E. Woo, J. Laurie, C. Le, *manuscript in preparation*)

Chapter 3 describes the palladium-catalyzed intermolecular Suzuki cross-coupling of 2-pyridyl CMFs with arylboronic acids to form medicinally relevant 2-pyridyl amides. The Chapter examines the role of the 2-pyridyl substituent in directing activation of the carbamoyl C–F bond, investigates organometallic intermediates relevant to the proposed catalytic cycle, and evaluates the possible role of triphenylphosphine oxide as a reaction additive.

Chapter 4 subsequently describes the nickel-catalyzed intermolecular Suzuki cross-coupling of unactivated CMFs with alkylboranes to afford *N*,*N*-disubstituted aliphatic amides through formation of C(O)–C(sp^3) bonds. Reaction development involved thorough optimization studies, followed by evaluation across a broad range of CMF and alkylborane substrates. Beyond reaction development, comprehensive mechanistic studies investigate catalyst activation, oxidative addition into the carbamoyl C–F bond, transmetalation, and the effects of base, water, and solvent selection on productive catalysis. Together, these studies provide insight into both the elementary organometallic steps and the reaction parameters required to maintain productive catalysis. (J. LeBlanc, S. Galea, M Jabbarpoor, D. Nelson, C. Le, *manuscript in preparation*)

Overall, the studies presented in this dissertation expand on the synthetic utility of CMFs and establish a foundation for their broader application as practical, bench-stable electrophiles in transition-metal-catalyzed amide synthesis.

1.5. References

(1) Pitzer, J.; Steiner, K. Amides in Nature and Biocatalysis. *J. Biotechnol.* **2016**, *235*, 32–46. https://doi.org/10.1016/j.jbiotec.2016.03.023.

(2) Seavill, P. W.; Wilden, J. D. The Preparation and Applications of Amides Using Electrosynthesis. *Green Chem.* **2020**, *22* (22), 7737–7759. https://doi.org/10.1039/d0gc02976a.

(3) Rajamanickam, K. R.; Rajan, R. P. S.; Pootheri, N.; Lee, C.-F.; Lee, S. Recent Advances in Transition Metal-Free Strategies for the Transformation of Amides into Carbonyl Compounds. *Eur. J. Org. Chem.* **2025**, *28* (23), e202500210. https://doi.org/10.1002/ejoc.202500210.

(4) Kaiser, D.; Bauer, A.; Lemmerer, M.; Maulide, N. Amide Activation: An Emerging Tool for Chemoselective Synthesis. *Chem. Soc. Rev.* **2018**, *47* (21), 7899–7925. https://doi.org/10.1039/c8cs00335a.

(5) de Figueiredo, R. M.; Suppo, J.-S.; Campagne, J.-M. Nonclassical Routes for Amide Bond Formation. *Chem. Rev.* **2016**, *116* (19), 12029–12122. https://doi.org/10.1021/acs.chemrev.6b00237.

(6) Pattabiraman, V. R.; Bode, J. W. Rethinking Amide Bond Synthesis. *Nature* **2011**, *480* (7378), 471–479. https://doi.org/10.1038/nature10702.

(7) Ojeda-Porras, A.; Gamba-Sánchez, D. Recent Developments in Amide Synthesis Using Nonactivated Starting Materials. *J. Org. Chem.* **2016**, *81* (23), 11548–11555. https://doi.org/10.1021/acs.joc.6b02358.

(8) Allen, C. L.; Williams, J. M. J. Metal-Catalysed Approaches to Amide Bond Formation. *Chem. Soc. Rev.* **2011**, *40* (7), 3405–3415. https://doi.org/10.1039/c0cs00196a.

(9) Mujika, J. I.; Matxain, J. M.; Eriksson, L. A.; Lopez, X. Resonance Structures of the Amide Bond: The Advantages of Planarity. *Chem. – Eur. J.* **2006**, *12* (27), 7215–7224. https://doi.org/10.1002/chem.200600052.

(10) Serrano, E.; Martin, R. Forging Amides Through Metal-Catalyzed C–C Coupling with Isocyanates. *Eur. J. Org. Chem.* **2018**, *2018* (24), 3051–3064. https://doi.org/10.1002/ejoc.201800175.

(11) Charville, H.; Jackson, D.; Hodges, G.; Whiting, A. The Thermal and Boron-Catalysed Direct Amide Formation Reactions: Mechanistically Understudied yet Important Processes. *Chem. Commun.* **2010**, *46* (11), 1813–1823. https://doi.org/10.1039/b923093a.

(12) Palmer, R. J. Polyamides, Plastics. In *Encyclopedia of Polymer Science and Technology*; John Wiley & Sons, Ltd, 2001. https://doi.org/10.1002/0471440264.pst251.

(13) Lundberg, H.; Tinnis, F.; Selander, N.; Adolfsson, H. Catalytic Amide Formation from Non-Activated Carboxylic Acids and Amines. *Chem. Soc. Rev.* **2014**, *43* (8), 2714–2742. https://doi.org/10.1039/c3cs60345h.

(14) Yoshida, T.; Irizawa, T.; Ogura, K.; Komido, T. Process for Producing Dimethylacetamide. CA2329241A1, October 28, 1999. https://patents.google.com/patent/CA2329241A1/en (accessed 2026-07-25).

(15) Fergusson, S. B.; Marchildon, E. K.; Mutel, A. T. Process for Making Nylon 6,6. US6472501B1, October 29, 2002. https://patents.google.com/patent/US6472501B1/en (accessed 2026-07-25).

(16) Magano, J. Large-Scale Amidations in Process Chemistry: Practical Considerations for Reagent Selection and Reaction Execution. *Org. Process Res. Dev.* **2022**, *26* (6), 1562–1689. https://doi.org/10.1021/acs.oprd.2c00005.

(17) Fujita, T.; Suto, M.; Ogura, K. Process for Production of Dimethylformamide. US4251460A, February 17, 1981. https://patents.google.com/patent/US4251460A/en (accessed 2026-07-25).
(18) Grafmans, H.; Maas, S.; Weck, A.; Rütter, H.; Schulz, M.; Roβ, K.-H. Method for the Production of N,N-Dimethylacetamide (DMAC). US8193390B2, June 5, 2012. https://patents.google.com/patent/US8193390B2/en (accessed 2026-07-25).
(19) Magano, J. Large-Scale Amidations in Process Chemistry: Practical Considerations for Reagent Selection and Reaction Execution. *Org. Process Res. Dev.* **2022**, *26* (6), 1562–1689. https://doi.org/10.1021/acs.oprd.2c00005.
(20) Dunetz, J. R.; Magano, J.; Weisenburger, G. A. Large-Scale Applications of Amide Coupling Reagents for the Synthesis of Pharmaceuticals. *Org. Process Res. Dev.* **2015**, *20* (2), 140–177. https://doi.org/10.1021/op500305s.
(21) Valeur, E.; Bradley, M. Amide Bond Formation: Beyond the Myth of Coupling Reagents. *Chem. Soc. Rev.* **2009**, *38* (2), 606–631. https://doi.org/10.1039/b701677h.
(22) Hansen, S. V. F.; Ulven, T. Oxalyl Chloride as a Practical Carbon Monoxide Source for Carbonylation Reactions. *Org. Lett.* **2015**, *17* (11), 2832–2835. https://doi.org/10.1021/acs.orglett.5b01252.
(23) Montalbetti, C. A. G. N.; Falque, V. Amide Bond Formation and Peptide Coupling. *Tetrahedron* **2005**, *61* (46), 10827–10852. https://doi.org/10.1016/j.tet.2005.08.031.
(24) Shi, M.; Ye, N.; Chen, W.; Wang, H.; Cheung, C.; Parmentier, M.; Gallou, F.; Wu, B. Simple Synthesis of Amides via Their Acid Chlorides in Aqueous TPGS-750-M. *Org. Process Res. Dev.* **2020**, *24* (8), 1543–1548. https://doi.org/10.1021/acs.oprd.0c00303.
(25) Sabatini, M. T.; Boulton, L. T.; Sneddon, H. F.; Sheppard, T. D. A Green Chemistry Perspective on Catalytic Amide Bond Formation. *Nat. Catal.* **2019**, *2* (1), 10–17. https://doi.org/10.1038/s41929-018-0211-5.
(26) Liu, L.; Gu, Y.-C.; Zhang, C.-P. Recent Advances in the Synthesis and Transformation of Carbamoyl Fluorides, Fluoroformates, and Their Analogues. *Chem. Rec.* **2023**, *23* (9), e202300071. https://doi.org/10.1002/tcr.202300071.
(27) Jabbarpoor, M.; Le, C. M. Carbamoyl Fluorides: A Platform to Interrogate Fluoride-Enabled Reactivity. *Synthesis* **2025**, *57* (16), 2399–2410. https://doi.org/10.1055/a-2557-7635.
(28) Jäger, P.; Rentzea, C. N.; Kieczka, H. Carbamates and Carbamoyl Chlorides. In *Ullmann's Encyclopedia of Industrial Chemistry*; John Wiley & Sons, Ltd, 2000. https://doi.org/10.1002/14356007.a05_051.
(29) Shrestha, M.; Wu, X.; Huang, W.; Qu, J.; Chen, Y. Recent Advances in Transition Metal-Catalyzed Reactions of Carbamoyl Chlorides. *Org. Chem. Front.* **2021**, *8* (14), 4024–4045. https://doi.org/10.1039/d0qo01648a.
(30) Bonnefoy, C.; Chefdeville, E.; Tourvieille, C.; Panossian, A.; Hanquet, G.; Leroux, F.; Toulgoat, F.; Billard, T. Study of Carbamoyl Fluoride: Synthesis, Properties and Applications. *Chem. – Eur. J.* **2022**, *28* (43), e202201589. https://doi.org/10.1002/chem.202201589.
(31) Varjosaari, S. E.; Suating, P.; Adler, M. J. One-Pot Synthesis of O-Aryl Carbamates. *Synthesis* **2016**, *48* (01), 43–47. https://doi.org/10.1055/s-0035-1560726.
(32) Ganiu, M. O.; Nepal, B.; Van Houten, J. P.; Kartika, R. A Decade Review of Triphosgene and Its Applications in Organic Reactions. *Tetrahedron* **2020**, *76* (47), 131553. https://doi.org/10.1016/j.tet.2020.131553.
(33) Eckert, H.; Forster, B. Triphosgene, a Crystalline Phosgene Substitute. *Angew. Chem. Int. Ed. Engl.* **1987**. https://doi.org/10.1002/anie.198708941.

(34) Eckert, H.; Auerweck, J. Solvent-Free and Safe Process for the Quantitative Production of Phosgene from Triphosgene by Deactivated Imino-Based Catalysts. *Org. Process Res. Dev.* **2010**, *14* (6), 1501–1505. https://doi.org/10.1021/op100239n.
(35) Semler, G.; Schaeffer, G. Process for the Preparation of Carbamoyl Chlorides Derived from Secondary Amines. US4770820A, September 13, 1988. https://patents.google.com/patent/US4770820A/en (accessed 2026-07-26).
(36) D'Souza, M. J.; Kevill, D. N. Mechanistic Studies of the Solvolyses of Carbamoyl Chlorides and Related Reactions. *Int. J. Mol. Sci.* **2016**, *17* (1), 111. https://doi.org/10.3390/ijms17010111.
(37) Stare, M.; Laniewski, K.; Westermark, A.; Sjögren, M.; Tian, W. Investigation on the Formation and Hydrolysis of N,N-Dimethylcarbamoyl Chloride (DMCC) in Vilsmeier Reactions Using GC/MS as the Analytical Detection Method. *Org. Process Res. Dev.* **2009**, *13* (5), 857–862. https://doi.org/10.1021/op900018f.
(38) Rodis, N. P.; Digenis, G. A. Synthesis and In-Vitro Evaluation of Novel Low Molecular Weight Thiocarbamates as Inhibitors of Human Leukocyte Elastase. *J. Enzym. Inhib.* **2001**, *16* (2), 95–105. https://doi.org/10.1080/14756360109162359.
(39) Wang, G. T.; Chen, Y.; Wang, S.; Sciotti, R.; Sowin, T. Solid Phase Synthesis of Ureas of Secondary Amines via Carbamoyl Chloride. *Tetrahedron Lett.* **1997**, *38* (11), 1895–1898. https://doi.org/10.1016/S0040-4039(97)00245-1.
(40) Lemoucheux, L.; Rouden, J.; Ibazizene, M.; Sobrio, F.; Lasne, M.-C. Debenzylation of Tertiary Amines Using Phosgene or Triphosgene: An Efficient and Rapid Procedure for the Preparation of Carbamoyl Chlorides and Unsymmetrical Ureas. Application in Carbon-11 Chemistry. *J. Org. Chem.* **2003**, *68* (19), 7289–7297. https://doi.org/10.1021/jo0346297.
(41) Wu, S.; Chen, G.; Zhang, Q.; Wang, G.; Chen, Q.-H. 3-O-Carbamoyl-5,7,20-O-Trimethylsilybins: Synthesis and Preliminary Antiproliferative Evaluation. *Molecules* **2021**, *26* (21), 6421. https://doi.org/10.3390/molecules26216421.
(42) Brimble, M. A.; Bryant, C. J. Synthesis and Assignment of the Absolute Configuration of the Anti-Helicobacter Pylori Agents CJ-12,954 and CJ-13,014. *Org. Biomol. Chem.* **2007**, *5* (17), 2858–2866. https://doi.org/10.1039/b709932k.
(43) Gayke, M.; Hirapara, N.; Narode, H.; Bhosle, S. D.; Bhosale, R. S.; Yadav, J. S. Zinc Chloride-Catalyzed Synthesis of Carbamates: An Application for the Synthesis of the Anti-Alzheimer's Drug Rivastigmine. *ACS Omega* **2022**, *7* (40), 36017–36027. https://doi.org/10.1021/acsomega.2c05350.
(44) Mandava, V. N. B. R.; Vajrala, V. R.; Varanasi, G.; Adla, V. K.; Jambula, M. R.; Reddy, V. R. K. Preparation of Rivastigmine and Its Salts. US8013181B2, September 6, 2011. https://patents.google.com/patent/US8013181B2/en (accessed 2026-07-26).
(45) Cuevas, J.-C.; Patil, P.; Snieckus, V. A′,A′-Disilylated Tertiary Benzamides as Dual Ortho- and A′-Carbanion Synthons: Amide Peterson Olefination Routes to N-Benzoyl Enamines, Isoquinolines, and Dibenzazocines. *Tetrahedron Lett.* **1989**, *30* (43), 5841–5844. https://doi.org/10.1016/S0040-4039(01)93485-9.
(46) Snieckus, V. Directed Ortho Metalation. Tertiary Amide and O-Carbamate Directors in Synthetic Strategies for Polysubstituted Aromatics. *Chem. Rev.* **2002**, *90* (6), 879–933. https://doi.org/10.1021/cr00104a001.
(47) Mills, R. J.; Taylor, N. J.; Snieckus, V. Directed Ortho Metalation of N,N-Diethylbenzamides. Silicon Protection of Ortho Sites and the o-Methyl Group. *J. Org. Chem.* **2002**, *54* (18), 4372–4385. https://doi.org/10.1021/jo00279a028.

(48) Comins, D. L.; Hong, H. Chiral Dihydropyridones as Synthetic Intermediates. Asymmetric Synthesis of (+)-Elaeokanine A and (+)-Elaeokanine C. *J. Am. Chem. Soc.* **2002**, *113* (17), 6672–6673. https://doi.org/10.1021/ja00017a047.
(49) Pichette Drapeau, M.; Tlili, A. Modern Synthesis of Carbamoyl Fluorides. *Tetrahedron Lett.* **2020**, *61* (47), 152539. https://doi.org/10.1016/j.tetlet.2020.152539.
(50) Onida, K.; Tlili, A. Direct Synthesis of Carbamoyl Fluorides by CO2 Deoxyfluorination. *Angew. Chem. Int. Ed.* **2019**, *58* (36), 12545–12548. https://doi.org/10.1002/anie.201907354.
(51) Bonnefoy, C.; Chefdeville, E.; Tourvieille, C.; Panossian, A.; Hanquet, G.; Leroux, F.; Toulgoat, F.; Billard, T. Study of Carbamoyl Fluoride: Synthesis, Properties and Applications. *Chem. – Eur. J.* **2022**, *28* (43), e202201589. https://doi.org/10.1002/chem.202201589.
(52) Cadwallader, D.; Tiburcio, T. R.; Cieszynski, G. A.; Le, C. M. Synthesis of Carbamoyl Fluorides Using a Difluorophosgene Surrogate Derived from Difluorocarbene and Pyridine N-Oxides. *J. Org. Chem.* **2022**, *87* (17), 11457–11468. https://doi.org/10.1021/acs.joc.2c01017.
(53) Hatch, C. E., III. Synthesis of N,N-Dialkylaminosulfenylcarbamate Insecticides via Carbamoyl Fluorides. *J. Org. Chem.* **2002**, *43* (20), 3953–3957. https://doi.org/10.1021/jo00414a033.
(54) Cadwallader, D.; Shevchuk, D.; Tiburcio, T. R.; Le, C. M. Fluoride-Catalyzed Cross-Coupling of Carbamoyl Fluorides and Alkynylsilanes. *Org. Lett.* **2023**, *25* (40), 7369–7373. https://doi.org/10.1021/acs.orglett.3c02871.
(55) McKnight, E. A.; Arora, R.; Pradhan, E.; Fujisato, Y. H.; Ajayi, A. J.; Lautens, M.; Zeng, T.; Le, C. M. BF3-Catalyzed Intramolecular Fluorocarbamoylation of Alkynes via Halide Recycling. *J. Am. Chem. Soc.* **2023**, *145* (20), 11012–11018. https://doi.org/10.1021/jacs.3c03982.
(56) Metzger, H. P.; Wilson, I. B. Evidence for an Electrophilic Mechanism in Catalysis by Hydrolytic Enzymes*. *Biochemistry* **2002**, *3* (7), 926–931. https://doi.org/10.1021/bi00895a013.
(57) Augustinsson, K. B.; Casida, J. E. Enzymic Hydrolysis of N:N-Dimethylcarbamoyl Fluoride. *Biochem. Pharmacol.* **1959**, *3* (1), 60–67. https://doi.org/10.1016/0006-2952(59)90009-7.
(58) Randall, G.; Meden, A.; Rutledge, M. T.; Prestreši, L.; Rambaher, M. H.; Chen, S.; Zdovc, I.; Gobec, S.; Knez, D.; Fellner, M. Carbamoyl Fluorides as Serine Hydrolase Inhibitors: A Case Study on FphI from *Staphylococcus Aureus*. *Bioorganic Chem.* **2026**, *176*, 109834. https://doi.org/10.1016/j.bioorg.2026.109834.
(59) Miyaura, Norio.; Suzuki, Akira. Palladium-Catalyzed Cross-Coupling Reactions of Organoboron Compounds. *Chem. Rev.* **2002**, *95* (7), 2457–2483. https://doi.org/10.1021/cr00039a007.
(60) Lennox, A. J. J.; Lloyd-Jones, G. C. Selection of Boron Reagents for Suzuki–Miyaura Coupling. *Chem. Soc. Rev.* **2014**, *43* (1), 412–443. https://doi.org/10.1039/c3cs60197h.
(61) Roughley, S. D.; Jordan, A. M. The Medicinal Chemist's Toolbox: An Analysis of Reactions Used in the Pursuit of Drug Candidates. *J. Med. Chem.* **2011**, *54* (10), 3451–3479. https://doi.org/10.1021/jm200187y.
(62) Brown, D. G.; Boström, J. Analysis of Past and Present Synthetic Methodologies on Medicinal Chemistry: Where Have All the New Reactions Gone?: Miniperspective. *J. Med. Chem.* **2015**, *59* (10), 4443–4458. https://doi.org/10.1021/acs.jmedchem.5b01409.

(63) Schneider, N.; Lowe, D. M.; Sayle, R. A.; Tarselli, M. A.; Landrum, G. A. Big Data from Pharmaceutical Patents: A Computational Analysis of Medicinal Chemists' Bread and Butter. *J. Med. Chem.* **2016**, *59* (9), 4385–4402. https://doi.org/10.1021/acs.jmedchem.6b00153.
(64) Duan, Y.-Z.; Deng, M.-Z. Palladium-Catalyzed Cross-Coupling Reaction of Arylboronic Acids with Chloroformate or Carbamoyl Chloride. *Synlett* **2005**, *2005* (02), 355–357. https://doi.org/10.1055/s-2004-837211.
(65) Magano, J.; Dunetz, J. R. Large-Scale Applications of Transition Metal-Catalyzed Couplings for the Synthesis of Pharmaceuticals. *Chem. Rev.* **2011**, *111* (3), 2177–2250. https://doi.org/10.1021/cr100346g.
(66) Blangetti, M.; Rosso, H.; Prandi, C.; Deagostino, A.; Venturello, P. Suzuki-Miyaura Cross-Coupling in Acylation Reactions, Scope and Recent Developments. *Molecules* **2013**, *18* (1), 1188–1213. https://doi.org/10.3390/molecules18011188.
(67) Krishnamoorthy, R.; Lam, S. Q.; Manley, C. M.; Herr, R. J. Palladium-Catalyzed Preparation of Weinreb Amides from Boronic Acids and N-Methyl-N-Methoxycarbamoyl Chloride. *J. Org. Chem.* **2010**, *75* (4), 1251–1258. https://doi.org/10.1021/jo902647h.
(68) Yasui, Y.; Tsuchida, S.; Miyabe, H.; Takemoto, Y. One-Pot Amidation of Olefins through Pd-Catalyzed Coupling of Alkylboranes and Carbamoyl Chlorides. *J. Org. Chem.* **2007**, *72* (15), 5898–5900. https://doi.org/10.1021/jo070724u.
(69) Christian, A. H.; Müller, P.; Monfette, S. Nickel Hydroxo Complexes as Intermediates in Nickel-Catalyzed Suzuki–Miyaura Cross-Coupling. *Organometallics* **2014**, *33* (9), 2134–2137. https://doi.org/10.1021/om5001327.
(70) Carrow, B. P.; Hartwig, J. F. Distinguishing Between Pathways for Transmetalation in Suzuki−Miyaura Reactions. *J. Am. Chem. Soc.* **2011**, *133* (7), 2116–2119. https://doi.org/10.1021/ja1108326.
(71) Payard, P.-A.; Perego, L. A.; Ciofini, I.; Grimaud, L. Taming Nickel-Catalyzed Suzuki-Miyaura Coupling: A Mechanistic Focus on Boron-to-Nickel Transmetalation. *ACS Catal.* **2018**, *8* (6), 4812–4823. https://doi.org/10.1021/acscatal.8b00933.
(72) Shrestha, M.; Wu, X.; Huang, W.; Qu, J.; Chen, Y. Recent Advances in Transition Metal-Catalyzed Reactions of Carbamoyl Chlorides. *Org. Chem. Front.* **2021**, *8* (14), 4024–4045. https://doi.org/10.1039/d0qo01648a.
(73) Le, C. M.; Sperger, T.; Fu, R.; Hou, X.; Lim, Y. H.; Schoenebeck, F.; Lautens, M. Stereoselective Synthesis of Methylene Oxindoles via Palladium(II)-Catalyzed Intramolecular Cross-Coupling of Carbamoyl Chlorides. *J. Am. Chem. Soc.* **2016**, *138* (43), 14441–14448. https://doi.org/10.1021/jacs.6b08925.
(74) Sperger, T.; Le, C. M.; Lautens, M.; Schoenebeck, F. Mechanistic Insights on the Pd-Catalyzed Addition of C–X Bonds across Alkynes – a Combined Experimental and Computational Study. *Chem. Sci.* **2017**, *8* (4), 2914–2922. https://doi.org/10.1039/c6sc05001h.
(75) Le, C. M.; Hou, X.; Sperger, T.; Schoenebeck, F.; Lautens, M. An Exclusively Trans-Selective Chlorocarbamoylation of Alkynes Enabled by a Palladium/Phosphaadamantane Catalyst. *Angew. Chem. Int. Ed.* **2015**, *54* (52), 15897–15900. https://doi.org/10.1002/anie.201507883.
(76) Balas, L.; Jousseaume, B.; Shin, H.; Verlhac, J. B.; Wallian, F. Palladium-Catalyzed Carbamoylation and Alkoxycarbonylation of Vinyl- and Arylorganotins: An Easy Entry into Vinyl or Aryl Amides and Esters. *Organometallics* **2002**, *10* (1), 366–368. https://doi.org/10.1021/om00047a077.

(77) Lemoucheux, L.; Rouden, J.; Lasne, M.-C. Cross-Coupling Reactions of Carbamoyl Chlorides and Grignard Reagents: A New Rapid Synthesis of Tertiary Amides. *Tetrahedron Lett.* **2000**, *41* (51), 9997–10001. https://doi.org/10.1016/S0040-4039(00)01783-4.
(78) Lysén, M.; Kelleher, S.; Begtrup, M.; Kristensen, J. L. Synthesis of Tertiary Benzamides via Pd-Catalyzed Coupling of Arylboronic Esters and Carbamoyl Chlorides. *J. Org. Chem.* **2005**, *70* (13), 5342–5343. https://doi.org/10.1021/jo050459h.
(79) He, F.; Hou, L.; Wu, X.; Ding, H.; Qu, J.; Chen, Y. Enantioselective Synthesis of α-Alkenylated γ-Lactam Enabled by Ni-Catalyzed 1,4-Arylcarbamoylation of 1,3-Dienes. *CCS Chem.* **2022**, *5* (2), 341–349. https://doi.org/10.31635/ccschem.022.202202010.
(80) Nielsen, C. D.-T.; Zivkovic, F. G.; Schoenebeck, F. Synthesis of N-CF3 Alkynamides and Derivatives Enabled by Ni-Catalyzed Alkynylation of N-CF3 Carbamoyl Fluorides. *J. Am. Chem. Soc.* **2021**, *143* (33), 13029–13033. https://doi.org/10.1021/jacs.1c07780.
(81) Li, Y.; Zhang, F.-P.; Wang, R.-H.; Qi, S.-L.; Luan, Y.-X.; Ye, M. Carbamoyl Fluoride-Enabled Enantioselective Ni-Catalyzed Carbocarbamoylation of Unactivated Alkenes. *J. Am. Chem. Soc.* **2020**, *142* (47), 19844–19849. https://doi.org/10.1021/jacs.0c09949.
(82) Han, L.; Boshevski, V.; Yang, Y.; Louvel, D.; Colombo, M.; Tran, G.; Lacôte, E.; Amgoune, A.; Tlili, A. Enabling Nickel-Catalyzed Suzuki–Miyaura Cross-Coupling of Carbamoyl Fluorides: Mechanism and Scope. *Chem. Eur. J.* **2025**, *3* (5), e202500213. https://doi.org/10.1002/ceur.202500213.

Chapter 2: Scalable Synthesis of Carbamoyl Fluorides

2.1. Author contributions

This chapter describes the synthesis of carbamoyl fluorides from secondary amines using 4-methylpyridine *N*-oxide, and the difluorocarbene precursor (triphenylphosphonio)difluoroacetate (PDFA). The initial report and reaction development was done by previous PhD student Dusty Cadwallader in 2022.[1] Undergraduate students, Emily Woo and Justin Laurie, have developed greener reaction conditions and work up procedures for synthesizing carbamoyl fluorides, as outlined in Section 2.3.4, using lower molecular weight reagents that allow for column-free purification. The work reported herein further expands on the initial report by introducing a modified protocol for efficient scale-up and work-up, while also expanding the substrate scope of the method.

2.2. Motivation and Research Plans

Historically, the carbamoyl fluoride (CMF) motif has been used far less extensively than CMCls, in part because CMCls are well-established and sufficient for many synthetic applications. Additionally, CMCls can be prepared from secondary amines using phosgene ($COCl_2$), which although highly toxic and subject to stringent controls, is commercially available and has long supported the preparation of CMCls, particularly in industrial settings.[2] In research settings, triphosgene is commonly employed as a solid phosgene surrogate that can be more easily handled compared to gaseous phosgene. However, triphosgene is itself highly toxic, and generates phosgene in situ, therefore retains many of the associated hazards and should not be considered as an inherently safe alternative.[3]

When CMFs are specifically required, they can be prepared readily from the corresponding CMCl through halide exchange, however this approach still requires prior preparation of the CMCl.[4] Direct preparation using difluorophosgene (COF_2) avoids the halide-exchange step but is similarly limited by the highly toxic gas and lack of commercial availability. Unlike phosgene, difluorophosgene has historically lacked a comparably safer alternative for use in research settings. Over time, alternative methods have been developed to circumvent the use of gaseous carbonyl halides, but these approaches often require hazardous, expensive and/or specialized reagents (e.g. DAST, $AgOCF_3$, DNTFB, etc.) (Figure 2.1).[5] Thus, although access to CMFs is not inherently prohibitive, the absence of a broadly practical and scalable method for their direct preparation from secondary amines has limited their wider adoption.

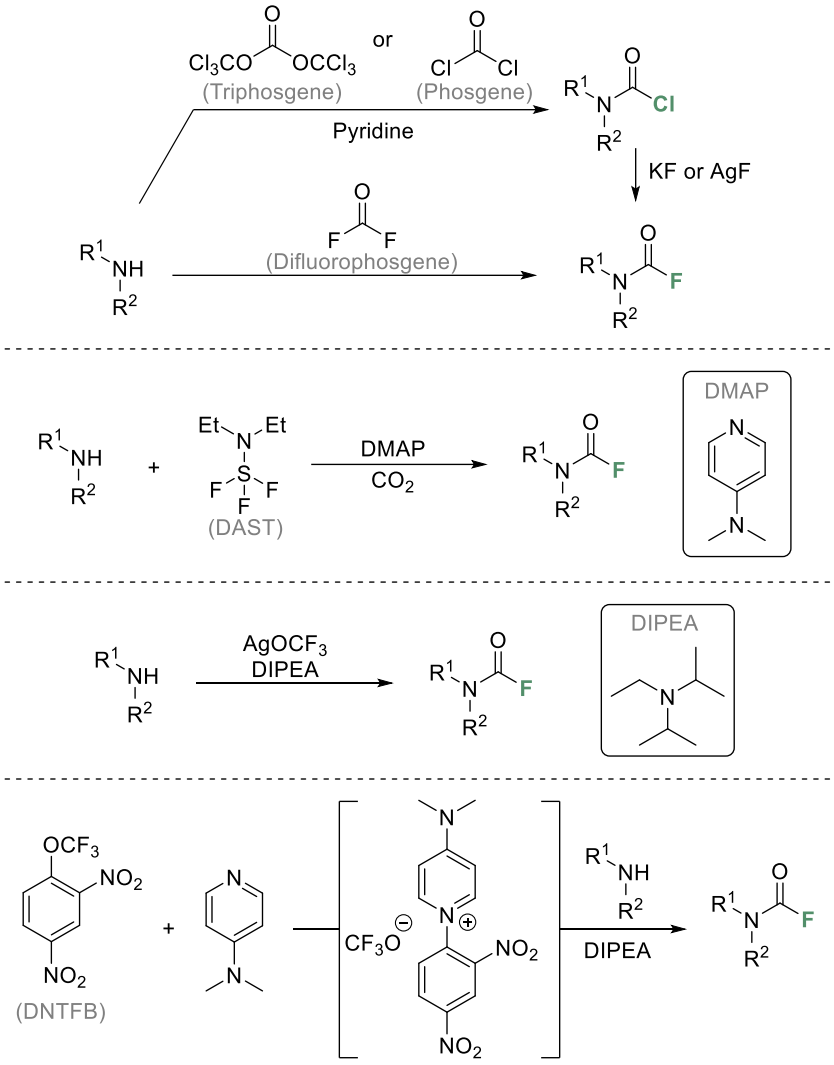

Figure 2.1: Typical methods of preparing CMFs.

Recently, our group reported the one-step synthesis of CMFs from secondary amines via the in situ generation of COF_2 using the difluorocarbene (DFC) precursor, (triphenylphosphonio)difluoroacetate (PDFA), and mild organic oxidant, 4-methylpyridine *N*-oxide (Scheme 2.1).[1,6] The proposed reaction mechanism proceeds through the thermally induced decarboxylation of PDFA to give phosphonium ylide **A**, which exists in equilibrium with free DFC (**B**). Nucleophilic attack of DFC by 4-methylpyridine *N*-oxide forms zwitterion **C**, which subsequently collapses to generate COF_2 and one equivalent of 4-methylpyridine. COF_2 then

undergoes a typical nucleophilic acyl substitution reaction with the secondary amine, forming the desired CMF and one equivalent of HF, which is quenched in situ by the 4-methylpyridine byproduct (Scheme 2.1).[1]

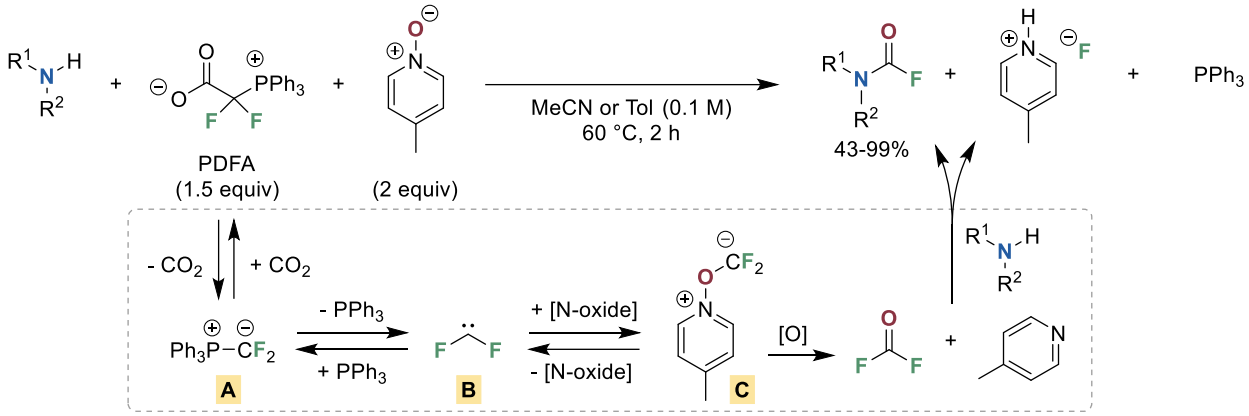

Scheme 2.1: Proposed mechanism for the synthesis of CMFs.

While this method provides a direct and high-yielding access to CMFs, its principal advantage is the in situ generation of and consumption of COF_2 from readily handled reagents, thereby avoiding the storage, transport, and direct manipulation of highly toxic gaseous COF_2. Nevertheless, one notable shortcoming is the challenge of product purification on larger reaction scales (>2 g). On small scales (<1 g), purification by column chromatography remains straightforward, as we previously reported.[1] However, as the reaction scale approaches and exceeds 2 g, column chromatography becomes increasingly resource-intensive and is generally insufficient to completely separate the CMF product from reaction by-products. The associated consumption of silica and solvent, together with the time and cost of repeated or extensive chromatographic purification, substantially limits the practicality of this synthetic approach on larger scales. To address these limitations, further reaction development and safety considerations are described herein.

2.3. Results and Discussion

2.3.1. Evaluation of Reaction and Reagent Safety

There are several factors that must be considered when increasing the scale of a reaction to preserve both reaction performance and ensure safety, including thermal hazards, gas evolution and subsequent pressure accumulation, changes in mixing and heat transfer, reagent addition rates, and the practicality of work-up and product isolation procedures.[7–10] For example, industrial processes that generate CO_2 in situ manage the rate of gas evolution through careful temperature control and/or metered reagent addition rates and by confirming that the available reactor headspace and venting capacity are sufficient for the anticipated gas volume.[11,12] For the present reaction, the most pertinent considerations are the generation of gaseous products and byproducts (e.g. COF_2 and CO_2), the resulting potential for pressure accumulation, the heat release during PDFA decomposition and its associated potential for thermal runaway, and the thermal stability of all reagents employed. Additionally, due to the high toxicity of COF_2, any larger-scale implementation would additionally require appropriate containment and/or treatment of the reactor off-gas.

To establish a baseline for both pressure and heat generation, the reaction was monitored under standard reaction conditions using *N*-phenylbenzylamine **2.1a** (1.0 equiv), PDFA (1.5 equiv) and 4-methylpyridine *N*-oxide (2.0 equiv) in toluene at 60 °C on a 2.7 g (15 mmol) scale (i.e., amount of limiting reagent) (Scheme 2.2). Thermal data (obtained using a Vernier LabQuest 2, equipped with a stainless-steel temperature probe and gas pressure sensor) showed no indication of any type of rapid exothermic event, suggesting minimal concern regarding thermal runaway upon moderate scale-up of the reaction (Figure 2.2 **A**). Further thermal evaluation will be

conducted as the reaction scale approaches 1 kg. However, the internal pressure of the reaction vessel increased rapidly approximately 8 minutes after the start of the reaction, reaching a maximum of nearly 18 psi after 20 minutes (Figure 2.2 **B**). This observation suggests that the majority of the PDFA present decomposes rapidly during the first 8-20-minute period of the reaction.

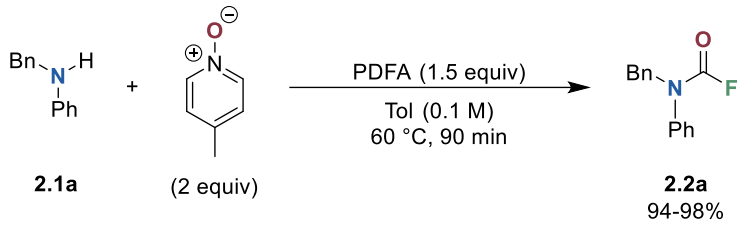

2.1a (2 equiv) **2.2a** 94-98%

Scheme 2.2: Standard reaction conditions used to evaluate reaction pressure and heat generation.

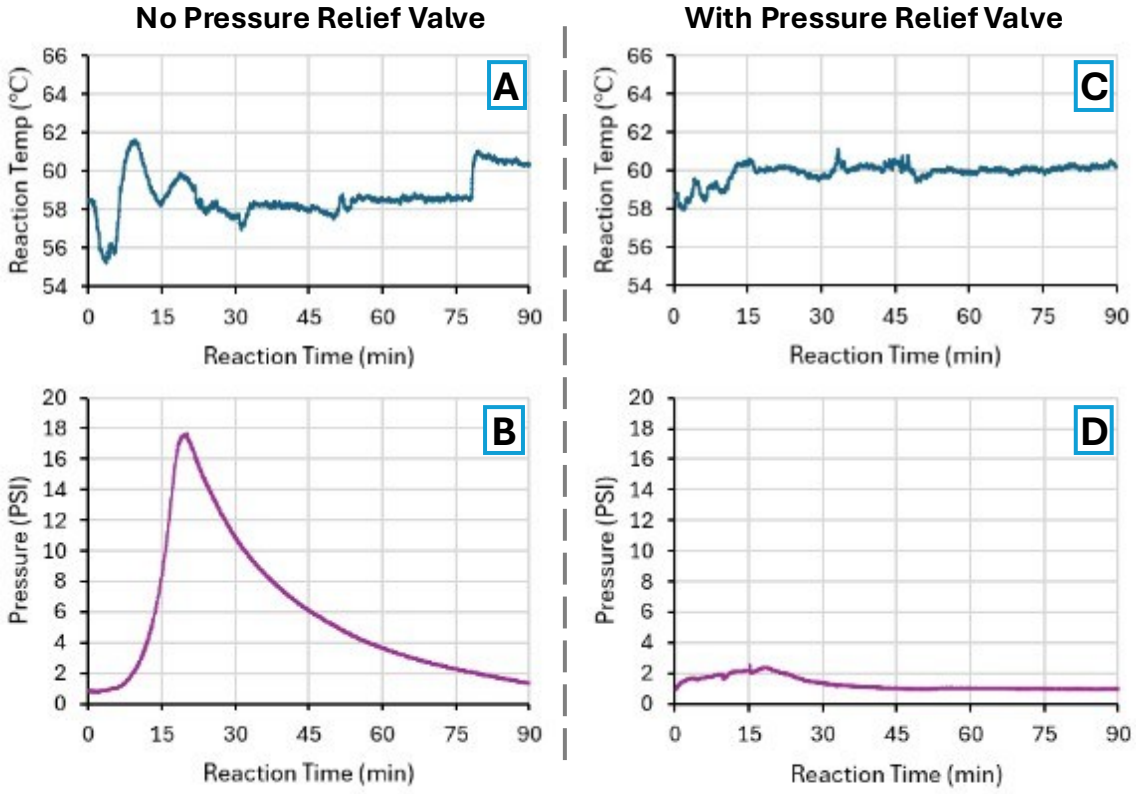

Figure 2.2: Graphs of reaction temperature and pressure of standard CMF synthesis with and without a pressure relief check valve.

At the outset of this project, the internal laboratory protocol for the synthesis of CMFs on scales greater than 1 g involved periodically venting the reaction vessel approximately every 10 minutes using a bleed needle to release excess pressure. Although effective, this procedure was

neither ideal nor practical and raised safety concerns due to the release of a gaseous mixture of CO_2 and COF_2. The latter is particularly problematic due to the highly toxic of COF_2, possessing a lethal concentration 50 (LC_{50}) of 37 ppm over 4 hr.[13] To address this concern, pressure-relief check valves were investigated as a means of maintaining an inert atmosphere while allowing for excess gas to be vented in a safer and controlled manner. This would also prevent backflow of ambient air and moisture, thereby limiting moisture-induced decomposition of DFC and COF_2. To scrub any excess COF_2 released from the reaction vessel, the exhaust stream was passed through a gas bubbler containing 10% aqueous NaOH, which hydrolyzes COF_2 to CO_2 (Figure 2.3).

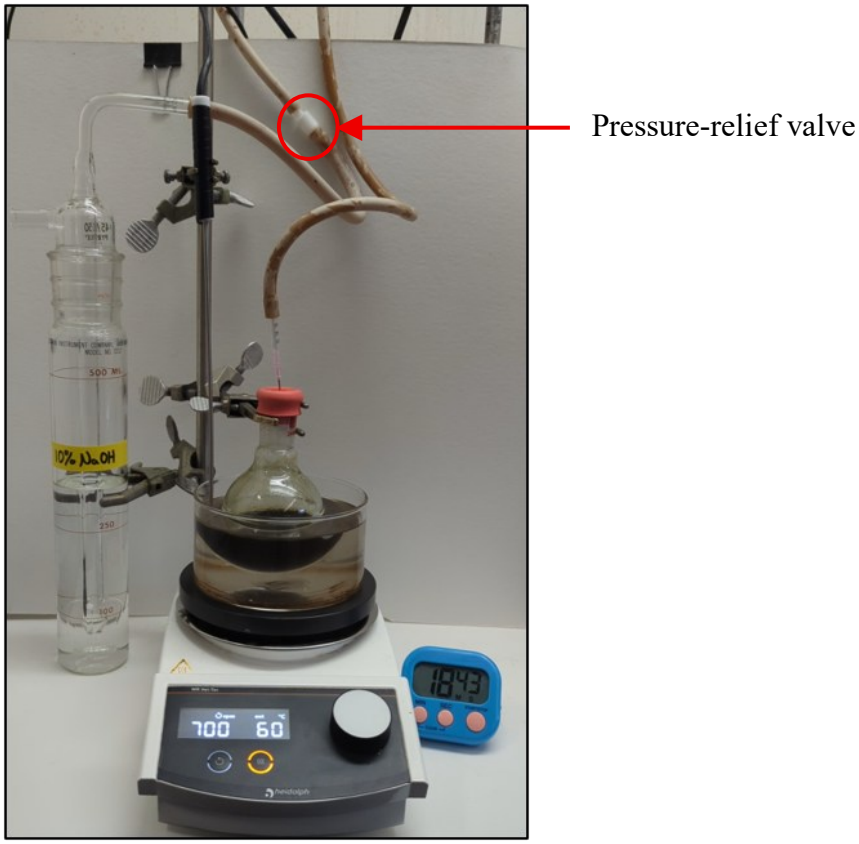

Figure 2.3: Standard reaction apparatus with pressure relief valve and bubbler.

A cost-effective and readily available pressure-relief valve manufactured by Chemglass (part no. CLS-1436-01) was selected for evaluation. Once the reaction vessel was equipped with both the pressure-relief valve and gas bubbler, both the pressure and heat generation were re-examined. While no notable change in temperature was observed (Figure 2.2 **C**), a substantial reduction in pressure buildup was identified (Figure 2.2 **D**). Furthermore, the reaction equipped with the pressure-relief valve afforded the desired product **2.2a** in a slightly improved yield of 98%, compared to 94% under otherwise identical conditions without the valve.

The final safety consideration evaluated was the thermal stability of the reagents employed in the reaction, as well as that of the precursor reagents (Scheme 2.3). Evaluating thermal stability is important to ensure that these materials can be safely stored for extended periods without the risk of decomposition. Differential scanning calorimetry (DSC) was used to assess the thermal stability of 4-methylpyridine *N*-oxide, PDFA and KCO_2CF_2Br (the precursor to PDFA) in the solid-state.

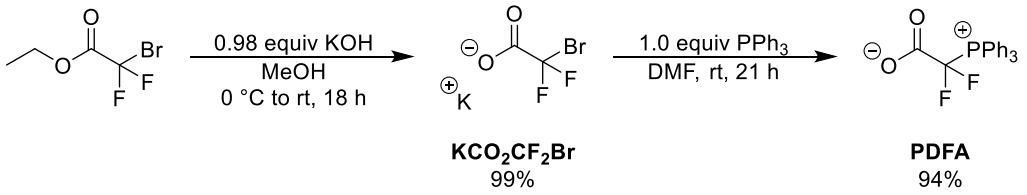

Scheme 2.3: Synthetic route to prepare PDFA.

For 4-methylpyridine *N*-oxide, the only thermal event observed was a melting transition at approximately 180 °C, which is consistent with its literature reported melting point (Figure 2.4 **A**). The PDFA precursor, KCO_2CF_2Br, was found to be stable up to approximately 110 °C, at which point a minor exothermic event was observed, follow by a second more pronounced exothermic event at 145 °C (Figure 2.4 **B**). Indicating that KCO_2CF_2Br becomes thermally unstable at temperatures exceeding 100 °C.

The primary concern regarding thermal stability arises from PDFA, as it readily decomposes at 60 °C under the standard reaction conditions. Surprisingly, DSC analysis revealed that PDFA is relatively thermally stable in the solid state and exhibits thermal behaviour comparable to KCO_2CF_2Br, with the onset of exothermic decomposition occurring at approximately 110 °C (Figure 2.4 **C**). These results suggest that PDFA is significantly more stable in the solid state than when suspended in solution, likely due to solvent effects that facilitate its decomposition under the reaction conditions. Overall, these findings indicate that, in the absence of residual solvent, PDFA and its precursor should be suitable for long-term storage on moderate laboratory scale.

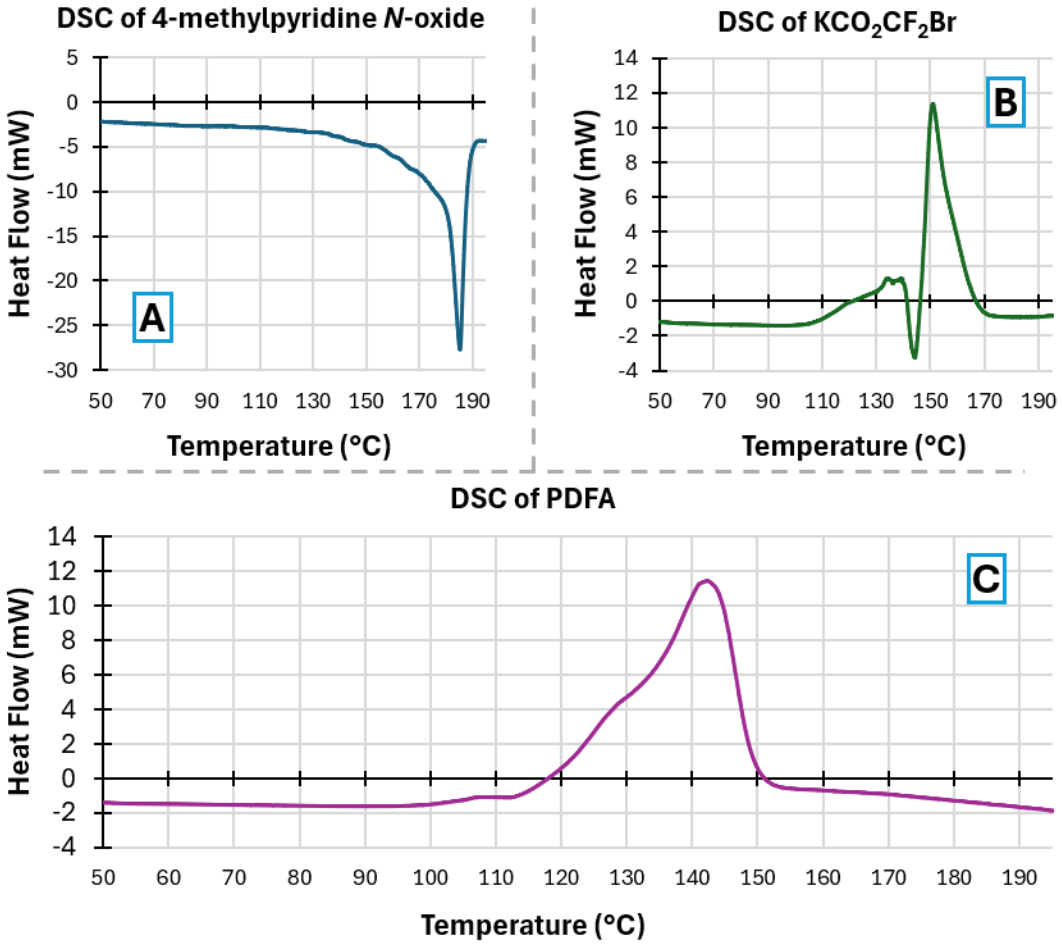

Figure 2.4: DSC traces of 4-methylpyridine *N*-oxide (**A**), KCO_2CF_2Br (**B**) and PDFA (**C**). Obtained using Thermal Advantage Q20 Differential Scanning Calorimeter.

2.3.2. Work-up Optimization

Our group previously reported an optimized synthesis of CMFs in 2022, in which reaction optimization and substrate scope studies were conducted on a 0.4 mmol scale. Along with a representative substrate subsequently prepared on a 9.3 mmol (1.0 g) scale, the generation of stoichiometric quantities of PPh_3 as a byproduct complicated the reaction work-up.[1] On reaction scales exceeding 1 g, purification by silica gel column chromatography can become increasingly difficult and impossible in some instances. This issue stems from the severe tailing exhibited by PPh_3 when eluting the product, resulting in significant cross-contamination with the desired CMF product. Consequently, repeated purification by column chromatography, sometimes up to four times, is required to achieve an acceptable degree of purity. This process requires substantial solvent volumes, rendering it both cost-inefficient and time-consuming, and represents the primary limitation to further scaling of this synthetic method.

As CMFs are being increasingly used as synthetic reagents in our research program, a more time- and cost-efficient work-up procedure was required to enable multi-gram scale synthesis of various derivatives. Such a procedure would eliminate the need for repeated small-scale, batch preparations of commonly used substrates and instead allow for the synthesis of larger quantities of material in a single operation. Because the reaction itself proceeds in high yield with relatively few side products, our initial efforts were focused on improving the purification process while maintaining the established reaction conditions.

Where the solubility profile of PPh_3 is nearly identical to that of many CMFs, and because most CMFs are isolated as oils, purification by recrystallization was not considered a practical solution. It therefore became apparent that efficient removal of PPh_3 would require chemical modification of the phosphine byproduct to alter its physical properties to enable easier removal.

Oxidation of phosphines is well understood and results in a substantial increase in polarity and corresponding changes in solubility. Accordingly, oxidation was investigated as a strategy for facilitating the removal of phosphine from the crude reaction mixture.

Hydrogen peroxide (H_2O_2) was selected as an obvious candidate due to its widespread use for the rapid oxidation of phosphines to the corresponding phosphine oxide in a matter of seconds. However, because of the possibility of undesired side reactions with the carbamoyl fluoride product (particularly those substituted with sensitive functional groups), a milder oxidant was also investigated. Elemental sulfur (S_8) was selected as a safer, less expensive, and milder alternative that is known to convert PPh_3 into triphenylphosphine sulfide (TPPS), providing a similar change in chemical properties to that observed with as triphenylphosphine oxide (TPPO).[14] Prior to evaluating these oxidants in post-reaction modification, their ability to efficiently and completely oxidize PPh_3 was examined. As anticipated, both H_2O_2 and S_8 achieved complete conversion to the corresponding oxide or sulfide under the conditions examined, as confirmed by ^{1}H and ^{31}P nuclear magnetic resonance (NMR) spectroscopy (Scheme 2.4).

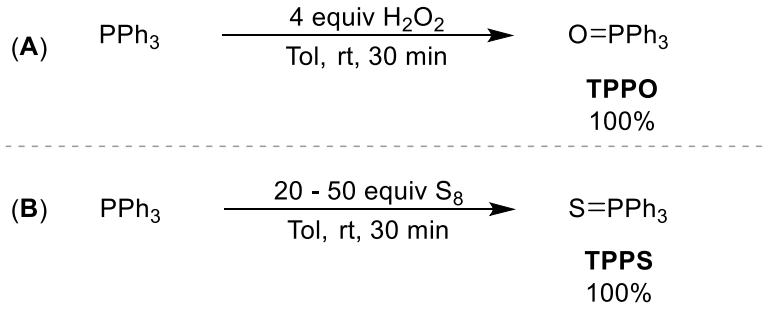

Scheme 2.4: Reaction schemes for the oxidation of PPh_3.

Based on these preliminary results, S_8 was first evaluated as a post-reaction oxidant and was found to completely convert PPh_3 into TPPS within 30 minutes (Scheme 2.5). As anticipated, the more polar phosphine sulfide did not elute significantly by column chromatography using the typical solvent eluent system, allowing for simpler separation of the CMF from this byproduct. Despite this apparent success, the isolated yield of **2.2a** obtained following purification was

approximately 120%. Analysis of the isolated material by both NMR spectroscopy and gas chromatography-mass spectrometry (GC-MS) suggested that the isolated product appeared to be pure; however, the apparent yield exceeding 100% strongly suggest the presence of a non-volatile, NMR silent impurity. Subsequent investigations revealed that S_8 could be readily eluted through silica gel and was responsible for the observed contamination. Because elemental sulfur was not detected by NMR or GC-MS, its presence was not initially recognized. Consequently, S_8 was deemed unsuitable for this application and H_2O_2 was explored next (Scheme 2.6).

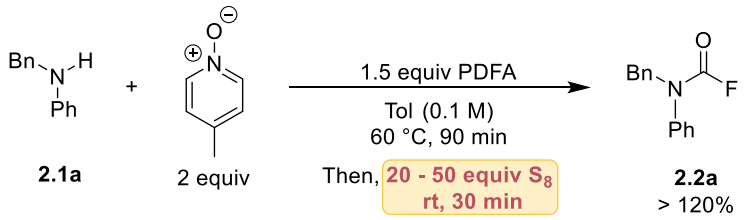

Scheme 2.5: Reaction conditions implemented including post-reaction modifications with S_8 to oxidize phosphine byproduct.

Implementation of H_2O_2 as a post-reaction oxidant proved highly successful, with no unanticipated side reactions observed, and isolated yields comparable to those obtained using the original procedure (Scheme 2.6). When the reaction was performed on approximately a 1 g scale, it was found that the crude reaction mixture should first be concentrated to approximately one-quarter of its original volume prior to oxidation to allow for efficient and complete oxidation of PPh_3. Additionally, vigorous stirring was required to ensure efficient mixing of the biphasic reaction mixture. Failure to sufficiently concentrate the reaction mixture or provide adequate mixing resulted in incomplete phosphine oxidation.

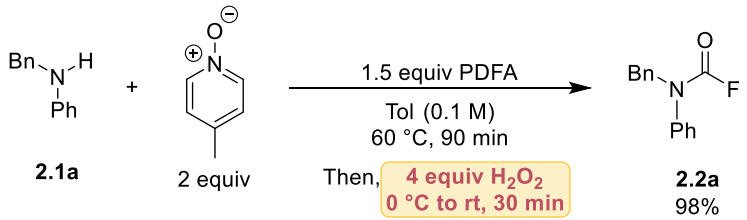

Scheme 2.6: Reaction conditions implemented including post-reaction modifications with H_2O_2 to oxidize phosphine byproduct.

During addition of H_2O_2, the reaction mixture was maintained at 0 °C, and the oxidant was added slowly over 1-15 minutes, depending on reaction scale, to minimize the heat generation associated with the oxidation of PPh_3. Because the oxidation of PPh_3 can be highly exothermic, rapid addition of H_2O_2 can and likely will result in thermal runaway during the oxidation process. The implications of this safety concern for further scale-up and alternative reaction conditions to mitigate these challenges are discussed in Section 2.3.4. Furthermore, it was found that TPPO could be removed if the oxidation step was performed in an alkyl hydrocarbon solvent such as hexanes. In such non-polar solvents, TPPO directly precipitates from the reaction mixture and can be removed by simple vacuum filtration.

Further improvements to the purification process were also realized. Following H_2O_2 oxidation, purification by column chromatography typically revealed only two compounds that eluted under the solvent system employed: the desired CMF **2.2a** and residual unreacted amine **2.1a**. This observation enabled a substantial reduction in the quantity of silica gel and solvent required for purification. To further simplify the purification process, the organic phase was first washed with 4 M aqueous HCl following oxidation. This treatment protonates any residual amine to form the corresponding ammonium salt. Although the ammonium salt generally remains in the organic phase, its strong ionic interactions with silica gel prevents its elution, allowing only the desired CMF and trace amounts of the F_2PPh_3 byproduct to elute during chromatography. The F_2PPh_3 byproduct is likely being formed through oxidative fluorination of PPh_3 with COF_2, followed by decarbonylation to afford F_2PPh_3 as described by Shreeve in 1984.[15] As a result, the product-containing organic phase could be simply passed though a small quantity of silica gel, reducing silica consumption by 50-90% while simultaneously decreasing solvent usage and purification time.

Collectively, these modifications transformed an otherwise purification-limited methodology into a practical and scalable process for the preparation of CMFs up to decagram scale. The optimized procedure significantly reduces purification time, solvent consumption, and silica usage while maintaining the high yields characteristic of the original reaction conditions.

2.3.3. Scaled up Substrate Scope

With the optimized procedure in hand, a scaled-up substrate scope and diversification study was conducted to evaluate the generality of the modified procedure. The primary objective was to determine whether the developed work-up protocol remained effective on larger reaction scales and across a broader range of substrates. A secondary objective was to establish whether the use of H_2O_2 during the work-up generally reduced yields or degraded CMF products. Note that the substrate scope for the original communication was done on a 0.4 mmol scale.[1]

Initial studies focused on substrates derived from a *N*-phenylbenzylamine scaffold, with derivatives bearing electron-donating, electron-withdrawing, and halogen substituents (Scheme 2.7). The model substrate **2.2a** was successfully isolated in 98% yield (10.0 g, 43.6 mmol) using the modified work-up procedure developed. Electron-donating substituents (**2.2b**, **2.2c**, **2.2h**) and halogen atoms (**2.2d-g**) at the *para*-position of the benzyl ring were all well tolerated, affording the corresponding products in isolated yields ranging from 80-99%. Likewise, both electron-donating methoxy (**2.2i**) and electron-withdrawing trifluoromethyl (**2.2j**) substituents at the *para* position on the aniline ring furnished the desired CMFs in excellent isolated yields of 97% and 92% respectively.

The developed conditions also proved compatible with unsaturated alkene-containing substrates. Phenyl (**2.2l**), benzyl (**2.2k**) 3-methylbut-3-en-1-yl, and 2-isopropenyl phenyl (**2.2s**)

carbamoyl fluoride derivatives were synthesized in isolated yields ranging from 84-87%, demonstrating that the reaction tolerates isolated alkene functionalities with no observable side reactions. To examine the influence of steric congestion, *tert*-butyl (**2.2p**) and 2,4-dimethylphenyl (**2.2n**) derivatives were evaluated, and isolated in yields of 73% and 83%, respectively. These results suggest that moderate steric hinderance at the amine nucleophile is well tolerated under the reaction conditions.

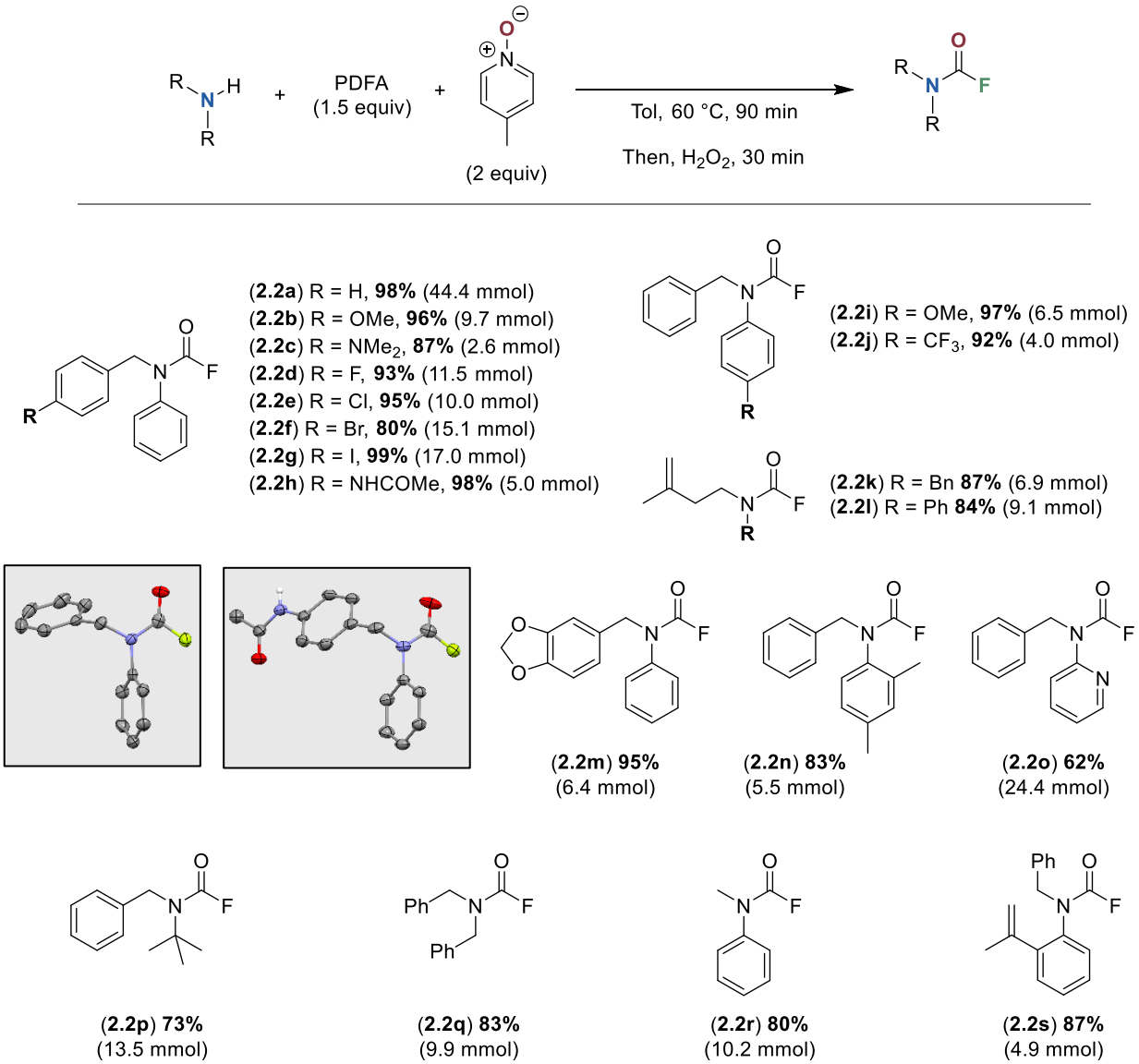

Scheme 2.7: Substrate scope of *N*-phenylbenzylamine derivatives. ORTEP drawn at 50% probability, select hydrogen atoms have been omitted for clarity.

Having established the utility of the method for acyclic substrates, our attention was directed toward the synthesis of cyclic CMFs (Scheme 2.8). A variety of cyclic amines possessing differing degrees of steric congestion and functionalities were successfully converted to the corresponding CMFs. Moderately hindered substrates such as **2.2t** and **2.2u** were isolated in good yields. In contrast, low-molecular weight amines, including 1-indoline (**2.2x**) and morpholine (**2.2w**), afforded reduced yields. In the case of morpholine-derived CMF **2.2w**, product volatility further complicated isolation. Future optimization may therefore benefit from the use of more volatile reaction solvents followed by purification via distillation.

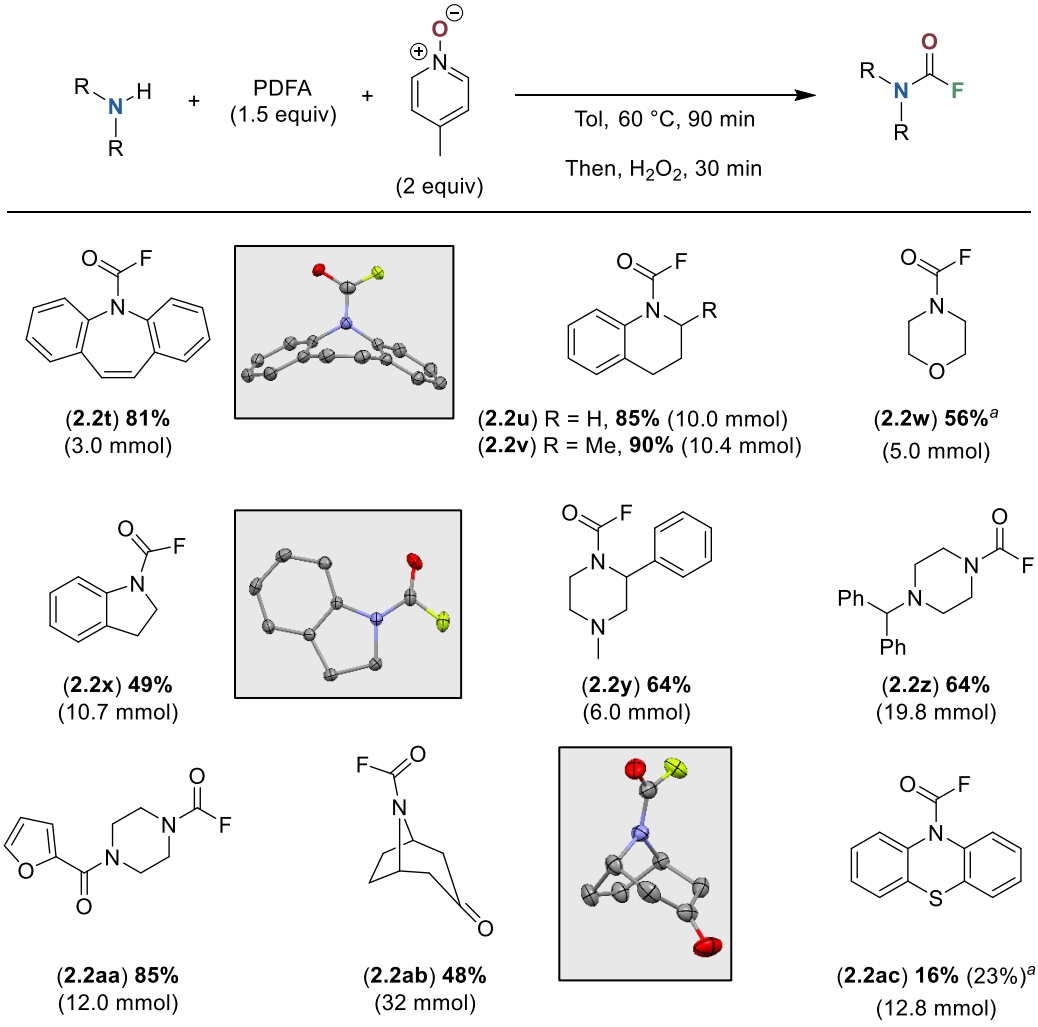

Scheme 2.8: Substrate scope of various cyclic CMFs. ORTEP drawn at 50% probability, hydrogen atoms have been omitted for clarity. [a]: Yield determined by quantitative NMR with trimethoxybenzene as internal standard.

Several piperazine derivatives were also prepared successfully. Comparison of substrates **2.2y** and **2.2z** or **2.2u** and **2.2v** suggests that steric congestion adjacent to the piperazine nitrogen exerts little influence on reaction efficiency. Furthermore, substrate **2.2aa** was isolated in 85% yield, demonstrating tolerance toward both tertiary amides and furan-containing motifs. To probe the compatibility of a ketone-containing functionality, the reaction was performed using 7-azabicyclo[4.1.1]octane, affording product **2.2ab** in an isolated 50% yield on a 32 mmol scale. While the desired product was successfully obtained, the reduced yield may indicate the presence of competing side reactions under the reaction conditions. A Wittig-type transformation was considered as a possible side reaction; however, no evidence for such a transformation was observed. To further evaluate the substrate scope, phenothiazine was investigated as a representative heterocyclic substrate of interest in materials chemistry. The corresponding CMF **2.2ac** was isolated in a 23% yield. The diminished reactivity observed for this substrate is likely attributed to reduced nucleophilicity of the amine resulting from extensive delocalization of the nitrogen lone pair into the conjugated π-system.

Finally, the generality of the modified procedure was examined using structurally complex substrates, including several active pharmaceutical ingredients (**APIs**) (Scheme 2.9). Substrate **2.2ad** was selected to evaluate the reactivity of a substrate containing two secondary amines. In this case, the loadings of PDFA and 4-methylpyridine *N*-oxide were doubled to accommodate functionalization of both nitrogen atoms. Under these conditions, the desired bis-CMF product was isolated in 61% yield, with less than 15% of the monosubstituted product observed.

The tolerance of more complex heterocyclic functionality was next explored through the synthesis of 1,3,5-oxdiazole-containing substrate **2.2ae**, which was isolated in an excellent 91% yield. Finally, several pharmaceutical agents, including Duloxetine (**2.2af**), Desloratadine (**2.2ag**),

and Ciprofloxacin (**2.2ah**), were converted to their corresponding CMF derivatives to demonstrate the suitability of this methodology for late-stage functionalization of API precursors. Notably, the successful preparation of substrate **2.2ah** demonstrates overall compatibility with carboxylic acid functionality. Although the carboxylic acid is expected to undergo transient conversion to the corresponding acyl fluoride under the reaction conditions, this intermediate is readily hydrolyzed during aqueous work-up to regenerate the carboxylic acid. Collectively, these results highlight the broad substate scope of the method and demonstrate the potential utility of CMFs in medicinal chemistry and pharmaceutical API synthesis.

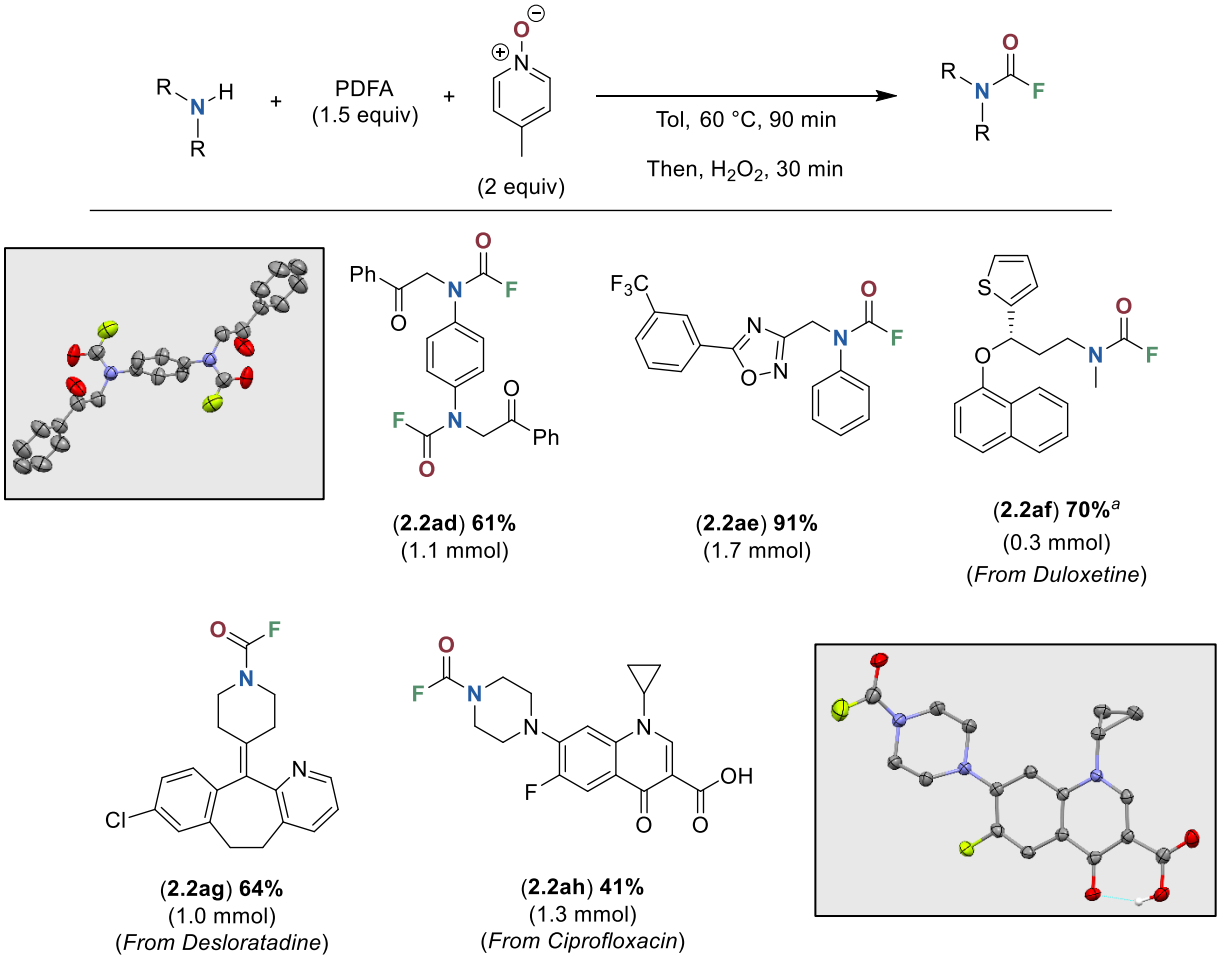

Scheme 2.9: Substrate scope of miscellaneous and drug related CMFs. ORTEP drawn at 50% probability, select hydrogen atoms have been omitted for clarity. [a]: Yield determined by quantitative ^{1}H NMR spectroscopy with 1,3,5-trimethoxybenzene as internal standard.

2.3.4. Alternative Reaction Conditions for Further Scale Up

Although the modifications developed for reaction safety and work-up optimization have enabled the synthesis of CMFs on a decagram scale, additional improvements are required before the method can be considered suitable for large-scale industrial implementation. Several limitations remain associated with the current process. Most notably is the waste generated during the preparation of PDFA from KCO_2CF_2Br. Although PDFA is prepared in an excellent 94% isolated yield, its preparation and purification require substantial volumes of solvent, resulting in an estimated E-factor of 22 kg/kg, including water and assuming no solvent recovery. This estimate excludes waste generated during the preparation of KCO_2CF_2Br, which itself has an estimated E-factor of 6.9 kg/kg. Accounting for both steps increases the overall estimated E-factor for PDFA to approximately 27kg/kg, before its use in the synthesis of CMFs. Additionally, the synthesis of CMF also suffers from a poor atom economy when employing PDFA, as only a single fluorine and carbon atom from the reagent end up ultimately incorporated into the product.

Furthermore, as discussed in Section 2.3.2, the oxidation of PPh_3 with H_2O_2 is highly exothermic and may present significant safety concerns upon further scale-up. Finally, despite the improvements to the purification procedure, column chromatography remains necessary to remove minor quantities of F_2PPh_3 generated during the reaction as a minor side product. Elimination of chromatographic purification would be highly desirable from both an economic and process-development perspective.

To address these shortcomings, our group has continued to investigate greener reaction conditions with the goal of developing a more scalable and industrially viable synthesis of CMFs. Initial reaction development and optimization studies were undertaken by undergraduate student Emily Woo, with particular emphasis on evaluating greener solvents selected using the GSK

solvent sustainability guides.[20] Additional optimization studies were subsequently conducted by undergraduate student Justin Laurie. The revised process uses KCO_2CF_2Br (PDFA precursor), as the DFC source with and employs dimethyl sulfoxide (DMSO) as a cost-effective oxidant in place of 4-methylpyridine *N*-oxide (Scheme 2.10).[16]

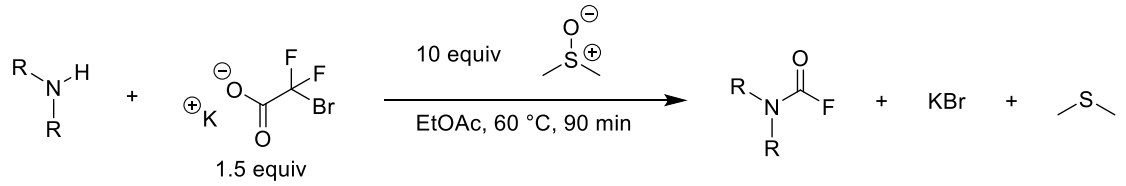

Scheme 2.10: Improved reaction conditions for the synthesis of CMFs with KCO_2CF_2Br and DMSO in place of PDFA and 4-methylpyridine *N*-oxide.

The direct use of KCO_2CF_2Br eliminates the additional step of preparing and purifying PDFA, as well as the challenges associated with CMF purification. Moreover, the principal by-products are CO_2 (volatile) and KBr (removed during aqueous work-up), thus improving both the atom economy and purification efficiency. Replacement of 4-methylpyridine *N*-oxide with DMSO further reduces reagent costs while simplifying purification. Unreacted DMSO can be removed during aqueous work-up, whereas the resulting dimethyl sulfide (DMS) possesses a sufficiently low boiling point (38 °C) to permit removal under reduced pressure or by distillation. Consequently, all major byproducts formed during the reaction should, in principle, be removable from the desired product, without requiring chromatographic purification. Under these conditions, residual unreacted amine represents the primary potential source of contamination.

To date, the largest-scale reaction employing these modified conditions in our lab has been performed using 3.5 mmol of *N*-benzylaniline (**2.1a**) as the substrate. The reaction afforded a ^1H NMR yield of 92%, and following two sequential recrystallizations in boiling heptane, **2.2a** was isolated in 68% yield (Scheme 2.11). Although modest in scale, this result serves as an important proof-of-concept for implementing these conditions in the preparation of CMFs.

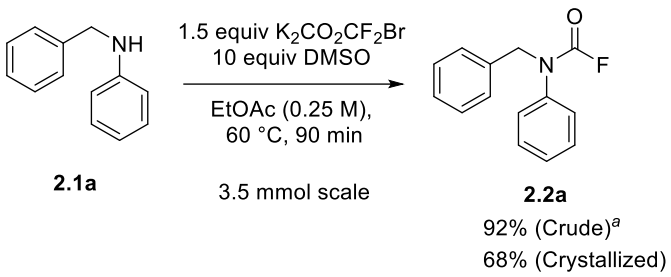

2.1a **2.2a**

92% (Crude)[a]

68% (Crystallized)

Scheme 2.11: Reaction conditions and yields on 3.5 mmol scale using KCO_2CF_2Br and DMSO. [a]: Yield determined by quantitative NMR with trimethoxybenzene as internal standard.

Despite these advantages, several challenges remain. One unexpected difficulty has been the complete removal of trace quantities of DMS from the final product, even after repeated recrystallization, resulting in contaminated products possessing a persistent sulfurous odor. More significantly, the modified conditions currently exhibit reduced robustness relative to the established PDFA/4-methylpyridine *N*-oxide system. Preliminary substrate scope studies conducted by undergraduate Emily Woo demonstrated consistently lower yields across all substrates examined (Scheme 2.12). The origin of this reduced reactivity remains unclear and is currently under investigation. Ongoing work focuses on improving reaction efficiency, identifying factors responsible for reduced yields, and developing purification strategies capable of completely removing residual DMS.

Nevertheless, these preliminary results demonstrate the potential of the KCO_2CF_2Br/DMSO system as a scalable and atom-economical alternative to the current method. Continued optimization of these conditions may ultimately provide a practical route to the larger-scale synthesis of CMFs, while eliminating several of the economic, safety, and purification challenges associated with the existing process.

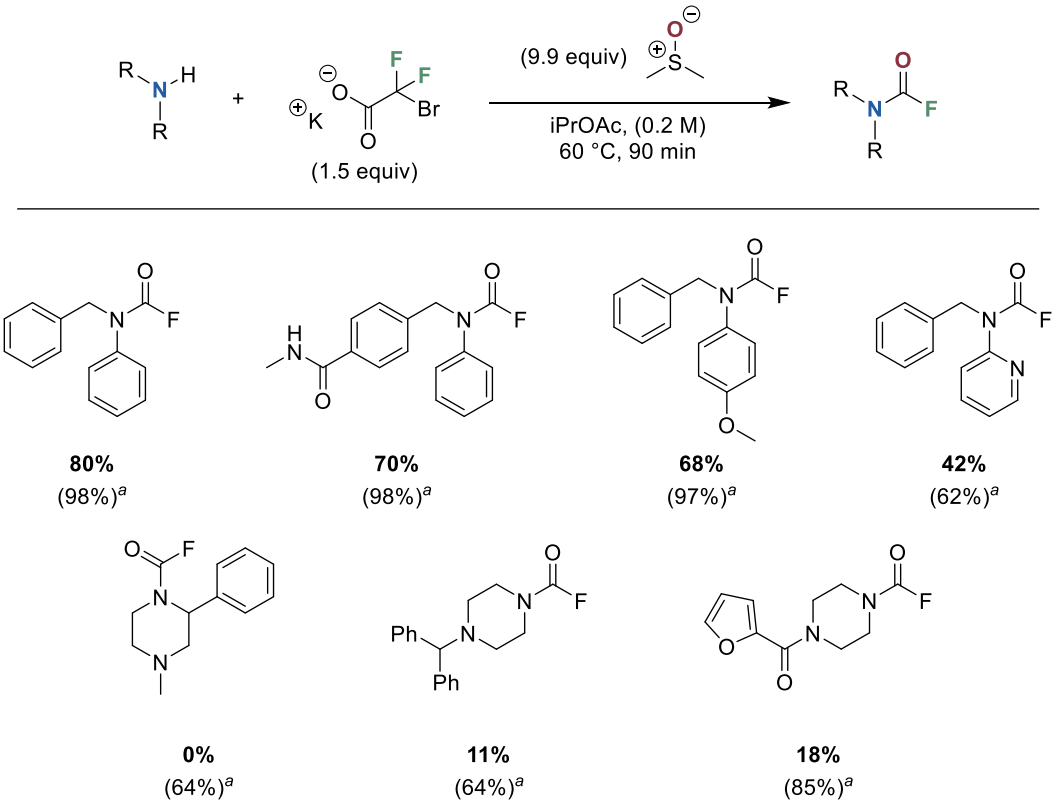

Scheme 2.12: CMF substrate scope using modified reaction conditions, done by undergraduate student Emily Woo. [a]: Yields obtained when using previously established reaction conditions using PDFA and 4-methylpyridine *N*-oxide.

2.4. References

(1) Cadwallader, D.; Tiburcio, T. R.; Cieszynski, G. A.; Le, C. M. Synthesis of Carbamoyl Fluorides Using a Difluorophosgene Surrogate Derived from Difluorocarbene and Pyridine N-Oxides. *J. Org. Chem.* **2022**, *87* (17), 11457–11468. https://doi.org/10.1021/acs.joc.2c01017.

(2) Semler, G.; Schaeffer, G. Process for the Preparation of Carbamoyl Chlorides Derived from Secondary Amines. US4770820A, September 13, 1988. https://patents.google.com/patent/US4770820A/en (accessed 2026-07-29).

(3) Cotarca, L.; Geller, T.; Répási, J. Bis(Trichloromethyl)Carbonate (BTC, Triphosgene): A Safer Alternative to Phosgene? *Org. Process Res. Dev.* **2017**, *21* (9), 1439–1446. https://doi.org/10.1021/acs.oprd.7b00220.

(4) Liu, L.; Gu, Y.-C.; Zhang, C.-P. Recent Advances in the Synthesis and Transformation of Carbamoyl Fluorides, Fluoroformates, and Their Analogues. *Chem. Rec.* **2023**, *23* (9), e202300071. https://doi.org/10.1002/tcr.202300071.

(5) Jabbarpoor, M.; Le, C. M. Carbamoyl Fluorides: A Platform to Interrogate Fluoride-Enabled Reactivity. *Synthesis* **2025**, *57* (16), 2399–2410. https://doi.org/10.1055/a-2557-7635.

(6) Lin, J.-H.; Xiao, J.-C. Fluorinated Ylides/Carbenes and Related Intermediates from Phosphonium/Sulfonium Salts. *Acc. Chem. Res.* **2020**, *53* (8), 1498–1510. https://doi.org/10.1021/acs.accounts.0c00244.

(7) Zhao, R.; Furman, T. R.; Roth, M. MSD's Process Safety Scale-Up Methodology for Pilot Plant Scale and Beyond. *Org. Process Res. Dev.* **2021**, *25* (11), 2566–2577. https://doi.org/10.1021/acs.oprd.1c00360.

(8) Armstrong, B. M.; Behre, T.; Turnbull, B. W. H.; Bishara, D.; Hartmanshenn, C.; McCarthy, E.; Whittington, M.; Ji, Y.; Jenks, A.; Desmond, R.; Muzzio, D. J.; Corry, J.; Zhao, R.; Kuhl, N.; Chung, C. K. Integrating Process Development and Safety Analysis for Scale-Up of a Diborane-Generating Reduction Reaction. *Org. Process Res. Dev.* **2023**, *27* (4), 763–774. https://doi.org/10.1021/acs.oprd.3c00018.

(9) Constable, D. J. C.; Jimenez-Gonzalez, C.; Henderson, R. K. Perspective on Solvent Use in the Pharmaceutical Industry. *Org. Process Res. Dev.* **2006**, *11* (1), 133–137. https://doi.org/10.1021/op060170h.

(10) Selekman, J. A.; Tran, K.; Xu, Z.; Dummeldinger, M.; Kiau, S.; Nolfo, J.; Janey, J. High-Throughput Extractions: A New Paradigm for Workup Optimization in Pharmaceutical Process Development. *Org. Process Res. Dev.* **2016**, *20* (10), 1728–1737. https://doi.org/10.1021/acs.oprd.6b00225.

(11) Allwein, S. P.; Roemmele, R. C.; Haley, J. J., Jr.; Mowrey, D. R.; Petrillo, D. E.; Reif, J. J.; Gingrich, D. E.; Bakale, R. P. Development and Scale-Up of an Optimized Route to the ALK Inhibitor CEP-28122. *Org. Process Res. Dev.* **2011**, *16* (1), 148–155. https://doi.org/10.1021/op200313v.

(12) Tran, D. N.; Zhdanko, A.; Barroso, S.; Nieste, P.; Rahmani, R.; Holan, J.; Hoefnagels, R.; Reniers, P.; Vermoortele, F.; Duguid, S.; Cazanave, L.; Figlus, M.; Muir, C.; Elliott, A.; Zhao, P.; Paden, W.; Diaz, C. H.; Bell, S. J.; Hashimoto, A.; Phadke, A.; Wiles, J. A.; Vogels, I.; Farina, V. Development of a Commercial Process for Odalasvir. *Org. Process Res. Dev.* **2021**, *26* (3), 832–848. https://doi.org/10.1021/acs.oprd.1c00237.

(13) Committee on Acute Exposure Guideline Levels; Committee on Toxicology; Board on Enviromental Studies and Toxicology; Devision on Earth and Life Studies. *Acute Exposure*

Guideline Levels for Selected Airborne Chemicals: Volume 18; National Academics Press, 2014.

(14) Kumar, R.; Kumar, S.; Pandey, M. K.; Kashid, V. S.; Radhakrishna, L.; Balakrishna, M. S. Synthesis of Phosphine Chalcogenides Under Solvent-Free Conditions Using a Rotary Ball Mill. *Eur. J. Inorg. Chem.* **2018**, *2018* (8), 1028–1037. https://doi.org/10.1002/ejic.201701414.

(15) Gupta, O. D.; Shreeve, J. M. Carbonyl Difluoride: A Versatile Fluorinating Reagent. *J. Chem. Soc. Chem. Commun.* **1984**, *20* (7), 416–417. https://doi.org/10.1039/C39840000416.

(16) Xiang, J.-C.; Gao, Q.-H.; Wu, A.-X. The Applications of DMSO. In *Solvents as Reagents in Organic Synthesis*; John Wiley & Sons, Ltd, 2017; pp 315–353. https://doi.org/10.1002/9783527805624.ch7.

(17) Jabbarpoor, M.; LeBlanc, J.; Chen, Z.; Cadwallader, D.; Le, C. M. Pd-Catalyzed Suzuki-Type Cross-Coupling of 2-Pyridyl Carbamoyl Fluorides. *Chem. Commun.* **2024**, *60* (66), 8700–8703. https://doi.org/10.1039/D4CC02431A.

(18) Tang, H.-J.; Shi, X.-M.; Zhu, X.-Y.; Wang, C.-Q.; Feng, C. Oxidation of Difluorocarbene by Pyridine N-Oxide and Ensuing Access to Carbamoyl Fluorides†. *Chin. J. Chem.* **2023**, *41* (22), 2981–2987. https://doi.org/10.1002/cjoc.202300316.

(19) Song, H.-X.; Han, Z.-Z.; Zhang, C.-P. Concise and Additive-Free Click Reactions between Amines and CF3SO3CF3. *Chem. – Eur. J.* **2019**, *25* (46), 10907–10912. https://doi.org/10.1002/chem.201901865.

(20) Alder, C. M.; Hayler, J. D.; Henderson, R. K.; Redman, A. M.; Shukla, L.; Shuster, L. E.; Sneddon, H. F. Updating and Further Expanding GSK's Solvent Sustainability Guide. *Green Chem.* **2016**, 18

(21) Pauluhn, J. Acute Nose-Only Exposure of Rats to Phosgene. Part I: Concentration × Time Dependence of LC50s, Nonlethal-Threshold Concentrations, and Analysis of Breathing Patterns. *Inhalation Toxicology* **2006**, 18 (6), 423–435.

2.5. Chapter 2 Appendix

Caution!

Difluorophosgene (carbonyl fluoride, COF_2), generated in situ during the reaction, is a highly toxic gas (LC_{50} = 37 ppm, 4 h)[21] that can cause severe respiratory injury and in some instances be fatal. It also reacts with moisture to release hydrogen fluoride (HF). Once the reaction has begun all operations should be performed in a fume hood until all possible gaseous material has been sparged from the reaction vessel through an aqueous NaOH gas bubbler to scrub any residual difluorophosgene.

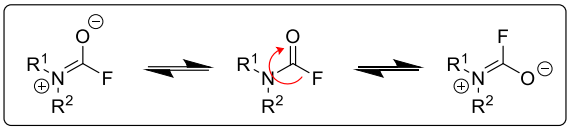

Note: *In accordance with previous reports, carbamoyl fluorides show restricted rotation about the N-C_{acyl} bond, resulting in rotamers in solution. Resonances for rotamers can be observed for unsymmetrically substituted carbamoyl fluorides (R'≠ R) in all ^{19}F NMR spectra, Chemical shifts reported in* ***bold*** *font indicate the* ***major rotamer****.*

A reaction vessel was charged with amine substrate, PDFA (1.5 equiv) and 4-methylpyridine N-oxide (2.0 equiv). The vessel was sealed with a rubber septum, evacuated under vacuum for approximately 10 min and subsequently backfilled with N_2. The septum was then pierced with a needle connected to a 3-psi pressure-relief check valve (Chemglass, Part Number: CLS-1436-01), which was attached to a gas bubbler containing 10% NaOH. The system was then purged with N_2 gas for approximately 5 min before the addition of anhydrous toluene. The resulting mixture was heated at 60 °C for 90 min.

Upon completion, air was bubbled though the reaction mixture and the attached check-valve/gas-bubble apparatus for 30 minutes to facilitate the removal of residual dissolved gaseous byproducts, including CO_2 and trace amounts of COF_2. The solvent was then removed under reduced pressure to afford a dark tar-like residue. The residue was then dissolved in DCM or hexanes and cooled in an ice bath for 5 min. Once sufficiently cold, 30 wt% H_2O_2 (2 mL per 5 mmol of amine) was then added dropwise over 5 min while maintaining the reaction temperature at 0 °C to minimize the exotherm associated with oxidation of residual PPh_3. The biphasic mixture

was stirred vigorously at 0 ℃ for 10 min and then allowed to warm to room temperature and continuous mixing for an additional 30 min to ensure complete oxidation of PPh_3.

The reaction mixture was then diluted with H_2O and transferred to a separatory funnel. The organic layer was separated and washed with water (2 ×) followed by brine. The organic phase was then collected, dried over $MgSO_4$, filtered, and concentrated under reduced pressure. The resulting residue was then purified by flash chromatography (EtOAc/hexanes) to afford the desired product.

***N*-benzyl-*N*-phenyl-carbamoyl fluoride**

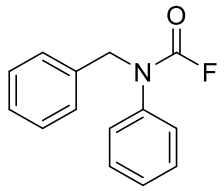

The title compound was prepared and worked up according to the general procedure from *N*-benzylaniline (4.58 g, 25.0 mmol, 1.0 equiv.), 4-methylpyridine *N*-oxide (5.48 g, 50.2 mmol, 2.0 equiv.), and PDFA (13.9 g, 38.8 mmol, 1.6 equiv.). The product was purified by flash chromatography (2% EtOAc/Hexanes), to yield a colorless viscous oil which crystallized into a white solid when dried under high vacuum for several days (5.25 g, 22.9 mmol, 92%).

^{1}H NMR (600 MHz, $CDCl_3$): δ 7.40 – 7.22 (m, 8.5H), 7.08 (d, *J* = 7.5 Hz, 1.5H), 4.86 (s, 2H). **^{13}C NMR** (151 MHz, $CDCl_3$): δ 55.0, 55.5, 125.9, 126.8, 127.4, 127.5, 128.0, 128.0, 128.5, 128.6, 128.7, 129.3, 135.6, 135.9, 139.2, 140.4, 146.6 (d, *J* = 291.3 Hz), 146.8 (d, *J* = 288.0 Hz). **^{19}F {^{1}H} NMR** (282 MHz, $CDCl_3$): δ **-14.59**, -16.97**.**

***N*-[(4-methoxyphenyl)methyl]-*N*-phenyl-carbamoyl fluoride**

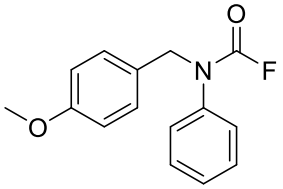

The title compound was prepared and worked up according to the general procedure from *N*-[(4-methoxyphenyl)methyl]aniline (2.06 g, 9.65 mmol, 1.0 equiv.), 4-methylpyridine *N*-oxide (2.13 g, 19.5 mmol, 2.0 equiv.), and PDFA (5.20 g, 14.6 mmol, 1.5 equiv.). The product was purified by flash chromatography (10% EtOAc/Hexanes) and was isolated as a pale-yellow oil (2.41 g, 9.28 mmol, 96%).

^{1}H NMR (600 MHz, $CDCl_3$): δ 7.39 – 7.26 (m, 3H), 7.20 (d, *J* = 7.8 Hz, 0.5H), 7.17 – 7.09 (m, 2H), **7.03** (d, *J* = 7.5 Hz, 1.5H), 6.88 – 6.79 (m, 2H), 4.76 (s, 2H), 3.79 (s, 3H). **^{13}C NMR** (151 MHz, $CDCl_3$): δ 54.6, 55.1, 55.2, 114.0, 114.1, 126.3, 127.1, 127.7, 127.8, 127.9, 128.1, 129.1,

129.30, 129.34, 130.1, 139.2, 140.4, 146.8 (d, J = 287.6 Hz), 159.4. **^{19}F {^{1}H} NMR** (282 MHz, $CDCl_3$): δ **-14.49**, -17.63.

***N*-[[4-(dimethylamino)phenyl]methyl]-*N*-phenyl-carbamoyl fluoride**

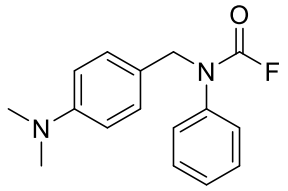

The title compound was prepared and worked up according to the general procedure from 4-(anilinomethyl)-*N*,*N*-dimethyl-aniline (577 mg, 2.55 mmol, 1.0 equiv.), 4-methylpyridine *N*-oxide (571 mg, 5.23 mmol, 2.1 equiv.), and PDFA (1.41 g, 3.94 mmol, 1.5 equiv.). The product was purified by flash chromatography (10% EtOAc/Hexanes) and was isolated as a colorless oil (606 mg, 2.23 mmol, 87%) which eventually turned orange in color upon sitting for weeks in a nitrogen filled glovebox.

^{1}H NMR (600 MHz, $CDCl_3$): δ 7.38 – 7.25 (m, 3H), 7.21 (d, J = 7.9 Hz, 0.5H), **7.08** (d, J = 8.5 Hz, 1.5H), 7.04 (d, J = 7.5 Hz, 2H), 6.68 – 6.61 (m, 2H), 4.72 (s, 2H), 2.94 (s, 6H). **^{13}C NMR** (151 MHz, $CDCl_3$): δ 40.4, 54.8, **55.3**, 112.3, 112.4, 123.3, 123.4, 126.4, 127.2, 127.5, 127.9, 128.9, 129.2, 129.3, 129.8, 139.4, 146.8 (d, J = 287.6 Hz), 150.3. **^{19}F {^{1}H} NMR** (282 MHz, $CDCl_3$): δ **-14.69**, -16.46.

HRMS (ESI) m/z: $[M+H]^+$ calc'd for $[C_{16}H_{18}FN_2O]$ 273.1403; found 273.1400.

***N*-[(4-fluorophenyl)methyl]-*N*-phenyl-carbamoyl fluoride**

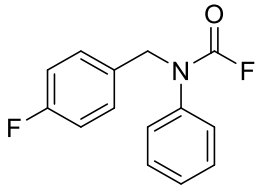

The title compound was prepared and worked up according to the general procedure from *N*-[(4-fluorophenyl)methyl]aniline (2.31 g, 11.5 mmol, 1 equiv.), 4-methylpyridine *N*-oxide (2.53 g, 23.2

mmol, 2.0 equiv.), and PDFA (6.16 g, 17.2 mmol, 1.5 equiv.). The product was purified by flash chromatography (8% EtOAc/Hexanes) and was isolated as a yellow oil (2.63 g, 10.6 mmol, 93%).

^{1}H NMR (600 MHz, $CDCl_3$): δ 7.44 – 7.28 (m, 3H), 7.24 – 6.91 (m, 6H), 4.80 (s, 2H). **^{13}C NMR** (151 MHz, $CDCl_3$): δ 54.4, **54.8**, 115.5, 115.6, 115.8, 126.1, 126.9, 127.8, 128.2, 129.4, 129.5, 130.4, 130.5, 131.48, 131.50, 131.7, 139.0, 140.2, 146.5 (d, J = 292.4 Hz), **146.8** (d, J = 288.2 Hz), 162.46 (d, J = 247.1 Hz), **162.53** (d, J = 246.9 Hz). **^{19}F {^{1}H} NMR** (282 MHz, $CDCl_3$): δ **-14.57**, -17.29, **-113.71**, -113.76.

HRMS (ESI) m/z: $[M+H]^+$ calc'd for $[C_{14}H_{12}F_2NO]$ 248.0887; found 248.0882.

***N*-[(4-chlorophenyl)methyl]-*N*-phenyl-carbamoyl fluoride**

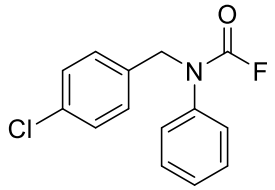

The title compound was prepared and worked up according to the general procedure from *N*-[(4-chlorophenyl)methyl]aniline (2.18 g, 10.0 mmol, 1.0 equiv.), 4-methylpyridine *N*-oxide (2.22 g, 20.4 mmol, 2.0 equiv.), and PDFA (5.39 g, 15.1 mmol, 1.5 equiv.). The product was purified by flash chromatography (7% EtOAc/Hexanes) and was isolated as a colorless oil (2.50 g, 9.50 mmol, 95%).

^{1}H NMR (600 MHz, $CDCl_3$): δ 7.40 – 7.24 (m, 5H), 7.22 (d, J = 7.7 Hz, 0.6H), 7.16 (m, 3H), 7.05 (d, J = 7.4 Hz, 1.4H), 4.79 (s, 2H). **^{13}C NMR** (151 MHz, $CDCl_3$): δ 54.4, **54.9**, 125.9, 126.8, 127.8, 128.2, 128.8, 129.0, 129.4, 130.0, 134.06, 134.12, 134.4, 139.0, 140.2, 146.4 (d, J = 291.0 Hz), **146.8** (d, J = 288.3 Hz). **^{19}F {^{1}H} NMR** (282 MHz, $CDCl_3$) δ **-17.01**, -14.60.

HRMS (ESI) m/z: $[M+H]^+$ calc'd for $[C_{14}H_{12}ClFNO]$ 264.0591; found 264.0585.

***N*-[(4-bromophenyl)methyl]-*N*-phenyl-carbamoyl fluoride**

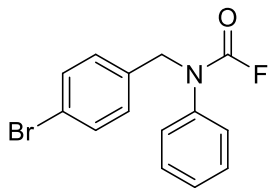

The title compound was prepared and worked up according to the general procedure from *N*-[(4-bromophenyl)methyl]aniline (3.96 g, 15.1 mmol, 1.0 equiv.), 4-methylpyridine *N*-oxide (3.35 g, 30.7 mmol, 2.0 equiv.), and PDFA (8.09 g, 22.6 mmol, 1.5 equiv.). The product was purified by flash chromatography (7% EtOAc/Hexanes) and was isolated as a colorless oil (3.71 g, 12.0 mmol, 80%).

^{1}H NMR (600 MHz, $CDCl_3$): δ 7.46 (d, *J* = 7.9 Hz, 0.4H), **7.43** (d, *J* = 8.1 Hz, 1.6H), 7.39 – 7.32 (m, 2H), 7.32 – 7.27 (m, 1H), 7.23 (d, *J* = 7.9 Hz, 0.4H), **7.12** (d, *J* = 8.1 Hz, 1.6H), 7.09 (d, *J* = 7.8 Hz, 0.4H), **7.06** (d, *J* = 7.6 Hz, 1.6H), 4.78 (s, 2H). **^{13}C NMR** (151 MHz, $CDCl_3$): δ 54.3, **54.8**, 122.0, 122.1, 125.8, 126.7, 127.7, 128.1, 129.2, 129.3, 130.2, 131.7, 131.8, 134.6, 134.8, 138.9, 140.1, 146.3 (d, *J* = 292.4 Hz), **146.6** (d, *J* = 288.4 Hz). **^{19}F {^{1}H} NMR** (282 MHz, $CDCl_3$): δ **-14.60**, -16.93.

HRMS (ESI) m/z: $[M+H]^+$ calc'd for $[C_{14}H_{12}BrFNO]$ 308.0086; found 308.0080.

***N*-[(4-iodophenyl)methyl]-*N*-phenyl-carbamoyl fluoride**

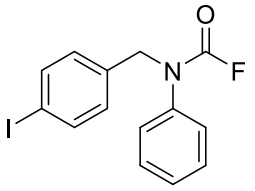

The title compound was prepared and worked up according to the general procedure from *N*-[(4-iodophenyl)methyl]aniline (5.25 g, 17.0 mmol, 1.0 equiv.), 4-methylpyridine *N*-oxide (3.72 g, 34.1 mmol, 2.0 equiv.), and PDFA (9.17 g, 25.7 mmol, 1.5 equiv.). The product was purified by flash chromatography (5% EtOAc/Hexanes) and was isolated as a yellow oil (5.95 g, 16.8 mmol, 99%).

^{1}H NMR (600 MHz, $CDCl_3$): δ 7.69 – 7.62 (m, 2H), 7.38 – 7.27 (m, 3H), 7.22 (d, *J* = 7.7 Hz, 0.4H), **7.05** (d, *J* = 7.5 Hz, 1.6H), 7.01 – 6.94 (m, 2H), 4.76 (s, 2H). **^{13}C NMR** (151 MHz, $CDCl_3$): δ 54.5, **55.0**, 93.7, **93.9**, 125.8, 126.7, 127.7, 128.2, 129.4, 130.4, 135.2, 135.5, 137.7, 137.9, 138.9, 140.2, 146.4 (d, *J* = 291.7 Hz), **146.7** (d, *J* = 288.6 Hz). **^{19}F {^{1}H} NMR** (282 MHz, $CDCl_3$): δ **-14.58**, -16.80.

HRMS (ESI) m/z: $[M+H]^+$ calc'd for $[C_{14}H_{12}IFNO]$ 355.9948; found 355.9943.

***N*-[(4-acetamidophenyl)methyl]-*N*-phenyl-carbamoyl fluoride**

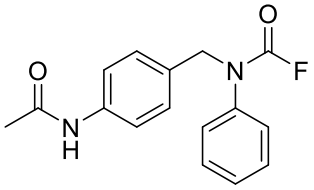

The title compound was prepared according to the general procedure without the H_2O_2 oxidation step from *N*-benzyl-4-(trifluoromethyl)aniline (1.02 g, 4.23 mmol, 1.0 equiv.), 4-methylpyridine *N*-oxide (2.09 g, 19.2 mmol, 4.5 equiv.), and PDFA (4.56 g, 12.8 mmol, 3.0 equiv.). The product was purified by flash chromatography (60% EtOAc/Hexanes) and was recrystallized in ether then washed with pentane yielding a pale yellow crystalline powder (1.19 g, 4.14 mmol, 98%).

^{1}H NMR (600 MHz, $CDCl_3$): δ 7.61 – 7.50 (m, br, 1H), 7.50 – 7.42 (m, 2H), 7.37 – 7.26 (m, 3H), 7.22 – 7.10 (m, 2.5H), **7.03** (d, *J* = 7.4 Hz, 1.5H), 4.77 (s, 2H), 2.15 (s, 3H). **^{13}C NMR** (151 MHz, $CDCl_3$): δ 24.5, 54.7, **55.1**, **119.8**, 120.0, 126.1, 126.9, 127.8, 128.1, 128.4, 129.3, 129.4, 131.3, 131.5, 137.9, 139.1, 140.2, 146.7 (d, *J* = 290.1 Hz), **146.9** (d, *J* = 288.2 Hz), 168.5. **^{19}F {^{1}H} NMR** (282 MHz, $CDCl_3$): δ **-14.55**, -17.32.

HRMS (ESI) m/z: $[M+H]^+$ calc'd for $[C_{16}H_{16}FN_2O_2]$ 287.1196; found 287.1192.

m.p.: 113 - 114 °C

***N*-benzyl-*N*-(4-methoxyphenyl)carbamoyl fluoride**

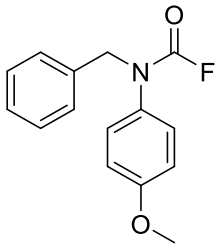

The title compound was prepared and worked up according to the general procedure from *N*-benzyl-4-methoxy-aniline (1.38 g, 6.47 mmol, 1 equiv.), 4-methylpyridine *N*-oxide (1.41 g, 12.9 mmol, 2.0 equiv.), and PDFA (3.47 g, 9.72 mmol, 1.5 equiv.). The product was purified by flash chromatography (10% EtOAc/Hexanes) and was isolated as a pale orange-yellow oil (1.63 g, 6.28 mmol, 97 %).

^{1}H NMR (600 MHz, $CDCl_3$): δ 7.37 – 7.27 (m, 3H), 7.25 – 7.18 (m, 2H), 7.11 (d, *J* = 8.8 Hz, 0.5H), **6.95** (d, *J* = 8.9 Hz, 1.5H), 6.86 (d, *J* = 8.7 Hz, 0.5H), **6.82** (d, *J* = 8.9 Hz, 1.5H), 4.78 (s, 2H), 3.78 (s, 3H). **^{13}C NMR** (151 MHz, $CDCl_3$): δ **55.4**, 55.8, 114.4, 114.5, 127.5, 127.8, 128.06, 128.12, 128.6, 128.7, 128.8, 131.9, 133.1, 135.7, 135.9, 147.0 (d, *J* = 289.3 Hz), **147.1** (d, *J* = 286.9 Hz), 158.8, 159.0. **^{19}F {^{1}H} NMR** (282 MHz, $CDCl_3$): δ **-15.11**, -18.40.

***N*-benzyl-*N*-[4-(trifluoromethyl)phenyl]carbamoyl fluoride**

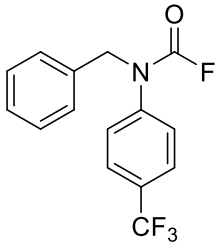

The title compound was prepared and worked up according to the general procedure from *N*-benzyl-4-(trifluoromethyl)aniline (1.01 g, 4.02 mmol, 1 equiv.), 4-methylpyridine *N*-oxide (1.78 g, 16.3 mmol, 4.0 equiv.), and PDFA (4.35 g, 12.2 mmol, 3.0 equiv.). The product was purified by flash chromatography (10% EtOAc/Hexanes) and was isolated as a colorless oil (1.10 g, 3.71 mmol, 92%).

^{1}H NMR (600 MHz, $CDCl_3$): δ 7.61 (d, *J* = 8.1 Hz, 2H), 7.47 – 7.29 (m, 3.7H), 7.25 – 7.18 (m, 3.3H), 4.88 (s, 2H). **^{13}C NMR** (151 MHz, $CDCl_3$): δ 54.7, **55.4**, 123.6 (q, *J* = 272.2 Hz), 125.8, 126.5, 127.2, 128.4, 128.9, 129.0, 130.2 (q, *J* = 32.6 Hz), **135.1**, 135.3, 142.3, 143.5, 146.2 (d, *J* = 290.3 Hz). **^{19}F {^{1}H} NMR** (282 MHz, $CDCl_3$): δ **-13.83** (s, br, 0.7F), -15.50 (s, br, 0.3F), -62.67 (s, 3F).

HRMS (ESI) m/z: $[M+H]^+$ calc'd for $[C_{15}H_{12}F_4NO]$ 298.0855; found 298.0850.

***N*-benzyl-*N*-(3-methylbut-3-enyl)carbamoyl fluoride**

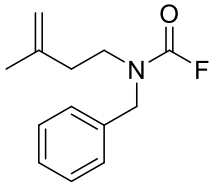

The title compound was prepared and worked up according to the general procedure from *N*-benzyl-3-methyl-but-3-en-1-amine (1.21 g, 6.93 mmol, 1.0 equiv.), 4-methylpyridine *N*-oxide (1.62 g, 14.9 mmol, 2.1 equiv.), and PDFA (3.74 g, 10.5 mmol, 1.5 equiv.). The product was purified by flash chromatography (10% EtOAc/Hexanes) and was isolated as a colorless oil (1.34 g, 6.04 mmol, 87%).

^{1}H NMR (600 MHz, $CDCl_3$): δ 7.40 – 7.28 (m, 4H), 7.26 – 7.23 (m, 1H), 4.81 (h, *J* = 1.6 Hz, 1H), 4.71 (dq, *J* = 2.0, 1.1 Hz, 0.46H), **4.69** (dq, *J* = 2.0, 1.0 Hz, 0.54H), **4.49** (s, 1.1H), 4.44 (s, 0.9H), 3.40 – 3.34 (m, 0.9H), **3.31 – 3.25** (m, 1.1H), 2.28 (t, *J* = 6.8 Hz, 0.9H), **2.22** (t, *J* = 7.3 Hz, 1.1H), 1.74 (t, *J* = 1.2 Hz, 1.4H), **1.71** (t, *J* = 1.2 Hz, 1.6H). **^{13}C NMR** (151 MHz, $CDCl_3$): δ 22.1, **22.2**, 35.0, **36.2**, **45.3** (d, *J* = 2.5 Hz), 46.2 (d, *J* = 1.6 Hz), 51.0 (d, *J* = 3.4 Hz), **51.5**, 112.6, 112.9, 127.4, 128.0, 128.1, **128.8**, 128.9, 135.75, **135.78**, **141.5**, 141.8, 147.3 (d, *J* = 288.4 Hz), 148.3 (d, *J* = 287.5 Hz). **^{19}F {^{1}H} NMR** (564 MHz, $CDCl_3$): δ -21.61, **-22.34**.

HRMS (ESI) m/z: $[M+H]^+$ calc'd for $[C_{13}H_{17}FNO]$ 222.1294; found 222.1290.

***N*-(3-methylbut-3-enyl)-*N*-phenyl-carbamoyl fluoride**

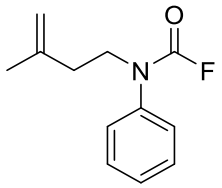

T The title compound was prepared and worked up according to the general procedure from *N*-(3-methylbut-3-enyl)aniline (1.47 g, 9.12 mmol, 1.0 equiv.), 4-methylpyridine *N*-oxide (2.06 g, 18.9 mmol, 2.1 equiv.), and PDFA (5.00 g, 14.0 mmol, 1.5 equiv.). The product was purified by flash chromatography (5% Ether/Hexanes) and was isolated as a colorless oil (1.59 g, 7.70 mmol, 84%).

^{1}H NMR (600 MHz, $CDCl_3$): δ 7.41 (t, *J* = 7.6 Hz, 2H), 7.37 – 7.29 (m, 1.5H), 7.21 (d, *J* = 7.8 Hz, 1.5H), 4.84 (s, 0.25H), 4.82 (s, 0.75H), 4.72 (s, 1H), 3.82 (t, *J* = 7.5 Hz, 1.5H), 3.79 (t, *J* = 7.4 Hz, 0.5H), 2.29 (t, *J* = 7.5 Hz, 2H), 1.72 (s, 2.25H), 1.71 (s, 0.75H). **^{13}C NMR** (151 MHz, $CDCl_3$): δ 22.05, **22.14**, **35.2**, 36.5, 49.5, **49.8**, 112.6, 112.9, 126.3, 126.8, 127.6, 127.9, 129.3, 139.1, 140.1, 141.3, 141.6, **146.1** (d, *J* = 287.2 Hz), 146.7 (d, *J* = 290.2 Hz). **^{19}F {^{1}H} NMR** (564 MHz, $CDCl_3$): δ -13.82, -18.80.

HRMS (ESI) m/z: $[M+H]^+$ calc'd for $[C_{12}H_{15}FNO]$ 208.1138; found 208.1134.

***N*-(1,3-benzodioxol-5-ylmethyl)-*N*-phenyl-carbamoyl fluoride**

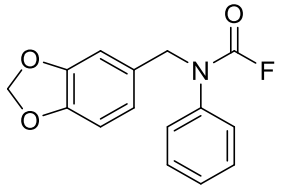

The title compound was prepared and worked up according to the general procedure from *N*-(1,3-benzodioxol-5-ylmethyl)aniline (1.46 g, 6.40 mmol, 1.0 equiv.), 4-methylpyridine *N*-oxide (1.46 g, 13.4 mmol, 2.1 equiv.), and PDFA (3.43 g, 9.60 mmol, 1.5 equiv.). The product was purified by flash chromatography (100% DCM) and was isolated as a pale-yellow oil (1.68 g, 6.09 mmol, 95%).

^{1}H NMR (600 MHz, $CDCl_3$): δ 7.40 – 7.27 (m, 3H), 7.22 (d, *J* = 7.8 Hz, 0.5H), **7.05** (d, *J* = 7.6 Hz, 1.5H), 6.79 – 6.68 (m, 2H), 6.64 (d, *J* = 8.0 Hz, 1H), 5.95 (s, 2H), 4.72 (s, 2H). **^{13}C NMR** (151 MHz, $CDCl_3$): δ 54.9, 55.4, 101.1, 101.2, 108.2, 108.4, 109.0, 121.4, 122.3, 126.2, 127.0, 127.7, 128.1, 128.9, 129.35, 129.42, 139.1, 140.3, 147.0 (d, *J* = 288.8 Hz), 147.5, 147.9. **^{19}F {^{1}H} NMR** (282 MHz, $CDCl_3$): δ **-14.49**, -17.51.

HRMS (ESI) m/z: $[M+H]^+$ calc'd for $[C_{15}H_{13}FNO_3]$ 274.0879; found 274.0872.

***N*-benzyl-*N*-(2,4-dimethylphenyl)carbamoyl fluoride**

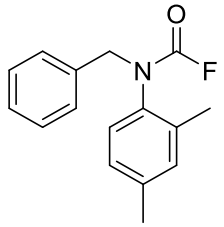

The title compound was prepared and worked up according to the general procedure from *N*-benzyl-2,4-dimethyl-aniline (1.17 g, 5.52 mmol, 1 equiv.), 4-methylpyridine *N*-oxide (1.26 g, 11.5 mmol, 2.1 equiv.), and PDFA (3.09 g, 8.65 mmol, 1.6 equiv.). The product was purified by flash chromatography (6% EtOAc/Hexanes) and was isolated as a colorless oil (1.18 g, 4.57 mmol, 83%).

^{1}H NMR (600 MHz, $CDCl_3$): δ 7.36 – 7.27 (m, 3H), 7.26 – 7.16 (m, 2H), 7.06 – 7.01 (m, 1H), 6.99 – 6.91 (m, 1H), 6.87 (d, *J* = 8.0 Hz, 0.2H), **6.76** (d, *J* = 8.0 Hz, 0.8H), 4.91 – 4.81 (m, 1H), 4.54 (d, *J* = 14.2 Hz, 1H), 2.31 (s, 3H), 2.04 (s, 0.6H), **2.00** (s, 2.4H). **^{13}C NMR** (151 MHz, $CDCl_3$): δ 17.16, 17.24, 20.98, 21.00, 55.28, 55.29, 55.34, 55.35, 127.4, 127.5, 127.6, 127.7, 128.2, 128.3, 128.6, 128.7, 128.8, 129.3, 131.8, 132.0, 135.19, 135.23, 135.51, 135.54, 136.1, 138.49, 138.52, 145.18 (d, *J* = 292.1 Hz), 147.16 (d, *J* = 286.2 Hz). **^{19}F {^{1}H} NMR** (282 MHz, $CDCl_3$): δ **-16.07**, -19.98.

HRMS (ESI) m/z: $[M+H]^+$ calc'd for $[C_{16}H_{17}FNO]$ 258.1294; found 258.1289.

***N*-Benzyl-*N*-(2-pyridyl)carbamoyl fluoride**

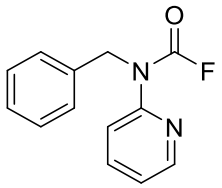

The title compound was prepared and worked up according to the general procedure from ciprofloxacin (4.50 g, 24.4 mmol, 1.0 equiv), 4-methylpyridine N-oxide (5.44 g, 49.8 mmol, 2.0 equiv), and PDFA (13.6 g, 39.1 mmol, 1.6 equiv). The product was purified by flash chromatography (10% EtOAc/Hexanes) and was isolated as a colorless oil (3.48 g, 15.1 mmol, 62%). Spectral data are consistent with literature values.[17]

***N*-benzyl-*N*-tert-butyl-carbamoyl fluoride**

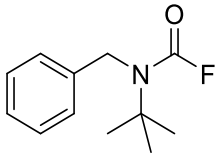

The title compound was prepared and worked up according to the general procedure from *N*-tert-butylbenzylamine (2.20 g, 13.5 mmol, 1.0 equiv.), 4-methylpyridine *N*-oxide (3.24 g, 29.6 mmol, 2.2 equiv.) and PDFA (8.55 g, 23.9 mmol, 1.8 equiv.). The product was purified by flash chromatography (5% EtOAc/Hexane) to yield a colorless crystalline solid (2.06 g, 9.86 mmol, 73%).

^{1}H NMR (600 MHz, $CDCl_3$): δ 7.35 (t, *J* = 7.6 Hz, 2H), 7.27 (t, *J* = 7.6 Hz, 1H), 7.23 (d, *J* = 7.6 Hz, 2H), 4.59 (s, br, 2H), 1.41 (s, br, 9H). **^{13}C NMR** (151 MHz, $CDCl_3$): δ **28.1** (br), 29.6 (br), **48.9** (br), 50.0 (br), 58.0, 126.1 (br), 127.2, 128.7, 138.3, **146.1** (d, br, *J* = 291.2 Hz), 150.1 (d, br, *J* = 282.4 Hz). **^{19}F {^{1}H} NMR** (282 MHz, $CDCl_3$): δ **-7.12** (br), -9.54 (br).

HRMS (ESI) m/z: $[M+H]^+$ calc'd for $[C_{12}H_{17}FNO]$ 210.1294; found 210.1290.

m.p.: 38 - 39 °C

***N*,*N*-dibenzylcarbamoyl fluoride**

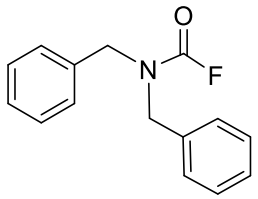

The title compound was prepared and worked up according to the general procedure from dibenzylamine (1.90 mL, 9.88 mmol, 1.0 equiv.), 4-methylpyridine *N*-oxide (2.21 g, 20.2 mmol, 2.0 equiv.) and PDFA (5.40 g, 15.1 mmol, 1.5 equiv.). The product was purified by flash chromatography (2% EtOAc/Hexane) to yield a pale-yellow oil (2.00 g, 8.23 mmol, 83%).

^{1}H NMR (600 MHz, $CDCl_3$): δ 7.46 – 7.33 (m, 6H), 7.31 (d, *J* = 6.7 Hz, 2H), 7.24 (d, *J* = 7.4 Hz, 2H), 4.45 (s, 2H), 4.37 (s, 2H). **^{13}C NMR** (151 MHz, $CDCl_3$): δ 49.6 (d, *J* = 3.3 Hz), 50.4, 127.6, 128.07, 128.10, 128.3, 128.8, 128.9, 135.2, 135.3, 148.1 (d, *J* = 288.0 Hz). **^{19}F {^{1}H} NMR** (282 MHz, $CDCl_3$): δ -22.67 (s).

***N*-methyl-*N*-phenyl-carbamoyl fluoride**

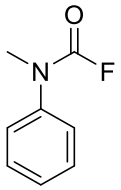

The title compound was prepared and worked up according to the general procedure from *N*-methylaniline (1.10 mL, 10.2 mmol, 1.0 equiv.), 4-methylpyridine *N*-oxide (2.19 g, 20.1 mmol, 2.0 equiv.) and PDFA (5.38 g, 15.1 mmol, 1.5 equiv.). The product was purified by flash chromatography (5% EtOAc/Hexane) to yield a volatile orange liquid (1.24 g, 8.12 mmol, 80%).

^{1}H NMR (600 MHz, $CDCl_3$): δ 7.40 (t, *J* = 7.9 Hz, 2H), 7.36 (d, *J* = 8.0 Hz, 0.6H), **7.32** (t, *J* = 7.5 Hz, 0.7H), 7.29 (t, *J* = 7.3 Hz, 0.3H), **7.23** (d, *J* = 7.9 Hz, 1.4H), 3.37 (s, 0.9H), **3.35** (s, 2.1H). **^{13}C NMR** (151 MHz, $CDCl_3$): δ 37.8, **38.8**, 124.5, 125.5, 127.0, 127.6, 129.2, 129.3, **140.7**, 141.5, **146.3** (d, *J* = 287.0 Hz), 146.6 (d, *J* = 290.9 Hz). **^{19}F {^{1}H} NMR** (282 MHz, $CDCl_3$): δ **-15.91**, -16.06.

***N*-benzyl-*N*-(2-isopropenylphenyl)carbamoyl fluoride**

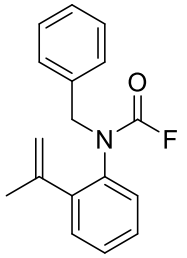

The title compound was prepared and worked up according to the general procedure from *N*-benzyl-2-isopropenyl-aniline (1.09 g, 4.87 mmol, 1.0 equiv.), 4-methylpyridine *N*-oxide (2.18 g, 20.0 mmol, 4.1 equiv.), and PDFA (5.35 g, 15.0 mmol, 3.1 equiv.). The product was purified by flash chromatography (3% EtOAc/Hexanes) and isolated as a colorless oil (1.14 g, 4.22 mmol, 87%).*Note: One of the minor broad alkene resonances with an integration of 0.2 overlaps with the benzylic resonances between 4.9 - 5.1 ppm.*

^{1}H NMR (600 MHz, $CDCl_3$): δ 7.36 – 7.27 (m, 5H), 7.25 – 7.21 (m, 1.6H), 7.20 – 7.17 (m, 0.6H), 7.14 (ddt, *J* = 6.1, 5.2, 3.2 Hz, 0.8H), 6.93 (d, *J* = 7.9 Hz, 0.2H), **6.78** (d, *J* = 7.9 Hz, 0.8H), 5.33 – 5.28 (m, 1H), **5.20** (dt, *J* = 14.5, 2.0 Hz, 0.8H), 5.07 (s, 0.2H), **5.03** (s, 0.8H), 4.27 (s, br, 0.2H), **4.21** (dt, *J* = 14.6, 2.1 Hz, 0.8H), 2.13 (s, 0.6H), **2.11** (s, 2.4H).

^{13}C NMR (151 MHz, $CDCl_3$): δ 23.3, 23.4, 54.95 (d, *J* = 2.3 Hz), **55.0**, 116.4, **116.7**, 127.7, 127.9, 128.1, 128.4, 128.49, 128.51, 128.52, 128.6, 129.0, 129.09, 129.14, 129.58, 129.63, 135.57, 135.65, 135.8, 136.8, **141.1**, 141.2, **142.5**, 142.6, 146.9 (d, *J* = 291.3 Hz), **147.0** (d, *J* = 286.4 Hz).
^{19}F {^{1}H} NMR (564 MHz, $CDCl_3$): δ **-12.86**, -19.25.

HRMS (ESI) m/z: $[M+H]^+$ calc'd for $[C_{17}H_{17}FNO]$ 270.1294; found 270.1290.

benzo[b][1]benzazepine-11-carbonyl fluoride

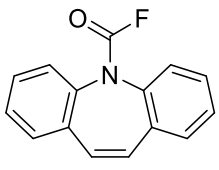

The title compound was prepared and worked up according to the general procedure from iminostilbene (578 mg, 3.00 mmol, 1.0 equiv.), 4-methylpyridine *N*-oxide (656 mg, 6.01 mmol, 2.0 equiv.) and PDFA (1.63 g, 4.57 mmol, 1.5 equiv.). The product was purified by flash chromatography (5% EtOAc/Hexane) to yield a colorless crystalline solid (584 mg, 2.44 mmol, 81%), which slowly became brown in color after several weeks in a nitrogen filled glovebox but was easily recrystallized from the slow evaporation of a saturated pentane solution.

^{1}H NMR (600 MHz, $CDCl_3$): δ 7.54 (d, *J* = 8.0 Hz, 1H), 7.49 (ddd, *J* = 8.0, 5.3, 2.8 Hz, 1H), 7.46 – 7.42 (m, 2H), 7.42 – 7.35 (m, 4H), 6.98 (dd, *J* = 14.1, 2.6 Hz, 2H). **^{13}C NMR** (151 MHz, $CDCl_3$): δ 127.15, 127.16, 127.26, 128.30, 128.35, 129.36 (d, *J* = 27.0 Hz), 129.6 (d, *J* = 25.9 Hz), 130.0, 130.5, 133.68, 133.71, 137.58, 137.60, 138.3, 145.8 (d, *J* = 291.2 Hz). **^{19}F {^{1}H} NMR** (282 MHz, $CDCl_3$): δ -16.63 (s).

HRMS (ESI) m/z: $[M+H]^+$ calc'd for $[C_{15}H_{11}FNO]$ 240.0825; found 240.0821.

m.p.: 159 - 160 °C

3,4-dihydro-2*H*-quinoline-1-carbonyl fluoride

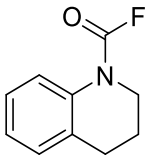

The title compound was prepared and worked up according to the general procedure from 1,2,3,4-tetrahydroquinoline (1.33 g, 9.96 mmol, 1.0 equiv.), 4-methylpyridine *N*-oxide (2.25 g, 20.6 mmol, 2.1 equiv.), and PDFA (5.39 g, 15.1 mmol, 1.5 equiv.). The product was purified by flash chromatography (5% EtOAc/Hexanes) and was isolated as a pale-yellow oil (1.51 g, 8.43 mmol, 85%).

^{1}H NMR (600 MHz, $CDCl_3$): δ 7.61 (d, *J* = 367.9 Hz, 1H), 7.21 (d, *J* = 8.0 Hz, 1H), 7.16 – 7.08 (m, 2H), 3.80 (t, *J* = 6.1 Hz, 2H), 2.83 (t, *J* = 6.6 Hz, 2H), 2.03 (p, *J* = 6.4 Hz, 2H). **^{13}C NMR** (151 MHz, $CDCl_3$): δ **22.9**, 23.1, 26.8, **27.0**, 45.9, 122.4, 123.6, 124.9, 125.4, 126.6, **128.9**, 129.7, 130.8, 135.9, **136.2**, **145.0** (d, *J* = 293.1 Hz), 146.6 (d, *J* = 298.0 Hz). **^{19}F {^{1}H} NMR** (282 MHz, $CDCl_3$): δ **-11.72**, -16.93.

HRMS (ESI) m/z: $[M+H]^+$ calc'd for $[C_{10}H_{11}FNO]$ 180.0825; found 180.0821.

2-methyl-3,4-dihydro-2*H*-quinoline-1-carbonyl fluoride

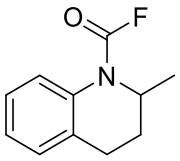

The title compound was prepared and worked up according to the general procedure from 2-methyl-1,2,3,4-tetrahydroquinoline (1.50 mL, 10.4 mmol, 1.0 equiv.), 4-methylpyridine *N*-oxide (2.23 g, 20.4 mmol, 2.0 equiv.), and PDFA (5.46 g, 15.3 mmol, 1.5 equiv.). The product was purified by flash chromatography (10% EtOAc/Hexanes) and was isolated as a pale-yellow oil (1.81 g, 9.39 mmol, 90%).

^{1}H NMR (600 MHz, $CDCl_3$): δ 7.54 (d, *J* = 310.4 Hz, 1H), 7.23 (td, *J* = 7.5, 2.1 Hz, 1H), 7.17 – 7.09 (m, 2H), 4.50 (hd, *J* = 6.7, 1.7 Hz, 1H), 2.78 – 2.65 (m, 2H), 2.31 (s, 1H), 1.59 (s, 1H), 1.25 (d, *J* = 6.6 Hz, 3H). **^{13}C NMR** (151 MHz, $CDCl_3$) δ 19.1, 24.7, 25.3, 30.2, 31.2, 51.3, 51.9, 123.9, 124.7, 125.5, 126.7, 128.0, 133.0, 134.5, 145.6 (d, *J* = 291.6 Hz). **^{19}F {^{1}H} NMR** (282 MHz, $CDCl_3$): δ -14.00, **-16.51**.

HRMS (ESI) m/z: $[M+H]^+$ calc'd for $[C_{11}H_{13}FNO]$ 194.0981; found 194.0977.

indoline-1-carbonyl fluoride

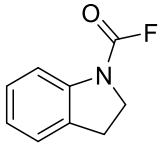

The title compound was prepared and worked up according to the general procedure from 1-indoline (1.2 mL, 10.7 mmol, 1.0 equiv.), 4-methylpyridine *N*-oxide (2.21 g, 20.3 mmol, 1.9 equiv.) and PDFA (5.37 g, 15.0 mmol, 1.9 equiv.). The product was purified by flash chromatography (2% EtOAc/Hexane) to yield a white crystalline solid (2.00 g, 8.23 mmol, 83%) which eventually turned pale pink in color upon sitting for weeks in a nitrogen filled glovebox.

^{1}H NMR (600 MHz, $CDCl_3$): δ **7.77** (dt, *J* = 8.0, 1.4 Hz, 0.7H), 7.31 (dd, *J* = 6.5, 2.5 Hz, 0.3H), 7.26 (d, *J* = 7.5 Hz, 0.6H), 7.24 – 7.19 (m, 1.4H), 7.11 – 7.04 (m, 1H), 4.12 – 4.03 (m, 2H), 3.20 (td, *J* = 8.6, 5.2 Hz, 2H). **^{13}C NMR** (151 MHz, $CDCl_3$): δ 27.3, **27.4**, **47.6**, 48.2, 114.95, 115.02, 115.06, 124.3, 124.5, 124.9, 125.5, **127.8**, 127.9 (d, *J* = 3.0 Hz), **131.1** (d, *J* = 4.4 Hz), 131.4, 139.6 (d, *J* = 5.3 Hz), **140.3**, **143.1** (d, *J* = 289.3 Hz), 144.1 (d, *J* = 294.6 Hz). **^{19}F {^{1}H} NMR** (282 MHz, $CDCl_3$): δ **-4.96**, -13.08.

HRMS (ESI) m/z: $[M+H]^+$ calc'd for $[C_9H_9FNO]$ 166.0668; found 166.0664.

m.p.: 71 - 72 °C

morpholine-4-carbonyl fluoride

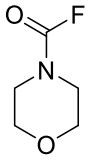

The title compound was prepared with a modified general procedure from morpholine (439 mg, 5.04 mmol, 1.0 equiv), 4-methylpyridine N-oxide (1.15 g, 10.5 mmol, 2.1 equiv), and PDFA (2.72 g, 7.61 mmol, 1.5 equiv). The yield was determined by quantitative ^{1}H NMR (56%) of the crude reaction mixture, with spectral data being consistent with literature values.[18]

4-methyl-2-phenyl-piperazine-1-carbonyl fluoride

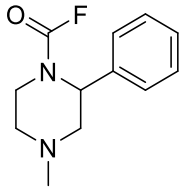

The title compound was prepared and worked up according to the general procedure from 1-methyl-3-phenyl-piperazine (1.05 g, 5.97 mmol, 1.0 equiv.), 4-methylpyridine *N*-oxide (1.43 g, 13.1 mmol, 2.2 equiv.), and PDFA (3.21 g, 8.99 mmol, 1.5 equiv.). The product was purified by

flash chromatography (50% EtOAc/Hexanes) and was isolated as an orange oil (857 mg, 3.85 mmol, 64%).

^{1}H NMR (600 MHz, $CDCl_3$): δ **7.57** (s, br, 1.1H), 7.48 (s, br, 0.9H), 7.36 (t, *J* = 7.6 Hz, 2H), 7.30 (t, *J* = 7.3 Hz, 1H), **5.21** (s, br, 0.55H), 5.07 (s, br, 0.45H), 3.87 (d, br, *J* = 13.3 Hz, 0.45H), **3.73** (d, br, *J* = 11.5 Hz, 0.55H), 3.33 (d, *J* = 12.2 Hz, 1H), 3.21 (ddd, *J* = 13.5, 12.3, 3.3 Hz, 1H), 2.82 (s, br, 1H), 2.49 (dd, *J* = 12.2, 4.4 Hz, 1H), 2.32 (s, 3H), 2.17 (s, br, 1H). **^{13}C NMR** (151 MHz, $CDCl_3$): δ **41.2**, 41.3, 46.2, 54.3, 54.6, 54.9, **56.6**, 57.2, 127.3, 127.7, 127.8, 128.6, 138.3, **146.5** (d, *J* = 285.7 Hz), 146.9 (d, *J* = 286.3 Hz). **^{19}F {^{1}H} NMR** (282 MHz, $CDCl_3$): δ -23.66, **-24.14.**

4-benzhydrylpiperazine-1-carbonyl fluoride

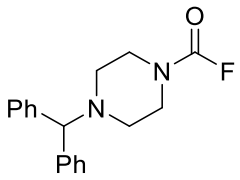

The title compound was prepared and worked up according to the general procedure from 1-benzhydrylpiperazine (5.01 g, 19.8 mmol, 1.0 equiv.), 4-methylpyridine *N*-oxide (4.39 g, 40.2 mmol, 2.0 equiv.), and PDFA (10.6 g, 29.8 mmol, 1.5 equiv.). The product was purified by flash chromatography (5% EtOAc/Hexanes) and was isolated as a white crystalline solid (3.78 g, 12.7 mmol, 64%).

^{1}H NMR (600 MHz, $CDCl_3$): δ 7.41 (d, *J* = 7.5 Hz, 4H), 7.30 (t, *J* = 7.6 Hz, 4H), 7.21 (t, *J* = 7.4 Hz, 2H), 4.28 (s, 1H), 3.50 (dt, *J* = 20.1, 5.1 Hz, 4H), 2.43 (dt, *J* = 22.2, 5.1 Hz, 4H). **^{13}C NMR** (151 MHz, $CDCl_3$): δ 44.9 (d, *J* = 3.4 Hz), 45.0, 51.0, 51.2, 75.8, 127.3, 127.8, 128.7, 141.8, 146.3 (d, *J* = 285.8 Hz). **^{19}F {^{1}H} NMR** (282 MHz, $CDCl_3$): δ -24.38.

m.p.: 113 - 114 °C

4-(furan-2-carbonyl)piperazine-1-carbonyl fluoride

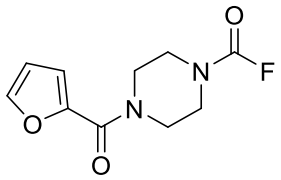

The title compound was prepared and worked up according to the general procedure from 2-furyl(piperazin-1-yl)methanone (2.16 g, 12.0 mmol, 1.0 equiv.), 4-methylpyridine *N*-oxide (2.63 g, 24.8 mmol, 2.0 equiv.), and PDFA (6.48 g, 18.2 mmol, 1.5 equiv.). The product was purified by flash chromatography (50% EtOAc/Hexanes) and was isolated as a pale-yellow solid (2.12 g, 10.2 mmol, 85%).

^{1}H NMR (600 MHz, $CDCl_3$): δ 7.52 – 7.48 (m, 1H), 7.09 (d, *J* = 3.5 Hz, 1H), 6.51 (dd, *J* = 3.6, 1.8 Hz, 1H), 3.87 (br, d, *J* = 22.3 Hz, 4H), 3.58 (dt, *J* = 16.0, 5.4 Hz, 4H). **^{13}C NMR** (151 MHz, $CDCl_3$): δ 44.8, 44.9, 111.6, 117.6, 144.1, 146.1 (d, *J* = 287.4 Hz), 147.4, 159.1. **^{19}F {^{1}H} NMR** (282 MHz, $CDCl_3$) δ -23.35.

HRMS (ESI) m/z: $[M+H]^+$ calc'd for $[C_{10}H_{12}FN_2O_3]$ 227.0832; found 227.0828.

m.p.: 97 - 98 °C

3-oxo-8-azabicyclo[3.2.1]octane-8-carbonyl fluoride

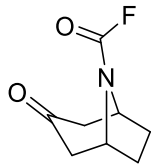

The title compound was prepared and worked up according to the general procedure from 8-azabicyclo[3.2.1]octan-3-one hydrochloride (5.17 g, 32.0 mmol, 1.0 equiv.), 4-methylpyridine *N*-oxide (10.5 g, 96.1 mmol, 3.0 equiv.), PDFA (23.0 g, 64.3 mmol, 2.0 equiv.) and NEt_3 (6.7 mL, 48.1 mmol, 1.5 equiv.). The product was purified by flash chromatography (20% EtOAc/Hexanes) and was isolated as an off-white crystalline solid (2.65 g, 15.5 mmol, 48%).

^{1}H NMR (600 MHz, $CDCl_3$): δ 4.52 (br, dq, *J* = 11.8, 4.9 Hz, 2H), 2.77 (dd, *J* = 16.3, 4.6 Hz, 1H), 2.66 (dd, *J* = 16.4, 4.7 Hz, 1H), 2.42 (d, *J* = 16.2 Hz, 2H), 2.23 – 2.11 (br, m, 2H), 1.79 – 1.70 (m, 2H). **^{13}C NMR** (151 MHz, $CDCl_3$): δ 28.3, 29.2, 48.4, 49.3, 53.9, 54.0, 143.8 (d, *J* = 289.5 Hz), 205.6. **^{19}F {^{1}H} NMR** (282 MHz, $CDCl_3$): δ -17.43.

HRMS (ESI) m/z: $[M+H]^+$ calc'd for $[C_8H_{11}FNO_2]$ 172.0774; found 172.0768.

m.p.: 106 - 107 °C

phenothiazine-10-carbonyl fluoride

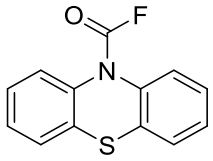

The title compound was prepared and worked up according to the general procedure from 10*H*-phenothiazine (2.50 g, 12.5 mmol, 1.0 equiv.), 4-methylpyridine *N*-oxide (2.74 g, 25.1 mmol, 2.0 equiv.), and PDFA (6.72 g, 18.8 mmol, 1.5 equiv.). The product was purified by flash chromatography (5% EtOAc/Hexanes) and was isolated as a pale-yellow solid (0.505 g, 2.06 mmol, 16%).

^{1}H NMR (600 MHz, $CDCl_3$): δ 7.57 (br, d, *J* = 90.2 Hz, 2H), 7.42 (dd, *J* = 7.8, 1.5 Hz, 2H), 7.35 (t, *J* = 7.8 Hz, 2H), 7.27 (td, *J* = 7.6, 1.3 Hz, 2H). **^{13}C NMR** (151 MHz, $CDCl_3$): δ 125.78, 125.80, 127.4, 127.5, 127.8, 131.9, 136.5, 144.6 (d, *J* = 294.7 Hz). **^{19}F {^{1}H} NMR** (282 MHz, $CDCl_3$): δ -15.39.

HRMS (ESI) m/z: $[M+H]^+$ calc'd for $[C_{13}H_9FNOS]$ 246.0389; found 246.0381.

m.p.: 155 - 157 °C

***N*-[4-[fluorocarbonyl(phenacyl)amino]phenyl]-*N*-phenacyl-carbamoyl fluoride**

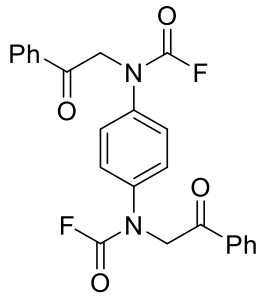

The title compound was prepared and worked up according to the general procedure from N,N'-diphenacyl-p-phenylenediamine (363 mg, 1.05 mmol, 1.0 equiv), 4-methylpyridine N-oxide (476 mg, 4.36 mmol, 4.2 equiv), and PDFA (1.17 g, 3.28 mmol, 3.1 equiv). The product was purified by flash chromatography (40% EtOAc/Hexanes) and was isolated as a colorless crystalline solid (281.7 mg, 0.645 mmol, 61%).

^{1}H NMR (600 MHz, $CDCl_3$): δ 7.92 (q, *J* = 6.7 Hz, 4H), 7.67 – 7.59 (m, 2H), 7.54 – 7.41 (m, 8H), 5.09 – 5.03 (m, 4H). **^{13}C NMR** (151 MHz, $CDCl_3$): δ 57.51, 57.53, 57.7, 127.1, 127.2, 127.90, 127.93, 127.95, 129.0, 129.1, 133.9, 134.18, 134.21, 134.27, 134.29, 134.41, 134.45, 139.2, 139.7, 140.3, 140.8, 145.39, 145.45, 145.5, 147.3, 147.4, 191.47, 191.50, 191.69, 191.75. **^{19}F NMR** (564 MHz, $CDCl_3$): δ -15.64, -15.65, -16.64, -16.87.

***N*-phenyl-*N*-[[5-[3-(trifluoromethyl)phenyl]-1,2,4-oxadiazol-3-yl]methyl]carbamoyl fluoride**

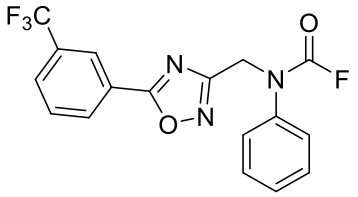

The title compound was prepared and worked up according to the general procedure from *N*-[[5-[3-(trifluoromethyl)phenyl]-1,2,4-oxadiazol-3-yl]methyl]aniline (544 mg, 1.73 mmol, 1.0 equiv.), 4-methylpyridine *N*-oxide (414 mg, 3.80 mmol, 2.2 equiv.), and PDFA (938 mg, 2.63 mmol, 1.5 equiv.). The product was purified by flash chromatography (20% EtOAc/Hexanes) and was isolated as a pale-yellow highly viscous oil (573 mg, 1.57 mmol, 91%).

^{1}H NMR (600 MHz, $CDCl_3$): δ 8.39 (s, 1H), 8.33 (d, *J* = 7.5 Hz, 1H), 7.87 (d, *J* = 7.5 Hz, 1H), 7.73 – 7.67 (m, 1H), 7.47 (d, *J* = 8.0 Hz, 0.5H), 7.45 – 7.31 (m, 4.5H), **5.06** (s, 1.5H), 5.02 (s,

0.5H). **^{13}C NMR** (151 MHz, $CDCl_3$): δ 47.0, **47.4**, 113.4, 124.1 (q, *J* = 272.7 Hz), 124.5, 124.6, 125.1 (q, *J* = 3.9 Hz), 126.0, 126.7, 128.2, 128.6, 129.5 (q, *J* = 3.7 Hz), 129.6, **129.9**, 130.0, **131.26**, 131.29, **131.9** (q, *J* = 33.4 Hz), 132.0 (q, *J* = 33.9 Hz), **139.1**, 140.2, 146.2 (d, *J* = 293.3 Hz), **146.4** (d, *J* = 289.6 Hz), **167.1**, 167.5, **175.1**, 175.3. **^{19}F {^{1}H} NMR** (564 MHz, $CDCl_3$): δ -14.88, -16.13, -62.98, -62.99.

HRMS (ESI) m/z: $[M+H]^+$ calc'd for $[C_{17}H_{12}F_4N_3O_2]$ 366.0866; found 366.0861.

4-(13-chloro-4-azatricyclo[9.4.0.0^{3,8}]pentadeca-1(11),3(8),4,6,12,14-hexaen-2-ylidene) piperidine-1-carbonyl fluoride

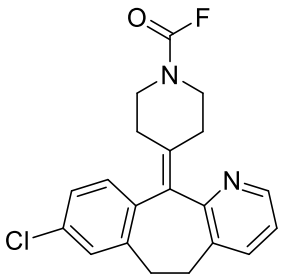

The title compound was prepared and worked up according to the general procedure from desloratadine (316 mg, 1.02 mmol, 1.0 equiv), 4-methylpyridine N-oxide (222 mg, 2.04 mmol, 2.0 equiv), and PDFA (557 mg, 1.56 mmol, 1.5 equiv). The product was purified by flash chromatography (40% EtOAc/Hexanes) and was isolated as a yellow crystalline solid (281.7 mg, 0.645 mmol, 61%). Spectral data are consistent with literature values.[18]

1-Cyclopropyl-6-fluoro-7-(4-(fluorocarbonyl)piperazin-1-yl)-4-oxo-1,4-dihydroquinoline-3-carboxylicacid

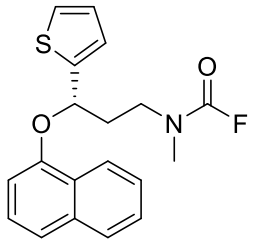

The title compound was prepared with a modified general procedure from duloxetine hydrochloride (85.2 mg, 0.26 mmol, 1.0 equiv), 4-methylpyridine N-oxide (64.9 mg, 0.59 mmol, 2.3 equiv), PDFA (138 mg, 0.39 mmol, 1.5 equiv), and NEt_3 (72.6 mg, 0.72 mmol, 2.8 equiv). The crude reaction mixture had volatiles removed under reduced pressure, and the product was extracted with hexanes (3 × 10 mL), passed through a plug of cotton and solvent removed under reduced pressure. Yield was determined by quantitative ^{1}H and ^{19}F $\{^{1}H\}$ NMR with trimethoxybenzene or trifluorotoluene used as an internal standard respectively.

_N_-methyl-_N_-[(3S)-3-(1-naphthyloxy)-3-(2-thienyl)propyl]carbamoyl fluoride

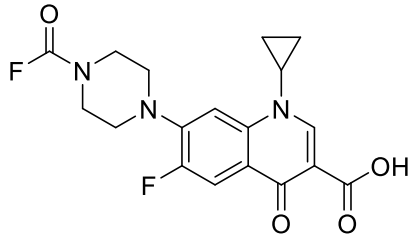

The title compound was prepared and worked up according to the general procedure from ciprofloxacin (436 mg, 1.32 mmol, 1.0 equiv), 4-methylpyridine N-oxide (619 mg, 5.67 mmol, 4.3 equiv), and PDFA (1.50 g, 4.2 mmol, 3.2 equiv). The product was purified by flash chromatography (40% EtOAc/Hexanes) and was isolated as a colorless crystalline solid (281.7 mg, 0.645 mmol, 61%). Spectral data are consistent with literature values.[19]

Chapter 3: Palladium Catalyzed Cross-Coupling of Carbamoyl Fluorides

3.1. Author contributions

This chapter describes the palladium-catalyzed Suzuki cross-coupling of 2-pyridyl carbamoyl fluorides (CMFs) with aryl boronic acids. This work was done in collaboration with graduate student Maryam Jabbarpoor, who developed and optimized reaction conditions, as well as performed the substrate scope studies. The project was conceptualized by former undergraduate student Zichuan Chen, who identified the initial hit for further reaction screening. Several of the CMF substrates used in this study were synthesized by former PhD student Dusty Cadwallader.

The author's contributions to this project focused primarily on mechanistic investigations. These studies included the synthesis and characterization of various catalytically relevant organometallic intermediates, evaluating the role of triphenylphosphine oxide (TPPO) as a reaction additive, and the synthesis of several CMF substrates required for the substrate scope and mechanistic investigations. The contributions of each co-author are stated within the text or labelled in the relevant schemes throughout the chapter where applicable. Most of the contents within this chapter are published in the journal *Chemical Communications*.

Citation: Jabbarpoor, M.; LeBlanc, J.; Chen, Z.; Cadwallader, D.; Le, C. M. Pd-Catalyzed Suzuki-Type Cross-Coupling of 2-Pyridyl Carbamoyl Fluorides. *Chem. Commun.* **2024**, *60* (66), 8700–8703.

3.2. Motivation and Research Plans

Although numerous synthetic routes towards pyridyl amides have been reported, many require the use of toxic reagents, strong oxidants, and/or harsh reaction conditions (Scheme 3.1).[1–4] Carbamoyl halides represent a unique class of electrophiles that provide an alternative retrosynthetic bond disconnection for amide synthesis via C–C bond formation rather than traditional C–N bond-forming approaches.[5] Among the various methods available for C–C bond formation, the Suzuki-Miyaura cross-coupling reaction is one of the most widely used transformations in the pharmaceutical industry.[6] However, Suzuki cross-coupling reactions of carbamoyl halides remain underdeveloped and are largely limited to carbamoyl chlorides (CMCls), with existing methods exhibiting limited substrate diversity.

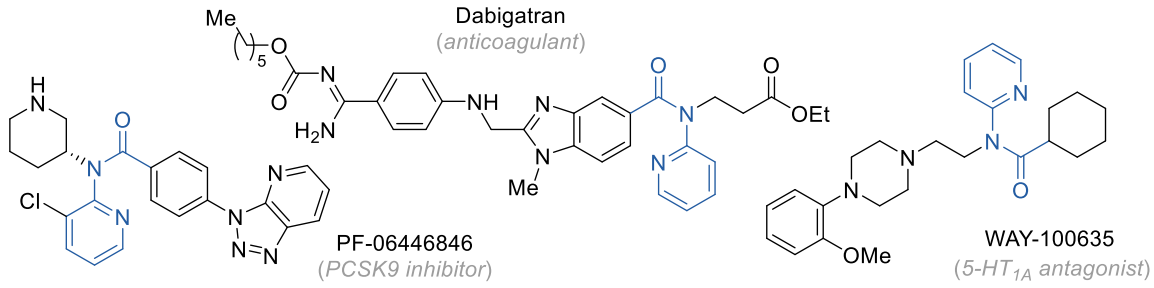

Figure 3.1: Representative examples of APIs containing 2-pyridyl amides.

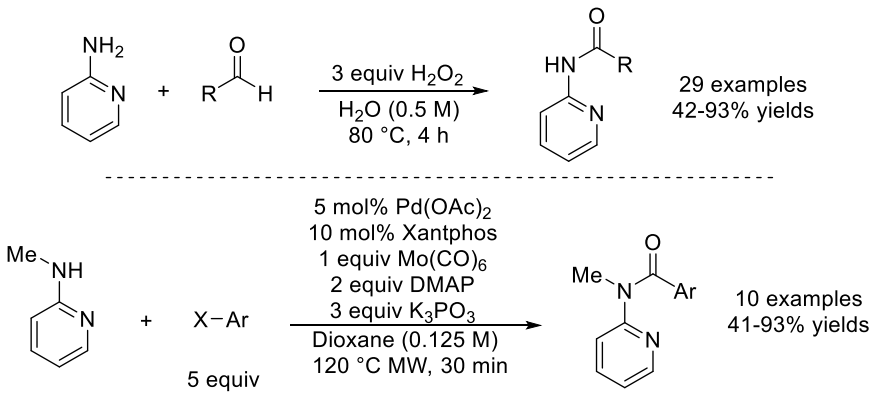

Scheme 3.1: Representative examples of the synthesis of 2-pyridyl amides.

Although CMFs are generally less electrophilic than their CMCl counterparts, they exhibit unique fluoride-enabled reactivity as mentioned in Chapter 1, in some reported Lewis acid- and Lewis base-catalyzed transformations.[7] Furthermore, in the context of transition metal-catalyzed reactions, CMFs have been shown to provide improved yields and enantioselectivities relative to the corresponding CMCls in nickel-catalyzed intramolecular carbocarbamoylation reactions.[8] These observations suggest that CMFs may serve as attractive electrophiles for the development of new cross-coupling methodologies.

At the time this work was initiated, no examples of the direct intermolecular cross-coupling of boronic acids with CMFs had been reported. This absence likely stems from the challenges associated with activation of the strong C–F bond, as well as the need to outcompete substrate decomposition pathways such as decarbonylation and hydrolysis. To address these challenges, we sought to develop the first metal-catalyzed intermolecular Suzuki cross-coupling reaction of CMFs. It was anticipated that incorporation of a 2-pyridyl directing group would facilitate oxidative addition through coordination to palladium while simultaneously promoting the formation of a five-membered palladacyclic intermediate. Such chelation was hypothesized to stabilize reactive intermediates and suppress unproductive decomposition pathways, thereby enabling efficient cross-coupling of CMF and aryl boronic acid substrates.

3.3. Introduction

3.3.1. Directing Groups for C–F bond activation

The use of carbamoyl halides as electrophiles for the synthesis of amides through C-C bond formation provides an attractive alternative to traditional methods for amide synthesis. Carbamoyl chlorides (CMCl) have been extensively studied in metal-catalyzed reactions, and have been shown to be competent electrophiles in a variety of cross-coupling reactions.[9–15] However, as discussed in Chapter 1 many reported examples rely on intramolecular cyclization, while comparatively few intermolecular cross-couplings have been described. This limitation largely arises from successful intermolecular coupling being dependent on the rate of transmetalation and subsequent reductive elimination relative to decarbonylation. The impact of decarbonylation also depends on its reversibility: reversible CO loss may permit re-formation of the metal-carbamoyl intermediate, whereas irreversible decarbonylation or loss of CO from the reaction systems results in intermediate decomposition. Because intramolecular reactions generally proceed more rapidly than intermolecular processes, productive bond formation can often outcompete decomposition pathways. Although CMCls are considerably more stable than the corresponding acyl chlorides, they remain relatively sensitive to moisture and can undergo hydrolysis after several days to the parent amine.

Carbamoyl fluorides (CMFs), in contrast, are significantly more stable analogues of carbamoyl chlorides and therefore represent an attractive alternative for metal-catalyzed cross-coupling reactions. Despite their enhanced stability, CMFs remain largely underexplored as electrophiles in cross-coupling chemistry, likely due to their limited synthetic accessibility until recently. Prior to the work reported herein, only three examples of metal-catalyzed cross-couplings

involving CMFs had been reported. In 2020, Ye and Luan reported the first cross-coupling reaction of CMFs in a nickel-catalyzed Suzuki-type intramolecular cyclization reaction.[8] Subsequently, Schoenebeck and co-workers reported the first intermolecular cross-coupling of a CMF through the nickel-catalyzed alkynylation of *N*–CF_3 CMFs to afford alkynamides.[16] Lastly, Chen and co-workers reported the intramolecular nickel-catalyzed enantioselective 1,4-arylcarbamoylation of 1,3-dienes using boronic acids, providing access to α-alkenylated γ-lactams.[17] Although these studies demonstrate the synthetic utility of CMFs, their broader application remains challenging. Although activation of the exceptionally strong C–F bond typically requires forcing reaction conditions, oxidative addition does not eliminate competing decomposition pathways, as the resulting metal-carbamoyl intermediate may still undergo decarbonylation. These challenges have substantially limited the widespread use of CMFs as electrophiles in metal-catalyzed reactions.

Historically, the use of directing groups has been an effective strategy for promoting otherwise challenging C–F bond activation processes. Directing groups are functional groups capable of interacting with a reagent or catalyst to facilitate bond activation or reactivity at a specific site within a molecule.[18] In transition-metal catalysis, directing groups frequently function as transient ligands that coordinate to a metal center and guide the target bond into close proximity to the metal, thereby facilitating bond activation (Figure 3.2). With an ideal directing group coordinating sufficiently to promote selective bond activation while allowing for subsequent catalytic steps and product release. Its effectiveness depends on both its binding affinity and ability to position the target bond in a favourable geometry. From a practical perspective, directing groups should also be compatible with the reaction conditions and either remain useful in the final product or be readily installed and removed.

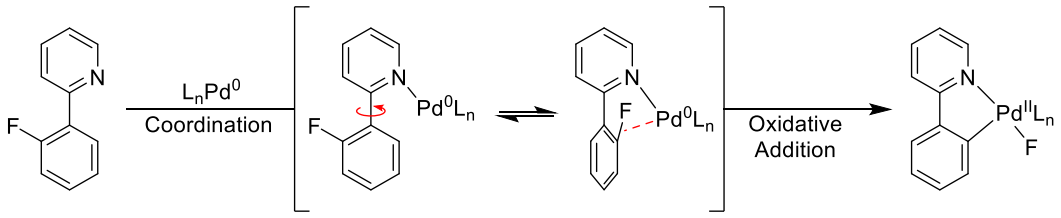

Figure 3.2: Example illustrating how a directing group can position a target bond in close proximity to a metal center, facilitating bond activation.

Common directing groups include imines, ketones, hydroxyl groups, and *N*-heterocycles, all of which possess donor atoms capable of coordinating to transition metals.[18,19] Among these, pyridyl directing groups have proven particularly effective due to the strong σ-donation provided by the nitrogen lone pair. As a result, pyridyl substituents have been widely used to facilitate challenging bond activations, including numerous examples of C–F bond activation.[19–21]

In addition to promoting oxidative addition, directing groups can stabilize reactive organometallic intermediates through chelation to the metal center. For substrates that are prone to decomposition following oxidative addition, such stabilization may help suppress unproductive pathways. In the context of cross-coupling of carbamoyl halides, coordination of a suitably positioned directing group can generate a five-membered palladacyclic intermediate. Decarbonylation of this intermediate would produce a metal-amido species containing a highly strained four-member palladacycle, thereby disfavoring decarbonylation (Figure 3.3). Consequently, the incorporation of suitable directing groups represents a potentially attractive strategy for enabling metal-catalyzed transformations of CMFs.

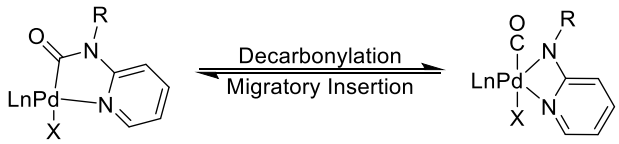

Figure 3.3: Formation of a highly strained four-member palladacycle upon decarbonylation.

3.4. Results and Discussion

3.4.1. Reaction Optimization and Scope

All reactions discussed in Section 3.4.1 were performed by Maryam Jabbarpoor and the results presented herein are included only to provide context for my contributions to the mechanistic studies. Prior to this work, no examples of the intermolecular Suzuki cross-coupling of CMFs had been reported. Based on the established ability of directing groups to facilitate challenging C–F bond activation processes, it was anticipated that incorporating 2-pyridyl substituents into the CMF substrates would promote oxidative addition to palladium. The resulting palladacycle intermediate was anticipated to suppress decarbonylation pathways, leading to the formation of undesired secondary amine and catalytically inactive Pd–CO complexes.[22]

Investigation into reaction conditions revealed that the target 2-pyridyl amide (**3.3a**) could be isolated in a 90% yield using $PdCl_2(PPh_3)_2$ as the pre-catalyst under the conditions outlined in Table 3.1 (entry 1). These conditions resulted in complete conversion of CMF **2.2o** with only trace formation of the corresponding amine.

A particularly noteworthy observation was the beneficial effect of triphenylphosphine oxide (TPPO) as a reaction additive. After observing the excellent performance of $PdCl_2(PPh_3)_2$, the commonly used cross-coupling pre-catalyst $Pd(PPh_3)_4$ was evaluated for comparison. Surprisingly, pristine $Pd(PPh_3)_4$ provided **3.3a** in only 10% yield, whereas an older batch that had been stored in open atmosphere provided drastically improved reactivity, (Table 3.1, entries 2 and 3), comparable to the standard catalyst. Subsequent investigation found that the older batch contained a significant amount of TPPO as an impurity. Interestingly, the addition of TPPO (30 mol%) as an additive to the reaction employing fresh $Pd(PPh_3)_4$ led to improved yields relative to

the TPPO-free system (Table 3.1, entry 4 vs 2). Additionally, it was found that the presence of TPPO in sub-stoichiometric amounts under the "standard conditions" (Table 3.1, entry 5) consistently led to slightly improved yields and improved reaction reproducibility in some substrate-dependent cases. Consequently, TPPO was incorporated into all subsequent cross-coupling reactions reported in Section 3.4.1, and our studies to elucidate its exact role in the reaction is discussed detail in Section 3.4.2.1.

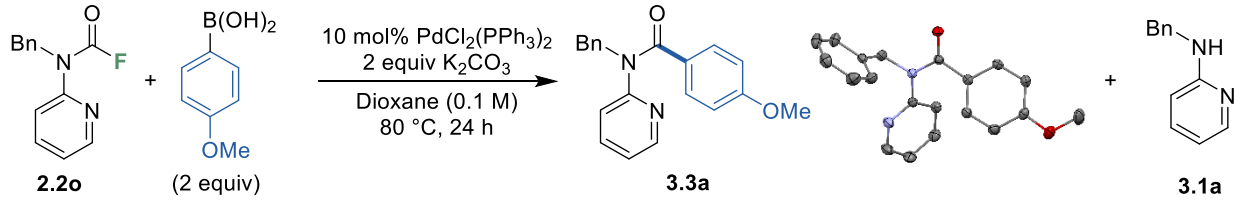

Entry	Deviation from Conditions Above	Conversion (%)[a]	Yield of **3.3a**[a] (%)	Yield of **3.1a**[a] (%)
1	None	100	90	8
2	$Pd(PPh_3)_4$[d]	97	10	72
3	$Pd(PPh_3)_4$[e]	100	84	7
4	$Pd(PPh_3)_4$[d] + TPPO (30 mol%)	98	42	38
5	**TPPO (30 mol%)**	**100**	**95**	**4**

Table 3.1: Catalyst screening for Suzuki-type cross-coupling of CMF **2.2o** conducted by Maryam Jabbarpoor. [a]: Conversions and yields acquired by ^{1}H NMR with 1,3,5 trimethoxybenzene as an internal standard. [d]: Batch stored in Argon-filled glovebox at -35 °C. [e]: Batch stored under N_2 at 4 °C. Hydrogen atoms have been omitted for clarity. ORTEP drawn at 50% probability.

3.4.2. Mechanistic Studies

3.4.2.1. Role of TPPO

During optimization studies, it was discovered that the addition of TPPO as a sub-stoichiometric additive (30 mol%) resulted in improved yields of the desired product (Table 3.1, entry 1). While beneficial to the reaction, the exact role of TPPO and the origin of its positive effect on reaction yield were not immediately apparent. Several possible explanations have been proposed in the literature, although few appear directly applicable to the present system. Given the

impact of TPPO on reaction performance, increasing yields by more than 30% for certain substrates (Table 3.2, entries **7** and **8**), its role in the reaction was herein thoroughly investigated in detail.

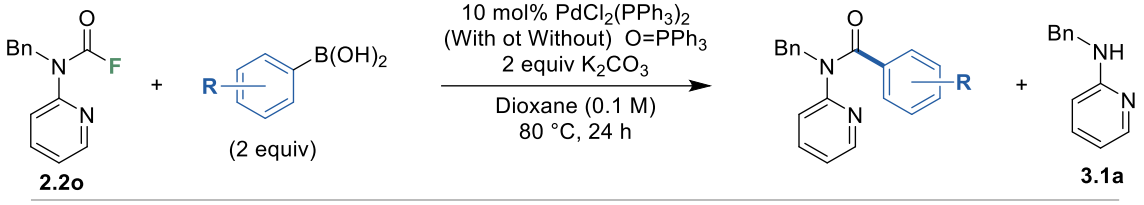

Entry	Boronic Acid	TPPO (mol%)	Conversion (%)[a]	Yield of Amide[a]	Yield of Amine[a]
1	R = *p*-H	-	100	50%	37%
2		**30%**	**99**	**76%**	**23%**
3	R = *p*-Me	-	100	65%	17%
4		**30%**	**99**	**78%**	**12%**
5	R = *m*-OMe	-	88	39%	9%
6		**30%**	**97**	**59%**	**29%**
7	R = *p*-F	-	100	52%	38%
8		**30%**	**100**	**84%**	**9%**

Table 3.2: The effect of TPPO with various boronic acid substrates. Reactions reported were conducted by Maryam Jabbarpoor. [a]: Conversions and yields acquired by ^{1}H NMR with 1,3,5 trimethoxybenzene as an internal standard.

Phosphine oxides are generally regarded as weakly coordinating ligands for late transitions metals such as palladium (Pd). Their relatively labile coordination arises primarily from the mismatch between the hard oxygen donor and the comparatively soft palladium center, resulting in weaker metal–ligand interactions than those formed with phosphine ligands. Furthermore, phosphine oxides lack the strong bonding interactions characteristic of phosphines, which combine significant σ-donation with the ability to accept electron density through π-backbonding. As a result, phosphine oxide ligands typically exhibit hemilabile behaviour in palladium complexes.[23,24]

Nevertheless, a handful of palladium complexes have been reported wherein a phosphine oxide oxygen coordinates directly to the metal center. However, most examples require bidentate ligands containing both a phosphine oxide and a typical phosphine donor (i.e., bisphosphine mono-

oxide). In these systems, the phosphine serves as an anchoring group, positioning the phosphine oxide in close proximity to the palladium center and facilitating coordination.[25–27]

Denmark and co-workers proposed that phosphine oxides may function as weakly coordinating additives capable of stabilizing palladium catalysts, particularly in non-coordinating solvents such as toluene, where solvent stabilization is minimal. Under these conditions, phosphine oxides could serve as labile ligands to stabilize sensitive catalytic intermediates, and reduce catalyst decomposition.[28]

To investigate whether TPPO was acting as a ligand in the present system, several phosphine oxides possessing different steric and electronic characteristics were evaluated using CMF **2.2o** (Table 3.3). Substrate **3.3b** was selected because the addition of TPPO produced the greatest improvement in yield and its fluorine containing substituent provided a convenient spectroscopic handle for reaction analysis. Our hypothesis was that if the phosphine oxides were functioning as a ligand on palladium, changes in the electronic and steric properties would be expected to influence reaction performance. Despite these differences, all phosphine oxides provided similar reaction outcomes, affording product yields between 78% and 82%. These results provide little evidence that TPPO functions primarily as a ligand on palladium under the reaction conditions employed. Reactions were performed by Maryam Jabbarpoor.

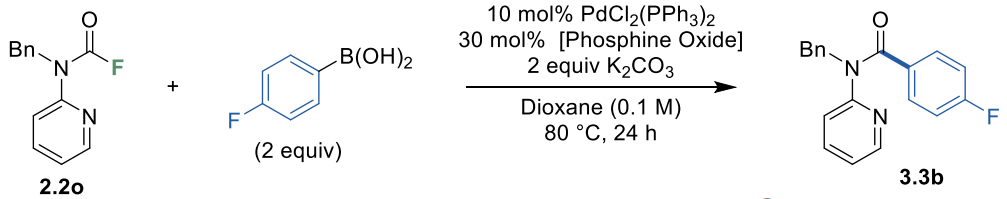

Entry	Phosphine Oxide (30 mol%)	Yield of **3.3b**[a] (%)
1	$O{=}PPh_3$	82
2	$O{=}PEt_3$	78
3	$O{=}P(o\text{-tol})_3$	82

Table 3.3: Phosphine oxide screening. [a]: Conversions and yields acquired by ^{1}H NMR with 1,3,5 trimethoxybenzene as an internal standard. Reactions performed by Maryam Jabbarpoor.

Denmark and Altan have proposed that phosphine oxides may stabilize highly active palladium nanoparticles in solution and prevent the formation of catalytically inactive palladium clusters.[28,29] Determining whether a metal-catalyzed reaction proceeds through homogenous molecular catalysis or heterogenous metal nanoparticles remains a challenging problem that has generated considerable debate in the literature. The "*mercury drop test"* is a classic experiment that is considered a diagnostic tool for distinguishing between homogeneous and heterogenous catalysis.[30] The principle of the test is that elemental mercury (Hg^0) will readily amalgamate with metal nanoparticles, significantly reducing or eliminating their catalytic activity and thereby effectively poisoning the reaction. The absence of reaction inhibition is often interpreted as evidence for homogenous catalysis, because homogenous metal complexes bearing protective ancillary ligands are assumed to be unaffected by Hg^0.[31]

Accordingly, the mercury drop test was performed under the standard reaction conditions. The reaction was found to be strongly inhibited in the presence of Hg^0, resulting in a 67% conversion of CMF **2.2o** and only 6% yield of amide **3.3a**, with the mass balance corresponding to amine **3.1a** (Scheme 3.2). At first glance, these results appear consistent with the formation of catalytically relevant palladium nanoparticles. However, the validity of the mercury drop test relies on several important assumptions. Recently, McIndoe and co-workers demonstrated that Hg^0 can interact with both L_nPd^0 and $Pd^{II}ArX$ intermediates.[31] In such cases, mercury was found to accelerate the consumption of homogeneous $Pd^{0/II}$ catalyst resting states, leading to the formation of organomercuric ions, mercuric halides, and catalyst deactivation through Pd^0 nanoparticle formation and amalgamation. In addition, transmetalation between organopalladium intermediates and Hg^0 was observed.[31] These findings refute the widely held assumption that protective ligands, such as triphenylphosphine, prevent Hg^0 from interacting with homogeneous palladium

complexes.[31] Consequently, while the present results do not rule out the formation of palladium nanoparticles, neither do they provide definitive evidence for their involvement in catalysis. Therefore, the mercury drop test alone cannot be considered sufficient evidence for or against a nanoparticle-mediated pathway.

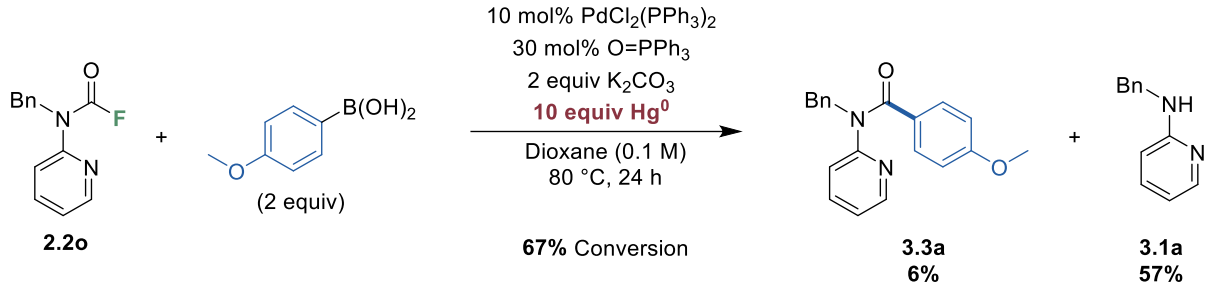

Scheme 3.2: Reaction conditions used to carry out mercury drop test.

It has been long been recognized that boronic acids exist in equilibrium with their corresponding boroxine (Figure 3.4).[32–34] Recent mechanistic studies have sown that this interconversion occurs through a three-stage dynamic process involving two transient acyclic anhydride intermediates.[35] However, under the hydrolytic equilibrium conditions examined it was found that boronic acid and boroxine together accounted for more than 95% of the total aryl-boron speciation. Accordingly, only these two predominate species are considered in the following discussion. The position of this equilibrium is influenced by the electronic and steric properties of the boronic acid, solvent, concentration, and water content. Consequently, commercial or aged boronic acid samples often contain variable quantities of both water and the less-reactive boroxine.

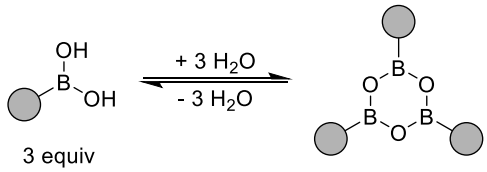

Figure 3.4: Boronic acid - boroxine equilibrium.

In 2012, Raţ and co-workers reported the solid-state structure of a hydrogen-bonding adduct between (2,4,6-trimethylphenyl)boronic acid and TPPO (Figure 3.5).[36] This observation prompted us to consider whether TPPO could influence the boronic acid-boroxine equilibrium

under the reaction conditions by acting as a hydrogen-bond acceptor. Such an effect could explain both the beneficial influence of TPPO on the reaction yield and the substrate-dependent nature of this improvement.

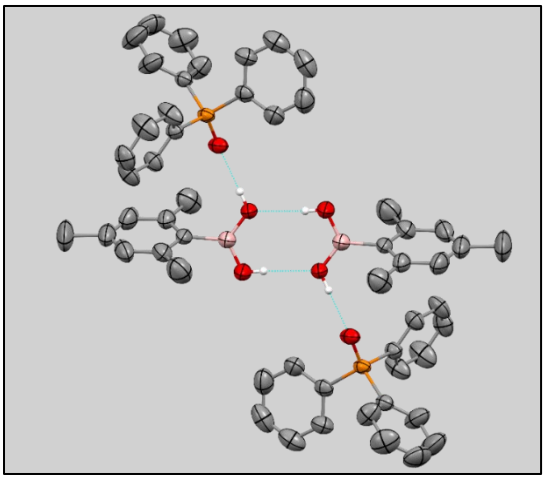

Figure 3.5: Solid state structure of boronic acid dimer stabilized by hydrogen bonding with TPPO. Crystallographic data obtained from CCDC reference number: 861749. Select hydrogen atoms have been omitted for clarity. ORTEP drawn at 50% probability.

Our working hypothesis is that TPPO increases the concentration of available boronic acid by perturbing the boronic acid:boroxine equilibrium. One possibility is that TPPO acts as a hydrogen bond acceptor through its phosphoryl oxygen, forming O–H···O=P interactions with the B–OH groups of boronic acid or the acyclic anhydride intermediates and thereby preferentially stabilizing these hydrolyzed species relative to boroxine.[35,37,38] Alternatively, TPPO could interact with water through O–H···O=P hydrogen bonds and participate in the hydrogen-bonded water networks that mediate hydrolytic B–O–B cleavage, potentially facilitating the accompanying proton-transfer steps.[35,39,40] A further possibility is that TPPO could function as a Lewis base and donate a lone pair from its phosphoryl oxygen into the vacant p-orbital of a Lewis-acidic boron in the boroxine. Such coordination could perturb the bonding within the ring and potentially facilitate hydrolytic B–O–B cleavage. These interactions could increase the effective concentration of the proposed transmetalation-active boronic acid with simultaneous consumption of water. Because water promotes hydrolysis of the CMF substrates under the basic reaction conditions, its

consumption would be expected to suppress this competing side reactions and improve reaction efficiency. Although these pathways provide plausible explanations for the beneficial effect of TPPO, other interactions or roles of TPPO in perturbing the boronic acid:boroxine equilibrium cannot be excluded.

To test this hypothesis, a known quantity of commercial 4-methylphenylboronic acid was analyzed by quantitative ^{1}H NMR spectroscopy in the presence of increasing concentrations of TPPO (Figure 3.6). Notably, the addition of less than 0.05 equivalent of TPPO resulted in a substantial increase in solubility of the commercial boronic acid in $CDCl_3$. Upon the addition of 1 equiv. of TPPO, an increase of boronic acid concentration from 9% to 26% was observed (Table 3.4).

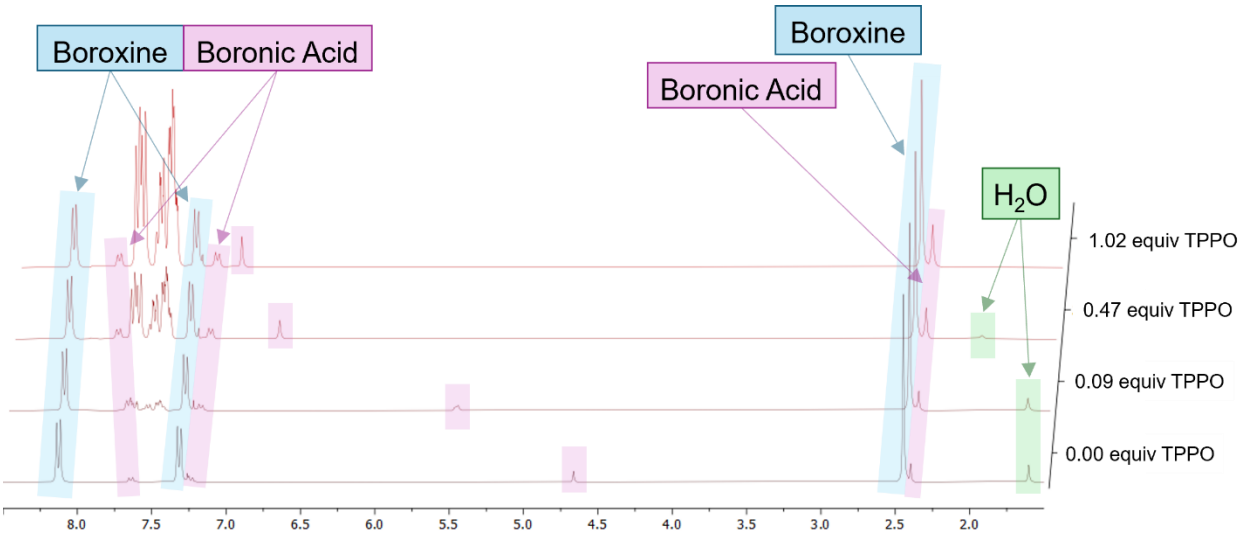

Figure 3.6: ^{1}H NMR spectra of commercial 4-methylphenylboronic acid with varying amounts of TPPO. Spectra were acquired in $CDCl_3$.

Entry	TPPO equiv	Boronic acid (mol%)	Boroxine (mol%)
1	0.00	9%	91%
2	0.09	12%	88%
3	0.47	18%	82%
4	1.02	26%	74%

Table 3.4: Quantification of the influence of TPPO on the boronic acid–boroxine equilibrium. The relative mol% of boronic acid and boroxine were determined based on the total number of boron atoms present in solution. Accordingly, one equivalent of boroxine was counted as three boron equivalents.

In addition to shifting the boroxine:boronic acid equilibrium, the concentration of water in solution decreased substantially, resulting in the complete disappearance of the water peak in the ^{1}H NMR spectrum (Figure 3.6). Even with more than 1 equiv. of TPPO, the boroxine still remains the dominant species in solution, suggesting that this hypothesis alone cannot fully account for the impact of this additive on the reaction yield. Nevertheless, it is anticipated that the impact of TPPO on the boroxine:boronic acid equilibrium should be more pronounced under the catalytic reaction conditions, where additional water and base are present, and a more polar solvent (dioxane) is employed.

Collectively, these results support a role for TPPO beyond its possible coordination to palladium. Rather than acting primarily as a ligand on palladium, TPPO appears to increase the concentration of transmetalation active-boronic acid by perturbing the boronic acid:boroxine equilibrium. This simultaneously reduces the concentration of free water in solution, as seen by quantitative NMR spectroscopy, thereby minimizing competitive hydrolysis of the CMF substrate. To the best of our knowledge, this represents a previously unreported explanation for the beneficial effects of TPPO additives in Suzuki cross-coupling reactions. Nevertheless, the possibility that TPPO additionally contributes to catalyst stabilization, including stabilization of palladium nanoparticles, cannot be entirely ruled out.

3.4.2.2. Synthesis and Evaluation of Proposed Catalytic Intermediates

To explore whether the proposed 2-pyridyl directing group participates in directed oxidative addition, efforts were undertaken to identify and isolate the catalytically relevant carbamoyl Pd–F complex. Based on the proposed catalytic cycle, it was anticipated that oxidative

addition of a 2-pyridyl CMF to a Pd(0) species would generate palladium complex **A** (Scheme 3.3). Coordination of the pyridyl nitrogen to the palladium center was expected to facilitate C–F bond activation, resulting in the formation of a favourable five-membered palladacycle **A**. The resulting chelated intermediate was expected to mitigate possible decomposition pathways, particularly decarbonylation.

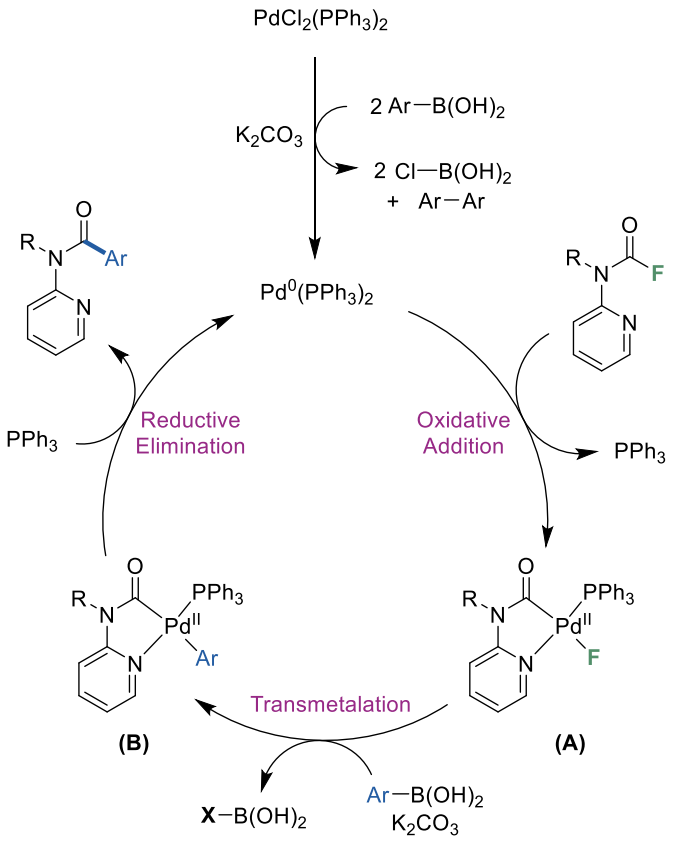

Scheme 3.3: Proposed catalytic cycle for the Suzuki cross-coupling of CMFs with boronic acids.

Initial attempts were made to synthesize complex **3.4** from $Pd(PPh_3)_4$ as a convenient and commercially available Pd(0) precursor. Treatment of $Pd(PPh_3)_4$ with CMF **2.2o** in C_6D_6 (Scheme 3.4) was monitored by ^{1}H, ^{19}F, and ^{31}P NMR spectroscopy. Formation of the desired complex **3.4** was observed upon heating the reaction to 60 °C (Figure 3.7). This was further supported by the emergence of a characteristic Pd–F resonance in the ^{19}F NMR spectrum at -255 ppm. Notably, no formation of amine was detected during the reaction, suggesting that oxidative addition of the

CMF does not immediately result in decarbonylation. This observation is consistent with the proposed stabilization effect of the 2-pyridyl directing group. Upon heating the reaction mixture for 2 days at 75 °C, the relative quantity of **3.4** remained constant compared to residual CMF, corresponding to an approximately 30% conversion of $Pd(PPh_3)_4$ to **3.4**. A possible cause for low conversion of $Pd(PPh_3)_4$ to **3.4** is the accumulation of free PPh_3 in solution which disfavors formation of the $Pd(PPh_3)_2$ species required for oxidative addition. Providing a possible explanation to the poor catalytic performance of $Pd(PPh_3)_4$ compared to $Pd(PPh_3)_2Cl_2$.

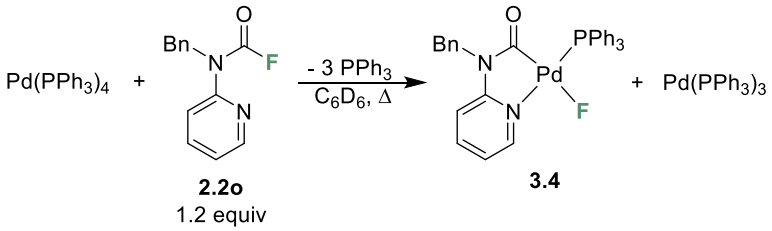

Scheme 3.4: Reaction scheme used to attempt the synthesis of complex **3.4**.

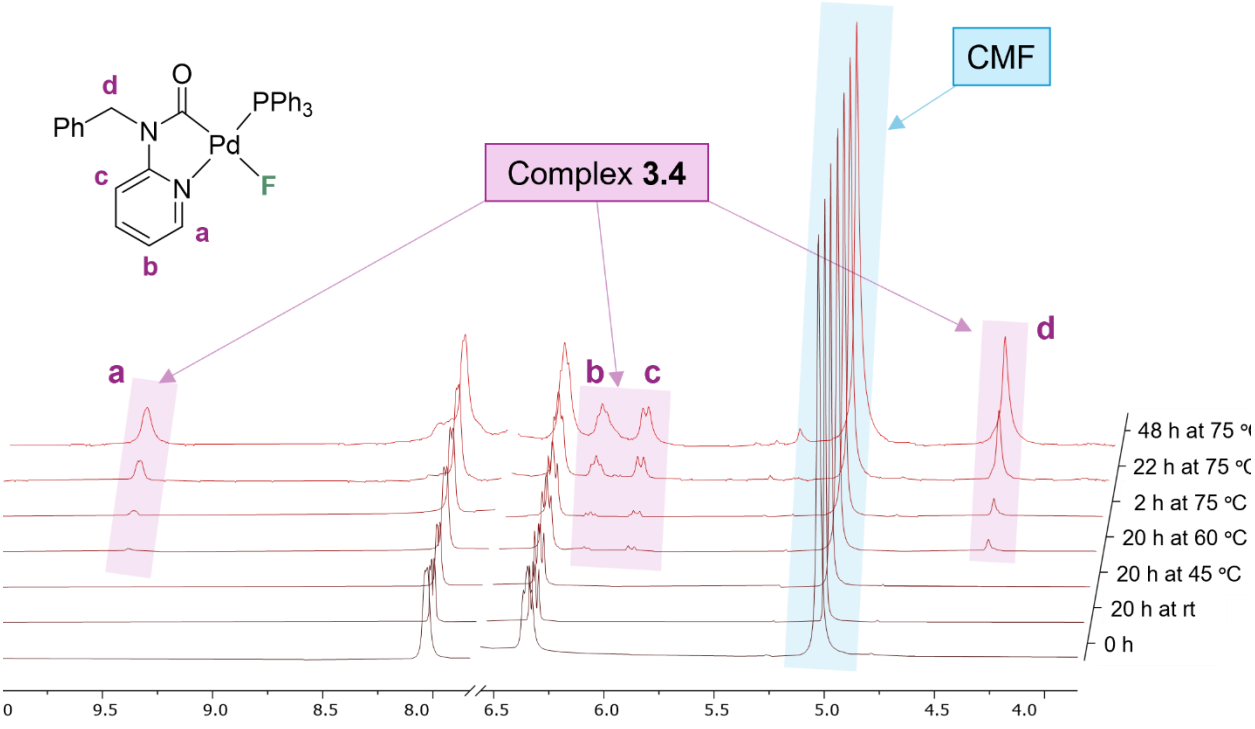

Figure 3.7: Series of ^{1}H NMR spectra from heating reaction mixture described in Scheme 3.4**:** Reaction scheme used to attempt the synthesis of complex **3.4**.

A after various amounts of time at the indicated temperatures. For clarity aromatic resonances between

Although the spectroscopic data supported the formation of **3.4**, all attempts to isolate the complex were unsuccessful. During concentration and crystallization of the reaction mixture, PPh_3 and $Pd(PPh_3)_3$ preferentially precipitates and were the only species that could be isolated (Figure 3.8), whereas **3.4** could not be induced to precipitate cleanly. Moreover, **3.4** progressively decomposed throughout its attempted isolation, further preventing its enrichment and purification. Consequently, alternative synthetic approaches were explored to obtain pure oxidative addition complexes and evaluate their relevance to the catalytic reaction.

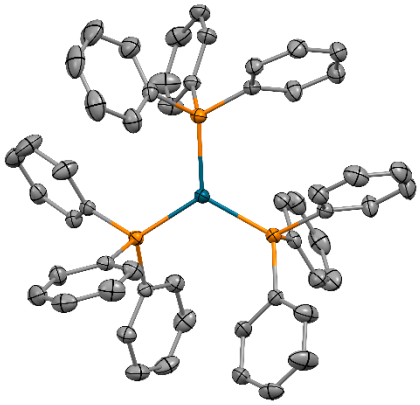

Figure 3.8: Solid state structure of $Pd(PPh_3)_3$ isolated from reaction outlined in Scheme 3.4

As definitive structural confirmation through single crystal X-ray diffraction (SC-XRD) could not be obtained for **3.4** using $Pd(PPh_3)_4$ due to purification challenges, an analogous complex bearing tri(*o*-tolyl)phosphine was instead targeted. $Pd[P(o\text{-tol})_3]_2$ was selected as an alternative Pd(0) pre-cursor due to its commercial availability and high reactivity towards oxidative addition. Reaction of $Pd[P(o\text{-tol})_3]_2$ with CMF **2.2o** afforded oxidative addition complex **3.5** in an isolated yield of 52% (Scheme 3.5). The complex showed a diagnostic ^{19}F NMR resonance at -255 ppm (broad singlet) and a ^{31}P NMR resonance at 29 ppm (broad singlet).

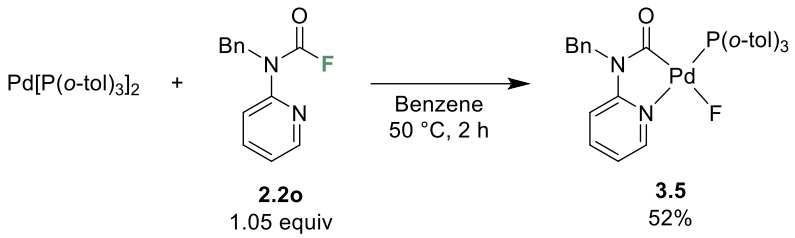

Scheme 3.5: Reaction scheme for the synthesis of complex **3.5**.

Single crystals suitable for X-ray diffraction of **3.5** were obtained by slow evaporation of a saturated benzene/ether mixture (Figure 3.9). The solid-state structure confirmed oxidative addition at palladium and revealed coordination of the 2-pyridyl group to the metal center, forming the anticipated five-membered palladacycle. With only one phosphine ligand bound, the complex adopts a slightly distorted square-planar, four-coordinate geometry. This provides structural evidence that the pyridyl substituent is capable of functioning as an effective directing group and supports the mechanistic rationale proposed for the catalytic reaction.

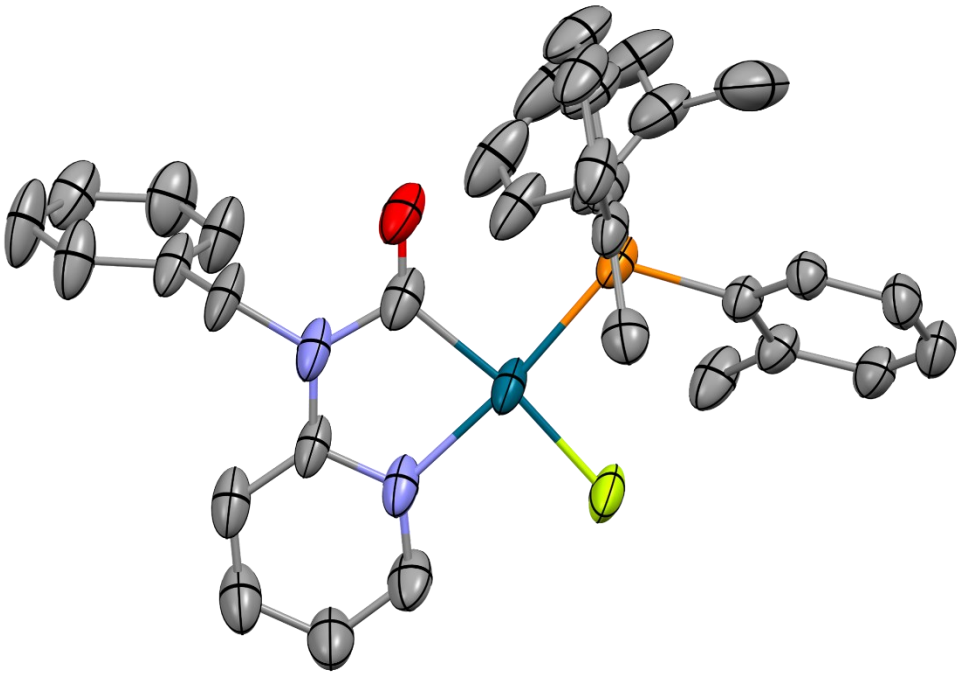

Figure 3.9: Solid-state structure of complex **3.5**. Hydrogen atoms have been omitted for clarity. ORTEP drawn at 50% probability.

With complex **3.5** in hand, we wanted to evaluate whether this complex could be used as a catalyst for the Suzuki cross-coupling in the presence of 10% P(*o*-tol)$_3$. These conditions resulted in the formation of **3.3a** in 5% yield along with amine in 92% yield (Scheme 3.6 **A**). In parallel, Pd[P(*o*-tol)$_3$]$_2$ was evaluated under identical conditions and was found to be catalytically inactive (Scheme 3.6 **B**) (reaction performed by Maryam Jabbarpoor). This inactivity accounts for the poor performance of **3.5** in the catalytic reaction and suggests that the bulky phosphine ligand inhibits productive catalysis.

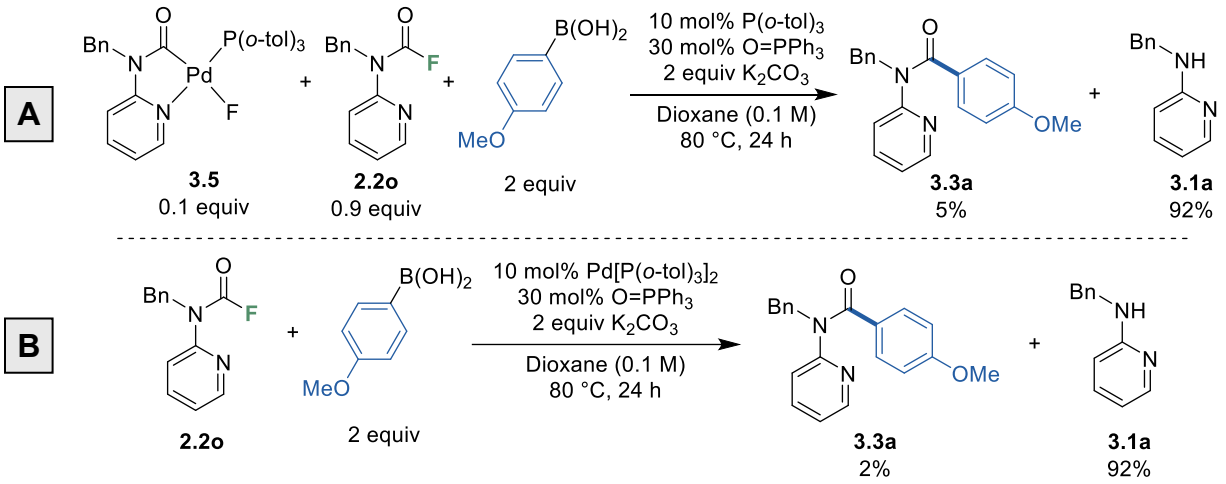

Scheme 3.6: (**A**) Catalytic reaction conditions used to evaluate complex **3.5** as a potential on-cycle catalytic intermediate. (**B**) Catalytic reaction conditions evaluating Pd[P(*o*-tol)$_3$]$_2$ as a pre-catalyst. (**B**) Reaction performed by Maryam Jabbarpoor.

Given the inactivity of the bulky phosphine system, attention returned to the original PPh$_3$ based framework to obtain **3.4** in an isolable form. PdMe$_2$(PPh$_3$)$_2$ was selected as the precursor due to its ability to readily undergo reductive elimination of ethane, generating a highly reactive 14-electron Pd(PPh$_3$)$_2$ species in situ. The precursor was synthesized by refluxing PdCl$_2$ in MeCN to generate (MeCN)$_2$PdCl$_2$ in situ, followed by addition of tetramethylethylenediamine (TMEDA) to afford complex **3.6** in 97% yield (Scheme 3.7). Subsequent methylation was performed with MeLi, by transmetalation providing complex **3.7** in 43% yield. Ligand exchange with PPh$_3$ in benzene resulted in the precipitation of complex **3.8** as a white solid in 94% yield.

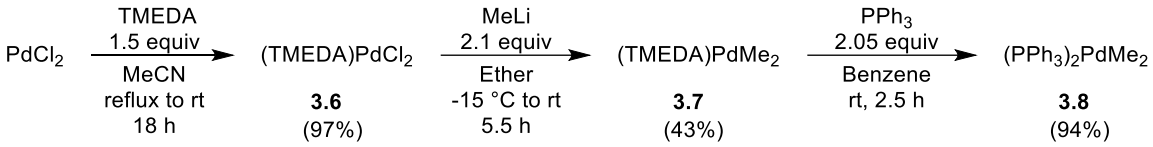

Scheme 3.7: Reaction scheme for the synthesis of complex **3.8**.

Reaction of **3.8** with CMF **2.2o** at room temperature produced a diagnostic ^{19}F NMR resonance at -255 ppm, consistent with the formation of oxidative addition complex **3.4**. However, attempted purification of this mixture yielded crystals of $Pd(PPh_3)_3$ and an unexpected complex, $PdF_2(PPh_3)_2$—the structure of which was verified by single crystal X-ray analysis (**3.9**) (Scheme 3.8). The formation of $Pd(PPh_3)_3$ suggests that **3.8** can act as a phosphine scavenger, sequestering excess PPh_3 generated during the reaction. Accordingly, subsequent reactions employed two equivalents of **3.8**.

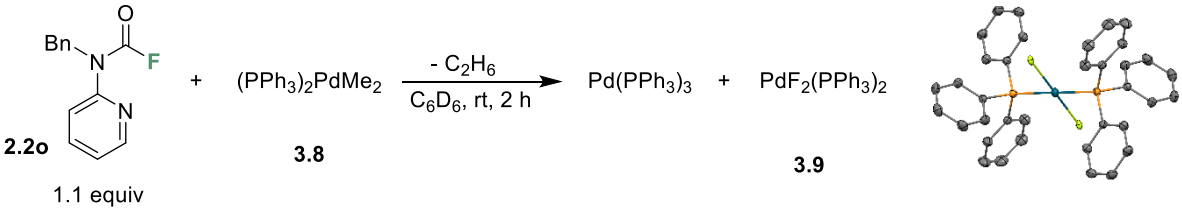

Scheme 3.8: Synthetic conditions for the attempted synthesis of complex **3.4**. Hydrogen atoms have been omitted for clarity. ORTEP drawn at 50% probability.

Intrigued by the formation of **3.9**, the fate of the organic CMF fragment was investigated, since C–F bond activation had clearly occurred. During attempted purification by column chromatography under air, clear colorless crystals were obtained upon standing overnight. Shockingly, these were identified as an oxidative addition complex; however, instead of a metal fluoride, the complex was found to be the analogous metal chloride (**3.10**), with residual EtOAc also observed in the unit cell (Figure 3.10).

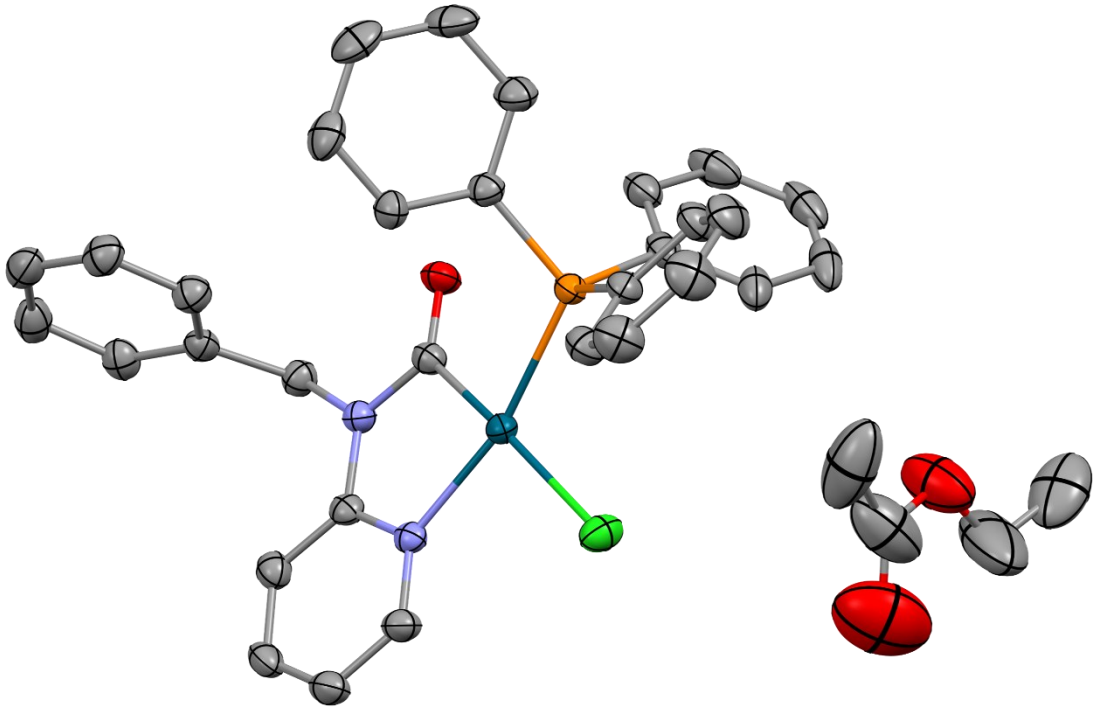

Figure 3.10: Solid state structure of complex **3.10**. Hydrogen atoms have been omitted for clarity. ORTEP drawn at 50% probability.

To identify the origin of chloride, earlier synthetic intermediates were re-examined. ^{1}H NMR analysis of **3.7** ((TMEDA)$PdCl_2$) revealed incomplete methylation had occurred, as the expected integration of the two methyl groups of the Pd complex at -0.13 ppm was reduced to 5.56. This indicated that residual Pd–Cl species were carried through the synthetic sequence, which explains the origin of the chloride ion in complex **3.10** (Figure 3.11).

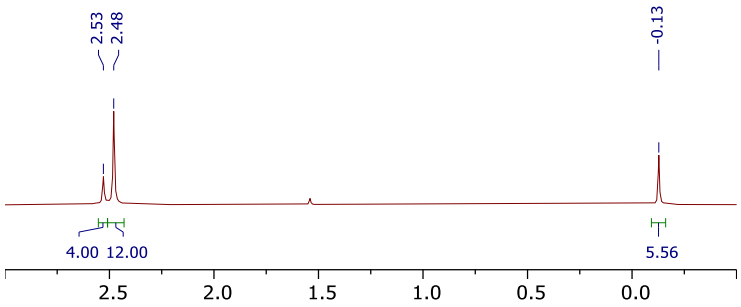

Figure 3.11: ^{1}H NMR spectra of **3.7** showing incomplete methylation of precursor **3.6**.

To salvage some amount of **3.8**, recrystallization was attempted. Crystals obtained were found to be the monomethylated complex **3.11** (Figure 3.12). Further supporting the conclusion that incomplete methylation of **3.6** was responsible for chloride incorporation.

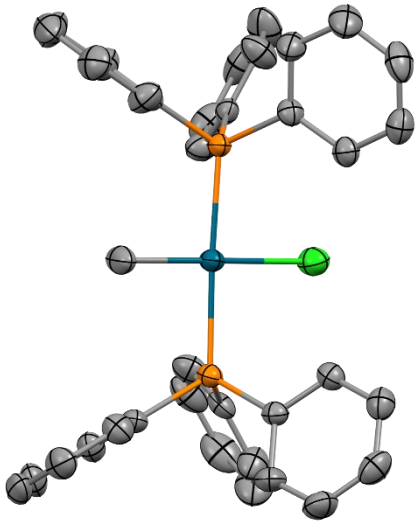

Figure 3.12: Solid-state structure of complex **3.11**. Hydrogen atoms have been omitted for clarity. ORTEP drawn at 50% probability.

The methylation of **3.6** was then repeated using four equivalents of MeLi, ensuring complete conversion to **3.7**, which was obtained in 86% yield. Subsequent ligand exchange with PPh_3 afforded **3.8** in 96% yield (Scheme 3.9).

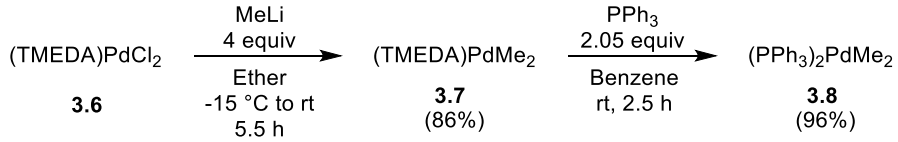

Scheme 3.9: Modified reaction scheme for the synthesis of precursor complex **3.8**.

Oxidative addition complex **3.4** was then prepared from two equivalents of pure **3.8** and CMF **2.2o**, with one equivalent serving of **3.8** serving as a sacrificial phosphine scavenger. Gas evolution was observed during the reaction, consistent with ethane formation. This procedure afforded **3.4** in 61% yield with moderate purity (Scheme 3.10). Single crystals obtained from a

saturated toluene solution confirmed the formation of the expected five-membered palladacycle with coordination of the pyridyl group to palladium. The complex adopts a slightly distorted square-planar geometry with a single PPh_3 ligand (Figure 3.13).

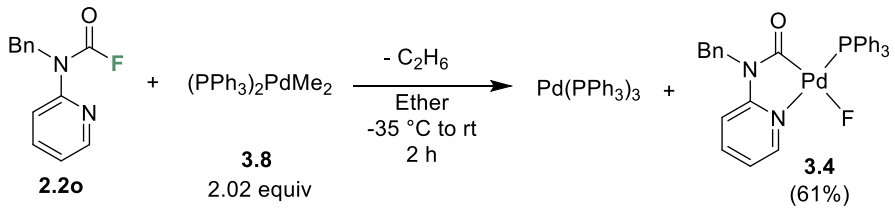

Scheme 3.10: Reaction scheme for the successful synthesis of **3.4**.

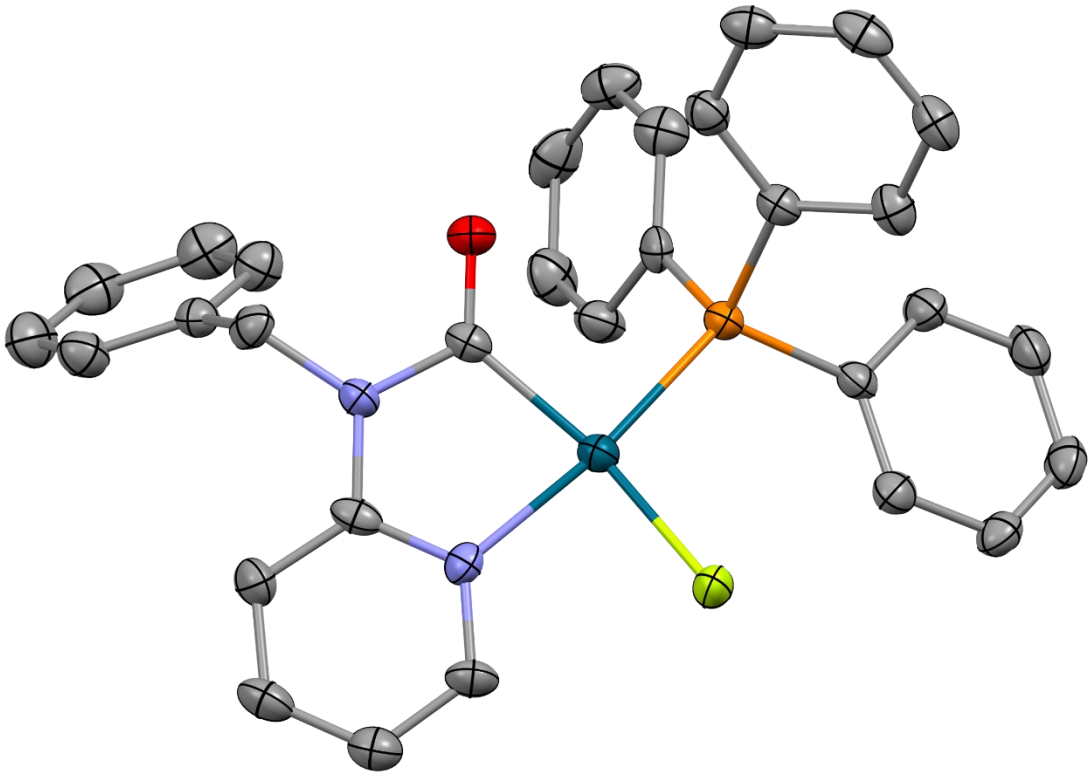

Figure 3.13: Solid state structure of complex **3.4**. Hydrogen atoms have been omitted for clarity. ORTEP drawn at 50% probability.

Although we were able to validate the structure of **3.4**, the product remained contaminated with inseparable $Pd(PPh_3)_n$ species, which would be problematic when assessing the stoichiometric or catalytic reactivity of this complex in the cross-coupling. Thus, an alternative

strategy was developed based on the previously isolated chloride complex **3.10**. Because the analogous CMCl oxidative addition complex could be easily accessed and purified by column chromatography to remove $Pd(PPh_3)_n$ impurities. It was hypothesized that its isolation and chromatographic purification would provide a viable route to the corresponding Pd–F complex through subsequent halide exchange. Complex **3.10** was prepared by reacting CMCl **3.2b** with $Pd(PPh_3)_4$ in toluene at 80 °C for 24 hours. Upon cooling, the product precipitated from solution and was isolated by vacuum filtration, followed by washing with cold toluene and ether, to afford the pure product in 86% yield (Scheme 3.11).

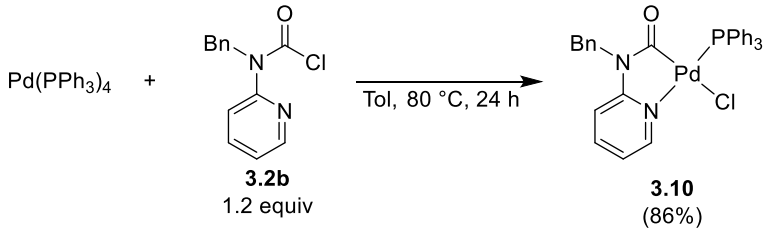

Scheme 3.11: Reaction conditions for the synthesis of complex **3.10**.

Halide exchange was then investigated using AgF and CsF; however, neither metal fluoride successfully generated **3.4**. An analogous Pd–I complex (**3.12**) was also prepared via a Finkelstein-type exchange, but fluoride incorporation by halide exchange with AgF remained unsuccessful (Scheme 3.12).

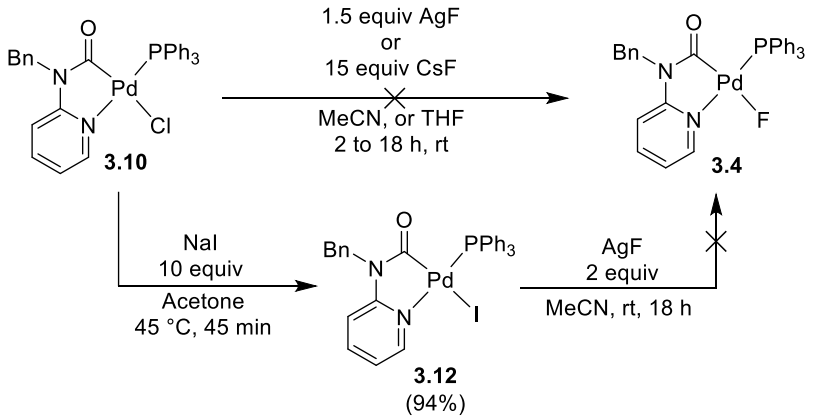

Scheme 3.12: Attempted synthetic methods for preparing **3.4** from **3.10** via halide exchange.

To overcome this barrier, more forcing conditions were employed via in situ generation of a cationic palladium triflate complex. Treatment of complex **3.10** with TMS-OTf in DCM for 1 hour generated the cationic intermediate, after which excess CsF was added to initially to quench residual TMS-OTf. Removal of volatiles eliminated the TMS-containing byproducts, and then THF was added to solubilize the remaining CsF, enabling the smooth and clean formation of **3.4**. The product was then isolated in 88% yield as a white solid (Scheme 3.13).

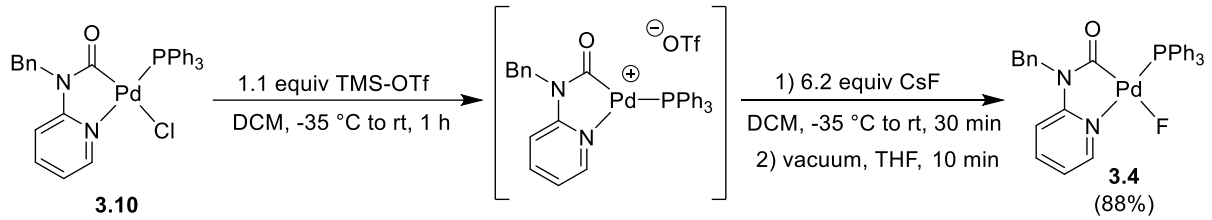

Scheme 3.13: Synthetic conditions used to prepare complex **3.4**.

With complex **3.4** in hand, its catalytic competence was evaluated. When employed as a catalyst at a loading of 10 mol%, amide **3.3a** was formed in a 54% yield, supporting its role as a viable intermediate in the catalytic cycle (Scheme 3.14 **A**). The stoichiometric reactivity of **3.4** was then evaluated in the presence of four equivalents of boronic acid. Under these conditions, **3.3a** was formed in a comparable 56% yield, indicating that both transmetalation and reductive elimination from **3.4** are feasible steps within the catalytic cycle (Scheme 3.14 **B**) (Reactions described in Scheme 3.14 were performed by Maryam Jabbarpoor). Collectively, these results support a Pd(0)/Pd(II) redox cycle for the Suzuki-type cross-coupling reaction (Scheme 3.3).

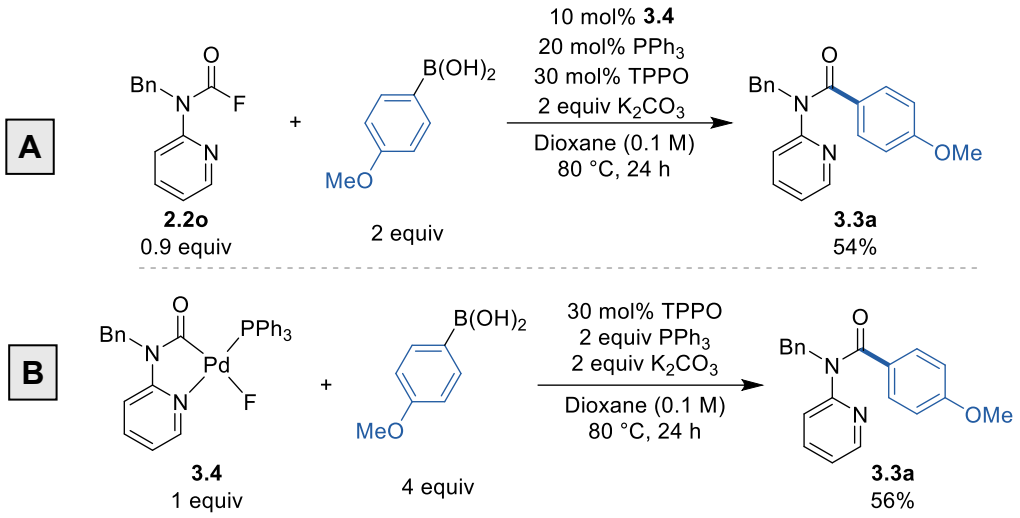

Scheme 3.14: (**A**) Stoichiometric reaction conditions used to evaluate complex **3.4** as a potential on-cycle catalytic intermediate. (**B**) Catalytic reaction conditions used to evaluate complex **3.4** as a potential on-cycle catalytic intermediate. Both reactions were performed by Maryam Jabbarpoor.

3.5. Conclusion and Future Work

In conclusion, an efficient Suzuki cross-coupling of CMFs enabled by a 2-pyridyl directing group was developed. Mechanistic studies demonstrated the importance of the 2-pyridyl moiety and established its key role in facilitating catalysis. Additionally, the role of TPPO as an additive was investigated and found to be multifaceted, increasing the concentration of boronic acid in solution while simultaneously reducing the concentration of water, thereby minimizing substrate hydrolysis. Overall, a broad range of 2-pyridyl amides were accessed from commercially available boronic acids, providing a complementary route to these medicinally important scaffolds.

Since this work represents the first example of an intermolecular Suzuki cross-coupling of CMFs, significant opportunities remain for further development. Future efforts could focus on enabling the cross-coupling of CMFs that lack a directing group, expanding the method to use earth-abundant nickel catalysts in place of palladium, and exploring alkyl nucleophiles to further diversify the range of accessible amide products. These objectives form the basis of the investigation described in Chapter 4.

3.6. References

(1) Devi, E. S.; Alanthadka, A.; Tamilselvi, A.; Nagarajan, S.; Sridharan, V.; Maheswari, C. U. Metal-Free Oxidative Amidation of Aldehydes with Aminopyridines Employing Aqueous Hydrogen Peroxide. *Org. Biomol. Chem.* **2016**, *14* (35), 8228–8231. https://doi.org/10.1039/C6OB01454B.

(2) Abramovitch, R. A.; Singer, G. M. Direct Acylamination of Pyridine 1-Oxides. *J. Org. Chem.* **1974**, *39* (13), 1795–1802. https://doi.org/10.1021/jo00927a001.

(3) Kathiravan, S.; Ghosh, S.; Hogarth, G.; A. Nicholls, I. Copper Catalysed Amidation of Aryl Halides through Chelation Assistance. *Chem. Commun.* **2015**, *51* (23), 4834–4837. https://doi.org/10.1039/C4CC09940K.

(4) Więckowska, A.; Fransson, R.; Odell, L. R.; Larhed, M. Microwave-Assisted Synthesis of Weinreb and MAP Aryl Amides via Pd-Catalyzed Heck Aminocarbonylation Using Mo(CO)6 or W(CO)6. *J. Org. Chem.* **2011**, *76* (3), 978–981. https://doi.org/10.1021/jo102151u.

(5) Shrestha, M.; Wu, X.; Huang, W.; Qu, J.; Chen, Y. Recent Advances in Transition Metal-Catalyzed Reactions of Carbamoyl Chlorides. *Org. Chem. Front.* **2021**, *8* (14), 4024–4045. https://doi.org/10.1039/D0QO01648A.

(6) Brown, D. G.; Boström, J. Analysis of Past and Present Synthetic Methodologies on Medicinal Chemistry: Where Have All the New Reactions Gone? *J. Med. Chem.* **2016**, *59* (10), 4443–4458. https://doi.org/10.1021/acs.jmedchem.5b01409.

(7) McKnight, E. A.; Arora, R.; Pradhan, E.; Fujisato, Y. H.; Ajayi, A. J.; Lautens, M.; Zeng, T.; Le, C. M. BF3-Catalyzed Intramolecular Fluorocarbamoylation of Alkynes via Halide Recycling. ChemRxiv April 19, 2023. https://doi.org/10.26434/chemrxiv-2022-464nx-v2.

(8) Li, Y.; Zhang, F.-P.; Wang, R.-H.; Qi, S.-L.; Luan, Y.-X.; Ye, M. Carbamoyl Fluoride-Enabled Enantioselective Ni-Catalyzed Carbocarbamoylation of Unactivated Alkenes. *J. Am. Chem. Soc.* **2020**, *142* (47), 19844–19849. https://doi.org/10.1021/jacs.0c09949.

(9) Yasui, Y.; Tsuchida, S.; Miyabe, H.; Takemoto, Y. One-Pot Amidation of Olefins through Pd-Catalyzed Coupling of Alkylboranes and Carbamoyl Chlorides. *J. Org. Chem.* **2007**, *72* (15), 5898–5900. https://doi.org/10.1021/jo070724u.

(10) Le, C. M.; Sperger, T.; Fu, R.; Hou, X.; Lim, Y. H.; Schoenebeck, F.; Lautens, M. Stereoselective Synthesis of Methylene Oxindoles via Palladium(II)-Catalyzed Intramolecular Cross-Coupling of Carbamoyl Chlorides. *J. Am. Chem. Soc.* **2016**, *138* (43), 14441–14448. https://doi.org/10.1021/jacs.6b08925.

(11) Sperger, T.; Le, C. M.; Lautens, M.; Schoenebeck, F. Mechanistic Insights on the Pd-Catalyzed Addition of C–X Bonds across Alkynes – a Combined Experimental and Computational Study. *Chem. Sci.* **2017**, *8* (4), 2914–2922. https://doi.org/10.1039/C6SC05001H.

(12) Le, C. M.; Hou, X.; Sperger, T.; Schoenebeck, F.; Lautens, M. An Exclusively Trans-Selective Chlorocarbamoylation of Alkynes Enabled by a Palladium/Phosphaadamantane Catalyst. *Angew. Chem. Int. Ed.* **2015**, *54* (52), 15897–15900. https://doi.org/10.1002/anie.201507883.

(13) Acosta-Guzmán, P.; Ojeda-Porras, A.; Gamba-Sánchez, D. Contemporary Approaches for Amide Bond Formation. *Adv. Synth. Catal.* **2023**, *365* (24), 4359–4391. https://doi.org/10.1002/adsc.202301018.

(14) Imaizumi, T.; Otsubo, S.; Komai, M.; Takada, H.; Maemoto, M.; Kobayashi, A.; Otsubo, N. The Design, Synthesis and Evaluation of 2-Aminobenzoxazole Analogues as Potent and

Orally Efficacious ChemR23 Inhibitors. *Bioorg. Med. Chem.* **2020**, *28* (17), 115622. https://doi.org/10.1016/j.bmc.2020.115622.
(15) Duan, Y.-Z.; Deng, M.-Z. Palladium-Catalyzed Cross-Coupling Reaction of Arylboronic Acids with Chloroformate or Carbamoyl Chloride. *Synlett* **2005**, *2005* (02), 355–357. https://doi.org/10.1055/s-2004-837211.
(16) Nielsen, C. D.-T.; Zivkovic, F. G.; Schoenebeck, F. Synthesis of N-CF3 Alkynamides and Derivatives Enabled by Ni-Catalyzed Alkynylation of N-CF3 Carbamoyl Fluorides. *J. Am. Chem. Soc.* **2021**, *143* (33), 13029–13033. https://doi.org/10.1021/jacs.1c07780.
(17) He, F.; Hou, L.; Wu, X.; Ding, H.; Qu, J.; Chen, Y. Enantioselective Synthesis of α-Alkenylated γ-Lactam Enabled by Ni-Catalyzed 1,4-Arylcarbamoylation of 1,3-Dienes. *CCS Chem.* **2022**, *5* (2), 341–349. https://doi.org/10.31635/ccschem.022.202202010.
(18) Sambiagio, C.; Schönbauer, D.; Blieck, R.; Dao-Huy, T.; Pototschnig, G.; Schaaf, P.; Wiesinger, T.; Zia, M. F.; Wencel-Delord, J.; Besset, T.; Maes, B. U. W.; Schnürch, M. A Comprehensive Overview of Directing Groups Applied in Metal-Catalysed C–H Functionalisation Chemistry. *Chem. Soc. Rev.* **2018**, *47* (17), 6603–6743. https://doi.org/10.1039/C8CS00201K.
(19) Ahrens, T.; Kohlmann, J.; Ahrens, M.; Braun, T. Functionalization of Fluorinated Molecules by Transition-Metal-Mediated C–F Bond Activation To Access Fluorinated Building Blocks. *Chem. Rev.* **2015**, *115* (2), 931–972. https://doi.org/10.1021/cr500257c.
(20) Das, A.; Chatani, N. The Directing Group: A Tool for Efficient and Selective C–F Bond Activation. *ACS Catal.* **2021**, *11* (21), 12915–12930. https://doi.org/10.1021/acscatal.1c03896.
(21) Yu, D.; Lu, L.; Shen, Q. Palladium-Catalyzed Coupling of Polyfluorinated Arenes with Heteroarenes via C–F/C–H Activation. *Org. Lett.* **2013**, *15* (4), 940–943. https://doi.org/10.1021/ol303567t.
(22) Suggs, J. W. Isolation of a Stable Acylrhodium(III) Hydride Intermediate Formed during Aldehyde Decarbonylation. Hydroacylation. *J. Am. Chem. Soc.* **1978**, *100* (2), 640–641. https://doi.org/10.1021/ja00470a054.
(23) Grushin, V. V. Mixed Phosphine−Phosphine Oxide Ligands. *Chem. Rev.* **2004**, *104* (3), 1629–1662. https://doi.org/10.1021/cr030026j.
(24) Grushin, V. V. Synthesis of Hemilabile Phosphine−Phosphine Oxide Ligands via the Highly Selective Pd-Catalyzed Mono-Oxidation of Bidentate Phosphines: Scope, Limitations, and Mechanism. *Organometallics* **2001**, *20* (18), 3950–3961. https://doi.org/10.1021/om010454k.
(25) Yang, S.; Deng, M.; Daley, R. A.; Darù, A.; Wolf, W. J.; George, D. T.; Ma, S.; Werley, B. K.; Samolova, E.; Bailey, J. B.; Gembicky, M.; Marshall, J.; Wisniewski, S. R.; Blackmond, D. G.; Engle, K. M. Palladium Bisphosphine Monoxide Complexes: Synthesis, Scope, Mechanism, and Catalytic Relevance. *J. Am. Chem. Soc.* **2025**, *147* (1), 409–425. https://doi.org/10.1021/jacs.4c10718.
(26) Marshall, W. J.; Grushin, V. V. Palladium(II) and Palladium(0) Complexes of BINAP(O) (2-(Diphenylphosphino)-2‘-(Diphenylphosphinyl)-1,1‘-Binaphthyl). *Organometallics* **2003**, *22* (3), 555–562. https://doi.org/10.1021/om020838q.
(27) Gowrisankar, S.; Neumann, H.; Gördes, D.; Thurow, K.; Jiao, H.; Beller, M. A Convenient and Selective Palladium-Catalyzed Aerobic Oxidation of Alcohols. *Chem. – Eur. J.* **2013**, *19* (47), 15979–15984. https://doi.org/10.1002/chem.201302526.

(28) Denmark, S. E.; Smith, R. C.; Tymonko, S. A. Phosphine Oxides as Stabilizing Ligands for the Palladium-Catalyzed Cross-Coupling of Potassium Aryldimethylsilanolates. *Tetrahedron* **2007**, *63* (26), 5730–5738. https://doi.org/10.1016/j.tet.2007.02.017.
(29) Altan, O. A Rare Example of the in Situ Formation of Palladium Nanoparticles: The Emergence of Catalytically Active Palladium Nanoparticles from Pd (II) Phosphine Complexes in the Suzuki–Miyaura Coupling Reaction. *Appl. Organomet. Chem.* **2022**, *36* (6), e6690. https://doi.org/10.1002/aoc.6690.
(30) Molnár, Á. Efficient, Selective, and Recyclable Palladium Catalysts in Carbon−Carbon Coupling Reactions. *Chem. Rev.* **2011**, *111* (3), 2251–2320. https://doi.org/10.1021/cr100355b.
(31) Chagunda, I. C.; Fisher, T.; Schierling, M.; McIndoe, J. S. Poisonous Truth about the Mercury Drop Test: The Effect of Elemental Mercury on Pd(0) and Pd(II)ArX Intermediates. *Organometallics* **2023**, *42* (19), 2938–2945. https://doi.org/10.1021/acs.organomet.3c00340.
(32) Lennox, A. J. J.; Lloyd-Jones, G. C. Selection of Boron Reagents for Suzuki–Miyaura Coupling. *Chem. Soc. Rev.* **2014**, *43* (1), 412–443. https://doi.org/10.1039/c3cs60197h.
(33) Tokunaga, Y.; Ueno, H.; Shimomura, Y.; Seo, T. Formation of Boroxine: Its Stability and Thermodynamic Parameters in Solution. *HETEROCYCLES* **2002**. https://doi.org/10.3987/com-02-9464.
(34) Tokunaga, Y. Boroxine Chemistry: From Fundamental Studies to Applications in Supramolecular and Synthetic Organic Chemistry. *HETEROCYCLES* **2013**. https://doi.org/10.3987/rev-13-767.
(35) Li, C.; Sotorrios, L.; Boaler, P. J.; Olikauskas, V.; Amico, M.; García-Domínguez, A.; Leach, A. G.; Lloyd-Jones, G. C. The Boroxine–Boronic Acid Equilibrium. *J. Am. Chem. Soc.* **2025**, *147* (42), 38237–38253. https://doi.org/10.1021/jacs.5c10835.
(36) Roşca, S.; Olaru, M.; Raţ, C. I. (2,4,6-Trimethylphenyl)Boronic Acid–Triphenylphosphine Oxide (1/1). *Acta Crystallogr. Sect. E Struct. Rep. Online* **2012**, *68* (1), o31–o31. https://doi.org/10.1107/S1600536811051609.
(37) Guadalupe Vasquez-Ríos, M.; Campillo-Alvarado, G.; MacGillivray, L. R. Mechanochemical Mediated Coexistence of B←N Coordination and Hydrogen Bonding. *Angew. Chem. Int. Ed.* **2023**, *62* (35), e202308350. https://doi.org/10.1002/anie.202308350.
(38) Georgiou, I.; Kervyn, S.; Rossignon, A.; De Leo, F.; Wouters, J.; Bruylants, G.; Bonifazi, D. Versatile Self-Adapting Boronic Acids for H-Bond Recognition: From Discrete to Polymeric Supramolecules. *J. Am. Chem. Soc.* **2017**, *139* (7), 2710–2727. https://doi.org/10.1021/jacs.6b11362.
(39) Begimova, G.; Tupikina, E. Yu.; Yu, V. K.; Denisov, G. S.; Bodensteiner, M.; Shenderovich, I. G. Effect of Hydrogen Bonding to Water on the 31P Chemical Shift Tensor of Phenyl- and Trialkylphosphine Oxides and α-Amino Phosphonates. *J. Phys. Chem. C* **2016**, *120* (16), 8717–8729. https://doi.org/10.1021/acs.jpcc.6b01140.
(40) Ng, S. W. A Second Monoclinic Modification of Triphenylphosphine Oxide Hemihydrate. *Acta Crystallogr. Sect. E Struct. Rep. Online* **2009**, *65* (6), o1431–o1431. https://doi.org/10.1107/S1600536809019254.
(41) De Graaf, Wim.; Boersma, Jaap.; Smeets, W. J. J.; Spek, A. L.; Van Koten, Gerard. Dimethyl(N,N,N',N'-Tetramethylethanediamine)Palladium(II) and Dimethyl[1,2-Bis(Dimethylphosphino)Ethane]Palladium(II): Syntheses, x-Ray Crystal Structures, and Thermolysis, Oxidative-Addition and Ligand-Exchange Reactions. *Organometallics* **1989**, *8* (12), 2907–2917. https://doi.org/10.1021/om00114a028.

(42) King, R. P.; Buchwald, S. L. Synthesis of (MeCN)2Pd(CF3)OTs, a General Precursor to Palladium(II) Trifluoromethyl Complexes LPd(CF3)X. *Organometallics* **2019**, *38* (19), 3490–3493. https://doi.org/10.1021/acs.organomet.9b00516.

3.7. Chapter 3 Appendix

Commercial reagents were purchased from Acros-Organics, Alfa Aesar, Combi-Blocks, Fisher, SigmaAldrich, STREM, or TCI and used without further purification. Unless otherwise stated, all reactions were carried out under an inert atmosphere of nitrogen or argon using glassware that was oven- (175 °C) or flame-dried, whereas the work-up and isolation of the products were conducted on the benchtop using standard techniques. Solvents and solutions were transferred by a syringe or cannula. Anhydrous THF, toluene, DCM, Pentane, MeCN and Et_2O were obtained from an MBraun MB-SPS 800 solvent drying system under a N_2 atmosphere and stored in a Strauss flask. C_6D_6 and $CDCl_3$ were purchased from Sigma-Aldrich, degassed using three freeze-pump-thaw cycles, vacuum–distilled from CaH_2 for C_6D_6 and $CDCl_3$ and stored under argon or nitrogen. The remaining anhydrous solvents were purchased directly from Milipore-Sigma (sure-seal bottle). Boronic acids were purchased from Combi-Blocks and used directly without further purification. Reactions were monitored by thin layer chromatography (TLC) using SiliaPlate glass-backed silica gel plates (hard layer) with F254 indicator. Visualization was accomplished using 250 nm UV light, followed by immersion in $KMnO_4$ stain. Unless otherwise stated, flash chromatography was performed using SiliaFlash P60 40−63 μm (230−400 mesh) 60 Å irregular silica gel. NMR characterization data were collected at 296 K on a Bruker 700 MHz spectrometer, Bruker DRX 600 MHz spectrometer, Bruker ARX 400 MHz spectrometer, or Bruker ARX 300 MHz spectrometer. For samples in $CDCl_3$, ^1H NMR spectra were internally referenced to the residual solvent signal (7.26 ppm) or TMS (0 ppm) and ^{13}C NMR spectra were internally referenced to the residual solvent signal (77.16 ppm) and are reported as observed. Data for ^1H NMR are reported as follows: chemical shift (δ ppm), multiplicity (s = singlet, d = doublet, t = triplet, q = quartet, m = multiplet, dd = double of doublets, dt = doublet of triplets, b = broad), coupling constant (Hz), and integration. NMR yields were obtained by analysis of the crude reaction mixtures by ^1H NMR spectroscopy using a 10 s relaxation delay and 1,3,5-trimethoxybenzene as the internal standard or by ^{19}F NMR spectroscopy using a 30 s relaxation delay and 2-fluoro-4-nitrotoluene as the internal standard. Solid-state structure .cif files are available upon request.

Complexes synthesized but not reported here (**3.6**, **3.7**, and **3.8**) were characterized and consistent with literature values.[41,42]

Direct Synthesis of Carbamoyl Pd–F, (3.4)

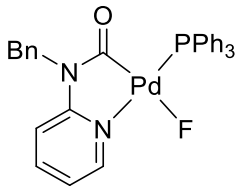

In a N_2-filled glovebox, $PdMe_2(PPh_3)_2$ (0.090 g, 0.137 mmol, 2.03 equiv) was added to a 20 mL vial equipped with a stir bar. A separate 20 mL vial was charged with carbamoyl fluoride **2.2o** (0.009 g, 0.040 mmol, 1.0 equiv) and Et_2O (0.01 M, 5 mL) was added. Both vials were cooled to -35 °C in the glovebox freezer. The solution of carbamoyl fluoride in ether was added to the solid $PdMe_2(PPh_3)_2$ resulting in a white suspension. The mixture was stirred for 3 hours and slowly came to room temperature, with periodic venting every hour to prevent gas build-up. With constant stirring, 10 mL of cold pentane was then added resulting in a brown precipitate. The supernatant was decanted, and the resulting solid was washed with ether until the washes became colourless. The resulting brown solid was then dried under reduced pressure to yield **3.4** as a brown powder (0.025 mg, 0.041 mmol, 61%). The product was crystallized by cooling a saturated toluene solution to yield colourless crystals suitable for XRD analysis. Although this method was suitable to obtain **3.4**, we found that purification of the residual $Pd(PPh_3)_n$ species from the reaction mixture was challenging and the yields were not reproducible. Hence, we opted for a two-step approach starting from carbamoyl chloride **3.10** (see method below).

Synthesis of Carbamoyl Pd–F Complex via Cl-to-F Exchange, Carbamoyl Pd–Cl, (3.10)

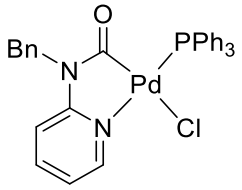

In a N_2-filled glovebox, $Pd(PPh_3)_4$ (0.762 g, 0.659 mmol, 1 equiv), carbamoyl chloride **3.2b** (0.195 g, 0.792 mmol, 1.2 equiv) and toluene (0.05 M, 12 mL) were added to a 50 mL round bottom flask equipped with a stir bar. The vial was submerged in an 80 °C oil bath and heated for 24 h. The reaction mixture was cooled down to -10 °C, the precipitate was isolated by suction

filtration and washed with cold toluene and ether. Carbamoyl Pd–Cl complex **3.10** was isolated as a white solid (0.347 g, 0.564 mmol, 86%).

Characterization data for **3.10**:

^{1}H NMR (400 MHz, $CDCl_3$): δ 9.33 (dd, 1H), 7.87 – 7.71 (m, 6H), 7.66 (ddd, J = 8.6, 7.3, 1.8 Hz, 1H), 7.49 – 7.33 (m, 9H), 7.32 – 7.21 (m, 3H), 7.14 – 7.07 (m, 2H), 6.95 (ddd, J = 7.1, 5.7, 1.2 Hz, 1H), 6.72 (d, J = 8.4 Hz, 1H), 4.75 (s, 2H). **^{13}C NMR** (101 MHz, $CDCl_3$): δ 176.9, 155.3, 148.6, 140.9, 135.8, 134.8, 134.7, 131.4, 130.9, 130.4, 130.3, 128.6, 128.0, 127.9, 127.3, 126.5, 116.5, 108.3, 44.2. **^{31}P NMR** (162 MHz, $CDCl_3$): δ 37.95 (s, 1P).

HRMS (ESI) m/z: [M–Cl]+ calc'd for [$C_{31}H_{26}N_2OPPd$+] 579.0812 found 579.0824. Note: Ionization of **3.10** for HRMS analysis resulted in fragmentation (via loss of halide) and a very weak parent ion signal.

Synthesis of Carbamoyl Pd–F Complex via Cl-to-F Exchange, Carbamoyl Pd–F, (3.4)

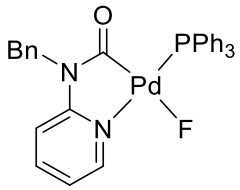

In a N_2-filled glovebox, a 20 mL vial equipped with a stir bar was charged with **3.10** (0.068 g, 0.110 mmol, 1 equiv) and DCM (0.04 M, 3 mL). To separate 1-dram vial, a solution of TMS-OTf (0.027 g, 0.122 mmol, 1.1 equiv) in DCM (0.12 M, 1 mL) was prepared. Both vials were cooled in the glovebox freezer (-35 °C). After 30 minutes, both vials were removed from the glovebox freezer and the solution of TMS-OTf in DCM was added dropwise to the vial containing **3.10** in DCM and stirred for 1 h at room temperature. CsF (0.104 g, 0.680 mmol, 5 equiv) was then added to the reaction mixture as a solid. After stirring for 15 minutes, DCM was removed under reduced pressure, THF (0.11 M, 1 mL) was added, and the solution was mixed for 10 minutes. The reaction was concentrated, washed with toluene, filtered through glass filter paper, and dried under reduced pressure to yield **3.4** as a white solid (0.042 g, 0.070 mmol, 64%).

Characterization data for **3.4** (trans isomer):

^{1}H NMR (700 MHz, $CDCl_3$): δ 8.85 (s, 1H), 7.72 (dd, J = 11.8, 7.4 Hz, 6H), 7.60 (t, J = 7.9 Hz, 1H), 7.42 – 7.38 (m, 3H), 7.37 – 7.32 (m, 6H), 7.23 (t, J = 7.5 Hz, 2H), 7.18 (t, J = 7.4 Hz, 1H), 7.07 (d, J = 7.3 Hz, 2H), 6.90 (t, J = 6.5 Hz, 1H), 6.66 (d, J = 8.5 Hz, 1H), 4.69 (s, 2H). **^{13}C NMR** (176 MHz, $CDCl_3$): δ 175.8 (d, J = 80.96 Hz), 155.1, 146.2 (d, J = 8.8 Hz), 140.9, 136.0, 134.7 (d, J = 12.32 Hz), 130.6 (d, J = 1.76 Hz), 130.3, 128.7, 128.3 (d, J = 10.56 Hz), 127.3, 126.6, 116.2, 108.2, 44.0. **^{19}F NMR** (659 MHz, CDCl3): δ -250.48 (s, 1F). **^{31}P NMR** (121 MHz, $CDCl_3$): δ 32.65 (s, 1P).

HRMS (ESI) m/z: [M–F]+calc'd for [$C_{31}H_{26}N_2OPPd$+] 579.0812 found 579.0822. Note: Ionization of **3.4** for HRMS analysis resulted in fragmentation (via loss of halide) and a very weak parent ion signal.

Synthesis of Carbamoyl Pd–F Complex via Cl-to-I Exchange, Carbamoyl Pd–I, (3.12)

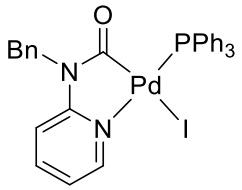

In open atmosphere, a 25 mL RBF equipped with a stir bar was charged with **3.10** (45.0 mg, 0.073 mmol, 1 equiv), NaI (145.4 mg, 0.970 mmol, 13 equiv), and acetone (10 mL). The reaction was heated at 45 °C for 30 minutes, solvent was removed under reduced pressure. The product was extracted with $CHCl_3$ (3 × 2 mL), filtered, and solvent removed to afford **3.12** as an orange solid (48.6 mg, 0.069 mmol, 94%).

Characterization data for **3.12**:

^{1}H NMR (300 MHz, $CDCl_3$): δ 9.85 (ddd, *J* = 5.8, 1.8, 0.7 Hz, 1H), 7.86 – 7.77 (m, 6H), 7.69 (ddd, *J* = 10.2, 6.3, 1.9 Hz, 3H), 7.44 – 7.37 (m, 10H), 7.15 – 7.06 (m, 2H), 6.88 (ddd, *J* = 7.1, 5.8, 1.2 Hz, 1H), 6.75 (dt, *J* = 8.5, 1.0 Hz, 1H), 4.76 (s, 2H). **^{13}C NMR** (75 MHz, $CDCl_3$): δ 44.8, 108.7, 117.4, 126.7, 127.5, 127.8, 128.0, 128.2, 128.8, 130.3, 130.4, 130.5, 132.5, 133.2, 134.9, 135.0, 135.3, 135.8, 141.2, 154.4, 155.6, 175.4. **^{31}P NMR** (121 MHz, $CDCl_3$): δ 40.52.

Chapter 4: Nickel Catalyzed Cross-Coupling of Carbamoyl Fluorides

4.1. Author contributions

The final chapter of this dissertation describes the first nickel-catalyzed intermolecular Suzuki cross-coupling of carbamoyl fluorides with alkylboranes. This work was conducted in collaboration with former undergraduate student Samantha Galea, who identified the initial reaction conditions, synthesized substrates **2.2p** and **2.2x**, and assisted with preliminary reaction optimization. The author's contributions include all other experiments, analyses, and data detailed in this chapter.

4.2. Motivation and Research Plans

At the outset of this project, only two examples of metal-catalyzed intermolecular cross-coupling reactions involving CMFs had been reported: the nickel-catalyzed alkynylation described by Schoenebeck and co-workers in 2021, followed by the palladium-catalyzed Suzuki cross-coupling developed by our group in 2024 (Chapter 3).[1,2] Despite these advances, several important aspects of metal-catalyzed CMF cross-coupling remain unexplored. In particular, no general cross-coupling method for CMFs had been developed, and the use of alkyl nucleophiles remained entirely unexplored. Because the use of CMFs as competent electrophiles remains in its infancy, significant opportunities exist to expand both the fundamental understanding of their reactivity and their broader synthetic applicability.

To address these gaps in the field, we sought to build upon the work described in Chapter 3 by developing the first general Suzuki cross-coupling of CMFs that does not rely on directing groups or electronically activated CMF substrates. In addition, we aimed to establish the use of alkyl nucleophiles in CMF cross-coupling chemistry, thereby substantially broadening the range of molecular scaffolds accessible from these electrophiles. It is anticipated that the successful development of such a method would greatly expand the synthetic utility of CMFs and provide a foundation for further developing diverse metal-catalyzed cross-coupling reactions employing this emerging class of electrophile.

4.3. Introduction

4.3.1. Carbamoyl Fluorides in Metal-Catalyzed Cross-Coupling Reactions

Although Chapter 3 demonstrated that the palladium-catalyzed Suzuki cross-coupling of CMFs could be achieved by incorporating a 2-pyridyl directing group, the requirement for substrates to contain this functionality limited the generality of the method. Coordination of the pyridyl nitrogen facilitates oxidative addition of the C–F bond to palladium, while also suppressing decarbonylation though the formation of a five-membered palladacycle, ultimately enabling the first intermolecular Suzuki cross-coupling of a CMF.[2] Despite this advance, the development of a general cross-coupling method for unactivated CMFs remained an important outstanding challenge to be addressed.

Well into the development of the work described in this chapter, Tlili and co-workers reported a nickel-catalyzed Suzuki cross-coupling of unactivated CMFs with aryl boronic acids. Using a catalyst system comprised of 20 mol% $Ni(COD)_2$ and 40 mol% tri(4-methoxyphenyl)phosphine, various CMFs and aryl boronic acids were coupled in synthetically useful yields ranging from 25-90% (Scheme 4.1). Although a modest range of dialkyl CMFs were successfully coupled, only a single aryl-substituted CMF was examined, affording the desired product in a modest 25% yield. This may suggest that aryl-substituted substrates are a more challenging class of CMFs, highlighting opportunities for further catalyst development. Furthermore, the optimized reaction conditions employed 1.5 equivalents of CMF while the boronic acid was used as the limiting reagent. Given the equilibrium between boronic acids and boroxines discussed in detail in Chapter 3, precise control over the concentration of boronic acid

can be exceedingly challenging. Together, these observations illustrate opportunities to both expand the substrate scope and increase reaction efficiency.

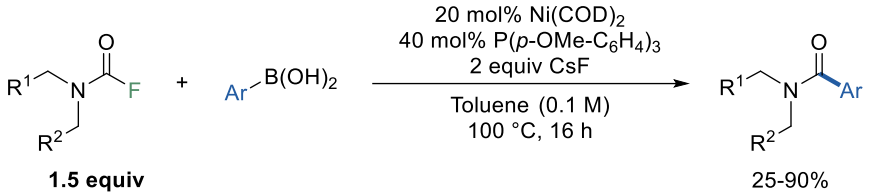

Scheme 4.1: General reaction scheme for the cross-coupling conditions developed by Tlili and co-workers.

Successful implementation of alkyl nucleophiles presents additional challenges compared to aryl systems, including generally slower transmetalation, competitive *β*-hydride elimination, and catalyst decomposition. Following transmetalation, the resulting alkyl-Ni intermediate typically contains accessible *β*-hydrogens and can undergo *β*-hydride elimination to form a nickel hydride and stable alkene. Which can remain coordinated to nickel and, in suitable cases can lead to formation of an η^3-allyl species, further stabilizing the resulting off-cycle species. In contrast, analogous *β*-hydride elimination from an aryl-Ni intermediate would generate a highly strained, high-energy aryne and is therefore generally noncompetitive.

This chapter describes the development of the first nickel-catalyzed Suzuki cross-coupling between unactivated CMFs and alkyl-9-BBN nucleophiles. The broad goal is to develop a general catalytic system that is compatible with a wide range of functionalities through the systematic optimization of reaction conditions. This will be followed by mechanistic investigations aimed at understanding factors governing productive C–F bond activation and cross-coupling under nickel catalysis.

4.4. Results and Discussion

4.4.1. Reaction Discovery

In 2007, Takemoto and co-workers reported the successful palladium-catalyzed Suzuki cross-coupling of CMCls with alkyl-9-BBN coupling partners. In this two-step protocol, alkene substrates underwent hydroboration with H-9BBN to generate the corresponding alkyl-9-BBN coupling partner and the resulting solution was used directly in the cross-coupling reaction using $Pd(PPh_3)_4$ as the catalyst. This method afforded excellent yields ranging from 62-87% across a limited substrate scope consisting of only eight examples (Scheme 4.2).[3]

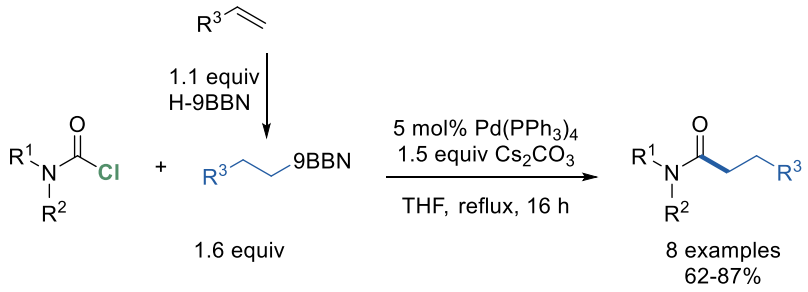

Scheme 4.2: Reaction conditions developed by Takemoto and co-workers.

Inspired by this work, similar reaction conditions were employed in an attempt to couple CMF substrates with alkyl-9-BBN coupling partners. Unfortunately, no cross-coupled product was detected when either *N*-benzyl-*N*-2-pyridyl (**2.2o**) or *N*-benzyl-*N*-phenyl (**2.2a**) CMFs were employed (Scheme 4.3). This outcome cannot be attributed solely to the intrinsic difficulty of C–F oxidative addition, because $Pd(PPh_3)_4$ had also exhibited poor activity in the cross-coupling of 2-pyridyl CMFs with arylboronic acids described in Chapter 3. As a coordinatively saturated Pd(0) complex, $Pd(PPh_3)_4$ must first dissociate one or more phosphine ligands to generate the lower-coordinate species required for oxidative addition. Thus, the absence of product may primarily reflect the limitations of this particular catalyst system rather than a fundamental incompatibility between CMFs and lakyl-9-BBN coupling partners.[4–10]

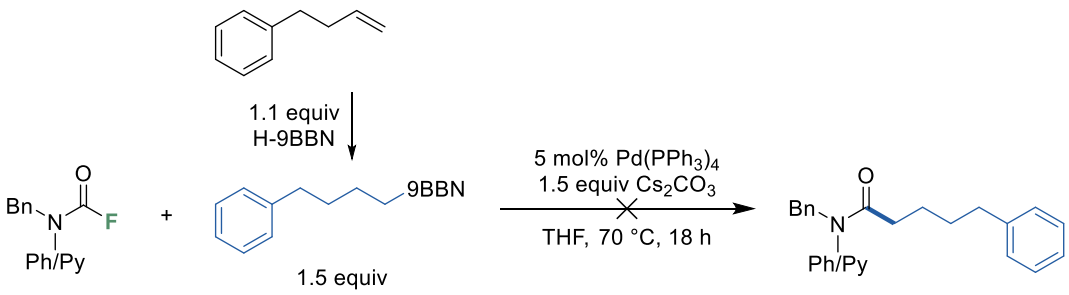

Scheme 4.3: Reaction conditions used in attempted cross-coupling reaction.

To overcome the limitations of the $Pd(PPh_3)_4$ system, nickel was investigated as an alternative metal for catalysis. Low-valent nickel complexes often undergo oxidative addition with lower activation barriers and more favourable thermodynamics than analogous palladium complexes, enabling the activation of comparatively unreactive electrophiles, including strong C–F bonds.[11–14] Accordingly, an initial organometallic approach was taken to assess the viability of oxidative addition of CMFs to electron-rich nickel(0) complexes. Therefore, $[Ni(PCy_3)_2]_2(\mu\text{-}N_2)$ (**4.4**) was first synthesized by reduction of the readily available Ni(II) complex $(PCy_3)_2NiCl_2$ (**4.5**) with excess sodium metal to afford the highly reactive Ni(0) complex **4.4**, which is highly active towards oxidative addition (Scheme 4.4).[15] Initially, 2-pyridyl CMF **2.2o** was selected to allow the directing group to facilitate rapid oxidative addition through formation of a stable five-membered nickellacycle, while simultaneously minimizing the likelihood of decarbonylation as discussed in Chapter 3. Treatment of complex **4.4** with an excess of CMF **2.2o** in pentane at –35 °C resulted in the rapid precipitation of oxidative addition complex **4.6** in an excellent isolated yield of 84% (Scheme 4.4).

Single crystals suitable for SC-XRD were obtained by cooling a saturated diethyl ether solution of **4.6** to –35 °C. The solid-state structure clearly confirmed oxidative addition of the CMF to nickel, affording a slightly distorted square planar complex bearing a single phosphine ligand, analogous to palladium complex **3.4** described in Chapter 3 (Figure 4.1). NMR analysis of complex

4.6 revealed a sharp doublet at –304 ppm in the ^{19}F $\{^1H\}$ NMR spectrum with a $^2J_{FP}$ value of 34 Hz, together with a corresponding sharp doublet at 40.9 ppm in the ^{31}P $\{^1H\}$ NMR spectrum possessing the same coupling constant.

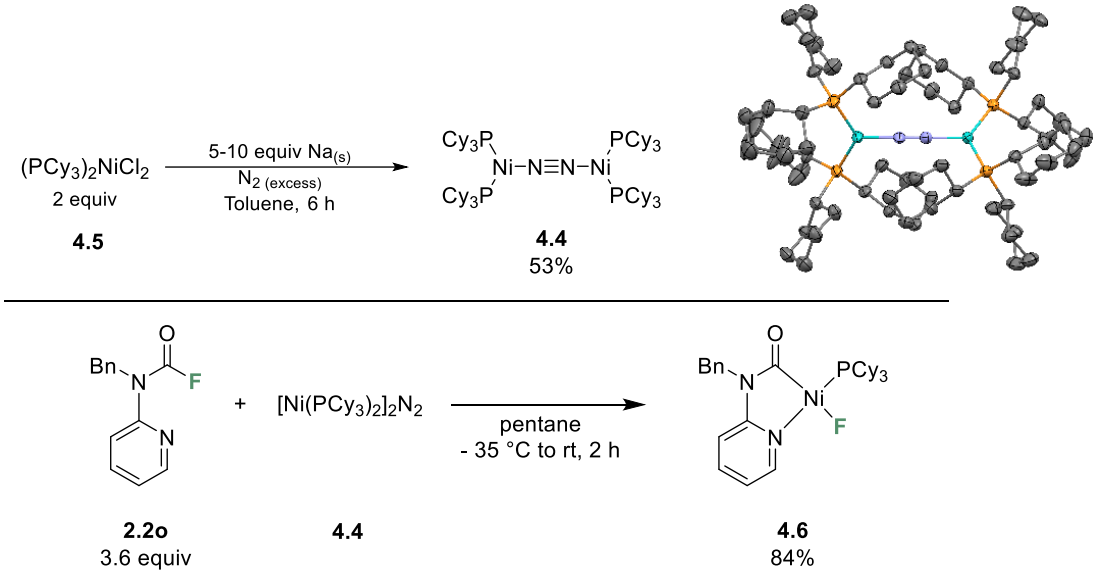

Scheme 4.4: Synthesis of complexes **4.4** and **4.6** (ORTEP drawn at 50% probability, hydrogen atoms have been omitted for clarity)

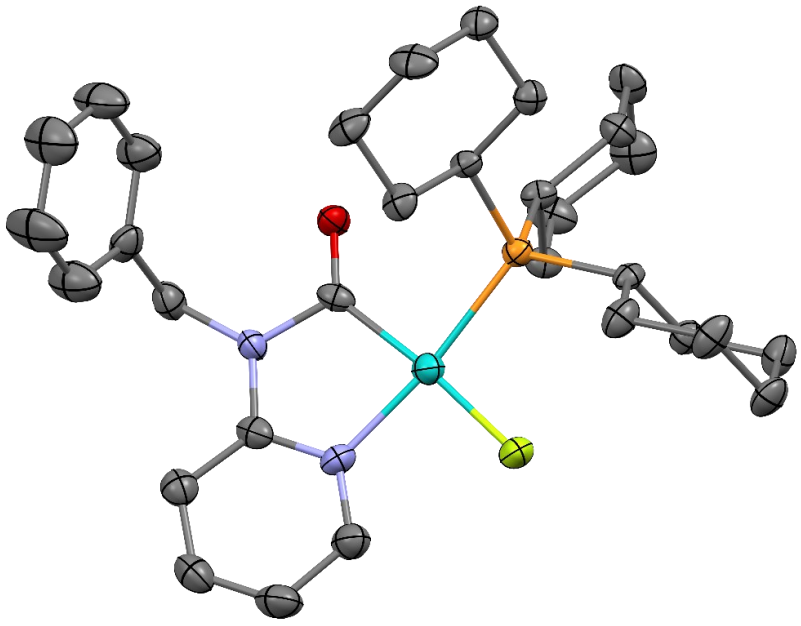

Figure 4.1: Solid state structure of oxidative addition complex **4.6** (ORTEP drawn at 50% probability, hydrogen atoms have been omitted for clarity)

Having established that CMF **2.2o** undergoes oxidative addition to complex **4.4**, the catalytic viability of **4.4** was then evaluated. Complex **4.4** (5 mol%) was premixed with CMF **2.2o** for several minutes prior to addition of phenylboronic acid, and the resulting reaction mixture was heated at 60 °C for 18 hours. These conditions afforded amide **3.3c** in 19% yield (Scheme 4.5), confirming that catalytic turnover was feasible.

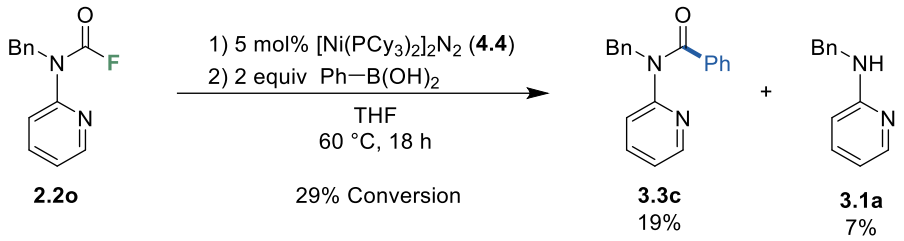

Scheme 4.5: Reaction conditions used in cross-coupling of **2.2o** and phenyl boronic acid.

As one of the principal objectives of this project was to develop conditions capable of coupling CMFs lacking directing groups, analogous studies were next performed using *N*-benzyl-*N*-phenyl CMF **2.2a**. Treatment of complex **4.4** with CMF **2.2a** at –35 °C over one hour afforded oxidative addition complex **4.7** in approximately 90% yield (Scheme 4.6 **A**). However, all attempts to isolate or purify complex **4.7** resulted in decomposition. To establish if oxidative addition of a CMF without a directing group was possible, CMF **2.2x** was treated with complex **4.4** at –35 °C. Immediate gas evolution, color change, and precipitate formation were observed, with the reaction appearing complete within approximately 30 seconds. Oxidative addition complex **4.8** was successfully isolated in 85% yield (Scheme 4.6 **B**). NMR analysis revealed a sharp triplet at –357 ppm in the ^{19}F NMR spectrum with a $^{2}J_{FP}$ value of 41 Hz, together with a corresponding doublet at 16.0 ppm in the ^{31}P NMR spectrum possessing the same coupling constant. The triplet observed in the ^{19}F NMR spectrum suggested the presence of two equivalent phosphine ligands coordinated to nickel. This assignment was subsequently confirmed by SC-XRD, which revealed oxidative

addition into the C–F bond did occur to afford a slightly distorted square planar complex bearing two phosphine ligands *trans* to one another (Figure 4.2).

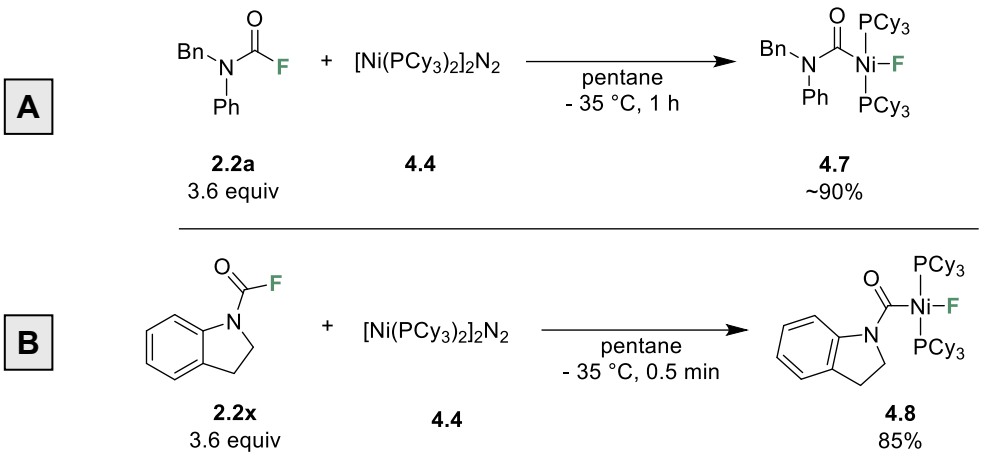

Scheme 4.6: (**A**) Reaction conditions used to synthesize complex **4.7**. (**B**) Reaction conditions used to synthesize complex **4.8**.

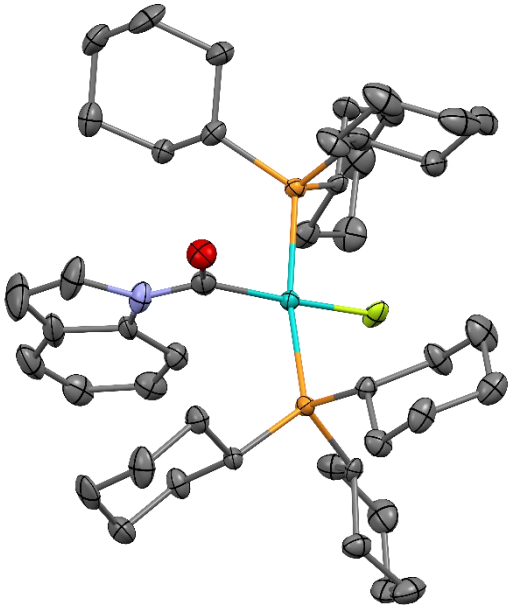

Figure 4.2: Solid state structure of oxidative addition complex **4.8**. ORTEP drawn at 50% probability, hydrogen atoms have been omitted for clarity.

Having confirmed that oxidative addition of an unactivated CMF was feasible, the reactivity of complex **4.7** was next investigated. Treatment of crude complex **4.7** with 2.2 equivalents of 4-methoxyphenylboronic acid at 60 °C for 18 hours afforded amide **4.3a** in 10%

yield, demonstrating that transmetalation and reductive elimination were feasible, even in the absence of base (Scheme 4.7 **A**). Catalytic reactivity was next evaluated under analogous conditions using CMF **2.2a**. Complex **4.4** (5 mol%) was premixed with CMF **2.2a** for several minutes prior to addition of the organoboron coupling partner, and the resulting reaction mixture was heated at 60 °C for 18 hours. Unfortunately, regardless of the organoboron nucleophile employed, no detectable quantity of the desired product was observed (Scheme 4.7 **B**).

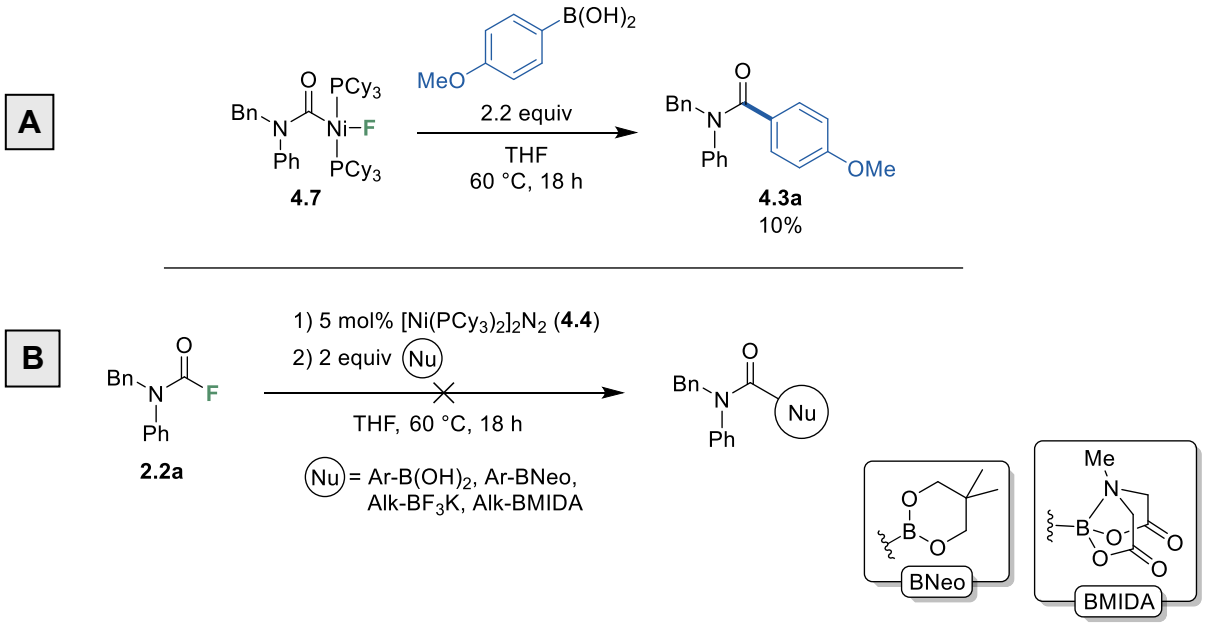

Scheme 4.7: (**A**) Conditions for the stoichiometric reaction of **4.7** with 4-methoxyphenylboronic acid. (**B**) Conditions used in the attempted cross-coupling of CMF **2.2a** and various borane nucleophiles.

These experiments demonstrate that oxidative addition, transmetalation and reductive elimination were all individually feasible. The inability to achieve catalytic turnover therefore suggests that catalyst generation or catalyst stability, rather than fundamental organometallic reactivity, represents the principal limitation of the system. Consequently, attention was shifted toward identifying a more robust Ni(II) pre-catalyst capable of generating the active catalyst under catalytic conditions.

Because the principal objective of this work was to develop cross-coupling conditions employing alkyl nucleophiles, alkyl-9-BBN reagents were selected as coupling partners due to their exceptional nucleophilicity. Initial catalyst screening was first conducted using 2-pyridyl CMF **2.2o** to facilitate reaction discovery, after which the more challenging *N*-benzyl-*N*-phenyl CMF **2.2a** would be re-evaluated under the determined catalytic conditions. Accordingly, several phosphine-ligated $NiCl_2$ pre-catalysts were examined under reaction conditions. It was found that pre-catalysts bearing PPh_3 or dppf as ligands successfully afforded amide **4.3b** in moderate yields of 20% and 49% respectively (Table 4.1, entries 1, 3).

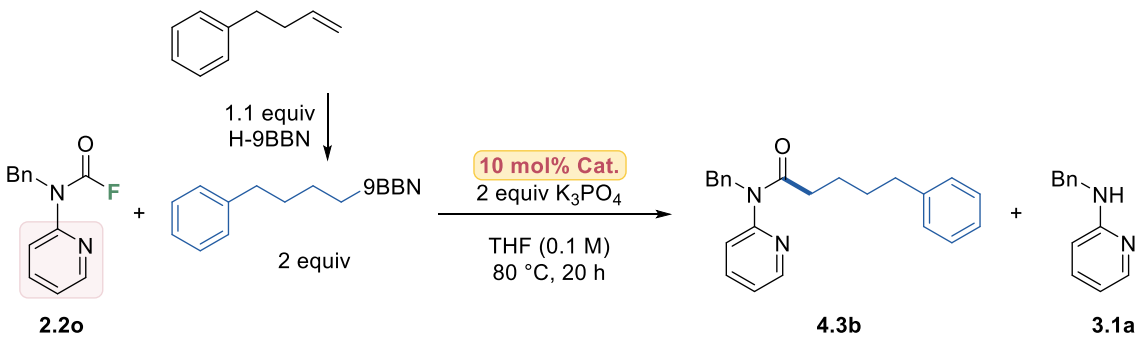

Entry	Pre-catalyst	Conversion	Amide	Amine
1	$(PPh_3)_2Ni^{II}Cl_2$	93%	20%	71%
2	$(PCy_3)_2Ni^{II}Cl_2$	84%	0%	76%
3	$(dppf)Ni^{II}Cl_2$	100%	49%	48%
4	$(dppe)Ni^{II}Cl_2$	95%	0%	89%
5	$(SPhos)Ni^{II}Cl_2$	98%	0%	92%
6	$(DavePhos)Ni^{II}Cl_2$	97%	0%	96%

Table 4.1: Reaction conditions used to evaluate various pre-catalysts for the cross-coupling of CMF **2.2o** with an alkyl-9-BBN coupling partner. Conversions and yields acquired by quantitative ^1H NMR with 1,3,5 trimethoxybenzene as an internal standard.

Having identified two pre-catalysts capable of facilitating the cross-coupling 2-pyridyl CMF **2.2o** with an alkyl-9-BBN coupling partner, the more challenging *N*-benzyl-*N*-phenyl CMF **2.2a** was subsequently re-evaluated under these conditions. Gratifyingly, both systems successfully afford the desired amide **4.3c**, with the dppf-based catalyst proving superior, providing the desired product in 44% yield (Table 4.2, entry 2). Notably, in both cases, secondary amine **2.1a** was formed in significant quantities. Having identified reaction conditions capable of promoting the cross-coupling unactivated CMFs with alkyl-9-BBN reagents, these conditions were adopted as a starting point for the optimization studies described in the following section.

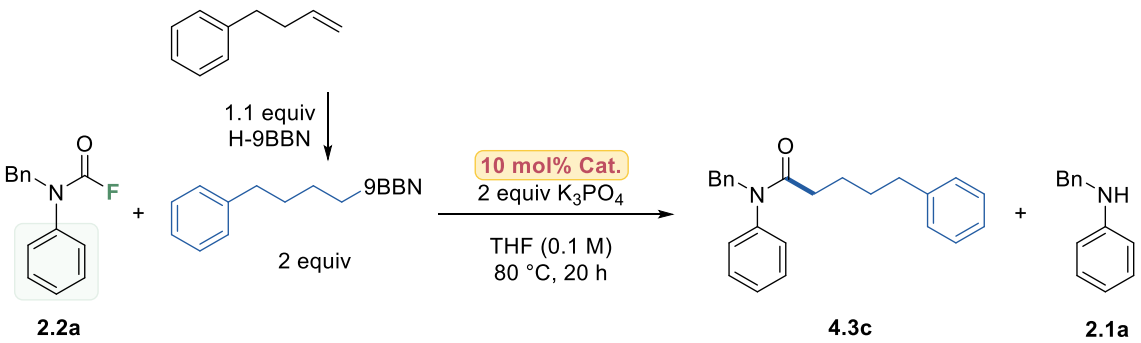

Entry	Pre-catalyst	Conversion	Amide	Amine
1	$(PPh_3)_2Ni^{II}Cl_2$	43%	8%	32%
2	$(dppf)Ni^{II}Cl_2$	87%	44%	39%

Table 4.2: Reaction conditions used to evaluate pre-catalysts for the cross-coupling of CMF **2.2a** with an alkyl-9-BBN coupling partner. Conversions and yields acquired by quantitative ^{1}H NMR with 1,3,5 trimethoxybenzene as an internal standard.

4.4.2. Reaction Optimization

4.4.2.1. Ligand Screen

With initial reaction conditions capable of producing the desired amide in hand and dppf identified as a promising ligand, a broader range of ligands were evaluated to determine if performance could be further improved. Because only a limited number of preligated Ni(II) complexes are commercially available, rapid screening was facilitated by generating the corresponding nickel complex in situ from $(DME)NiCl_2$ and the indicated ligand. Control experiments performed prior to this study established that $(DME)NiCl_2$ combined with 10 mol% dppf afforded the same yields of amide and amine as $(dppf)NiCl_2$. These control experiments were again performed with the optimized conditions and again found to afford the same yields of amide and amine (Table 4.15). Accordingly, $(DME)NiCl_2$ and the indicated mol% of ligand were premixed for 10 minutes and used in place of pre-ligated complexes for simplicity and to facilitate a larger and more rapid ligand screen.

A variety of monodentate phosphine ligands were evaluated at a loading of 20 mol%, ranging from triaryl- to trialkyl-substituted phosphines with varying donor strengths. Most monodentate ligands afforded less than 10% yield of amide and between 44-53% yield of amine, with **L5** providing a marginally improved yield of 14% (Table 4.3, entries 2-7, 9-12). While $P(Oct)_3$ afforded only 5% amide, it also produced 8% of the corresponding formamide. The mechanism by which formamide is generated is later discussed in Section 4.4.5.6. Interestingly, $EtPPh_2$ (**L8**) afforded the desired amide in 28% yield, making it the most efficient non-ferrocene-based ligand system evaluated (Table 4.3, entry 8). However, the increased performance of **L8** cannot be attributed solely to steric effects as the analogous $MePPh_2$ (**L10**) produced only 7% amide under otherwise identical conditions (Table 4.3, entry 10). Presently, it is unclear why **L8**

provides notably higher yields than the other monodentate phosphines examined. All other non-ferrocene-based ligands evaluated resulted in amide yields below 5%, with the consumed CMF being converted almost exclusively into amine (Table 4.3, entries 13-31).

Given that dppf (**L32**) was the only ligand to afford the desired amide in greater than 30% yield, we hypothesized that ferrocene-based ligands may provide a uniquely favourable coordination environment around nickel that promotes the desired reactivity. To investigate this possibility, several readily available ferrocene-based ligands were evaluated. Analogues of dppf bearing isopropyl (**L33**), cyclohexyl (**L34**), or *tert*-butyl (**L35**) substituents on phosphorus were found to provide little to no amide, with **L33** giving the highest yield of 14% (Table 4.3, entries 32-35). To determine whether the phosphorus donor atoms must reside on opposing cyclopentadienyl rings of the ferrocene scaffold, JosiPhos ligand (**L37**) was examined and produced no detectable amide (Table 4.3, entry 37). These results suggest that the structural features unique to dppf play a crucial role in enabling the desired reactivity with CMFs.

To further probe this hypothesis, an electron-poor dppf derivative bearing *p*-CF_3-C_6H_4 substituents on both phosphorus atoms (**L36**) was synthesized. Evaluation of this ligand afforded a 54% yield of amide, nearly twice that of any non-ferrocenyl ligand (Table 4.3, entry 36). This indicated that dppf-type ligands bearing aryl substituents on phosphorus represent a privileged ligand class for promoting the desired cross-coupling reaction. Accordingly, dppf was selected as the optimal ligand in all subsequent reactions, either in combination with (DME)$NiCl_2$ as the pre-catalyst or using the pre-ligated complex (dppf)$NiCl_2$ directly.

Finally, In the control experiment, where no ligand was employed, 53% of CMF **2.2a** was consumed and converted exclusively into amine **2.1a**, likely via base-promoted hydrolysis in the absence of a competent catalyst (Table 4.3, entry 1).

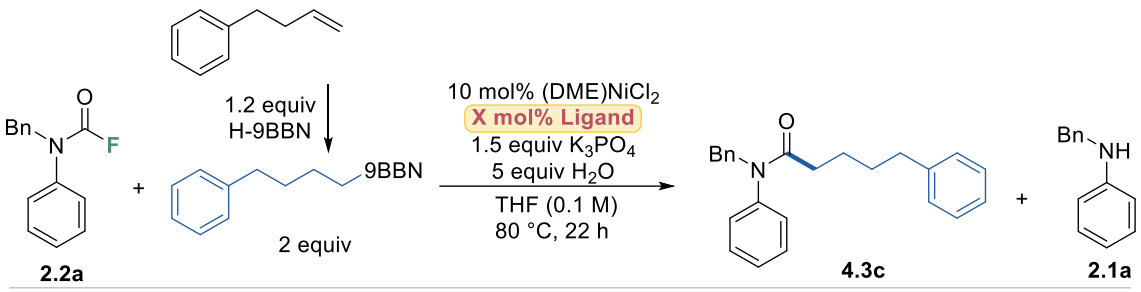

Entry	Ligand Class	Ligand		mol % Ligand	Conversion	Amide	Amine
1	Control	None		0	53%	0%	53%
2	Monodentate Phosphine	PPh_3	(L2)	20%	55%	9%	44%
3		PCy_3	(L3)	20%	63%	6%	53%
4		P(*o*-tol)$_3$	(L4)	20%	50%	1%	45%
5		P(*p*-F-Ph)$_3$	(L5)	20%	54%	14%	38%
6		P(*p*-OMe-Ph)$_3$	(L6)	20%	52%	3%	47%
7		P(*o*-OMe-Ph)$_3$	(L7)	20%	50%	0%	50%
8		$EtPPh_2$	(L8)	20%	66%	28%	36%
9		^{n}BuP(Ad)$_2$	(L9)	20%	60%	8%	49%
10		$MePPh_2$	(L10)	20%	62%	7%	52%
11		P(Oct)$_3$	(L11)	20%	59%	5%	45%
12		(F_5-Ph)PPh_2	(L12)	20%	54%	0%	52%
13	NHC	IPr	(L13)	10%	54%	0%	54%
14		IMes	(L14)	10%	47%	0%	47%
15	Buchwald-Type	SPhos	(L15)	10%	51%	2%	48%
16		RuPhos	(L16)	10%	51%	3%	48%
17		PhDave Phos	(L17)	10%	53%	0%	51%
18	N-N Bidentate	bpy	(L18)	10%	53%	0%	51%
19		dtbpy	(L19)	10%	68%	0%	51%
20		phen	(L20)	10%	50%	0%	50%
21	P-N Bidentate	PyPhos	(L21)	10%	57%	4%	53%
22		TrippyPhos	(L22)	10%	57%	0%	57%
23		(*o*-NMe_2Ph)PPh_2	(L23)	10%	51%	0%	50%
24		PPh_2Py	(L24)	10%	48%	0%	46%
25	P-P Bidentate	dppe	(L25)	10%	48%	0%	48%
26		dppb	(L26)	10%	43%	2%	41%
27		dppbz	(L27)	10%	42%	0%	42%
28		DPEPhos	(L28)	10%	49%	4%	43%
29		DCEPhos	(L29)	10%	25%	3%	21%
30		Xantphos	(L30)	10%	45%	3%	42%
31		*rac*-BINAP	(L31)	10%	49%	5%	42%
32	Ferrocene Based P-P Bidentate	dppf	(L32)	10%	82%	69%	11%
33		dipf	(L33)	10%	47%	14%	32%
34		dcpf	(L34)	10%	44%	2%	42%
35		dtbpf	(L35)	10%	49%	0%	44%
36		*p*-CF_3-dppf	(L36)	10%	88%	54%	31%
37		JosiPhos	(L37)	10%	66%	0%	46%

Table 4.3: Ligand screen, conversions and yields acquired by quantitative ^{1}H NMR with 1,3,5 trimethoxybenzene as an internal standard.

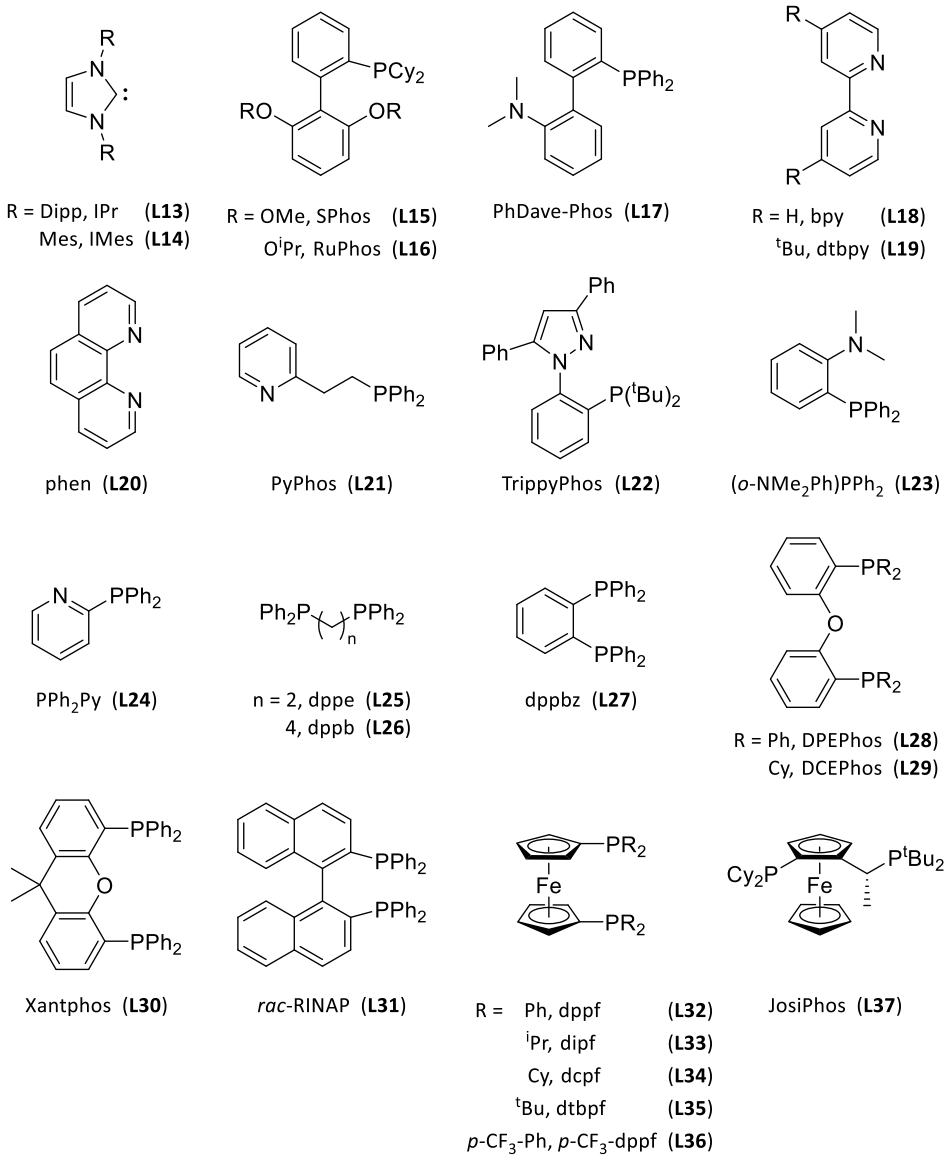

Figure 4.3: List of ligands with abbreviations and ligand codes used in **Table 4.3:** Ligand screen, conversions and yields acquired by quantitative ^{1}H NMR with 1,3,5

4.4.2.2. Alkene to H-9BBN Ratio Screen

During the initial reaction development, it became apparent that the presence of excess H-9BBN was beneficial for the formation of the desired amide product. In the standard procedure, alkyl-9-BBN reagents were prepared via hydroboration using H-9BBN in slight excess and the resulting solution was used directly without purification. As one equivalent of H-9BBN is

consumed during the hydroboration, varying the amount employed in this step provided a convenient means of controlling the amount of residual H-9BBN present in the resulting stock solution. Because the presence of residual H-9BBN was found to have a significant influence on the reaction performance, optimization studies were conducted to determine the ideal excess amount.

To establish a baseline, the hydroboration was first performed using 0.9 equivalents of H-9BBN, ensuring no residual H-9BBN remained upon completion of the hydroboration step. Under these conditions, incomplete conversion of **2.2a** was observed, affording amide **4.3c** in only 20% yield (Table 4.4, entry 1). Increasing the amount of H-9BBN to 1.0 equivalent resulted in a substantial improvement, with conversion increasing to 94% and the yield of **4.3c** rising to 41% (Table 4.4, entry 2).

Further increasing the amount of H-9BBN resulted in continued improvement, with the maximum yields being obtained when 1.2-1.4 equivalents were used during the hydroboration step (Table 4.4, entries 4-6). However, increasing the loading beyond 1.4 equivalents led to diminished yields (Table 4.4, entry 7). As identical yields were obtained using 1.2 to 1.4 equivalents of H-9BBN, we opted to use 1.2 equivalents for all subsequent reactions, as it provided optimal reaction performance while simplifying the reaction workup by forming less byproducts. These results indicate that while residual H-9BBN is not strictly required for reactivity, its presence is highly beneficial and leads to significantly improved reaction efficiency. The specific role of H-9BBN is further described in detail throughout Section 4.4.5.

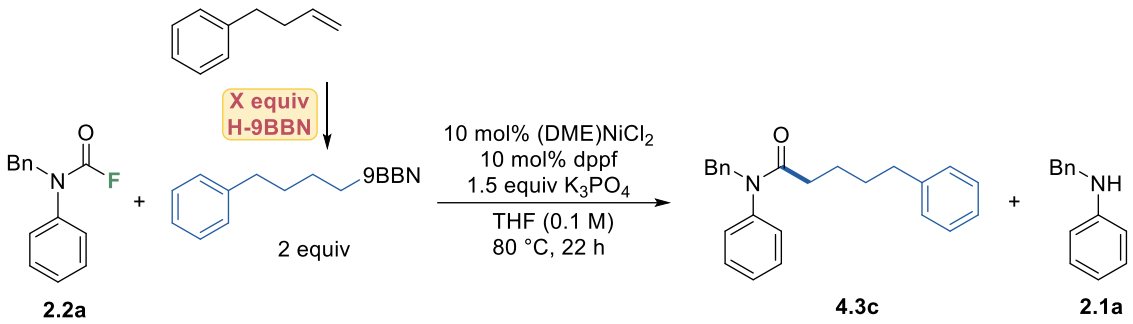

	Ratio Alkene : H-9BBN				
Entry	Alkene	H-9BBN	Conversion	Amide	Amine
1	1	0.9	77%	20%	58%
2	1	1.0	94%	41%	48%
3	1	1.1	99%	51%	43%
4	1	1.2	100%	64%	33%
5	1	1.3	100%	64%	33%
6	1	1.4	100%	63%	32%
7	1	1.5	93%	54%	34%

Table 4.4: Optimization of alkene and H-9BBN ratio for the Ni-catalyzed cross-coupling reaction. Conversions and yields acquired by ^{1}H NMR spectroscopy using 1,3,5 trimethoxybenzene as an internal standard.

4.4.2.3. Base and Water Cross-Screen

During the initial stages of the reaction development, substantial and unanticipated reproducibility issues were encountered. As discussed in Chapter 1 Section 1.3 nickel-catalyzed Suzuki cross-coupling reactions can be exceptionally sensitive to the relative quantities of water and base present. Following a thorough investigation, a correlation was observed between the ambient laboratory humidity and the corresponding reaction yields. In some cases, yields varied from 50-70% when reactions were conducted on different days. Because inorganic bases are hydroscopic and readily absorb moisture from the atmosphere, it was hypothesized that variable amounts of water introduced by the base were responsible for these observed inconsistencies.

To determine whether ambient humidity was indeed the source of the reproducibility issues, accurately weighed quantities of base were prepared on the same day and transferred into a nitrogen-filled glovebox at the same time. This was to ensure that each sample was prepared

under identical handling conditions. Once inside the glovebox, the vials were sealed with Teflon-lined caps and stored at –35 °C until used, thereby maintaining a consistent water content across all samples. When these pre-prepared vials were used under the reaction conditions outlined in Scheme 4.8, reaction yields became highly reproducible, varying by only ±1% across eight replicate experiments performed on different days (Table 4.5). Although these precautions were excessive from a practical standpoint, they provided strong evidence that variable water content introduced through the base was the primary source of the observed reproducibility issues. Such effects are generally more pronounced at smaller reaction scales, where minor variation in water and/or base content represent larger differences relative to the quantities of the other reaction components.

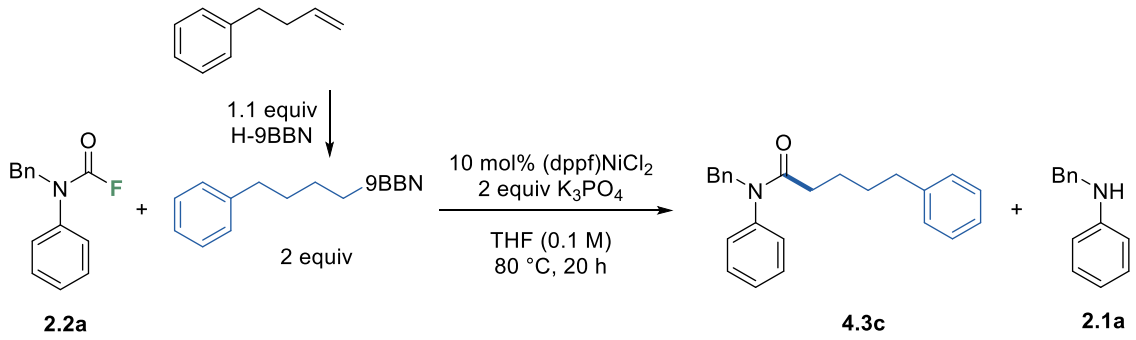

Scheme 4.8: Reaction conditions used for replicate runs in Table 4.5**:** Yields for replicate runs using reaction conditions outlined in Scheme 4.8**:** Reaction conditions

Replicate	Conversion	Amide	Amine
1	98%	62%	32%
2	98%	62%	31%
3	98%	63%	33%
4	97%	63%	32%
5	98%	62%	32%
6	97%	62%	32%
7	98%	62%	31%
8	97%	62%	33%
Average	98%	62%	32%

Table 4.5: Yields for replicate runs using reaction conditions outlined in Scheme 4.8**:** Reaction conditions used for replicate runs in Table 4.5.

Because inorganic bases can absorb atmospheric moisture and can exist as mixtures of hydrated species, both the water content and effective molecular weight of the base can vary over time. This can result in inconsistent quantities of both base and water being introduced to the reaction. To eliminate this source of variability, all inorganic bases used herein were thoroughly dried under dynamic vacuum (<10 mTorr) at 180-240 °C for a minimum of four days to ensure complete removal of residual water. Following drying, the bases were stored in a nitrogen-filled glovebox, and all reactions were similarly prepared in a nitrogen-filled glovebox to maintain the anhydrous reaction conditions.

As the reaction requires water to be productive (discussed in Chapter 1, Section 1.3), all subsequent reactions herein were conducted using carefully controlled amounts of water. To ensure accurate and reproducible addition a 5.0 M stock solution of degassed H_2O in THF was prepared and used to transfer the indicated equivalents of water to each reaction vessel within the glovebox.

Because reaction performance was highly sensitive to the base and water content, these variables could not be considered independently. In addition to its direct involvement in the reaction, water influences the extent that inorganic bases can dissolve, with different bases exhibiting different degrees of solubility. This interdependence motivated a cross-optimization of the base and water content to identify the optimal combination (Table 4.6). The optimal base loading was found to be 1.5 equivalents. In general, increasing the amount of base beyond this amount resulted in decreased yields, likely due to promotion of competing hydrolysis. Conversely, reducing the amount of base below 1.5 equivalents also led to diminished yields, indicating that a minimum threshold of base is required for efficient catalysis.

Evaluation of the water content revealed a similar trend. In general, reactions containing insufficient water provided lower yields, with the optimum amount determined to be 5 equivalents. Slightly increasing the water loading beyond this point had only a modest effect, with a slight decrease in yield and conversion when 7 equivalents were used. These results indicate that the reaction tolerates a slight excess of water better than insufficient water, and that reaction performance is particularly dependent on maintaining an appropriate base loading. With the greater degree of hydrolysis observed at higher base loadings likely a result from a corresponding increase in the concentration of hydroxide in solution, which promoted hydrolysis of the CMF substrate. Ultimately, the optimal combination was found to be 1.5 equivalents of base and 5 equivalents of water (Table 4.6).

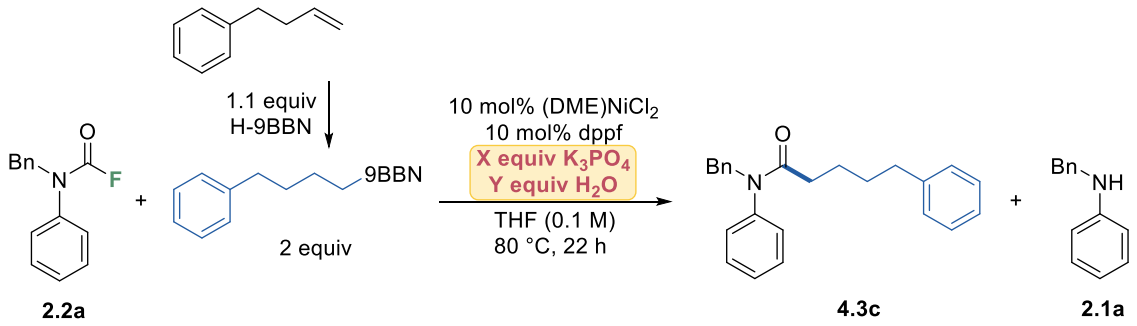

Equiv K_3PO_4	Amide / Amine	Equiv H_2O = 1	3	5	7
1.0	Amide	42%	55%	59%	67%
	Amine	35%	32%	11%	17%
1.5	Amide	36%	58%	72%	71%
	Amine	55%	39%	26%	21%
2.0	Amide	29%	41%	55%	57%
	Amine	68%	57%	43%	38%
2.5	Amide	20%	35%	37%	45%
	Amine	79%	62%	62%	52%
3.0	Amide	13%	21%	24%	31%
	Amine	86%	78%	74%	67%

Table 4.6: Base and water cross-optimization. Conversions and yields acquired by ^{1}H NMR spectroscopy with 1,3,5 trimethoxybenzene as an internal standard.

4.4.2.4. Base-Solvent Cross-Screen

Given that the solubility and effective concentration of an inorganic base can vary with both solvent and counter cation choice, a second cross-optimization was conducted to identify the optimal base-solvent combination. The previously optimized loadings of 1.5 equivalents of base and 5 equivalents if water were maintained throughout the screen. Three commonly used solvents in Suzuki cross-couplings were selected for evaluation: THF and 1,4-dioxane, which are polar aprotic solvents capable of coordinating to transition metals, and toluene, a non-polar solvent. A wide variety of bases were subsequently evaluated, with inorganic bases selected to also encompass a range of count cations (Table 4.7, Table 4.8).

Four carbonate bases were evaluated across the three solvents. With the exception of Tl_2CO_3, each carbonate was reasonably effective, although pronounced solvent dependencies were observed. Na_2CO_3 performed best in 1,4-dioxane, K_2CO_3 in THF, and Cs_2CO_3 in toluene. Although Cs_2CO_3 provided complete conversion in every solvent, it afforded considerably more amine in ethereal solvents (Table 4.7, entries 7 and 8). Among the carbonate conditions evaluated, K_2CO_3 in THF provided the best overall results, affording amide **4.3c** in 88% yield (Table 4.7, entry 4). Tl_2CO_3 was evaluated because Tl(I) bases have been reported to promote challenging Suzuki cross-coupling reactions, likely by sequestering halide ions as insoluble TlX salts and thereby facilitating transmetalation.[77-79] However, Tl_2CO_3 was consistently ineffective across all solvents.

Among the phosphate bases, Li_3PO_4 was ineffective in all three solvents, consistent with its limited solubility under the reaction conditions (Table 4.7, entries 13-15). Na_3PO_4 was generally effective across all three solvents, providing consistent high conversions and amide yield with minimal amine formation. In contrast, K_3PO_4 exhibited a strong solvent dependence, performing

comparably to Na_3PO_4 in ethereal solvents but poorly in toluene. With THF providing the highest amide yield for both Na_3PO_4 and K_3PO_4 (Table 4.7, entries 16-21).

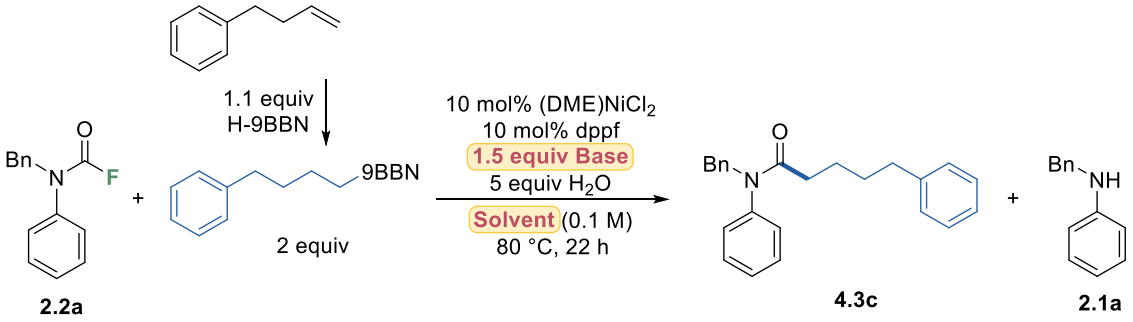

Entry	Base	Solvent	Conversion	Amide	Amine
1	Na_2CO_3	THF	58%	52%	5%
2		Dioxane	85%	76%	6%
3		Toluene	53%	45%	6%
4	K_2CO_3	THF	100%	88%	9%
5		Dioxane	85%	53%	29%
6		Toluene	50%	38%	12%
7	Cs_2CO_3	THF	100%	59%	39%
8		Dioxane	100%	52%	40%
9		Toluene	100%	80%	16%
10	Tl_2CO_3	THF	16%	6%	10%
11		Dioxane	30%	21%	10%
12		Toluene	20%	12%	8%
13	Li_3PO_4	THF	1%	0%	0%
14		Dioxane	4%	0%	0%
15		Toluene	0%	0%	0%
16	Na_3PO_4	THF	90%	80%	7%
17		Dioxane	82%	71%	6%
18		Toluene	78%	67%	9%
19	K_3PO_4	THF	91%	78%	10%
20		Dioxane	85%	67%	12%
21		Toluene	31%	19%	12%

Table 4.7: Carbonate and phosphate bases evaluated in THF, 1,4-dioxane, and toluene in the base-solvent cross-optimization. Conversions and yields acquired by ^{1}H NMR with 1,3,5 trimethoxybenzene as an internal standard.

Various fluoride and miscellaneous bases were subsequently evaluated (Table 4.8). KF exhibited a strong solvent dependence, providing a moderate yield in THF but performed poorly in 1,4-dioxane and toluene. CsF was more broadly effective across all solvents, likely owing to greater solubility in organic solvents; CsF in THF provided the best fluoride-based conditions, affording amide **4.3c** in 78% yield. Nevertheless, conversion never exceeded 85% with any

fluoride-solvent combination. Tetra-n-butylammonium fluoride (TBAF) was ineffective in THF, affording no detectable amide, and was therefore not evaluated in the other solvents (Table 4.8, entries 1-7).

The remaining bases were generally ineffective or poorly selective. 2,6-lutidine provided essentially no conversion in any solvent, whereas potassium *tert*-butoxide (KO^tBu) gave high conversion in ethereal solvents but produced substantial amounts of amine, suggesting that CMF hydrolysis strongly competes with productive coupling. Both conversion and yield were lower when KO^tBu was employed in toluene. Finally, no conversion was observed in the absence of base in any of the three solvents, confirming that base is required for productive catalysis (Table 4.8, entries 10-18). Collectively, these results demonstrate that neither the base nor the solvent could be optimized independently; rather, reaction performance depended on the specific base-solvent combination, with K_2CO_3 in THF providing the optimal combination

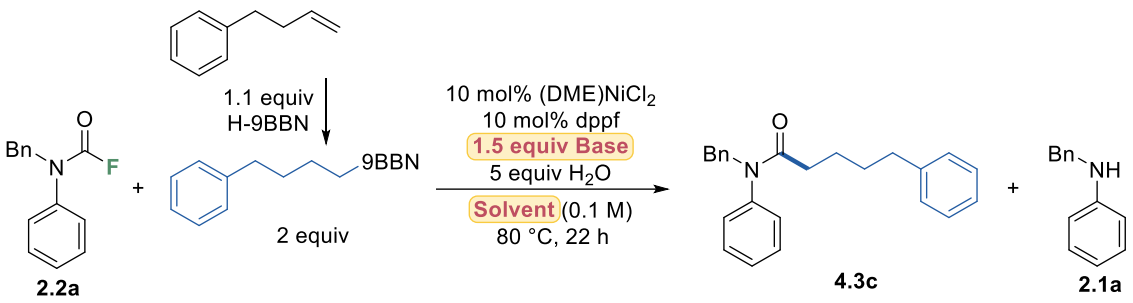

Entry	Base	Solvent	Conversion	Amide	Amine
1	KF	THF	78%	68%	8%
2		Dioxane	20%	12%	6%
3		Toluene	11%	7%	4%
4	CsF	THF	85%	78%	6%
5		Dioxane	85%	57%	25%
6		Toluene	77%	67%	14%
7	TBAF	THF	11%	0%	8%
8		Dioxane			
9		Toluene			
10	2,6-lutidine	THF	0%	0%	0%
11		Dioxane	6%	0%	0%
12		Toluene	1%	0%	0%
13	KO^{t}Bu	THF	100%	48%	40%
14		Dioxane	89%	35%	46%
15		Toluene	49%	28%	22%
16	None	THF	0%	0%	0%
17		Dioxane	0%	0%	0%
18		Toluene	0%	0%	0%

Table 4.8: Fluoride and miscellaneous bases evaluated in THF, 1,4-dioxane, and toluene in the base-solvent cross-optimization. Conversions and yields acquired by ^{1}H NMR with 1,3,5 trimethoxybenzene as an internal standard.

4.4.2.5. Borane Nucleophile Screen

To determine whether the developed system was general for different classes of organoboron nucleophiles, a variety of boron coupling partners were evaluated. The nucleophiles examined included potassium organotrifluoroborates (BF_3K), boronic acids, boronic acid pinacol esters (BPin), boronic acid neopentylglycol esters (BNeo), aryl boroxines, and an alkyl 9-borabicyclo[3.3.1]nonane (9-BBN). Under the optimized conditions, all boron nucleophiles other than alkyl-9-BBN resulted exclusively in formation of the corresponding amine, with no detectable cross-coupled product (Table 4.9, entries 1-8). In contrast, the alkyl-9-BBN coupling partner afforded the desired amide in an excellent 88% yield (Table 4.9, entry 9). These results suggest that, under the developed reaction conditions, productive reactivity is unique to 9-BBN containing coupling partners.

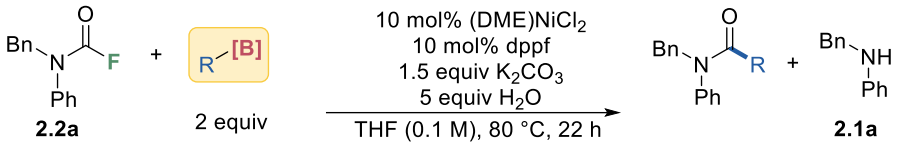

Entry	Borane	Conversion	Amide	Amine
1	BF_3K	3%	0%	3%
2	BF_3K	2%	0%	2%
3	$B(OH)_2$	23%	0%	23%
4	$B(OH)_2$	34%	0%	34%
5	BPin	9%	0%	8%
6	BPin	35%	0%	35%
7	BNeo	24%	0%	24%
8	$B(O)_3$	26%	0%	26%
9	9BBN	100%	88%	9%

Table 4.9: Borane nucleophile screening. Conversions and yields acquired by ^{1}H NMR spectroscopy using 1,3,5 trimethoxybenzene as an internal standard.

4.4.2.6. Concentration and Catalyst Loading Screen

The influence of catalyst loading and reaction concentration on the reaction efficiency was next investigated. Catalyst loadings were evaluated first, with both 10 mol% and 20 mol% loadings providing identical reaction outcomes, affording the desired amide in 89% yield (Table 4.10, entries 1 and 2). Reducing the catalyst loading to 5 mol% led to a substantial decrease in both conversion and product yield, furnishing only 56% yield of the desired amide while increasing amine formation to 24% (Table 4.10, entry 3).

To determine whether the reduced catalyst loading could be compensated for by increasing reaction concentration, the reaction was subsequently evaluated at concentrations of 0.2 M and 0.4 M while maintaining a catalyst loading of 5 mol%. Increasing the concentration provided only modest improvements in yield, increasing product formation to 68% and 67% respectively. However, significant quantities of amine (25-28%) were still produced under these conditions (Table 4.10, entries 4, 5). As increasing reaction concentration failed to fully compensate for the lower catalyst loading, the optimal conditions were determined to be 10 mol% catalyst loading at a reaction concentration of 0.1 M.

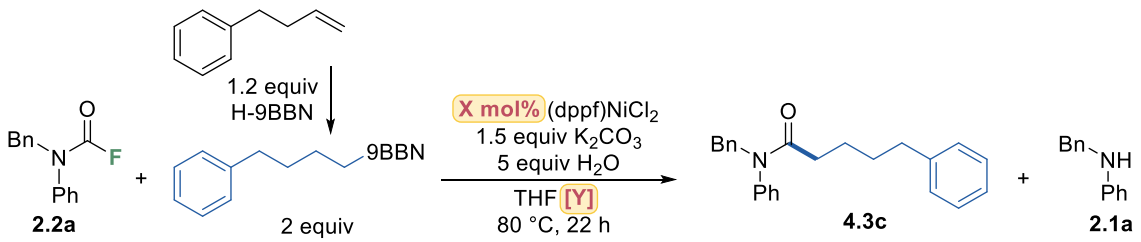

Entry	Concentration	Cat. Loading	Conversion	Amide	Amine
1	(0.1 M)	20 mol%	100%	89%	7%
2		10 mol%	100%	89%	8%
3		5 mol%	83%	56%	24%
4	(0.2 M)	5 mol%	95%	68%	25%
5	(0.4 M)	5 mol%	96%	67%	28%

Table 4.10: Optimization table screening reaction concentrations and catalyst loadings. Conversions and yields acquired by ^{1}H NMR spectroscopy using 1,3,5 trimethoxybenzene as an internal standard.

4.4.2.7. Reaction Temperature Screen

The effect of reaction temperature was investigated to determine whether milder conditions could be used, as the existing conditions employed THF at 80 °C, well above the solvent's boiling point of 66 °C. Lowering the reaction temperature to 60 °C afforded amide **4.3c** in 66% yield with only a slight increase of amine formation (Table 4.11, entry 2). Because conversion reached only 80% under these conditions, extending the reaction time may permit complete conversion while allowing the reaction to be performed at lower temperatures. Further reductions in temperature proved detrimental to reaction performance, with product yields falling below 10% at temperatures of ≤ 40 °C (Table 4.11, entries 3, 4). Overall, the original reaction temperature of 80 °C remained optimal, providing complete conversion of the CMF together with an excellent product yield and minimal amine formation.

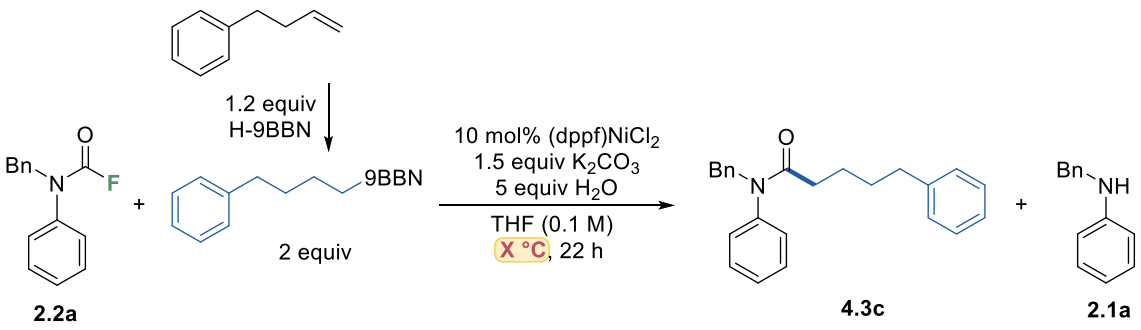

Entry	Temperature	Conversion	Amide	Amine
1	80 °C	100%	89%	9%
2	60 °C	80%	66%	12%
3	40 °C	14%	6%	7%
4	Room Temp	3%	0%	4%

Table 4.11: Reaction temperature screening, conversions and yields acquired by ^{1}H NMR with 1,3,5 trimethoxybenzene as an internal standard.

4.4.2.8. Reaction Time Screen

Having established that complete conversion was achieved after 22 hours under the optimized conditions, reaction time was next investigated to determine whether shorter reaction durations could provide comparable yields. The reaction proceeded relatively rapidly during the initial period, affording approximately half of the desired amide within 90 minutes, and 77% after 6 hours. Product formation subsequently slowed, with the remaining increase to 88% yield and complete CMF conversion requiring an additional 16 hours (Table 4.12). Accordingly, a reaction time of 22 hours was retained for subsequent studies to ensure complete substrate conversion.

The decreasing rate of conversion over time, together with the incomplete conversion observed upon reducing the catalyst loading from 10 to 5 mol% (Section 4.4.2.6.), may be consistent with rapid generation of an active catalyst during the reaction onset, followed by gradual catalyst deactivation over time. However, the data collected cannot distinguish catalyst deactivation from other factors that could slow the reaction at later time points, including depletion of the CMF substrate or changes in the composition of the heterogeneous reaction mixture.

Interestingly, amine formation remained remarkably constant at 8-9% across all time points examined (Table 4.12, entries 1-4). Because no amine was detected in the starting CMF, the byproduct must be formed under the reaction conditions. Its lack of accumulation over time suggests that amine formation occurs predominantly during the early stages of the reaction, within the first 90 minutes, rather than through continuous CMF hydrolysis throughout the reaction. At present, the origin of this amine formation remains unclear.

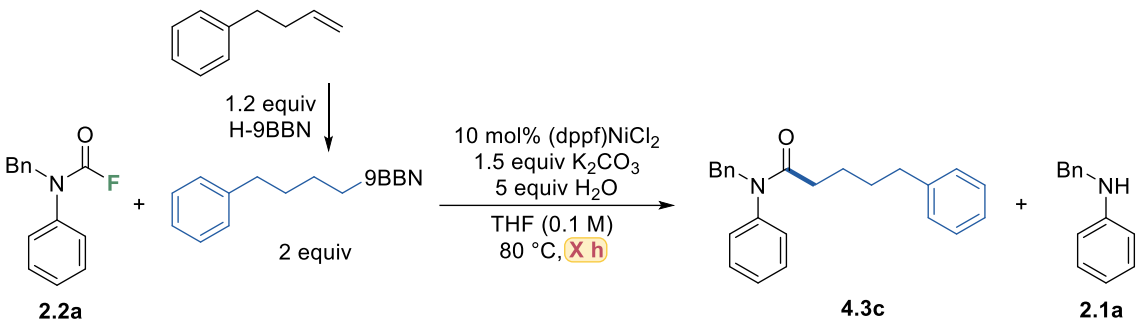

Entry	Time	Conversion	Amide	Amine
1	90 min	59%	49%	8%
2	3 h	78%	67%	9%
3	6 h	89%	77%	9%
4	22 h	100%	88%	9%

Table 4.12: Evaluation of optimal reaction time. Conversions and yields acquired by ^{1}H NMR spectroscopy using 1,3,5 trimethoxybenzene as an internal standard.

4.4.2.9. Equivalents of Alkylborane Screen

The influence of alkylborane loading was next investigated to determine the optimal quantity required for efficient cross-coupling. Using one equivalent of alkyl-9-BBN resulted in incomplete conversion (85%), affording only 66% of the desired amide while increasing amine formation to 16% (Table 4.13, entry 1). Increasing the alkylborane loading to either 1.5 or 2.0 equivalents resulted in complete conversion and identical product yields of 87% (Table 4.13, entries 2, 3). Further increasing the amount of alkylborane beyond two equivalents proved detrimental, leading to reduced conversion, diminished product yields, and increased formation of the corresponding amine (Table 4.13, entries 4, 5).

Although 1.5 and 2.0 equivalents afforded identical reaction outcomes, 1.5 equivalents were selected for all subsequent studies to minimize purification challenges arising from alkylborane-derived by-products. These purification difficulties are discussed further in Section 4.4.3.

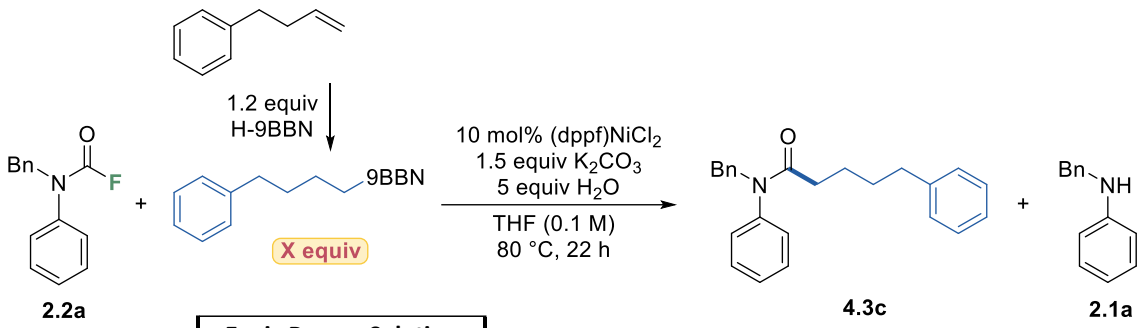

Entry	Equiv Borane Solution (1 : 1.2, Alkene : H-9BBN)	Conversion	Amide	Amine
1	1.0	85%	66%	16%
2	1.5	100%	87%	10%
3	2.0	100%	87%	11%
4	2.5	89%	67%	19%
5	3.0	86%	58%	21%

Table 4.13: Optimization of equivalents of alkylborane. Conversions and yields acquired by ^{1}H NMR with 1,3,5 trimethoxybenzene as an internal standard.

4.4.2.10. Premixing of Pre-catalyst and Alkylborane

During the reaction discovery process, it was observed that premixing (dppf)$NiCl_2$ with the alkyl-9-BBN reagent for 1-10 minutes transformed the initial deep green suspension into a homogenous yellow solution (Figure 4.4). Addition of this premixed solution to the remaining reaction components consistently afforded higher yields than simply combining all reagents prior to solvent addition. Throughout the optimization studies described in Sections 4.4.2.1-4.4.2.9, the catalyst and alkylborane were routinely premixed until a homogenous yellow solution had formed. The nature of the species generated during this premixing step is discussed in Section 4.4.5. and will not be further discussed here.

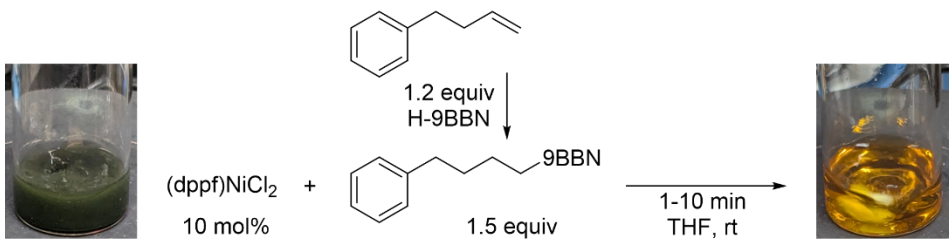

Figure 4.4: Visual cue observed during premixing.

The premixing time was systematically investigated next. When no premixing was employed and all reagents were combined simultaneously followed by addition of solvent, only 40% conversion was achieved, producing just 9% of the desired amide (Table 4.14, entry 1). In contrast, simply allowing the pre-catalyst and alkylborane to premix for 30 seconds prior to addition to the remaining reaction components increased the yield to 57% (Table 4.14, entry 2). Premixing for between 1 and 10 minutes afforded nearly identical reaction outcomes, providing 86-89% yields of the desired amide (Table 4.14, entry 3-6). These results demonstrate that premixing of the pre-catalyst with the alkylborane was essential for efficient catalyst generation and productive cross-coupling. Consequently, premixing times between 1 and 10 minutes were employed for all subsequent reactions. Interestingly, successful catalyst activation could be assessed visually post-reaction. Reactions that underwent insufficient premixing appeared yellow upon completion, whereas successful reactions consistently produced black reaction mixtures (Figure 4.5).

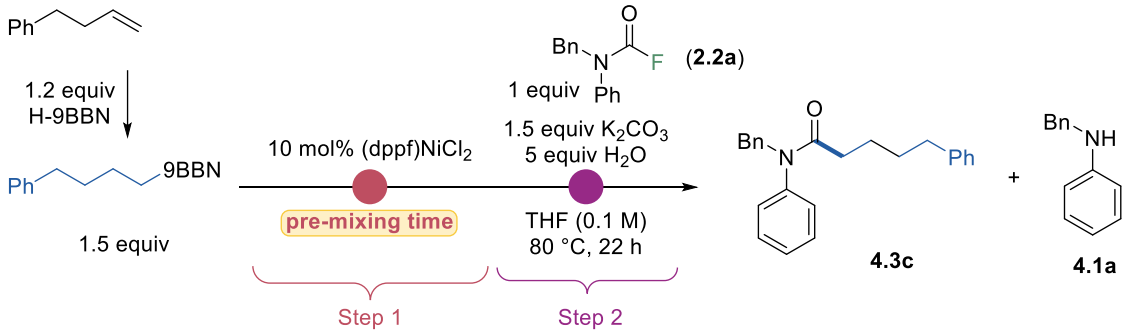

Entry	Pre-Mixing Time	Conversion	Amide	Amine
1	0 min	41%	9%	31%
2	0.5 min	76%	57%	18%
3	1 min	95%	86%	9%
4	2 min	96%	89%	6%
5	5 min	95%	89%	6%
6	10 min	91%	87%	6%

Table 4.14: Optimization of premixing times. Conversions and yields acquired by ^{1}H NMR spectroscopy using 1,3,5 trimethoxybenzene as an internal standard.

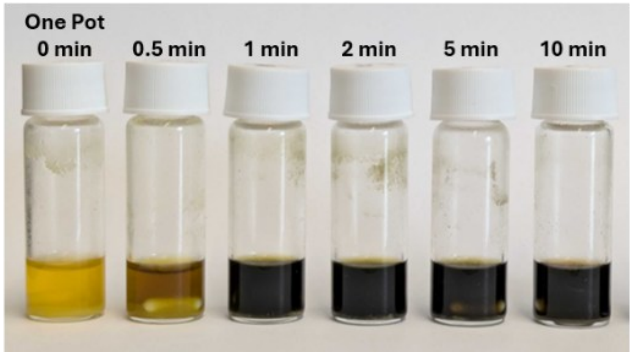

Figure 4.5: Appearance of reactions solutions after 22 hours with varying premixing times.

4.4.2.11. Pre-catalyst Screen

Finally, a range of nickel and palladium pre-catalysts were evaluated under the optimized reaction conditions. For pre-catalysts that did not contain pre-ligated dppf, 10 mol% dppf was added separately and the resulting mixture was premixed for 30 minutes prior to use.

Both (dppf)$NiCl_2$ and (DME)$NiCl_2$ afforded identical reaction outcomes, producing the desired amide in 89% yield with only 10% amine formation (Table 4.15, entries 1, 8). In contrast, the considerably less soluble $NiCl_2$ afforded only 28% (Table 4.15, entry 2). (TMEDA)Ni(*o*-tolyl)Cl (Doyle's catalyst) performed reasonably well, providing 82% conversion and a moderate 60% yield (Table 4.15, entry 4). All remaining Ni(II) pre-catalysts examined reacted poorly, affording no more than 23% product (Table 4.15, entry 3, 9).

Interestingly, every pre-catalyst containing a 1,5-cyclooctadiene (COD) ligand exhibited poor catalytic performance, even when dppf was pre-ligated to the nickel center, with product yields not exceeding 43% (Table 4.15, entries 5-7). These observations suggest that displacement of the COD ligand may be too challenging under the reaction conditions, thereby limiting formation of the catalytically active Ni(0) species capable of undergoing oxidative addition.

To assess whether palladium could also catalyze this transformation, two palladium pre-catalysts were evaluated. (dppf)$PdCl_2$ was selected as a direct palladium analogue of the optimal nickel catalyst, while $(PPh_3)_2PdCl_2$ was chosen because it proved to be the optimal catalyst for the palladium-catalyzed Suzuki cross-coupling of CMFs described in Chapter 3. Neither palladium pre-catalysts produced detectable quantities of the desired amide, instead giving only moderate conversion accompanied by amine formation (Table 4.15, entries 10, 11). These results demonstrate that the developed transformation is highly specific to nickel catalysis, with analogous palladium catalyst systems proving ineffective under otherwise identical reaction conditions.

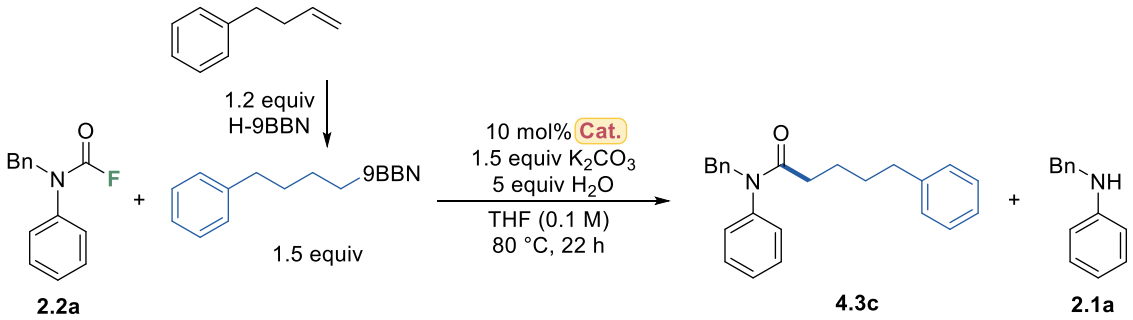

Entry	Pre-Catalyst	Ligand	Conversion	Amide	Amine
1	$(DME)NiCl_2$	10 mol% dppf	100%	89%	10%
2	$NiCl_2$	10 mol% dppf	55%	28%	27%
3	$Ni(acac)_2$	10 mol% dppf	49%	23%	26%
4	(TMEDA)Ni(*o*-tolyl)Cl	10 mol% dppf	82%	60%	18%
5	$Ni(COD)_2$	10 mol% dppf	66%	21%	40%
6	Ni(COD)(DQ)	10 mol% dppf	82%	43%	34%
7	(dppf)Ni(COD)	-	76%	19%	49%
8	$(dppf)NiCl_2$	-	100%	89%	10%
9	$(PCy_3)_2NiCl_2$	-	42%	6%	36%
10	$(dppf)PdCl_2$	-	37%	0%	23%
11	$(PPh_3)_2PdCl_2$	-	29%	0%	30%

Table 4.15: Pre-catalyst screening. Conversions and yields acquired by ^1H NMR spectroscopy using 1,3,5 trimethoxybenzene as an internal standard.

4.4.2.12. Summary of Reaction Optimization Studies

Collectively, these optimization studies established a robust set of reaction conditions for the nickel-catalyzed Suzuki cross-coupling of unactivated CMFs with alkyl-9-BBN nucleophiles. The optimized reaction conditions are summarized in Scheme 4.9 and include premixing of the pre-catalyst with the alkyl-9-BBN for 1-10 minutes prior to addition to the remaining reaction components. These conditions were subsequently employed throughout the substrate scope described in Section 4.4.4.

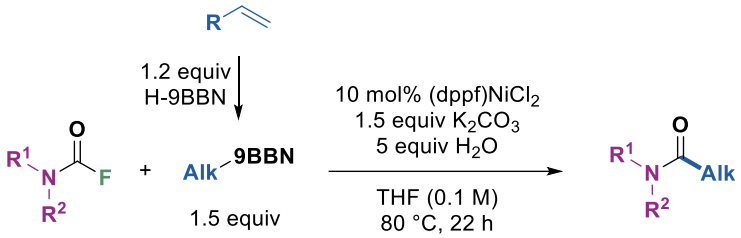

Scheme 4.9: Reaction scheme of the optimized reaction conditions established in Section 4.4.2.

4.4.3. Substrate Purification

Accurate determination of reaction conversion and product yields was essential throughout the optimization studies and was performed by quantitative NMR (qNMR) spectroscopy using an internal standard. However, the ^{1}H NMR of the crude reaction mixtures consistently exhibited extensive signal broadening that rendered the spectra unsuitable for quantitative analysis (Figure 4.6, **A**). This broadening was initially believed to arise from paramagnetic nickel species present in the crude reaction mixture. After a thorough investigation, it was found that the addition of approximately 0.5 mL of D_2O to the crude NMR sample, followed by vigorous mixing of the biphasic system for several minutes and brief manual centrifugation to separate the aqueous and organic phases, removed the paramagnetic species responsible for the signal broadening. This simple procedure produced well-resolved spectra suitable for quantitative analysis and was subsequently employed for all qNMR measurements throughout the optimization studies (Figure 4.6, **B**).

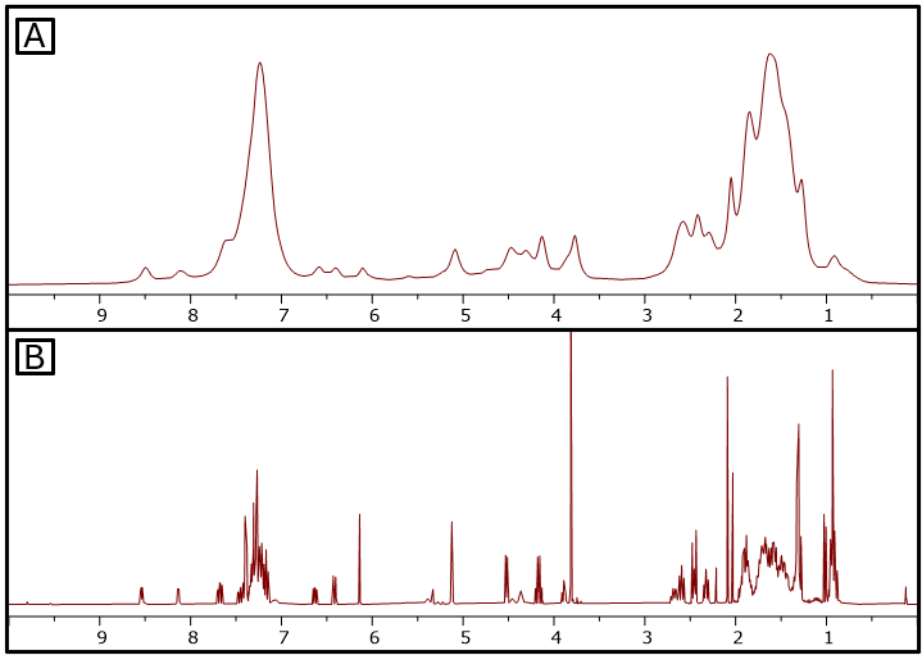

Figure 4.6: ^{1}H NMR spectra of crude cross-coupling reaction mixture. (**A**) Spectra acquired in $CDCl_3$. (**B**) ^{1}H NMR spectra acquired after extensive mixing of biphasic crude mixture of $CDCl_3/D_2O$, followed by centrifugation.

Once the reaction conditions had been optimized, efforts were directed towards developing reliable purification conditions prior to investigating the substrate scope. Initial attempts to isolate products by column chromatography proved exceedingly challenging due to the presence of numerous unexpected impurities, most of which were not visible by thin layer chromatography TLC under UV light. Only upon staining with phosphomolybdic acid (PMA) did impurities become visible (Figure 4.7).

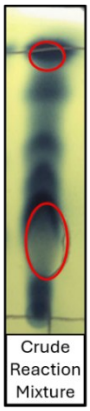

Figure 4.7: Representative example of a typical TLC plate from a crude reaction mixture once stained in PMA. Spots circled in **red** indicate all spots visible under UV light.

Investigation into the origin of these impurities led to a report by Chung and co-workers describing the aerobic oxidation of alkyl-9-BBN derivatives. Exposure of alkyl-9-BBN compounds to atmospheric oxygen at ambient temperature results in the formation of a peroxyborane (**I**) (Figure 4.8).[16,17] Peroxyborane (**I**) was found to be unstable and readily undergoes homolytic O–O bond cleavage to generate an alkoxy radical (**II**) and relatively persistent borinate radical (**III**) (Figure 4.8).[16] Alkoxy radicals are highly reactive and can undergo numerous degradation pathways with surrounding functional groups.[17–22] In contrast, borinate radical (**III**) exhibits enhanced stability through back-donation of electron density from oxygen into the vacant boron p-orbital.[16] At elevated temperatures, peroxyborane (**I**) may alternatively undergo asymmetric peroxide cleavage to generate an alkyl radical (**IV**) together with a peroxyborane radical (**V**), both of which rapidly decompose (Figure 4.8).[16]

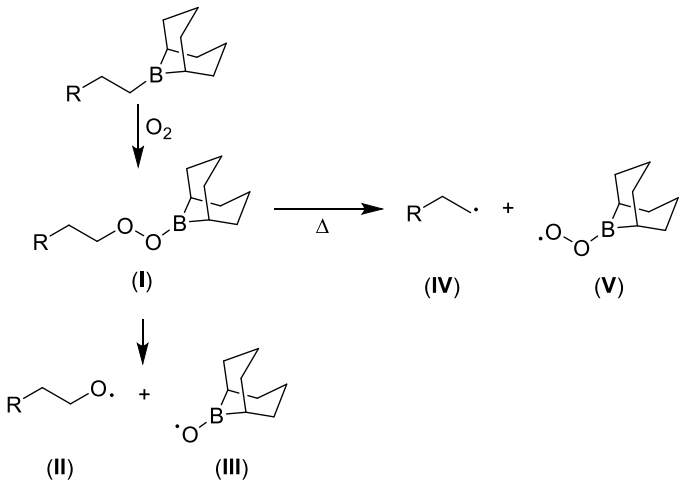

Figure 4.8: General oxidation and radical generation pathways of alkyl-9-BBN.

Formation of these radical intermediates was highly consistent with the experimental observations. Generation of highly reactive radicals (**I**, **II**, **IV**, and **V**) would be expected to produce numerous decomposition products through secondary reactions with compounds present in solution, consistent with the large number of species observed by TLC (Figure 4.7). Furthermore, the persistence of borinate radical (**III**) provides a plausible explanation for the extensive signal broadening observed in crude qNMR spectra (Figure 4.6, **A)**.

To further investigate this hypothesis, a standard cross-coupling reaction was completed and the solvent removed under an inert atmosphere. The crude residue was transferred directly into an NMR tube inside a nitrogen-filled glovebox to prevent exposure to atmospheric oxygen. Under these conditions, only minor signal broadening was observed (Figure 4.9, **A**), likely arising from a small population of paramagnetic nickel species. The NMR tube was then briefly exposed to air by removing the cap for approximately 30 seconds before resealing and vigorously shaking the sample for 1-2 minutes. Reanalysis revealed moderate signal broadening throughout the spectrum following this brief exposure to air (Figure 4.9, **B**). These observations strongly suggest that much of the signal broadening observed in crude reaction mixtures originates from radical species

generated by oxidation of residual alkyl-9-BBN upon exposure to atmospheric oxygen, rather than solely from paramagnetic nickel complexes.

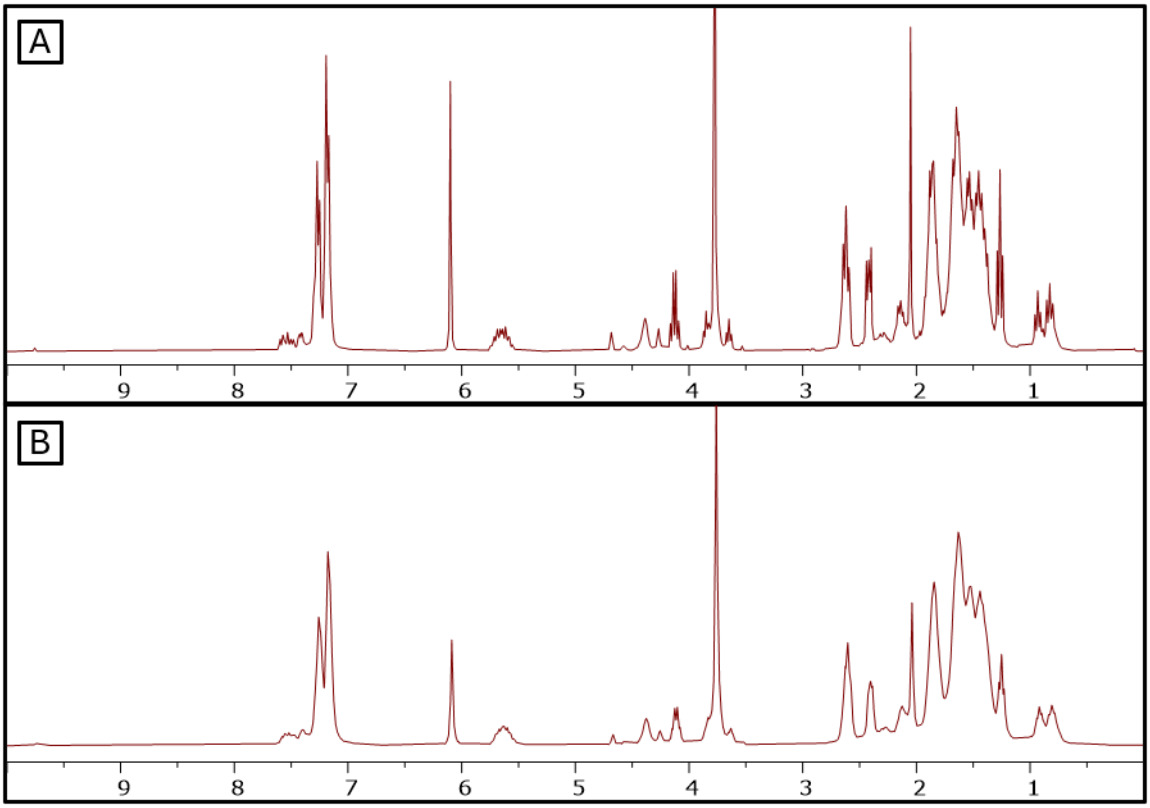

Figure 4.9: ^{1}H NMR spectra of crude cross-coupling reaction mixture. (**A**) NMR sample prepared in a nitrogen filled glovebox, spectra acquired in $CDCl_3$. (**B**) NMR sample prepared in a nitrogen filled glovebox and NMR tube cap removed for 30 seconds, recapped, and vigorously shaken for 1-2 minutes, spectra acquired in $CDCl_3$.

Additionally, an aliquot of the alkyl-9-BBN reagent was combined with (2,2,6,6-tetramethylpiperidin-1-yl)oxyl (TEMPO) under an inert atmosphere and subsequently exposed to air. Gas chromatography-mass spectrometry (GC-MS) analysis of the resulting mixture revealed the corresponding 4-phenylbutyl-TEMPO adduct (**4.9**) (Figure 4.10), further supporting the generation of 4-phenylbutyl radicals upon aerobic oxidation of the alkyl-9-BBN reagent.

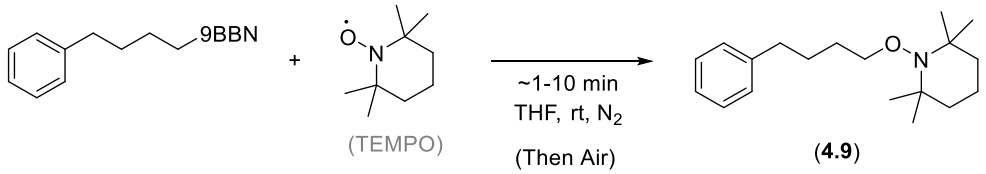

Figure 4.10: Formation of TEMPO adduct **4.9** under aerobic conditions.

Having identified the likely origin of these decomposition products, efforts were directed towards the developing a suitable method for quenching residual alkyl-9-BBN prior to exposure of the reaction mixture to aerobic conditions. A wide variety of quenching methods were investigated under oxygen-free conditions using literature procedures for borane oxidation or Lewis acid deactivation (Figure 4.11).[23–37] Of all methods evaluated, only aqueous $NaOH/H_2O_2$ effectively quenched residual alkyl-9-BBN (Figure 4.11, **J**). This reagent combination generates sodium hydroperoxide ($NaHO_2$) in situ, an extremely reactive oxidant that presented both safety concerns and the possibly of undesired oxidation of sensitive functional groups during substrate scope investigations. Consequently, a milder alternative oxidant was sought.

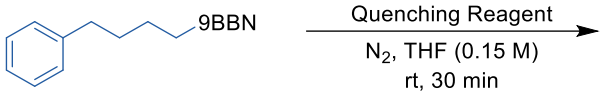

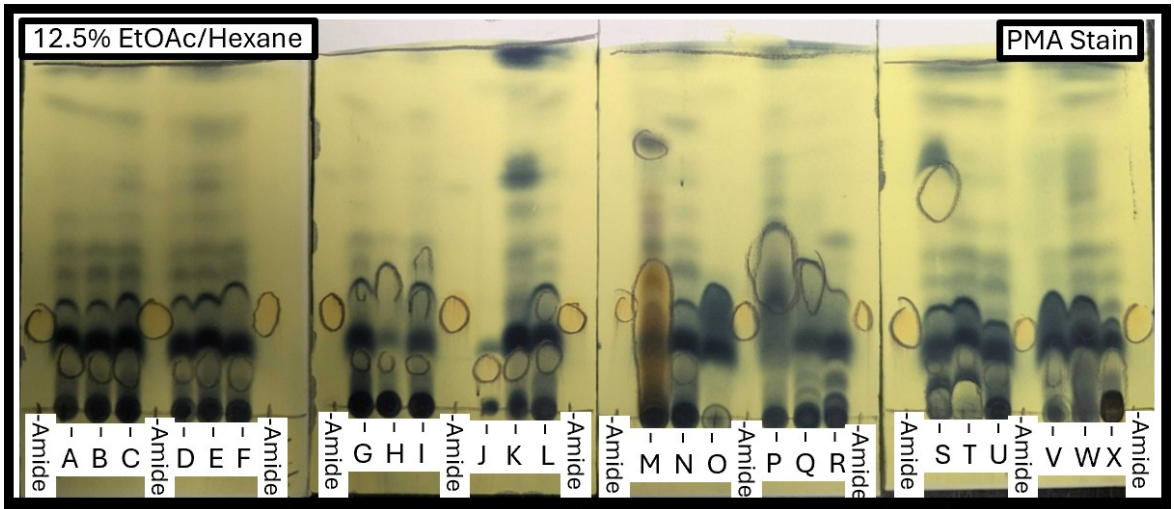

Entry	Quenching Reagent	Entry	Quenching Reagent	Entry	Quenching Reagent	Entry	Quenching Reagent
A	None (Control)	**G**	Sat. $NaOAc_{(aq)}$	**M**	Dibenzylideneacetone	**S**	Neopentylene glycol
B	H_2O	**H**	Sat. $K_2CO_{3(aq)}$	**N**	MeI	**T**	TPPO
C	Sat. $NH_4Cl_{(aq)}$	**I**	10% $NaOH_{(aq)}$	**O**	Pivalic acid	**U**	MeOH
D	0.5 M $HCl_{(aq)}$	**J**	(1:3) $NaOH/H_2O_{2(aq)}$	**P**	Phenol	**V**	2-Pyridone
E	1.0 M $Na_2S_2O_{3(aq)}$	**K**	30% $H_2O_{2(aq)}$	**Q**	2-Aminoethanol	**W**	2,3-Butanedione
F	Sat. $NaHCO_{3(aq)}$	**L**	4-Picoline *N*-oxide	**R**	Pyridine	**X**	Curcumin

Figure 4.11: TLC experiments used to evaluated effectiveness of various alkyl-9-BBN quenching experiments. Lanes titled **Amide** are of shown as a reference representing the desired products R_f.

Subsequent literature investigation revealed that *N*-methylmorpholine *N*-oxide (NMO) selectively oxidizes alkyl-9-BBN derivatives to the corresponding oxaborabicyclo[3.3.2]decane species (**I**) which is stable under ambient conditions (Figure 4.12).[38–40] When employed to quench crude reaction mixtures, NMO proved highly effective and substantially reduced the number of decomposition products observed during purification (Figure 4.13). Accordingly, NMO was adopted as the standard quenching reagent for all substrate scope reactions and was added under an inert atmosphere prior to workup under ambient conditions.

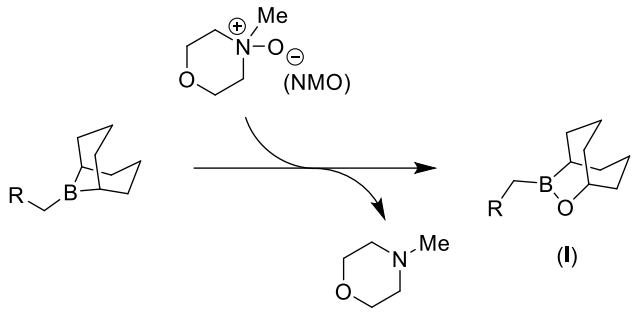

Figure 4.12: General reaction scheme for the oxidation of alkyl-9-BBNs with NMO.

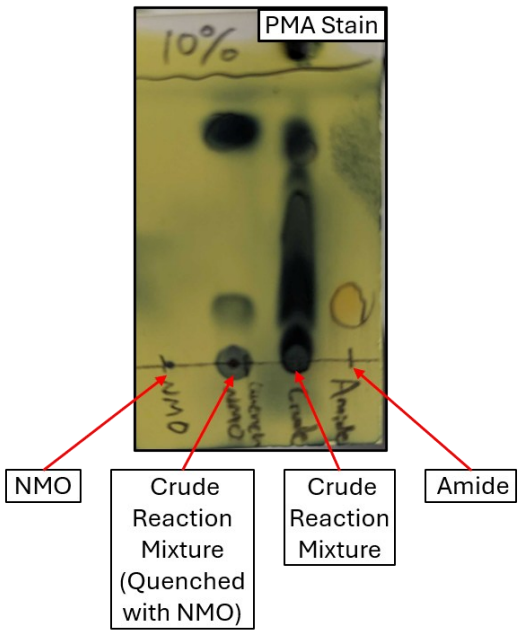

Figure 4.13: TLC plate illustrating the ability of NMO to quench residual alkyl-9-BBN in crude a reaction mixture.

Despite successful quenching of residual alkyl-9-BBN, purification by column chromatography remained challenging because of the poor UV absorbance of the standard amide product. Product-containing fractions could not be readily identified by TLC, even after application of various visualization stains or use of automated flash chromatography. Only after fractions were allowed to concentrate over several days to approximately 10% of their initial volume did product spots become detectable by TLC. Consequently, to maintain a consistent purification procedure, all products described in Section 4.4.4 were purified by preparatory TLC.

4.4.4. Substrate Scope

With optimized reaction conditions established, the generality of the developed conditions ware evaluated through a comprehensive substrate scope investigation. Both the alkyl-9-BBN nucleophile and CMF components were systematically varied to examine the influence of electronic, steric, and functional group on reaction performance.

The alkylborane scope was investigated first using the optimized reaction conditions, with isolated yields reported throughout (Scheme 4.10). Two CMF substrates were employed during this study because purification of several products proved challenging when using the standard substrate **2.2a**. In these instances, the corresponding *p*-methoxybenzyl (PMB) analogue **2.2b** afforded products that could be purified considerably more easily. Importantly, both CMFs exhibited nearly identical reactivity, affording **4.3c** and **4.3d** in isolated yields of 82% and 89%, respectively (Scheme 4.10). Consequently, CMFs **2.2a** and **2.2b** were used interchangeably throughout the alkylborane scope to facilitate product isolation.

The unsubstituted 3-phenyl-propyl-9-BBN derivative afforded the desired amide in 79% isolated yield (**4.3e**). A variety of substituted analogues containing *para*-methoxy (**4.3f**, **4.3g**), *meta*-trifluoromethyl (**4.3i**), *para*-fluoro (**4.3v**), and 1,3-benzodioxole (**4.3q**) substituents also performed well, providing isolated yields ranging from 63-77% (Scheme 4.10). In contrast, alkylboranes containing either *para*-cyanophenyl group (**4.3h**) or a pyrazole substituent (**4.3s**) afforded more modest yields of 44% (**4.3h**) and 32% (**4.3s**) respectively, possibly due to coordination of the nitrogen-containing functionality to Lewis acidic boron center. Naphthyl (**4.3o**) and cyclohexyl (**4.3p**) derivatives likewise furnished the corresponding amides in moderate yields of 57% and 58% (Scheme 4.10).

Styrene-derived alkylboranes proved considerably less reactive. The unsubstituted styrene derivative afforded only a 29% isolated yield (**4.3j**). Introduction of electron-donating substituents to the aromatic ring resulted in modest improvements, with the *para*-methyl derivative affording 36% yield (**4.3k**) and the *para*-methoxy analogue providing 41% yield (**4.3l**) (Scheme 4.10), suggesting that increased electron density marginally benefits these substrates.

To further evaluate the synthetic utility of this developed method, alkylboranes containing motifs commonly encountered in materials chemistry were examined. Carbazole- and ferrocene-containing substrates afforded the corresponding amides in moderate isolated yields of 64% (**4.3t**) and 54% (**4.3u**), respectively (Scheme 4.10).

Because potassium fluoride is expected to be generated as a byproduct of transmetalation, two silyl-containing alkylboranes were investigated to evaluate silane compatibility. The trimethylsilane (TMS) derivative afforded the corresponding amide (**4.3m**) in a near-quantitative 98% isolated yield. Surprisingly, the *tert*-butyldimethylsilyl ether (OTBS) derivative also proved highly compatible, furnishing amide **4.3n** in 73% isolated yield (Scheme 4.10). Because OTBS protecting groups are generally susceptible to fluoride-mediated deprotection, these results suggest that free fluoride is unlikely to accumulate under the reaction conditions. This observation is discussed further in Section 4.4.5.

Lastly, an alkyl-9-BBN derivative bearing a *tert*-butyl carbamate (NHBoc) substituent afforded the desired amide (**4.3r**) in a quantitative yield (Scheme 4.10). The increased polarity imparted by the NHBoc group also greatly simplified purification by preparative TLC. Given its excellent yield, broad synthetic utility, and straightforward purification, *tert*-butyl 3-propylcarbamate-9-BBN was employed as the standard alkylborane for evaluation of the CMF substrate scope.

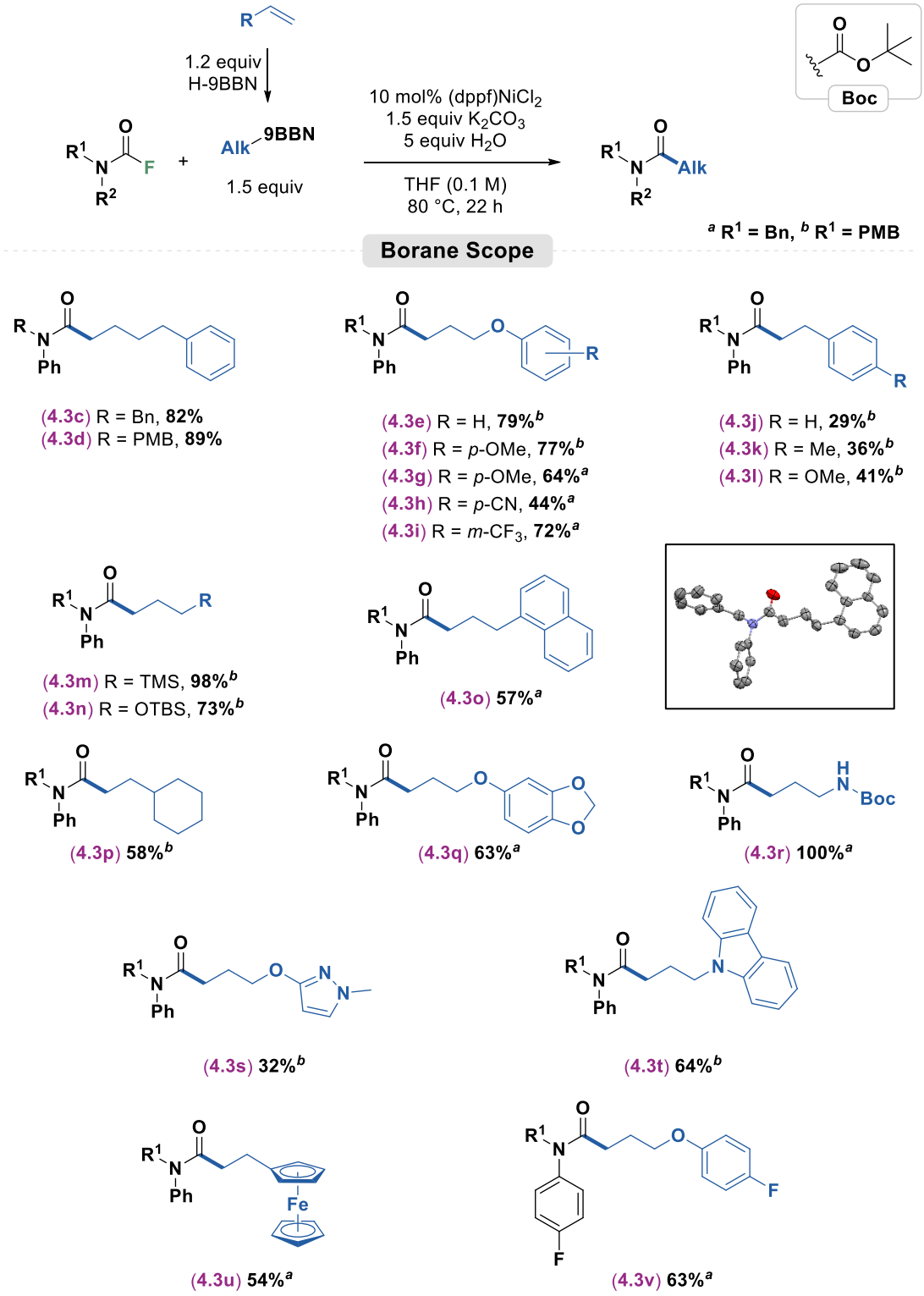

Scheme 4.10: Alkylborane substrate scope. Isolated yields are reported (ORTEP drawn at 50% probability, hydrogen atoms have been omitted for clarity)

For the CMF scope, the initial core scaffold consisted of *N*-phenyl-*N*-benzyl based CMFs, while *tert*-butyl 3-propylcarbamate-9-BBN served as the standard alkylborane coupling partner. Substituents positioned on the *para*-position of the benzyl fragment were first investigated. Electron-donating substituents including methoxy (**4.3x**), dimethylamino (**4.3y**), acetamide (**4.3z**), and 1,3-benzodioxole (**4.3ad**) all afforded excellent isolated yields ranging from 84-88%, while the *para*-fluoro derivative (**4.3w**) provided a near-quantitative 99% yield (Scheme 4.11). These results indicate that substitution on the benzyl CMF fragment exerts little influence on reaction productivity.

The electronic properties of the CMF itself were next investigated by introducing substituents at the *para*-position of the *N*-phenyl ring, thereby modulating the electronics of the CMF while maintaining similar steric properties. The electron-rich methoxy-substituted substrate afforded an excellent 89% isolated yield (**4.3aa**), whereas the electron-deficient trifluoromethyl analogue gave a substantially lower yield to 48% (**4.3ab**) (Scheme 4.11). These observations suggest that electron-rich CMFs are readily tolerated, whereas electron-deficient CMFs are less effective substrates, possibly reflecting increased susceptibility toward hydrolysis.

Substrates analogous to those employed in the seminal nickel-catalyzed intramolecular cyclization reported by Ye and Luan were then investigated to determine whether the developed reaction conditions would promote intermolecular cross-coupling or competitive cyclization. Gratifyingly, both the *N*-phenyl (**4.3af**) and *N*-benzyl (**4.3ag**) substrates afforded exclusively the desired intermolecular products in isolated yields of 88% and 52%, respectively, with no cyclized products detected (Scheme 4.11).

The influence of steric hinderance surrounding the CMF was subsequently examined. Moderately congested substrates including *N*,*N*-diphenyl (**4.3aj**), *N*-benzyl-*N*-*tert*-butyl (**4.3ai**),

N-benzyl-*N*-2,4-dimethyl-phenyl (**4.3ak**) derivatives afforded modest isolated yields ranging from 30-38% (Scheme 4.11). Despite these modest yields, these examples represent some of the most sterically demanding CMFs employed in metal-catalyzed cross-coupling reactions to date, demonstrating that the developed reaction conditions tolerate moderate steric congestion.

Several cyclic CMFs were also evaluated. The 1-indoline-derived substrate afforded the desired amide in a good 67% isolated yield (**4.3ao**), while both 1,2,3,4-tetrahydroquinoline derivatives provided excellent yields ranging from 84-99% (**4.3an**, **4.3am**). Piperazine-derived substrates likewise proved broadly compatible. The benchmark piperazine CMF substrate **2.2z** afforded amide **4.3ap** in 78% isolated yield, while introduction of a phenyl substituent slightly reduced the yield to 67% (**4.3al**), indicating that increased steric hinderance modestly impedes reaction efficiency. A more structurally complex piperazine derivative containing both amide and furan functionalities (**2.2aa**) afforded product **4.3aq** in 49% yield (Scheme 4.11).

Materials-relevant CMFs derived from dibenzazepine and phenothiazine were also examined. The dibenzazepine derivative afforded an excellent 82% isolated yield (**4.3as**), whereas the phenothiazine analogue furnished only a 28% yield (**4.3ar**) (Scheme 4.11), possibly reflecting coordination of sulfur to the alkylborane reagent.

Finally, the standard 2-pyridyl CMF employed throughout Chapter 3 was evaluated under the nickel-catalyzed conditions. The corresponding amide (**4.3at**) was isolated in 92% yield (Scheme 4.11), demonstrating that substrates containing 2-pyridyl directing groups are compatible with the reaction conditions developed in this chapter.

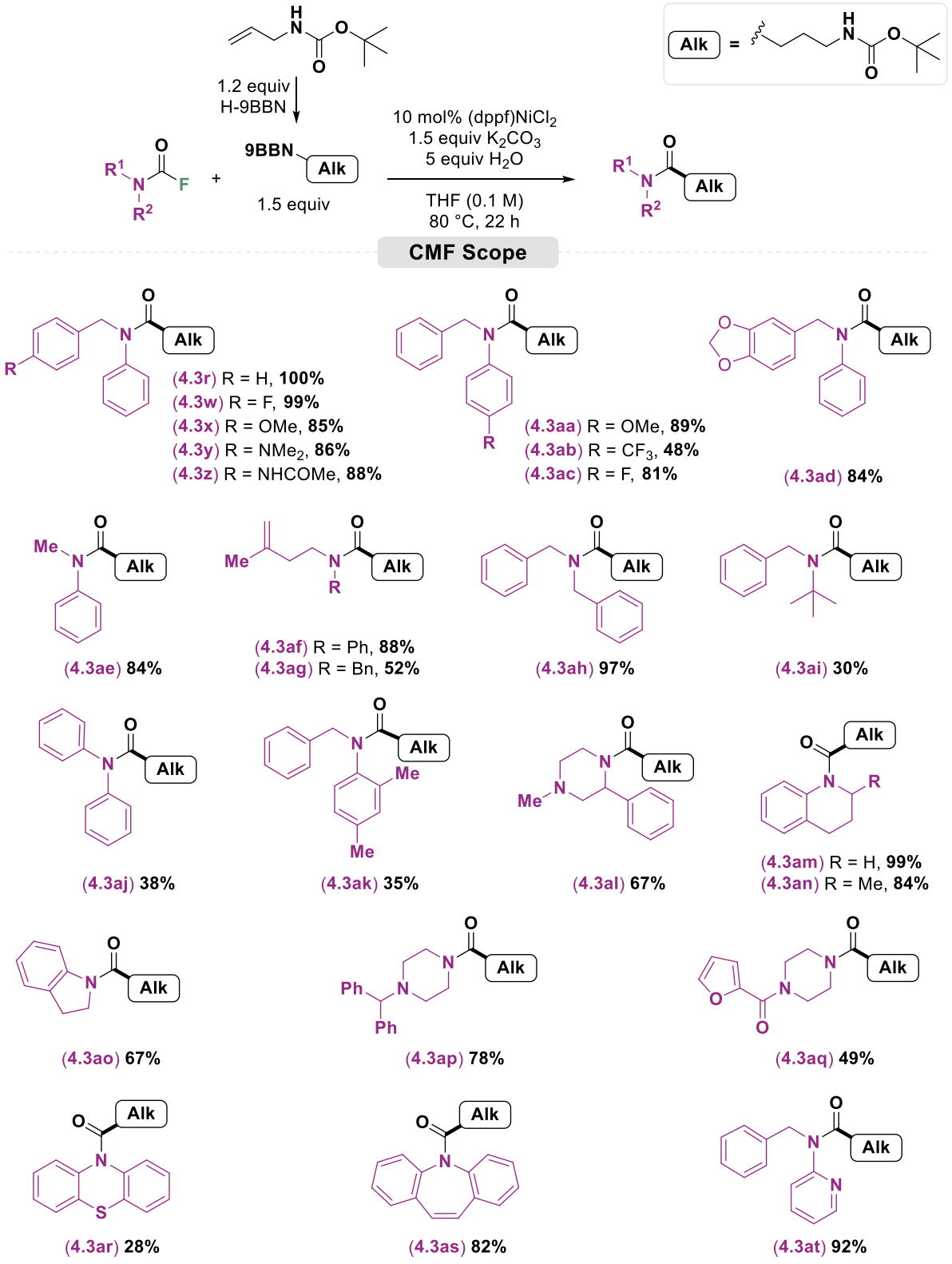

Scheme 4.11: Carbamoyl fluoride substrate scope. Isolated yields are reported.

Throughout the substrate scope investigation, several additional substrates were examined but ultimately classified as unsuccessful due to purification difficulties or inconclusive characterization. Naphthyl (**4.3au**) and cyclohexyl (**4.3av**) derivatives could not be fully purified because residual borane impurities could not be completely removed. Nevertheless, crude qNMR spectra contained resonances consistent with the desired products in approximately 12% and 10% yield, respectively (Scheme 4.12).

Nitro (**4.3aw**), phenol (**4.3ay**) and bicyclic (**4.3az**) containing substrates were also investigated. Complete conversion of CMF was observed when nitro-containing alkyl-9-BBN was employed, with amine being afforded in 85% and resonances tentatively assigned to the desired product (**4.3aw**) (approximately 15% yield). When phenol-containing alkyl-9-BBN was employed, CMF substrate only resulted in 20% conversion, with no detectable amine formation and resonances provisionally assigned to product in approximately 20% yield (**4.3ay**). Complete consumption of bicyclic CMF was observed without detectable amine formation, although the identity of several new resonances could be observed, non could be conclusively determined to be of the desired product (**4.3az**) (Scheme 4.12).

An alkyl-9-BBN substrate containing a BPin substituent appeared particularly promising. Crude qNMR analysis indicated complete CMF consumption, formation of 22% amine, and resonances consistent with approximately 68% of the desired product (Scheme 4.12, **4.3ax**). However, attempted isolation consistently resulted in decomposition during workup following addition of NMO. Because NMO has been reported to oxidatively cleave both 9-BBN and BPin functional groups,[41,42] it is believed that the desired product was successfully generated but subsequently decomposed during the quenching procedure. As definitive isolation and characterization were not possible, these substrates were conservatively classified as unsuccessful.

Several additional substrates, including acetate (**4.3ba**), norborane (**4.3bb**), and phthalimide (**4.3bc**) derivatives, produced inconclusive results. Although conversions of 64-75% were observed together with 55-65% amine formation, only minor resonances tentatively assigned to the desired products (4-10%) were detected, making purification impractical. Other substrates (**4.3bd**, **4.3be**, **4.3bf**, and **4.3bg**) generated spectra too complex to permit reliable determination of conversion or product formation (Scheme 4.12). Finally, when alkyl-9-BBN substrates containing either an epoxide (**4.3bh**) or morpholine (**4.3bi**) were evaluated incomplete conversion was observed, with all consumed CMF converted exclusively to the corresponding amine, indicating the productive cross-coupling did not occur (Scheme 4.12).

During the evaluation of the CMF substrate scope, substrates containing *para*-substituted aryl halides on the benzyl fragment exhibited pronounced chemoselectivity that depended on the aryl halide present. The *para*-fluoro CMF derivative (**2.2d**) underwent efficient cross-coupling to afford amide **4.3w** in near-quantitative yield (Scheme 4.13). In contrast, CMF substrates containing aryl chloride (**2.2e**), bromide (**2.2f**), or iodide (**2.2g**) failed to selectively produce the desired amide products. Instead, oxidative addition occurred preferentially at the aryl halide, resulting in conventional Suzuki coupling products. For both the chloride and bromide derivatives, the major isolated products arose from cross-coupling at both the aryl halide and CMF positions, affording doubly functionalized product **4.3bl** in 50% and 44% yields, respectively (Scheme 4.13). In contrast, the aryl iodide substrate reacted almost exclusively at the aryl iodide, furnishing Suzuki product **4.3bk** in 66% yield while leaving the CMF functionality largely intact, with only 19% of the doubly coupled product formed (Scheme 4.13). Collectively, these results indicate that although cross-coupling occurs preferentially at the aryl halide, the CMF remains a competent electrophile and can also undergo productive coupling under the reaction conditions.

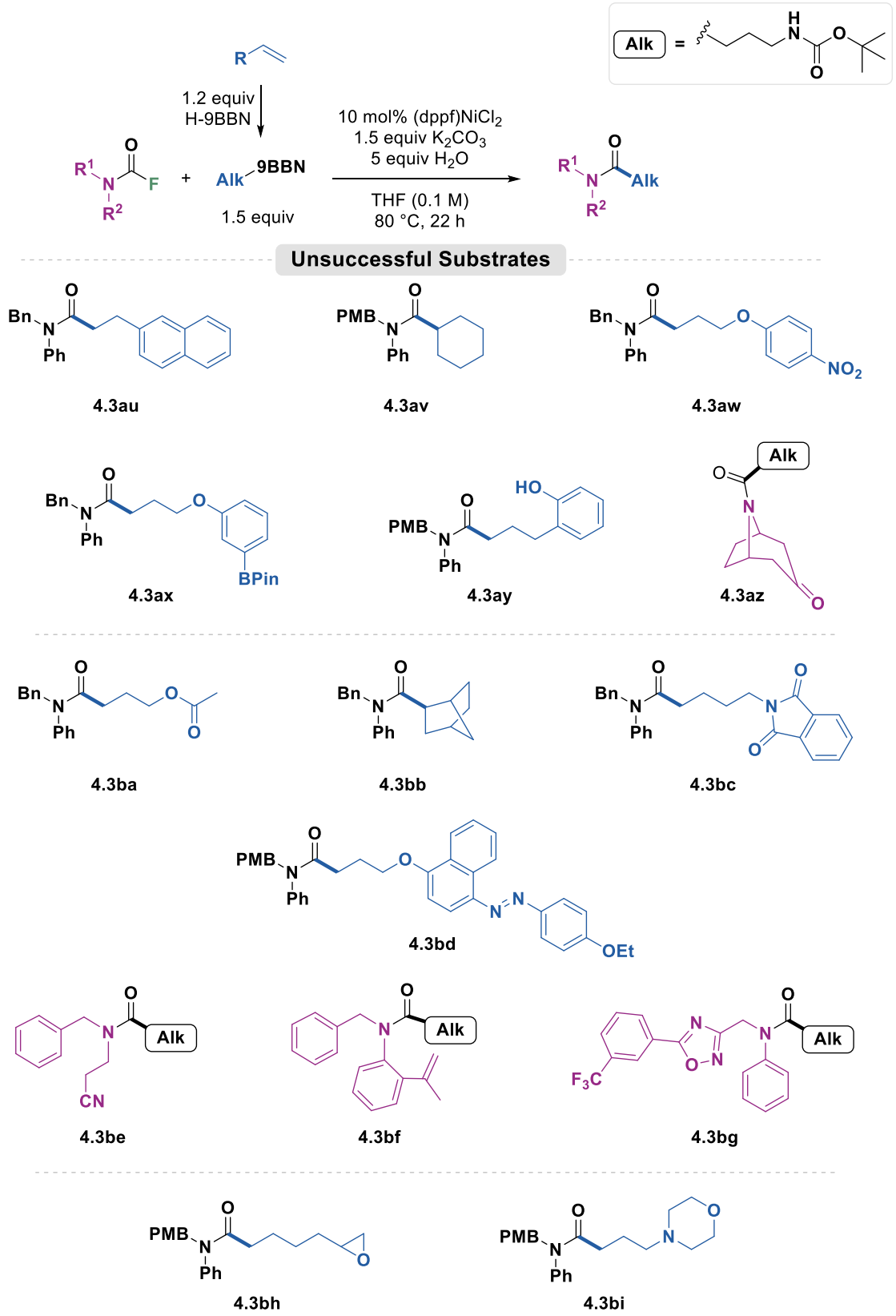

Scheme 4.12: Unsuccessful or inconclusive substrates attempted during scope.

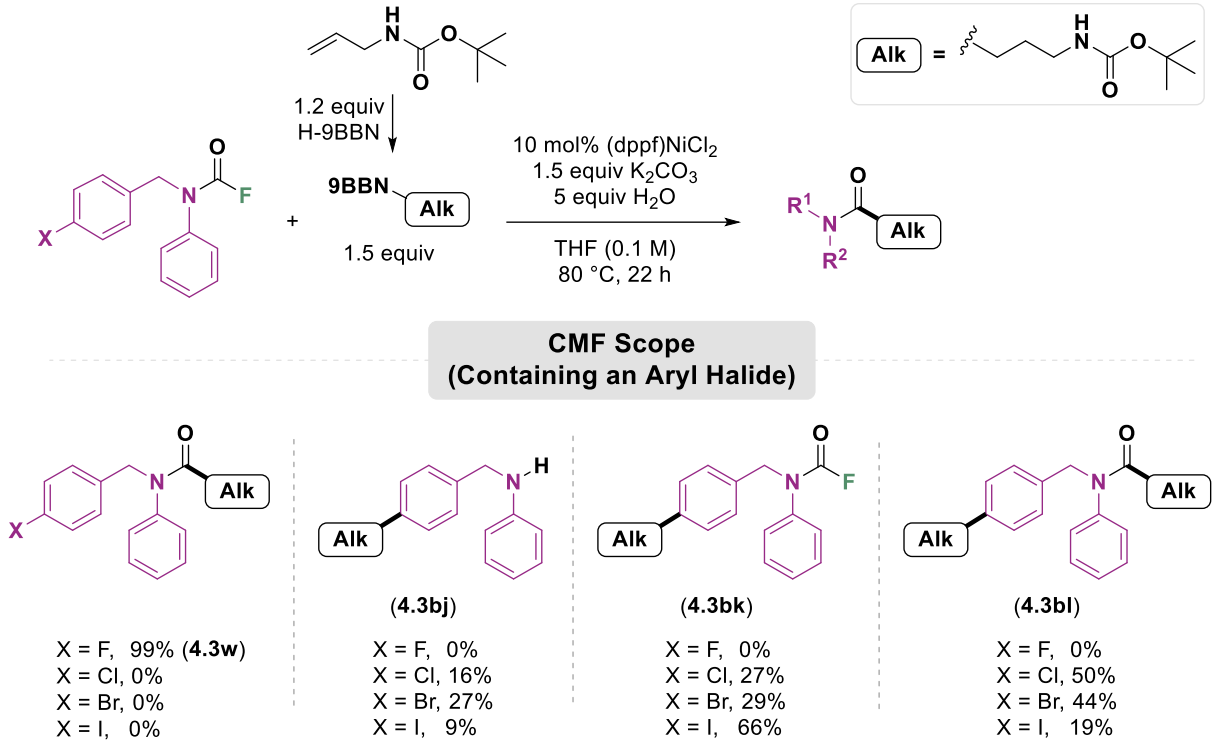

Scheme 4.13: Substrate scope of aryl halide containing CMFs.

Mechanistic Studies

4.4.4.1. Pre-mixing Investigation

As described in Section 4.4.2.10, it was observed that premixing (dppf)$Ni^{II}Cl_2$ (**4.10**) with alkyl-9-BBN reagent (**4.11**) for 1-10 minutes transformed the initial deep green suspension into a homogenous yellow solution. When this premixed solution was then added to the remaining reaction components, it consistently afforded higher yields than simply combining all reagents at the same time prior to solvent addition.

Analysis of the yellow solution by ^{1}H NMR spectroscopy revealed peak broadness indicative of the presence of a paramagnetic compound. Single crystals suitable for SC-XRD were obtained from cooling a saturated ether solution, which revealed that during this premixing step complex **4.10** was being selectively reduced to (dppf)$Ni^{I}Cl$ (**4.12**) in the presence of the alkyl borane (Scheme 4.14). Upon further investigation, it was found that H-9BBN was able to perform this reduction alone, and that even in the presence of excess H-9BBN, only complex **4.12** is generated (i.e., no further reduction to Ni(0) takes place). This presents a previously unknown method for the selective reduction of **4.10** to **4.12** using H-9BBN, allowing for the simple and high yielding preparation of (dppf)$Ni^{I}Cl$ (**4.12**) (Scheme 4.15).

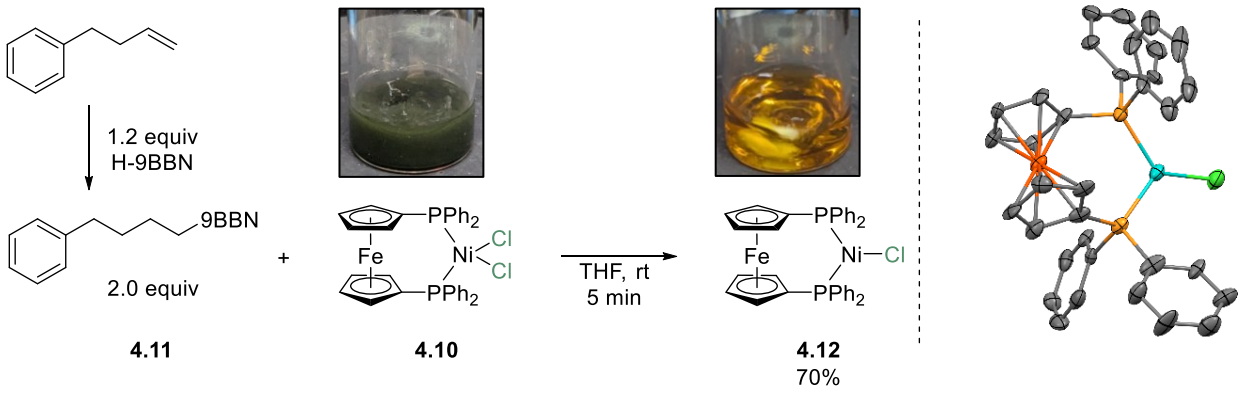

4.11 **4.10** **4.12** 70%

Scheme 4.14: Generation of **4.12** during reaction premixing step. ORTEP drawn at 50% probability, hydrogen atoms have been omitted for clarity.

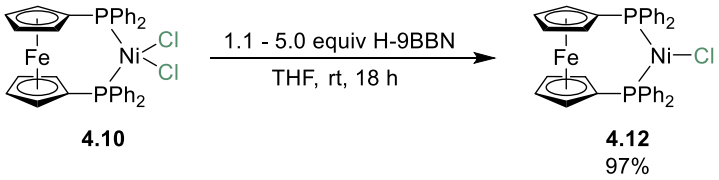

Scheme 4.15: Selective reduction of **4.10** to **4.12** with H-9BBN.

The generation of (dppf)Ni^{I}Cl (**4.12**) is proposed to occur through a comproportionation pathway (Figure 4.14). (dppf)Ni^{II}Cl$_2$ (**4.10**) first undergoes transmetalation with two equivalents of H-9BBN, followed by reductive elimination to generate highly reactive Ni(0) (complex **4.13**), along with H_2 and two equivalents of Cl-9-BBN. Owing to its high reactivity, complex **4.13** is proposed to rapidly react with an equivalent of Ni(II) (complex **4.10**) in a comproportionation step to afford the dinuclear Ni(I) complex **4.14**, which exists in equilibrium with the monomeric Ni(I) complex (dppf)Ni^{I}Cl (**4.12**) (Figure 4.14).

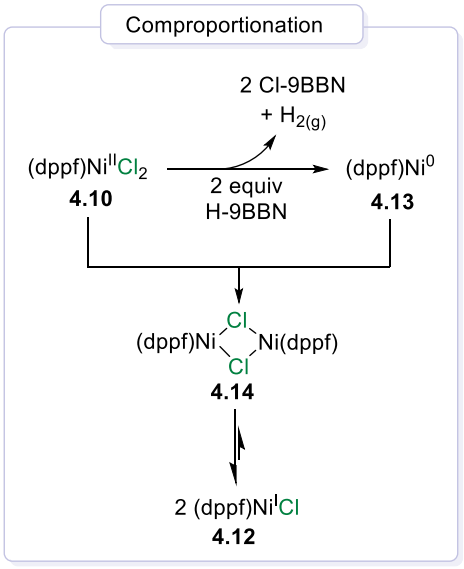

Figure 4.14: Proposed comproportionation mechanism for reduction of (dppf)Ni^{II}Cl$_2$.

Because reaction outcomes were drastically improved by the in situ generation of (dppf)Ni^{I}Cl during the premixing step, as described in Section 4.4.2.10, the potential role of this complex in catalysis was investigated further. As established in Section 4.4.2.10, 60 seconds of premixing time improved yields from 9% to 86%, suggesting that it is crucial to generate (dppf)Ni^{I}Cl prior to the addition of the carbamoyl fluoride and base. The catalytic efficiency of

(dppf)Ni^{I}Cl is later evaluated in Section 4.4.5.5. Based on established literature precedence on the Ni-catalyzed Suzuki cross-couplings, our reaction could proceed through either a typical Ni(0)/Ni(II) cycle, a Ni(I)/Ni(III) cycle, or a direct Ni(I) cycle.[12,43–49]

Most Suzuki cross-coupling reactions proceed through a Ni(0)/Ni(II) catalytic cycle (Figure 4.15). Pre-catalyst activation occurs by sequential transmetalation with two equivalents of sacrificial alkyl-9-BBN, followed by reductive elimination, to yield one equivalent of homo-coupled dialkyl product and the highly reactive Ni(0) complex (**I**). Oxidative addition with the CMF generates Ni(II) complex (**II**), which then undergoes a base-assisted transmetalation with the alkyl-9-BBN coupling partner resulting in intermediate **III**. Reductive elimination affords the amide product and regenerates Ni(0) (**I**).

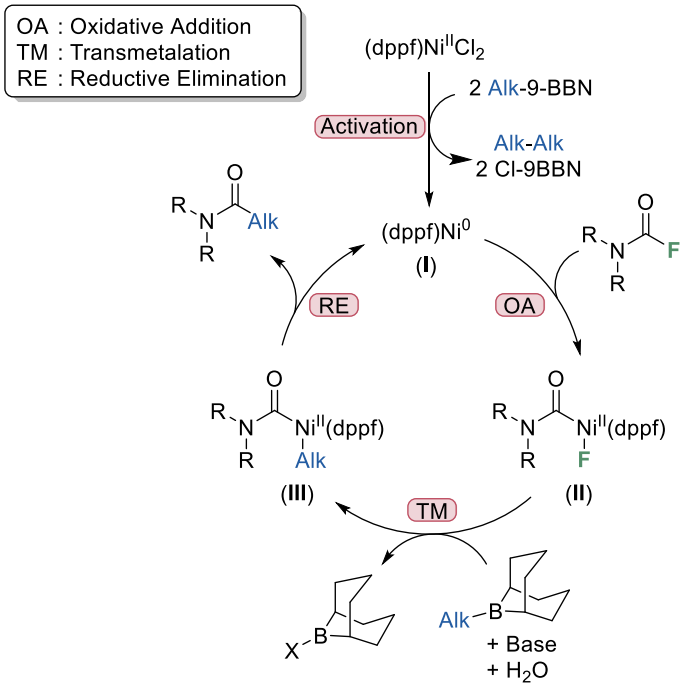

Figure 4.15: Proposed mechanism for a Ni(0)/Ni(II) Suzuki cross-coupling.

Although most nickel-catalyzed Suzuki cross-coupling reactions proceed through a Ni(0)/Ni(II) catalytic cycle (Figure 4.16), there are a handful of examples in which a Ni(I)/Ni(III)

cycle is proposed.[50–53] The Ni(II) pre-catalyst undergoes comproportionation as described in Figure 4.14 to generate a Ni(I) species (**IV**), which then transmetalates with Alkyl-9-BBN to furnish intermediate (**V**). Oxidative addition to the CMF substrate forms an unstable Ni(III) complex (**VI**), which then rapidly reductively eliminates to afford the desired product and complex (**VI**). While Pd(IV) species are accessible via oxidative addition to carbamoyl chlorides, there is no literature precedent for the generation of high-valent Ni complexes with acyl or carbamoyl halide electrophiles.[54]

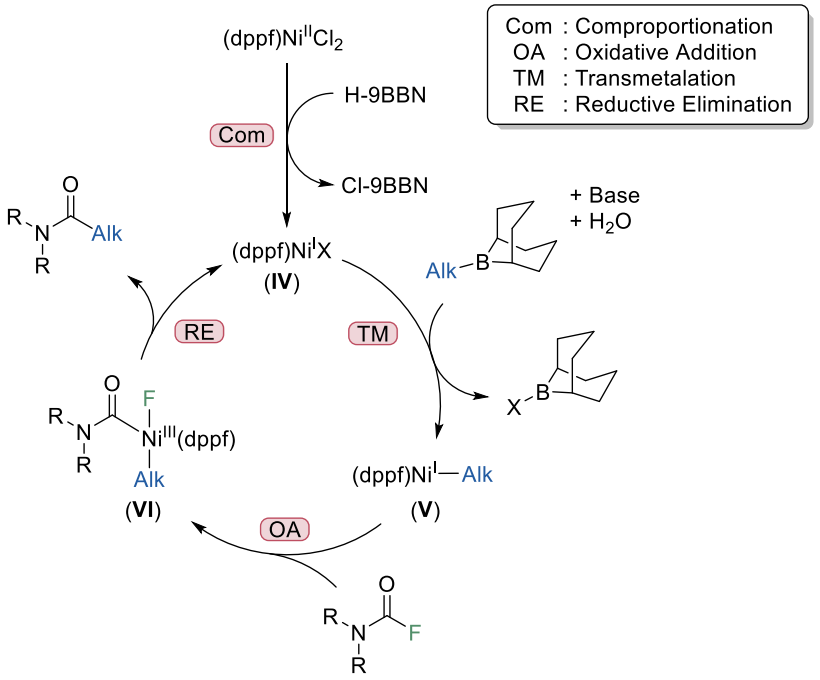

Figure 4.16: Proposed mechanism for a Ni(I)/Ni(III) Suzuki cross-coupling.

Additionally, direct Ni(I) cross-coupling may occur, similar to a Ni(I)/Ni(III) cycle, complex (**V**) is formed. Followed by subsequent coordination to the CMF carbonyl and 1,2-migratory insertion forming complex (**VII**), which can then undergo β-fluoride elimination furnishing the desired amide and complex (**IV**) (Figure 4.17). Although X would initially be fluoride following β-fluoride elimination, subsequent salt metathesis under the reaction conditions could generate the corresponding chloride- or hydroxide- ligated species (X = Cl or OH).

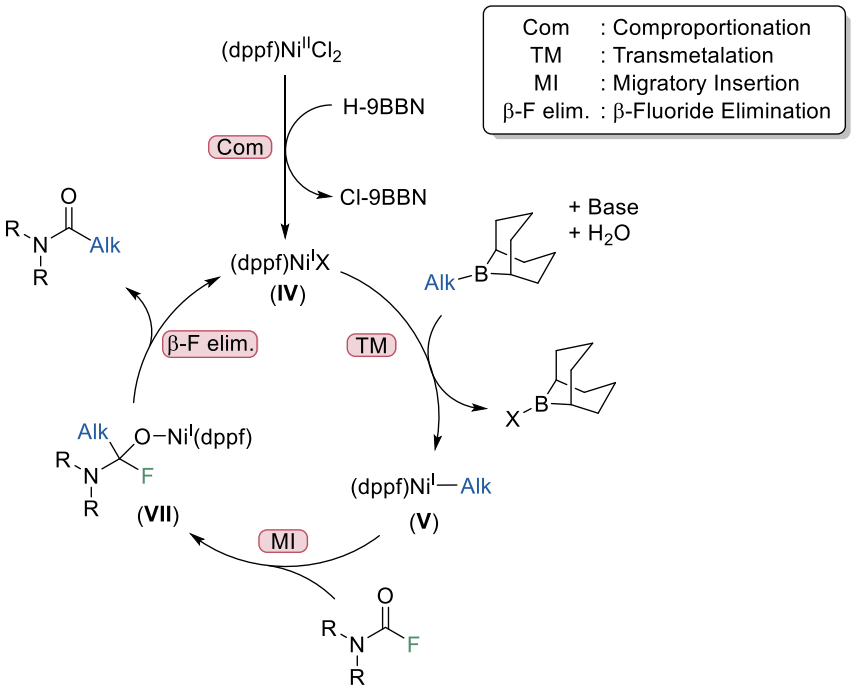

Figure 4.17: Proposed mechanism for direct Ni(I) Suzuki cross-coupling.

Due to several mechanistic possibilities, a synthetic organometallic approach was taken to assess the viability of each catalytic cycle, similar to what was carried out in Chapter 3. Complexes (**II**), (**IV**), and (**V**) were of particular interest for gaining a better mechanistic understanding of the reaction. Specifically, oxidative addition complex (**II**) would be used to assess the viability of a Ni(0)/Ni(II) catalytic cycle, and complex (**IV**) and (**V**) would give insight into a possible Ni(I)/Ni(III) or direct Ni(I) cycle. Therefore, several Ni(I) and Ni(II) derivatives were synthesized as described in Sections 4.4.5.2 and 4.4.5.3, and the reactivity of relevant complexes were evaluated in Section 4.4.5.5.

4.4.4.2. Synthesis of Catalytically Relevant Ni(I) Complexes

Owing to the paramagnetic nature of many Ni(I) complexes, characterization by NMR spectroscopy was often not possible. Although NMR spectroscopy proved useful in some cases for identifying diamagnetic byproducts, characterization of the target complexes relied primarily on SC-XRD.

Initial synthetic efforts focused on the direct preparation of an alkyl–Ni(I) complex through alkylation of Ni(I) chloride complex **4.12** using organometallic alkylating reagents, such as Grignard reagents (Scheme 4.16). Treatment of (dppf)Ni^{I}Cl (**4.12**) with isopropylmagnesium bromide (*i*-PrMgBr) afforded $(dppf)_2Ni(0)$ (**4.15**) in 90% isolated yield (relative to nickel) together with a small quantity of $[(dppf)Ni^{I}(Cl)]_2$(μ-dppf) (**4.14**).[55] Complex **4.15** was identified by both SC-XRD (Figure 4.19 **A**) and its diagnostic ^{31}P NMR resonance at 15.7 ppm. We proposed it forms through disproportionation following alkylation of **4.12** (Figure 4.18). A small quantity of **4.14** is proposed to form via the coordination of two equivalents of (dppf)Ni^{I}Cl (**4.12**) with free dppf, affording the corresponding bridged dinuclear complex.[48] Although **4.14** was not isolated, its identity was confirmed by SC-XRD (Figure 4.19 **B**). When benzylmagnesium chloride (BnMgCl) was employed instead, numerous unidentified diamagnetic species were formed, with $(dppf)_2Ni(0)$ (**4.15**) being the only identifiable product based on the crude ^{31}P NMR spectrum (Figure 4.20). As it became apparent that Grignard reagents were unsuitable for preparing the desired alkyl-Ni(I) complex, alternative alkylation strategies were investigated.

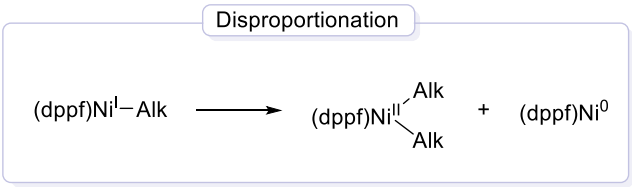

Figure 4.18: Proposed disproportionation mechanism of Alkyl-Ni(I).

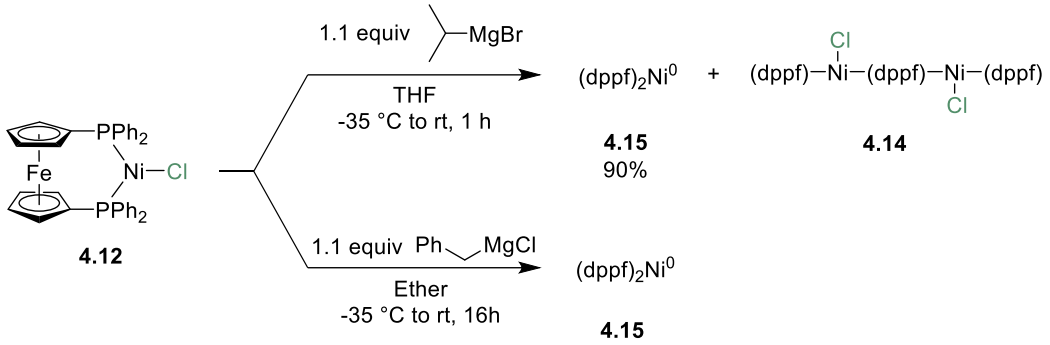

Scheme 4.16: Attempted synthesis of an alkyl-Ni(I) complex using Grignard reagents.

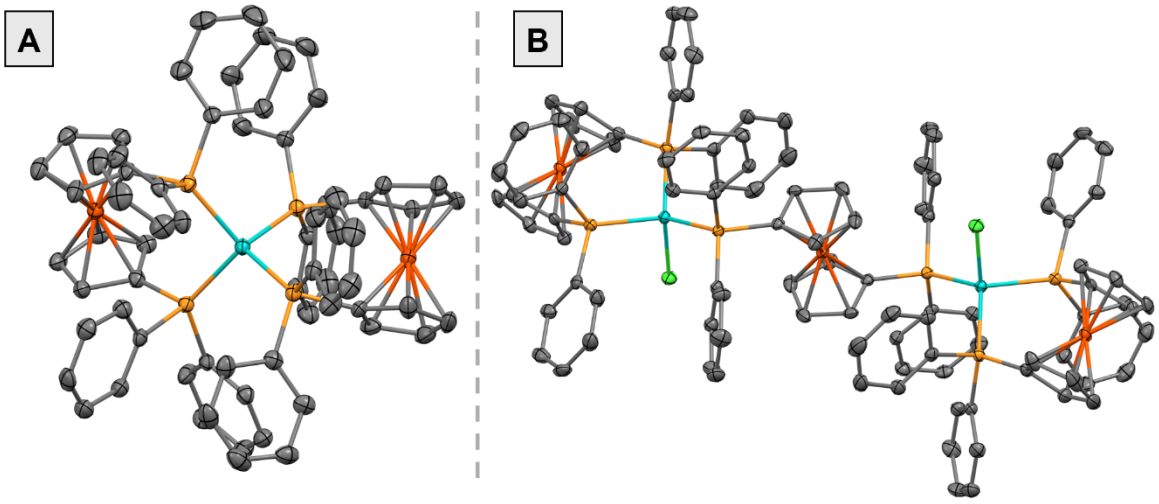

Figure 4.19: Solid-state structures of **4.15** (**A**) and **4.14** (**B**). ORTEP drawn at 50% probability, hydrogen atoms have been omitted for clarity.

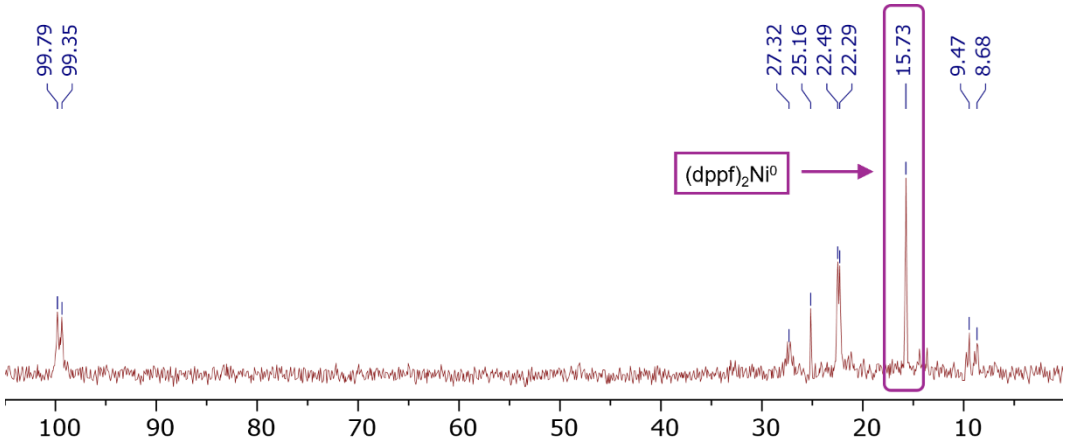

Figure 4.20: ^{31}P $\{^{1}H\}$ NMR spectrum of crude reaction mixture using **4.12** and BnMgCl, spectra acquired in C_6D_6.

Organolithium reagents were subsequently explored, beginning with methyllithium (MeLi), which resulted predominantly in the formation of two complexes (Scheme 4.17). The first was $(dppf)_2Ni(0)$ (**4.15**), which was the only species observed by ^{31}P NMR spectroscopy, while the second was **4.16**, which readily crystallized from a saturated diethyl ether solution. Complex **4.16** was found to be both thermally sensitive and unstable under ambient atmosphere, decomposing with evolution of ethane gas. The solid-state structure reveled a dimeric complex in which each nickel center adopts a slightly distorted square-planar geometry, with the two nickel centers bridged through four μ_2-lithium cations with an average Ni–Li distance of 2.509(2) Å and separated by a Ni···Ni of 3.1597(12) Å (Figure 4.21). When *n*-butyllithium (*n*-BuLi) was employed, a complex mixture of products was obtained, with $(dppf)_2Ni(0)$ (**4.15**) again being the only identifiable species based on the crude ^{31}P NMR spectrum (Figure 4.22).

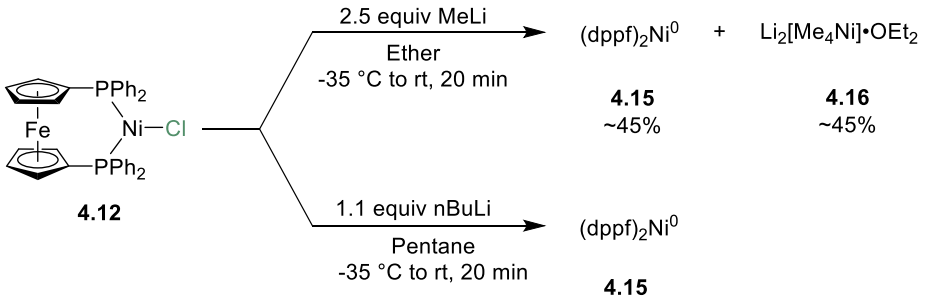

Scheme 4.17: Attempted synthesis of alkyl-Ni(I) complexes using organolithium reagents.

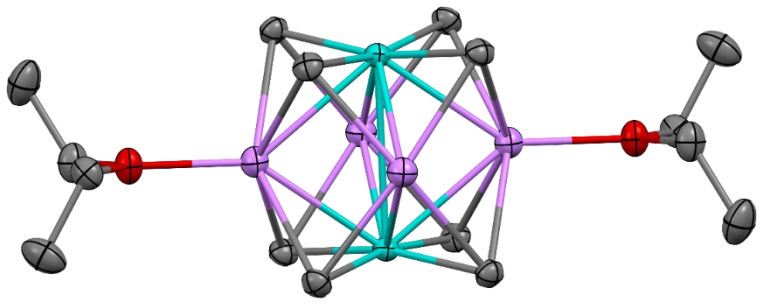

Figure 4.21: Solid state structure of complex **4.16**. ORTEP drawn at 50% probability, hydrogen atoms have been omitted for clarity.

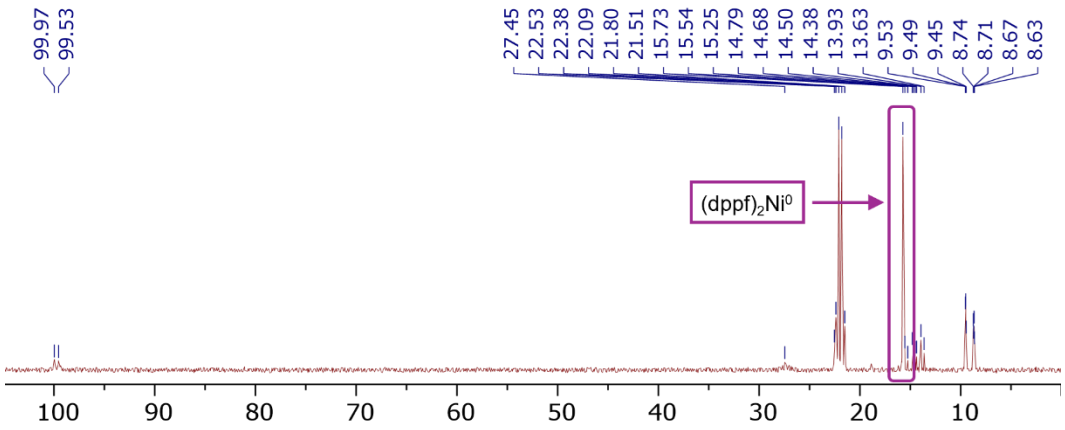

Figure 4.22: ^{31}P $\{^{1}H\}$ NMR spectrum of crude reaction mixture using **4.12** and *n*-BuLi, spectra acquired in C_6D_6.

These results demonstrate that highly reactive, harsh alkylating reagents such as Grignard and organolithium reagents were unsuitable for the direct synthesis of alkyl-Ni(I) complexes, instead promoting extensive decomposition and formation of undesired products. Consequently, milder alkylating reagents were next explored, specifically organoalanes (Scheme 4.18).

Reaction of (dppf)Ni^{I}Cl (**4.12**) with trimethylaluminum ($AlMe_3$) afforded a paramagnetic crude reaction mixture. Crystallization of this mixture yielded complex **4.17** (Scheme 4.18). SC-XRD of **4.17** revealed a cationic dinuclear nickel complex containing a $Ni_2(\mu_2\text{-}CH_2)$ core, in which each nickel center is supported by a dppf ligand and paired with an $AlMeCl_3$ counteranion (Figure 4.23). The hydrogen atoms associated with both the bridging methylene ligand and the counteranion were successfully located in the residual electron density map, confirming the identity of the μ_2-methylene ligand.

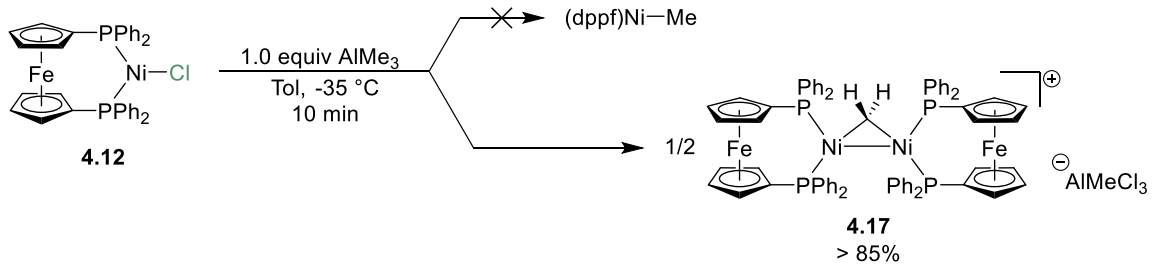

Scheme 4.18: Attempted synthesis of an alkyl-Ni(I) complex using $AlMe_3$.

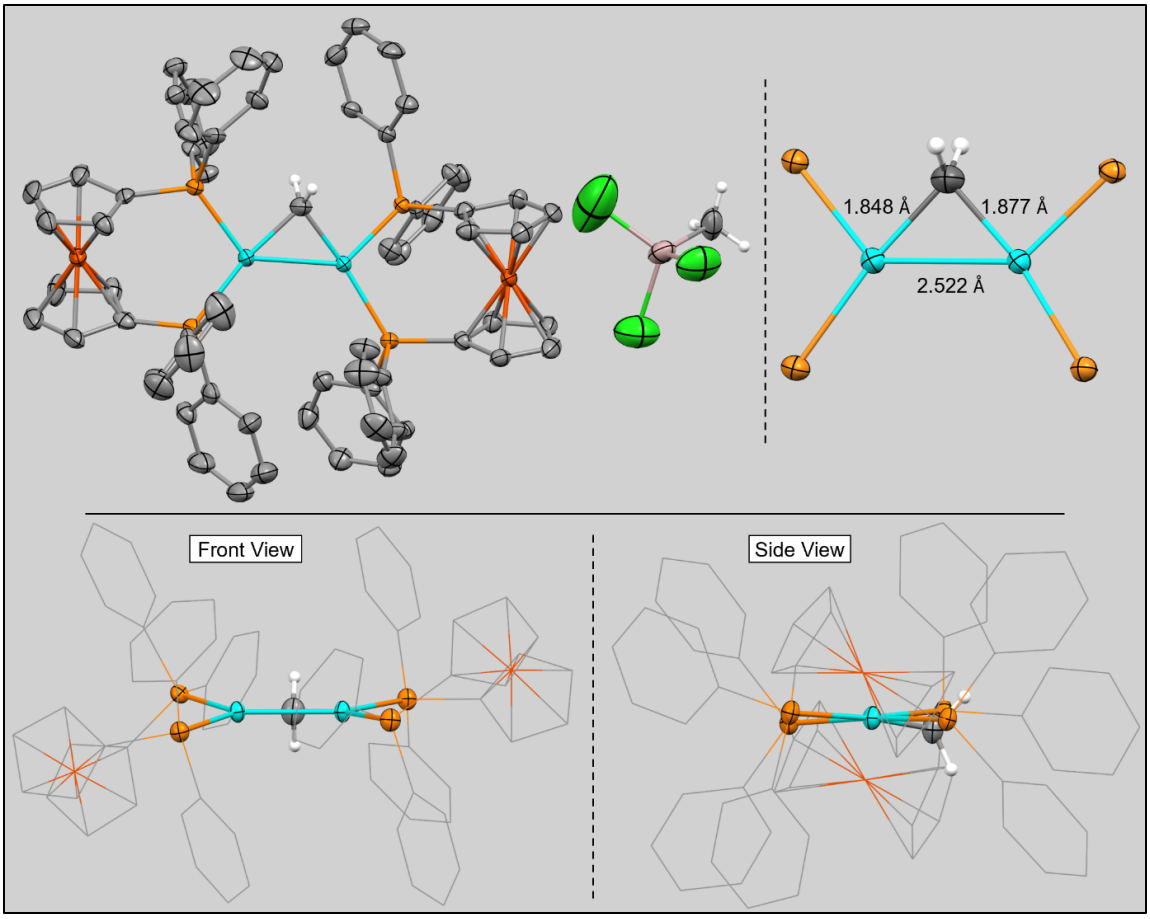

Figure 4.23: Solid state structure of complex **4.17**. ORTEP drawn at 50% probability, select hydrogen atoms and solvent molecules have been omitted for clarity, and hydrogen atoms shown were located with residual electron density.

The solid-state structure of complex **4.17** exhibits a short Ni···Ni separation of 2.522(11) Å, together with nearly equivalent Ni–C bond distances of 1.848(7) Å and 1.877(7) Å (Figure 4.23). The close similarity in the Ni–C bond lengths indicate that the methylene ligand interacts almost symmetrically with both nickel centers, consistent with significant electron delocalization across the $Ni_2(\mu_2\text{-}CH_2)$ core. Although the short Ni···Ni distance is highly suggestive of a direct Ni–Ni bonding interaction, crystallographic data alone is insufficient to definitively establish the presence of a formal Ni–Ni bond. Accordingly, the core is more appropriately described as a delocalized dinuclear system in which the bridging methylene ligand mediates strong electronic coupling between the two nickel centers.

Dinuclear nickel complexes containing unsupported Ni–Ni interactions are themselves exceptionally uncommon because of their inherent instability and high reactivity. Furthermore, the relatively few structurally characterized examples reported are consistently stabilized through multiple bridging ligands, such as halides and hydrides, or by multidentate bridging ligands the reinforce the dinuclear structure.[56–58] In contrast, complexes in which two nickel centers are connected by only a single bridging atom are exceedingly rare, reflecting the difficulty of stabilizing such electron rich metal cores without additional bridging ligand supports.

The electronic structure of **4.17** is equally unusual. Based on the formal bonding description, the $Ni_2(\mu_2\text{-}CH_2)$ core possesses and average nickel oxidation state +1.5, while the similar coordination environments and symmetric Ni–C bond distances indicate extensive electron delocalization between the two metal centers. This description is generally consistent with a Robin-Day Class II or III mixed-valence complex, in which the valence electrons are fully delocalized across both nickel atoms, giving rise to equivalent metal sites with intermediate oxidation states. Robin-Day Class II or III behaviour is generally observed only when metal centers possess highly similar coordination environments and are connected through ligands that are highly conjugated with the metal centers.[59,60] Although definitive assignment of either a Class II or III electronic structure would require further complementary spectroscopic or computational studies. Nevertheless, a localized mixed-valent Ni(I)/Ni(II) complex or presence of a Fe(III) center cannot be conclusively excluded at this time.

Perhaps the most remarkable structural feature of **4.17** is the nature of the bridging ligand itself. Although μ-methylene ligands are well established in organometallic chemistry, they are most commonly encountered in complexes of early transition metals or within multinuclear carbonyl clusters and are typically accompanied by one or more additional bridging ligands.[57,58,61–

[64] To the best of our knowledge, **4.17** represents the first structurally characterized dinuclear nickel complex in which a single μ_2-methylene ligand serves as the sole bridge between two nickel centers. Furthermore, should the short Ni···Ni contact ultimately be confirmed as a formal Ni–Ni bond through complementary computational or spectroscopic investigation, **4.17** would also constitute the first reported example of an unsupported mixed-valence Ni_2 complex bridged exclusively by a methylene ligand. The combination of an unsupported Ni_2 core, a symmetrically bridging μ_2-methylene ligand, and a highly delocalized mixed-valence electronic structure therefore makes **4.17** an exceptionally unusual organometallic complex with no obvious structural precedent in the nickel literature.

To determine if the formation of the unusual $Ni_2(\mu_2\text{-}CH_2)$ core depended on the organoalane stoichiometry, the reaction was repeated using excess $AlMe_3$. Gratifyingly, crystallization again afforded the closely related dinuclear complex **4.18**, differing from **4.17** only in the identity of the organoaluminate counteranion (Scheme 4.19). SC-XRD revealed that **4.18** contains an essentially identical motif, comprising a μ_2-methylene-bridged dinickel core with an average Ni···Ni separation of 2.5119(5) Å and nearly equivalent Ni–C bond lengths of 1.896(11) Å and 1.920(11) Å (Figure 4.24).

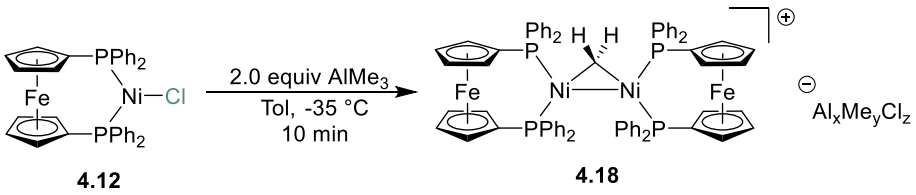

4.12 **4.18**

Scheme 4.19: Attempted synthesis of alkyl-Ni(I) complexes using excess $AlMe_3$.

The reproducible isolation of both **4.17** and **4.18** demonstrates that reaction of **4.12** with $AlMe_3$ consistently converges on formation of the same unprecedented dinuclear framework rather than the desired mononuclear alkyl-Ni(I) intermediate. A plausible mechanism for formation of the $Ni_2(\mu_2\text{-}CH_2)$ core is proposed in Figure 4.25. Initial alkyl transfer from $AlMe_3$ is proposed to

generate a transient alkyl-Ni(I) complex, which subsequently associates to form a dimeric intermediate. This intermediate may then undergo α-hydrogen abstraction, or a related dehydrogenative process, converting one methyl ligand into a bridging μ_2-methylene ligand while transferring the abstracted hydrogen atom to the second bridging methyl ligand. Subsequent elimination of methane would then afford the methylene-bridged dinickel complex **4.17** (Scheme 4.24).

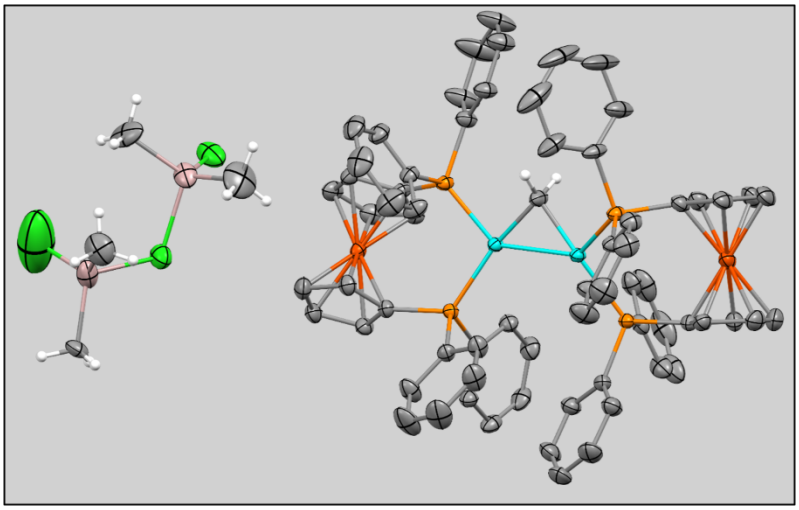

Figure 4.24: Solid state structure of complex **4.18**. ORTEP drawn at 50% probability, select hydrogen atoms and solvent molecules have been omitted for clarity. Hydrogen atoms shown were located with residual electron density. Only one independent molecule per unit cell is drawn

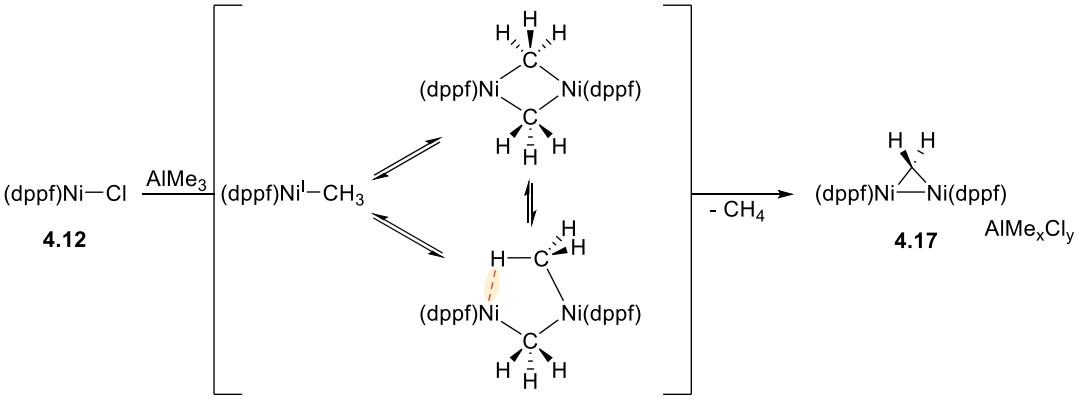

Figure 4.25: Proposed mechanism for the formation of complex **4.17**

To investigate whether steric hinderance could suppress methylene bridge formation and instead favor formation of mononuclear alkyl-Ni(I) complex, triisobutylaluminum (TIBA) was employed as a bulkier alkylating reagent in place of $AlMe_3$ (Scheme 4.20). It was anticipated that the increased steric demand of the isobutyl substituent would inhibit dimerization of the initially formed alkyl-Ni(I) complex while still permitting alkyl transfer to nickel. Unfortunately, reaction of (dppf)$Ni^{I}Cl$ (**4.12**) with TIBA afforded a complex mixture of predominantly paramagnetic species. Despite repeated attempts, no crystalline products suitable for SC-XRD could be obtained, and analysis by NMR spectroscopy failed to identify any diamagnetic byproducts. Consequently, the outcome of the reaction could not be conclusively established.

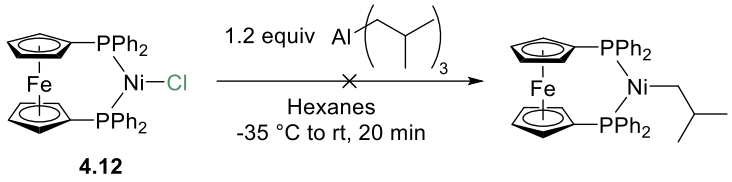

Scheme 4.20: Attempted synthesis of alkyl-Ni(I) complexes using TIBA.

Collectively, these experiments demonstrated that although trialkylalane reagents readily react with (dppf)$Ni^{I}Cl$ (**4.12**), they do not provide a practical route to the desired isolable alkyl-Ni(I) complexes. Instead, under the conditions examined, $AlMe_3$ reproducibly promotes formation of the unprecedented μ_2-methylene-bridged dinickel complexes **4.17** and **4.18**, whereas increasing the steric bulk of the organoalane reagent results in only ill-defined paramagnetic mixtures.

As direct synthesis of an alkyl-Ni(I) complex proved challenging due to the unanticipated reactivity of organometallic alkylating reagents, an alternative strategy was pursued. Rather than attempting to prepare the alkyl-Ni(I) complex directly, attention was instead directed toward the synthesis of a mechanistically relevant surrogate complex.

Under the proposed Ni(I)/Ni(III) catalytic cycle, complex (**IV**) undergoes base promoted transmetalation with the alkyl borane to generate the corresponding alkyl-Ni(I) species (**V**) (Figure 4.26). This transformation is not expected to occur through a single concerted step, but rather through a sequence of elementary processes.

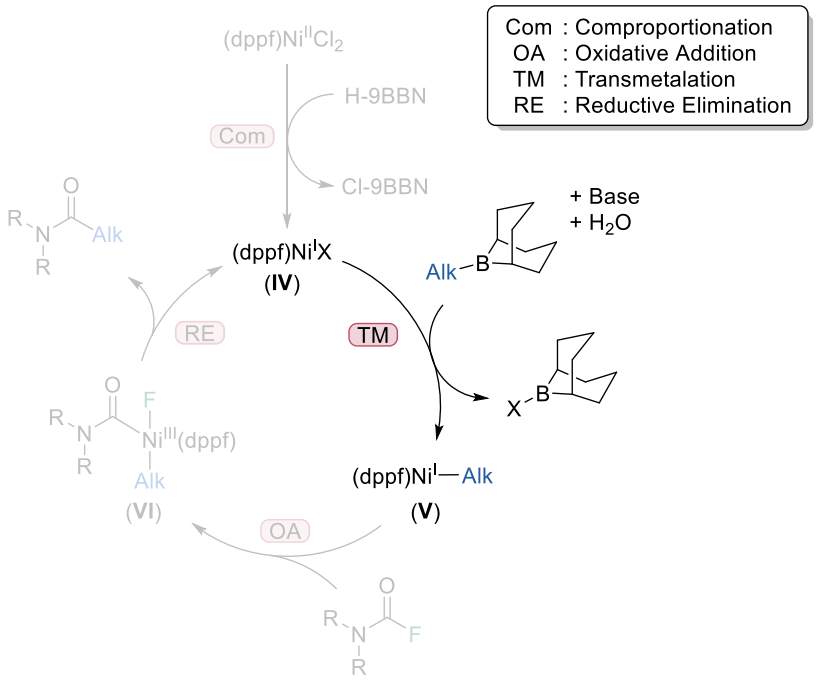

Figure 4.26: Proposed mechanism for a Ni(I)/Ni(III) Suzuki cross-coupling.

Two plausible transmetalation pathways are proposed and illustrated in Figure 4.27. Both pathways require the in situ generation of potassium hydroxide (KOH), which arises from the equilibrium between K_2CO_3 and H_2O. In Path A, Ni(I)–X complex **IV** first undergoes ligand exchange with KOH to generate Ni(I)-OH complex **IV-A** together with KX. The hydroxide ligand of **IV-A** subsequently coordinates to the Lewis acidic alkyl-9-BBN reagent to form hydroxoborate complex **IV-C**. Transfer of the alkyl fragment from boron to nickel then occurs, liberating 9-bora-bicyclo[3.3.1]nonan-9-ol (HO-9-BBN) and producing alkyl-Ni(I) complex **V**.

Alternatively, Path B proceeds through initial reaction of KOH with alkyl-9-BBN to generate a hydroxoborate species, which subsequently coordinates to Ni(I)–X complex **IV** to form

intermediate **IV-B**. Elimination of KX then affords the common hydroxoborate complex **IV-C**, after which alkyl transfer to nickel proceeds identically to Path A, yielding alkyl-Ni(I) complex **V**.

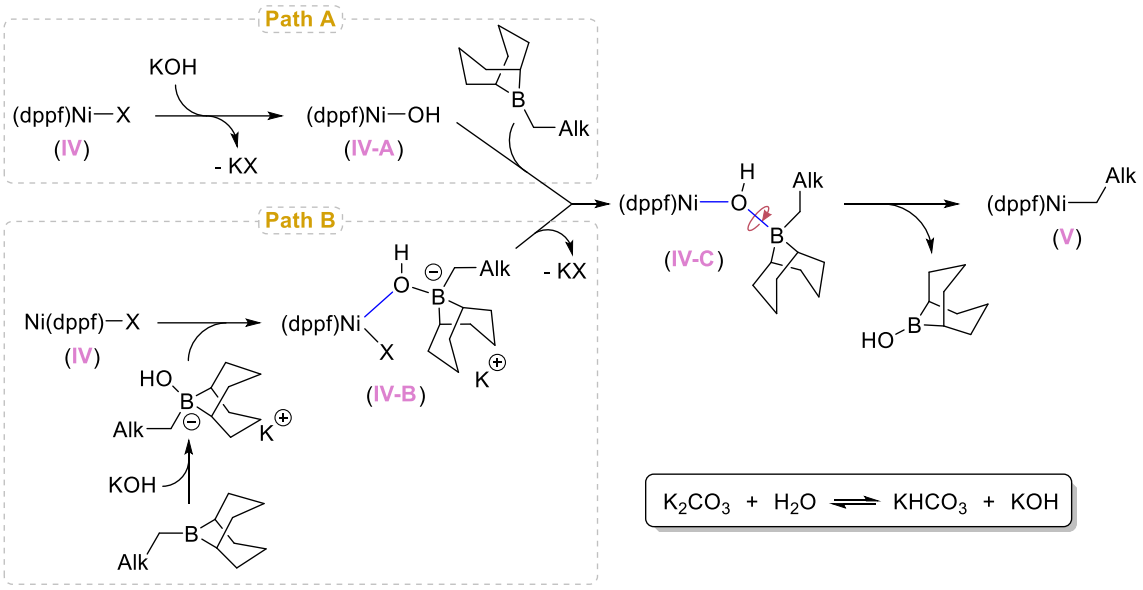

Figure 4.27: Proposed mechanism for transmetalation in a Ni(I)/Ni(III) catalytic cycle.

Importantly, although Paths A and B differ in the order of elementary steps, both converge at the common hydroxoborate intermediate complex **IV-C** prior to alkyl transfer. Because this intermediate is common to both proposed transmetalation pathways, efforts were directed toward its synthesis as a mechanistically relevant surrogate for the otherwise highly reactive alkyl-Ni(I) intermediate **V**.

In anticipation that the targeted hydroxoborate-Ni(I) complex would be paramagnetic and therefore difficult to characterize be NMR spectroscopy, SC-XRD served as the primary means of characterization. Accordingly, a series of alkyl-9-BBN reagents and corresponding hydroxoborate salts bearing different alkyl substituents were prepared. Variation of the alkyl substituents was expected to alter the solubility, intermolecular interactions, and crystal-packing behaviour of the resulting complex while preserving the proposed hydroxoborate-Ni(I) core, thereby maximizing the likelihood that at least one derivative would afford crystals suitable for SC-XRD analysis.

Hydroboration of several alkenes with 0.98 equivalents of H-9BBN furnished the corresponding alkyl-9-BBN derivatives in excellent isolated yields ranging from 60-96% (Scheme 4.21). The products were isolated as either colorless oils or powdery solids, all of which exhibited considerable pyrophoricity upon exposure to air. Single crystals suitable for SC-XRD were readily obtained by cooling of a near saturated THF solution of **4.22** to -35 °C for several days (Figure 4.28 **A**).

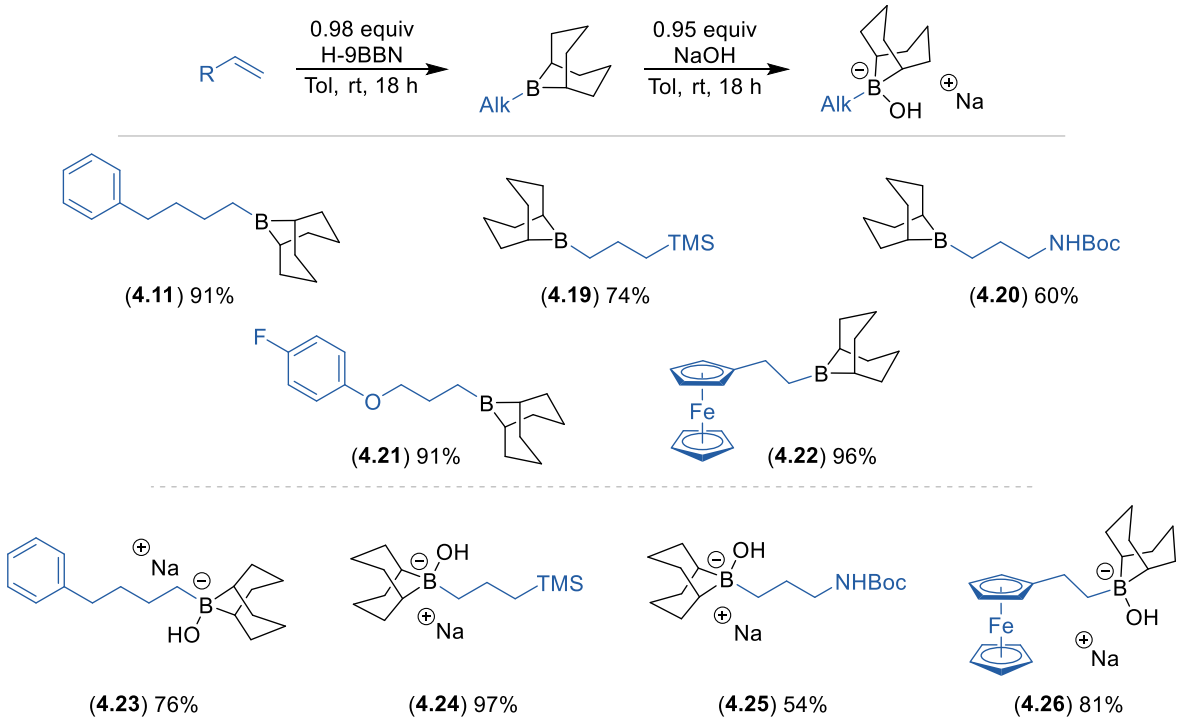

Scheme 4.21: Scope of synthesized alkyl-9-BBN and hydroxoborate salts. Reported are isolated yields.

The corresponding hydroxoborate salts were subsequently prepared by treatment of the alkyl-9-BBN derivatives with 0.95 equivalents of NaOH, affording the desired products in excellent isolated yields ranging from 54 to 97% (Scheme 4.21). All hydroxoborate salts readily purified by recrystallization from pentane at -35 °C overnight to give solid products that were moderately stable to ambient atmosphere for several hours. Single crystals suitable for SC-XRD were acquired by cooling a saturated THF solution of **4.26** to -35 °C overnight. The solid-state

structure revealed the presence of an OH bound to the borane with the hydrogen atom being successfully located in the residual electron density map, additionally it was found that the hydroxoborate product exists as a dimer in the solid state (Figure 4.28 **B**).

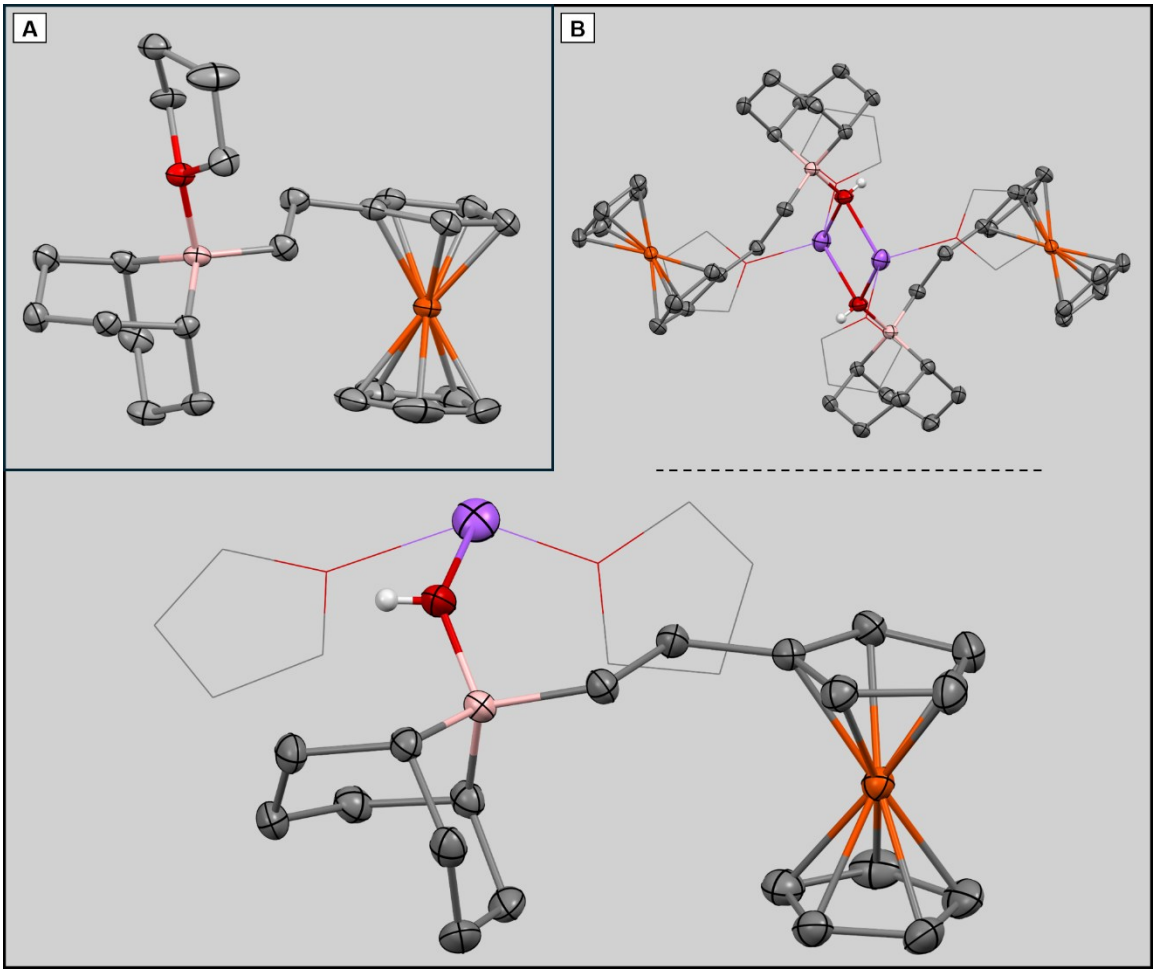

Figure 4.28: Solid-state structures of **4.22** (**A**) and **4.26** (**B**). ORTEP drawn at 50% probability, select hydrogen atoms have been omitted for clarity. Hydrogen atoms shown were successfully located in the residual electron density map.

Interestingly, when excess H-9BBN was not removed following hydroboration and the crude alkyl-9-BBN product was treaded directly with excess of NaOH, formation of both the desired hydroxoborate salt (**4.26**) and boroxane salt (**4.27**) was observed (Scheme 4.22).

It was found that dissolution of either the alkyl-9-BBN derivatives or hydroxoborate salts in ethereal solvents resulted in irreversible coordination of solvent molecules to either the Lewis

acidic boron center or the sodium cation. Once coordinated, these solvent molecules could not be displaced, even after prolonged evacuation under high vacuum (<10 mTorr). Consequently, synthesis and purification of these compounds was restricted to hydrocarbon-based solvents such as pentane and toluene.

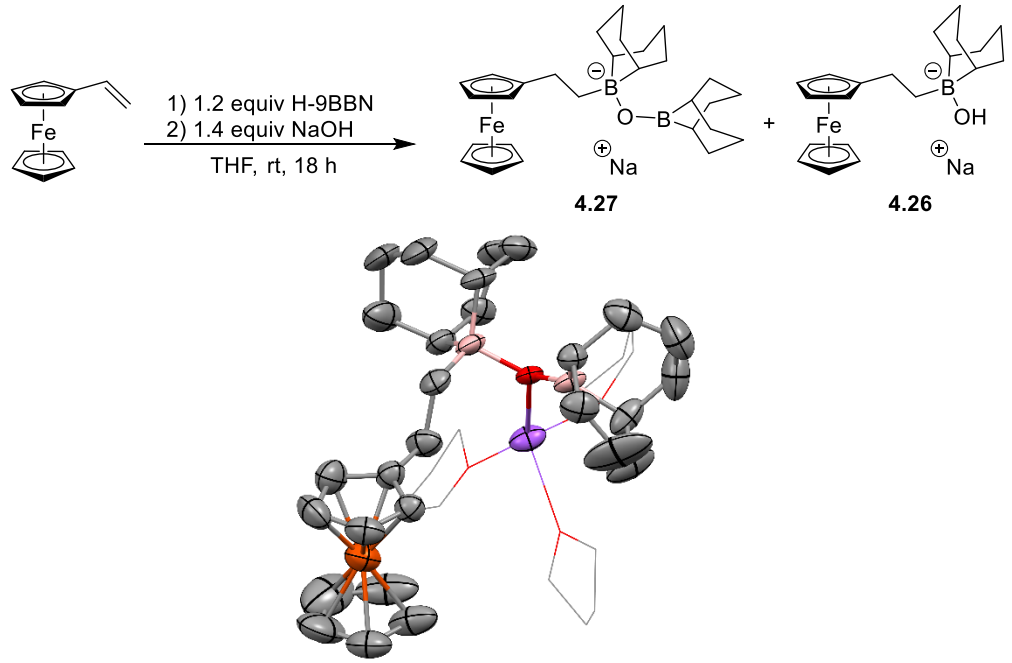

Scheme 4.22: Accidental synthesis of boroxane **4.27** due to the presence of excess H-9BBN and hydroxide when attempting to synthesize hydroxoborate salt **4.26**. ORTEP drawn at 50% probability, hydrogen atoms have been omitted for clarity.

With several hydroxoborate salts in hand, efforts were directed towards the synthesis of hydroxoborate-Ni(I) complexes. Owing to the paramagnetic nature of both starting Ni(I) complex and the anticipated products, NMR spectroscopy was unsuitable for reaction monitoring. Instead, the work-up of the reaction mixtures involved complete removal of solvent, followed by sequential extraction with solvents of increasing polarity. The extraction procedure started with pentane and finished with THF, which typically resulted in the complete dissolution of any remaining residue. Each extract was filtered through oven-dried glass filter paper to remove any insoluble material, concentrated, and cooled to –35 °C for several days. To identify the crystalline species formed, at least one representative of every visually distinct crystal type (distinguished by color, morphology,

or both) was selected and analyzed by SC-XRD. Thus, when crystals of different colors and/or morphologies (e.g., blocks, plates, needles) were present, at least one representative of each distinct type was examined.

Unfortunately, all salt metathesis reactions between (dppf)Ni^{I}Cl (**4.12**) and hydroxoborate salts **4.23**, **4.25** or **4.26** were either unsuccessful or inconclusive. The only crystalline material that could be definitively identified was the recovered starting material **4.12**, indicating that ligand exchange with the hydroxoborate salts did not occur to any appreciable extent under the conditions investigated (Scheme 4.23).

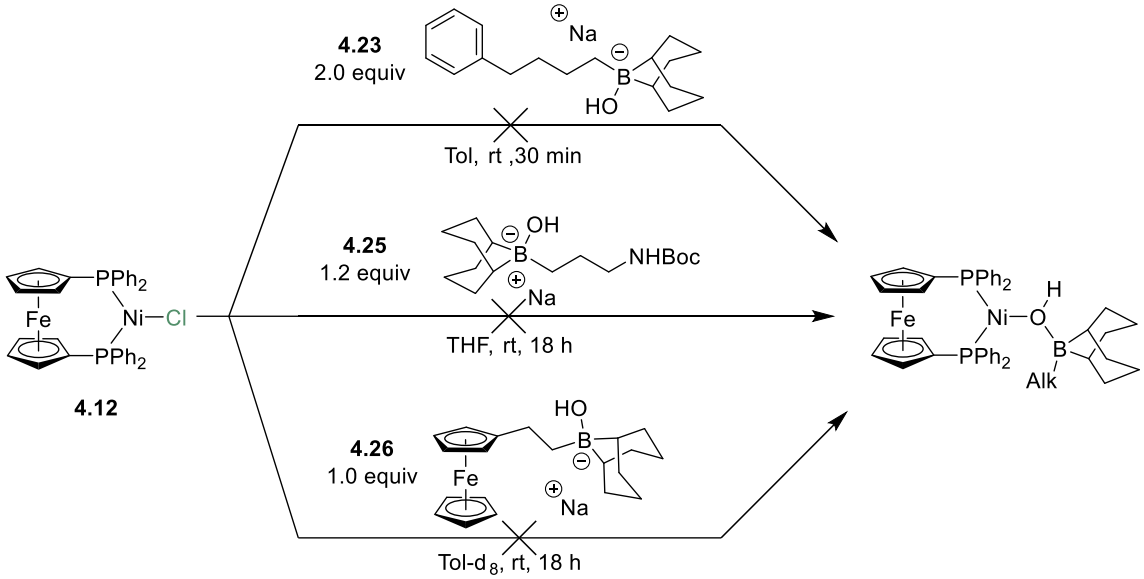

Scheme 4.23: Reaction conditions used to attempt the synthesis of hydroxoborate-Ni(I) complexes.

It was therefore hypothesized that increasing the electrophilicity of the nickel center by generating a cationic Ni(I) species would facilitate coordination of the hydroxoborate salt. Accordingly, (dppf)Ni^{I}-OTf complex (**4.28**) was prepared by reaction of (dppf)Ni^{I}Cl (**4.12**) with an excess amount of trimethylsilyl trifluoromethanesulfonate (TMSOTf), producing **4.28** and trimethylsilyl chloride (TMSCl) as a byproduct (Scheme 4.24). Upon mixing (dppf)Ni^{I}Cl (**4.12**) with TMSOTf, the initially pale-yellow suspension gradually turned to a tan colour over

approximately 30 minutes. The mixture was further stirred for an additional 18 hours to ensure complete conversion of **4.12**. The product was purified by removal of all volatiles under reduced pressure, followed by repeated washing with pentane, and drying under high vacuum (<10 mTorr) for at least 24 hours to remove residual TMSOTf and TMSCl. This procedure afforded **4.28** as a pale tan solid in 90% isolated yield.

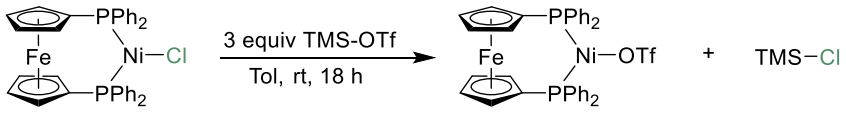

4.12 **4.28** 90%

Scheme 4.24: Synthesis of **4.28** from **4.12** with excess TMS-OTf.

With **4.28** in hand, the reaction with hydroxoborate salt **4.24** in hexanes at room temperature afforded the desired product hydroxoborate-Ni(I) complex **4.29** in a 48% isolated yield (Scheme 4.25). Complex **4.29** was successfully crystallized and analyzed by SC-XRD. However, the collected diffraction data exhibited significant complex disorder that could not be satisfactorily modeled, preventing location of the hydroxyl hydrogen atom using residual electron density. Consequently, the solid-state structure of **4.29** is presented only to illustrate the structural connectivity of the complex (Figure 4.29). Nevertheless, the structure clearly demonstrates that coordination of the hydroxoborate ligand to the Ni(I) center had occurred, confirming that synthesis of the targeted hydroxoborate-Ni(I) complex was feasible. These results suggested that improved crystallization conditions, rather than an alternative synthetic approach, would likely be required to conclusively establish the hydroxoborate-Ni(I) complex connectivity.

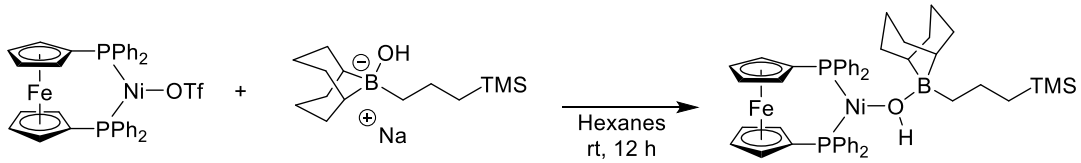

4.28 **4.24** 1.1 equiv **4.29** 48%

Scheme 4.25: Reaction conditions to prepare complex **4.29**.

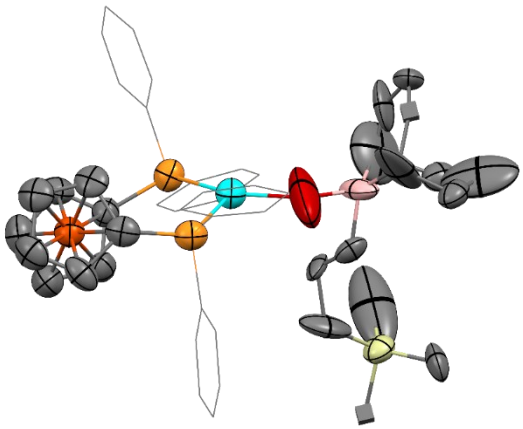

Figure 4.29: Solid-state structures of **4.29**. ORTEP drawn at 50% probability. Due to poor data quality and significant disorder, solid-state structure shown only for structural connectivity.

In an attempt to improve crystal quality, hydroxoborate salt **4.25**, bearing an NHBoc functionality, was next investigated. It was anticipated that intermolecular hydrogen-bonding between carbamate groups might aid in reducing structural disorder and promote higher-quality crystal growth. A product tentatively assigned as hydroxoborate-Ni(I) complex **4.30** was isolated in 86% yield (Scheme 4.26). Preliminary SC-XRD analysis provided some support for the proposed structure; however, severe disorder in the alkylborane portion of the complex prevented complete structural refinement. The EPR spectroscopic data for **4.30** was consistent with that of complexes **4.29** and **4.31**, further supporting the assignment of **4.30**. Further characterization by elemental analysis is planned to assess the bulk composition and purity, while HRMS is expected to provide additional support for the proposed molecular formula of **4.30**.

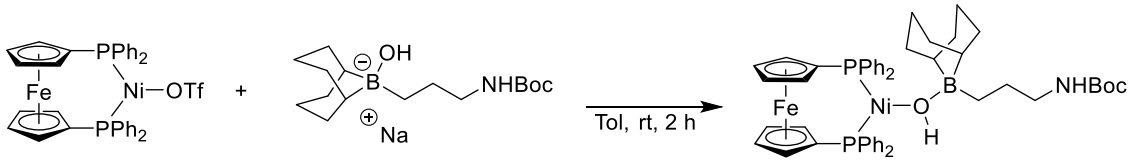

4.28 | **4.25** 1.5 equiv | **4.30** 86%

Scheme 4.26: Reaction conditions to prepare complex **4.30**.

Attention was next directed toward ferrocene-containing hydroxoborate salt **4.26**, with the expectation that the larger and more rigid alkyl substituent would promote improved crystal

packing. Gratifyingly, treatment of complex **4.28** with hydroxoborate **4.26** afforded hydroxoborate-Ni(I) complex **4.31** in a 75% yield (Scheme 4.27).

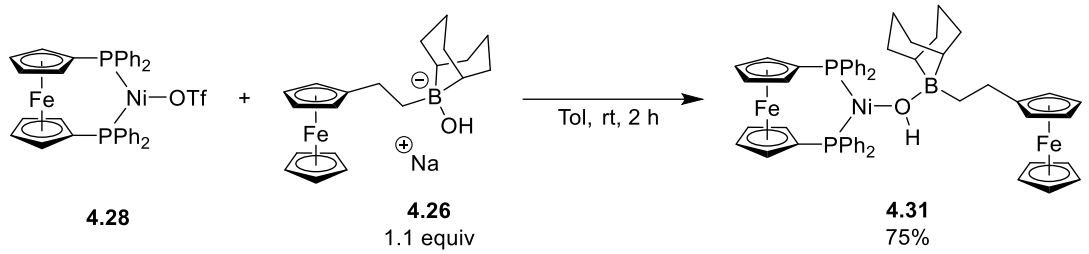

4.28 | **4.26** 1.1 equiv | **4.31** 75%

Scheme 4.27: Reaction conditions to prepare complex **4.31**.

Single crystals suitable for SC-XRD were successfully grown by slow cooling of a saturated toluene solution of complex hydroxoborate-Ni(I) complex (**4.31**) to –35 °C over several days. The solid-state structure unambiguously confirmed formation of the anticipated hydroxoborate-Ni(I) complex with no observable structural disorder present within the crystal lattice (Figure 4.30). Importantly, the hydrogen atom associated with the hydroxoborate ligand was located directly from the residual electron density map rather than being positioned geometrically, providing definitive crystallographic confirmation that the ligand remains protonated upon coordination to nickel.

The nickel center adopts a trigonal planar geometry, with a sum of angles around nickel of 358.8°, consistent with the three-coordinate Ni(I) complexes described throughout this work. The Ni–O bond distance of 1.907(5) Å, together with Ni–P bond lengths of 2.202(2) Å and 2.222(2) Å, confirms strong coordination of the hydroxoborate oxygen to the Ni(I) center while maintaining an intact B–O bond (1.581(10) Å). Furthermore, the large Ni–O–B bond angle of 134.4(4) ° indicates efficient orbital overlap between the oxygen donor and both the Lewis acidic boron and electron-rich Ni(I) center, providing an arrangement primed for subsequent alkyl transfer.

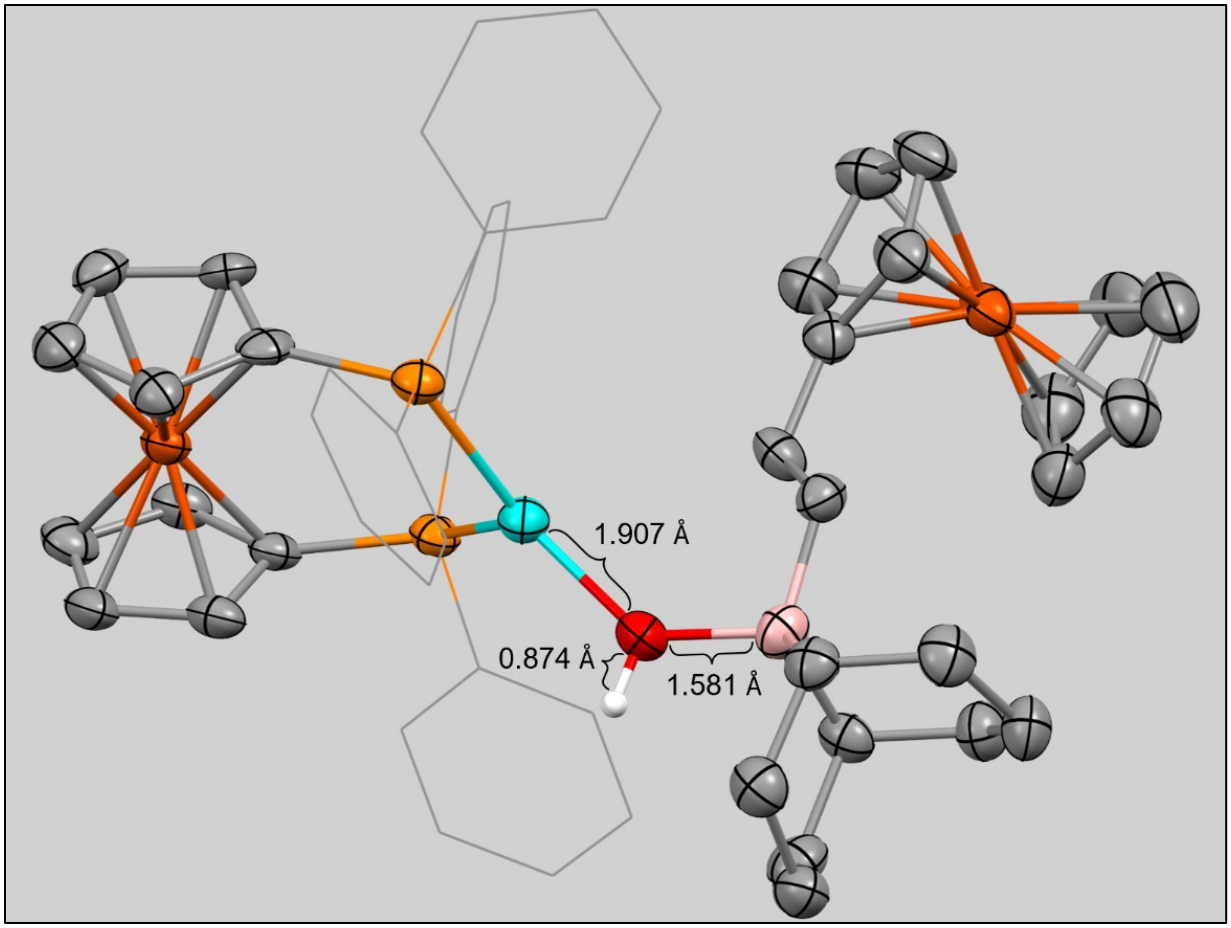

Figure 4.30: Solid-state structures of complex **4.31**. ORTEP drawn at 50% probability, select hydrogen atoms have been omitted for clarity. Hydrogen atoms shown were located from the residual electron density map.

To the best of our knowledge, hydroxoborate-Ni(I) complex (**4.31**) represents the first structurally characterized hydroxoborate-Ni(I) complex. Metal-hydroxoborate intermediates have frequently been proposed as potential intermediates in Suzuki cross-coupling reactions proceeding through either M(0)/M(II) and M(I)/M(III) catalytic cycles. Accordingly, isolation of **4.31** provides direct experimental evidence that Ni(I) hydroxoborate complexes can be synthesized and isolated, and that they possess sufficient stability to permit full structural characterization. Although, hydroxoborate-Ni(I) complex (**4.31**) is not itself the targeted alkyl-Ni(I) intermediate, it constitutes a well-defined surrogate complex that closely models the proposed transmetalation intermediate preceding C–B bond cleavage. The successful isolation and crystallographic characterization of

hydroxoborate-Ni(I) complex (**4.31**) provide valuable experimental support for the feasibility of this key step in the proposed Ni(I)/Ni(III) catalytic cycle.

To determine whether complex **4.31** (**IV-C**) could undergo conversion to the corresponding alkyl-Ni(I) species in situ, a solution of **4.31** was heated at 70 °C and periodically monitored by ^{11}B $\{^{1}H\}$ NMR spectroscopy. Owing to the paramagnetic nature of both **4.31** (**IV-C**) and the proposed alkyl-Ni(I) intermediate (**V**), direct observation of either species by NMR spectroscopy was not possible. Instead, the formation of HO-9-BBN, the expected byproduct of transmetalation, was monitored as an indirect probe for generation of the alkyl-Ni(I) complex (Figure 4.31).

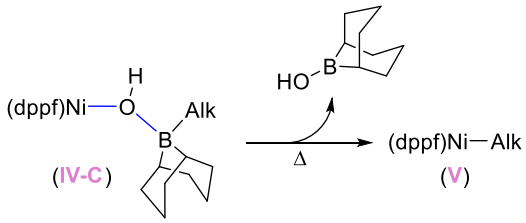

Figure 4.31: Proposed mechanism for the formation of complex **V** from **IV-C**.

Initial analysis of hydroxoborate-Ni(I) complex (**4.31**) by ^{11}B $\{^{1}H\}$ NMR spectroscopy prior to heating indicated no detectable HO-9-BBN in solution and only a trace quantity of free alkyl-9-BBN (Figure 4.32). The absence of HO-9-BBN prior to heating indicates that any subsequently observed hydroxoborane may likely arise from the thermal decomposition of hydroxoborate-Ni(I) complex (**4.31**), supporting the possible in situ formation of alkyl-Ni(I) (**V**). Upon heating at 70 °C for 30 minutes, a distinct resonance corresponding to HO-9-BBN appeared with a chemical shift of 56 ppm, consistent with its reported chemical shift in C_6D_6.[65] Continued heating for 16 hours resulted in substantial formation of HO-9-BBN together with only a minor quantity of free alkyl-9-BBN (Figure 4.32). The appearance and progressive accumulation of HO-9-BBN suggests that the hydroxoborate-Ni(I) complex may undergo transmetalation upon heating to form the corresponding alkyl-Ni(I) complex. Such reactivity could allow **4.31** to serve as a

surrogate for the desired alkyl-Ni(I) intermediate. The catalytic performance of complex **4.31** is further discussed alongside other prepared catalytically related complexes in Section 4.4.5.5.

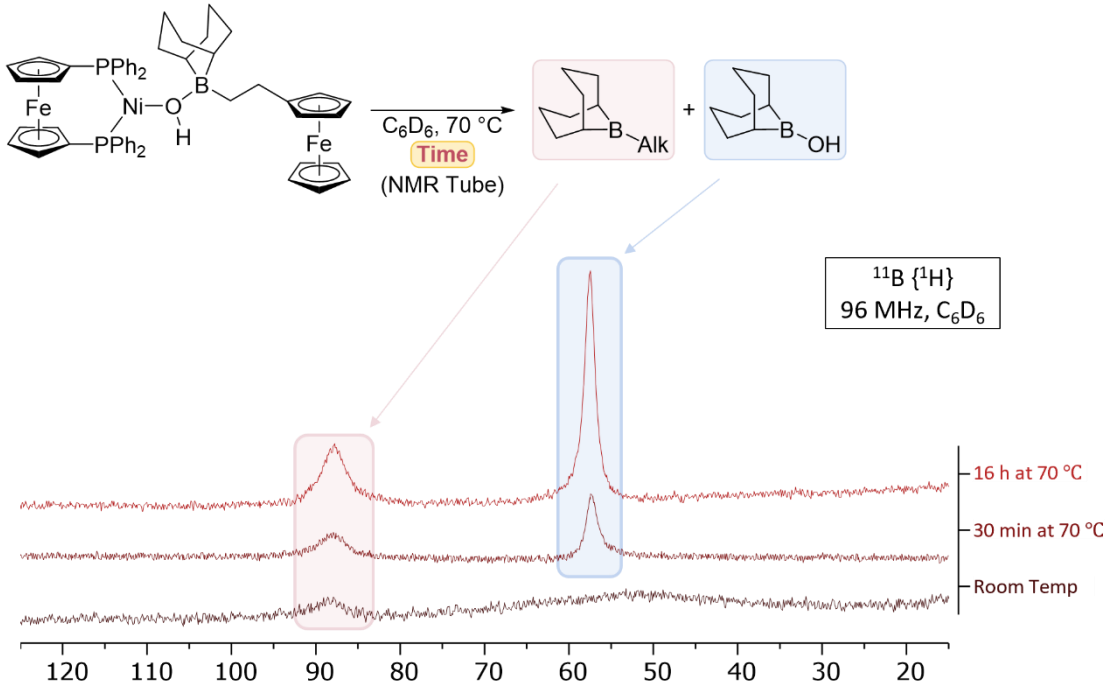

Figure 4.32: ^{11}B $\{^{1}H\}$ NMR spectra of complex **4.31** heated at 70 °C overtime. Spectra acquired in C_6D_6.

During the initial attempts to prepare an alkyl-Ni(I) complex using *i*-PrMgBr, formation of the dinuclear Ni(I) complex $[(dppf)Ni^{I}(Cl)]_2(\mu\text{-}dppf)$ (**4.14**) was also observed. Because generation of $(dppf)Ni^{I}Cl$ during the catalyst activation step is believed to be essential to catalytic activity, **4.14** was considered a potential catalytically relevant complex and was therefore synthesized independently. This was accomplished by first reducing $(dppf)NiCl_2$ (**4.10**) with two equivalents of sodium naphthalenide in the presence of one equivalent of free dppf to afford $(dppf)_2Ni^{0}$ (**4.15**) in a 46% isolated yield (Scheme 4.28).[55]

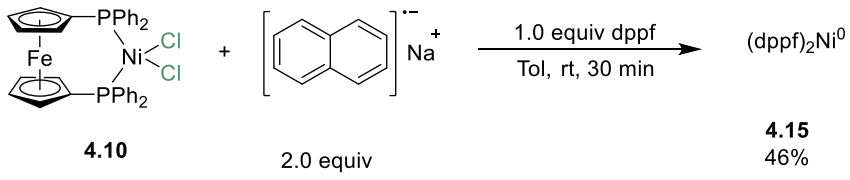

Scheme 4.28: Synthetic conditions for the preparation of complex **4.15**.

$(dppf)_2Ni(0)$ (**4.15**) was subsequently reacted with 1.2 equivalents of **4.10**, undergoing comproportionation to afford $[(dppf)Ni^{I}(Cl)]_2(\mu\text{-dppf})$ (**4.14**) in a 73% isolated yield (Scheme 4.29). As with hydroxoborate-Ni(I) complex **4.31**, catalytic performance of both $(dppf)_2Ni(0)$ (**4.15**) and **4.14** is discussed in Section 4.4.5.5.

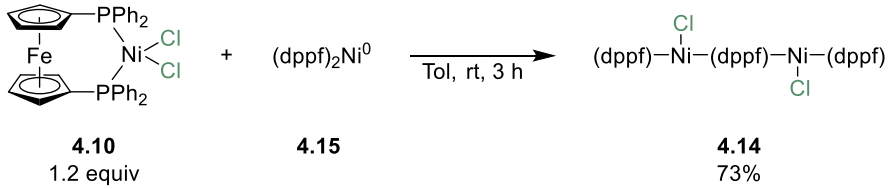

Scheme 4.29: Conditions used to synthesize complex **4.14**.

The final catalytically relevant Ni(I) complex which was targeted was $(dppf)Ni^{I}F$ (**4.32**), which is proposed to form following reductive elimination (Figure 4.33, **I**). Similar to $(dppf)Ni^{I}Cl$, this complex was expected to provide insight into the reactivity and catalytic competence of nickel(I) fluoride complex, particularly its direct transmetalation ability.[66,67]

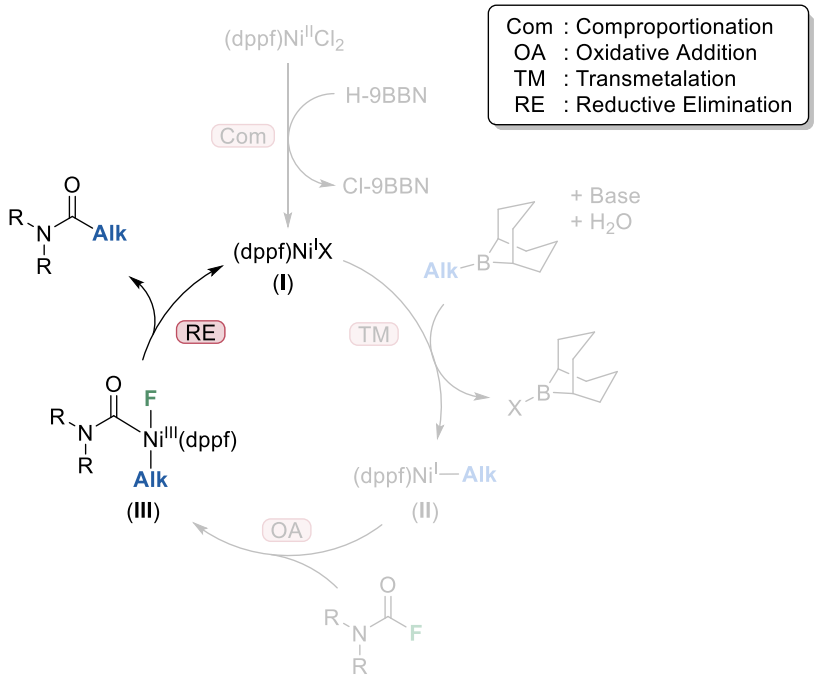

Figure 4.33: Proposed mechanism for a Ni(I)/Ni(III) Suzuki cross-coupling.

Initial attempts to prepare **4.32** involved carried direct halide exchange from **4.12** using a variety of inorganic and organic fluoride sources (Scheme 4.30). However, no detectable conversion was observed, even after several days of reaction. Because the successful synthesis of the hydroxoborate-Ni(I) complexes required first generation of the cationic triflate complex **4.28**, it was anticipated that a similar strategy might facilitate formation of **4.32**.

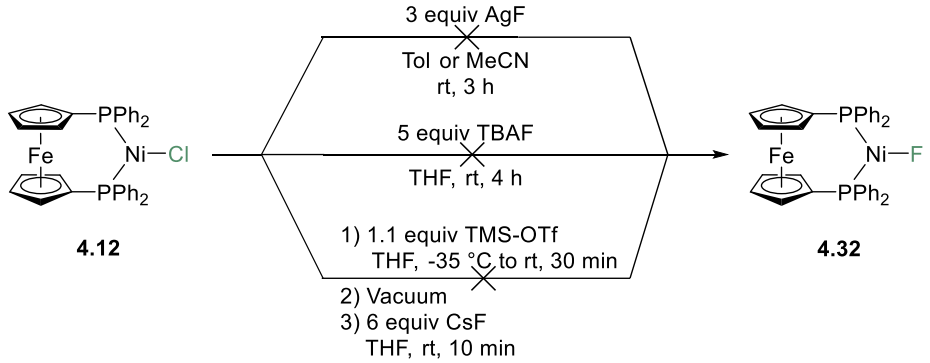

Scheme 4.30: Reaction conditions used to attempt the synthesis of complex **4.32**.

Accordingly, **4.28** was treated with excess KF or CsF for 20 hours (Scheme 4.31). Unfortunately, the formation of **4.32** was not detected. Instead, only trace quantities of complex $(dppf)_2Ni(0)$ (**4.15**) were observed, indicating decomposition rather than productive fluoride coordination. These results led to the abandonment of the ligand exchange strategy in favor of an alternative synthetic approach.

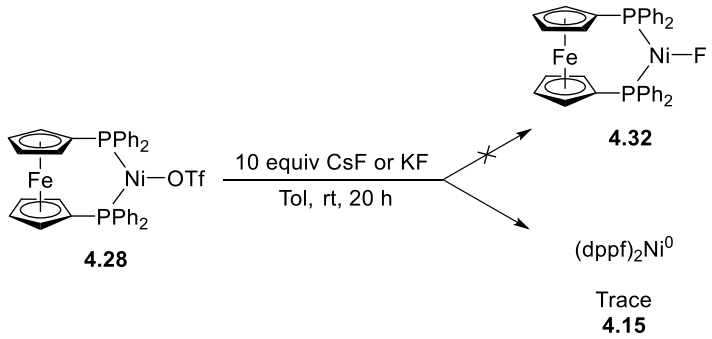

Scheme 4.31: Attempted synthesis of complex **4.32** from **4.28**.

Because H-9BBN was found to selectively reduce $(dppf)Ni^{II}Cl_2$ to $(dppf)Ni^{I}Cl$ (**4.12**), it was reasoned that an analogous reduction of $(dppf)Ni^{II}F_2$ (**4.33**) might provide direct access to

4.32. Accordingly, the synthesis of **4.33** was first attempted through direct coordination of dppf to NiF_2 in refluxing ethanol, using conditions analogous to those employed for preparation of $(dppf)Ni^{II}Cl_2$ (Scheme 4.32). However, no detectable reaction appeared to occur, even after two weeks of reflux. This lack of reactivity was speculated to be due to the exceptionally low solubility of NiF_2.

In an attempt to remediate this issue, efforts were directed toward preparing $(DME)NiF_2$, which was anticipated to convert NiF_2 into a more soluble form bearing a labile DME ligand (Scheme 4.32). This was attempted using conditions analogous to those employed for $(DME)NiCl_2$. Again, no detectable product formation was observed.

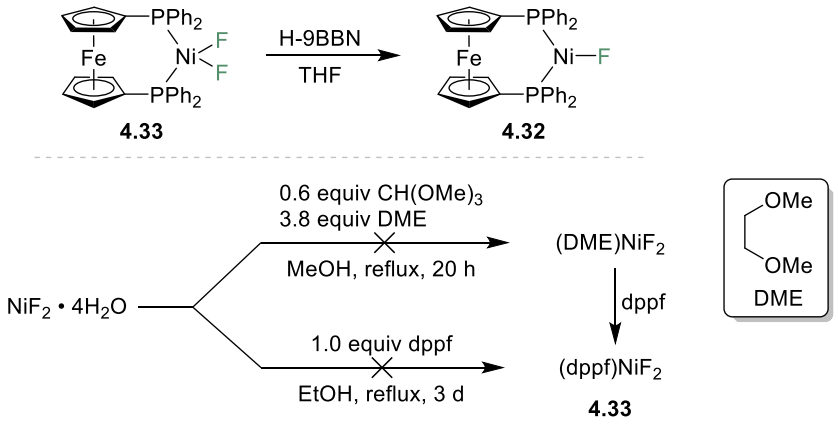

Scheme 4.32: Synthetic conditions used in the attempted synthesis of complex **4.33**.

Because TMEDA is a commonly employed labile bidentate ligand capable of improving metal salt solubility through ligation, coordination of TMEDA to NiF_2 was next explored. Refluxing NiF_2 in isopropanol (IPA) with two equivalents of TMEDA afforded a turquoise, highly soluble, diamagnetic fluorine-containing complex in 14% isolated yield (Scheme 4.33). SC-XRD analysis revealed that the product was not the anticipated mononuclear $(TMEDA)NiF_2$ (**4.34**), but instead the trinuclear nickel(II) fluoride cluster $[(Ni(TMEDA))_3(\mu_2\text{-}F)_3(\mu_3\text{-}F)_2]F{\bullet}3HF$ (**4.35**) (Figure 4.34).

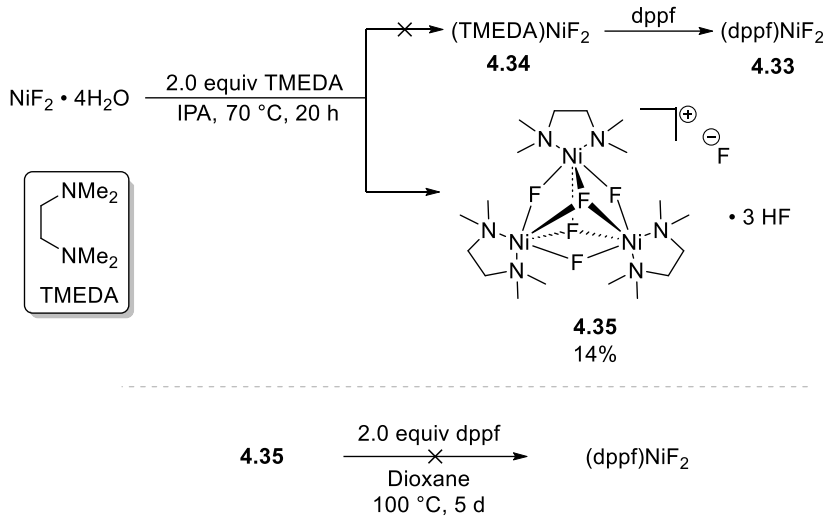

Scheme 4.33: Attempted synthesis of (TMEDA)NiF_2 and (dppf)NiF_2.

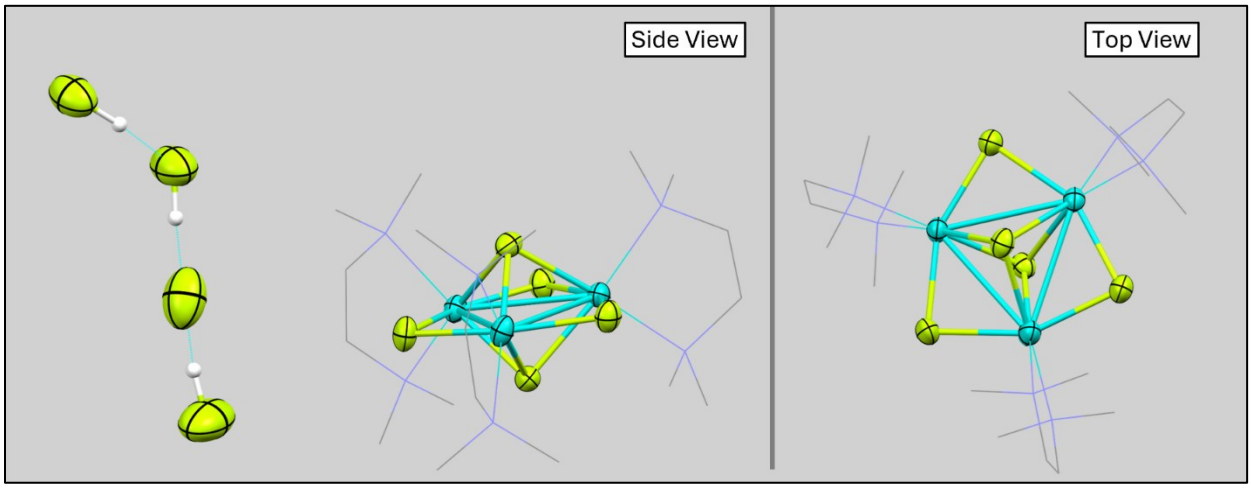

Figure 4.34: Solid state structure of complex **4.35**. ORTEP drawn at 50% probability, select hydrogen atoms have been omitted for clarity, and hydrogen atoms shown were located with residual electron density.

The cationic cluster consists of three nickel(II) centers, each chelated to a single TMEDA ligand and interconnected through a network of five bridging fluoride ligands. This structure is comprised of three μ_2-fluoride ligands spanning the edges of the triangular Ni_3 core, and two μ_3-fluoride ligands capping the cluster above and below the Ni_3 plane. As a result, each nickel center adopts a distorted octahedral coordination geometry. The cationic cluster is charge-balanced by an external fluoride anion and it co-crystallized with three equivalents of HF. Because repeated

attempts to prepare either **4.33** or **4.32** proved unsuccessful, no further investigation into nickel(I) fluoride complexes was undertaken.

Finally, during attempts to synthesize various Ni(I) complexes, it was observed that prolonged storage of (dppf)Ni^{I}Cl (**4.12**) in DCM resulted in the formation of emerald-green crystals from an initially homogenous yellow solution (Scheme 4.34). SC-XRD analysis identified these crystals as **4.36**, however the exact mechanism in which **4.36** formed is not presently clear (Figure 4.35).

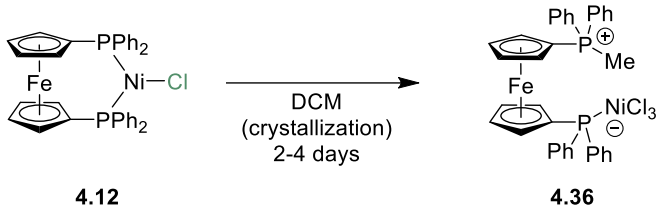

4.12 **4.36**

Scheme 4.34: Reaction conditions for the formation of complex **4.36**.

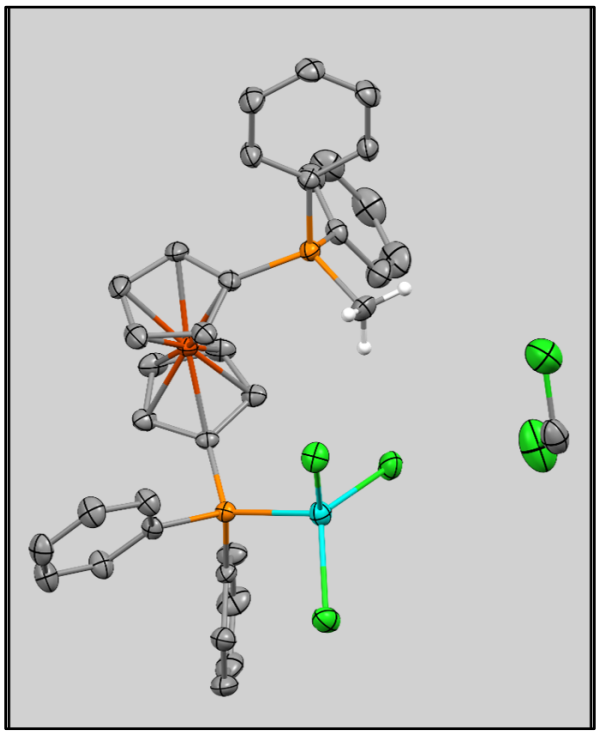

Figure 4.35: Solid state structure of complex **4.36**. ORTEP drawn at 50% probability, select hydrogen atoms have been omitted for clarity, and hydrogen atoms shown were located with residual electron density.

4.4.4.3. Synthesis of Catalytically Relevant Ni(II) Complexes

With the successful isolation of two Ni(II) oxidative addition complexes bearing tricyclohexylphosphine (PCy_3) ligands described in Section 4.4.1, PCy_3 was initially considered a promising ligand system for the mechanistic investigation of carbamoyl–NiF oxidative addition complexes. However, evaluation of PCy_3 in the ligand screening study (Section 4.4.2.1) revealed poor catalytic performance, affording the amide product in only 6% yield. Consequently, PCy_3 was deemed unsuitable as a representative ligand for mechanistic studies. In contrast, dppf was the only ligand evaluated that exhibited excellent catalytic activity, it was therefore selected as the ligand framework for future complex preparation and mechanistic studies. Initial efforts focused on the preparation of a CMF–Ni oxidative addition complex using *N*-benzyl-*N*-(2-pyridyl) CMF (**2.2o**), where the directing group was expected to facilitate oxidative addition.

Upon heating $Ni(COD)_2$, dppf and CMF **2.2o** at 50 °C for 1 hour, the desired oxidative addition complex **4.37** was obtained in 80% isolated yield (Scheme 4.35). Analysis of the afforded product by multinuclear NMR spectroscopy revealed broad singlets in both the ^{19}F spectra (–366 ppm) and ^{31}P spectra (–9 ppm) (Figure 4.36).

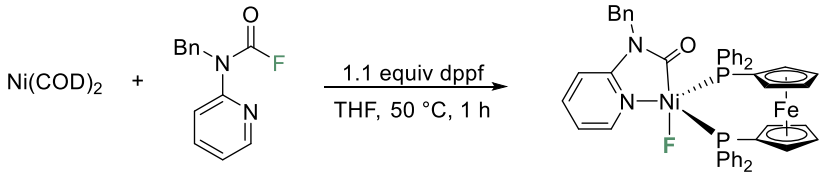

2.2o
1.2 equiv

4.37
80%

Scheme 4.35: Synthetic conditions for the preparation of complex **4.37**.

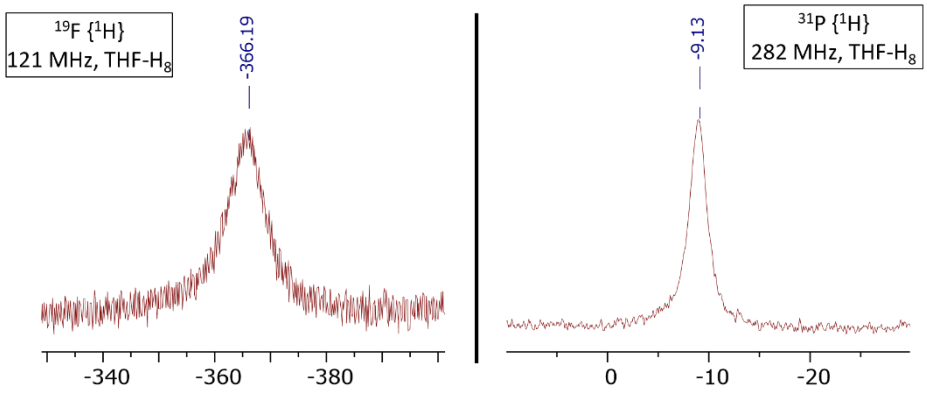

Figure 4.36: ^{19}F $\{^{1}H\}$ and ^{31}P $\{^{1}H\}$ NMR spectra of complex **4.37** acquired in THF-H_8.

SC-XRD analysis of complex **4.37** confirmed successful oxidative addition and revealed the formation of a five-coordinate nickel(II) complex adopting a slightly distorted trigonal bipyramidal geometry (Figure 4.38). This near-ideal trigonal bipyramidal geometry, coupled with the strong field ligands present in the complex, suggest that the complex likely exists in a thermally accessible high-spin to low-spin equilibrium (Figure 4.37). Such behavior would explain the observed line broadening and the loss of resolved P–F fine coupling in both the ^{31}P $\{^{1}H\}$ and ^{19}F $\{^{1}H\}$ NMR spectra.

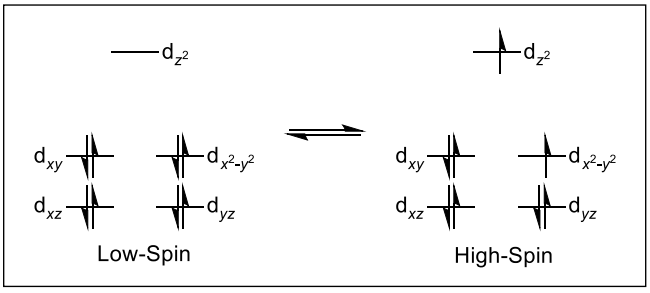

Figure 4.37: High-spin to low-spin equilibrium for an ideal trigonal bipyramidal complex.

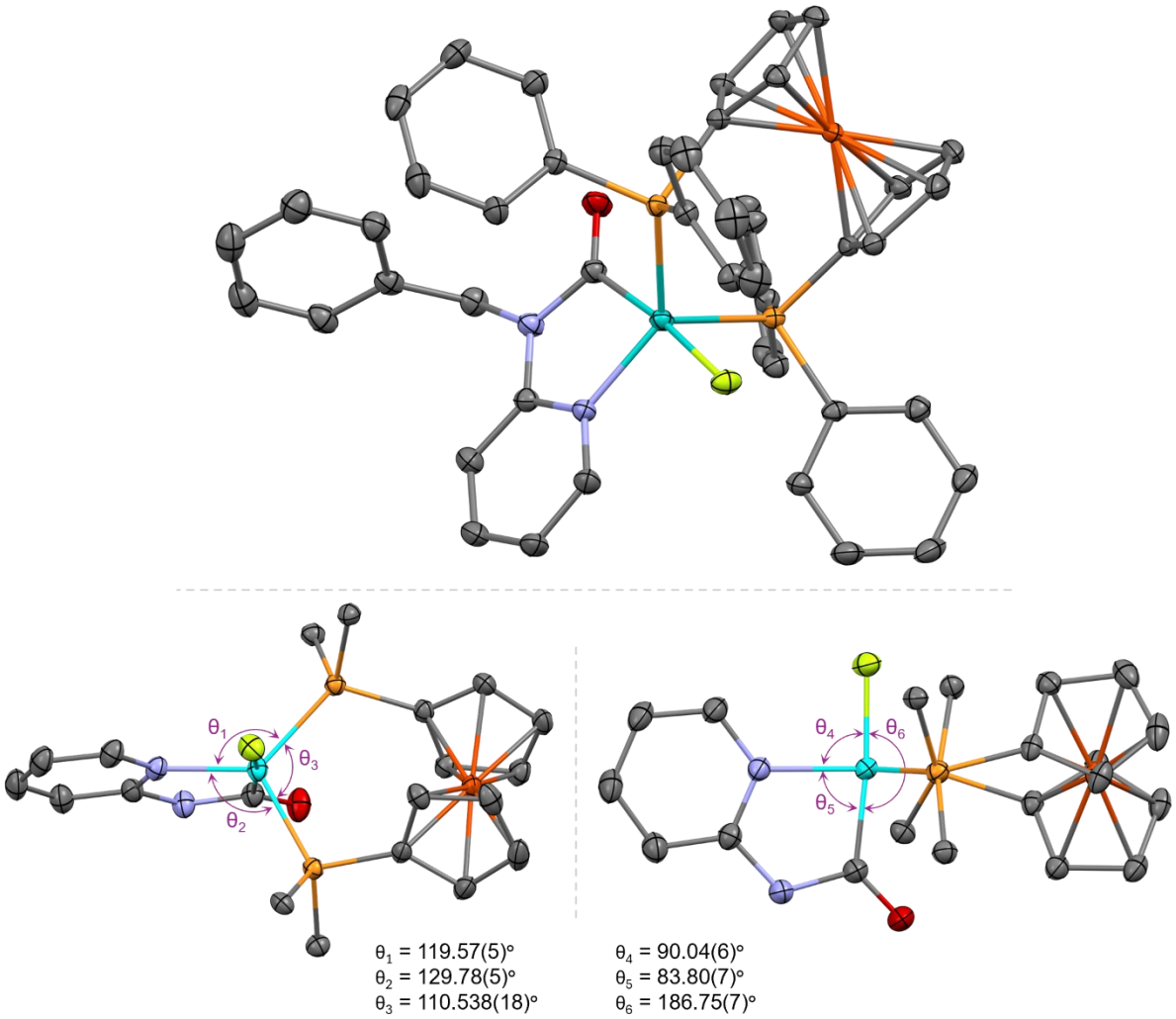

Figure 4.38: Solid state structure of complex **4.37**. ORTEP drawn at 50% probability, hydrogen atoms have been omitted for clarity. (Bottom) Select atoms have been removed for clarity.

With oxidative addition complex (**4.37**) successfully prepared, efforts were directed toward preparation of analogous oxidative addition complexes lacking the pyridyl directing group. Since *N*-benzyl-*N*-phenyl CMF **2.2a** served as the standard substrate throughout reaction optimization and much of the substrate scope, it was selected as the primary target.

Using conditions similar to those employed for the preparation of oxidative addition complex (**4.37**), $Ni(COD)_2$, dppf, and CMF **2.2a** were heated at 70 °C for 10 minutes (Scheme 4.36). Surprisingly only formation of (dppf)Ni(COD) (**4.38**) was observed. Similar results were

obtained when either the corresponding CMCl (**4.2a**) or dibenzyl CMF (**2.2q**) were employed. Formation of complex **4.38** was confirmed by both SC-XRD and the presence of a singlet resonance at 34.5 ppm in the ^{31}P $\{^{1}H\}$ NMR spectrum, consistent with its literature reported value (Scheme 4.36).

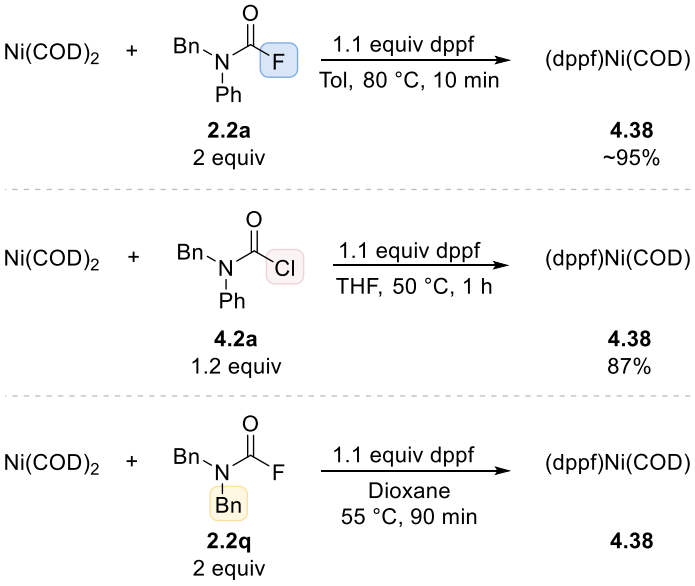

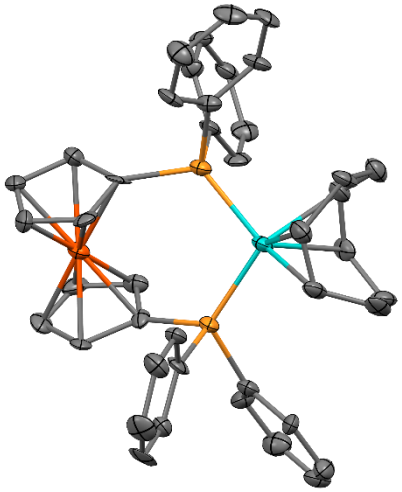

Scheme 4.36: Reaction conditions employed for the attempted synthesis of various oxidative addition complexes. ORTEP drawn at 50% probability, hydrogen atoms have been omitted for clarity.

To further investigate whether oxidative addition of CMF **2.2a** was occurring, complex **4.38** was independently prepared and reacted with CMF **2.2a** (Scheme 4.37). The reaction was analyzed by both ^{19}F $\{^{1}H\}$ and ^{31}P $\{^{1}H\}$ NMR spectroscopy before and after heating at 80 °C for one hour (Figure 4.39). Following heating, a new resonance appeared at 22.5 ppm in the ^{31}P $\{^{1}H\}$ NMR spectrum.

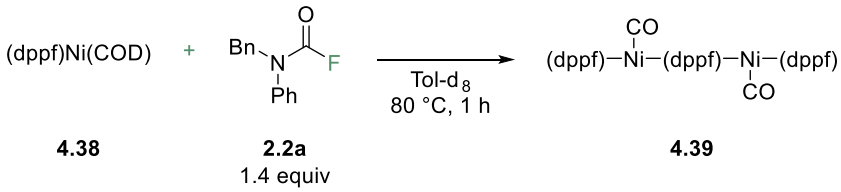

Scheme 4.37: Reaction conditions employed for the attempted synthesis of an oxidative addition complex.

Subsequent crystallization attempts afforded single crystals suitable for SC-XRD analysis, revealed the formation of the nickel carbonyl complex [(dppf)Ni(CO)]$_2$(μ-dppf) (**4.39**), which was found to correspond to the new ^{31}P {^{1}H} NMR resonance at 22.5 ppm (Figure 4.39). Formation of complex **4.39** provides strong evidence that oxidative addition of CMF **2.2a** had occurred, as formation of the nickel carbonyl complex requires liberation of CO through decarbonylation.

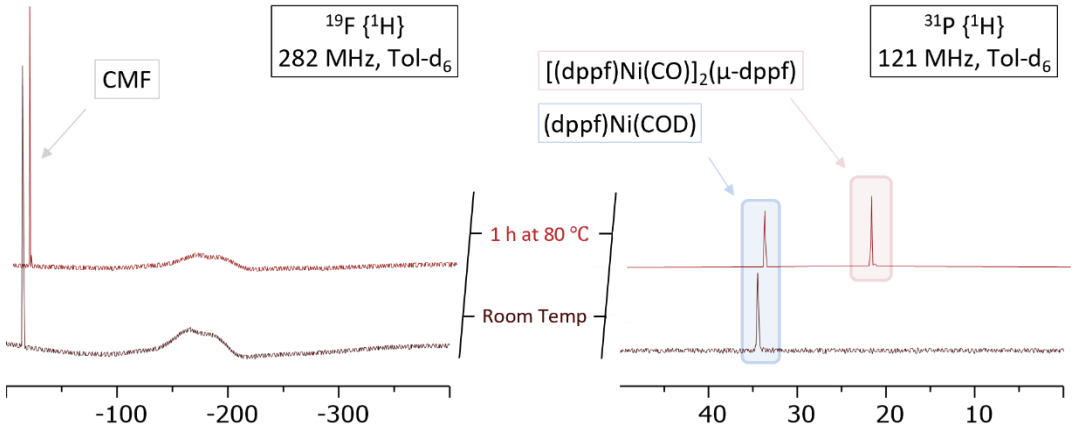

Figure 4.40: ^{19}F {^{1}H} and ^{31}P {^{1}H} NMR spectra of reaction described in **Scheme 4.37:** Reaction conditions employed for the attempted synthesis of an oxidative addition complex.

all spectra were acquired in Tol-d$_8$

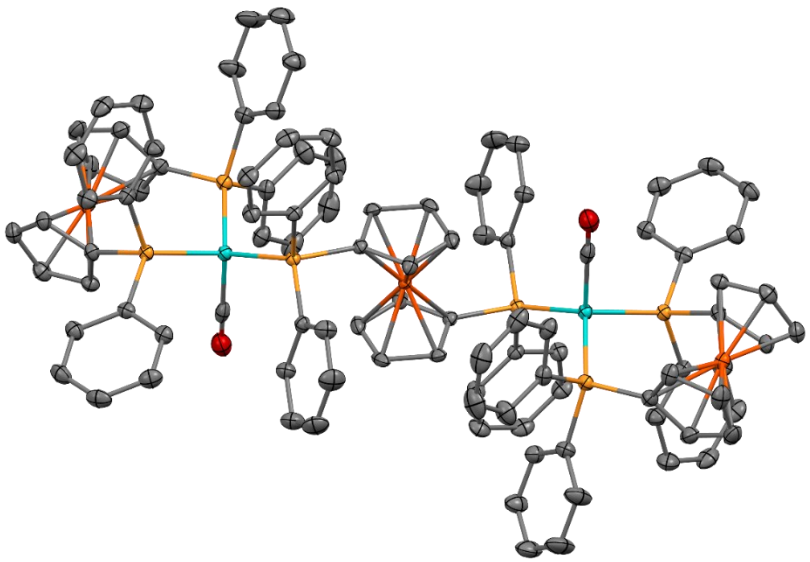

Figure 4.39: Solid-state structure of complex **4.39.** ORTEP drawn at 50% probability, hydrogen atoms have been omitted for clarity.

Additionally, because dppf possess a relatively large bite angle (~110°), the desired oxidative addition complex would be expected to adopt a tetrahedral geometry and therefore likely be paramagnetic (Figure 4.41). As a result, direct observation by NMR spectroscopy was not possible. Despite extensive efforts, all attempts to crystallize the desired oxidative addition complex were either unsuccessful or instead afforded complex **4.39**.

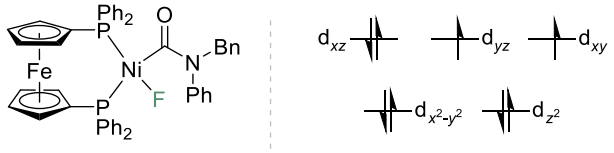

4.40

Figure 4.41: Anticipated crystal field diagram of oxidative addition complex **4.40**.

To determine whether less sterically demanding CMFs would permit isolation of the oxidative addition complex, both indoline (**2.2x**) and piperazine (**2.2z**) derived CMFs were investigated. When CMF **2.2x** was heated with complex **4.38** at 60 °C for 20 minutes (Scheme 4.38) and analyzed by ^{31}P $\{^{1}H\}$ NMR spectroscopy, only limited consumption of complex **4.38** was observed, together with the formation of **4.39** (Figure 4.43). Furthermore, all crystallization attempts only yielded **4.39** and the corresponding urea **4.41** (Figure 4.42).

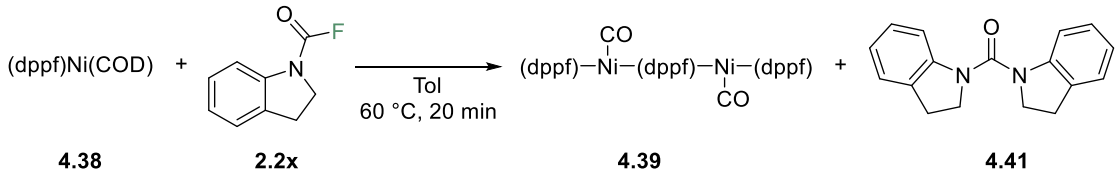

4.38 **2.2x** 2.0 equiv **4.39** **4.41**

Scheme 4.38: Reaction conditions employed for the attempted synthesis of an oxidative addition complex.

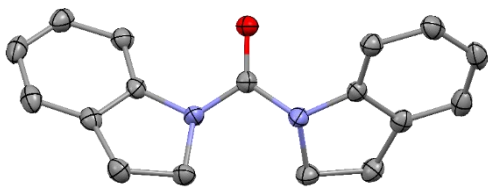

Figure 4.42: Solid-state structure of **4.41.** ORTEP drawn at 50% probability, hydrogen atoms have been omitted for clarity.

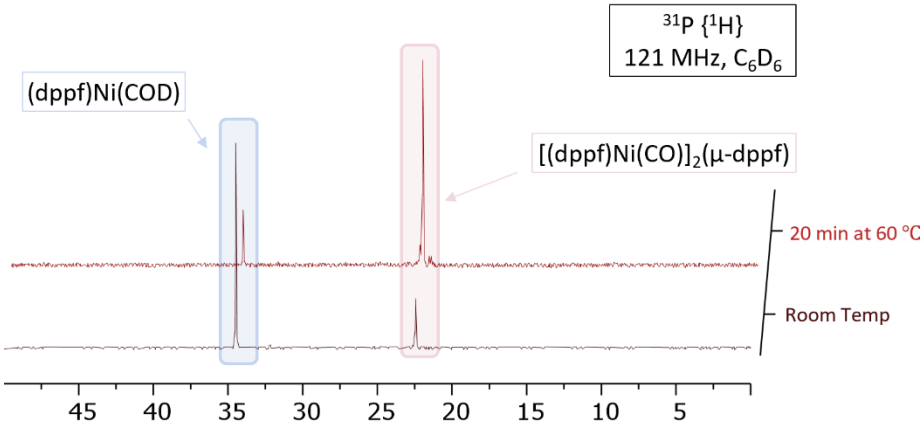

Figure 4.43: ^{31}P $\{^{1}H\}$ NMR spectra of the crude reaction mixture described in **Scheme 4.38:** Reaction conditions employed for the attempted synthesis of an oxidative addition complex.

Interestingly, it was found that when the reaction was performed directly from heating $Ni(COD)_2$, dppf, and CMF **2.2x** at 70 °C for 90 minutes (Scheme 4.39), a new resonance was observed in the ^{31}P $\{^{1}H\}$ NMR spectrum at 15.7 ppm (Figure 4.44). This resonance was later found to correlate to the formation of $(dppf)_2Ni^0$ (**4.15**).

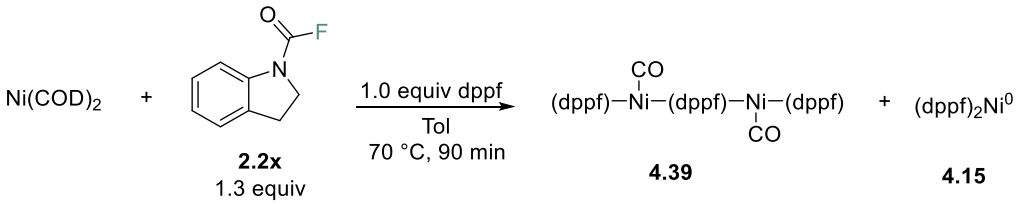

Scheme 4.39: Reaction conditions employed for the attempted synthesis of an oxidative addition complex containing CMF **2.2x**.

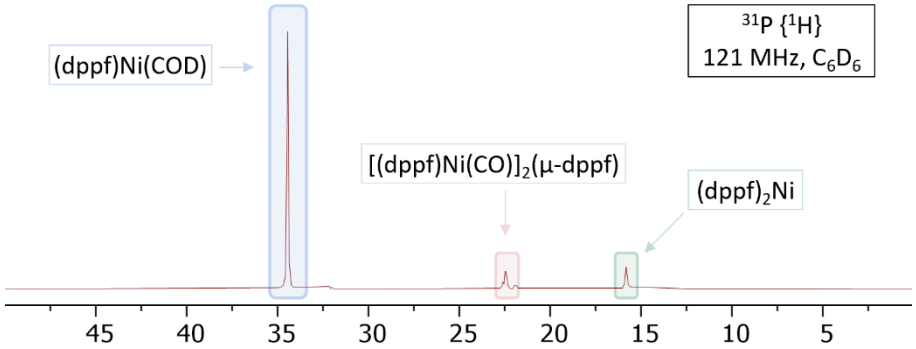

Figure 4.44: Crude ^{31}P $\{^{1}H\}$ NMR spectrum of reaction described in **Scheme 4.39**, spectrum was acquired in C_6D_6.

Next, piperazine-derived CMF **2.2z** was reacted with **4.38** in an attempt to generate oxidative addition complex **4.42** (Scheme 4.40). Analysis of the crude reaction mixture by ^{19}F $\{^{1}H\}$ NMR spectroscopy revealed the presence of an exceedingly small resonance at -387 ppm, tentatively assigned to the desired complex **4.42** (Figure 4.45). Unfortunately, all attempts to isolate this species were unsuccessful, with the only other compounds conclusively identified being **4.39** and $(dppf)_2Ni(0)$ (**4.15**).

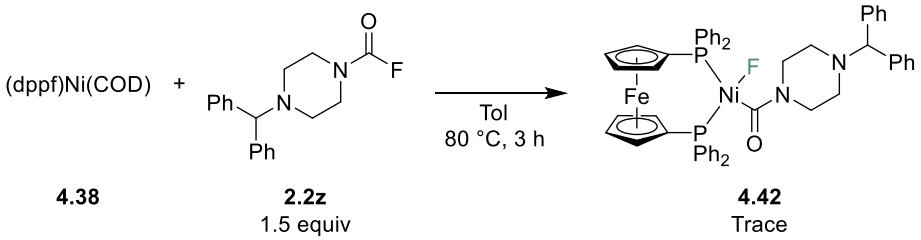

Scheme 4.40: Reaction conditions employed in the attempted synthesis of complex **4.42**.

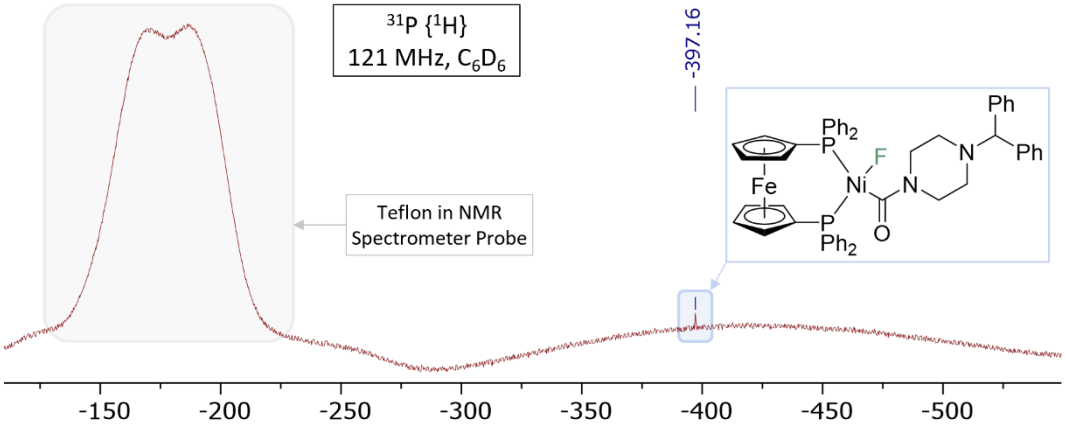

Figure 4.45: ^{19}F $\{^{1}H\}$ NMR spectrum from the attempted synthesis of **4.42** spectrum was acquired in C_6D_6.

Because the desired dppf-supported oxidative addition complexes were expected to be paramagnetic and therefore difficult to observe by NMR spectroscopy, alongside the extensive failed attempts to crystallize the desired product, an analogous system employing two PPh_3 ligands was investigated. In addition to favoring a square planar geometry resulting in a diamagnetic

complex observable by NMR, PPh_3 was selected because numerous nickel carbonyl complexes bearing PPh_3 ligands have been reported, facilitating identification of potential decomposition products. Although PPh_3 was found to be catalytically inferior, affording only a 9% yield in the catalytic reaction (Section 4.4.2.1), it was considered suitable for evaluating the fundamental feasibility of oxidative addition with a CMF lacking a directing group.

To investigate formation of the proposed oxidative addition complex, $Ni(COD)_2$, CMF **2.2a**, and a slight were combined and heated at 50 °C, with periodic analysis of the crude reaction mixture by ^{19}F $\{^1H\}$ excess of PPh_3 and ^{31}P $\{^1H\}$ NMR spectroscopy (Scheme 4.41, Figure 4.47, Figure 4.46). Upon mixing $Ni(COD)_2$ and PPh_3 at room temperature, rapid formation of $(PPh_3)_2Ni(COD)$ (**4.43**) and a small quantity of $(PPh_3)_3Ni^0$ was observed (Figure 4.46). After addition of CMF **2.2a** but prior to heating, trace quantities of the desired oxidative addition complex **4.45** could already be observed (Figure 4.46, Figure 4.47).

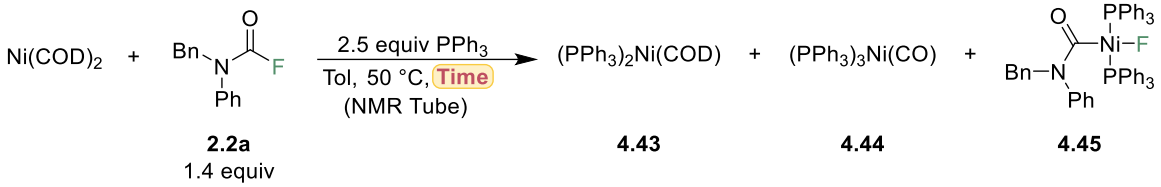

Scheme 4.41: Reaction conditions employed for the formation of complex **4.45**.

Upon heating to 50 °C, oxidative addition proceeded rapidly, resulting in significant formation of **4.45**. The complex was identified by a characteristic pair of mutually coupled resonances consisting of a sharp triplet in the ^{19}F $\{^1H\}$ NMR spectrum at -338.4 ppm ($^2J_{FP}$ = 50 Hz) and a corresponding doublet in the ^{31}P $\{^1H\}$ NMR spectrum at 15.0 ppm ($^2J_{PF}$ = 50 Hz). The concentration of **4.45** increased rapidly during the first 36 minutes before gradually decreasing upon prolonged heating. Simultaneously, nickel carbonyl complex $(PPh_3)_3Ni(CO)$ (**4.44**) appeared

after approximately 21 minutes and continued to increase throughout the experiment, while the concentration of **4.43** steadily decreased.

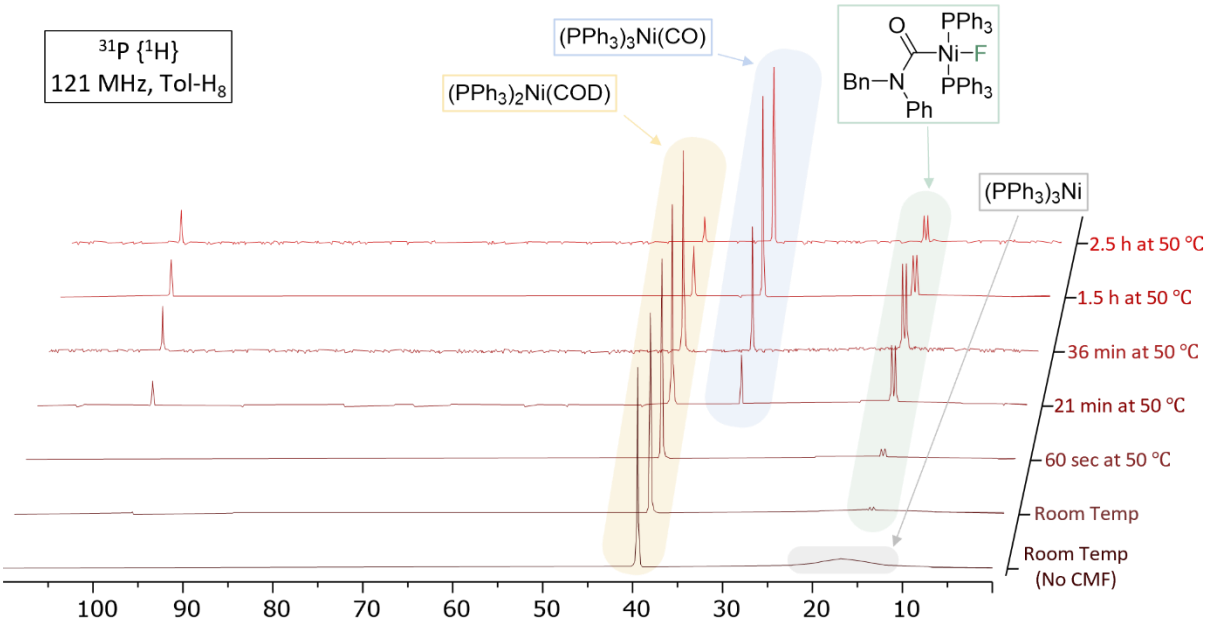

Figure 4.46: ^{31}P $\{^{1}H\}$ NMR spectra of the crude reaction mixture described in **Scheme 4.41:** Reaction conditions employed for the formation of complex **4.45**.

all spectra were acquired in Tol-H_8

The continuous growth of complex **4.44**, together with the gradual disappearance of oxidative addition complex **4.45**, is consistent with decomposition of **4.45** through decarbonylation. In this process, the liberated CO is trapped by Ni(0) to form the thermodynamically stable 18-electron carbonyl complex $(PPh_3)_3Ni(CO)$ (**4.44**). Collectively these results indicate that oxidative addition of unactivated CMFs to nickel readily occurs in the absence of a directing group. However, the resulting oxidative addition complex is only intermittently stable and gradually undergo decarbonylation upon prolonged heating.

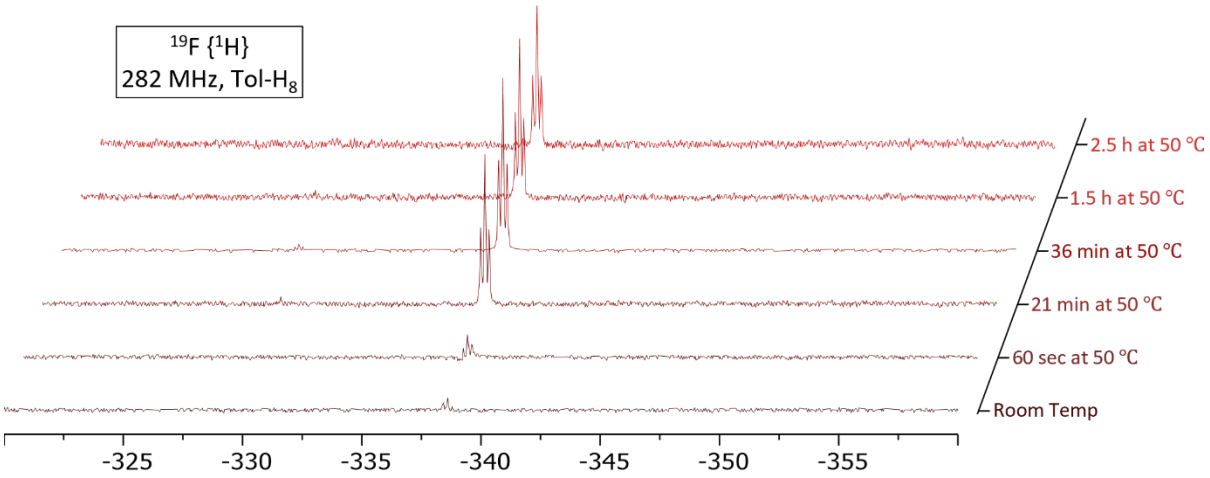

Figure 4.47: ^{19}F $\{^{1}H\}$ NMR showing the gradual generation of complex **4.45** after various amounts of time, all spectra were acquired in Tol-H_8.

4.4.4.4. Reaction Monitoring

To gain further insight into the reaction mechanism, the standard cross-coupling reaction was conducted in an NMR tube at 80 °C and periodically monitored by ^{11}B, ^{19}F, and ^{31}P NMR spectroscopy (Scheme 4.42). Although direct observation of many organometallic intermediates was considered unlikely because several species were anticipated to be both paramagnetic and present at exceedingly low concentrations, it was anticipated that the catalytic resting state and other diamagnetic species might provide valuable mechanistic insight.

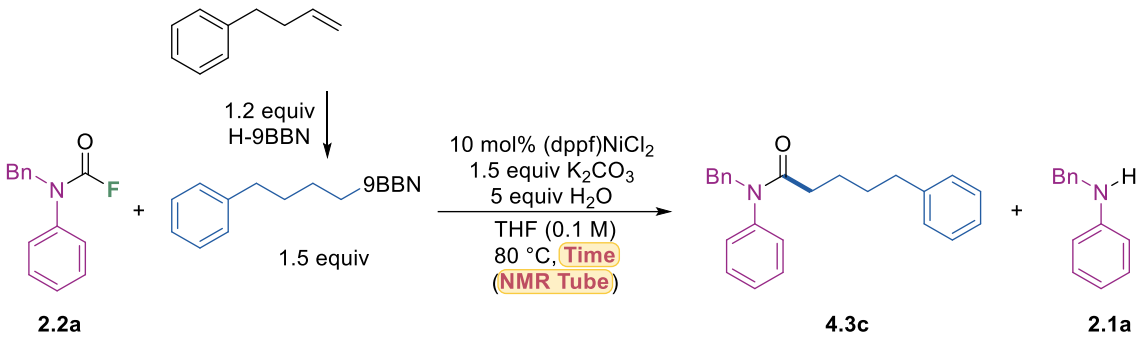

Scheme 4.42: Reaction conditions employed for reaction monitoring experiments.

Many Suzuki cross-coupling reactions are inherently heterogenous because they employ inorganic bases such as K_2CO_3, and our developed reaction similarly exhibits this heterogenous behaviour. Consequently, reproducing the optimized reaction conditions inside an NMR tube required efficient mixing throughout the experiment. Because conventional magnetic stirring could not be employed, a modular NMR spinning apparatus was designed in Fusion360 and fabricated using a resin 3D printer to provide continuous mixing of the reaction mixture (Figure 4.48). Using a readily available compressed air source, the NMR tube was maintained at a rotation rate of approximately 100 Hz (6000 rpm), providing efficient mixing throughout the course of the experiment to effectively mix the heterogenous reaction mixture.

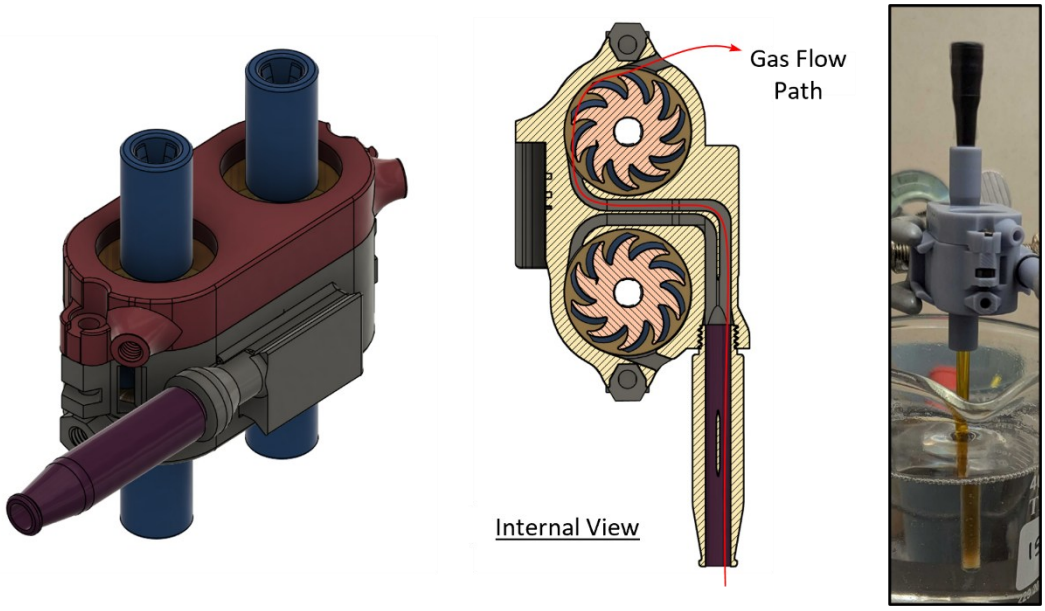

Figure 4.48: Apparatus designed and fabricated to allow for efficient mixing of NMR tube contents at elevated temperatures. Files are available upon request.

With a suitable means of mixing established, the reaction was conducted under the optimized catalytic conditions. Initial analysis of the ^{11}B $\{^{1}H\}$ NMR spectra revealed the presence of both HO-9-BBN and solvent-coordinated alkyl-9-BBN prior to heating the reaction mixture (Figure 4.49). The presence of HO-9-BBN before heating was expected, because addition of the premixed alkyl-9-BBN/Ni pre-catalyst solution to the remaining reaction components exposed excess H-9BBN to water. Hydrolysis of H-9BBN therefore readily occurred, producing HO-9-BBN with the simultaneous evolution of H_2 gas, which was visually observed upon mixing.[68]

As expected, the concentration of alkyl-9-BBN steadily decreased throughout the reaction, while the concentration of HO-9-BBN increased correspondingly. These observations are consistent with the progressive consumption of the alkylborane coupling partner during catalysis.

After approximately one hour of heating, a new resonance corresponding to 9,9-difluoro-9-borabicyclo-[3.3.1]-nonanate salt (F_2-9-BBN) appeared as a triplet at 10.3 ppm ($^{1}J_{BF}$ = 86.4 Hz). Formation of this species indicates that the fluoride released during catalysis can be trapped by the

Lewis acidic boron center rather than remaining as free fluoride in solution. This observation is consistent with the excellent tolerance of both TMS and OTBS functional groups observed during the substrate scope (Section 4.4.4), as significant concentrations of free fluoride would be expected to promote desilylation under the reaction conditions.

Finally, all ^{11}B $\{^1H\}$ NMR spectra contained a small broad resonance near 2.0 ppm, which was consistent with the in situ formation of a hydroxoborate species. Observation of this resonance is consistent with the proposed transmetalation pathways outlines in Figure 4.27, in which hydroxoborate intermediates are generated prior to coordination to nickel.

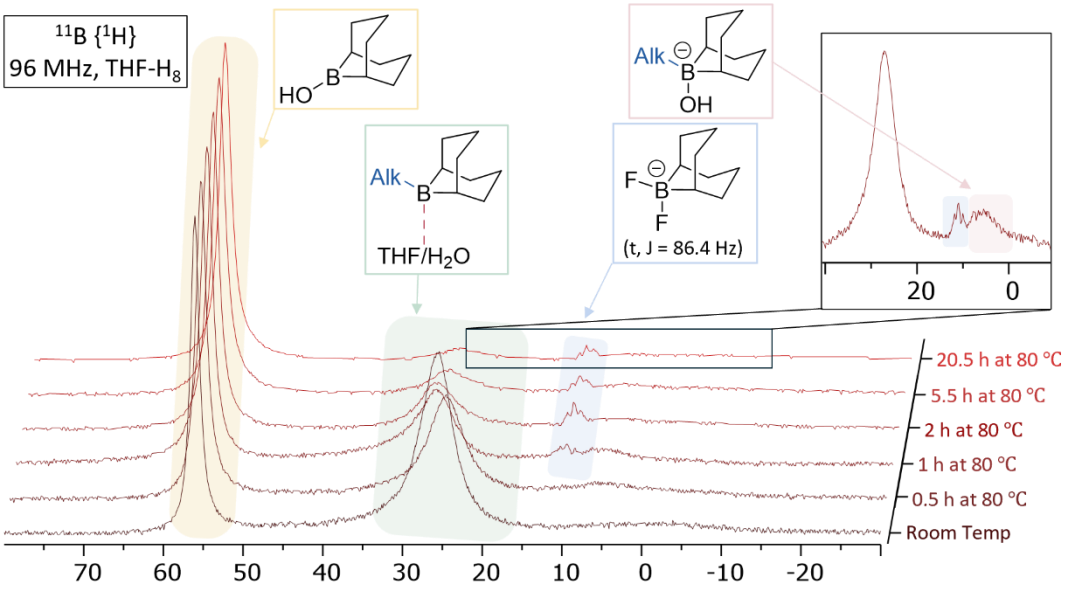

Figure 4.49: ^{11}B $\{^1H\}$ NMR spectra of the crude reaction mixture described in **Scheme 4.42:** Reaction conditions employed for reaction monitoring experiments.

after the indicated period of time, all spectra were acquired in THF-H_8.

Analysis of the ^{19}F $\{^1H\}$ NMR spectra revealed the progressive consumption of CMF **2.2a** throughout the course of the reaction (Figure 4.50). After approximately one hour of heating, gradual formation of F_2-9-BBN was observed as a quartet at -163.4 ppm ($^1J_{FB}$ = 86.4 Hz), spin-coupled with the resonance observed in the ^{11}B $\{^1H\}$ NMR spectrum, which results from the trapping of fluoride released after transmetalation. In addition, a small unidentified broad singlet at -190.7 ppm appeared after 30 minutes, reaching its highest relative concentration after 2 hours,

and subsequently decreased in concentration upon prolonged heating. Although this resonance could not be assigned, its transient nature suggests that it corresponds to a reactive intermediate or byproduct.

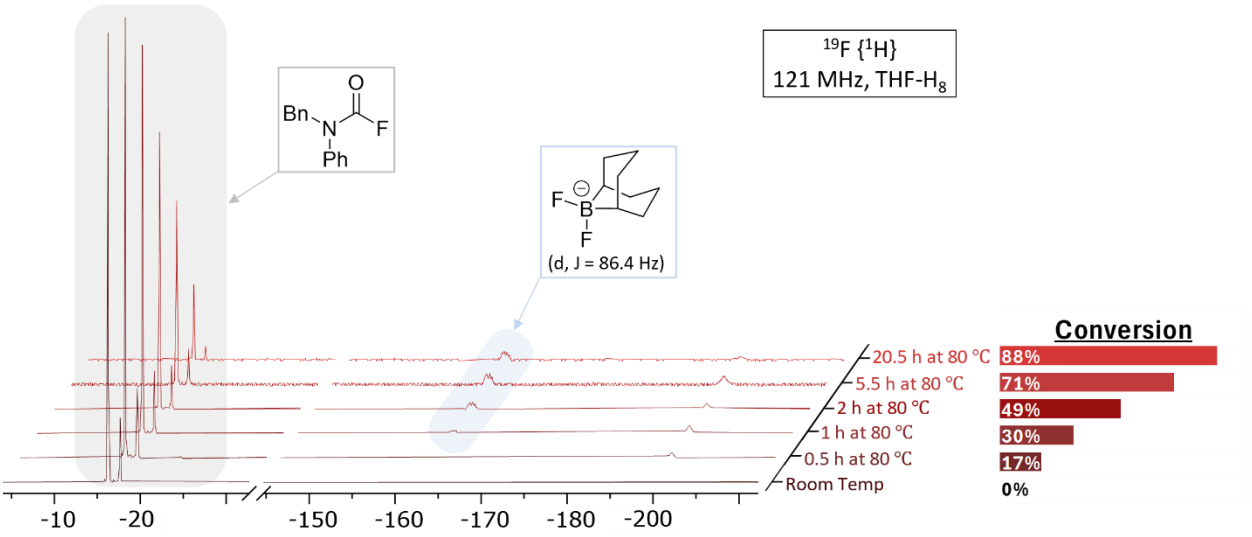

Figure 4.50: ^{19}F {^{1}H} NMR spectra of the crude reaction mixture described in **Scheme 4.42:** Reaction conditions employed for reaction monitoring experiments.

after the indicated period of time, all spectra were acquired in THF-H$_8$. Spectra region between -30 ppm and -145 ppm has been omitted for clarity. Conversion was determined by quantitative NMR with Trifluorotoluene used as an internal standard.

Analysis of the ^{31}P {^{1}H} NMR spectra proved particularly informative (Figure 4.51). Upon mixing the reaction components, a resonance corresponding to (dppf)$_2$Ni^0 (**4.15**) (δ = 15.6 ppm) was observed prior to heating the reaction mixture. The concentration of **4.15** remained relatively constant during the first 2 hours of the reaction before gradually decreasing. Simultaneously, several new phosphorus-containing species began to emerge. A previously unobserved doublet appeared at 99.2 ppm (J =53.8 Hz), although this species could not be confidently assigned. Two overlapping singlets also begun to emerge after 5.5 hours of heating appearing at -17.3 and -17.8 ppm. The former was identified as free dppf released during catalyst decomposition, while the latter was tentatively assigned to a Ni complex coordinated to a single phosphorus atom of a dppf ligand (i.e., κ^1-coordination).

A resonance at 22.3 ppm was tentatively assigned to a mixture of nickel carbonyl complexes, formulated as $(dppf)_xNi_y(CO)_z$. This resonance was absent prior to heating, first appeared after approximately 30 minutes, and gradually increased in concentration throughout the remainder of the experiment. Its formation is consistent with thermally induced decarbonylation occurring during catalysis, resulting in the gradual accumulation of catalytically nickel carbonyl species.

Of particular significance is the accumulation of $(dppf)_2Ni^0$ (**4.15**) prior to heating, followed by its gradual consumption as the reaction progresses. This behaviour suggests that $(dppf)_2Ni^0$ (**4.15**) may represent a catalytic resting state. Because the resting state generally precedes the turnover-limiting step (TLS) of the catalytic cycle, accumulation of **4.15** may therefore indicate that oxidative addition is the TLS. Consequently, $(dppf)_2Ni^0$ (**4.15**) was investigated further as a potential catalytically relevant species and is discussed in Section 4.4.5.5.

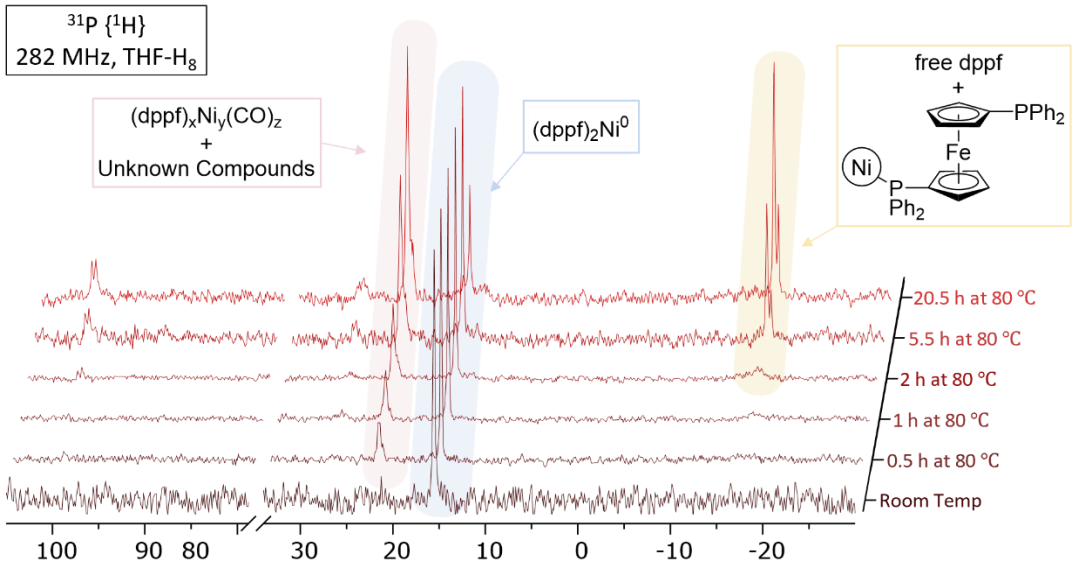

Figure 4.51: ^{31}P $\{^1H\}$ NMR spectra of the crude reaction mixture described in **Scheme 4.42:** Reaction conditions employed for reaction monitoring experiments.

after the indicated period of time, all spectra were acquired in THF-H_8. Spectra region between

4.4.4.5. Assessment of Catalytically Relevant Complexes

With several organometallic complexes in hand, their stoichiometric and catalytic reactivity was investigated to assess whether they are catalytically competent (Figure 4.52). If the complexes are not catalytically relevant, they would be expected to afford no product under the reaction conditions, thereby ruling them out as catalytically relevant intermediates.

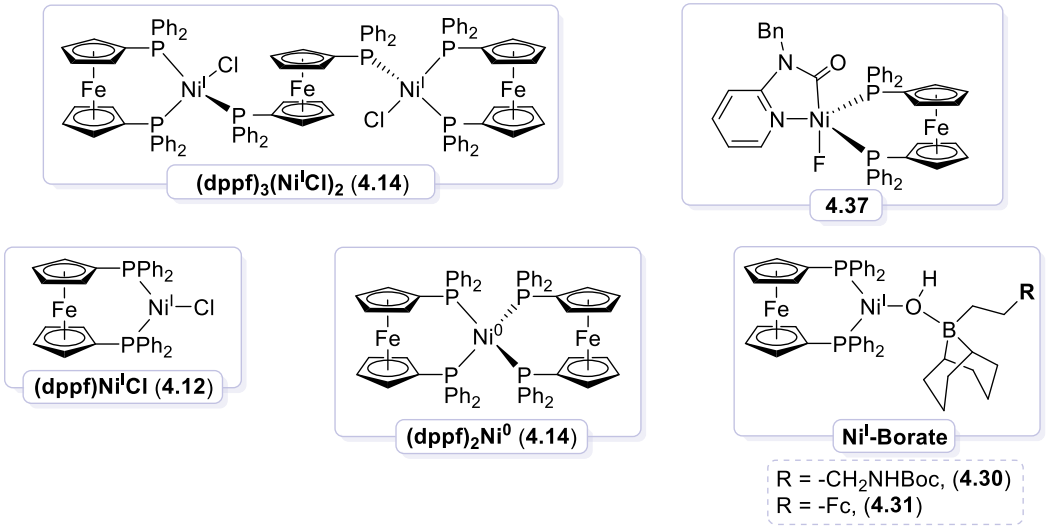

Figure 4.52: Complexes prepared to be evaluated for catalytic performance.

First, the stoichiometric reactivity of the prepared hydroxoborate-Ni(I) complexes was evaluated using a 1:1 molar ratio of the complex and CMF **2.2a** (Table 4.16). It was hypothesized that, because the hydroxoborate-Ni(I) complexes were previously found to be competent surrogates for the corresponding alkyl-Ni(I) species, formation of the desired amide in yields comparable to those obtained under the standard catalytic conditions would provide support for a Ni(I)/Ni(III) catalytic cycle.

Evaluation of the NHBoc-substituted hydroxoborate-Ni(I) complex (**4.30**) afforded the desired amide in a 36% yield, with 75% conversion of CMF **2.2a** and 36% amine formation (Table 4.16, entry 1). It was hypothesized that, following reductive elimination, the resulting nickel(I) species may undergo unproductive side reactions that limit productive turnover. To suppress this

possibility, one equivalent of dppf was added to the reaction mixture in an attempt to coordinate the resulting nickel species and inhibit an undesired reactivity (Table 4.16, entry 2). However, addition of dppf had little influence on the reaction outcome, providing the desired amide in a comparable 33% yield. These results contrast sharply with the quantitative formation of the identical product (**4.3r**) under the standard catalytic reaction conditions.

To verify that this behaviour was not unique to hydroxoborate-Ni(I) complex (**4.30**), an analogous experiment was performed using hydroxoborate-Ni(I) complex **4.31** (Table 4.16, entry 3). Under these conditions, the desired amide formed in a 13% yield, with 67% conversion of CMF **2.2a**. Although substantially lower than the 54% yield obtained for the corresponding product (**4.3u**) under the optimized catalytic conditions, productive formation of the desired amide nevertheless demonstrates that the prepared hydroxoborate-Ni(I) complexes could be chemically competent species capable of undergoing the transformation required to facilitate C–C bond formation.

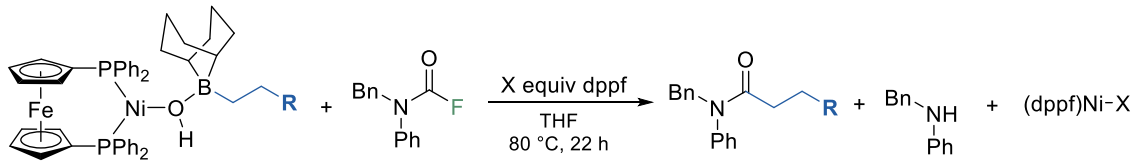

Entry	Pre-Catalyst		Conversion	Amide	Amine
1	R = -CH_2NHBoc	-	75%	36%	36%
2		10% dppf	83%	33%	52%
3	R = -Fc	-	67%	13%	54%

Table 4.16: Evaluation of the stoichiometric reactivity of various Ni^{I}-Borate complexes. Conversions and yields acquired by ^{1}H NMR with 1,3,5 trimethoxybenzene as an internal standard.

Although the observed stoichiometric reactivity may suggest that a Ni(I) catalytic pathway is possible, it does not definitively establish that these complexes are on-cycle intermediates. One alternative explanation is that, upon heating, the hydroxoborate-Ni(I) complexes first generate the

corresponding alkyl-Ni(I) species, which may rapidly undergo disproportionation to afford one equivalent of (dppf)Ni^0 and (dppf)$Ni^{II}(alkyl)_2$. The bis(alkyl)Ni(II) complex could then undergo reductive elimination to generate the alkyl–alkyl homocoupling product together with an additional equivalent of (dppf)Ni^0. The resulting Ni(0) species could subsequently enter the catalytic cycle through oxidative addition of the CMF, allowing the stoichiometric reaction to proceed through a conventional Ni(0)/Ni(II) pathway despite being initiated from a Ni(I) complex.

Consequently, these experiments alone cannot definitively distinguish between a Ni(I) pathway and one involving initial disproportionation to Ni(0). Additional mechanistic studies were therefore undertaken throughout Section 4.4.5.5 and 4.4.5.6 to further evaluate the viability of a Ni(I)/Ni(III) catalytic cycle.

Next, the stoichiometric reactivity of oxidative addition complex **4.37** was evaluated. Although the pyridyl directing group present is not representative of the substrates examined throughout this study, it was the only oxidative addition Ni(II) complex that could be isolated. Furthermore, to simplify the reaction and avoid the need for additional reagents such as water, K_2CO_3, and alkyl-9-BBN, hydroxoborate salt **4.25** was employed in place of the alkylborane. As discussed in Section 4.4.5.2, hydroxoborate salts are proposed to be a catalytically relevant intermediate in one of the possible transmetalation pathways and therefore serves as a suitable surrogate for evaluating the subsequent elementary steps of the catalytic cycle.

Accordingly, oxidative addition complex **4.37** and hydroxoborate **4.25** were reacted in a 1:1.5 molar ratio in the presence of one equivalent of dppf in THF at 80 °C for 22 hours (Scheme 4.43). Analysis of the crude reaction mixture revealed complete consumption of **4.37** and formation of the desired amide **4.3at** in a 55% yield, together with 34% of the corresponding amine. These results demonstrate that oxidative addition complex **4.37** is chemically competent

and capable of undergoing productive transmetalation and reductive elimination to afford the desired cross-coupled product.

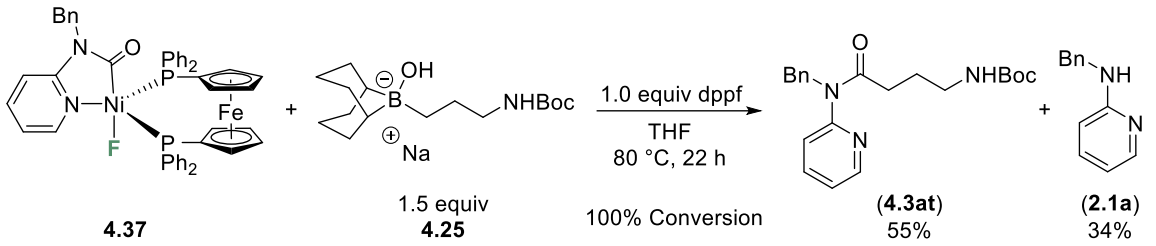

Scheme 4.43: Stoichiometric reaction condition used to evaluate complex **4.37** as a competent catalytic species.

To gain further mechanistic insight into the reactivity of oxidative addition complex (**4.37**), the reaction was repeated in an NMR tube without the addition of excess dppf, with the intention of monitoring the reaction by NMR spectroscopy (Scheme 4.44). Unexpectedly, approximately 45 seconds after addition of hydroxoborate **4.25** to the solution of oxidative addition complex (**4.37**) at room temperature, the reaction mixture underwent a striking color change from dark red-orange to a light clear yellow. This color persisted for approximately 2-3 minutes before gradually darkening to a red-brown color. Although the origin of this transient yellow species could not be established, the immediate color change upon addition of hydroxoborate **4.25** is consistent with the rapid formation of a new nickel-containing intermediate.

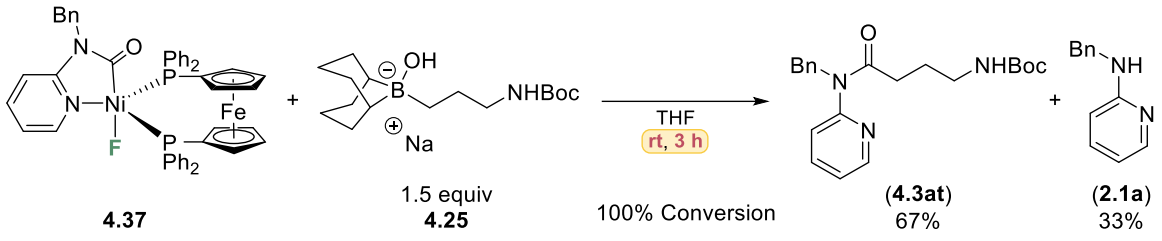

Scheme 4.44: Stoichiometric reaction condition used to evaluate complex **4.37** as a competent catalytic species.

By the time the initial NMR spectra had been acquired, the reaction had already appeared to have proceeded to completion, with complete consumption of oxidative addition complex (**4.37**). Analysis by ^{19}F $\{^{1}H\}$ NMR spectroscopy revealed complete disappearance of the

characteristic broad singlet of oxidative addition complex (**4.37**) at -366 ppm and the appearance of a new broadened resonance at -224 ppm (Figure 4.53). This previously unobserved fluorine-containing species had not been detected through the mechanistic studies, and unfortunately, its identity could not be determined. To be cautious and ensure complete conversion, the reaction mixture was allowed to continue mixing at room temperature for a total of 3 hours before final analysis. Quantitative NMR spectroscopy revealed formation of the desired amide **4.3at** in a 67% yield together with 33% of the corresponding amine.

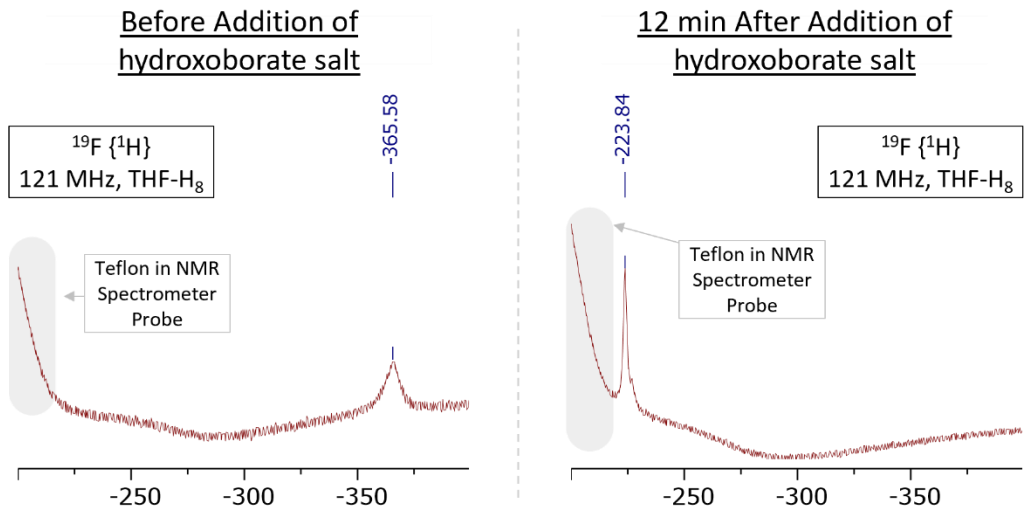

Figure 4.53: ^{19}F {^{1}H} NMR spectrum of complex **4.37** before and after addition of hydroxoborate **4.25.** Spectrum was acquired in THF-H$_8$

The rapid reaction observed at room temperature demonstrates that, once oxidative addition complex **4.37** and hydroxoborate salt **4.25** have formed, the subsequent transmetalation and reductive elimination steps may proceed readily without the need for heating. If considering a Ni(0)/Ni(II) cycle, these observations suggest that the TLS likely occurs before or during oxidative addition, at least for the 2-pyridyl substrate examined. This interpretation may also extend to CMF substrates not containing a directing group, although further investigation is required to establish whether the same kinetic behaviour applies.

With the stoichiometric studies completed, the catalytic competence of the prepared complexes was evaluated next. Hydroxoborate-Ni(I) complex (**4.30**) was first examined as a pre-catalyst by conducting the standard cross-coupling reaction using a 10 mol% catalyst loading under the standard reaction conditions (Scheme 4.45). Under these conditions, the desired amide was obtained 28% yield with 72% conversion of the CMF. These results contrast sharply with the quantitative yield previously obtained for the identical substrate under the optimized catalytic conditions (Section 4.4.4).

Although the formation of the desired product demonstrates that Ni(I)-borate complex (**4.30**) is capable of entering a productive catalytic pathway, its substantially diminished catalytic performance suggests that it is unlikely to represent the primary on-cycle catalyst. One possible explanation is that a small quantity of **4.30** undergoes disproportionation in the reaction to generate a small amount of catalytically active Ni(0), thereby accounting for the observed product formation. While these experiments do not exclude participation of Ni(I) species during catalysis,

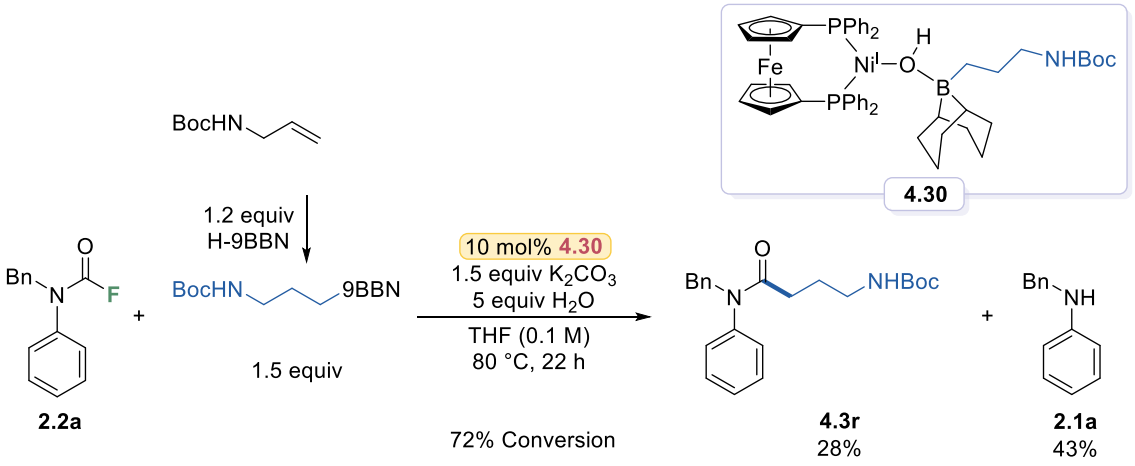

Scheme 4.45: Reaction conditions employed for evaluation of catalytic reactivity of complex **4.30**. Conversions and yields acquired by ^{1}H NMR with 1,3,5 trimethoxybenzene as an internal standard.

they provide little evidence that the hydroxoborate-Ni(I) complex itself functions as the active catalyst.

The catalytic competence of oxidative addition complex **4.37** was then evaluated. Because **4.37** is a product of oxidative addition with CMF **2.2o**, this substrate was employed to ensure that the CMF used in the reaction also matched that already bound to the nickel center. Accordingly, the reaction was conducted using 10 mol% of oxidative addition complex (**4.37**) as the catalyst precursor, together with 0.9 equivalents of CMF **2.2o**, thereby accounting for the additional 0.1 equivalents of substrate incorporated within the pre-catalyst (Scheme 4.46).

Under the standard optimized conditions, oxidative addition complex **4.37** afforded the desired product **4.3at** in a 71% yield with complete conversion of the CMF and 24% formation of the corresponding amine. Although this yield is somewhat lower than the 92% yield obtained using (dppf)$Ni^{II}Cl_2$ under the standard conditions, the comparable catalytic performance suggests that **4.37** may re-enter the catalytic cycle and undergoes multiple catalytic turnovers.

Collectively, the stoichiometric and catalytic evaluation of the prepared nickel complexes consistently favors a Ni(0)/Ni(II) catalytic cycle. While hydroxoborate-Ni(I) complexes are chemically competent and capable of producing the desired product, their comparatively poor catalytic performance contrasts with that of oxidative addition complex **4.37**, whose high stoichiometric and catalytic performance supports its assignment as an on-cycle intermediate. However, comprehensive kinetic studies are required to definitively establish which catalytic pathway is primarily responsible for product formation.

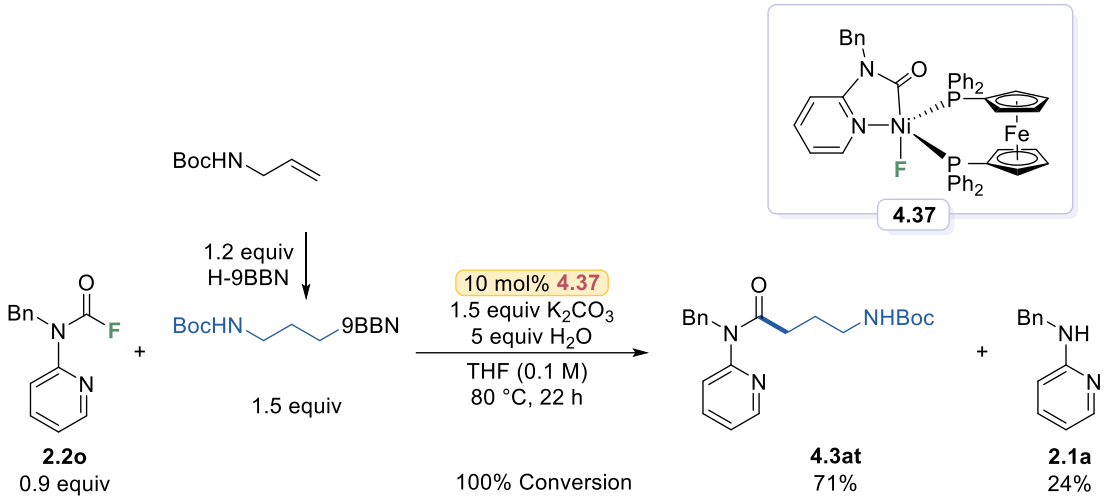

Scheme 4.46: Reaction conditions employed for evaluation of catalytic reactivity of complex **4.37**. Conversions and yields acquired by ^{1}H NMR with 1,3,5 trimethoxybenzene as an internal standard.

Following evaluation of the potential on-cycle catalytic species, several additional nickel complexes identified throughout the mechanistic investigation were assessed for their catalytic competence. These include the standard pre-catalyst (dppf)Ni^{II}Cl$_2$ (**4.10**), which served as benchmark, (dppf)Ni^{I}Cl (**4.12**), which was shown to form quantitatively during the crucial premixing step described in Section 4.4.5.1, the dinuclear Ni(I) complex [(dppf)Ni^{I}(Cl)]$_2$(μ-dppf) (**4.14**), which was repeatedly isolated during attempts to prepare various alkyl-Ni(I) complexes (Section 4.4.5.2), and (dppf)$_2$Ni^{0} (**4.15**), which was consistently observed during both the synthesis of catalytically relevant complexes and the reaction monitoring studies (4.4.5.4). Evaluation of these complexes was undertaken to determine whether they represent catalytically competent species or decomposition products.

Because [(dppf)Ni^{I}(Cl)]$_2$(μ-dppf) (**4.14**) is dinuclear in nature, containing two nickel centers. A catalyst loading of 5 mol% was employed to maintain the same overall nickel loading as the other catalyst systems. As expected, the benchmark pre-catalyst (dppf)Ni^{II}Cl$_2$ (**4.10**) afforded the desired amide in 89% yield together with 10% of the corresponding amine (Table 4.17, entry 1).

As discussed in Section 4.4.5.1, premixing **4.10** with alkyl-9-BBN resulted in quantitative formation of (dppf)$Ni^{I}Cl$ (**4.12**) prior to addition to the remaining reaction components. Consequently, if **4.12** is indeed the catalytically relevant species generated during the activation step, it would be expected to exhibit catalytic performance compatible to that of (dppf)$Ni^{II}Cl_2$ (**4.10**). Gratifyingly, use of (dppf)$Ni^{I}Cl$ (**4.12**) as a pre-catalyst afforded an identical 89% yield of amide together with 11% amine formation (Table 4.17, entry 2). These results provide independent experimental validation that catalyst activation during the premixing stage proceeds through formation of (dppf)$Ni^{I}Cl$ (**4.12**). Interestingly, although the collective mechanistic evidence presented thus far strongly favors a Ni(0)/Ni(II) catalytic cycle, these results indicate that formation (dppf)$Ni^{I}Cl$ (**4.12**) is nevertheless a crucial step during catalyst activation.

Because $[(dppf)Ni^{I}(Cl)]_2$(μ-dppf) (**4.14**) readily formed during attempts to prepare alkyl-Ni(I) complexes, its catalytic activity was evaluated to determine whether this accessible form of Ni(I) could enter the catalytic cycle. Complex **4.14** was found to afford the desired amide in a 93% yield with 6% amine formation. This excellent catalytic performance demonstrates that the dinuclear complex is a highly competent and can likely convert into a catalytically active nickel species under the reaction conditions. The origin of its slightly improved performance relative to (dppf)$Ni^{II}Cl_2$ (**4.10**) and (dppf)$Ni^{I}Cl$ (**4.12**) remains unclear but may reflect differences in catalyst activation, nickel speciation, or stability of catalytically active species. However, the available data does not permit a specific activation pathway to be assigned.

Finally, $(dppf)_2Ni^{0}$ **4.15** was evaluated and proved to be the most active pre-catalyst examined. At first glance, this result was surprising, as **4.15** is a coordinatively saturated 18-electron, four-coordinate Ni(0) complex bearing two strongly coordinating bidentate dppf ligands. We would therefore expect oxidative addition to be slow, given that dissociation of at least one of

the phosphine ligands would be required prior to this step. Nevertheless, $(dppf)_2Ni^0$ (**4.15**) afforded the desired amide in an excellent 97% yield, with only 3% formation of the corresponding amine (Table 4.17, entry 4). Owing to this unexpectedly high activity, the catalytic performance of $(dppf)_2Ni^0$ (**4.15**) was further investigated to better understand its potential role in the catalytic cycle.

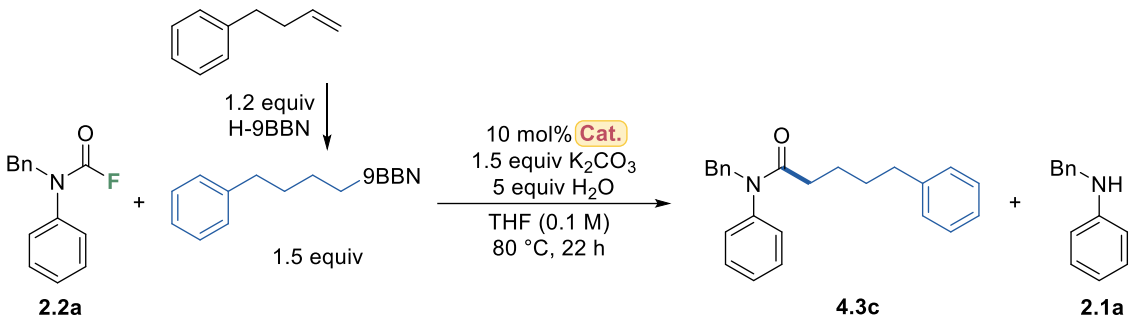

Entry	Pre-Catalyst	Conversion	Amide	Amine
1	$(dppf)Ni^{II}Cl_2$	100%	89%	10%
2	$(dppf)Ni^{I}Cl$	100%	89%	11%
3	$[(dppf)Ni^{I}(Cl)]_2(\mu\text{-}dppf)$	100%	93%	6%
4	$dppf_2Ni^0$	100%	97%	3%

Table 4.17: Evaluation of other catalytically related complexes. Entry 3 was conducted with a catalyst loading of 5 mol%. Conversions and yields acquired by ^1H NMR with 1,3,5 trimethoxybenzene as an internal standard.

Using the standard optimized reaction conditions, the catalyst loading of $(dppf)_2Ni^0$ (**4.15**) was systematically varied (Table 4.18). Reducing the loading from 10 to 5 mol% had only a minor effect on catalytic performance, affording the desired amide in 92% yield together with 7% amine formation (Table 4.18, entry 2). Only when the catalyst loading was further reduced to 2 mol% was a substantial decrease in reactivity observed. Under these conditions, the amide product was obtained in 75% yield along with 16% amine, and incomplete conversion of the CMF substrate was observed (92%) (Table 4.18, entry 3). These results demonstrate that $(dppf)_2Ni^0$ (**4.15**) remains a highly competent pre-catalyst even at reduced loadings. This behaviour contrasts sharply with that of $(dppf)Ni^{II}Cl_2$ (**4.10**), which afforded the desired amide in only 56% yield when employed at a 5 mol% catalyst loading (Section 4.4.2.6, Table 4.10, entry 3).

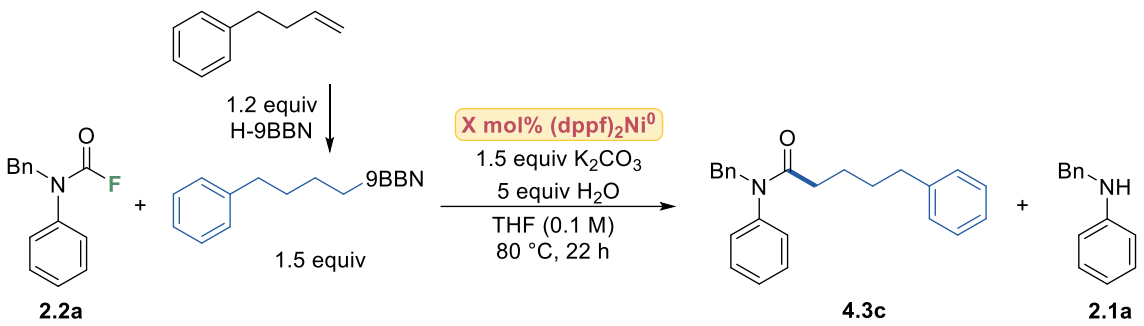

Entry	Pre-Catalyst	Conversion	Amide	Amine
1	10 mol% $(dppf)_2Ni^0$	100%	97%	3%
2	5 mol% $(dppf)_2Ni^0$	100%	92%	7%
3	2 mol% $(dppf)_2Ni^0$	92%	75%	16%

Table 4.18: Reaction screening with various catalyst loadings of $(dppf)_2Ni^0$. Conversions and yields acquired by ^1H NMR with 1,3,5 trimethoxybenzene as an internal standard.

Having established that $(dppf)_2Ni^0$ (**4.15**) remained effective at reduced catalyst loadings, its performance at lower reaction temperature was subsequently evaluated. Reactions were conducted at both 60 and 40 °C to assess whether the enhanced activity of $(dppf)_2Ni^0$ (**4.15**) would permit catalysis under milder conditions (Table 4.19). At 60 °C, the reaction proceeded to 80% conversion and afforded the desired amide in 69% yield (Table 4.19, entry 1). In contrast, decreasing the temperature to 40 °C substantially impeded the reaction, resulting in only 24% conversion and a yield of 16% of the desired product (Table 4.19, entry 2). Unlike the catalyst loading study, these results were comparable to those obtained during the reaction temperature screening using $(dppf)Ni^{II}Cl_2$ (**4.10**), for which reactions conducted at 60 and 40 °C afforded the desired amide in 66% and 6% yield, respectively (Section 4.4.2.7, Table 4.11, entries 2 and 3). Thus, although $(dppf)_2Ni^0$ (**4.15**) exhibits greater catalyst activity than $(dppf)Ni^{II}Cl_2$ (**4.10**) at reduced catalyst loadings, it does not substantially lower the temperature required for efficient catalysis.

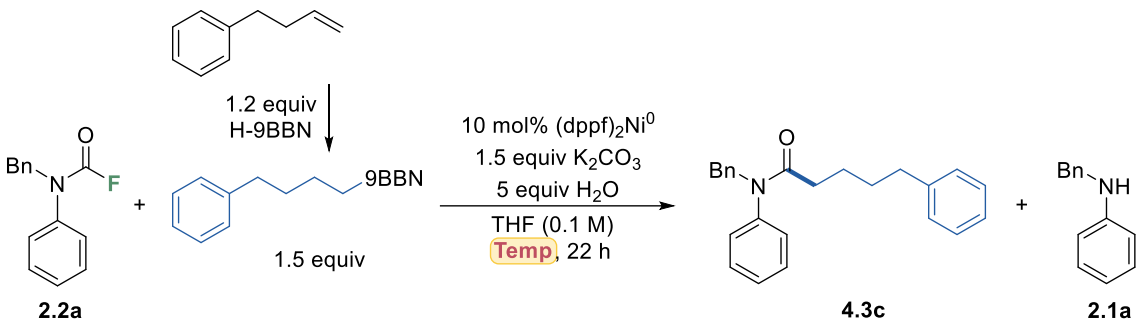

Entry	Pre-Catalyst	Temp	Conversion	Amide	Amine
1	10 mol% $(dppf)_2Ni^0$	60°C	80%	69%	10%
2		40°C	24%	16%	8%

Table 4.19: Reaction screening at reduced temperatures with $(dppf)_2Ni^0$ as the pre-catalyst. Conversions and yields acquired by ^1H NMR with 1,3,5 trimethoxybenzene as an internal standard.

To further investigate catalyst activation, the three principal catalytically relevant species identified throughout the mechanistic investigation, $(dppf)Ni^{II}Cl_2$ (**4.10**), $(dppf)Ni^{I}Cl$ (**4.12**), and $(dppf)_2Ni^0$ (**4.15**), were evaluated in parallel without performing the standard premixing procedure. In these experiments, the pre-catalyst and alkyl-9-BBN reagent were combined directly with the remaining reaction components, thereby preventing the activation process that normally occurs during premixing (Table 4.20). Accordingly, omission of the premixing step was expected to have little effect if the pre-catalyst was either catalytically active itself or could be converted rapidly into the active species under the complete reaction conditions.

$(dppf)Ni^{II}Cl_2$ (**4.10**) was first evaluated as a benchmark and as expected, it performed poorly in the absence of premixing, affording amide in only 9% yield together with 31% of the corresponding amine and overall conversion of 41% (Table 4.20, entry 1). This observation is consistent with the catalyst activation studies described in Section 4.4.5.1, which demonstrated that premixing is essential for conversion of $(dppf)Ni^{II}Cl_2$ (**4.10**) into the catalytically competent Ni(I) complex **4.12**.

In contrast, (dppf)Ni^{I}Cl (**4.12**) afforded the desired amide in a 78% yield together with 15% amine formation and 96% overall conversion (Table 4.20, entry 2). Although this represents a modest decrease in activity compared to the 89% amide yield obtained under the standard premixing conditions (Table 4.17, entry 2). This significantly improved performance relative to (dppf)Ni^{II}Cl$_2$ (**4.10**) demonstrates that (dppf)Ni^{I}Cl (**4.12**) must be more related to the catalytically active species than the original Ni(II) pre-catalyst. These results further support the proposal that generation of (dppf)Ni^{I}Cl (**4.12**) constitutes a crucial catalyst activation step.

Most notably, the catalytic performance of (dppf)$_2$Ni^{0} (**4.15**) was completely unaffected by omission of the premixing procedure. Under these conditions, the desire amide was again obtained in 97% yield along with only 3% amine formation (Table 4.20, entry 3), identical to that observed under the standard optimized conditions (Table 4.17, entry 4). This behaviour stands in stark contrast to both (dppf)Ni^{II}Cl$_2$ (**4.10**) and (dppf)Ni^{I}Cl (**4.12**) and indicates that (dppf)$_2$Ni^{0} (**4.15**) does not require the activation process associated with premixing to function as a highly competent pre-catalyst.

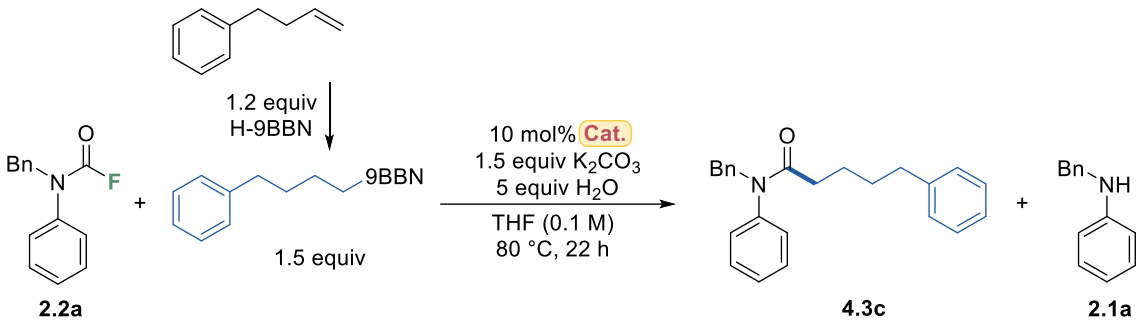

Entry	Pre-Cat	Pre-Mixing Time	Conversion	Amide	Amine
1	(dppf)Ni^{II}Cl$_2$	0 min	41%	9%	31%
2	(dppf)Ni^{I}Cl	0 min	96%	78%	15%
3	(dppf)$_2$Ni^{0}	0 min	100%	97%	3%

Table 4.20: Reaction screening with various pre-catalysts with no pre-mixing. Conversions and yields acquired by ^{1}H NMR with 1,3,5 trimethoxybenzene as an internal standard.

Collectively, these results suggest that **4.15** does not require a pre-activation step to produce an on cycle, catalytically competent species. This interpretation is consistent with the observation that omission of the premixing step had no measurable effect on its catalytic performance.

Furthermore, reaction of (dppf)$Ni^{II}Cl_2$ (**4.10**) with a large excess of either alkyl-9-BBN or H-9BBN afforded no detectable formation of $(dppf)_2Ni^0$ (**4.15**), instead producing (dppf)$Ni^{I}Cl$ (**4.12**) exclusively (Section 4.4.5.1). In contrast, the reaction-monitoring experiments demonstrated that $(dppf)_2Ni^0$ (**4.15**) was already present prior to heating once the complete reaction mixture had been assembled (Section 4.4.5.4). Together, these observations indicate that formation of **4.15** does not occur during the premixing stage and is only formed after all the reaction components are added. Although the precise pathway in which this transformation occurs remains unclear, any pathway converting (dppf)$Ni^{I}Cl$ (**4.12**) into $(dppf)_2Ni^0$ (**4.15**) would involve ligand redistribution, as each molecule of $(dppf)_2Ni^0$ (**4.15**) contains two dppf ligands. The catalyst loading studies for $(dppf)_2Ni^0$ (**4.15**) (Table 4.20) and (dppf)$Ni^{II}Cl_2$ (**4.10**) (Section 4.4.2.6, Table 4.10) provide additional support for this proposal.

Notably, reactions employing 10 mol% of either (dppf)$Ni^{II}Cl_2$ (**4.10**) or (dppf)$Ni^{I}Cl$ (**4.12**) afforded essentially identical yields of 89% (Table 4.17, entries 1 and 2), whereas use of only 5 mol% of **4.15** afforded a comparable 92% yield (Table 4.18, entry 2). The comparable catalytic performance of 10 mol% of Ni(I) complex **4.12** and 5 mol% of $(dppf)_2Ni$ (**4.15**) suggests the possibility that disproportionation of (dppf)$Ni^{I}Cl$ (**4.12**) under the reaction conditions, whereby 10 mol% of Ni(I) would generate 5 mol% of Ni(0) together with 5 mol% of Ni(II). However, further mechanistic studies are required to better understand the formation of the active catalytic species.

To investigate how **4.15** might be formed, the reactivity of (dppf)$Ni^{I}Cl$ (**4.12**) toward hydroxoborate salt **4.24** was re-examined. Although an analogous reaction was previously

investigated in Section 4.4.5.2, the primary objective of that study was the synthesis and isolation of a hydroxoborate-Ni(I) complex, rather than monitoring for the formation of $(dppf)_2Ni^0$ (**4.15**). Consequently, the reaction was repeated using five equivalents of hydroxoborate salt **4.24** and monitored by ^{31}P $\{^1H\}$ NMR spectroscopy to determine whether **4.15** was generated under these conditions. Upon treatment of $(dppf)Ni^ICl$ (**4.12**) with **4.24** at room temperature, trace formation of $(dppf)_2Ni^0$ (**4.15**) was already evident after only 1 minute. Continued monitoring further revealed an increase in intensity of the resonance belonging to **4.15** after 5 minutes, together with the appearance of several additional unidentified phosphorus-containing species (Figure 4.54). The effect of adding free dppf under the standard reaction conditions is evaluated in Section 4.4.5.6.

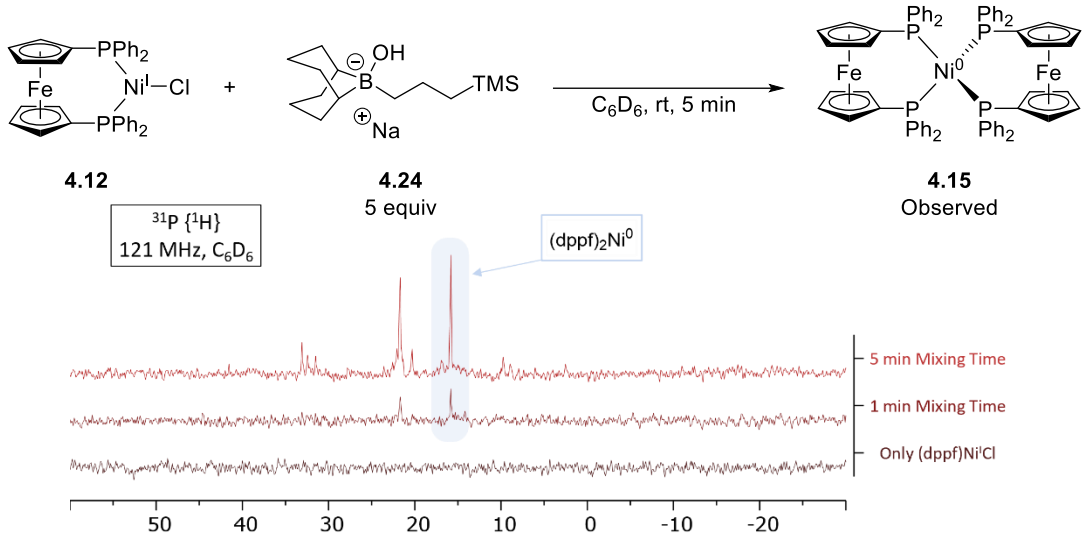

Figure 4.54: ^{31}P $\{^1H\}$ NMR spectra of reaction of **4.12** and **4.24** after the indicated period of time, all spectra were acquired in C_6D_6.

These observations demonstrate that $(dppf)_2Ni^0$ (**4.15**) can be generated from $(dppf)Ni^ICl$ (**4.12**) in the presence of hydroxoborate salt **4.24**. As hydroxoborate salts are proposed to form in situ under the catalytic conditions through reaction of alkyl-9-BBN with H_2O and K_2CO_3, these findings provide a plausible explanation for why $(dppf)_2Ni^0$ (**4.15**) is observed only after all reaction components have been combined and not during the premixing stage. Together, these results establish an experimental link between the catalyst activation and reaction-monitoring

studies, identifying hydroxoborate formation as a plausible promoter for the generation of $(dppf)_2Ni^0$ (**4.15**) under the catalytic reaction conditions.

Based on these observations, a plausible pathway for the formation of $(dppf)_2Ni^0$ (**4.15**) from hydroxoborate salt and $(dppf)Ni^ICl$ (**4.12**) is proposed. Initial transmetalation between hydroxoborate with $(dppf)Ni^ICl$ (**4.12**), followed by alkyl-group transfer, would generate HO-9-BBN together with an alkyl-Ni(I) intermediate. Subsequent disproportionation of this intermediate, accompanied by ligand redistribution, could then furnish complex $(dppf)_2Ni^0$ (**4.15**). Although the precise sequence of these transformations remains to be established, the observed reactivity is consistent with such a pathway.

Although these studies provide a plausible explanation for how $(dppf)_2Ni^0$ **(4.15**) may be generated under the reaction conditions, they do not explain its exceptional catalytic activity. The reactivity of $(dppf)_2Ni^0$ (**4.15**) in the absence of premixing suggests that this complex is either capable of undergoing oxidative addition directly (after dissociating one phosphine ligand) or can rapidly access a different, catalytically relevant species under the reaction conditions. Distinguishing between these possibilities is essential to understanding the role of $(dppf)_2Ni^0$ (**4.15**) within the catalytic cycle. To address this question, the stoichiometric reactivity of $(dppf)_2Ni^0$ (**4.15**) towards CMF **2.2a** was subsequently investigated.

Although the preceding study provides a plausible explanation for how $(dppf)_2Ni^0$ (**4.15**) may be generated under the catalytic reaction conditions, the manner in which **4.15** participates in oxidative addition remains unresolved. To investigate this question, $(dppf)_2Ni^0$ (**4.15**) was treated stoichiometrically with CMF **2.2a** at 80 °C, and the reaction was monitored by ^1H, ^{19}F, and ^{31}P NMR spectroscopy (Scheme 4.47). Although any paramagnetic intermediates or products formed during the reaction would likely remain undetected by NMR spectroscopy, it was anticipated that

observation of diamagnetic species could nevertheless provide insight into the reactivity of $(dppf)_2Ni^0$ (**4.15**) towards carbamoyl fluorides.

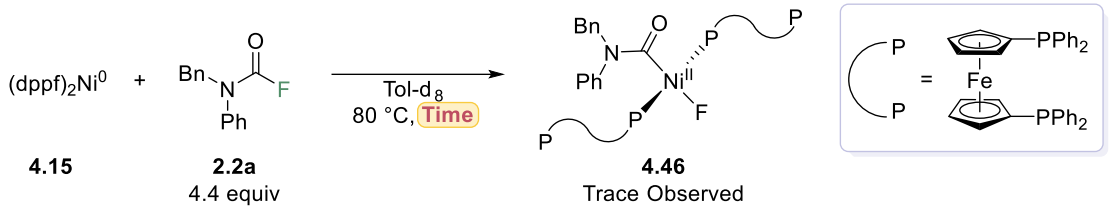

Scheme 4.47: Stoichiometric reaction condition used to evaluate reactivity between complex **4.15** and CMF **2.2a**.

Analysis of the ^1H and ^{31}P $\{^1H\}$ NMR spectra revealed the gradual consumption of $(dppf)_2Ni^0$ (**4.15**), accompanied by the appearance of several new phosphorus-containing species (Figure 4.56, Figure 4.55). Most notably, two resonances emerged at approximately 22 ppm in an apparent 2:1 ratio, with the ratio remaining constant as the signals increased in intensity. Although the identities of these new phosphorus-containing species could not be established, their growth directly paralleled the consumption of $(dppf)_2Ni^0$ (**4.15**), suggesting that Ni(0) complex **4.15** may be able to react with CMF substrate **2.2a**.

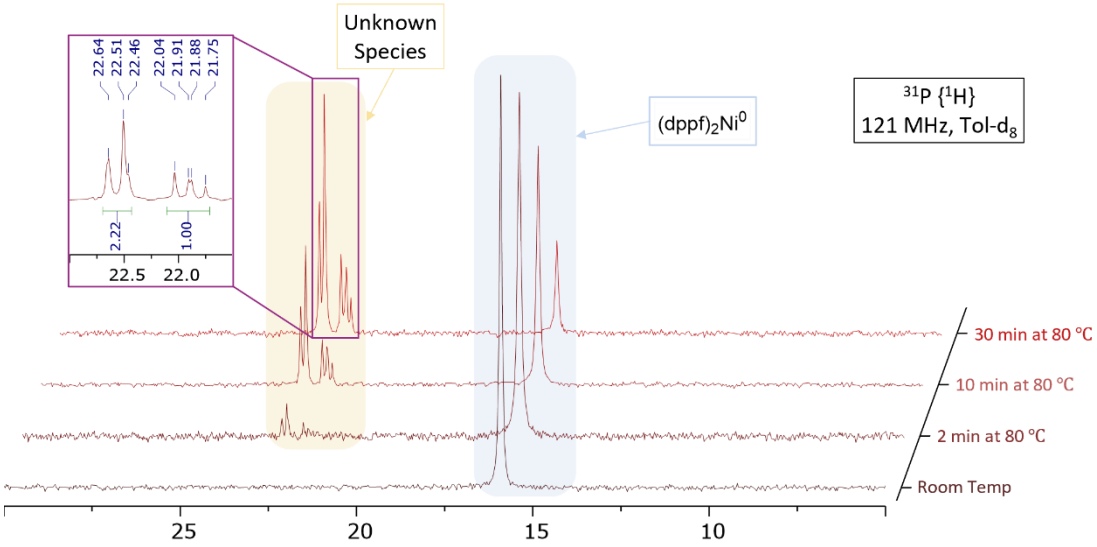

Figure 4.55: ^{31}P $\{^1H\}$ NMR spectra of reaction between **4.15** and **2.2a** after the indicated period of time at 80 °C, all spectra were acquired in Tol-d_8.

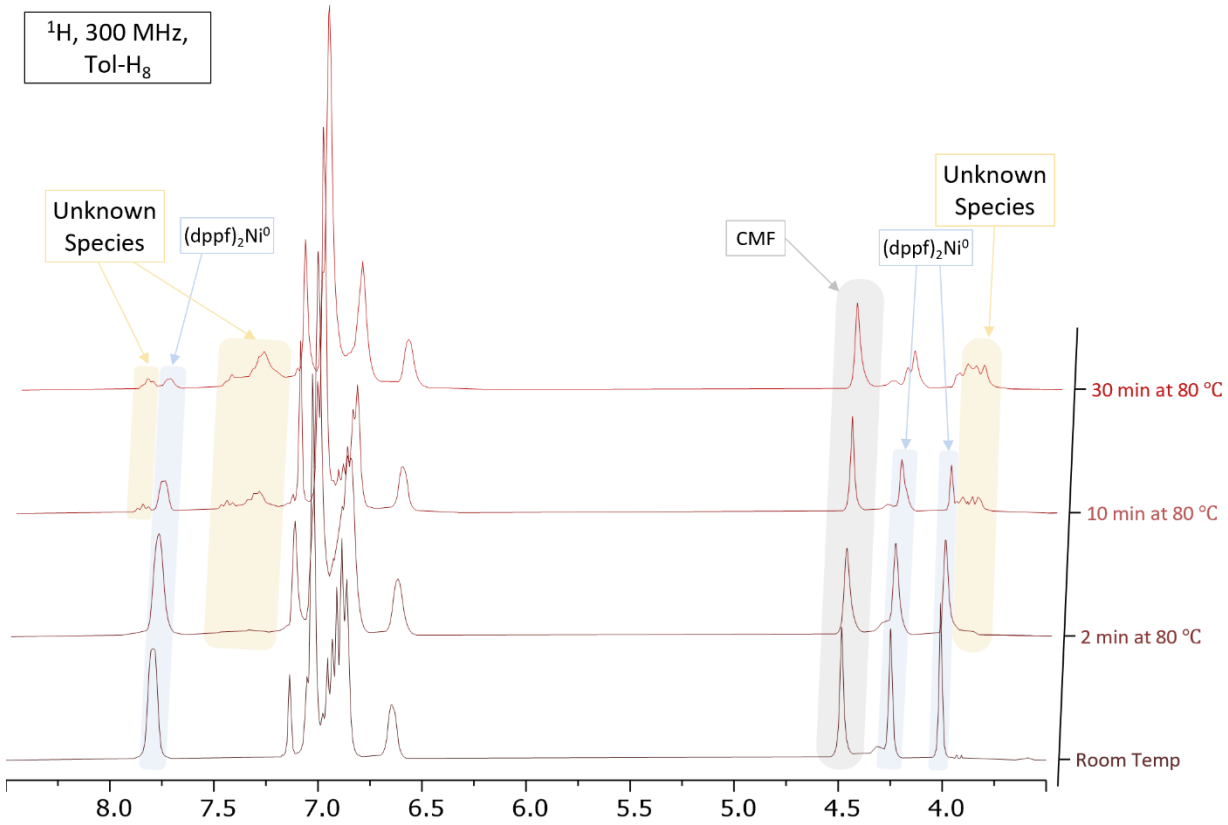

Figure 4.56: ^{1}H NMR spectra of reaction between **4.15** and **2.2a** after the indicated period of time at 80 °C, all spectra were acquired in Tol-d$_8$.

Although the ^{1}H and ^{31}P {^{1}H} NMR spectra indicated that a transformation was occurring, the ^{19}F {^{1}H} NMR spectrum proved to be considerably more informative. While initial inspection of the spectrum revealed no apparent transformation. Upon careful examination of the spectral region in which a fluorine-containing F–Ni(II) oxidative addition complex would be expected, the emergence of a transient, sharp triplet at -293 ppm ($^2J_{FP}$ of 82.8 Hz) was observed (Figure 4.57). This resonance was absent prior to heating and was first observed after heating the reaction mixture at 80 °C for 2 minutes. Continued heating for 10 or 30 minutes resulted in complete disappearance of the resonance, indicating that the fluorine-containing species is both transient and relatively unstable under the reaction conditions. Although the corresponding ^{31}P doublet expected for this species could not be identified, this is likely attributed to its extremely low concentration.

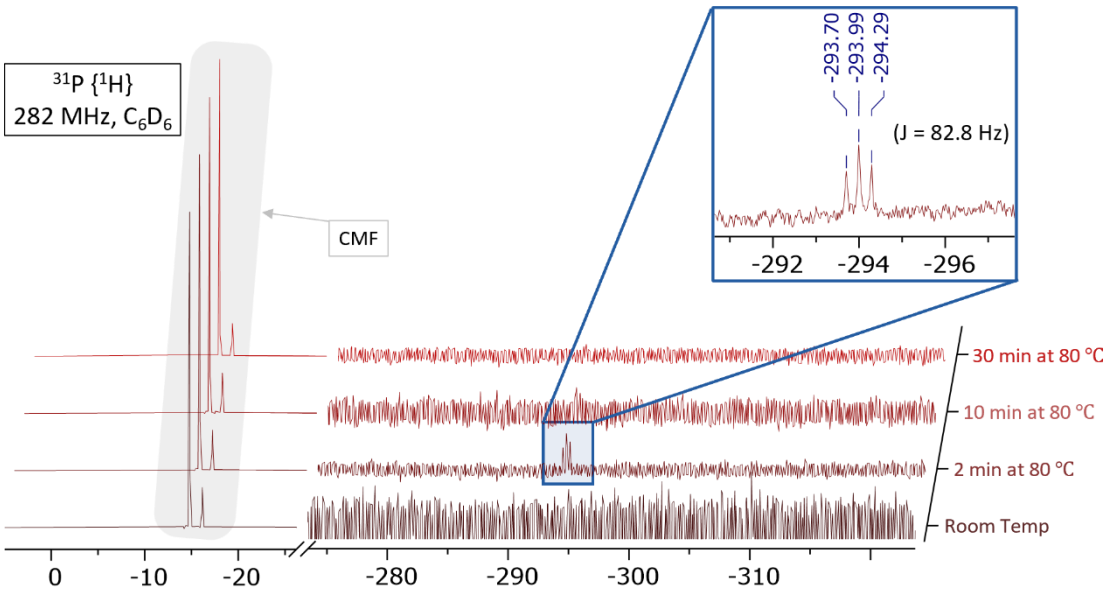

Figure 4.57: ^{19}F {^{1}H} NMR spectra of reaction between **4.15** and **2.2a** after the indicated period of time at 80 °C, all spectra were acquired in Tol-d_8. Spectrum region between -25 and -275 ppm have been omitted for clarity. Spectrum region between -275 and -320 ppm (right) has been significantly magnified relative to spectrum region between 5 and -25 ppm (left) for clarity.

Most importantly, the spectroscopic features of this transient fluorine-containing species provide substantial insight into its structure. First, the ^{19}F {^{1}H} NMR chemical shift at -293 ppm is suggestive of a nickel-bound fluorine ligand, as relatively few fluorine-containing species appear in this region. Furthermore, the presence of a sharp, well-defined, symmetric triplet demonstrates coupling of the fluorine to two equivalent phosphorus atoms. The well-resolved nature of the resonance further indicates that the species is diamagnetic, ruling out the possibility of a paramagnetic Ni(I) complex. A diamagnetic d^8 Ni(II) complex is therefore most consistent with a square-planar geometry rather than tetrahedral. When considering the approximate ~110° bite angle of dppf and presence of two equivalent phosphorus atoms on this new complex, the species at -293 ppm likely bears two κ^1-dppf ligands in a trans orientation (Scheme 4.47) (**4.46**). Notably, these chemical shifts and coupling constants are consistent with the analogous oxidative addition

complex bearing two PPh_3 ligands described in Section 4.4.5.3, providing additional support for the proposed structure.

Collectively, the stoichiometric and catalytic evaluation of the isolated nickel complexes establishes a coherent picture of the catalytic cycle. Although the hydroxoborate-Ni(I) complexes **4.30** and **4.31** were capable of promoting amide formation, their comparatively poor stoichiometric and catalytic reactivity suggests that they are unlikely to represent the principal on-cycle intermediates. In contrast, oxidative addition complex **4.37** demonstrated both excellent stoichiometric and catalytic competence, providing strong support that Ni(II) oxidative addition complexes are catalytically relevant intermediates, in line with a likely Ni(0)/Ni(II) catalytic cycle.

Within these mechanistic studies, $(dppf)_2Ni^0$ (**4.15**) emerged as a key catalytic species, which can be formed through the reaction of $(dppf)Ni^ICl$ (**4.12**) and hydroxoborate intermediates under the reaction conditions, accounting for its appearance only after assembly of the complete reaction mixture. Once formed, $(dppf)_2Ni^0$ (**4.15**) functions as a highly competent catalyst precursor that is capable of undergoing oxidative addition with CMFs. Although the transient oxidative addition complex could not be isolated, its spectroscopic features are consistent with formation of a square-planar Ni(II) carbamoyl fluoride complex and closely parallels that of the independently prepared PPh_3 analogue. These findings rationalize both how $(dppf)_2Ni^0$ (**4.15**) is able to participate in catalysis, wherein both dppf ligands likely remain bound to the Ni center, with the full proposed catalytic cycle illustrates in Section 4.4.5.7.

4.4.4.6. Miscellaneous Mechanistic Studies

Several additional mechanistic experiments were conducted to gain further insight into the reaction mechanism. As a benchmark, the standard cross-coupling was performed under the optimized reaction conditions, resulting in complete conversion of CMF **2.2a** and afforded the desired amide in 89% yield, together with 10% amine (Table 4.21, entry 1).

To investigate whether THF plays a role in coordinating and stabilizing organometallic intermediates or coordinating to the Lewis acidic borane species, the reaction was repeated using 2-methyltetrahydrofuran (2-MeTHF) as the solvent. It was hypothesized that the increased steric bulk of 2-MeTHF would reduce its coordinating ability relative to THF, thereby diminishing its capacity to stabilize reactive intermediates during the catalytic cycle. Under these conditions, a significant reduction in amide was observed with only 49% yield (Table 4.21, entry 2).

However, preparation of the reaction mixture revealed that H_2O exhibits significantly lower solubility in 2-MeTHF than in THF, resulting in the formation of a biphasic solution when the H_2O/2-MeTHF stock solution was prepared. At first glance, this reduced solubility appeared to provide a plausible explanation for the diminished reaction performance. However, during the base-solvent screening (Section 4.4.2.4), the reaction proceeded in 80% yield when conducted in toluene with Cs_2CO_3 (Table 4.7, entry 8), a solvent that is essentially immiscible with water. This observation suggests that reduced water solubility alone is unlikely to account for the diminished reactivity observed in 2-MeTHF. Nevertheless, because the effects of solvent coordination and water availability cannot be fully deconvoluted in the present work, no definitive conclusion can be drawn.

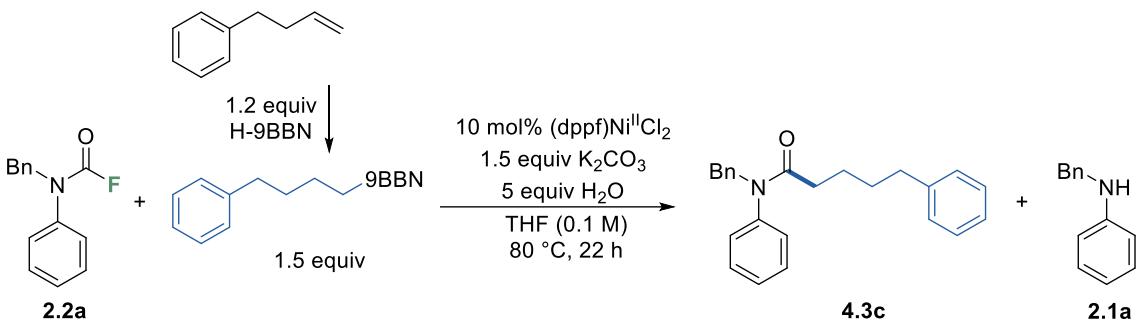

Entry	Deviation from STD conditions	Conversion	Amide	Amine
1	N/A	100%	89%	10%
2	2-MeTHF Instead of THF	54%	49%	4%

Table 4.21: Evaluation of deviations from optimized reaction conditions. Conversions and yields acquired by ^{1}H NMR with 1,3,5 trimethoxybenzene as an internal standard.

To further probe the viability of the proposed catalytic pathways, D_2O was used in place of H_2O under the standard reaction conditions. This experiment was designed to evaluate the extent to which β-hydride elimination occurs during catalysis. If β-hydride elimination is occurring, the alkyl-nickel species generated in situ is expected to exist in equilibrium with the corresponding nickel-hydride through β-hydride elimination and the reverse process of migratory insertion (Figure 4.58). Because metal hydrides can undergo hydrogen-deuterium exchange (HDX) with D_2O, this equilibrium provides a pathway for deuterium incorporation into the catalytic cycle and ultimately into the cross-coupling product.[69,70]

The extent of deuterium incorporation was anticipated to provide insight into the identity of catalytically relevant species. Under a Ni(I)/Ni(III) catalytic cycle and assuming that oxidative addition is slow, β-hydride elimination from the alkyl-Ni(I) intermediate is proposed to generate the corresponding nickel(I) hydride, which is expected to undergo reversible migratory insertion and HDX with D_2O prior to productive C–C bond formation. Consequently, appreciable deuterium incorporation into the amide product would be anticipated. In contrast, although β-hydride elimination is also possible for a Ni(II) alkyl intermediate, rapid C–C bond reductive elimination

to form the desired amide is expected to outcompete β-hydride elimination in a Ni(0)/Ni(II) catalytic cycle. Furthermore, any Ni(II) hydride generated may itself undergo reductive elimination to afford the corresponding formamide by-product. Consequently, substantially lower levels of deuterium incorporation would be expected if catalysis proceeds predominantly though a Ni(0)/Ni(II) cycle.

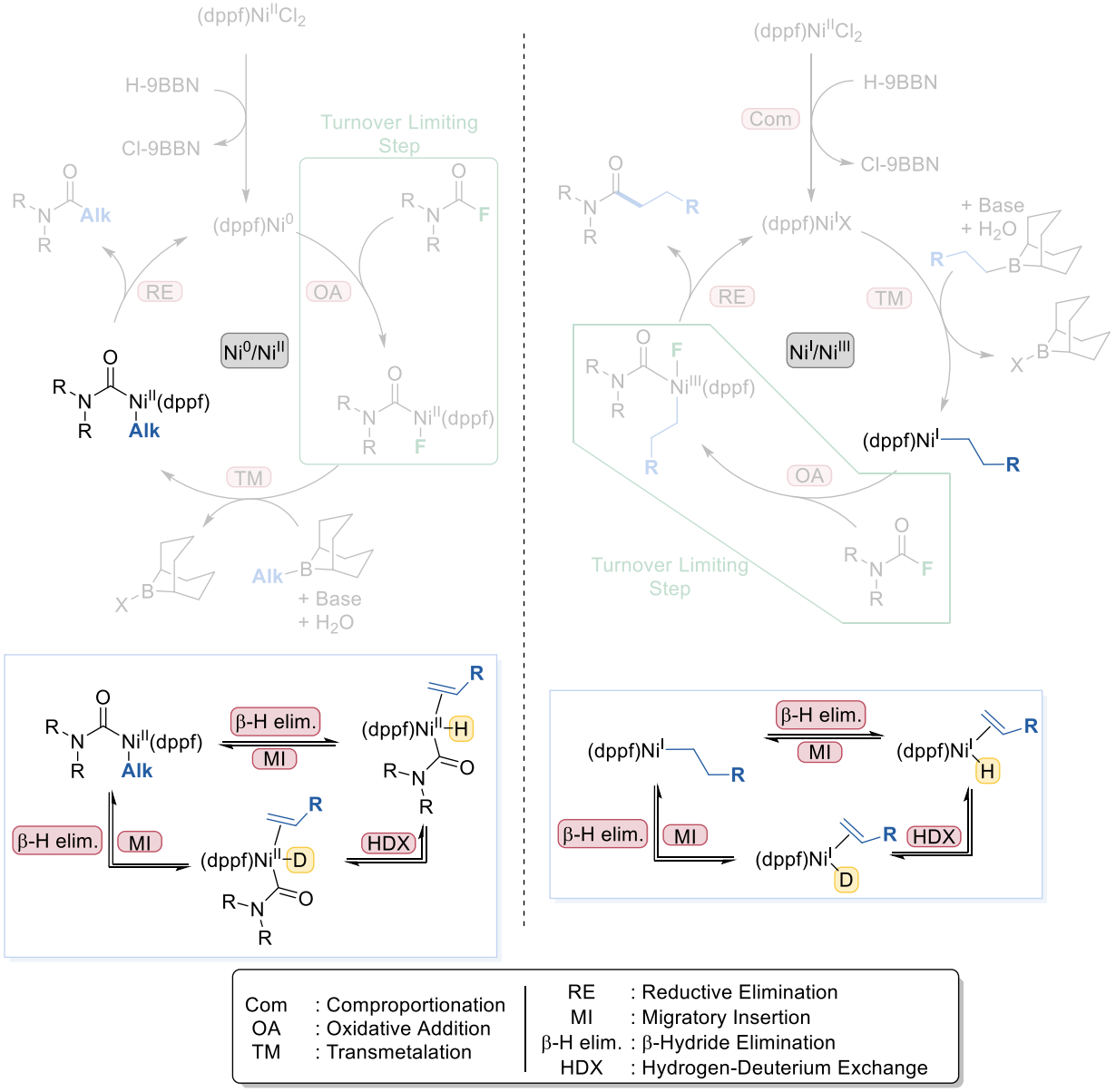

Figure 4.58: Proposed catalytic pathways in which HDX can occur.

Upon conducting the reaction using 5 equivalents of D_2O in place of H_2O under the standard reaction conditions, a surprising and entirely unanticipated result was obtained. The desired amide was formed in only 16% yield with a conversion of 41%, in stark contrast to the standard reaction employing H_2O, which affords the which affords the product in 89% yield with complete conversion (Table 4.22). This dramatic reduction in both product yield and substrate conversion is consistent with a substantial kinetic isotope effect (KIE), though its origin is not immediately apparent.

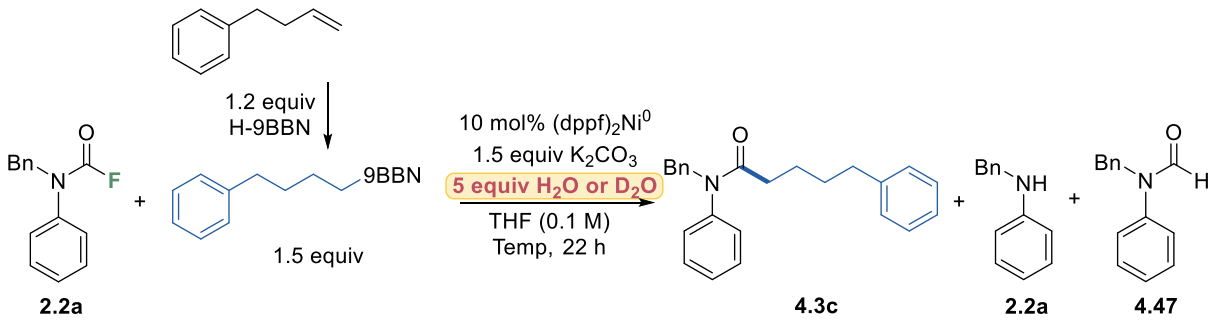

Entry	H_2O or D_2O	Conversion	Amide	Amine	Formamide
1	H_2O	100%	89%	10%	2%
2	D_2O	41%	16%	22%	3%

Table 4.22: Evaluation of specified deviations from optimized reaction conditions. Conversions and yields acquired by ^{1}H NMR with 1,3,5 trimethoxybenzene as an internal standard.

To determine whether HDX had occurred during catalysis, the crude reaction mixture was analysed by GC-MS and NMR spectroscopy (Figure 4.59). No deuterium incorporation being detected in the amide product. Instead, deuterium incorporation was observed in on the carbamoyl hydrogen of the corresponding formamide by-product, which is formed in approximately 2-3% under both the H_2O and D_2O reaction conditions. Analysis of the ^{1}H NMR spectrum revealed a significant decrease in the relative integration of the carbamoyl proton (8.58 ppm) with respect to the benzylic methylene protons (5.01 ppm), consistent with deuterium incorporation at the carbamoyl site (Figure 4.59 **B**). Because the protiated and deuterated formamides possess identical

retention times by GC-MS, the extent of deuterium incorporation was assessed by comparison of the observed molecular-ion isotope distribution with that expected from the natural isotope abundance of the non-deuterated formamide. The enhanced intensity of the *m/z* 212 molecular ion relative to the *m/z* 211 ion exceeded that expected from the natural abundance of ^{13}C, confirming the formation of the deuterated formamide (Figure 4.59). Together, the GC-MS and ^{1}H NMR data demonstrates the HDX occurs during formation of the formamide by-product.

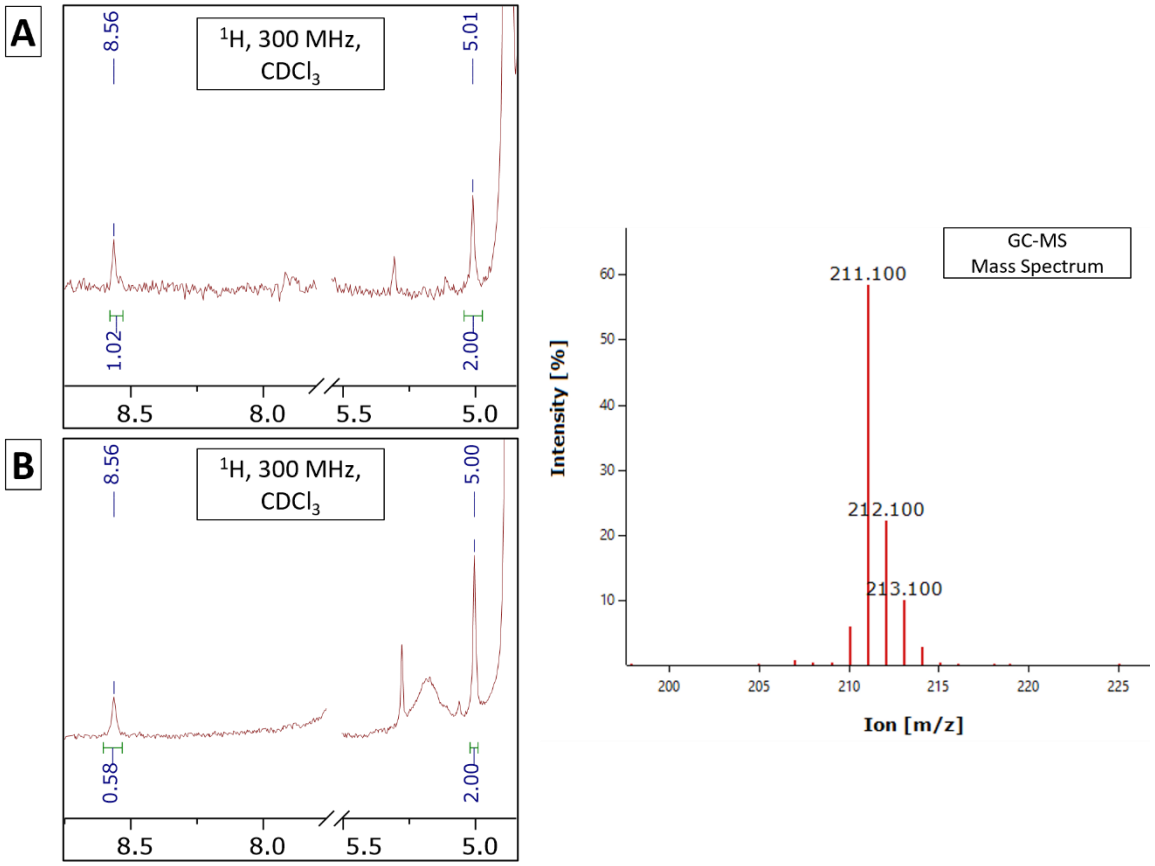

Figure 4.59: Crude ^{1}H NMR spectra of the standard cross-coupling reaction with H_2O (**A**) or D_2O (**B**), signals shown and integrated are of the benzylic and carbamoyl hydrogen atoms. All spectra were acquired in $CDCl_3$. Spectra region between -7.7 and 5.5 ppm have been omitted for clarity. GC-MS mass spectrum with retention time of 11.0 min (Right) from reaction employing D_2O.

Mechanistically, these observations provide important insight into the nature of the catalytic cycle. The incorporation of deuterium into the formamide, rather than the desired amide, is consistent with the formation of a Ni(II) hydride following β-hydride elimination from the

corresponding alkyl-Ni(II) intermediate. Subsequent HDX between the nickel hydride and D_2O, followed by reductive elimination, provides a straightforward path to the observed deuterated formamide (Figure 4.60). In contrast, the absence of detectable deuterium incorporation into the desired amide argues against reversible β-hydride elimination and migratory insertion prior to oxidative addition of CMF, as would be anticipated for a dominant Ni(I)/Ni(III) cycle. Consequently, these observations provide further support for a Ni(0)/Ni(II) catalytic cycle under the developed reaction conditions.

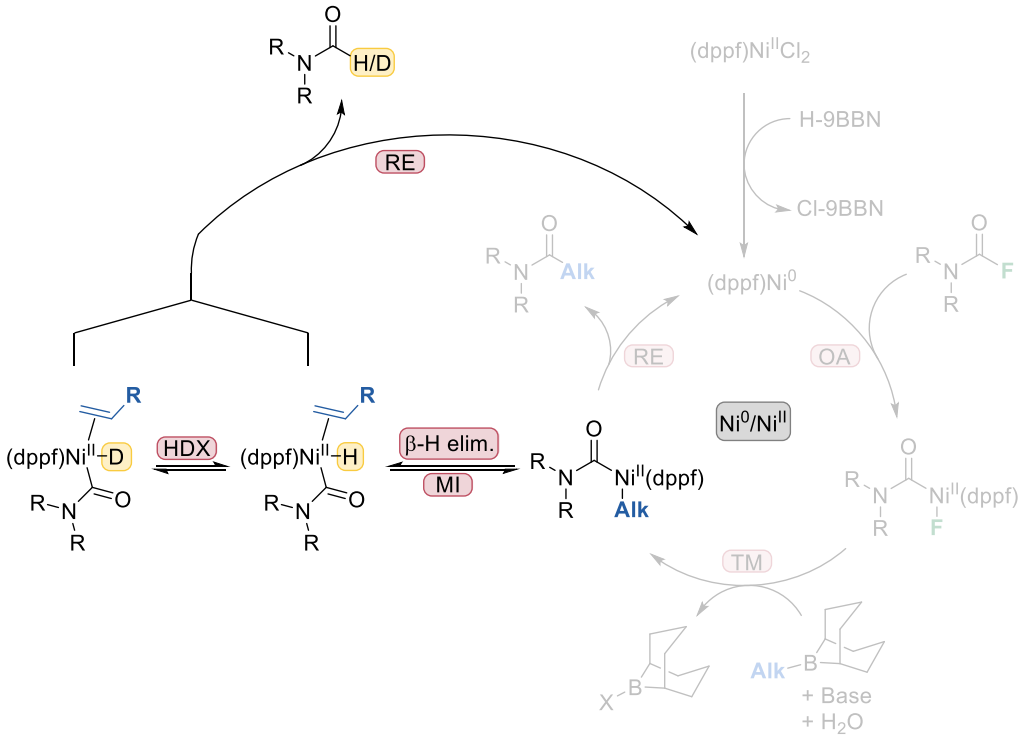

Figure 4.60: Proposed mechanism for how formamide may be generated in the catalytic cycle.

Although deuterium incorporation into the formamide supports the intermediacy of a nickel hydride, it does not explain the pronounced reduction in catalytic activity observed upon replacing H_2O with D_2O. The magnitude of the observed KIE indicates that substitution of H_2O with D_2O influences an important process required for efficient catalysis. Water is required throughout the

catalytic cycle, including its equilibrium with the carbonate base to generate hydroxide, which forms the catalytically relevant hydroxoborate species. Thus, several water-mediated steps could potentially contribute to the observed isotope effect. However, the available experimental data does not permit the origin of the KIE to be assigned unequivocally.

Next to further investigate the nature of the organometallic intermediates generated during catalysis, TEMPO was evaluated as a mechanistic probe. TEMPO has frequently been employed in nickel catalysis as both a radical trapping reagent and an oxidant capable of intercepting low-valent nickel species. Several Ni(I)-mediated catalytic transformations have been reported to undergo substantial inhibition, or complete suppression, upon addition of TEMPO, even when employed in quantities lower than the catalyst loading.[71–76] Consequently, TEMPO was investigated as a means of probing whether persistent Ni(I) intermediates or free organic radicals are required for productive catalysis. Before evaluating its effect under catalytic conditions, the reactivity of TEMPO towards (dppf)Ni^{I}Cl (**4.12**) was first examined to establish whether rapid oxidation to a Ni(II)-TEMPO adduct would occur.

Treatment of (dppf)Ni^{I}Cl (**4.12**) with two equivalents of TEMPO at room temperature resulted in an immediate reaction, evidenced by the transformation of the yellow-orange suspension of (dppf)Ni^{I}Cl (**4.12**) into a homogeneous dark red solution corresponding to **4.48**. The corresponding Ni(II)-TEMPO adduct **4.48** was isolated in 96% yield (Scheme 4.48). Single crystals suitable for SC-XRD were obtained by slow evaporation of a saturated benzene solution. Analysis by SC-XRD revealed the formation of a dinuclear Ni(II) complex in which two nickel centers, each bearing one chloride and a κ^2-(N,O)-coordinated TEMPO ligand, are bridged by a single dppf ligand through coordination of one phosphorus donor atom to each nickel center (Figure 4.61). The rapid and essentially quantitative formation of **4.48** demonstrates that TEMPO

readily reacts with (dppf)Ni^{I}Cl (**4.12**) at room temperature, confirming that it is capable of efficiently intercepting this Ni(I) species.

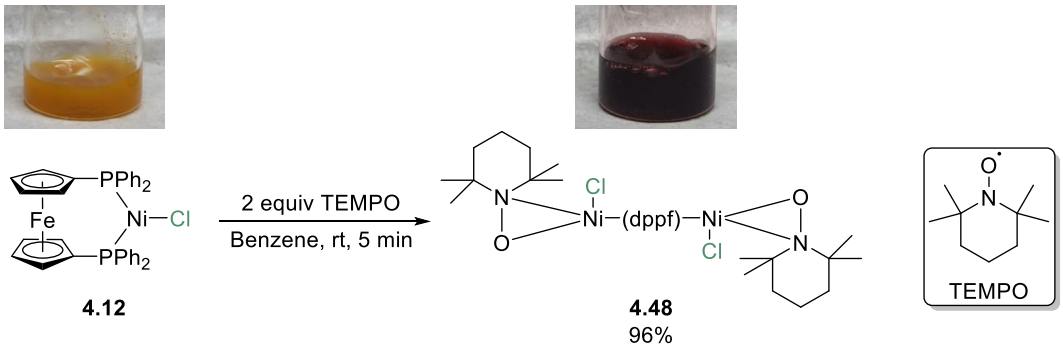

Scheme 4.48: Reaction conditions employed to synthesized Ni–TEMPO adduct **4.48**.

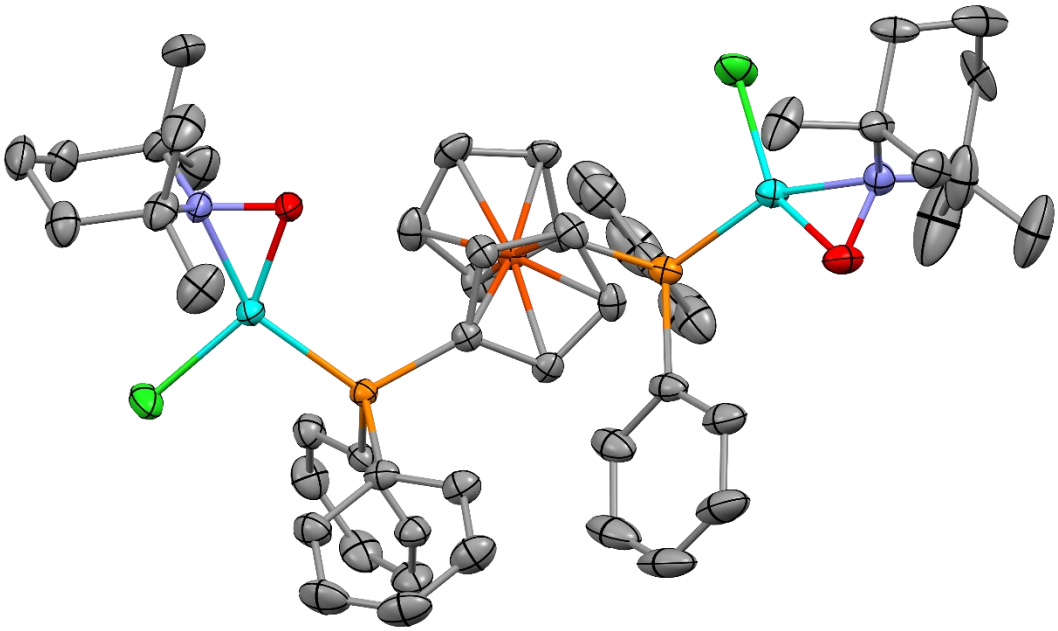

Figure 4.61: Solid-state structure of complex **4.48.** ORTEP drawn at 50% probability, hydrogen atoms have been omitted for clarity.

Having established the rapid reactivity of TEMPO toward (dppf)Ni^{I}Cl (**4.12**), its effect on the catalytic cross-coupling reaction was subsequently evaluated. The standard reaction was conducted using either (dppf)Ni^{II}Cl$_2$ (**4.10**) or (dppf)Ni^{I}Cl (**4.12**) as the pre-catalyst in the presence of one equivalent of TEMPO (10 equivalents relative to nickel). In both cases, catalytic activity

was moderately diminished, with (dppf)$Ni^{II}Cl_2$ (**4.10**) affording the desired product in 70% yield with 93% conversion, while (dppf)$Ni^{I}Cl$ (**4.12**) afforded 47% yield with 71% conversion (Table 4.23).

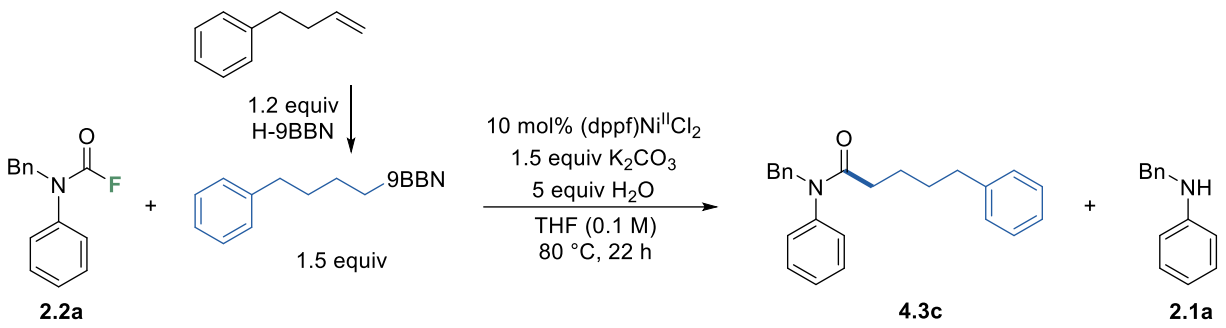

Entry	Pre-Cat	Additive	Conversion	Amide	Amine
1	(dppf)$Ni^{II}Cl_2$	1 equiv TEMPO	93%	70%	20%
2	(dppf)$Ni^{I}Cl$		71%	47%	23%

Table 4.23: Evaluation of specified deviations from optimized reaction conditions. Conversions and yields acquired by ^{1}H NMR with 1,3,5 trimethoxybenzene as an internal standard.

These observations indicate that TEMPO inhibits the catalytic process but does not completely suppress turnover. Although catalytic activity is reduced, substantial substrate conversion and product formation are still observed, even in the presence of a ten-fold excess of TEMPO relative to nickel. Furthermore, because TEMPO is capable of coordinating to the Lewis acidic boron species present under the reaction conditions, in addition to its demonstrated ability to rapidly oxidize (dppf)$Ni^{I}Cl$ (**4.12**), the observed reduction in activity cannot be definitively attributed to either the trapping of organic radicals or the oxidation of relevant Ni(I) species. Nevertheless, the relatively modest inhibition observed suggests that productive catalysis is unlikely to rely on persistent, readily accessible Ni(I) species or organic radicals throughout the catalytic cycle, as substantially greater inhibition would be anticipated if such intermediates were involved. Rather, these results are more consistent with a mechanism in which such species, if formed, are either short-lived and rapidly consumed or are not required for productive catalysis.

Lastly, as $(dppf)_2Ni^0$ (**4.15**) is proposed to be a key catalytically relevant species but its formation from $(dppf)Ni^{II}Cl_2$ (**4.10**) requires a sacrificial equivalent of the pre-catalyst. It was hypothesized that the addition of 10 mol% dppf to the standard reaction conditions would result in a greater concentration of the catalytically relevant **4.15** complex being generated in situ. Thus, we expected to see enhanced catalytic activity comparable to that observed when employing 10 mol% $(dppf)_2Ni^0$ (**4.15**) directly. Surprisingly, addition of 10 mol% dppf had no measurable effect on the reaction outcome, affording identical conversion and product yield to those obtained under the standard reaction conditions (Table 4.24). This observation suggests that simply increasing the concentration of free dppf may not promote the formation of additional $(dppf)_2Ni^0$ (**4.15**) under the catalytic conditions. Given that increasing the catalyst loading of independent prepared **4.15** was previously shown to improve catalytic performance (Section 4.4.5.5, Table 4.18), these results suggest that formation of $(dppf)_2Ni^0$ (**4.15**) may not be limited by the availability of free dppf. Further studies are therefore required to clarify the factors governing catalyst activation and the generation of the catalytically relevant Ni(0) species. In particular, evaluating the effect of additional dppf at lower catalyst loadings would help determine whether its lack of benefit is specific to the conditions examined.

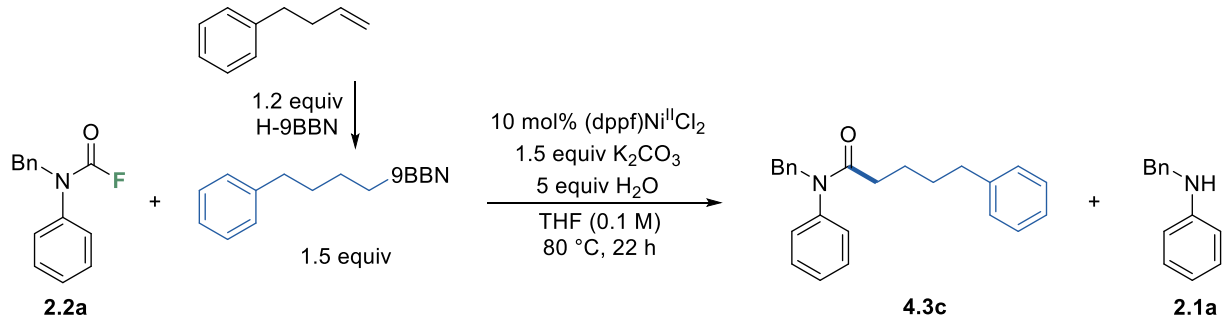

Entry	Deviation from STD conditions	Conversion	Amide	Amine
1	N/A	100%	89%	10%
2	10 mol% dppf added	100%	88%	12%

Table 4.24: Evaluation of specified deviations from optimized reaction conditions. Conversions and yields acquired by ^1H NMR with 1,3,5 trimethoxybenzene as an internal standard.

Collectively, these miscellaneous mechanistic studies provide additional support for the proposed catalytic cycle while highlighting the complexity of the catalyst activation process and speciation. Although several of the experiments did not provide definitive mechanistic answers, they nevertheless served to refine the current mechanistic picture. In particular, the studies employing D_2O further supporting a Ni(0)/Ni(II) catalytic cycle, through the identification of a possible Ni(II)-hydride pathway leading to the formamide by-product. The TEMPO inhibition experiments suggest that productive catalysis is unlikely to rely on persistent Ni(I) species or formation of organic radicals. Finally, the inability of free dppf to enhance the in situ generation of $(dppf)_2Ni^0$ suggests that catalyst activation is governed by factors beyond simple ligand availability. Together, the observed results are in line with a traditional Ni(0)/Ni(II) catalytic cycle. However, we are currently investigating the energetic feasibility of the other proposed pathways using DFT calculations in a collaboration with Prof. David Nelson.

4.4.4.7. Mechanistic Summary

The mechanistic investigations presented throughout this Chapter were undertaken to establish the identity of the catalytically relevant nickel species and their role in the developed cross-coupling reaction. Although several mechanistically distinct pathways were considered plausible at the outset of this study, including Ni(0)/Ni(II), Ni(I)/Ni(III), and direct Ni(I) catalytic cycles, the collective experimental evidence obtained throughout this work consistently favors a mechanism operating predominantly through a Ni(0)/Ni(II) cycle. Rather than relying on a single mechanistic observation, this conclusion is supported by numerous complementary experiments, including the synthesis and structural characterization of catalytically relevant intermediates, stoichiometric reactivity studies, pre-catalyst competence experiments, in situ reaction monitoring, as well as isotope and radical trapping studies. Together these separate lines of evidence provide a rough mechanistic picture (Figure 4.62), although they do not definitively establish the TLS. Although stoichiometric studies indicate a turnover-limiting event occurring before or during oxidative addition; this interpretation remains tentative because the relative rates of these steps under catalytic conditions have not been fully determined. Therefore, detailed kinetic studies and DFT calculations are required to establish a more complete understanding of the reaction.

Catalyst activation studies revealed that premixing (dppf)$NiCl_2$ with H-9BBN rapidly generates (dppf)$Ni^{I}Cl$ through rapid and selective reduction of Ni(II) to Ni(I). The dramatic improvement in catalytic performance observed upon premixing, together with the identical catalytic activity of independently prepared (dppf)$Ni^{I}Cl$, demonstrates that formation of the Ni(I) species represents a crucial activation step preceding productive catalysis. Despite its essential role in catalyst activation, no experimental evidence supports that (dppf)$Ni^{I}Cl$ itself is a principal catalytically relevant species. Instead, reaction monitoring experiments established that $(dppf)_2Ni^{0}$

forms once the reaction mixture is fully assembled, while subsequent mechanistic studies demonstrated that hydroxoborate intermediates are capable of promoting the formation of $(dppf)_2Ni^0$ from $(dppf)Ni^ICl$.

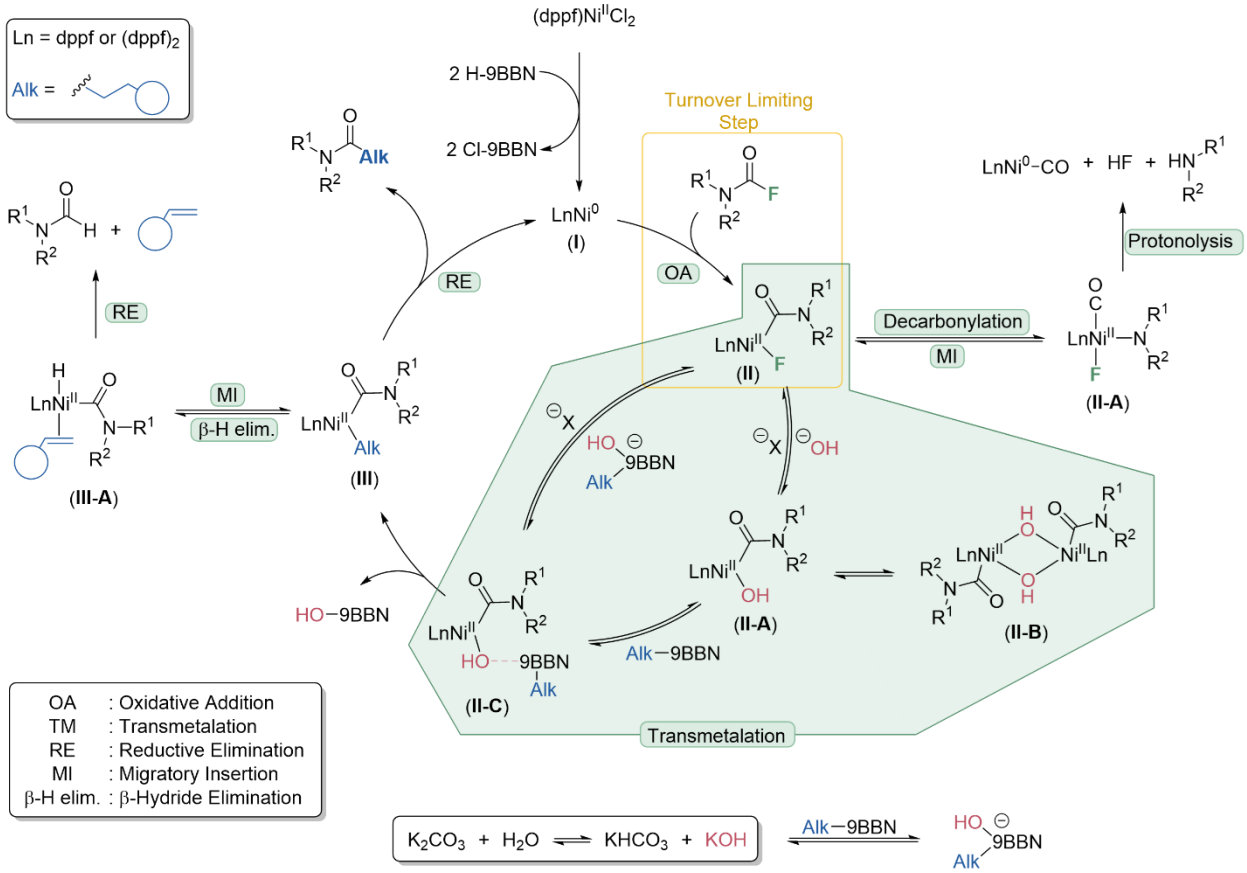

Figure 4.62: Complete proposed catalytic-cycle including mechanisms for by-product formation.

Perhaps the strongest evidence supporting a Ni(0)/Ni(II) catalytic cycle arises from the successful preparation and evaluation of oxidative addition complexes. The direct oxidative additions complex **4.37** was isolated and structurally characterized by SC-XRD, demonstrating that CMFs can undergo oxidative addition with Ni(0). Although isolation was not possible, analysis by NMR spectroscopy further established that CMFs lacking a directing group are likewise capable of undergoing oxidative addition to Ni(0). Stoichiometric reactions demonstrated that complex **4.37** readily undergoes transmetalation and reductive elimination to afford the

desired cross-coupled product, while catalytic evaluation confirmed that oxidative addition complex (**4.37**) can efficiently re-enter the catalytic cycle and supports multiple catalytic turnovers. The remarkable rapid reaction observed between **4.37** and hydroxoborate **4.25** at room temperature additionally indicates that, once oxidative addition has occurred, the subsequent elementary steps proceed readily under comparatively mild conditions. These observations, together with the accumulation of $(dppf)_2Ni^0$ (**4.15**) during the reaction monitoring studies, strongly suggests that oxidative addition represents the turnover limiting step of the catalytic cycle.

Although the mechanistic studies consistently favored a Ni(0)/Ni(II) pathway, considerable effort was devoted to evaluating the viability of alternative Ni(I)-mediated mechanisms. A series of novel hydroxoborate-Ni(I) complexes were successfully synthesized, culminating in the first crystallographically characterized hydroxoborate-Ni(I) complex **4.31**. These complexes demonstrated that hydroxoborate salts can coordinate to Ni(I) under the appropriate conditions, resulting in sufficiently stable species for structural characterization and providing direct experimental support for the feasibility of the proposed transmetalation intermediate. Furthermore, both hydroxoborate complexes underwent productive stoichiometric reactions with CMFs, confirming that they could be chemically competent species capable of facilitating C–C bond formation. However, catalytic evaluation revealed that these complexes exhibited drastically lower catalytic activity than either $(dppf)_2Ni^0$ (**4.15**) or oxidative addition complex **4.37**. Consequently, while these studies demonstrate that Ni(I) complexes are capable of promoting the reaction, they provide little evidence that such species are directly involved in productive catalysis.

One of the most unexpected findings to emerge from these studies was the identification of $(dppf)_2Ni^0$ (**4.15**) as an exceptionally active pre-catalyst. Unlike $(dppf)Ni^{II}Cl_2$ (**4.10**), its catalytic performance was completely independent of the premixing procedure, indicating that

$(dppf)_2Ni^0$ (**4.15**) bypasses the activation process required for the Ni(II) pre-catalyst. Stoichiometric reactions between $(dppf)_2Ni^0$ (**4.15**) and CMF **2.2a** further revealed formation of the proposed oxidative addition complex, providing direct experimental support for its role as a catalytically relevant species. These observations not only rationalize the exceptional catalytic activity of $(dppf)_2Ni^0$ (**4.15**) but also establish it as one of the most likely catalytically relevant Ni(0) species operating under the reaction conditions.

Collectively, the mechanistic investigations presented throughout this chapter establish a coherent description of the catalytic cycle. Catalyst activation proceeds initially through selective reduction of Ni(II) to Ni(I), followed by generation of a Ni(0) species under the complete reaction conditions. The resulting Ni(0) complex undergoes oxidative addition with CMF, followed by base-assisted transmetalation with alkyl-9-BBN and reductive elimination affording the desired amide product while regenerating the active catalyst. Although Ni(I) clearly participates during catalyst activation, the overwhelming body of experimental evidence indicates that productive turnover proceeds predominantly through a Ni(0)/Ni(II) catalytic cycle. The combination of synthetic organometallic chemistry, structural characterization by SC-XRD and NMR spectroscopy, stoichiometric reactivity studies, catalytic competence experiments, reaction monitoring, and complementary mechanistic probes provide a comprehensive experimental evaluation of the nickel-catalyzed Suzuki cross-coupling of carbamoyl fluoride.

4.5. Conclusion and Future Work

This Chapter has established the first general Suzuki cross-coupling of carbamoyl fluorides with alkyl boranes, providing an efficient method for the synthesis of aliphatic amides from easily prepared carbamoyl fluorides. Through extensive optimization studies, effective reaction conditions were identified, revealing several crucial factors for productive catalysis including catalyst premixing, strict control of the water-base ratio in the reaction, and suitable workup conditions for the reaction. Under the optimized reaction conditions, the method developed worked well across a large substrate scope, successfully coupling 45 combinations of carbamoyl fluorides and alkyl boranes encompassing a wide range of structural motifs, generally in excellent yields and with a broad functional group tolerance.

Beyond reaction development, extensive mechanistic investigations provided detailed insight into the catalytic pathway. Numerous catalytically relevant nickel complexes were successfully prepared and characterized, including oxidative addition complexes and hydroxoborate-Ni(I) complexes, enabling experimental evaluation of the proposed elementary steps. Collectively, these studies suggest that catalyst activation proceeds through initial reduction of Ni(II) to Ni(I), followed by generation of a catalytically competent Ni(0) species under the complete reaction conditions. With $(dppf)_2Ni^0$ identified as the most probable catalytic resting state and oxidative addition to the carbamoyl fluoride proposed to likely be the TLS. However, further detailed kinetic studies and DFT calculations are required to establish a more definitive mechanistic picture of the reaction.

Importantly, these studies also demonstrated that carbamoyl fluorides lacking directing groups remain competent substrates for oxidative addition to Ni(0), significantly advancing the

fundamental understanding of their reactivity with nickel. This insight further broadens the potential synthetic utility of carbamoyl fluorides and provides a strong foundation for future development of a wider range of transition-metal-catalyzed transformations employing carbamoyl fluorides as electrophilic coupling partners.

4.6. References

(1) Nielsen, C. D.-T.; Zivkovic, F. G.; Schoenebeck, F. Synthesis of N-CF3 Alkynamides and Derivatives Enabled by Ni-Catalyzed Alkynylation of N-CF3 Carbamoyl Fluorides. *J. Am. Chem. Soc.* **2021**, *143* (33), 13029–13033. https://doi.org/10.1021/jacs.1c07780.

(2) Jabbarpoor, M.; LeBlanc, J.; Chen, Z.; Cadwallader, D.; Le, C. M. Pd-Catalyzed Suzuki-Type Cross-Coupling of 2-Pyridyl Carbamoyl Fluorides. *Chem. Commun.* **2024**, *60* (66), 8700–8703. https://doi.org/10.1039/D4CC02431A.

(3) Yasui, Y.; Tsuchida, S.; Miyabe, H.; Takemoto, Y. One-Pot Amidation of Olefins through Pd-Catalyzed Coupling of Alkylboranes and Carbamoyl Chlorides. *J. Org. Chem.* **2007**, *72* (15), 5898–5900. https://doi.org/10.1021/jo070724u.

(4) Pearson, R. G. Hard and Soft Acids and Bases, HSAB, Part 1: Fundamental Principles. *J. Chem. Educ.* **1968**, *45* (9), 581. https://doi.org/10.1021/ed045p581.

(5) Pearson, R. G. Hard and Soft Acids and Bases. *J. Am. Chem. Soc.* **1963**, *85* (22), 3533–3539. https://doi.org/10.1021/ja00905a001.

(6) Moloto, B. P.; Vermeeren, P.; Dalla Tiezza, M.; Esterhuysen, C.; Bickelhaupt, F. M.; Hamlin, T. A. Palladium-Catalyzed Activation of Carbon–Halogen Bonds: Electrostatics-Controlled Reactivity. *Eur. J. Org. Chem.* **2022**, *2022* (26), e202200722. https://doi.org/10.1002/ejoc.202200722.

(7) Rio, J.; Liang, H.; Perrin, M.-E.; Perego, L.; Grimaud, L.; Payard, P.-A. We Already Know Everything about Oxidative Addition to Pd(0) - Do We? *ACS Catal.* **2023**, *13* (17), 11399–11421. https://doi.org/10.1021/acscatal.3c01943.

(8) Anjali, B. A.; Suresh, C. H. Interpreting Oxidative Addition of Ph–X (X = CH3, F, Cl, and Br) to Monoligated Pd(0) Catalysts Using Molecular Electrostatic Potential. *ACS Omega* **2017**, *2* (8), 4196–4206. https://doi.org/10.1021/acsomega.7b00745.

(9) Amii, H.; Uneyama, K. C−F Bond Activation in Organic Synthesis. *Chem. Rev.* **2009**, *109* (5), 2119–2183. https://doi.org/10.1021/cr800388c.

(10) Ariafard, A.; Lin, Z. Understanding the Relative Easiness of Oxidative Addition of Aryl and Alkyl Halides to Palladium(0). *Organometallics* **2006**, *25* (16), 4030–4033. https://doi.org/10.1021/om060236x.

(11) Chernyshev, V. M.; Ananikov, V. P. Nickel and Palladium Catalysis: Stronger Demand than Ever. *ACS Catal.* **2022**, *12* (2), 1180–1200. https://doi.org/10.1021/acscatal.1c04705.

(12) Lin; Liu, L.; Fu, Y.; Luo, S.-W.; Chen, Q.; Guo, Q.-X. Comparing Nickel- and Palladium-Catalyzed Heck Reactions. *Organometallics* **2004**, *23* (9), 2114–2123. https://doi.org/10.1021/om034067h.

(13) Cooper, A. K.; Burton, P. M.; Nelson, D. J. Nickel versus Palladium in Cross-Coupling Catalysis: On the Role of Substrate Coordination to Zerovalent Metal Complexes. *Synthesis* **2020**, *52* (04), 565–573. https://doi.org/10.1055/s-0039-1690045.

(14) Jasim, N. A.; Perutz, R. N.; Whitwood, A. C.; Braun, T.; Izundu, J.; Neumann, B.; Rothfeld, S.; Stammler, H.-G. Contrasting Reactivity of Fluoropyridines at Palladium and Platinum: C−F Oxidative Addition at Palladium, P−C and C−F Activation at Platinum. *Organometallics* **2004**, *23* (26), 6140–6149. https://doi.org/10.1021/om049448p.

(15) Mastrorilli, P.; Moro, G.; Nobile, C. F.; Latronico, M. New Nickel(O) Complexes with Bulky Diphosphine Ligands. *Inorganica Chim. Acta* **1992**, *192* (2), 183–187. https://doi.org/10.1016/S0020-1693(00)80757-4.

(16) Chung, T. C.; Janvikul, W.; Lu, H. L. A Novel "Stable" Radical Initiator Based on the Oxidation Adducts of Alkyl-9-BBN. *J. Am. Chem. Soc.* **1996**, *118* (3), 705–706. https://doi.org/10.1021/ja9527737.
(17) Ollivier, C.; Renaud, P. Organoboranes as a Source of Radicals. *Chem. Rev.* **2001**, *101* (11), 3415–3434. https://doi.org/10.1021/cr010001p.
(18) Chang, L.; An, Q.; Duan, L.; Feng, K.; Zuo, Z. Alkoxy Radicals See the Light: New Paradigms of Photochemical Synthesis. *Chem. Rev.* **2022**, *122* (2), 2429–2486. https://doi.org/10.1021/acs.chemrev.1c00256.
(19) Gehani, A. A. M. A. E.; A. Maashi, H.; Harnedy, J.; C. Morrill, L. Electrochemical Generation and Utilization of Alkoxy Radicals. *Chem. Commun.* **2023**, *59* (25), 3655–3664. https://doi.org/10.1039/D3CC00302G.
(20) Banoun, C.; Bourdreux, F.; Magnier, E.; Dagousset, G. Intermolecular C–O Bond Formation with Alkoxyl Radicals: Photoredox-Catalyzed α-Alkoxylation of Carbonyl Compounds. *Org. Lett.* **2021**, *23* (22), 8926–8930. https://doi.org/10.1021/acs.orglett.1c03444.
(21) He, X.; Zhao, Y.; Zhang, Z.; Shen, X. Tuning the Reactivity of Alkoxyl Radicals from Cyclization to 1,2-Silyl Transfer: Stereoselective Synthesis of β-Substituted Cycloalcohols. *Org. Lett.* **2022**, *24* (10), 1991–1995. https://doi.org/10.1021/acs.orglett.2c00428.
(22) Yang, Z.; Niu, Y.; He, X.; Chen, S.; Liu, S.; Li, Z.; Chen, X.; Zhang, Y.; Lan, Y.; Shen, X. Tuning the Reactivity of Alkoxyl Radicals from 1,5-Hydrogen Atom Transfer to 1,2-Silyl Transfer. *Nat. Commun.* **2021**, *12* (1), 2131. https://doi.org/10.1038/s41467-021-22382-y.
(23) Köster, R.; Seidel, G.; Wrackmeyer, B. Alkalimetall-Trialkylhydroxyborate Und (Alkalimetalloxy)Dialkylborane[1]. *Chem. Ber.* **1992**, *125* (3), 617–625. https://doi.org/10.1002/cber.19921250313.
(24) Bhagat, K. K.; Cheke, R. S.; Gavali, V. D.; Kharkar, P. S.; Arote, N. D. A Brief Review on Metal-Curcumin Complexes: Synthesis Approaches and Their Pharmaceutical Applications. *Discov. Chem.* **2025**, *2* (1), 119. https://doi.org/10.1007/s44371-025-00174-3.
(25) Amaya, T.; Maegawa, Y.; Masuda, T.; Osafune, Y.; Hirao, T. Selective Intermolecular Oxidative Cross-Coupling of Enolates. *J. Am. Chem. Soc.* **2015**, *137* (32), 10072–10075. https://doi.org/10.1021/jacs.5b05058.
(26) Yalpani, M.; Boese, R.; Seevogel, K.; Köuster, R. Monomeric and Dimeric Acyloxydialkylboranes. *J. Chem. Soc. Dalton Trans.* **1993**, No. 1, 47–50. https://doi.org/10.1039/DT9930000047.
(27) Bubnov, Yu. N.; Zheludeva, V. I.; Ignatenko, A. V. Synthesis of 1-Substituted 1-Vinylcycloalkanes by Allylboration of Carbonyl Compounds and Ethoxyacetylene with Diorganylborylethylidenecyclopentane and a Diorganylborylethylidenecyclohexane. *Bull. Acad. Sci. USSR Div. Chem. Sci.* **1989**, *38* (2), 366–372. https://doi.org/10.1007/BF00953631.
(28) Kliegel, W.; Nanninga, D. Borchelate von Salicylaldehydnitronen. *J. Organomet. Chem.* **1983**, *243* (4), 373–385. https://doi.org/10.1016/S0022-328X(00)98570-X.
(29) Hojoh, K.; Shido, Y.; Ohmiya, H.; Sawamura, M. Construction of Quaternary Stereogenic Carbon Centers through Copper-Catalyzed Enantioselective Allylic Cross-Coupling with Alkylboranes. *Angew. Chem. Int. Ed.* **2014**, *53* (19), 4954–4958. https://doi.org/10.1002/anie.201402386.
(30) Schäfer, F.; Lamm, J.-H.; Neumann, B.; Stammler, H.-G.; Mitzel, N. W. Silicon-Bridged Bi- and Tridentate Lewis Acidic Host Systems. *Eur. J. Inorg. Chem.* **2021**, *2021* (32), 3265–3271. https://doi.org/10.1002/ejic.202100497.

(31) Eisenberger, P.; Bestvater, B. P.; Keske, E. C.; Crudden, C. M. Hydrogenations at Room Temperature and Atmospheric Pressure with Mesoionic Carbene-Stabilized Borenium Catalysts. *Angew. Chem. Int. Ed.* **2015**, *54* (8), 2467–2471. https://doi.org/10.1002/anie.201409250.
(32) Bubnov, Yu. N.; Zheludeva, V. I.; Ignatenko, A. V. Synthesis of 1-Substituted 1-Vinylcycloalkanes by Allylboration of Carbonyl Compounds and Ethoxyacetylene with Diorganylborylethylidenecyclopentane and a Diorganylborylethylidenecyclohexane. *Bull. Acad. Sci. USSR Div. Chem. Sci.* **1989**, *38* (2), 366–372. https://doi.org/10.1007/BF00953631.
(33) W. Kramer, G.; C. Brown, H. Organoboranes: XIX. The Preparation and Some Unusual Chemistry of b-Allyl Derivatives of 9-Borabicyclo[3.3.1]Nonane. *J. Organomet. Chem.* **1977**, *132* (1), 9–27. https://doi.org/10.1016/S0022-328X(00)92510-5.
(34) Curran, D. P.; Moura-Letts, G.; Pohlman, M. Solution-Phase Mixture Synthesis with Fluorous Tagging En Route: Total Synthesis of an Eight-Member Stereoisomer Library of Passifloricins. *Angew. Chem. Int. Ed.* **2006**, *45* (15), 2423–2426. https://doi.org/10.1002/anie.200600041.
(35) O'Keefe, B. M.; Mans, D. M.; Kaelin, D. E. J.; Martin, S. F. Total Synthesis of Isokidamycin. *J. Am. Chem. Soc.* **2010**, *132* (44), 15528–15530. https://doi.org/10.1021/ja107926f.
(36) Benaissa, I.; Rialland, B.; Bennaamane, S.; Espada, M. F.; Saffon-Merceron, N.; Fustier-Boutignon, M.; Clot, E.; Mézailles, N. N2 Functionalization via Molybdenum-Nitride Complex: Stepwise BH Bond Additions. *Angew. Chem. Int. Ed.* **2024**, *63* (29), e202402586. https://doi.org/10.1002/anie.202402586.
(37) Köuster, R.; Seidel, G.; Schüuβler, W.; Wrackmeyer, B. Die Ersten Organobor-Tellur-Verbindungen[1]. *Chem. Ber.* **1995**. https://doi.org/10.1002/cber.19951280113.
(38) Soderquist, J. A.; Najafi, M. R. Selective Oxidation of Organoboranes with Anhydrous Trimethylamine N-Oxide. *J. Org. Chem.* **1986**, *51* (8), 1330–1336. https://doi.org/10.1021/jo00358a032.
(39) Matos, K.; Soderquist, J. A. Alkylboranes in the Suzuki−Miyaura Coupling: Stereochemical and Mechanistic Studies. *J. Org. Chem.* **1998**, *63* (3), 461–470. https://doi.org/10.1021/jo971681s.
(40) *Synthesis of Functionalized [3], [4], [5] and [6]Dendralenes through Palladium-Catalyzed Cross-Couplings of Substituted Allenoates - Lippincott - 2017 - Angewandte Chemie International Edition - Wiley Online Library*. https://onlinelibrary.wiley.com/doi/10.1002/anie.201609636 (accessed 2026-06-29).
(41) Jiang, Y.; Kwan, E. E.; Ping, Y.; Liu, R. Y. Synthesis of Diaryl Ethers by Formal Oxygen Insertion Between Suzuki–Miyaura Coupling Partners. *ACS Catal.* **2025**, *15* (15), 13588–13594. https://doi.org/10.1021/acscatal.5c03249.
(42) Zhu, C.; Wang, R.; Falck, J. R. Mild and Rapid Hydroxylation of Aryl/Heteroaryl Boronic Acids and Boronate Esters with N-Oxides. *Org. Lett.* **2012**, *14* (13), 3494–3497. https://doi.org/10.1021/ol301463c.
(43) Diccianni, J.; Lin, Q.; Diao, T. Mechanisms of Nickel-Catalyzed Coupling Reactions and Applications in Alkene Functionalization. *Acc. Chem. Res.* **2020**, *53* (4), 906–919. https://doi.org/10.1021/acs.accounts.0c00032.
(44) Diccianni, J. B.; Diao, T. Mechanisms of Nickel-Catalyzed Cross-Coupling Reactions. *Trends Chem.* **2019**, *1* (9), 830–844. https://doi.org/10.1016/j.trechm.2019.08.004.

(45) Mohadjer Beromi, M.; Nova, A.; Balcells, D.; Brasacchio, A. M.; Brudvig, G. W.; Guard, L. M.; Hazari, N.; Vinyard, D. J. Mechanistic Study of an Improved Ni Precatalyst for Suzuki–Miyaura Reactions of Aryl Sulfamates: Understanding the Role of Ni(I) Species. *J. Am. Chem. Soc.* **2016**, *139* (2), 922–936. https://doi.org/10.1021/jacs.6b11412.
(46) Christian, A. H.; Müller, P.; Monfette, S. Nickel Hydroxo Complexes as Intermediates in Nickel-Catalyzed Suzuki–Miyaura Cross-Coupling. *Organometallics* **2014**, *33* (9), 2134–2137. https://doi.org/10.1021/om5001327.
(47) Singh, S.; Sunoj, R. B. Mechanism and Origin of Enantioselectivity in Nickel-Catalyzed Alkyl–Alkyl Suzuki Coupling Reaction. *J. Phys. Chem. A* **2019**, *123* (31), 6701–6710. https://doi.org/10.1021/acs.jpca.9b04284.
(48) Mohadjer Beromi, M.; Banerjee, G.; Brudvig, G. W.; Hazari, N.; Mercado, B. Q. Nickel(I) Aryl Species: Synthesis, Properties, and Catalytic Activity. *ACS Catal.* **2018**, *8* (3), 2526–2533. https://doi.org/10.1021/acscatal.8b00546.
(49) Matsubara, K.; Fukahori, Y.; Inatomi, T.; Tazaki, S.; Yamada, Y.; Koga, Y.; Kanegawa, S.; Nakamura, T. Monomeric Three-Coordinate N-Heterocyclic Carbene Nickel(I) Complexes: Synthesis, Structures, and Catalytic Applications in Cross-Coupling Reactions. *Organometallics* **2016**, *35* (19), 3281–3287. https://doi.org/10.1021/acs.organomet.6b00419.
(50) Li, Z.; Jiang, Y.-Y.; Fu, Y. Theoretical Study on the Mechanism of Ni-Catalyzed Alkyl–Alkyl Suzuki Cross-Coupling. *Chem. Eur. J.* **2012**, *18* (14), 4345–4357. https://doi.org/10.1002/chem.201103882.
(51) West, M. J.; Watson, A. J. B. Ni vs. Pd in Suzuki–Miyaura Sp2–Sp2 Cross-Coupling: A Head-to-Head Study in a Comparable Precatalyst/Ligand System. *Org. Biomol. Chem.* **2019**, *17* (20), 5055–5059. https://doi.org/10.1039/c9ob00561g.
(52) Bena, A. R.; Pieber, B. Advances in NiI/NiIII-Catalyzed C(Sp2)–Heteroatom Cross-Couplings. *ACS Catal.* **2026**, *16* (2), 866–881. https://doi.org/10.1021/acscatal.5c07964.
(53) Fan, P.; Lan, Y.; Zhang, C.; Wang, C. Nickel/Photo-Cocatalyzed Asymmetric Acyl-Carbamoylation of Alkenes. *J. Am. Chem. Soc.* **2020**, *142* (5), 2180–2186. https://doi.org/10.1021/jacs.9b12554.
(54) Le, C. M.; Sperger, T.; Fu, R.; Hou, X.; Lim, Y. H.; Schoenebeck, F.; Lautens, M. Stereoselective Synthesis of Methylene Oxindoles via Palladium(II)-Catalyzed Intramolecular Cross-Coupling of Carbamoyl Chlorides. *J. Am. Chem. Soc.* **2016**, *138* (43), 14441–14448. https://doi.org/10.1021/jacs.6b08925.
(55) Pilloni, G.; Toffoletti, A.; Bandoli, G.; Longato, B. Homoleptic Complexes of Cobalt(0) and Nickel(0,I) with 1,1‘-Bis(Diphenylphosphino)Ferrocene (Dppf): Synthesis and Characterization. *Inorg. Chem.* **2006**, *45* (25), 10321–10328. https://doi.org/10.1021/ic061185z.
(56) Cleaves, P. A.; Ayres, A. J.; Vondung, L.; Stewart, J. C.; Cobb, P. J.; Wooles, A. J.; Liddle, S. T. Bridged and Unbridged Nickel–Nickel Bonds Supported by Cyclopentadienyl and Phosphine Ligand Sets. *Organometallics* **2020**, *39* (24), 4735–4746. https://doi.org/10.1021/acs.organomet.0c00708.
(57) Xu, W.; Li, M.; Qiao, L.; Xie, J. Recent Advances of Dinuclear Nickel- and Palladium-Complexes in Homogeneous Catalysis. *Chem. Commun.* **2020**, *56* (61), 8524–8536. https://doi.org/10.1039/d0cc02542a.
(58) Inatomi, T.; Koga, Y.; Matsubara, K. Dinuclear Nickel(I) and Palladium(I) Complexes for Highly Active Transformations of Organic Compounds. *Molecules* **2018**, *23* (1), 140. https://doi.org/10.3390/molecules23010140.

(59) Demadis, K. D.; Hartshorn, C. M.; Meyer, T. J. The Localized-to-Delocalized Transition in Mixed-Valence Chemistry. *Chem. Rev.* **2001**, *101* (9), 2655–2686. https://doi.org/10.1021/cr990413m.
(60) Robin, M. B.; Day, P. Mixed Valence Chemistry-A Survey and Classification. In *Advances in Inorganic Chemistry and Radiochemistry*; Emeléus, H. J., Sharpe, A. G., Eds.; Academic Press, 1968; Vol. 10, pp 247–422. https://doi.org/10.1016/S0065-2792(08)60179-X.
(61) Witzke, R. J.; Tilley, T. D. Synthesis and Reactivity of a Dimeric Ni(I) Methyl Complex. *Organometallics* **2022**, *41* (12), 1565–1571. https://doi.org/10.1021/acs.organomet.2c00188.
(62) Herrmann, W. A.; Krüger, C.; Goddard, R.; Bernal, I. Transition Metal Methylene Complexes: III. Methylene (CH2), a Carbonyl Analogous Ligand; Crystal Structure of μ-Methylenebis(Carbonyl-H5-Cyclopentadienylrhodium)(Rh—Rh. *J. Organomet. Chem.* **1977**, *140* (1), 73–89. https://doi.org/10.1016/S0022-328X(00)84398-3.
(63) Herrmann, W. A. The Methylene Bridge. *Adv. Organomet. Chem.* **1982**. https://doi.org/10.1016/S0065-3055(08)60522-5.
(64) Gao, Y.; Jennings, M. C.; Puddephatt, R. J. A Diruthenium μ-Methylene Complex. *Organometallics* **2001**, *20* (9), 1882–1888. https://doi.org/10.1021/om0010417.
(65) Wu, Y.; Shan, C.; Ying, J.; Su, J.; Zhu, J.; Liu, L. L.; Zhao, Y. Catalytic Hydroboration of Aldehydes, Ketones, Alkynes and Alkenes Initiated by NaOH. *Green Chem.* **2017**, *19* (17), 4169–4175. https://doi.org/10.1039/c7gc01632h.
(66) Malapit, C. A.; Bour, J. R.; Brigham, C. E.; Sanford, M. S. Base-Free Nickel-Catalysed Decarbonylative Suzuki–Miyaura Coupling of Acid Fluorides. *Nature* **2018**, *563* (7729), 100–104. https://doi.org/10.1038/s41586-018-0628-7.
(67) Ohashi, M.; Saijo, H.; Shibata, M.; Ogoshi, S. Palladium-Catalyzed Base-Free Suzuki–Miyaura Coupling Reactions of Fluorinated Alkenes and Arenes via a Palladium Fluoride Key Intermediate. *Eur. J. Org. Chem.* **2013**, *2013* (3), 443–447. https://doi.org/10.1002/ejoc.201201405.
(68) Köuster, R.; Seidel, G.; Schüuβler, W.; Wrackmeyer, B. Die Ersten Organobor-Tellur-Verbindungen[1]. *Chem. Ber.* **1995**, *128* (1), 87–89. https://doi.org/10.1002/cber.19951280113.
(69) Cypcar, A. D.; Kerr, T. A.; Yang, J. Y. Thermochemical Studies of Nickel Hydride Complexes with Cationic Ligands in Aqueous and Organic Solvents. *Organometallics* **2022**, *41* (18), 2605–2611. https://doi.org/10.1021/acs.organomet.2c00319.
(70) Connelly Robinson, S. J.; Zall, C. M.; Miller, D. L.; Linehan, J. C.; Appel, A. M. Solvent Influence on the Thermodynamics for Hydride Transfer from Bis(Diphosphine) Complexes of Nickel. *Dalton Trans.* **2016**, *45* (24), 10017–10023. https://doi.org/10.1039/c6dt00309e.
(71) Korch, K. M.; Watson, D. A. Cross-Coupling of Heteroatomic Electrophiles. *Chem. Rev.* **2019**, *119* (13), 8192–8228. https://doi.org/10.1021/acs.chemrev.8b00628.
(72) Knappke, C. E. I.; Grupe, S.; Gärtner, D.; Corpet, M.; Gosmini, C.; Jacobi von Wangelin, A. Reductive Cross-Coupling Reactions between Two Electrophiles. *Chem. – Eur. J.* **2014**, *20* (23), 6828–6842. https://doi.org/10.1002/chem.201402302.
(73) Diccianni, J. B.; Katigbak, J.; Hu, C.; Diao, T. Mechanistic Characterization of (Xantphos)Ni(I)-Mediated Alkyl Bromide Activation: Oxidative Addition, Electron Transfer, or Halogen-Atom Abstraction. *J. Am. Chem. Soc.* **2019**, *141* (4), 1788–1796. https://doi.org/10.1021/jacs.8b13499.
(74) Chakraborty, U.; Urban, F.; Mühldorf, B.; Rebreyend, C.; de Bruin, B.; van Velzen, N.; Harder, S.; Wolf, R. Accessing the CpArNi(I) Synthon: Reactions with N-Heterocyclic

Carbenes, TEMPO, Sulfur, and Selenium. *Organometallics* **2016**, *35* (11), 1624–1631. https://doi.org/10.1021/acs.organomet.6b00084.
(75) Rettenmeier, C.; Wadepohl, H.; Gade, L. H. Stereoselective Hydrodehalogenation via a Radical-Based Mechanism Involving T-Shaped Chiral Nickel(I) Pincer Complexes. *Chem. – Eur. J.* **2014**, *20* (31), 9657–9665. https://doi.org/10.1002/chem.201403243.
(76) Ma, Z.; Mahmudov, K. T.; Aliyeva, V. A.; Gurbanov, A. V.; Pombeiro, A. J. L. TEMPO in Metal Complex Catalysis. *Coord. Chem. Rev.* **2020**, *423*, 213482. https://doi.org/10.1016/j.ccr.2020.213482.
(77) Chaumeil, H.; Signorella, S.; Le Drian, C. Suzuki Cross-Coupling Reaction of Sterically Hindered Aryl Boronates with 3-Iodo-4-Methoxybenzoic Acid Methylester. Tetrahedron **2000**, 56 (49), 9655–9662. https://doi.org/10.1016/S0040-4020(00)00928-5
(78) Matos, K.; Soderquist, J. A. Alkylboranes in the Suzuki−Miyaura Coupling: Stereochemical and Mechanistic Studies. *J. Org. Chem.* **1998**, 63 (3), 461–470. https://doi.org/10.1021/jo971681s
(79) Sato, M.; Miyaura, N.; Suzuki, A. Cross-Coupling Reaction of Alkyl- or Arylboronic Acid Esters with Organic Halides Induced by Thallium(I) Salts and Palladium-Catalyst. *Chem. Lett.* **1989**, 18 (8), 1405–1408. https://doi.org/10.1246/cl.1989.1405

4.7. Chapter 4 Appendix

General Remarks

Unless otherwise stated, all reactions and manipulations were performed under an inert atmosphere of dry argon, using standard Schlenk techniques or in a nitrogen filled glovebox. Solid H-9BBN was obtained by the removal of solvent from a 0.53M solution in THF commercially purchased from Sigma-Aldrich. K_2CO_3, Na_2CO_3, Li_3PO_4, Na_3PO_4, K_3PO_4, KF, and CsF were all dried under high vacuum <50 mTorr at 185°C for 24 to 72 hours prior to use in Suzuki cross-coupling reactions. All other specified reagents were purchased from Sigma-Aldrich, TCI Chemicals, Combi-Blocks or Alfa Aesar and used as received. Toluene, Ether, THF and Pentane were dried over activated alumina columns, degassed with dry argon or nitrogen, and stored on molecular sieves prior to use. H_2O was degassed using three freeze-pump-thaw cycles. Dioxane, Benzene-H_6, C_6D_6 and $CDCl_3$ were purchased from Sigma-Aldrich, degassed using three freeze-pump-thaw cycles, vacuum–distilled from CaH_2 for C_6D_6 and $CDCl_3$ and stored under argon or nitrogen, all other solvents were used as received. Unless otherwise stated, ^1H NMR spectra were referenced to the residual protio solvent resonance (δ 7.26 ppm for $CDCl_3$, 7.15 ppm for C_6D_6). All glassware was oven dried at 175°C overnight prior to use. ^1H, ^{13}C, ^{19}F and ^{31}P NMR spectra were recorded on a Bruker 400 MHz, Bruker UltraShield 300 MHz, Bruker UltraShield 600 MHz NMR spectrometer at room temperature. NMR multiplicities are abbreviated as follows: s = singlet, d = doublet, t = triplet, q = quadruplet, m = multiplet, br = broad. Solid-state structure .cif files are available upon request.

Note: *Exposure of alkyl-9BBN to oxygen will result in rapid decomposition into multiple radical by-products. To simplify purification, controlled quenching is strongly recommended. In all instances herein reactions were quenched with and excess of* ***NMO*** (*N-Methylmorpholine N-oxide) (~75mg / 0.1mmol of CMF). If reactions are not quenched alkyl hydrocarbon-based solvents should be avoided as eluents for column chromatography as they promote co-elution of alkyl-borane byproducts with the desired amide products. Through many efforts we found using 100% DCM as an eluent allowed for separation of the desired product from byproducts with limited success requiring a substantial amount eluent and silica in the stationary phase. When purifying*

by column chromatography, amide products are typically insufficiently UV active and require fractions to be substantially concentrated to effectively see on TLC, even with the aid of stains.

Anhydrous K_2CO_3 used in cross-coupling reactions was prepared by drying under vacuum (~10 mTorr) at 180°C over the course of 3 days, then brought into a nitrogen filled glovebox for storage. 5.0M stock solution of H_2O in THF was carefully prepared in a nitrogen filled glovebox using degassed H_2O, and solution stored in a glovebox freezer at -35°C.

Caution: *alkyl-9BBN solutions will rapidly and exothermically decompose if allowed to come into contact with air, appropriate measures should be taken to ensure stock solutions are prepared and stored under inert conditions. Once prepared, stock solutions may be stored under inert conditions at -35 °C for up to 10 to 14 days with minimal degradation.* ***Isolation of pure alkyl boranes should be avoided as they may spontaneously ignite upon contact with air.***

Preparation of Alkyl Borane Solutions:

In a N_2-filled glovebox, a volumetric flask was charged with the appropriate amount of alkene (0.3 mmol for 1 mL stock solution, 1.5 mmol for 5 mL stock solution, 1.0 equiv.) followed by 1.2 equiv. of a commercial solution of H-9BBN in THF (0.36 mmol for 1 mL stock solution, 1.8 mmol for 5 mL stock solution). The flask was then filled to the calibration line (0.3 M) with THF and then equipped with a stir bar and sealed and mixed overnight at room temperature. To ensure complete conversion an aliquot of the solution was added to an NMR tube and analyzed by NMR spectroscopy (spectra acquired in THF-H_8). If no characteristic alkene resonances were observed (typically between 4 to 6 ppm) the reaction was assumed to be complete and was used as is without further purification.

General Procedure:

In a nitrogen filled glovebox, a 4 mL vial was charged with (dppf)$NiCl_2$ (6.8 mg, 0.01 mmol, 10 mol%) a stir bar, and 500 μL of a previously prepared 0.3 M alkyl borane solution (1 : 1.2 ratio of alkene : H-9BBN) (0.15 mmol, 1.5 equiv.) and mixed for 30 minutes, eventually turning from a dark green suspension to a clear homogenous orange-yellow solution.

A separate 4 mL vial was charged with K_2CO_3 (20.7 mg, 0.15 mmol, 1.5 equiv.), 275 μL of anhydrous THF, a 5.0M H_2O solution in THF (100 μL, 0.5 mmol, 5 equiv.), and a stir bar. The vial was then charged with 500 μL of the nickel-borane solution, followed by 125 μL of a 0.8M CMF (0.1 mmol, 1 equiv.) stock solution, for a total volume of 1.00 mL.

The reaction vessel was then sealed with a Teflon lined cap and removed from the glovebox and further secured with a minimum of two complete layers of electrical tape along the vial-cap interface and then partially submerged in an 80 °C oil bath and mixed for 22 hours.

NMR Yield Workup:

Upon completion, the reaction solution was brought to room temperature and in open atmosphere transferred into a 20 mL scintillation vial with EtOAc (4 × 3-4 mL), solvent was then removed by rotary evaporation, followed by high vacuum to at least 100 mTorr. Once dry the vial was charged with an accurately weighed amount of 1,3,5-trimethoxybenzene (minimum: 10 mg, internal standard), dissolved in ~ 1 mL of $CDCl_3$, sonicated for several seconds and then ~ 0.1 mL transferred into an NMR tube, followed by an additional 0.65 mL of $CDCl_3$, and ~ 0.7 mL of D_2O and the tube capped. The biphasic solution was then vigorously mixed for several minutes to thoroughly mix the two phases. Once mixed the bottom half of the tube was then submerged in a harm water bath for ~ 10 minutes and then the phases separated by manual centrifugation and analyzed by NMR. *A too concentrated sample or insufficient mixing will result in broadening of signals due to the presence of paramagnetic species.*

Product Isolation Workup:

Upon completion, the reaction was then brought back into a nitrogen filled glove box and charged with NMO (~75mg / 0.1mmol of CMF) and brought out of the glovebox and mixed for a minimum of 30 minutes to quench any residual borane. The reaction was then opened and approximately 2 mL of distilled H_2O was added and mixed for an additional 15 minutes. The biphasic mixture was then transferred to a separatory funnel using ~15mL of EtOAc and the organic phase washed with water (2 × 10 mL) followed by brine (1 × 5 mL). The organic phase was collected and dried over $MgSO_4$, filtered, and solvent removed by rotary evaporation followed by high vacuum (~50 mTorr). The product was then purified by preparatory plate thin-layer chromatography with the specified eluent system. In some instances, two preparatory plates were

required to fully purify products, by first eluting the product in EtOAc / Hexanes and secondly with an eluent of Ether / DCM.

***N*-benzyl-*N*,5-diphenyl-pentanamide**

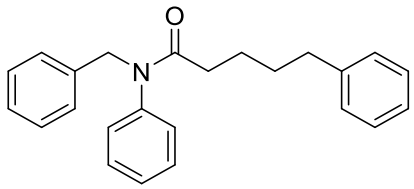

The title amide was synthesized according to the general procedure and purified by preparatory plate thin-layer chromatography (4% EtOAc/Hexanes), followed by a second preparatory plate to remove borane impurities (5% Ether/DCM). The product was isolated as a clear pale-yellow oil (28.1 mg, 0.082 mmol, 82 %).

^{1}H NMR (600 MHz, $CDCl_3$): δ 7.24 – 7.19 (m, 3H), 7.15 (t, *J* = 7.7 Hz, 3H), 7.12 – 7.09 (m, 2H), 7.07 (t, *J* = 7.3 Hz, 1H), 7.02 (d, *J* = 7.4 Hz, 2H), 6.85 (d, *J* = 6.8 Hz, 2H), 4.79 (s, 2H), 2.45 (t, *J* = 7.7 Hz, 2H), 2.01 (t, *J* = 7.4 Hz, 2H), 1.57 (p, *J* = 7.4 Hz, 2H), 1.45 (p, *J* = 7.9 Hz, 2H). **^{13}C NMR** (151 MHz, $CDCl_3$): δ 25.1, 31.0, 34.2, 35.6, 52.9, 125.6, 127.2, 127.8, 128.2, 128.28, 128.31, 128.4, 128.8, 129.4, 137.6, 142.3, 142.4, 172.7.

HRMS (ESI) m/z: $[M+H]^+$ calc'd for $[C_{24}H_{26}NO]$ 344.2014; found 344.2009.

***N*-[(4-methoxyphenyl)methyl]-*N*,5-diphenyl-pentanamide**

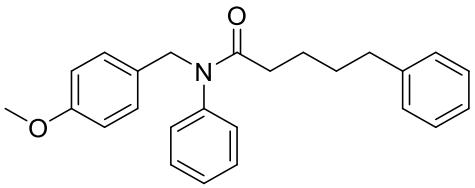

The title amide was synthesized according to the general procedure and purified by preparatory plate thin-layer chromatography (15% EtOAc/Hexanes) and isolated as a clear colorless oil (33.1 mg, 0.089 mmol, 89 %).

^{1}H NMR (600 MHz, $CDCl_3$): δ 7.34 – 7.28 (m, 3H), 7.24 (t, *J* = 7.6 Hz, 2H), 7.16 (tt, *J* = 7.4, 1.4 Hz, 1H), 7.10 (dt, *J* = 9.4, 2.7 Hz, 4H), 6.92 (dd, *J* = 7.9, 2.2 Hz, 2H), 6.78 (d, *J* = 8.5 Hz, 2H),

4.81 (s, 2H), 3.78 (s, 3H), 2.53 (t, *J* = 7.7 Hz, 2H), 2.06 (t, *J* = 7.4 Hz, 2H), 1.65 (p, *J* = 7.4 Hz, 2H), 1.53 (p, *J* = 7.6 Hz, 2H). **^{13}C NMR** (151 MHz, $CDCl_3$): δ 25.1, 31.0, 34.2, 35.6, 52.3, 55.2, 113.6, 125.6, 127.8, 128.2, 128.3, 128.5, 129.4, 129.9, 130.2, 142.3, 142.4, 158.8, 172.6.

HRMS (ESI) m/z: $[M+H]^+$ calc'd for $[C_{25}H_{28}NO_2]$ 374.2120; found 374.2112.

***N*-[(4-methoxyphenyl)methyl]-4-phenoxy-*N*-phenyl-butanamide**

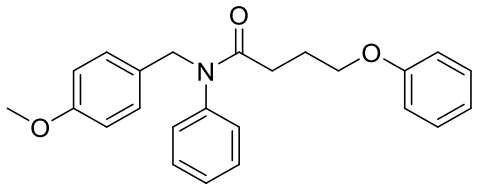

The title amide was synthesized according to the general procedure and purified by preparatory plate thin-layer chromatography (15% EtOAc/Hexanes) and isolated as a clear pale-yellow oil (29.7 mg, 0.079 mmol, 79 %).

^{1}H NMR (600 MHz, $CDCl_3$): δ 7.27 (dd, *J* = 5.2, 1.9 Hz, 3H), 7.24 – 7.18 (m, 2H), 7.05 (d, *J* = 8.4 Hz, 2H), 6.91 – 6.85 (m, 3H), 6.76 (d, *J* = 8.1 Hz, 2H), 6.72 (d, *J* = 8.4 Hz, 2H), 4.78 (s, 2H), 3.90 (t, *J* = 6.0 Hz, 2H), 3.73 (s, 3H), 2.21 (t, *J* = 7.1 Hz, 2H), 2.05 (p, *J* = 6.5 Hz, 2H). **^{13}C NMR** (151 MHz, $CDCl_3$): δ 25.1, 30.7, 52.3, 55.2, 66.6, 113.6, 114.4, 120.5, 127.9, 128.5, 129.3, 129.5, 129.7, 130.1, 142.2, 158.8, 172.1.

HRMS (ESI) m/z: $[M+H]^+$ calc'd for $[C_{24}H_{26}NO_3]$ 376.1913; found 376.1904.

4-(4-methoxyphenoxy)-*N*-[(4-methoxyphenyl)methyl]-*N*-phenyl-butanamide

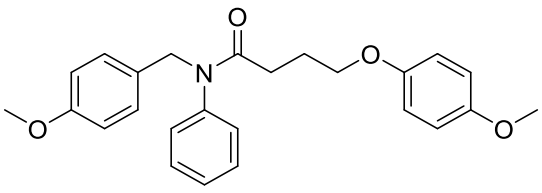

The title amide was synthesized according to the general procedure and purified by preparatory plate thin-layer chromatography (15% EtOAc/Hexanes) and isolated as a clear pale-yellow oil (31.2 mg, 0.077 mmol, 77 %).

^{1}H NMR (600 MHz, $CDCl_3$): δ 7.33 – 7.27 (m, 3H), 7.12 – 7.06 (m, 2H), 6.96 – 6.89 (m, 2H), 6.82 – 6.70 (m, 6H), 4.81 (s, 2H), 3.88 (t, *J* = 6.0 Hz, 2H), 3.77 (s, 3H), 3.75 (s, 3H), 2.23 (t, *J* = 7.1 Hz, 2H), 2.06 (p, *J* = 6.5 Hz, 2H). **^{13}C NMR** (151 MHz, $CDCl_3$): δ 25.1, 30.7, 52.3, 55.2, 55.7, 67.4, 113.6, 114.5, 115.3, 127.9, 128.5, 129.5, 129.7, 130.1, 142.3, 153.0, 153.7, 158.8, 172.1.

HRMS (ESI) m/z: $[M+H]^+$ calc'd for $[C_{25}H_{28}NO_4]$ 406.2018; found 406.2013.

***N*-benzyl-4-(4-methoxyphenoxy)-*N*-phenyl-butanamide**

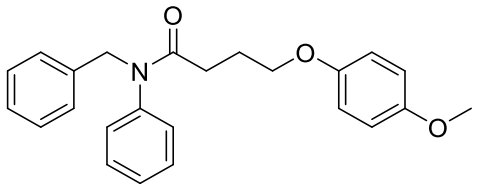

The title amide was synthesized according to the general procedure and purified by preparatory plate thin-layer chromatography (10% EtOAc/Hexanes) and isolated as an off-white solid (24.2 mg, 0.064 mmol, 64 %).

^{1}H NMR (600 MHz, $CDCl_3$): δ 7.34 – 7.27 (m, 3H), 7.25 – 7.21 (m, 3H), 7.17 (dd, *J* = 6.9, 2.5 Hz, 2H), 6.94 (dd, *J* = 6.9, 2.6 Hz, 2H), 6.79 (d, *J* = 9.1 Hz, 2H), 6.73 (d, *J* = 8.9 Hz, 2H), 4.88 (s, 2H), 3.89 (t, *J* = 6.1 Hz, 2H), 3.76 (s, 3H), 2.26 (t, *J* = 7.2 Hz, 2H), 2.07 (p, *J* = 6.6 Hz, 2H). **^{13}C NMR** (151 MHz, $CDCl_3$): δ 25.2, 30.7, 53.0, 55.7, 67.4, 114.6, 115.3, 127.3, 127.9, 128.3, 128.4, 128.8, 129.5, 137.5, 142.3, 153.0, 153.7, 172.3.

HRMS (ESI) m/z: $[M+H]^+$ calc'd for $[C_{24}H_{26}NO_3]$ 376.1913; found 376.1906.

m.p.: 86-87 °C

***N*-benzyl-4-(4-cyanophenoxy)-*N*-phenyl-butanamide**

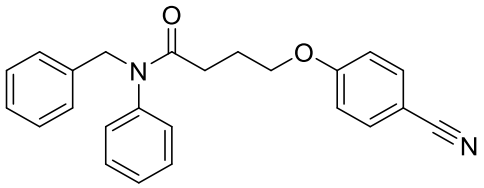

The title amide was synthesized according to the general procedure and purified by preparatory plate thin-layer chromatography (30% EtOAc/Hexanes) followed by a second preparatory plate to remove borane impurities (6% Ether/DCM). The product was isolated as a clear pale-yellow oil (16.2 mg, 0.044 mmol, 44 %).

^{1}H NMR (600 MHz, $CDCl_3$): δ 7.54 (d, *J* = 8.8 Hz, 2H), 7.31 (dd, *J* = 5.2, 1.8 Hz, 3H), 7.25 – 7.19 (m, 3H), 7.17 (dd, *J* = 6.7, 2.9 Hz, 2H), 6.93 (dd, *J* = 6.8, 2.9 Hz, 2H), 6.85 (d, *J* = 8.8 Hz, 2H), 4.88 (s, 2H), 4.00 (t, *J* = 6.1 Hz, 2H), 2.25 (t, *J* = 7.0 Hz, 2H), 2.10 (p, *J* = 6.6 Hz, 2H). **^{13}C NMR** (151 MHz, $CDCl_3$): δ 24.7, 30.4, 53.1, 67.3, 103.8, 115.1, 119.2, 127.4, 128.1, 128.4, 128.8, 129.6, 133.9, 137.4, 142.2, 162.1, 171.8.

HRMS (ESI) m/z: $[M+H]^+$ calc'd for $[C_{24}H_{23}N_2O_2]$ 371.1760; found 371.1756.

***N*-benzyl-*N*-phenyl-4-[3-(trifluoromethyl)phenoxy]butanamide**

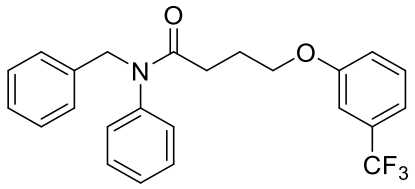

The title amide was synthesized according to the general procedure and purified by preparatory plate thin-layer chromatography (8% EtOAc/Hexanes) followed by a second preparatory plate to remove borane impurities (20% EtOAc/Hexanes). The product was isolated as a clear pale-yellow oil (29.8 mg, 0.072 mmol, 72 %).

^{1}H NMR (600 MHz, $CDCl_3$): δ 7.35 (t, *J* = 8.0 Hz, 1H), 7.32 – 7.28 (m, 3H), 7.26 – 7.21 (m, 3H), 7.18 (dd, *J* = 7.4, 2.2 Hz, 3H), 7.03 (t, *J* = 2.1 Hz, 1H), 6.97 (dd, *J* = 8.3, 2.5 Hz, 1H), 6.94 (dd, *J* = 6.7, 3.0 Hz, 2H), 4.89 (s, 2H), 3.98 (t, *J* = 6.0 Hz, 2H), 2.28 (t, *J* = 7.1 Hz, 2H), 2.11 (p, *J* = 6.5

Hz, 2H). **^{13}C NMR** (151 MHz, $CDCl_3$): δ 24.9, 30.5, 53.0, 67.1, 111.34 (q, *J* = 3.9 Hz), 117.20 (q, *J* = 4.0 Hz), 117.8, 123.95 (q, *J* = 272.3 Hz), 127.3, 128.0, 128.3, 128.4, 128.8, 129.6, 129.9, 131.73 (q, *J* = 32.2 Hz), 137.4, 142.2, 158.9, 172.0. **^{19}F NMR** (282 MHz, $CDCl_3$): δ -62.68.

HRMS (ESI) m/z: $[M+H]^+$ calc'd for $[C_{24}H_{23}F_3NO_2]$ 414.1681; found 414.1674.

_N_-[(4-methoxyphenyl)methyl]-_N_,3-diphenyl-propanamide

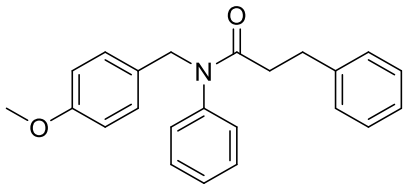

The title amide was synthesized according to the general procedure and purified by preparatory plate thin-layer chromatography (10% EtOAc/Hexanes) and isolated as a clear pale-yellow oil (10.0 mg, 0.029 mmol, 29 %).

^{1}H NMR (600 MHz, $CDCl_3$): δ 7.26 (d, *J* = 4.0 Hz, 3H), 7.21 (t, *J* = 7.4 Hz, 2H), 7.16 (t, *J* = 7.4 Hz, 1H), 7.05 (dd, *J* = 8.2, 3.6 Hz, 4H), 6.81 – 6.73 (m, 4H), 4.80 (s, 2H), 3.78 (s, 3H), 2.93 (t, *J* = 7.8 Hz, 2H), 2.34 (t, *J* = 7.7 Hz, 2H). **^{13}C NMR** (151 MHz, $CDCl_3$): δ 31.7, 36.1, 52.4, 55.2, 113.6, 126.0, 127.9, 128.3, 128.47, 128.49, 129.4, 129.7, 130.2, 141.2, 142.2, 158.8, 171.9.

HRMS (ESI) m/z: $[M+H]^+$ calc'd for $[C_{23}H_{24}NO_2]$ 346.1807; found 346.1802.

_N_-[(4-methoxyphenyl)methyl]-_N_-phenyl-3-(p-tolyl)propanamide

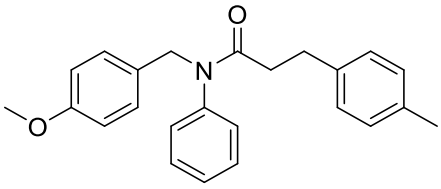

The title amide was synthesized according to the general procedure and purified by preparatory plate thin-layer chromatography (10% EtOAc/Hexanes) and isolated as a clear pale-yellow oil (13.1 mg, 0.036 mmol, 36 %).

^{1}H NMR (600 MHz, $CDCl_3$): δ 7.30 – 7.23 (m, 3H), 7.08 – 7.00 (m, 4H), 6.95 (d, *J* = 7.6 Hz, 2H), 6.80 (dd, *J* = 6.7, 3.0 Hz, 2H), 6.79 – 6.74 (m, 2H), 4.80 (s, 2H), 3.78 (s, 3H), 2.89 (t, *J* = 7.8 Hz, 2H), 2.32 (t, *J* = 7.8 Hz, 2H), 2.29 (s, 3H). **^{13}C NMR** (151 MHz, $CDCl_3$): δ 21.0, 31.3, 36.3, 52.3, 55.2, 113.6, 127.8, 128.3, 128.5, 129.0, 129.4, 129.7, 130.2, 135.4, 138.1, 142.2, 158.8, 171.9.

HRMS (ESI) m/z: $[M+H]^+$ calc'd for $[C_{24}H_{26}NO_2]$ 360.1964; found 360.1957.

3-(4-methoxyphenyl)-*N*-[(4-methoxyphenyl)methyl]-*N*-phenyl-propanamide

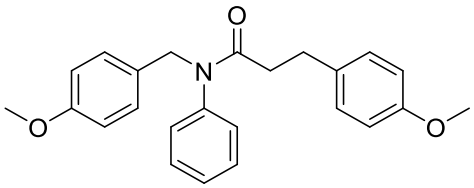

The title amide was synthesized according to the general procedure and purified by preparatory plate thin-layer chromatography (15% EtOAc/Hexanes) and isolated as a clear pale-yellow oil (15.3 mg, 0.041 mmol, 41 %).

^{1}H NMR (600 MHz, $CDCl_3$): δ 7.30 – 7.23 (m, 3H), 7.07 – 7.02 (m, 2H), 7.00 – 6.94 (m, 2H), 6.82 – 6.73 (m, 6H), 4.79 (s, 2H), 3.78 (s, 3H), 3.76 (s, 3H), 2.87 (t, *J* = 7.7 Hz, 2H), 2.31 (t, *J* = 7.7 Hz, 2H). **^{13}C NMR** (151 MHz, $CDCl_3$): δ 30.8, 36.4, 52.3, 55.17, 55.21, 113.6, 113.7, 127.8, 128.5, 129.4, 129.7, 130.2, 133.2, 142.3, 157.9, 158.8, 171.9.

HRMS (ESI) m/z: $[M+H]^+$ calc'd for $[C_{24}H_{26}NO_3]$ 376.1913; found 376.1905.

***N*-[(4-methoxyphenyl)methyl]-*N*-phenyl-4-trimethylsilyl-butanamide**

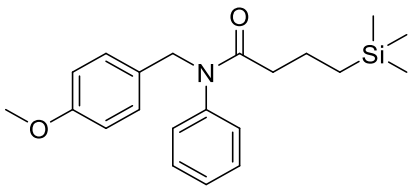

The title amide was synthesized according to the general procedure and purified by preparatory plate thin-layer chromatography (25% EtOAc/Hexanes) and isolated as a clear pale-yellow oil (34.9mg, 0.098 mmol, 98 %).

^{1}H NMR (600 MHz, $CDCl_3$): δ 7.34 – 7.27 (m, 3H), 7.10 (d, *J* = 8.5 Hz, 2H), 6.94 (d, *J* = 7.4 Hz, 2H), 6.78 (d, *J* = 8.7 Hz, 2H), 4.81 (s, 2H), 3.77 (s, 3H), 2.06 (t, *J* = 7.5 Hz, 2H), 1.63 – 1.55 (m, 2H), 0.40 – 0.34 (m, 2H), -0.08 (s, 9H). **^{13}C NMR** (151 MHz, $CDCl_3$): δ -1.8, 16.5, 20.1, 38.1, 52.2, 55.2, 113.6, 127.7, 128.5, 129.4, 129.9, 130.2, 142.5, 158.8, 172.8.

HRMS (ESI) m/z: $[M+H]^+$ calc'd for $[C_{21}H_{30}NO_2Si]$ 356.2046; found 356.2040.

4-[tert-butyl(dimethyl)silyl]oxy-*N*-[(4-methoxyphenyl)methyl]-*N*-phenyl-butanamide

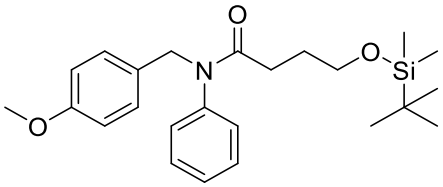

The title amide was synthesized according to the general procedure and purified by preparatory plate thin-layer chromatography (20% EtOAc/Hexanes) and isolated as a clear colorless oil (30.1 mg, 0.073 mmol, 73 %).

^{1}H NMR (600 MHz, $CDCl_3$): δ 7.34 – 7.27 (m, 3H), 7.10 (d, *J* = 8.3 Hz, 2H), 6.94 (d, *J* = 7.2 Hz, 2H), 6.78 (d, *J* = 8.2 Hz, 2H), 4.81 (s, 2H), 3.77 (s, 3H), 3.54 (t, *J* = 6.1 Hz, 2H), 2.11 (t, *J* = 7.5 Hz, 2H), 1.80 (p, *J* = 6.6 Hz, 2H), 0.79 (s, 9H), -0.06 (s, 6H). **^{13}C NMR** (151 MHz, $CDCl_3$): δ -5.4, 18.2, 25.9, 28.4, 30.9, 52.2, 55.2, 62.2, 113.6, 127.8, 128.5, 129.4, 129.9, 130.2, 142.4, 158.8, 172.6.

HRMS (ESI) m/z: $[M+H]^+$ calc'd for $[C_{24}H_{36}NO_3Si]$ 414.2464; found 414.2455.

***N*-benzyl-4-(1-naphthyl)-*N*-phenyl-butanamide**

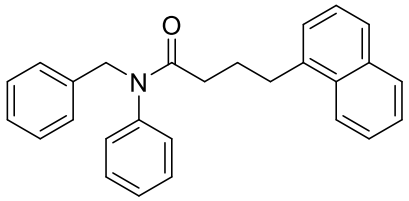

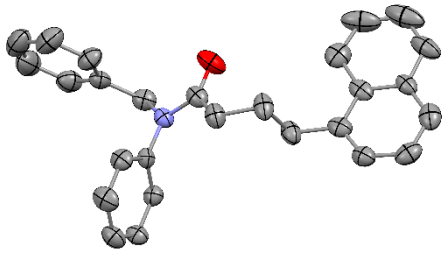

The title amide was synthesized according to the general procedure and purified by preparatory plate thin-layer chromatography (15% EtOAc/Hexanes) and isolated as a white crystalline solid (21.6 mg, 0.057 mmol, 57 %). The product was then able to be recrystallized by slow evaporation of a saturated solution of pentane.

^{1}H NMR (600 MHz, $CDCl_3$): δ 8.03 (d, *J* = 7.7 Hz, 1H), 7.85 (dd, *J* = 7.6, 1.9 Hz, 1H), 7.70 (d, *J* = 8.2 Hz, 1H), 7.53 – 7.45 (m, 2H), 7.35 (dd, *J* = 8.2, 6.9 Hz, 1H), 7.31 – 7.26 (m, 6H), 7.25 – 7.22 (m, 3H), 6.93 (dd, *J* = 7.2, 3.7 Hz, 2H), 4.93 (s, 2H), 3.06 (t, *J* = 7.7 Hz, 2H), 2.20 (t, *J* = 7.2 Hz, 2H), 2.09 (p, *J* = 7.3 Hz, 2H). **^{13}C NMR** (151 MHz, $CDCl_3$): δ 26.4, 32.3, 34.1, 52.9, 123.9, 125.365, 125.373, 125.7, 125.9, 126.6, 127.3, 127.8, 128.3, 128.4, 128.6, 128.8, 129.4, 131.9, 133.8, 137.6, 137.9, 142.3, 172.5.

HRMS (ESI) m/z: $[M+H]^+$ calc'd for $[C_{27}H_{26}NO]$ 380.2014; found 380.2007.

m.p.: 135-137 °C

3-cyclohexyl-*N*-[(4-methoxyphenyl)methyl]-*N*-phenyl-propanamide

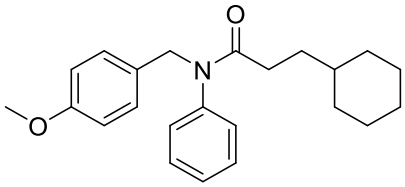

The title amide was synthesized according to the general procedure and purified by preparatory plate thin-layer chromatography (25% EtOAc/Hexanes) and isolated as a clear pale-yellow oil (20.3 mg, 0.058 mmol, 58 %).

^{1}H NMR (600 MHz, $CDCl_3$): δ 7.35 – 7.27 (m, 3H), 7.10 (d, *J* = 8.6 Hz, 2H), 6.94 (d, *J* = 7.1 Hz, 2H), 6.78 (d, *J* = 8.6 Hz, 2H), 4.80 (s, 2H), 3.77 (s, 3H), 2.04 (t, *J* = 7.9 Hz, 2H), 1.64 – 1.56 (m, 3H), 1.54 – 1.43 (m, 4H), 1.17 – 1.03 (m, 4H), 0.75 (qd, *J* = 12.0, 3.3 Hz, 2H). **^{13}C NMR** (151 MHz, $CDCl_3$): δ 26.2, 26.5, 31.9, 33.0, 33.0, 37.2, 52.3, 55.2, 113.6, 127.8, 128.5, 129.4, 129.9, 130.2, 142.5, 158.8, 173.2.

HRMS (ESI) m/z: $[M+H]^+$ calc'd for $[C_{23}H_{30}NO_2]$ 352.2277; found 352.2271.

4-(1,3-benzodioxol-5-yloxy)-*N*-benzyl-*N*-phenyl-butanamide

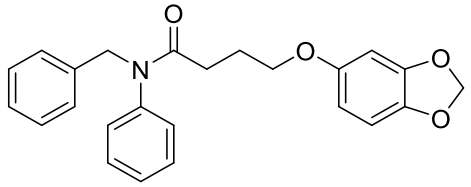

The title amide was synthesized according to the general procedure and purified by preparatory plate thin-layer chromatography (15% EtOAc/Hexanes) and isolated as an orange oil (24.6 mg, 0.063 mmol, 63 %).

^{1}H NMR (600 MHz, $CDCl_3$): δ 7.34 – 7.27 (m, 3H), 7.26 – 7.21 (m, 3H), 7.18 (dd, *J* = 7.2, 2.3 Hz, 2H), 6.99 – 6.93 (m, 2H), 6.66 (d, *J* = 8.5 Hz, 1H), 6.38 (d, *J* = 2.5 Hz, 1H), 6.22 (dd, *J* = 8.5, 2.5 Hz, 1H), 5.89 (s, 2H), 4.89 (s, 2H), 3.86 (t, *J* = 6.0 Hz, 2H), 2.25 (t, *J* = 7.1 Hz, 2H), 2.06 (p, *J* = 6.3 Hz, 2H). **^{13}C NMR** (151 MHz, $CDCl_3$): δ 25.1, 30.6, 53.0, 67.7, 98.0, 101.0, 105.5, 107.8, 127.3, 127.9, 128.3, 128.4, 128.7, 129.5, 137.5, 141.4, 142.3, 148.1, 154.3, 172.2.

HRMS (ESI) m/z: $[M+H]^+$ calc'd for $[C_{24}H_{24}NO_4]$ 390.1705; found 390.1700.

***tert*-butyl *N*-[4-(*N*-benzylanilino)-4-oxo-butyl]carbamate**

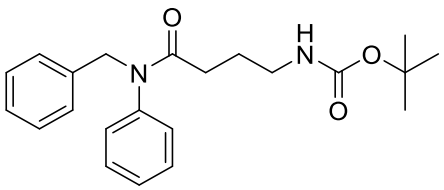

The title amide was synthesized according to the general procedure and purified by preparatory plate thin-layer chromatography (40% EtOAc/Hexanes) and isolated as a white solid (36.8 mg, 0.100 mmol, 100 %).

^{1}H NMR (600 MHz, $CDCl_3$): δ 7.31 (q, *J* = 7.2 Hz, 3H), 7.27 – 7.21 (m, 3H), 7.20 – 7.15 (m, 2H), 6.95 (d, *J* = 6.0 Hz, 2H), 4.87 (s, 2H), 4.71 (br, s, 1H), 3.06 (br, t, *J* = 6.7 Hz, 2H), 2.10 (t, *J* = 7.2 Hz, 2H), 1.77 (p, *J* = 7.0 Hz, 2H), 1.40 (s, 9H). **^{13}C NMR** (151 MHz, $CDCl_3$): δ 25.5, 28.4, 31.7, 40.1, 53.0, 78.9, 127.3, 128.0, 128.3, 128.4, 128.8, 129.6, 137.4, 142.2, 155.9, 172.3.

HRMS (ESI) m/z: $[M+H]^+$ calc'd for $[C_{22}H_{29}N_2O_3]$ 369.2178; found 369.2176.

m.p.: 101-103 ℃

***N*-[(4-methoxyphenyl)methyl]-4-(1-methylpyrazol-3-yl)oxy-*N*-phenyl-butanamide**

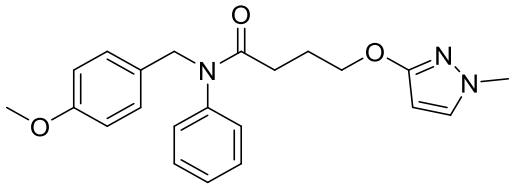

The title amide was synthesized according to the general procedure and purified by preparatory plate thin-layer chromatography (50% EtOAc/Hexanes) and isolated as a clear colorless oil (12.2 mg, 0.032 mmol, 32 %).

^{1}H NMR (600 MHz, $CDCl_3$): δ 7.34 – 7.26 (m, 3H), 7.13 – 7.03 (m, 3H), 6.93 (d, *J* = 6.1 Hz, 2H), 6.77 (d, *J* = 8.1 Hz, 2H), 5.52 (d, *J* = 2.3 Hz, 1H), 4.81 (s, 2H), 4.04 (t, *J* = 6.2 Hz, 2H), 3.77 (s, 3H), 3.69 (s, 3H), 2.20 (t, *J* = 7.4 Hz, 2H), 2.06 (p, *J* = 6.7 Hz, 2H). **^{13}C NMR** (151 MHz, $CDCl_3$): δ 25.1, 30.9, 38.8, 52.4, 55.2, 68.3, 89.9, 113.6, 127.8, 128.5, 129.5, 129.8, 130.2, 131.0, 142.2, 158.8, 163.3, 172.1.

HRMS (ESI) m/z: $[M+H]^+$ calc'd for $[C_{22}H_{26}N_3O_3]$ 380.1974; found 380.1971.

4-carbazol-9-yl-*N*-[(4-methoxyphenyl)methyl]-*N*-phenyl-butanamide

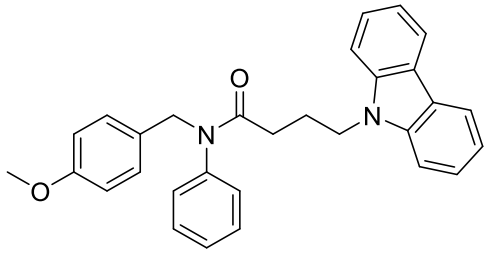

The title amide was synthesized according to the general procedure and purified by preparatory plate thin-layer chromatography (20% EtOAc/Hexanes) and isolated as an off-white solid (28.6 mg, 0.064 mmol, 64 %).

^{1}H NMR (600 MHz, $CDCl_3$): δ 8.08 (d, *J* = 7.7 Hz, 2H), 7.42 – 7.34 (m, 4H), 7.21 (ddd, *J* = 7.9, 6.6, 1.4 Hz, 2H), 7.18 – 7.08 (m, 5H), 6.85 – 6.79 (m, 2H), 6.58 (d, *J* = 7.5 Hz, 2H), 4.82 (s, 2H), 4.41 (t, *J* = 6.8 Hz, 2H), 3.80 (s, 3H), 2.17 (p, *J* = 6.7 Hz, 2H), 1.91 (t, *J* = 6.6 Hz, 2H). **^{13}C NMR** (151 MHz, $CDCl_3$): δ 23.9, 30.9, 41.6, 52.3, 55.2, 108.8, 113.7, 118.7, 120.2, 122.7, 125.5, 127.7, 128.3, 129.3, 129.7, 130.3, 140.4, 141.8, 158.9, 171.6.

HRMS (ESI) m/z: $[M+H]^+$ calc'd for $[C_{30}H_{29}N_2O_2]$ 449.2229; found 449.2221.

m.p.: 103-104 °C

***N*-benzyl-3-ferrocenyl-*N*-phenyl-propanamide**

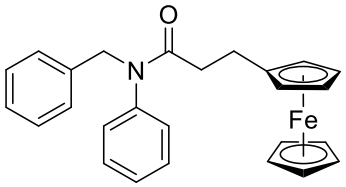

The title amide was synthesized according to the general procedure and purified by preparatory plate thin-layer chromatography (15% EtOAc/Hexanes) followed by a second preparatory plate to remove borane impurities (100% DCM). The product was isolated as a clear orange oil (22.7 mg, 0.054 mmol, 54 %).

^{1}H NMR (600 MHz, $CDCl_3$): δ 7.35 – 7.23 (m, 6H), 7.21 (d, *J* = 7.7 Hz, 2H), 6.92 (d, *J* = 5.8 Hz, 2H), 4.91 (s, 2H), 4.03 – 3.99 (m, 7H), 3.97 (s, 2H), 2.68 (dd, *J* = 9.1, 6.6 Hz, 2H), 2.32 (dd, *J* =

9.1, 6.6 Hz, 2H). **^{13}C NMR** (151 MHz, $CDCl_3$): δ 25.5, 36.0, 52.9, 67.1, 68.1, 68.4, 87.9, 127.3, 127.9, 128.3, 128.4, 128.8, 129.5, 137.5, 142.3, 172.3.

HRMS (ESI) m/z: $[M+H]^+$ calc'd for $[C_{26}H_{24}FeNO]$ 422.1201; found 422.1395.

***N*-benzyl-4-(4-fluorophenoxy)-*N*-(4-fluorophenyl)butanamide**

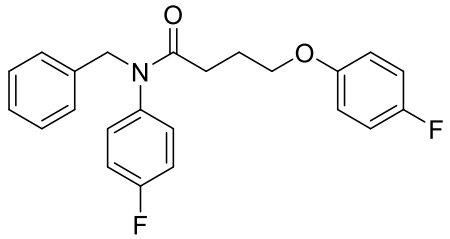

The title amide was synthesized according to the general procedure and purified by preparatory plate thin-layer chromatography (15% EtOAc/Hexanes) and isolated as a clear colorless oil (24.1 mg, 0.063 mmol, 63 %).

^{1}H NMR (600 MHz, $CDCl_3$): δ 7.26 – 7.20 (m, 3H), 7.16 (dd, *J* = 6.6, 2.9 Hz, 2H), 6.98 (t, *J* = 8.4 Hz, 2H), 6.93 (t, *J* = 8.7 Hz, 2H), 6.89 (dd, *J* = 8.8, 4.8 Hz, 2H), 6.76 – 6.70 (m, 2H), 4.85 (s, 2H), 3.91 (t, *J* = 6.0 Hz, 2H), 2.23 (t, *J* = 7.1 Hz, 2H), 2.08 (p, *J* = 6.5 Hz, 2H). **^{13}C NMR** (151 MHz, $CDCl_3$): δ 25.0, 30.6, 53.0, 67.3, 115.30 (d, *J* = 7.8 Hz), 115.71 (d, *J* = 23.0 Hz), 116.46 (d, *J* = 22.6 Hz), 127.5, 128.4, 128.8, 130.16 (d, *J* = 8.6 Hz), 137.2, 138.16 (d, *J* = 3.4 Hz), 154.90 (d, *J* = 2.1 Hz), 157.13 (d, *J* = 238.1 Hz), 161.87 (d, *J* = 248.4 Hz), 172.1. **^{19}F NMR** (282 MHz, $CDCl_3$): δ -113.10, -124.19.

HRMS (ESI) m/z: $[M+H]^+$ calc'd for $[C_{23}H_{22}F_2NO_2]$ 382.1619; found 382.1613.

***tert*-butyl *N*-[4-[*N*-[(4-fluorophenyl)methyl]anilino]-4-oxo-butyl]carbamate**

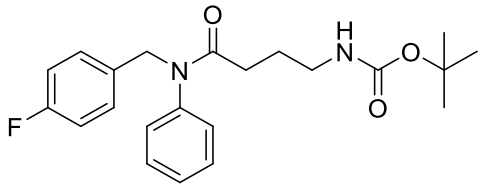

The title amide was synthesized according to the general procedure and purified by preparatory plate thin-layer chromatography (40% EtOAc/Hexanes) and isolated as a white solid (38.3 mg, 0.099 mmol, 99 %).

^{1}H NMR (600 MHz, $CDCl_3$): δ 7.35 – 7.29 (m, 3H), 7.14 (dd, *J* = 8.4, 5.5 Hz, 2H), 6.96 – 6.89 (m, 4H), 4.83 (s, 2H), 4.67 (br, s, 1H), 3.06 (br, q, *J* = 6.6 Hz, 2H), 2.08 (t, *J* = 7.1 Hz, 2H), 1.76 (p, *J* = 6.8 Hz, 2H), 1.40 (s, 9H). **^{13}C NMR** (151 MHz, $CDCl_3$): δ 25.5, 28.4, 31.7, 40.1, 52.3, 78.9, 115.18 (d, *J* = 21.3 Hz), 128.1, 128.4, 129.7, 130.55 (d, *J* = 8.0 Hz), 133.29 (d, *J* = 3.2 Hz), 142.0, 155.9, 162.12 (d, *J* = 245.5 Hz). 172.3. **^{19}F NMR** (282 MHz, $CDCl_3$): δ -115.10.

HRMS (ESI) m/z: $[M+H]^+$ calc'd for $[C_{22}H_{28}FN_2O_3]$ 387.2084; found 387.2080.

m.p.: 80-81 °C

***tert*-butyl *N*-[4-[*N*-[(4-methoxyphenyl)methyl]anilino]-4-oxo-butyl]carbamate**

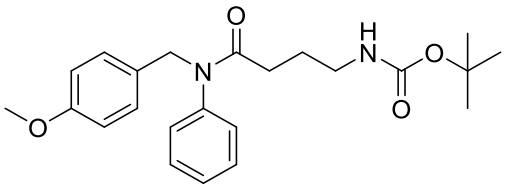

The title amide was synthesized according to the general procedure and purified by preparatory plate thin-layer chromatography (50% EtOAc/Hexanes) and isolated as an off-white solid (33.9 mg, 0.085 mmol, 85 %).

^{1}H NMR (600 MHz, $CDCl_3$): δ 7.36 – 7.27 (m, 3H), 7.09 (d, *J* = 8.6 Hz, 2H), 6.93 (d, *J* = 6.0 Hz, 2H), 6.77 (d, *J* = 8.5 Hz, 2H), 4.80 (s, 2H), 4.69 (s, br, 1H), 3.77 (s, 3H), 3.05 (t, br, *J* = 6.7 Hz, 2H), 2.07 (t, *J* = 7.1 Hz, 2H), 1.76 (p, *J* = 7.1 Hz, 2H), 1.40 (s, 9H). **^{13}C NMR** (151 MHz, $CDCl_3$):

δ 25.5, 28.4, 31.8, 40.1, 52.4, 55.2, 78.9, 113.7, 128.0, 128.5, 129.5, 129.7, 130.2, 142.1, 155.9, 158.8, 172.2.

HRMS (ESI) m/z: $[M+H]^+$ calc'd for $[C_{23}H_{31}N_2O_4]$ 399.2284; found 399.2278.

m.p.: 93-94 °C

***tert*-butyl *N*-[4-[*N*-[[4-(dimethylamino)phenyl]methyl]anilino]-4-oxo-butyl]carbamate**

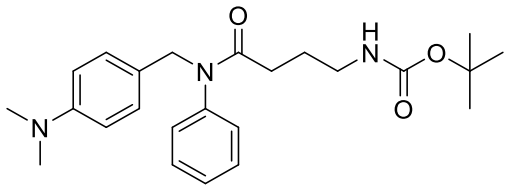

The title amide was synthesized according to the general procedure and purified by preparatory plate thin-layer chromatography (40% EtOAc/Hexanes) and isolated as a white solid (35.3 mg, 0.086 mmol, 86 %).

^{1}H NMR (600 MHz, $CDCl_3$): δ 7.34 – 7.27 (m, 3H), 7.03 (d, *J* = 8.6 Hz, 2H), 6.93 (d, *J* = 7.0 Hz, 2H), 6.61 (d, *J* = 8.5 Hz, 2H), 4.76 (s, 2H), 4.72 (s, 1H), 3.05 (br, q, *J* = 6.6 Hz, 2H), 2.91 (s, 6H), 2.06 (t, *J* = 7.1 Hz, 2H), 1.75 (p, *J* = 6.9 Hz, 2H), 1.40 (s, 9H). **^{13}C NMR** (151 MHz, $CDCl_3$): δ 25.5, 28.4, 31.8, 40.2, 40.5, 52.5, 78.9, 112.3, 125.4, 127.8, 128.6, 129.4, 129.9, 142.3, 149.9, 155.9, 172.1.

HRMS (ESI) m/z: $[M+H]^+$ calc'd for $[C_{24}H_{34}N_3O_3]$ 412.2600; found 412.2591.

m.p.: 97-98 °C

***tert*-butyl *N*-[4-[*N*-[(4-acetamidophenyl)methyl]anilino]-4-oxo-butyl]carbamate**

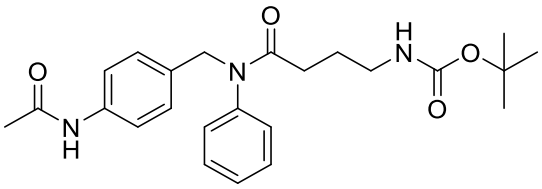

The title amide was synthesized according to the general procedure and purified by preparatory plate thin-layer chromatography (100% EtOAc) and isolated as a white solid (37.4 mg, 0.088 mmol, 88 %).

^{1}H NMR (600 MHz, $CDCl_3$): δ 7.98 (s, 1H), 7.40 (d, *J* = 8.2 Hz, 2H), 7.32 – 7.26 (m, 3H), 7.08 (d, *J* = 8.2 Hz, 2H), 6.93 (dd, *J* = 7.5, 2.0 Hz, 2H), 4.80 (s, 2H), 4.72 (br, t, *J* = 6.0 Hz, 1H), 3.03 (br, q, *J* = 6.7 Hz, 2H), 2.12 (s, 3H), 2.07 (t, *J* = 7.2 Hz, 2H), 1.74 (p, *J* = 7.0 Hz, 2H), 1.38 (s, 9H). **^{13}C NMR** (151 MHz, $CDCl_3$): δ 24.4, 25.5, 28.3, 31.7, 40.0, 52.5, 79.0, 119.7, 128.0, 128.3, 129.3, 129.6, 133.0, 137.4, 142.0, 155.9, 168.5, 172.3.

HRMS (ESI) m/z: $[M+H]^+$ calc'd for $[C_{24}H_{32}N_3O_4]$ 426.2393; found 426.2389.

m.p.: 71-73 °C

***tert*-butyl *N*-[4-(*N*-benzyl-4-methoxy-anilino)-4-oxo-butyl]carbamate**

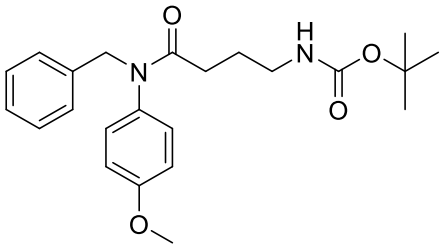

The title amide was synthesized according to the general procedure and purified by preparatory plate thin-layer chromatography (25% EtOAc/Hexanes) and isolated as a clear colorless oil (35.3 mg, 0.089 mmol, 89 %).

^{1}H NMR (600 MHz, $CDCl_3$): δ 7.28 – 7.19 (m, 3H), 7.19 – 7.14 (m, 2H), 6.87 – 6.77 (m, 4H), 4.82 (s, 2H), 4.72 (br, s, 1H), 3.77 (s, 3H), 3.06 (br, q, *J* = 6.5 Hz, 2H), 2.08 (t, *J* = 7.1 Hz, 2H), 1.76 (p, *J* = 7.0 Hz, 2H), 1.40 (s, 9H). **^{13}C NMR** (151 MHz, $CDCl_3$): δ 25.5, 28.4, 31.7, 40.2, 53.1, 55.3, 78.9, 114.6, 127.3, 128.3, 128.8, 129.4, 134.8, 137.6, 155.9, 158.9, 172.7.

HRMS (ESI) m/z: $[M+H]^+$ calc'd for $[C_{23}H_{31}N_2O_4]$ 399.2284; found 399.2276.

***tert*-butyl *N*-[4-[*N*-benzyl-4-(trifluoromethyl)anilino]-4-oxo-butyl]carbamate**

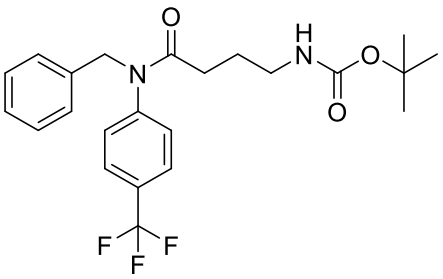

The title amide was synthesized according to the general procedure and purified by preparatory plate thin-layer chromatography (25% EtOAc/Hexanes) and isolated as a white solid (20.8 mg, 0.048 mmol, 48 %).

^{1}H NMR (600 MHz, $CDCl_3$): δ 7.59 (d, *J* = 8.2 Hz, 2H), 7.27 (d, *J* = 7.6 Hz, 3H), 7.19 – 7.15 (m, 2H), 7.10 (br, d, *J* = 7.8 Hz, 2H), 4.89 (s, 2H), 4.65 (br, s, 1H), 3.09 (br, q, *J* = 6.6 Hz, 2H), 2.10 (br, s, 2H), 1.79 (p, *J* = 6.9 Hz, 2H), 1.40 (s, 9H). **^{13}C NMR** (151 MHz, $CDCl_3$): δ 25.6, 28.4, 31.8, 40.0, 53.0, 79.1, 123.62 (q, *J* = 272.5 Hz), 126.8, 127.6, 128.6, 128.7, 128.9, 136.9, 145.4, 156.0, 171.9. **^{19}F NMR** (282 MHz, $CDCl_3$): δ -62.60.

HRMS (ESI) m/z: $[M+H]^+$ calc'd for $[C_{23}H_{28}F_3N_2O_3]$ 437.2052; found 437.2047.

m.p.: 75-77 °C

***tert*-butyl *N*-[4-(*N*-benzyl-4-fluoro-anilino)-4-oxo-butyl]carbamate**

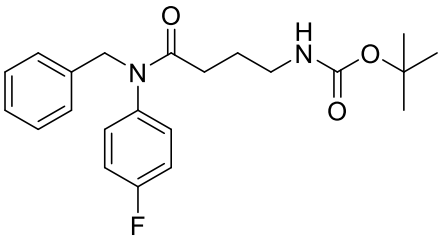

The title amide was synthesized according to the general procedure and purified by preparatory plate thin-layer chromatography (25% EtOAc/Hexanes) and isolated as an off-white solid (31.4 mg, 0.081 mmol, 81 %).

^{1}H NMR (600 MHz, $CDCl_3$): δ 7.29 – 7.22 (m, 3H), 7.18 – 7.13 (m, 2H), 6.99 (t, *J* = 8.3 Hz, 2H), 6.91 (dd, *J* = 8.6, 4.9 Hz, 2H), 4.84 (s, 2H), 4.69 (s, 1H), 3.07 (t, *J* = 6.7 Hz, 2H), 2.07 (t, *J* = 7.2 Hz, 2H), 1.77 (p, *J* = 6.8 Hz, 2H), 1.40 (s, 9H). **^{13}C NMR** (151 MHz, $CDCl_3$): δ 25.5, 28.4, 31.7, 40.1, 53.0, 79.0, 116.50 (d, *J* = 22.5 Hz), 127.5, 128.4, 128.8, 130.14 (d, *J* = 8.6 Hz), 137.2, 138.06 (d, *J* = 3.2 Hz), 155.9, 161.86 (d, *J* = 248.4 Hz), 172.3. **^{19}F NMR** (282 MHz, $CDCl_3$): δ -113.05.

HRMS (ESI) m/z: $[M+H]^+$ calc'd for $[C_{22}H_{28}FN_2O_3]$ 387.2084; found 287.2077.

m.p.: 72-73 °C

***tert*-butyl *N*-[4-[*N*-(1,3-benzodioxol-5-ylmethyl)anilino]-4-oxo-butyl]carbamate**

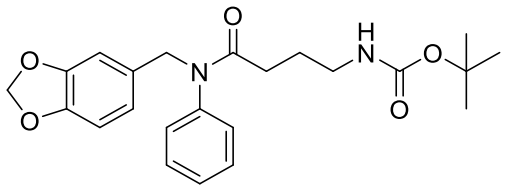

The title amide was synthesized according to the general procedure and purified by preparatory plate thin-layer chromatography (40% EtOAc/Hexanes) and isolated as a white solid (34.8 mg, 0.084 mmol, 84 %).

^{1}H NMR (600 MHz, $CDCl_3$): δ 7.36 – 7.27 (m, 3H), 6.95 (d, *J* = 6.4 Hz, 2H), 6.74 (d, *J* = 1.8 Hz, 1H), 6.65 (d, *J* = 7.9 Hz, 1H), 6.56 (dd, *J* = 7.9, 1.7 Hz, 1H), 5.91 (s, 2H), 4.76 (s, 2H), 4.69 (s, 1H), 3.05 (q, *J* = 6.6 Hz, 2H), 2.07 (t, *J* = 7.1 Hz, 2H), 1.75 (p, *J* = 7.9 Hz, 2H), 1.40 (s, 9H). **^{13}C NMR** (151 MHz, $CDCl_3$): δ 25.5, 28.4, 31.7, 40.1, 52.8, 78.9, 100.9, 107.9, 109.3, 122.3, 128.0, 128.4, 129.6, 131.4, 142.1, 146.8, 147.6, 155.9, 172.3.

HRMS (ESI) m/z: $[M+H]^+$ calc'd for $[C_{23}H_{29}N_2O_5]$ 413.2076; found 413.2071.

m.p.: 116-118 °C

tert-butyl *N*-[4-(*N*-methylanilino)-4-oxo-butyl]carbamate

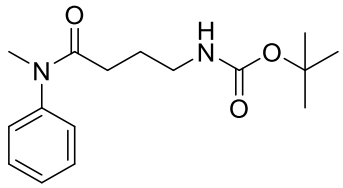

The title amide was synthesized according to the general procedure and purified by preparatory plate thin-layer chromatography (40% EtOAc/Hexanes) followed by a second preparatory plate to remove borane impurities (25% Ether/DCM). The product was isolated as an off-white solid (24.5 mg, 0.084 mmol, 84 %).

^{1}H NMR (600 MHz, $CDCl_3$): δ 7.35 (t, *J* = 7.6 Hz, 2H), 7.27 (t, *J* = 7.5 Hz, 1H), 7.10 (d, *J* = 7.7 Hz, 2H), 4.62 (br, s, 1H), 3.19 (s, 3H), 2.99 (br, q, *J* = 6.7 Hz, 2H), 2.03 (t, *J* = 7.2 Hz, 2H), 1.68 (p, *J* = 6.9 Hz, 2H), 1.34 (s, 9H). **^{13}C NMR** (151 MHz, $CDCl_3$): δ 25.5, 28.4, 31.5, 37.3, 40.1, 78.9, 127.3, 127.8, 129.8, 144.0, 155.9, 172.5.

HRMS (ESI) m/z: $[M+H]^+$ calc'd for $[C_{16}H_{25}N_2O_3]$ 293.1865; found 293.1858.

m.p.: 95-97 °C

***tert*-butyl *N*-[4-[*N*-(3-methylbut-3-enyl)anilino]-4-oxo-butyl]carbamate**

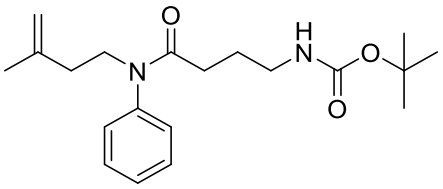

The title amide was synthesized according to the general procedure and purified by preparatory plate thin-layer chromatography (25% EtOAc/Hexanes) and isolated as a clear colorless oil (30.5 mg, 0.088 mmol, 88 %).

^{1}H NMR (600 MHz, $CDCl_3$): δ 7.41 (t, *J* = 7.6 Hz, 2H), 7.34 (t, *J* = 7.4 Hz, 1H), 7.14 (d, *J* = 7.1 Hz, 2H), 4.74 (s, 1H), 4.72 – 4.20 (m, 2H), 3.81 (t, *J* = 7.7 Hz, 2H), 3.04 (q, *J* = 6.5 Hz, 2H), 2.21 (t, *J* = 7.7 Hz, 2H), 2.03 (t, *J* = 7.2 Hz, 2H), 1.76 – 1.66 (m, 5H), 1.40 (s, 9H). **^{13}C NMR**

(151 MHz, $CDCl_3$): δ 22.4, 25.4, 28.4, 31.8, 35.7, 40.2, 47.7, 78.9, 111.7, 128.0, 128.4, 129.7, 142.4, 142.8, 155.9, 172.2.

HRMS (ESI) m/z: $[M+H]^+$ calc'd for $[C_{20}H_{31}N_2O_3]$ 347.2335; found 347.2329.

***tert*-butyl *N*-[4-[benzyl(3-methylbut-3-enyl)amino]-4-oxo-butyl]carbamate**

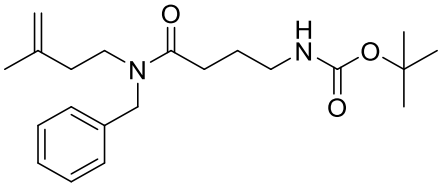

The title amide was synthesized according to the general procedure and purified by preparatory plate thin-layer chromatography (40% EtOAc/Hexanes) and isolated as a clear colorless oil (18.8 mg, 0.052 mmol, 52 %).

^{1}H NMR (600 MHz, $CDCl_3$): 7.35 (t, *J* = 7.5 Hz, 1H), 7.32 – 7.27 (m, 2H), 7.27 – 7.23 (m, 1H), 7.23 – 7.20 (m, 1H), 7.15 (d, *J* = 7.5 Hz, 1H), 4.85 (s, 0H), 4.80 – 4.76 (m, 1H), 4.74 (s, 1H), 4.69 – 4.65 (m, 1H), 4.60 (s, 1H), 4.51 (s, 1H), **Major Rotamer:** δ 3.48 (dd, *J* = 8.7, 6.5 Hz, 1.05H), 3.12 (q, *J* = 6.5 Hz, 1.05H), 2.35 (t, *J* = 7.1 Hz, 1.05H), 2.26 – 2.22 (m, 1.05H), 1.82 (p, *J* = 7.1 Hz, 1.05H), 1.73 (s, 1.57H), 1.40 (s, 4.73H), **Minor Rotamer:** δ 3.32 – 3.27 (m, 0.95H), 3.20 (q, *J* = 6.6 Hz, 0.95H), 2.44 (t, *J* = 7.1 Hz, 0.95H), 2.21 – 2.18 (m, 0.95H), 1.90 (p, *J* = 7.0 Hz, 0.95H), 1.71 (s, 1.43H), 1.43 (s, 4.27H). **^{13}C NMR** (151 MHz, $CDCl_3$): **Major Rotamer:** δ 172.7, 156.01, 143.0, 136.8, 128.9, 127.28, 126.16, 112.5, 78.92, 51.2, 45.0, 40.2, 35.6, 30.6, 28.36, 25.2, 22.4. **Minor Rotamer:** δ 172.4, 156.08, 141.9, 137.7, 128.6, 128.0, 127.6, 111.8, 79.0, 48.4, 45.7, 40.3, 36.5, 30.2, 28.39, 25.4, 22.6

HRMS (ESI) m/z: $[M+H]^+$ calc'd for $[C_{21}H_{33}N_2O_3]$ 361.2491; found 361.2485.

***tert*-butyl *N*-[4-(dibenzylamino)-4-oxo-butyl]carbamate**

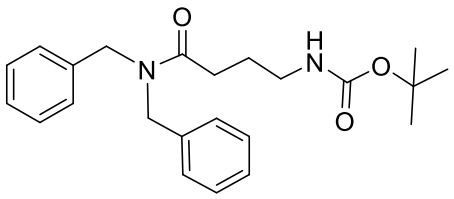

The title amide was synthesized according to the general procedure and purified by preparatory plate thin-layer chromatography (40% EtOAc/Hexanes) and isolated as a white solid (37.0 mg, 0.097 mmol, 97 %).

^{1}H NMR (600 MHz, $CDCl_3$): δ 7.36 (t, *J* = 7.5 Hz, 2H), 7.31 (t, *J* = 6.7 Hz, 3H), 7.29 – 7.25 (m, 1H), 7.21 (d, *J* = 7.4 Hz, 2H), 7.13 (d, *J* = 7.0 Hz, 2H), 4.83 – 4.79 (br, m, 1H), 4.61 (s, 2H), 4.44 (s, 2H), 3.17 (q, *J* = 6.5 Hz, 2H), 2.46 (t, *J* = 7.1 Hz, 2H), 1.90 (p, *J* = 7.0 Hz, 2H), 1.42 (s, 9H). **^{13}C NMR** (151 MHz, $CDCl_3$): δ 25.3, 28.4, 30.5, 40.2, 48.3, 49.9, 79.0, 126.3, 127.4, 127.6, 128.2, 128.6, 129.0, 136.4, 137.3, 156.0, 173.0.

HRMS (ESI) m/z: $[M+H]^+$ calc'd for $[C_{23}H_{31}N_2O_3]$ 383.2335; found 383.2333.

m.p.: 103-104 °C

***tert*-butyl *N*-[4-[benzyl(*tert*-butyl)amino]-4-oxo-butyl]carbamate**

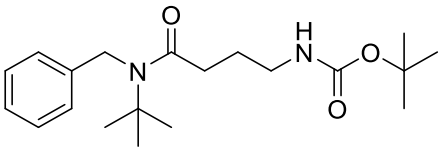

The title amide was synthesized according to the general procedure and purified by preparatory plate thin-layer chromatography (25% EtOAc/Hexanes) and isolated as a clear colorless oil (10.4 mg, 0.030 mmol, 30 %).

^{1}H NMR (600 MHz, $CDCl_3$): δ 7.35 (t, *J* = 7.6 Hz, 2H), 7.26 (t, *J* = 7.2 Hz, 1H), 7.18 (d, *J* = 7.6 Hz, 2H), 4.79 (br, s, 1H), 4.59 (s, 2H), 3.11 (br, q, *J* = 6.4 Hz, 2H), 2.32 (t, *J* = 6.9 Hz, 2H), 1.82 (p, *J* = 7.0 Hz, 2H), 1.43 (s, 9H), 1.40 (s, 9H). **^{13}C NMR** (151 MHz, $CDCl_3$): δ 25.1, 28.4, 28.8, 33.3, 40.4, 48.6, 57.9, 78.8, 125.4, 127.0, 128.9, 139.2, 156.0, 174.0.

HRMS (ESI) m/z: $[M+H]^+$ calc'd for $[C_{20}H_{33}N_2O_3]$ 349.2491; found 349.2484.

***tert*-butyl *N*-[4-oxo-4-(*N*-phenylanilino)butyl]carbamate**

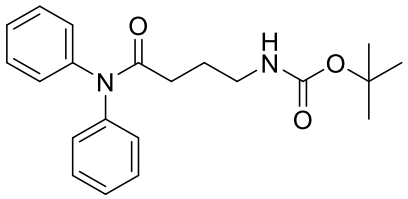

The title amide was synthesized according to the general procedure and purified by preparatory plate thin-layer chromatography (40% EtOAc/Hexanes) and isolated as an off-white solid (13.4 mg, 0.038 mmol, 38 %).

^{1}H NMR (600 MHz, $CDCl_3$): δ 7.52 – 7.09 (m, 10H), 4.70 (br, s, 1H), 3.14 (br, q, *J* = 6.5 Hz, 2H), 2.30 (t, *J* = 7.0 Hz, 2H), 1.84 (p, *J* = 6.9 Hz, 2H), 1.42 (s, 9H). **^{13}C NMR** (151 MHz, $CDCl_3$): δ 25.4, 28.4, 32.7, 40.2, 79.0, 126.4 (br), 128.8 (br), 129.8 (br), 142.7, 156.0, 172.7.

HRMS (ESI) m/z: $[M+H]^+$ calc'd for $[C_{21}H_{27}N_2O_3]$ 355.2022; found 355.2014.

m.p.: 112-114 °C

***tert*-butyl *N*-[4-(*N*-benzyl-2,4-dimethyl-anilino)-4-oxo-butyl]carbamate**

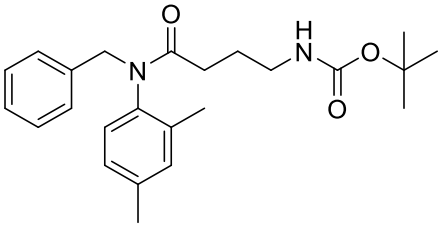

The title amide was synthesized according to the general procedure and purified by preparatory plate thin-layer chromatography (25% EtOAc/Hexanes) and isolated as a clear colorless oil (13.9 mg, 0.035 mmol, 35 %).

^{1}H NMR (600 MHz, $CDCl_3$): δ 7.25 – 7.22 (m, 3H), 7.21 – 7.15 (m, 2H), 7.04 (s, 1H), 6.89 (dd, *J* = 8.0, 2.1 Hz, 1H), 6.61 (d, *J* = 7.9 Hz, 1H), 5.23 (d, *J* = 13.9 Hz, 1H), 4.70 (br, s, 1H), 4.29 (d,

J = 13.9 Hz, 1H), 3.10 – 3.01 (br, m, 2H), 2.30 (s, 3H), 2.03 (dt, J = 16.1, 7.1 Hz, 1H), 1.99 (s, 3H), 1.90 (dt, J = 16.0, 7.1 Hz, 1H), 1.76 (p, J = 7.0 Hz, 2H), 1.40 (s, 9H). **^{13}C NMR** (151 MHz, $CDCl_3$): δ 17.3, 21.0, 25.2, 28.4, 31.4, 40.3, 52.1, 78.9, 127.4, 127.7, 128.3, 128.9, 129.3, 132.1, 135.3, 137.3, 138.0, 138.2, 155.9, 172.7.

HRMS (ESI) m/z: $[M+H]^+$ calc'd for $[C_{24}H_{33}N_2O_3]$ 397.2491; found 397.2480.

***tert*-butyl *N*-[4-(4-methyl-2-phenyl-piperazin-1-yl)-4-oxo-butyl]carbamate**

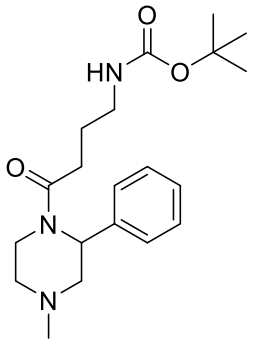

The title amide was synthesized according to the general procedure and purified by preparatory plate thin-layer chromatography (75% EtOAc/Hexanes) followed by a second preparatory plate to remove borane impurities (60% Ether/DCM). The product was isolated as a clear orange oil (24.3 mg, 0.067 mmol, 67 %).

^{1}H NMR (600 MHz, **55°C**, $CDCl_3$): δ 7.41 (br, s, 2H), 7.32 (t, J = 7.6 Hz, 2H), 7.23 (t, J = 7.4 Hz, 1H), 5.73 (br, s, 1H), 4.73 (br, s, 1H), 3.70 (br, s, 1H), 3.35 (d, J = 11.9 Hz, 1H), 3.18 (br, p, J = 6.2 Hz, 3H), 2.79 (dd, J = 11.4, 3.2 Hz, 1H), 2.46 – 2.34 (br, m, 3H), 2.29 (s, 3H), 2.07 (td, J = 11.6, 3.3 Hz, 1H), 1.92 – 1.82 (br, m, 2H), 1.43 (s, 9H). **^{13}C NMR** (151 MHz, **55°C**, $CDCl_3$): δ 25.6, 28.5, 30.6, 40.5, 41.0 (br), 46.2, 51.4 (br), 55.3, 57.4 (br), 76.8, 77.0, 77.2, 79.1, 127.1, 127.5, 128.6, 139.7, 156.1, 171.4.

HRMS (ESI) m/z: $[M+H]^+$ calc'd for $[C_{20}H_{32}N_3O_3]$ 362.2444; found 362.2436.

***tert*-butyl *N*-[4-(3,4-dihydro-*2H*-quinolin-1-yl)-4-oxo-butyl]carbamate**

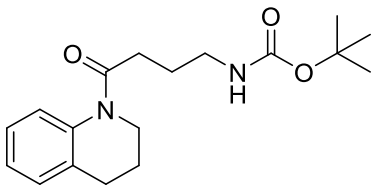

The title amide was synthesized according to the general procedure and purified by preparatory plate thin-layer chromatography (40% EtOAc/Hexanes) and isolated as a clear colorless oil (31.6 mg, 0.099 mmol, 99 %).

^{1}H NMR (600 MHz, $CDCl_3$): δ 7.20 – 7.07 (m, 4H), 4.71 (br, s, 1H), 3.77 (br, t, *J* = 6.6 Hz, 2H), 3.12 (br, s, 2H), 2.70 (br, t, *J* = 6.8 Hz, 2H), 2.52 (t, *J* = 7.2 Hz, 2H), 1.95 (p, *J* = 6.7 Hz, 2H), 1.84 (br, p, *J* = 6.3 Hz, 2H), 1.40 (s, 9H). **^{13}C NMR** (151 MHz, $CDCl_3$): δ 24.0, 25.9, 26.7, 28.4, 31.9, 40.2, 43.0, 70.8, 79.0, 124.6, 125.3, 126.1, 128.5, 139.0, 156.0, 172.3.

HRMS (ESI) m/z: $[M+H]^+$ calc'd for $[C_{18}H_{27}N_2O_3]$ 319.2022; found 319.2017.

***tert*-butyl *N*-[4-(2-methyl-3,4-dihydro-*2H*-quinolin-1-yl)-4-oxo-butyl]carbamate**

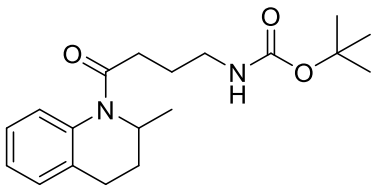

The title amide was synthesized according to the general procedure and purified by preparatory plate thin-layer chromatography (40% EtOAc/Hexanes) and isolated as a clear colorless oil (27.9 mg, 0.084 mmol, 84 %).

^{1}H NMR (600 MHz, **55°C**, $CDCl_3$): δ 7.22 – 7.09 (m, 4H), 4.84 (br, q, *J* = 7.1 Hz, 1H), 4.61 (br, s, 1H), 3.09 (br, q, *J* = 6.5 Hz, 2H), 2.63 – 2.45 (m, 3H), 2.39 – 2.30 (m, 2H), 1.90 – 1.59 (m, 3H), 1.41 (s, 9H), 1.10 (d, *J* = 6.5 Hz, 3H). **^{13}C NMR** (151 MHz, **55°C**, $CDCl_3$): δ 20.4, 26.0, 26.3, 28.4, 31.9, 32.8, 40.4, 48.5, 70.9, 79.0, 125.8, 126.1, 126.4, 127.5, 137.5, 156.0, 171.9.

HRMS (ESI) m/z: $[M+H]^+$ calc'd for $[C_{19}H_{29}N_2O_3]$ 333.2178; found 333.2170.

***tert*-butyl *N*-(4-indolin-1-yl-4-oxo-butyl)carbamate**

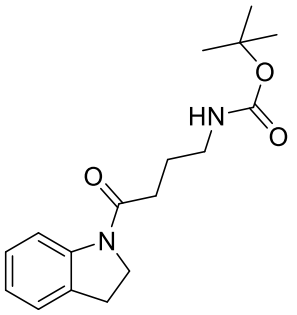

The title amide was synthesized according to the general procedure and purified by preparatory plate thin-layer chromatography (40% EtOAc/Hexanes) and isolated as an off-white solid (20.3 mg, 0.067 mmol, 67 %).

^{1}H NMR (600 MHz, $CDCl_3$): δ 8.21 (d, *J* = 8.1 Hz, 1H), 7.21 – 7.13 (m, 2H), 7.00 (t, *J* = 7.4 Hz, 1H), 4.80 (br, s, 1H), 4.03 (t, *J* = 8.5 Hz, 2H), 3.23 (q, *J* = 6.6 Hz, 2H), 3.18 (t, *J* = 8.5 Hz, 2H), 2.46 (t, *J* = 7.1 Hz, 2H), 1.93 (p, *J* = 7.0 Hz, 2H), 1.41 (s, 9H). **^{13}C NMR** (151 MHz, $CDCl_3$): δ 24.7, 28.0, 28.3, 33.2, 40.2, 47.9, 79.0, 117.0, 123.6, 124.5, 127.5, 131.0, 143.0, 156.1, 170.7.

HRMS (ESI) m/z: $[M+H]^+$ calc'd for $[C_{17}H_{25}N_2O_3]$ 305.1865; found 305.1859.

m.p.: 131-132 °C

***tert*-butyl *N*-[4-(4-benzhydrylpiperazin-1-yl)-4-oxo-butyl]carbamate**

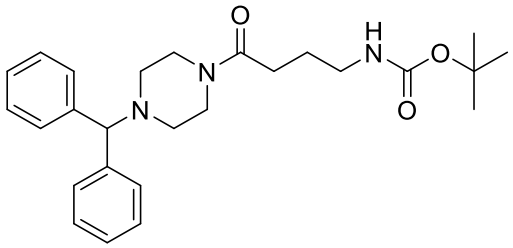

The title amide was synthesized according to the general procedure and purified by preparatory plate thin-layer chromatography (50% EtOAc/Hexanes) followed by a second preparatory plate to remove borane impurities (60% Ether/DCM). The product was isolated as an off-white solid (34.3 mg, 0.078 mmol, 78 %).

^{1}H NMR (600 MHz, **55°C**, $CDCl_3$): δ 7.40 (d, *J* = 7.5 Hz, 4H), 7.27 (t, *J* = 7.7 Hz, 4H), 7.19 (t, *J* = 7.4 Hz, 2H), 4.72 (br, s, 1H), 4.26 (s, 1H), 3.61 (br, s, 2H), 3.45 (br, s, 2H), 3.15 (q, *J* = 6.5 Hz, 2H), 2.38 (br, t, *J* = 5.0 Hz, 4H), 2.32 (t, *J* = 7.2 Hz, 2H), 1.81 (p, *J* = 7.0 Hz, 2H), 1.43 (s, 9H). **^{13}C NMR** (151 MHz, **55°C**, $CDCl_3$): δ 25.5, 28.5, 30.4, 33.0, 41.9, 45.8, 51.6, 52.1, 76.0, 79.1, 127.2, 128.0, 128.6, 142.1, 156.1, 170.9.

HRMS (ESI) m/z: $[M+H]^+$ calc'd for $[C_{26}H_{36}N_3O_3]$ 438.2757; found 438.2750.

m.p.: 155-157 °C

***tert*-butyl *N*-[4-[4-(furan-2-carbonyl)piperazin-1-yl]-4-oxo-butyl]carbamate**

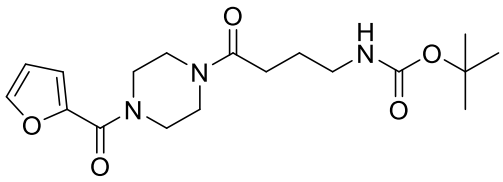

The title amide was synthesized according to the general procedure and purified by preparatory plate thin-layer chromatography (100% EtOAc) and isolated as an off-white solid (17.9 mg, 0.049 mmol, 49 %).

^{1}H NMR (600 MHz, $CDCl_3$): δ 7.49 (dd, *J* = 1.9, 0.9 Hz, 1H), 7.05 (dd, *J* = 3.5, 0.8 Hz, 1H), 6.49 (dd, *J* = 3.5, 1.7 Hz, 1H), 4.77 (br, s, 1H), 3.80 (br, s, 4H), 3.69 (br, dd, *J* = 6.7, 3.8 Hz, 2H), 3.56 – 3.52 (br, m, 2H), 3.18 (q, *J* = 6.5 Hz, 2H), 2.39 (t, *J* = 7.2 Hz, 2H), 1.85 (p, *J* = 7.0 Hz, 2H), 1.42 (s, 9H). **^{13}C NMR** (151 MHz, $CDCl_3$): δ 25.4, 28.4, 30.4, 40.1, 41.7, 45.4, 79.2, 111.5, 117.1, 143.9, 147.6, 156.1, 159.2, 171.2.

HRMS (ESI) m/z: $[M+H]^+$ calc'd for $[C_{18}H_{28}N_3O_5]$ 366.2029; found 366.2026.

m.p.: 94-95 °C

***tert*-butyl *N*-(4-oxo-4-phenothiazin-10-yl-butyl)carbamate**

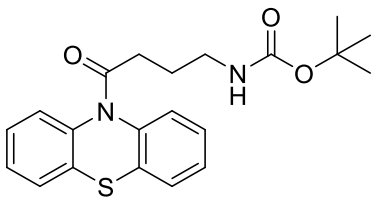

The title amide was synthesized according to the general procedure and purified by preparatory plate thin-layer chromatography (25% EtOAc/Hexanes) followed by a second preparatory plate to remove borane impurities (20% Ether/DCM). The product was isolated as a clear colorless oil (10.9 mg, 0.028 mmol, 28 %).

^{1}H NMR (600 MHz, $CDCl_3$): δ 7.50 (d, *J* = 8.0 Hz, 2H), 7.45 (dd, *J* = 7.8, 1.4 Hz, 2H), 7.33 (td, *J* = 7.7, 1.4 Hz, 2H), 7.23 (td, *J* = 7.6, 1.3 Hz, 2H), 4.59 (br, s, 1H), 3.11 (br, q, *J* = 6.6 Hz, 2H), 2.49 (br, t, *J* = 7.3 Hz, 2H), 1.79 (br, p, *J* = 6.9 Hz, 2H), 1.40 (s, 9H). **^{13}C NMR** (151 MHz, $CDCl_3$): δ 25.5, 28.4, 31.6, 39.9, 79.1, 126.9, 127.0, 127.3, 128.0, 133.3, 138.7, 156.0, 171.8.

HRMS (ESI) m/z: $[M+H]^+$ calc'd for $[C_{21}H_{25}N_2O_3S]$ 385.1586; found 385.1578.

***tert*-butyl *N*-(4-benzo[b][1]benzazepin-11-yl-4-oxo-butyl)carbamate**

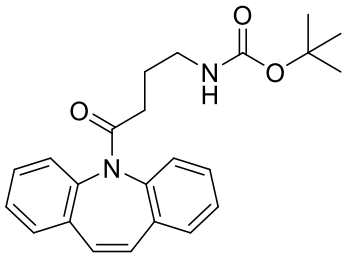

The title amide was synthesized according to the general procedure and purified by preparatory plate thin-layer chromatography (40% EtOAc/Hexanes) and isolated as a clear colorless oil (31.0 mg, 0.082 mmol, 82 %).

^{1}H NMR (600 MHz, $CDCl_3$): δ 7.47 – 7.41 (m, 3H), 7.40 – 7.34 (m, 4H), 7.32 (ddd, *J* = 8.1, 6.8, 1.7 Hz, 1H), 6.94 (dd, 2H), 4.63 (br, t, *J* = 6.0 Hz, 1H), 3.03 (br, q, *J* = 6.3 Hz, 2H), 2.28 (dt, *J* = 16.0, 7.0 Hz, 1H), 1.92 (dt, *J* = 16.0, 7.0 Hz, 1H), 1.69 (ddt, *J* = 34.4, 13.8, 6.9 Hz, 2H), 1.42 (s,

9H). **^{13}C NMR** (151 MHz, $CDCl_3$): δ 25.0, 28.4, 30.8, 40.0, 78.9, 127.4, 127.9, 128.0, 128.5, 129.0, 129.2, 129.3, 129.4, 131.5, 133.4, 134.8, 139.7, 140.3, 155.9, 172.9.

HRMS (ESI) m/z: $[M+H]^+$ calc'd for $[C_{23}H_{27}N_2O_3]$ 379.2022; found 379.2019.

***tert*-butyl *N*-[4-[benzyl(2-pyridyl)amino]-4-oxo-butyl]carbamate**

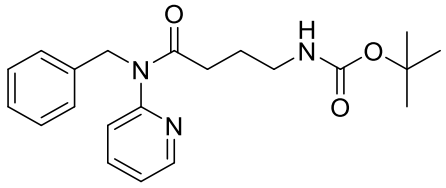

The title amide was synthesized according to the general procedure and purified by preparatory plate thin-layer chromatography (60% EtOAc/Hexanes) followed by a second preparatory plate to remove borane impurities (25% Ether/DCM). The product was isolated as a clear colorless oil (34.1 mg, 0.092 mmol, 92 %).

^{1}H NMR (600 MHz, $CDCl_3$): δ 8.52 – 8.48 (m, 1H), 7.65 (td, *J* = 7.7, 2.0 Hz, 1H), 7.27 – 7.23 (m, 2H), 7.22 – 7.17 (m, 4H), 7.05 (s, br, 1H), 5.06 (s, 2H), 4.92 (s, br, 1H), 3.10 (q, *J* = 6.5 Hz, 2H), 2.30 (t, *J* = 7.1 Hz, 2H), 1.82 (p, *J* = 6.9 Hz, 2H), 1.41 (s, 9H). **^{13}C NMR** (151 MHz, $CDCl_3$): δ 25.5, 28.4, 32.0, 39.9, 51.3, 78.9, 121.8, 122.3, 127.2, 127.9, 128.4, 137.5, 138.2, 149.3, 155.0, 155.9, 172.6.

HRMS (ESI) m/z: $[M+H]^+$ calc'd for $[C_{21}H_{28}N_3O_3]$ 370.2131; found 370.2128.

***N*-(1,3-benzodioxol-5-ylmethyl)-*N*,5-diphenyl-pentanamide**

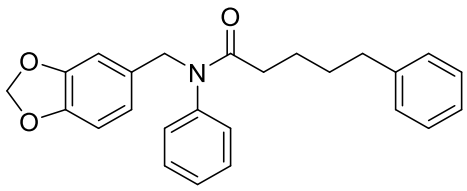

The title amide was synthesized according to the general procedure and purified by preparatory plate thin-layer chromatography (15% EtOAc/Hexanes) and isolated as a clear pale-yellow oil (34.2 mg, 0.088 mmol, 88 %).

^{1}H NMR (600 MHz, $CDCl_3$): δ 7.32 (q, *J* = 7.5 Hz, 3H), 7.24 (t, *J* = 7.5 Hz, 2H), 7.15 (t, *J* = 7.3 Hz, 1H), 7.11 (d, 2H), 6.94 (d, 2H), 6.76 (d, *J* = 1.7 Hz, 1H), 6.66 (d, *J* = 7.9 Hz, 1H), 6.57 (dd, *J* = 8.0, 1.7 Hz, 1H), 5.92 (s, 2H), 4.77 (s, 3H), 2.53 (t, *J* = 7.7 Hz, 2H), 2.07 (t, *J* = 7.4 Hz, 2H), 1.64 (p, *J* = 7.5 Hz, 2H), 1.53 (p, *J* = 7.8 Hz, 2H). **^{13}C NMR** (151 MHz, $CDCl_3$): δ 25.1, 31.0, 34.2, 35.6, 52.7, 100.9, 107.9, 109.3, 122.3, 125.6, 127.9, 128.2, 128.3, 128.4, 129.5, 131.6, 142.29, 142.33, 146.8, 147.6, 172.7.

HRMS (ESI) m/z: $[M+H]^+$ calc'd for $[C_{25}H_{26}NO_3]$ 388.1913; found 388.1905.

_N_-[[4-(dimethylamino)phenyl]methyl]-_N_,5-diphenyl-pentanamide

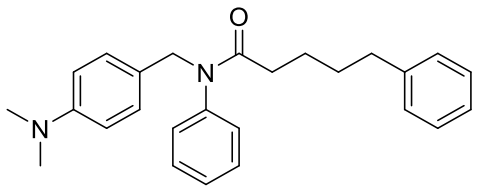

The title amide was synthesized according to the general procedure and purified by preparatory plate thin-layer chromatography (20% EtOAc/Hexanes) and isolated as a clear pale-orange oil (36.6 mg, 0.095 mmol, 95 %).

^{1}H NMR (300 MHz, $CDCl_3$): δ 7.35 – 7.19 (m, 5H), 7.19 – 7.13 (m, 1H), 7.13 – 7.07 (m, 2H), 7.07 – 7.00 (m, 2H), 6.99 – 6.87 (m, 2H), 6.66 – 6.55 (m, 2H), 4.77 (s, 2H), 2.91 (s, 6H), 2.53 (t, *J* = 7.5 Hz, 2H), 2.05 (t, *J* = 7.2 Hz, 2H), 1.63 (p, *J* = 7.6 Hz, 2H), 1.53 (p, *J* = 5.8 Hz, 2H). **^{13}C NMR** (75 MHz, $CDCl_3$): δ 25.2, 31.0, 34.2, 35.7, 40.6, 52.4, 112.3, 125.6, 127.6, 128.2, 128.3, 128.6, 129.3, 129.9, 142.4, 142.6, 149.8, 172.5.

HRMS (ESI) m/z: $[M+H]^+$ calc'd for $[C_{26}H_{31}N_2O]$ 387.2436; found 387.2431.

***tert*-butyl *N*-[3-[4-(anilinomethyl)phenyl]propyl]carbamate**

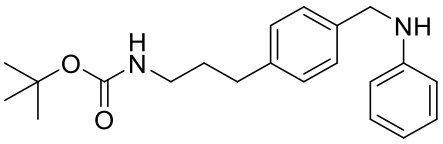

The title amine was synthesized according to the general procedure using CMF **2.2e** and purified by preparatory plate thin-layer chromatography (20% EtOAc/Hexanes) followed by a second preparatory plate to remove borane impurities (5% Ether/DCM). The product was isolated as a clear colorless oil (5.5 mg, 0.016 mmol, 16 %).

^{1}H NMR (300 MHz, $CDCl_3$): δ 7.29 (d, *J* = 7.8 Hz, 2H), 7.23 – 7.11 (m, 4H), 6.71 (tt, *J* = 7.3, 1.2 Hz, 1H), 6.64 (d, *J* = 7.8 Hz, 2H), 4.52 (s, 1H), 4.29 (s, 2H), 4.05 (s, 1H), 3.14 (q, *J* = 6.8 Hz, 2H), 2.63 (t, *J* = 7.7 Hz, 2H), 1.80 (p, *J* = 7.4 Hz, 2H), 1.45 (s, 9H).

HRMS (ESI) m/z: $[M+H]^+$ calc'd for $[C_{21}H_{29}N_2O_2]$ 341.2229; found 341.2222.

***tert*-butyl *N*-[3-[4-[(*N*-fluorocarbonylanilino)methyl]phenyl]propyl]carbamate**

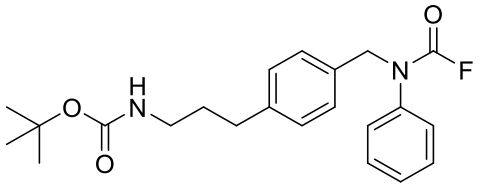

The title CMF was synthesized according to the general procedure using CMF **2.2g** and purified by preparatory plate thin-layer chromatography (20% EtOAc/Hexanes) followed by a second preparatory plate to remove borane impurities (5% Ether/DCM). The product was isolated as a clear colorless oil (25.5 mg, 0.066 mmol, 66 %).

^{1}H NMR (300 MHz, $CDCl_3$): δ 7.38 – 7.23 (m, 4H), 7.19 – 7.00 (m, 5H), 4.79 (s, 2H), 4.54 (s, 1H), 3.13 (q, *J* = 6.9 Hz, 2H), 2.62 (t, *J* = 7.8 Hz, 2H), 1.79 (p, *J* = 7.3 Hz, 2H), 1.44 (s, 9H). **^{19}F NMR** (282 MHz, $CDCl_3$): δ -14.58, -17.04.

HRMS (ESI) m/z: $[M+H]^+$ calc'd for $[C_{22}H_{28}FN_2O_3]$ 387.2084; found 387.2080.

***tert*-butyl *N*-[3-[4-[[*N*-[4-(*tert*-butoxycarbonylamino)butanoyl]anilino]methyl]phenyl] propyl] carbamate**

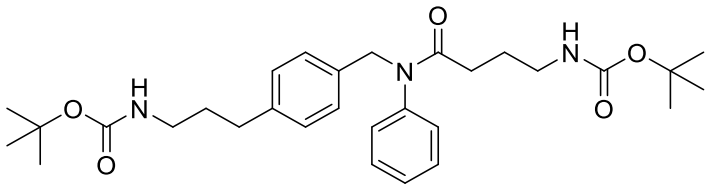

The title amide was synthesized according to the general procedure using CMF **2.2f** and purified by preparatory plate thin-layer chromatography (40% EtOAc/Hexanes) followed by a second preparatory plate to remove borane impurities (5% Ether/DCM). The product was isolated as a clear colorless oil (23.2mg, 0.044 mmol, 44 %).

^{1}H NMR (300 MHz, $CDCl_3$): δ 7.38 – 7.27 (m, 3H), 7.13 – 7.01 (m, 4H), 6.99 – 6.90 (m, 2H), 4.83 (s, 2H), 4.68 (s, 1H), 4.53 (s, 1H), 3.18 – 2.99 (m, 4H), 2.59 (t, *J* = 7.8 Hz, 2H), 2.08 (t, *J* = 7.1 Hz, 2H), 1.87 – 1.70 (m, 4H), 1.44 (s, 9H), 1.40 (s, 9H).

HRMS (ESI) m/z: $[M+H]^+$ calc'd for $[C_{20}H_{31}N_2O_3]$ 526.3281; found 526.3276.

$[(PCy_3)_2Ni]_2N_2$

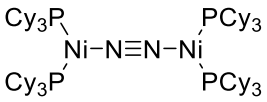

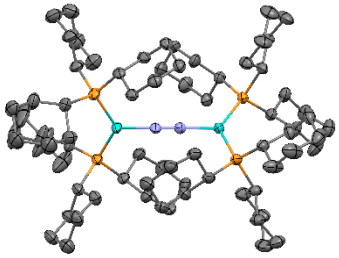

<u>Warning:</u> Extreme caution should be taken when working with $[(PCy_3)_2Ni]_2N_2$ as decomposition will occur if allowed contact with even the slightest amount of non-inert gas or any remotely functionalized compound. Contact with purely hydrocarbon-based solvents is strongly recommended. Handle only under an atmosphere of nitrogen! Prolonged exposure to strong vacuum may result in displacement of N_2 from the complex, resulting in a highly unstable complex which may spontaneously decompose resulting in significant amounts of inseparable side products. To minimize decomposition, prolonged storage of the product should be done at -35°C in a nitrogen filled glovebox.

A 250 mL oven-dried Schlenk tube was brought into a nitrogen filled glovebox and had sodium metal (172 mg, 7.5 mmol, 5 equiv) smeared as thinly as possible on the inner walls of the reaction

vessel. The flask was then charged with bis(tricyclohexylphosphine)nickel(II) dichloride (1.04 g, 1.53 mmol, 5 equiv) followed by 50 mL of toluene which had been previously degassed with nitrogen. The reaction was then vigorously stirred for 6 hours with a slow continuous stream of nitrogen gas bubbled though the mixture. Caution was taken to ensure the reaction mixture never touch the septum of the reaction vessel as it would result in decomposition of the product. Solvent was then removed under vacuum, ensuring to periodically backfill the reaction vessel with fresh N_2 gas and to allow the reaction mixture to return to room temperature. Once nearly all solvent was removed the reaction vessel was transferred into a nitrogen filled glovebox and the product was extracted with pentane (3 × 50 mL) mixing for 15 minutes prior to each decanting. The resulting intense deep red solution was then filtered through glass filter paper and volume carefully decreased by 75% under reduced pressure. The solution was then cooled to -35°C overnight, the mixture was carefully decanted and solids washed with -35°C pentane (2 × 5 mL). residual solvent was then removed under reduced pressure to give intense dark black-red crystals of the desired product (678 mg, 0.535 mmol, 70%) which was confirmed single crystal XRD.

^{1}H NMR (400 MHz, C_6D_6) δ 1.92 – 1.59 (m, 66H), 1.46 – 1.06 (m, 66H). **^{13}C NMR** (101 MHz, C_6D_6): δ 26.9, 27.2, 28.0, 28.0, 28.1, 28.2, 31.4, 31.5, 31.6, 31.7, 32.1, 32.3, 34.9, 35.1. **^{31}P {^{1}H} NMR** (162 MHz, C_6D_6): δ 46.02.

N-benzyl-N-(pyridin-2-yl)carbamoyl-tricyclohexyl Nickel (II) fluoride

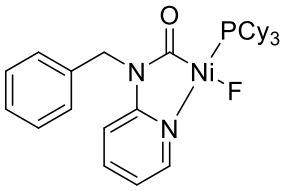

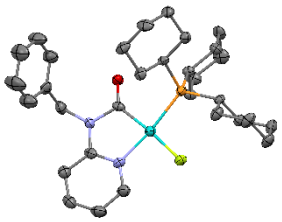

In nitrogen filled glovebox, a 20 mL scintillation was charged with N-benzyl-N-(pyridin-2-yl)carbamoyl fluoride (**2.2o**) (3.5 mg, 15.0 µmol, 2.4 equiv) followed by 2 mL of pentane and cooled to -35°C for 30 minutes. A cold solution of $[(PCy_3)_2Ni]_2N_2$ (8.0 mg, 6.3 µmol, 1 equiv) in pentane was then added dropwise, resulting in an immediate color change from deep black-red to yellow and the formation of a bright yellow precipitate. The reaction was then brought to room temperature and mixed for 3 hours. The precipitate was collected by decanting

the pentane layer and washing the subsequent solid with cold pentane (2 × 3 mL). The product was then dissolved in ether, filtered and dried under reduced pressure to yield a yellow solid (6.0 mg, 10.6 µmol, 84%). Single crystals suitable for XRD were grown from a cooling of a saturated ether solution at -35°C.

^{1}H NMR (300 MHz, $CDCl_3$): δ 8.50 – 8.42 (m, 1H), 7.57 (td, *J* = 7.9, 1.7 Hz, 1H), 7.32 – 7.26 (m, 1H), 7.25 – 7.10 (m, 4H), 6.82 (t, *J* = 6.5 Hz, 1H), 6.52 (d, *J* = 8.4 Hz, 1H), 4.64 (s, 2H), 2.11 (d, *J* = 12.5 Hz, 6H), 1.77 (d, *J* = 26.5 Hz, 17H), 1.36 – 1.28 (m, 10H). **^{19}F {^{1}H} NMR** (282 MHz, $CDCl_3$): δ -304.80 (d, *J* = 34.3 Hz). **^{31}P {^{1}H} NMR** (121 MHz, $CDCl_3$): δ 40.91 (d, *J* = 34.0 Hz).

Indoline-1-carbamoyl-bis(tricyclohexyl) Nickel (II) fluoride

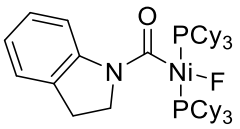

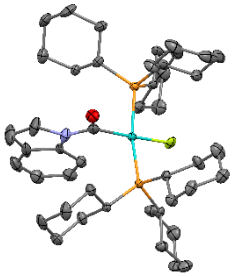

In nitrogen filled glovebox, a 20 mL scintillation was charged with Indoline-1-carbamoyl fluoride (**2.2x**) (2.4 mg, 14.5 µmol mmol, 8 equiv) followed by 1 mL of pentane and cooled to -35°C for 30 minutes. A cold solution of $[(PCy_3)_2Ni]_2N_2$ (2.3 mg, 1.8 µmol, 1 equiv) in pentane was then added dropwise, resulting in an immediate color change from deep black-red to yellow and the formation of a bright yellow precipitate. The reaction was then brought to room temperature and mixed for 5 min. The precipitate was collected by decanting the pentane layer and washing the subsequent solid with cold pentane (2 × 3 mL). The product was then dissolved in ether, filtered and dried under reduced pressure to yield a yellow solid (2.4 mg, 3.1 µmol, 85%). Single crystals suitable for XRD were grown from a cooling of a saturated ether solution at -35°C.

^{1}H NMR (300 MHz, $CDCl_3$) δ 11.22 (d, 1H, Ar), 7.34-7.04 (m, 2H, Ar), 6.93 (t, 1H, Ar), 3.86 (t, 2H, Ar-CH_2-), 2.92 (t, 2H, -CH_2-N), 2.35-1.08 (m, 66H, Ni-$(PCy_3)_2$ + PCy_3). **^{19}F {^{1}H} NMR** (282 MHz, $CDCl_3$) δ -357.2 (t, 1F, Ni-F). **^{31}P {^{1}H} NMR** (121 MHz, $CDCl_3$) δ 16.0 (d, 2P, Ni-$(PCy_3)_2$).

bis(tricyclohexylphosphine)nickel(II) dichloride

$(PCy_3)_2NiCl_2$

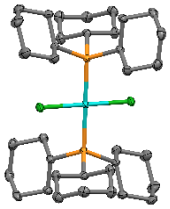

A 500 mL oven-dried RBF was brought into a nitrogen filled glovebox and charged with anhydrous nickel(II) chloride (3.01 g, 23.2 mmol, 1 equiv) and tricyclohexyl phosphine (14.0 g, 50.1 mmol, 2.2 equiv) and equipped with a septum. The vessel was then transferred out of the glovebox and equipped to a Schlenk line and 150 mL of anhydrous EtOH was then added and heated to 75°C for 18 hours. The resulting fine microcrystalline burgundy solid was collected by suction filtration and washed with EtOH (2 × 50 mL) and ether (2 × 50 mL). The product was then recrystallized in boiling toluene to give cubic burgundy crystals (15.8 g, 22.9 mmol, 99%) which were then confirmed by XRD to be the product and used as is without further purification.

bis(triphenylphosphine)nickel(II) dichloride

$(PPh_3)_2Ni^{II}Cl_2$

In open atmosphere, a 500 mL oven-dried RBF was charged with a fully dissolved solution of nickel(II) chloride hexahydrate (3.41 g, 14.3 mmol, 1 equiv) in 75 mL of EtOH followed by triphenylphosphine (11.5 g, 43.9 mmol, 3.1 equiv) dissolved in 100 mL of hot EtOH. The reaction was mixed at 40°C for 2 hours, and the resulting precipitate was collected by suction filtration and subsequently washed with EtOH (3 × 100 mL) and ether (2 × 100 mL). Residual solvent was removed by reduced pressure, resulting in a dark blue microcrystalline solid. The product was then further purified by dissolution in boiling MeCN which was then gravity filtered and allowed to sit overnight, which resulted in large dark blue cubic crystals of the desired product (8.74 g, 13.4 mmol, 93%).

[1,1′-Bis(diphenylphosphino)ferrocene]dichloronickel(II)

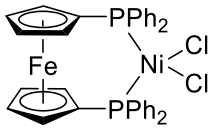

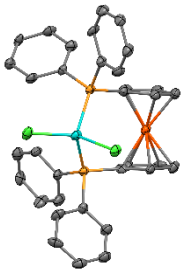

In open atmosphere, a 500 mL oven-dried RBF was charged with a fully dissolved solution of nickel(II) chloride hexahydrate (8.24 g, 34.7 mmol, 2.13 equiv) in 150 mL of EtOH and 1,1′-Ferrocenediyl-bis(diphenylphosphine) (9.03 g, 16.3 mmol, 1 equiv) which was added as a solid. The reaction was mixed at 50°C for 4 hours, and the resulting precipitate was collected by suction filtration and subsequently washed with EtOH (6 × 50 mL) and ether (5 × 100 mL). Residual solvent was removed by reduced pressure, resulting in a dark forest green microcrystalline solid (10.3 g, 15.0 mmol, 92%). The product could then be recrystalized using boiling toluene under an inert atmosphere.

[1,1′-Bis(diphenylphosphino)ferrocene]chloronickel(I)

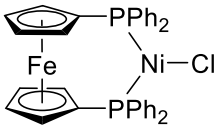

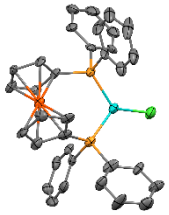

In nitrogen filled glovebox, a 20 mL scintillation was charged with [1,1′-Bis(diphenylphosphino)ferrocene]dichloronickel(II) (250 mg, 0.366 mmol, 1 equiv) followed by 4.5 mL of THF and cooled to -35°C for 10 minutes. A 0.53M solution of H-9BBN (1.51 mL, 0.800 mmol, 2.2 equiv) was then slowly added, the reaction was then brought to room temperature and mixed for 18 hours. Solvent was removed with reduced pressure and solids washed with pentane (3 × 10 mL) and ether (2 × 10 mL). Residual solids were dried with reduced pressure to yield the product as a yellow-orange powdery solid (231 mg, 0.356 mmol, 97%) which was used as is in subsequent reactions. Further purification was possible by recrystallization in a minimal amount of THF at -35°C however a notable amount of product is lost in the process.

N-benzyl-N-(pyridin-2-yl)carbamoyl-[1,1′-Bis(diphenylphosphino) ferrocene] Nickel (II) fluoride

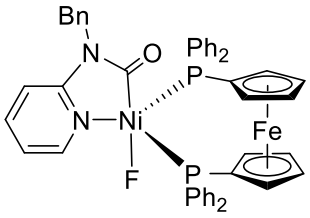

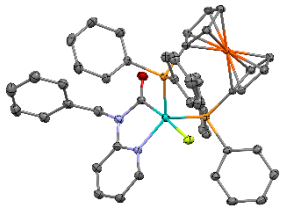

In nitrogen filled glovebox, a 20 mL scintillation was charged with $Ni(COD)_2$ (226 mg, 0.820 mmol, 1 equiv.), dppf (465 mg, 0.839 mmol, 1.02 equiv), N-benzyl-N-(pyridin-2-yl)carbamoyl fluoride (224 mg, 0.973 mmol, 1.2 equiv), followed by 10 mL of THF. The vial was secured with electrical tape and removed from the glovebox, the mixture was then heated to 50°C for 1 hour and brought back into a nitrogen filled glovebox. Solvent was removed by reduced pressure, and the resulting solids were repeatedly for a total of three times, had 10 mL of pentane added, followed by sonication for 2 minutes, the vial was then centrifuged, and pentane soluble fraction decanted. Residual solvent was then removed under reduced pressure, yielding a red powdery solid (310 mg, 0.367 mmol, 45%). Single crystals suitable for XRD were grown from a cooling of a saturated THF solution at -35°C.

^{1}H NMR (300 MHz, C_6D_6): δ 9.07 (d, J = 5.7 Hz, 1H), 7.87 (s, 9H), 7.09 – 6.88 (m, 15H), 6.79 (t, J = 7.7 Hz, 1H), 6.73 – 6.65 (m, 2H), 6.31 (t, J = 6.4 Hz, 1H), 6.08 (d, J = 8.2 Hz, 1H), 4.92 (s, 4H), 4.22 (s, 4H), 4.07 (s, 2H). **^{19}F {^{1}H}** NMR (282 MHz, THF-H_8): δ -366.19. **^{31}P {^{1}H}** NMR (121 MHz, THF-H_8): δ -8.99.

(dppf)Ni(I)OTf

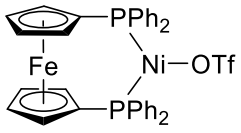

The title complex was prepared by treating a suspension of [1,1′-Bis(diphenylphosphino)ferrocene]chloronickel(I) (367 mg, 0.567 mmol, 1 equiv) in 5 mL of toluene with TMSOTf (514 µL, 2.83 mmol, 5.0 equiv) at room temperature for 2 hours. The

reaction volume was reduced to approximately 50% and centrifuged, decanted and residual solvent removed under reduced pressure. The resulting tan color solid was then washed with pentane (2 × 10 mL) and dried under reduced pressure to afford a tan color free flowing solid (388 mg, 0.508 mmol, 90% yield).

Alkyl Borane Synthesis

Isolated alkyl boranes were prepared by reacting the corresponding alkene with 0.98 equivalents of H-9BBN in toluene at room temperature for 18 hours. All solvent was removed under reduced pressure, the product was purified by recrystallization in a saturated pentane solution at -35 °C, to afford the product, which was used as is without further purification.

2-(9-borabicyclo[3.3.1]nonan-9-yl)ethylferrocene

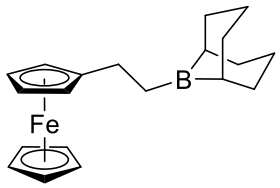

The title alkyl-borane was synthesized according to the general procedure using vinylferrocene (421 mg, 1.98 mmol, 1 equiv), which was then purified by recrystallization in pentane at -35 °C to afford the product as orange solid (629 mg, 1.89 mmol, 96 %).

^{1}H NMR (600 MHz, C_6D_6): δ 4.04 (s, 5H), 3.98 (s, 2H), 3.55 (t, *J* = 6.1 Hz, 2H), 2.56 (t, *J* = 7.9 Hz, 2H), 1.91 – 1.82 (m, 4H), 1.81 – 1.75 (m, 2H), 1.72 – 1.63 (m, 6H), 1.46 – 1.38 (m, 2H), 1.23 – 1.15 (m, 2H). **^{11}B {^{1}H}** NMR (192 MHz, C_6D_6): δ 87.82. **^{13}C NMR** (151 MHz, C_6D_6): δ 23.6, 24.5, 25.8, 33.5, 67.4, 67.8, 68.1, 68.8, 92.2, 128.3.

3-(9-borabicyclo[3.3.1]nonan-9-yl)propyl-trimethyl-silane

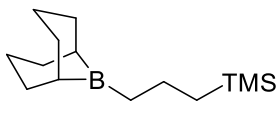

The title alkyl-borane was synthesized according to the general procedure using allyltrimethylsilane (600 µL, 3.78 mmol, 1 equiv), which was then purified by recrystallization in pentane at -35 ℃ to afford the product as colorless oil (659 mg, 2.78 mmol, 74 %).

^{1}H NMR (600 MHz, C_6D_6): δ 1.91 – 1.80 (m, 6H), 1.77 (p, *J* = 3.6 Hz, 2H), 1.74 – 1.67 (m, 4H), 1.65 – 1.56 (m, 2H), 1.50 (t, *J* = 7.4 Hz, 2H), 1.24 – 1.16 (m, 2H), 0.63 – 0.57 (m, 2H), 0.04 (s, 9H). **^{11}B {^{1}H} NMR** (192 MHz, C_6D_6): δ 88.21. **^{13}C NMR** (151 MHz, C_6D_6): δ -1.4, 19.3, 20.9, 23.7, 33.5, 128.3.

***tert*-butyl *N*-[3-(9-borabicyclo[3.3.1]nonan-9-yl)propyl]carbamate**

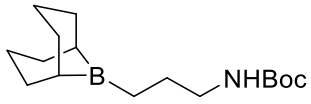

The title alkyl-borane was synthesized according to the general procedure using *tert*-Butyl *N*-allylcarbamate (632 mg, 4.02 mmol, 1 equiv), which was then purified by recrystallization in pentane at -35 ℃ to afford the product as a white powdery solid (679 mg, 2.43 mmol, 60 %).

^{1}H NMR (600 MHz, C_6D_6): δ 4.46 (t, *J* = 6.1 Hz, 1H), 2.97 (q, *J* = 6.7 Hz, 2H), 1.98 – 1.85 (m, 6H), 1.81 – 1.72 (m, 4H), 1.55 – 1.51 (m, 2H), 1.48 (p, *J* = 7.3 Hz, 2H), 1.41 (s, 9H), 1.38 – 1.30 (m, 2H), 1.12 (t, *J* = 7.6 Hz, 2H). **^{11}B {^{1}H} NMR** (192 MHz, C_6D_6): δ 72.86. **^{13}C NMR** (151 MHz, C_6D_6): δ 24.1, 25.2, 28.4, 30.6, 33.4, 43.2, 79.3, 128.3, 157.1.

Alkyl hydroxoborate salt General Synthesis

alkyl hydroxoborate salts were prepared by reacting the corresponding alkyl-borane with 0.95 equivalents of NaOH in toluene at room temperature for 18 hours. The resulting solution was then filtered through a pad of glass filter-paper, and all solvent removed under reduced pressure. The product was purified by recrystallization in a saturated pentane or toluene solution at -35 ℃, to afford the product, which was used as is without further purification.

Sodium 2-(9-hydroxy-9-boranuidabicyclo[3.3.1]nonan-9-yl)ethylferrocene

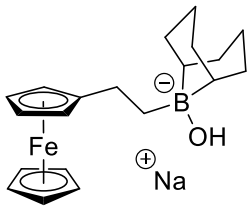

The title alkyl-hydroxoborate salts was synthesized according to the general procedure using 2-(9-borabicyclo[3.3.1]nonan-9-yl)ethylferrocene (286 mg, 0.856 mmol, 1 equiv), which was then purified by recrystallization in toluene at -35 °C to afford the product as an orange solid (260 mg, 0.695 mmol, 81 %).

^{11}B {^{1}H} NMR (192 MHz, C_6D_6): δ -2.78.

Sodium 3-(9-hydroxy-9-boranuidabicyclo[3.3.1]nonan-9-yl)propyl-trimethyl-silane

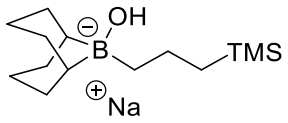

The title alkyl-hydroxoborate salts was synthesized according to the general procedure using 3-(9-borabicyclo[3.3.1]nonan-9-yl)propyl-trimethyl-silane (376 mg, 1.59 mmol, 1 equiv), which was then purified by recrystallization in pentane at -35 °C to afford the product as a white solid (426 mg, 1.54 mmol, 97 %).

^{1}H NMR (300 MHz, C_6D_6): δ 2.51 – 1.78 (m, 12H), 1.56 – 1.39 (m, 2H), 0.87 (t, *J* = 7.9 Hz, 2H), 0.72 – 0.61 (m, 2H), 0.56 (s, 2H), 0.24 (s, 1H), 0.15 (s, 9H). (Coordinated THF : δ 3.55 – 3.49, 1.43 – 1.23.). **^{11}B {^{1}H} NMR** (96 MHz, C_6D_6): δ -1.62. **^{13}C NMR** (75 MHz, C_6D_6): δ -1.1, 20.8, 22.9, 25.5, 32.6, 34.0, 68.2.

Sodium tert-butyl N-[3-(9-hydroxy-9-boranuidabicyclo[3.3.1]nonan-9-yl)propyl]carbamate

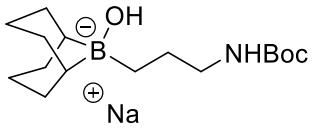

The title alkyl-hydroxoborate salts was synthesized according to the general procedure using *tert*-butyl *N*-[3-(9-borabicyclo[3.3.1]nonan-9-yl)propyl]carbamate (272.1 mL, 0.979 mmol, 1 equiv), which was then purified by recrystallization in pentane at -35 °C to afford the product as a white solid (164.5 mg, 0.515 mmol, 54 %).

^{1}H NMR (600 MHz, C_6D_6): δ 4.20 (s, 1H), 2.66 (s, 2H), 2.30 (s, 4H), 2.15 – 2.12 (m, 4H), 1.91 (s, 4H), 1.47 (p, *J* = 6.0 Hz, 2H), 1.31 (s, 9H), 0.69 – 0.52 (m, 2H), 0.42 (s, 2H), 0.11 (s, 1H). **^{11}B {^{1}H} NMR** (192 MHz, C_6D_6): δ -1.34. **^{13}C NMR** (151 MHz, C_6D_6): δ 21.9, 26.0, 26.5, 28.4, 28.9, 32.6, 33.9, 45.6, 79.9, 128.3, 158.1.

(dppf)Ni(I)[HO-B(9-BBN)(EtFc)]

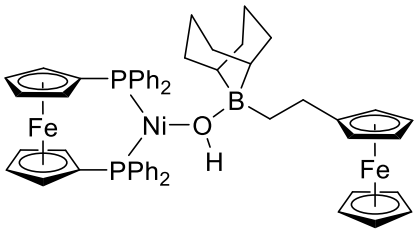

The title hydroxoborate-Ni(I) complex was prepared by charging a 20 mL vial with (dppf)Ni(I)OTf (261 mg, 0.342 mmol, 1 equiv), sodium 2-(9-hydroxy-9-boranuidabicyclo[3.3.1]nonan-9-yl)ethylferrocene (143 mg, 0.381 mmol, 1.1 equiv), and 6 mL of toluene, the resulting mixture was stirred at room temperature for 2 hours. Reaction volume was reduced to approximately 50% and the reaction mixture treated with 5 mL of hexanes and cooled to -35 °C for 30 minutes. The reaction vessel was then centrifuged, decanted, and residual solid dried under reduced pressure. The resulting solid was then washed with hexanes (2 × 10 mL) and dried under reduced pressure until free flowing, affording the product as a light brown solid (247 mg, 0.261 mmol, 76 %).

Appendix

Chapter 2 NMR Spectra

N-benzyl-*N*-phenyl-carbamoyl fluoride, (2.2a)

^{1}H NMR Spectrum $CDCl_3$ (600 MHz)

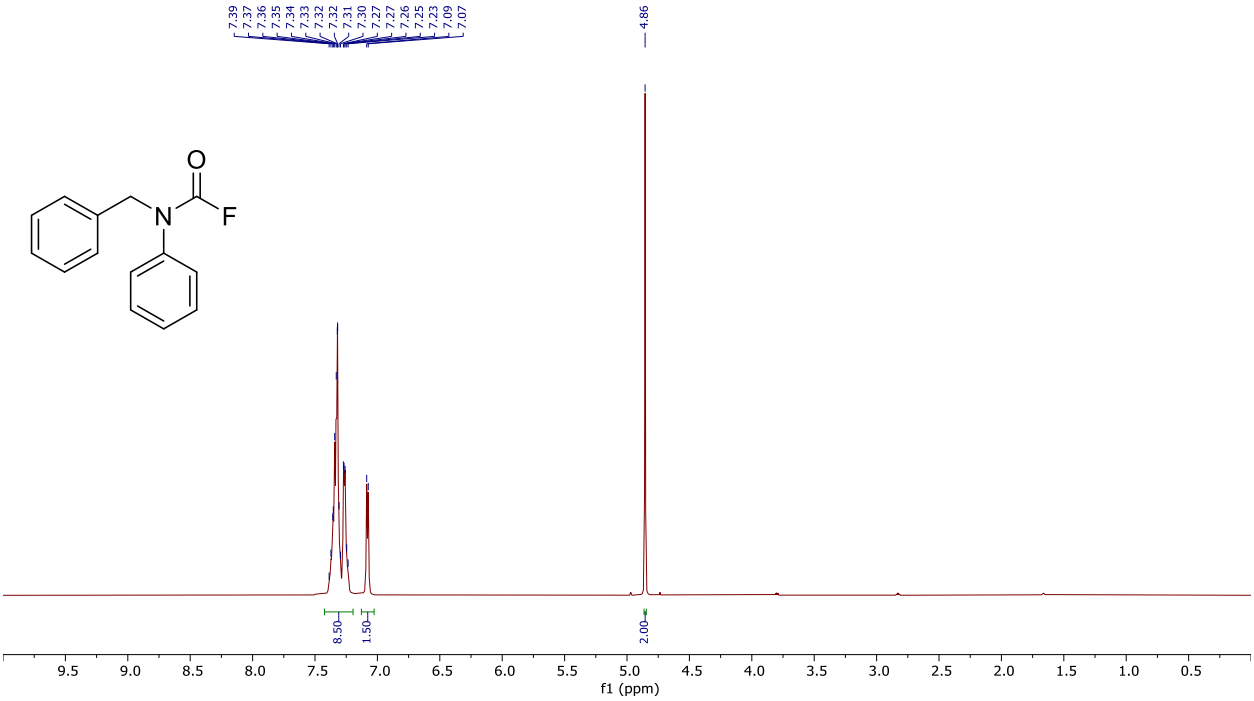

^{13}C NMR Spectrum $CDCl_3$ (151 MHz)

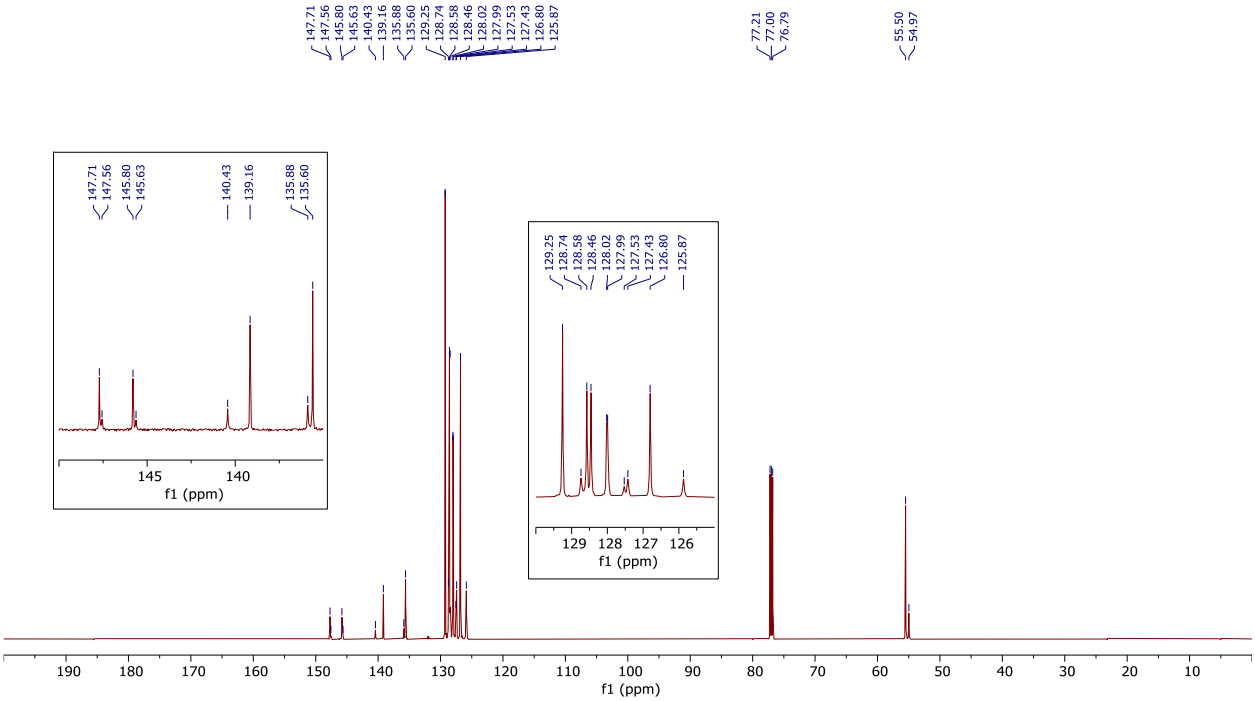

^{19}F {^{1}H} NMR Spectrum $CDCl_3$ (282 MHz)

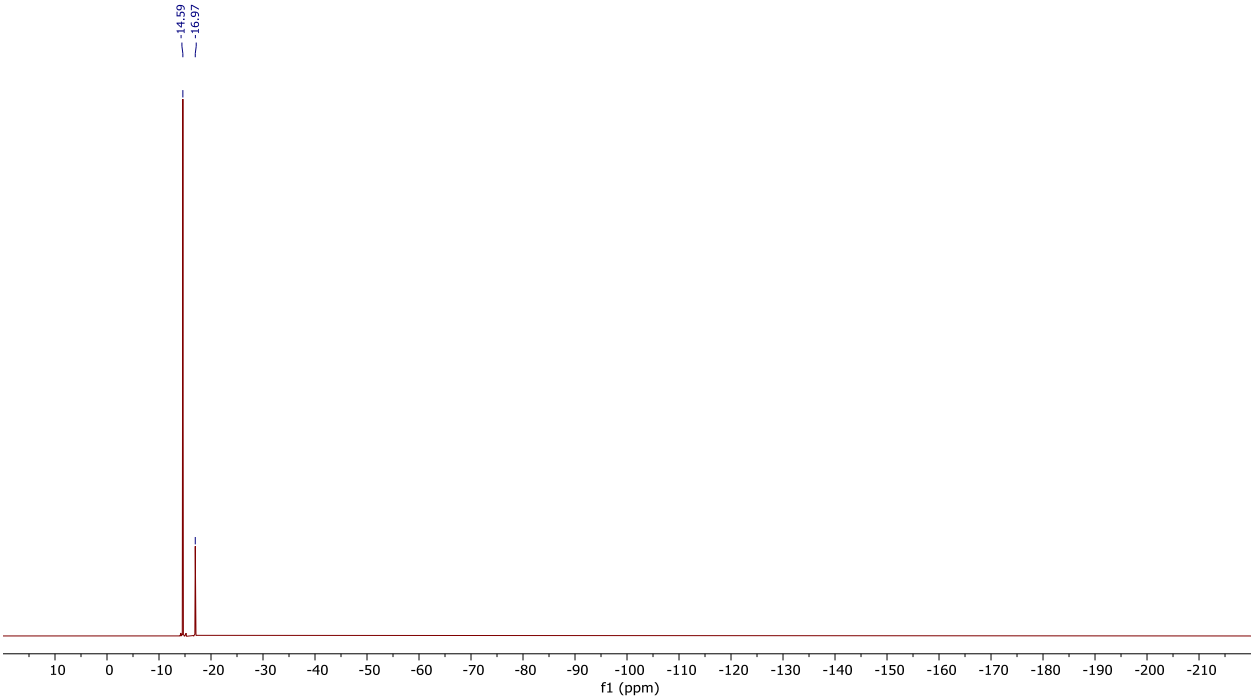

N-benzyl-*N*-(2,4-dimethylphenyl)carbamoyl fluoride, (2.2n)

^{1}H NMR Spectrum $CDCl_3$ (600 MHz)

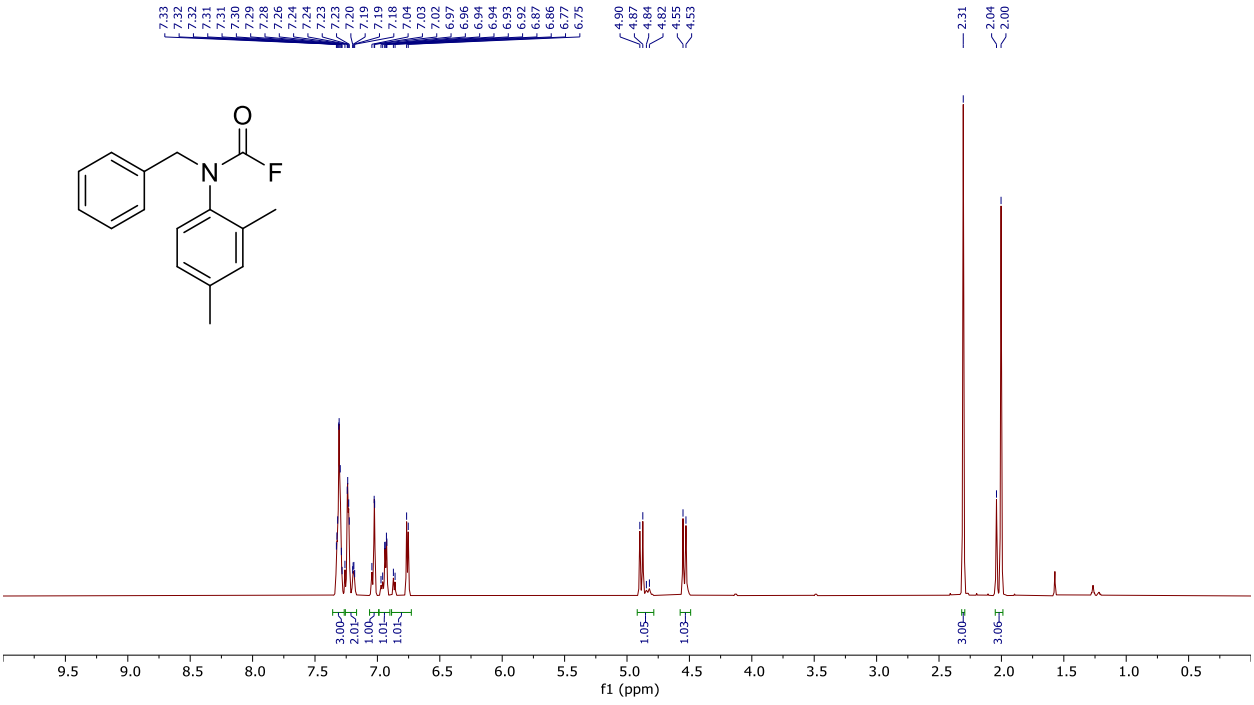

^{13}C NMR Spectrum $CDCl_3$ (151 MHz)

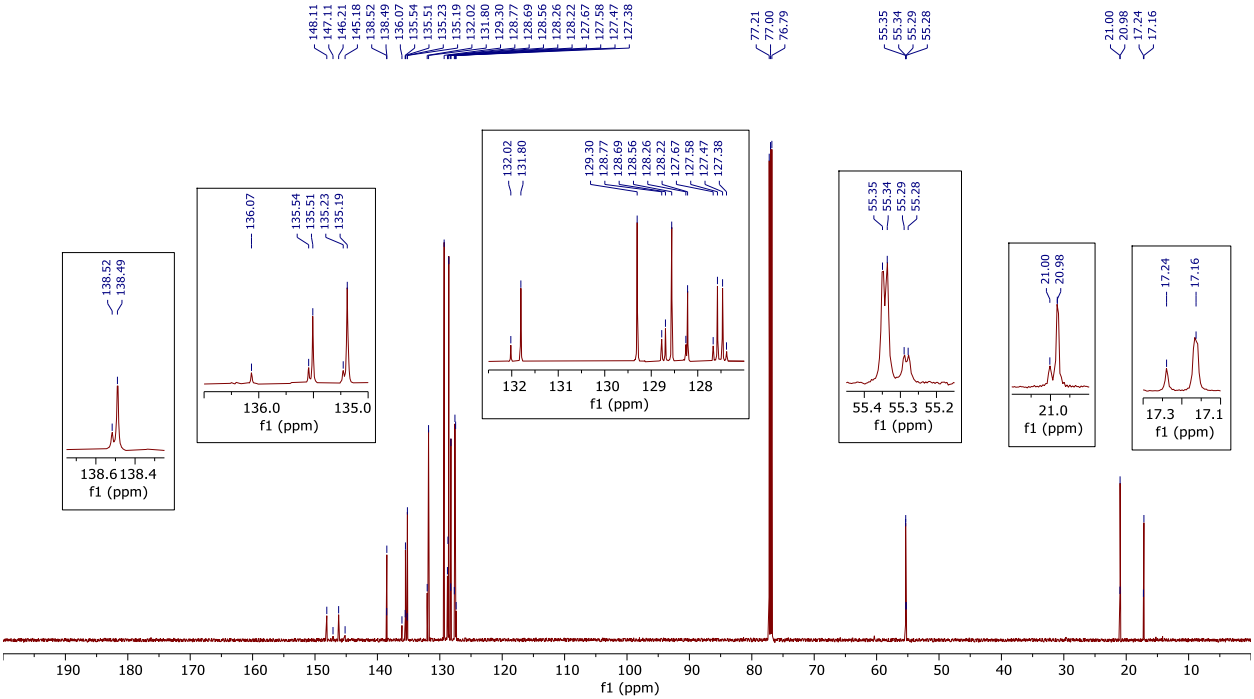

^{19}F {^{1}H} NMR Spectrum $CDCl_3$ (282 MHz)

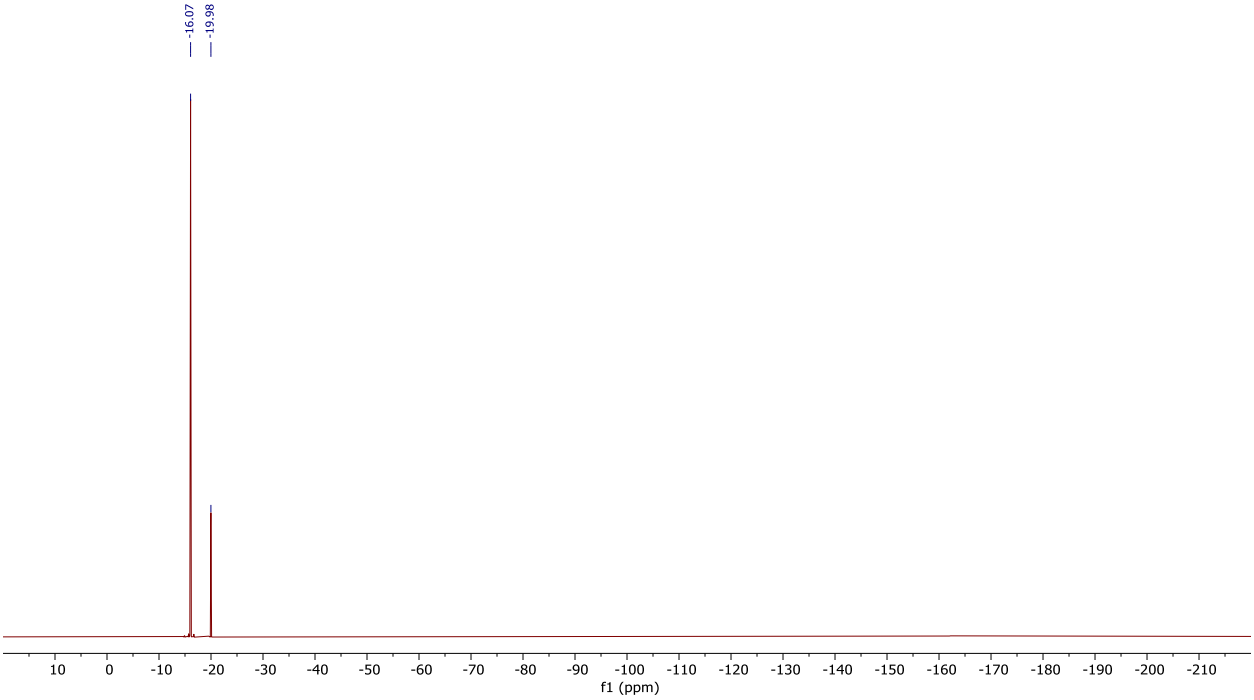

N-benzyl-*N*-(4-methoxyphenyl)carbamoyl fluoride, (2.2i)

^{1}H NMR Spectrum $CDCl_3$ (600 MHz)

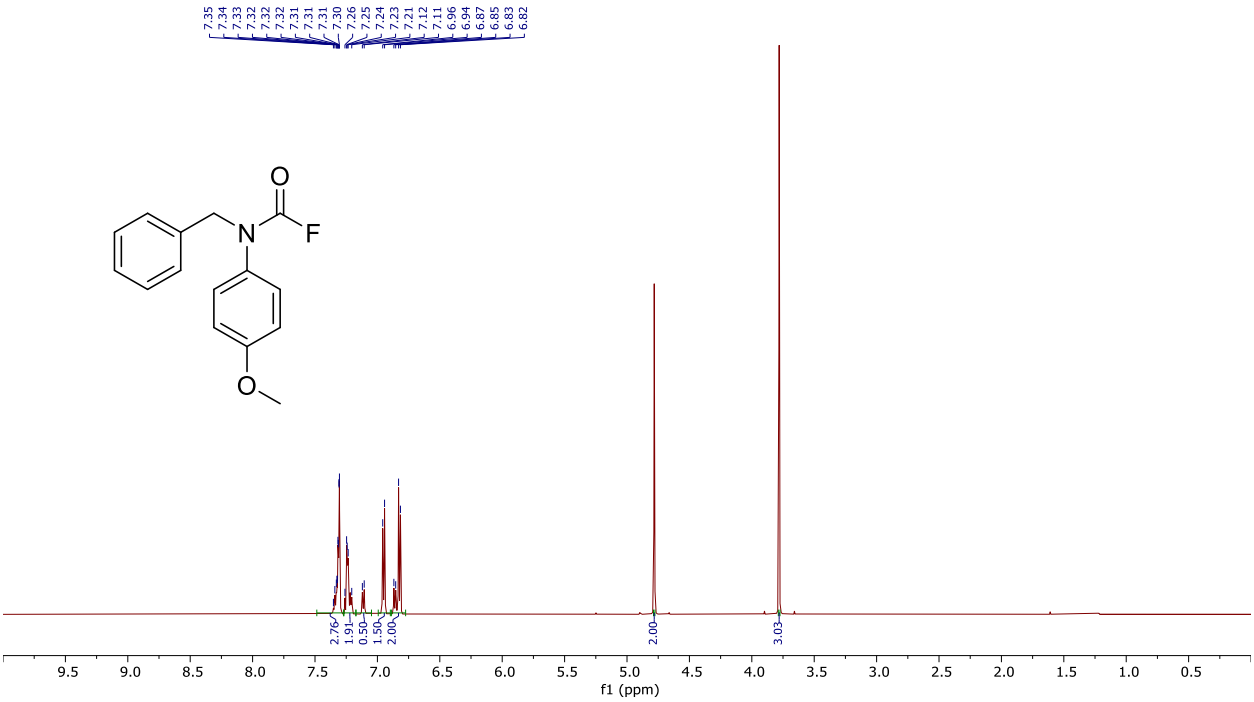

^{13}C NMR Spectrum $CDCl_3$ (151 MHz)

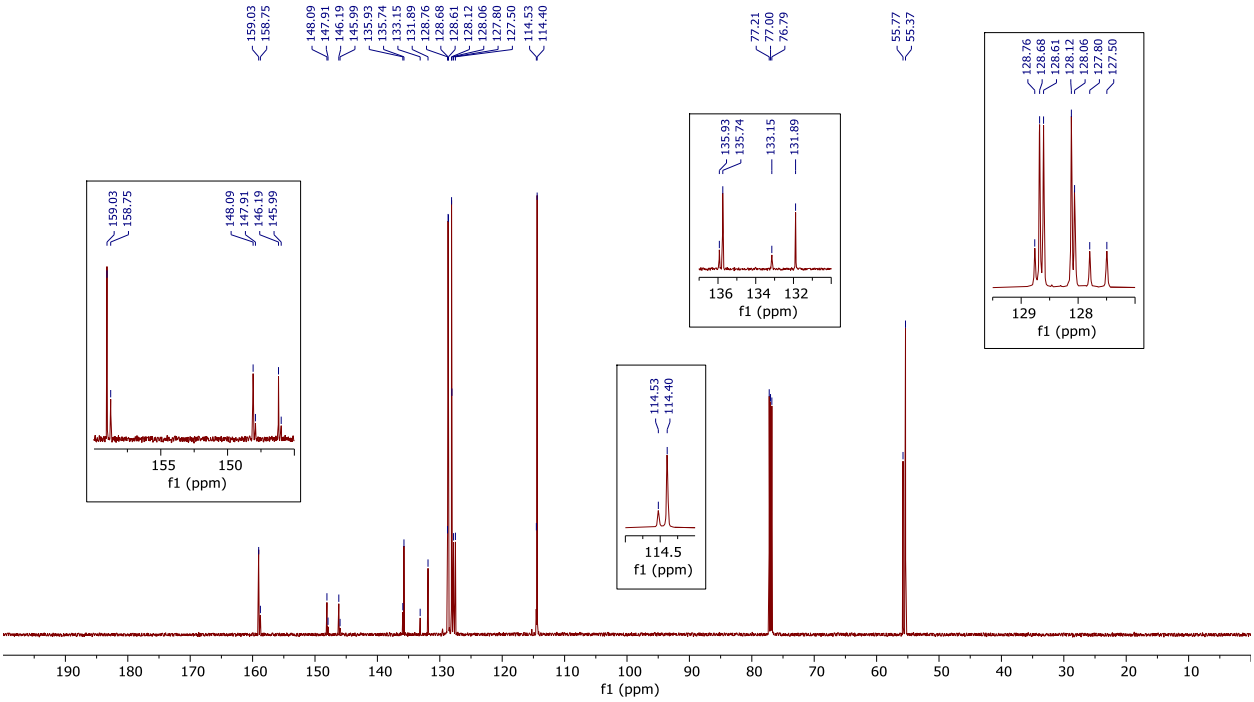

^{19}F {^{1}H} NMR Spectrum $CDCl_3$ (282 MHz)

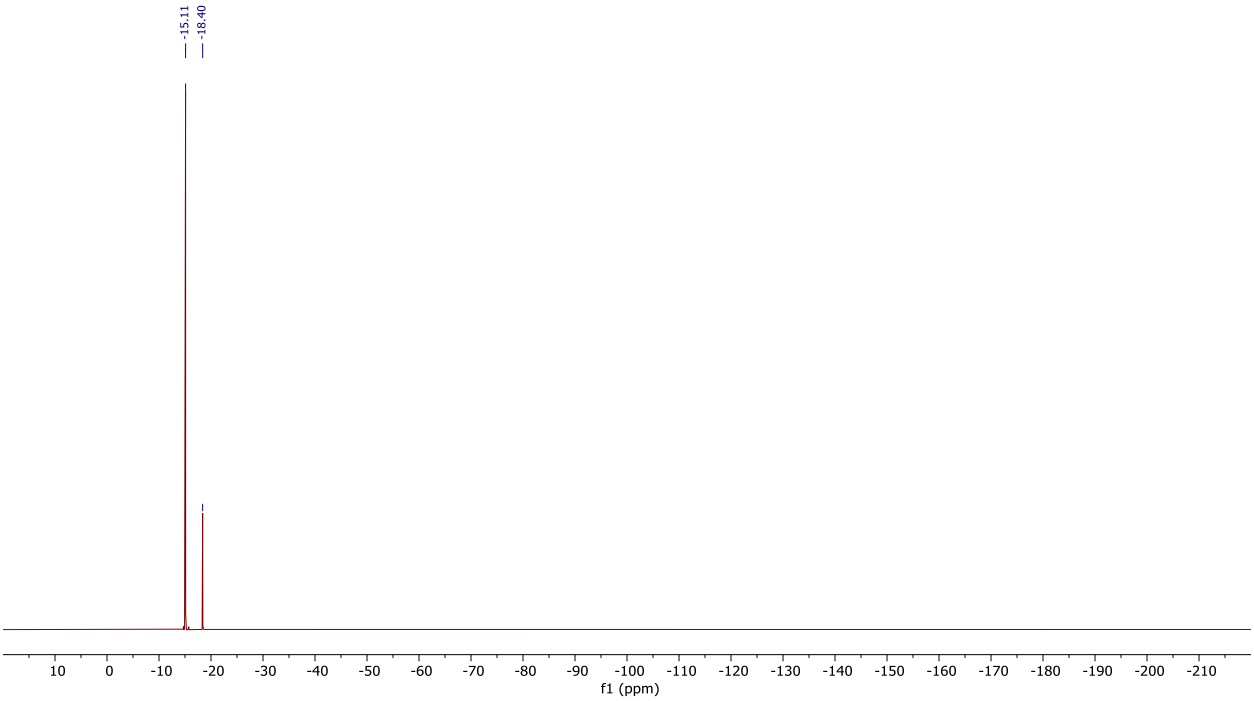

_N_-benzyl-_N_-[4-(trifluoromethyl)phenyl]carbamoyl fluoride, (2.2j)

^{1}H NMR Spectrum $CDCl_3$ (600 MHz)

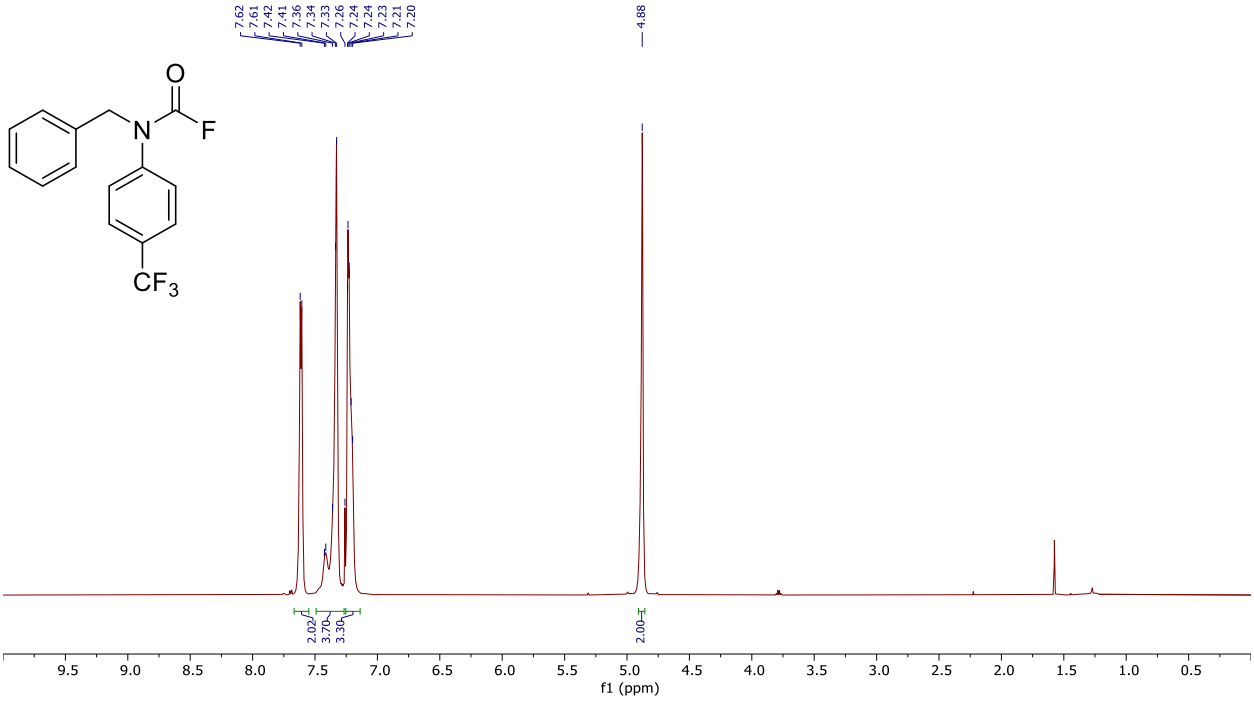

^{13}C NMR Spectrum $CDCl_3$ (151 MHz)

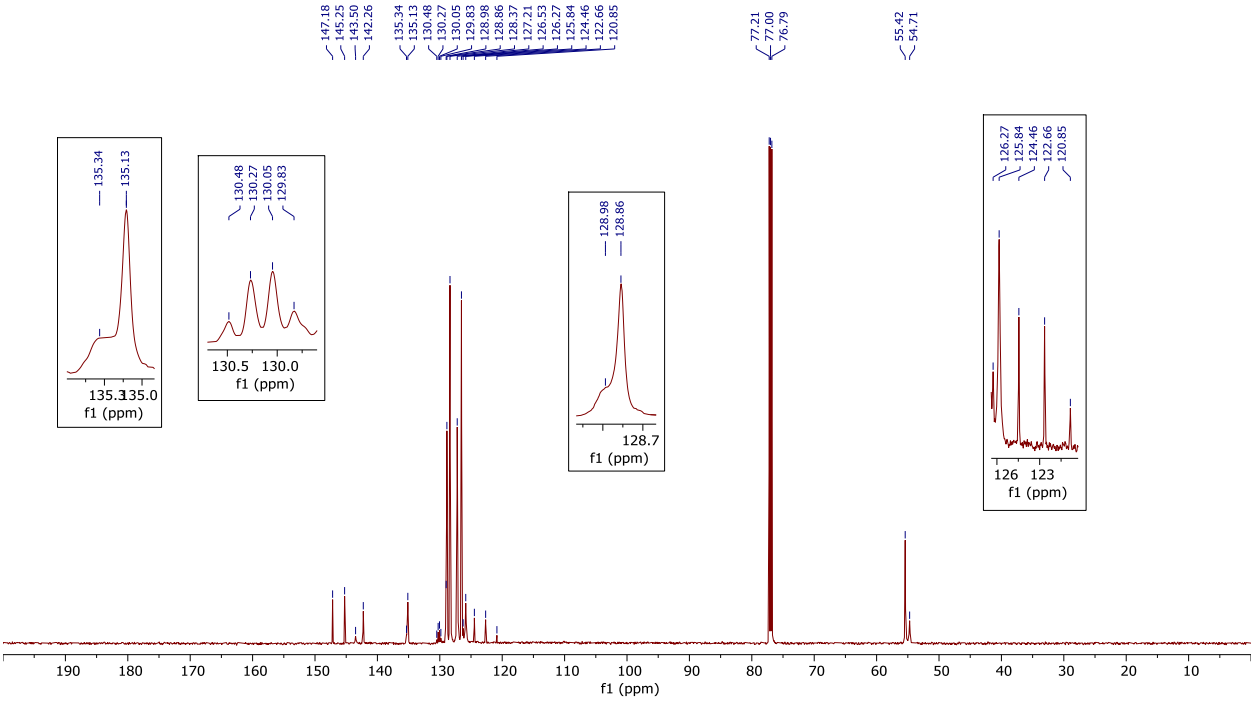

^{19}F {^{1}H} NMR Spectrum $CDCl_3$ (282 MHz)

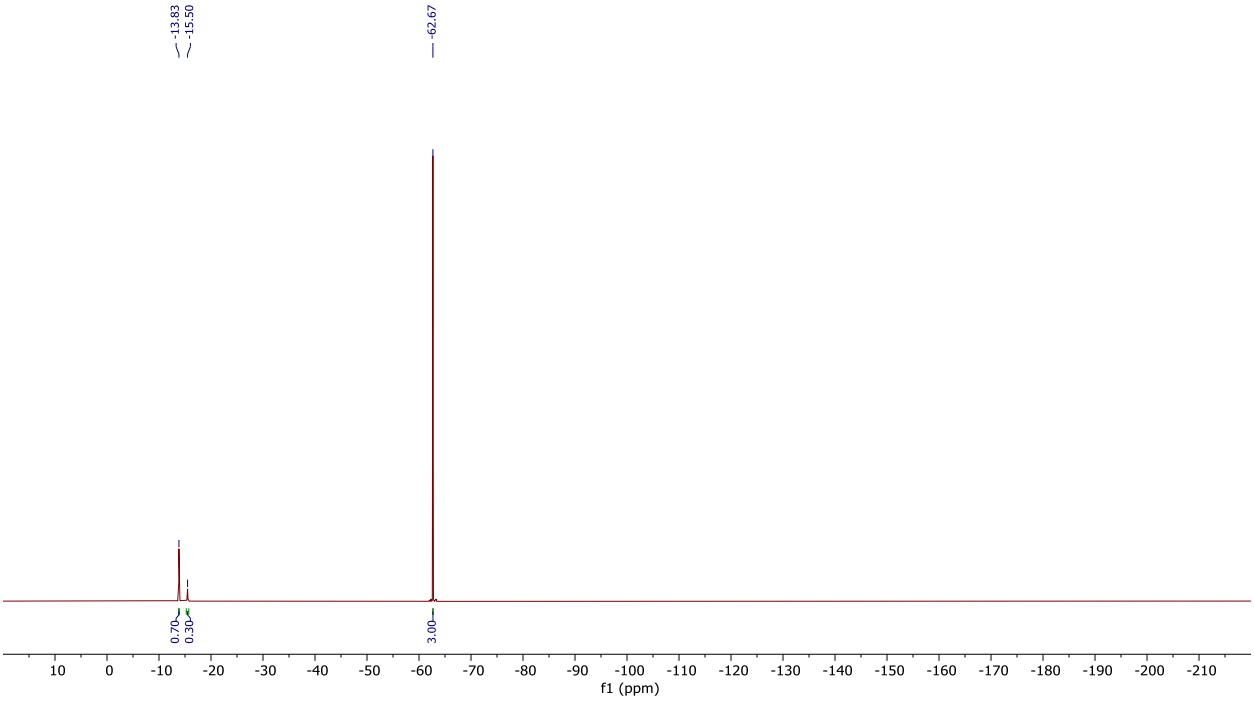

N-[(4-fluorophenyl)methyl]-*N*-phenyl-carbamoyl fluoride, (2.2d)

^{1}H NMR Spectrum $CDCl_3$ (600 MHz)

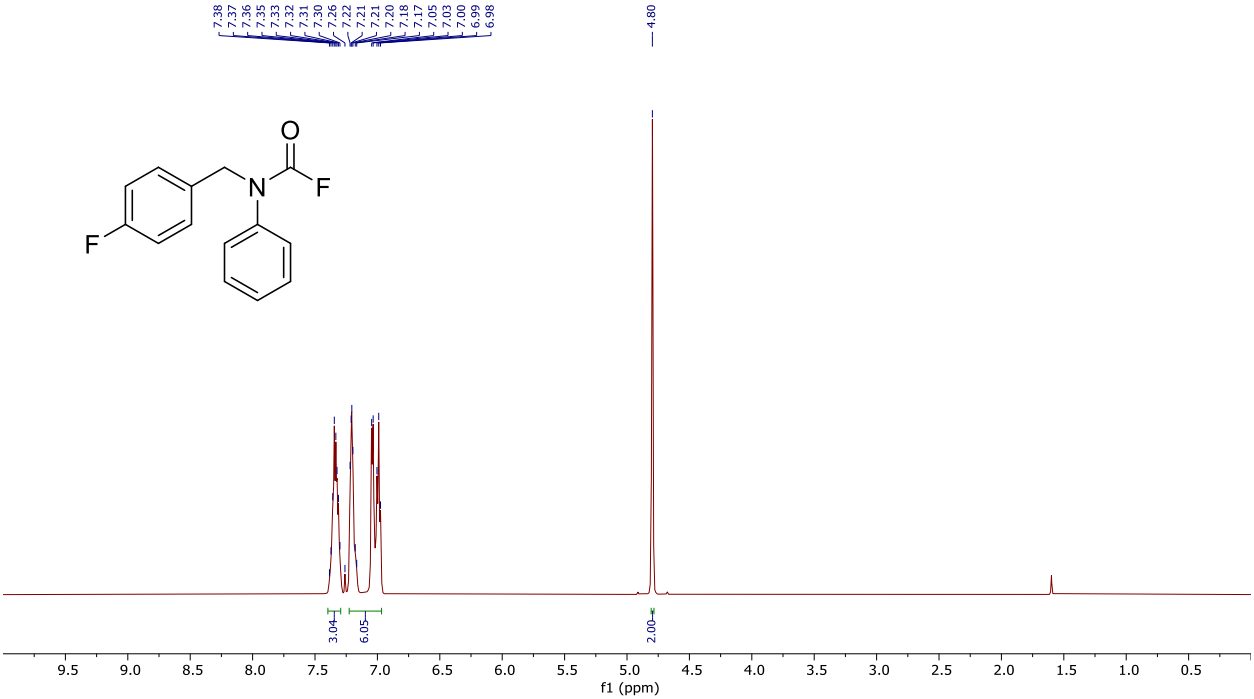

^{13}C NMR Spectrum $CDCl_3$ (151 MHz)

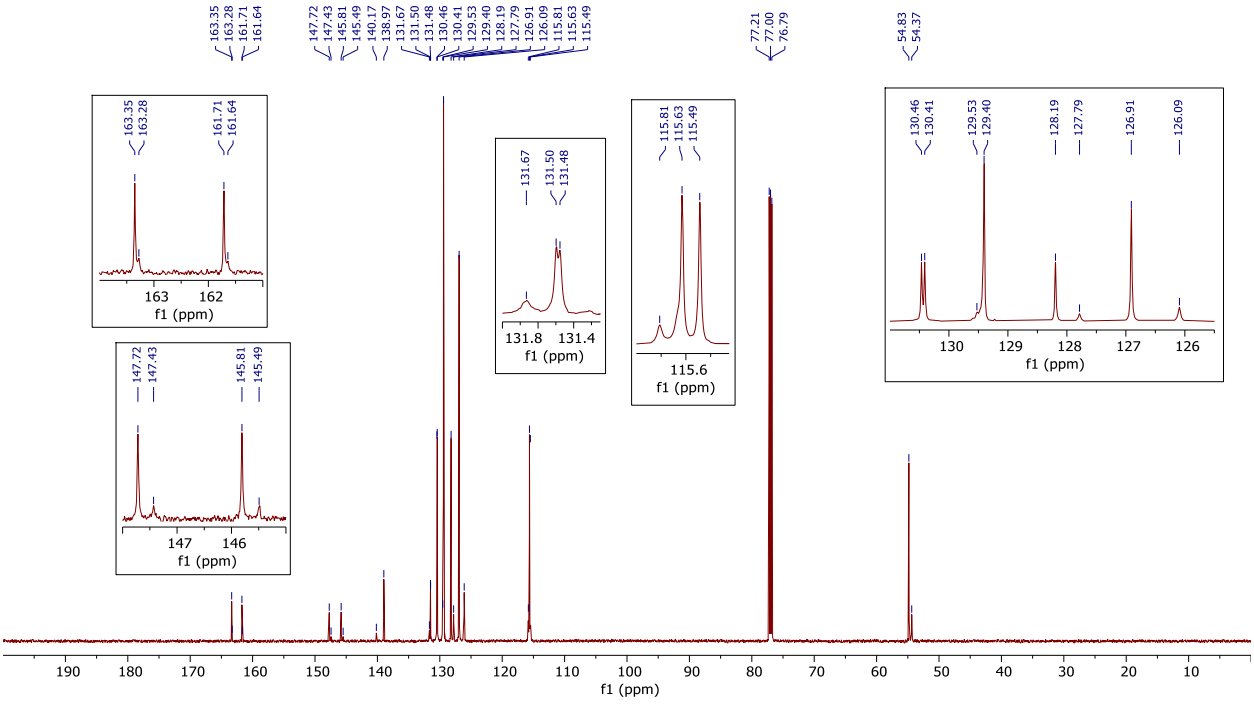

^{19}F {^{1}H} NMR Spectrum $CDCl_3$ (282 MHz)

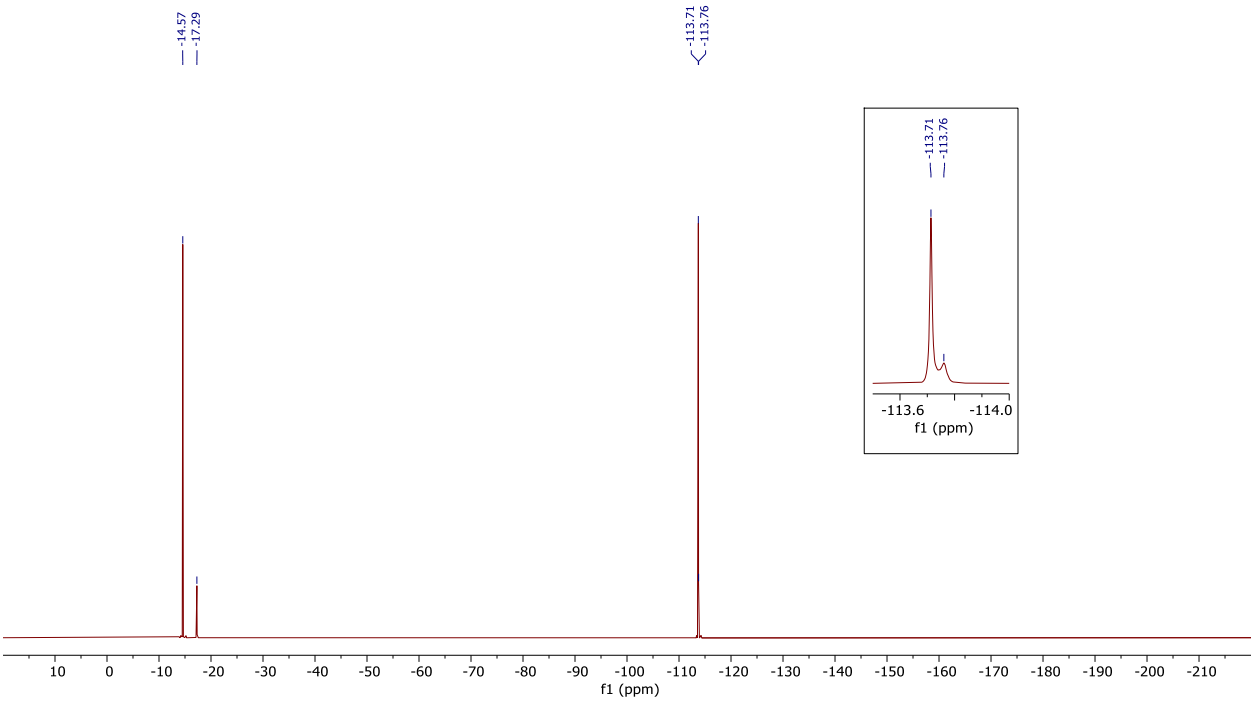

N-[(4-chlorophenyl)methyl]-*N*-phenyl-carbamoyl fluoride, (2.2e)

^{1}H NMR Spectrum $CDCl_3$ (600 MHz)

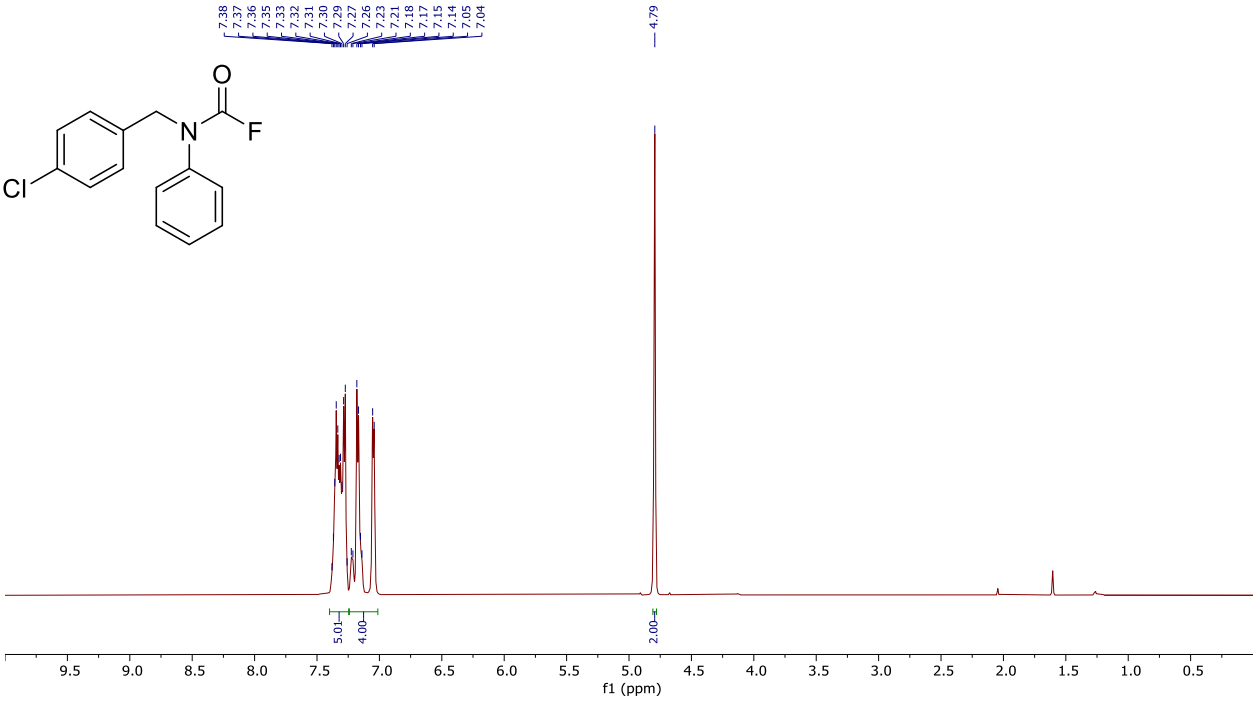

^{13}C NMR Spectrum $CDCl_3$ (151 MHz)

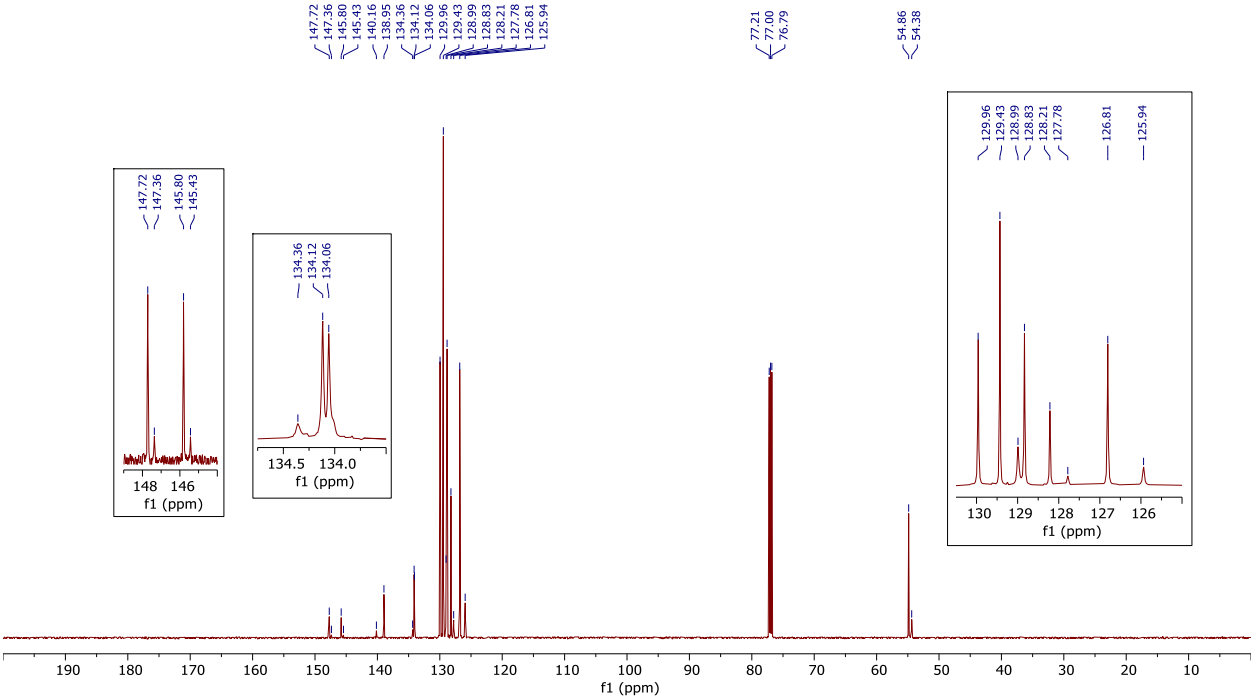

^{19}F {^{1}H} NMR Spectrum $CDCl_3$ (282 MHz)

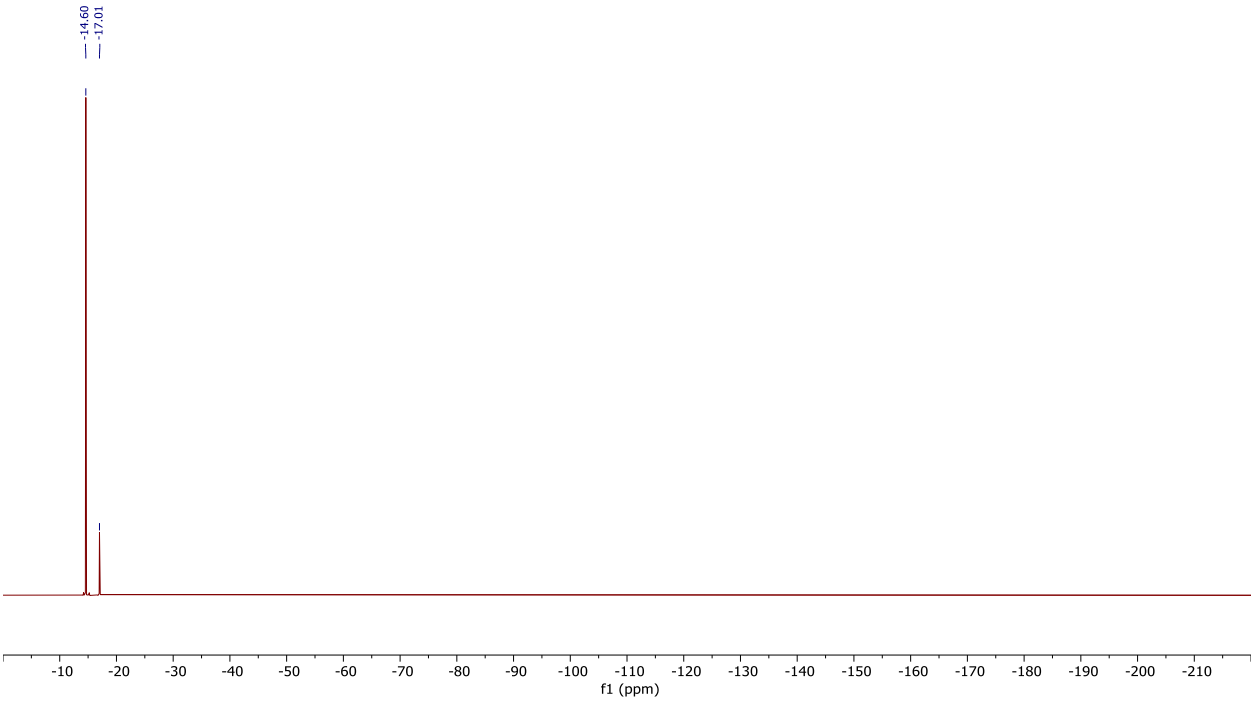

N-[(4-bromophenyl)methyl]-*N*-phenyl-carbamoyl fluoride, (2.2f)

^{1}H NMR Spectrum $CDCl_3$ (600 MHz)

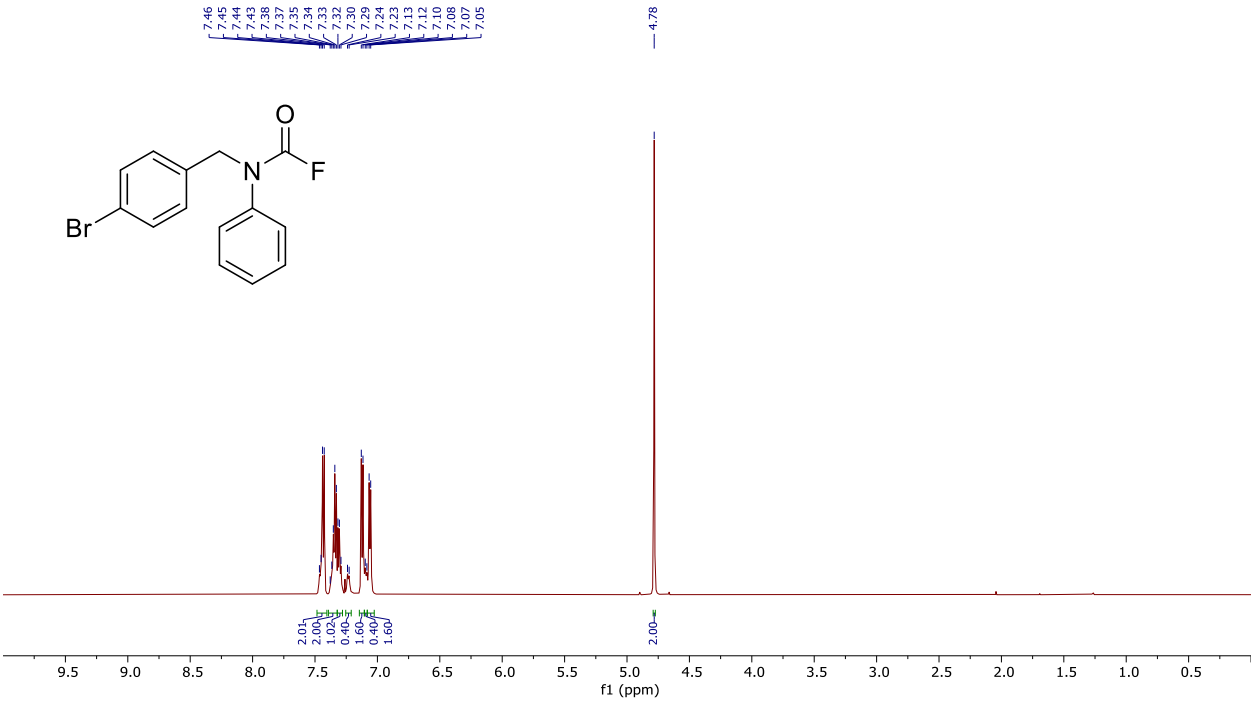

^{13}C NMR Spectrum $CDCl_3$ (151 MHz)

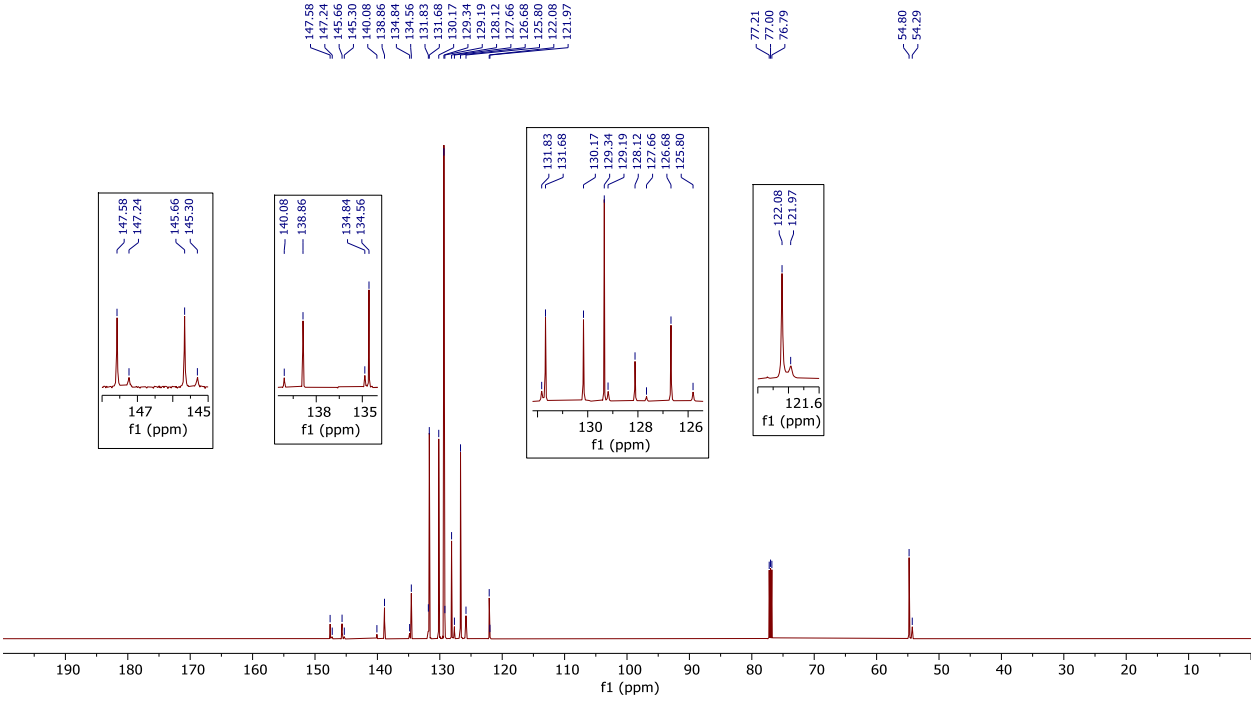

^{19}F {^{1}H} NMR Spectrum $CDCl_3$ (282 MHz)

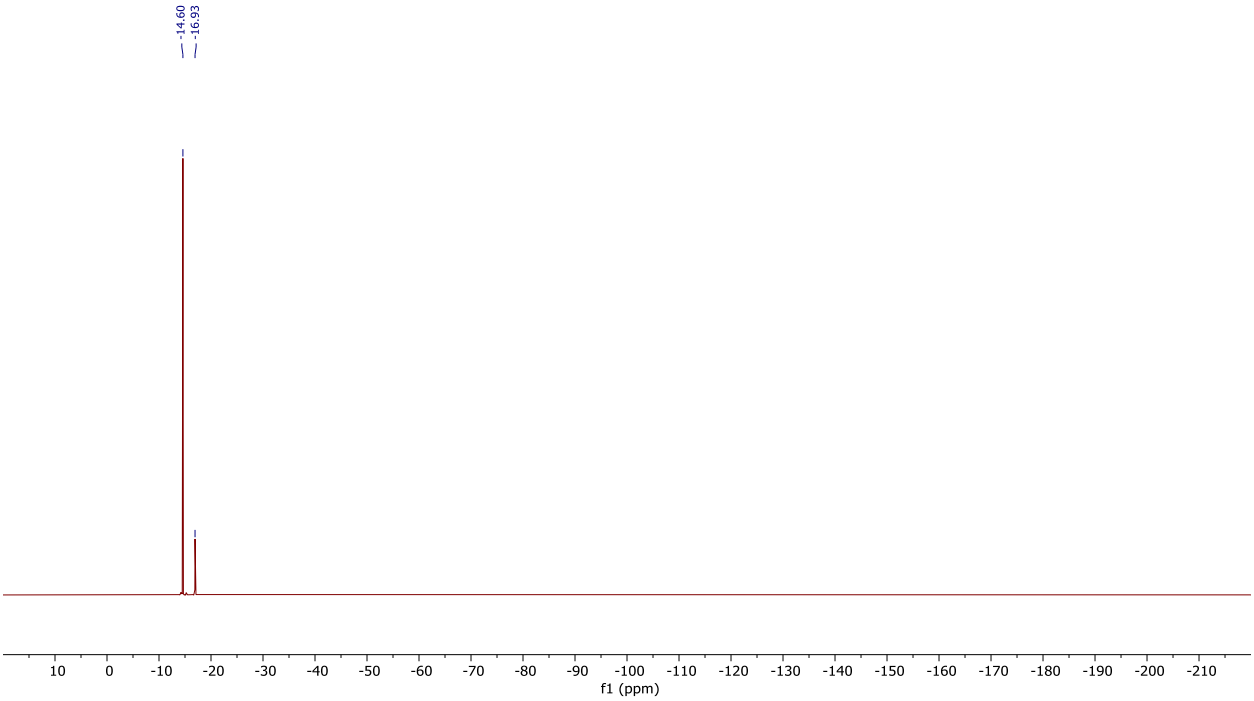

_N_-[(4-iodophenyl)methyl]-_N_-phenyl-carbamoyl fluoride, (2.2g)

^{1}H NMR Spectrum $CDCl_3$ (600 MHz)

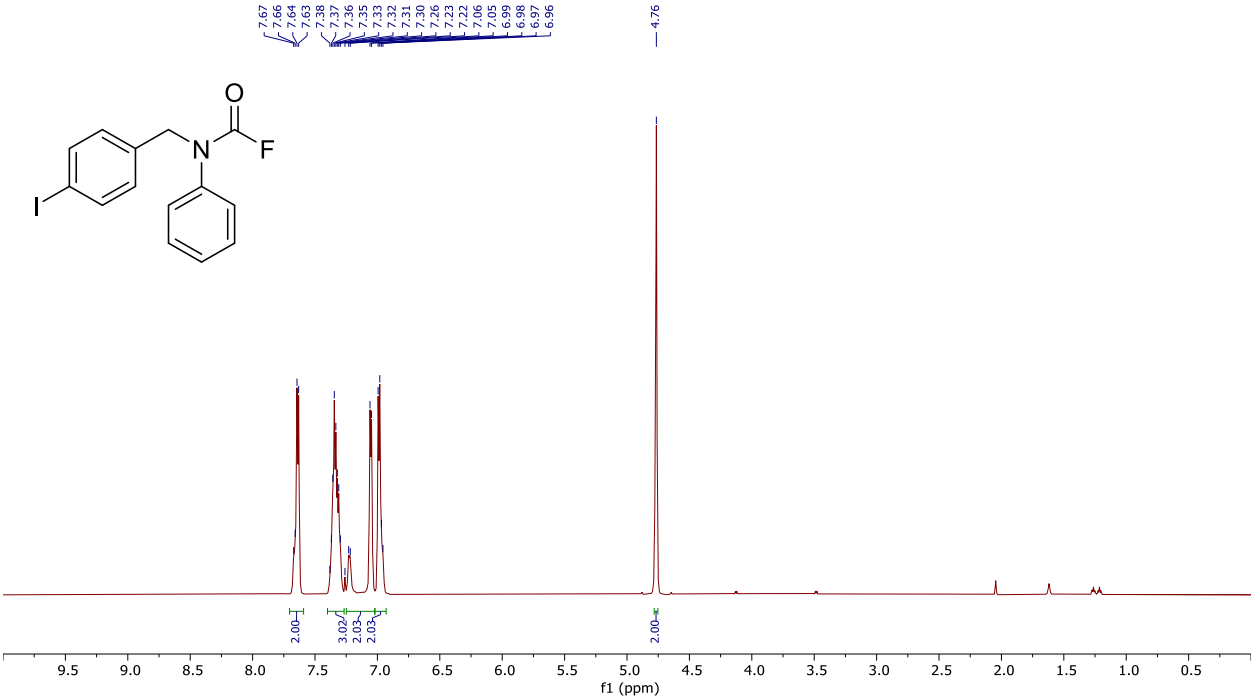

^{13}C NMR Spectrum $CDCl_3$ (151 MHz)

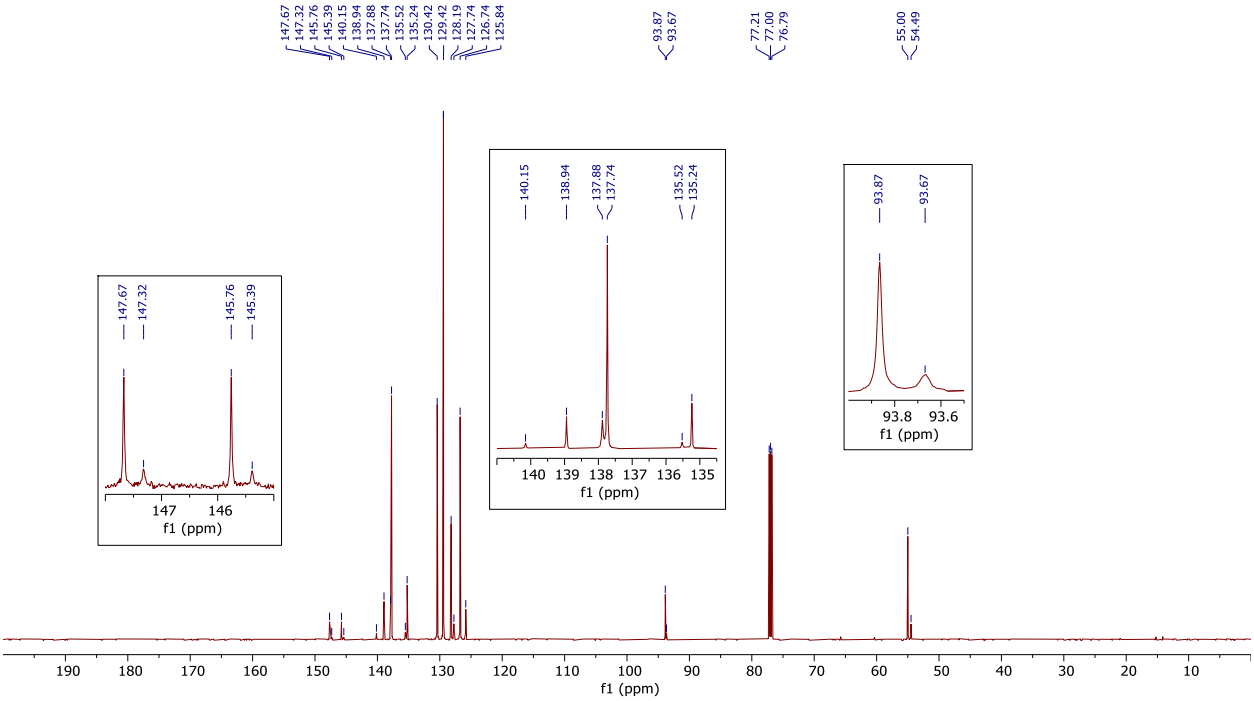

^{19}F {^{1}H} NMR Spectrum $CDCl_3$ (282 MHz)

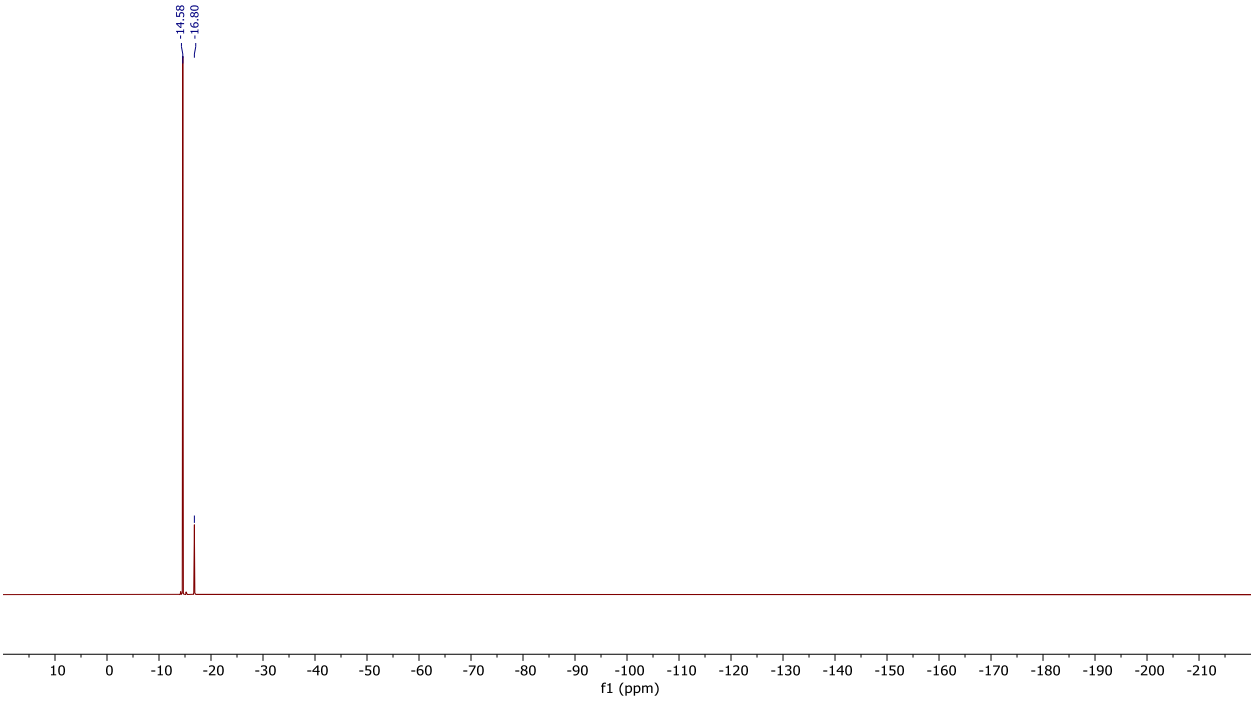

_N_-[[4-(dimethylamino)phenyl]methyl]-_N_-phenyl-carbamoyl fluoride, (2.2c)

^{1}H NMR Spectrum $CDCl_3$ (600 MHz)

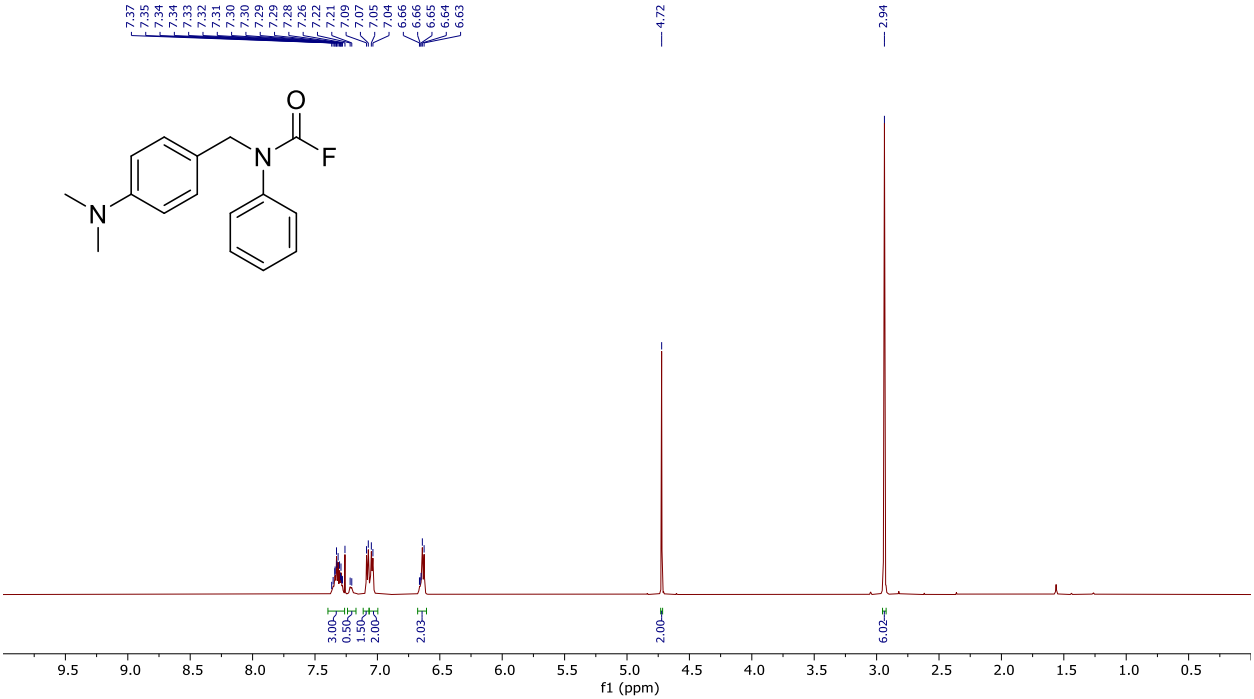

^{13}C NMR Spectrum $CDCl_3$ (151 MHz)

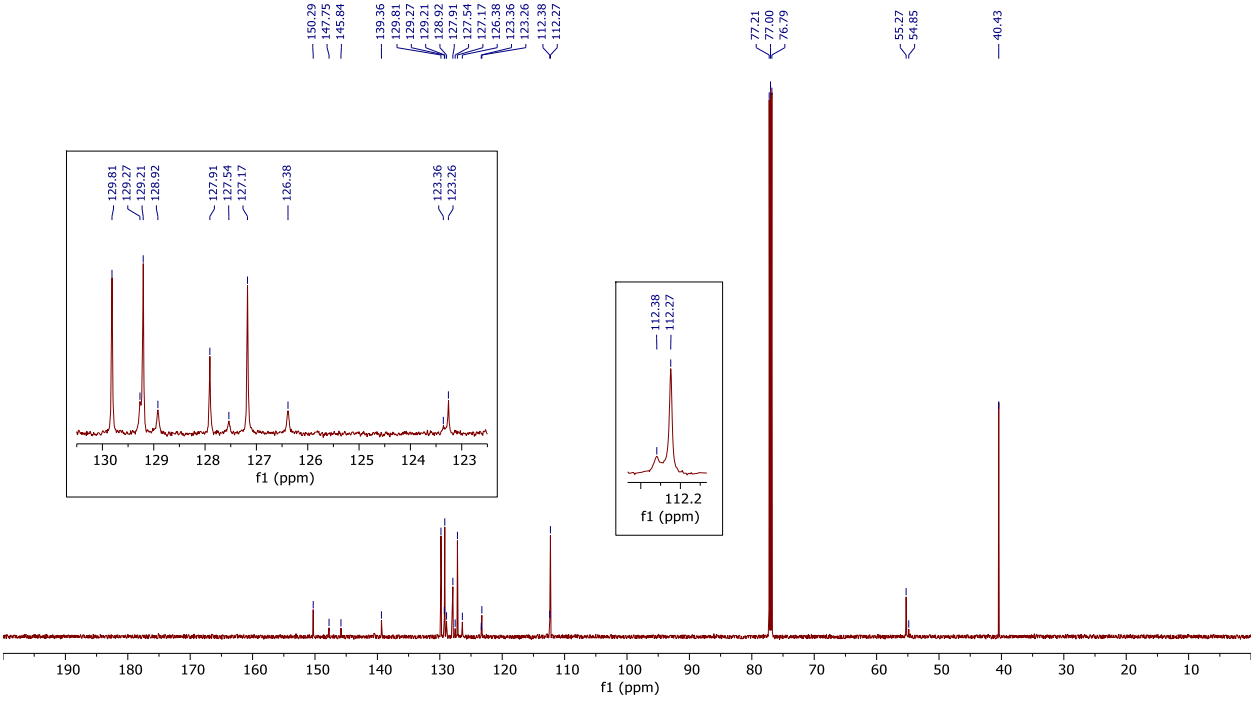

^{19}F {^{1}H} NMR Spectrum $CDCl_3$ (282 MHz)

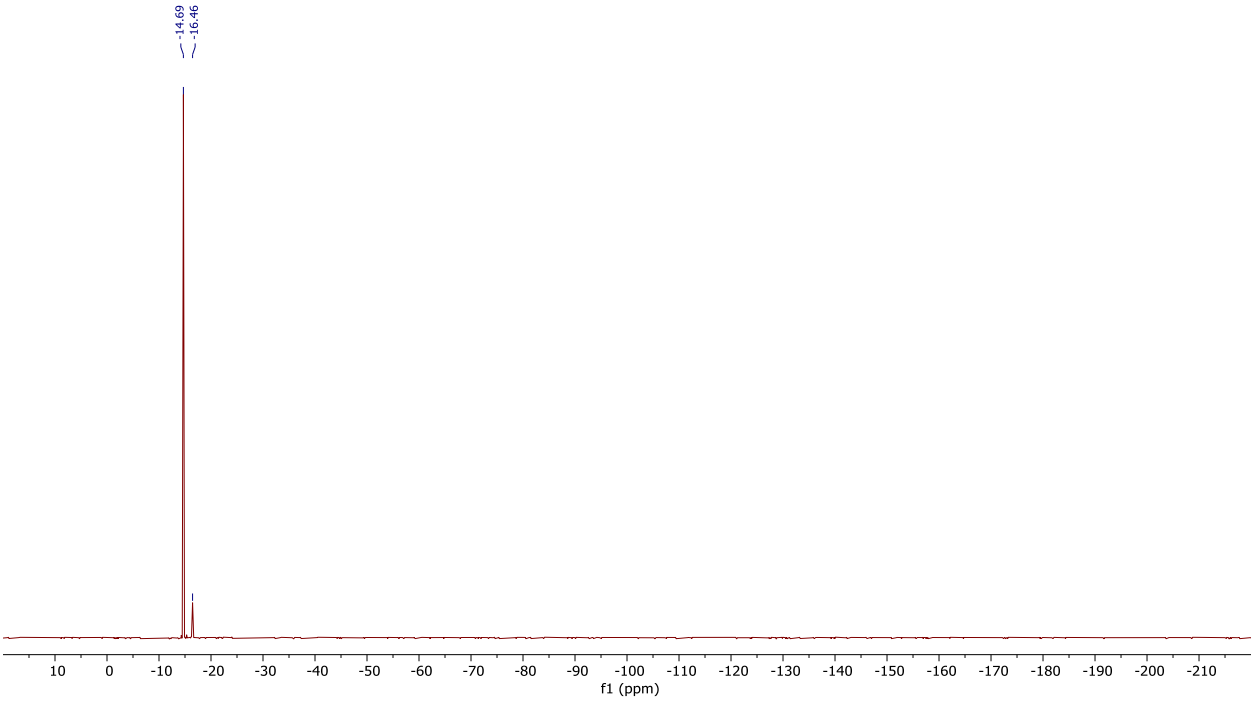

_N_-[(4-methoxyphenyl)methyl]-_N_-phenyl-carbamoyl fluoride, (2.2b)

^{1}H NMR Spectrum $CDCl_3$ (600 MHz)

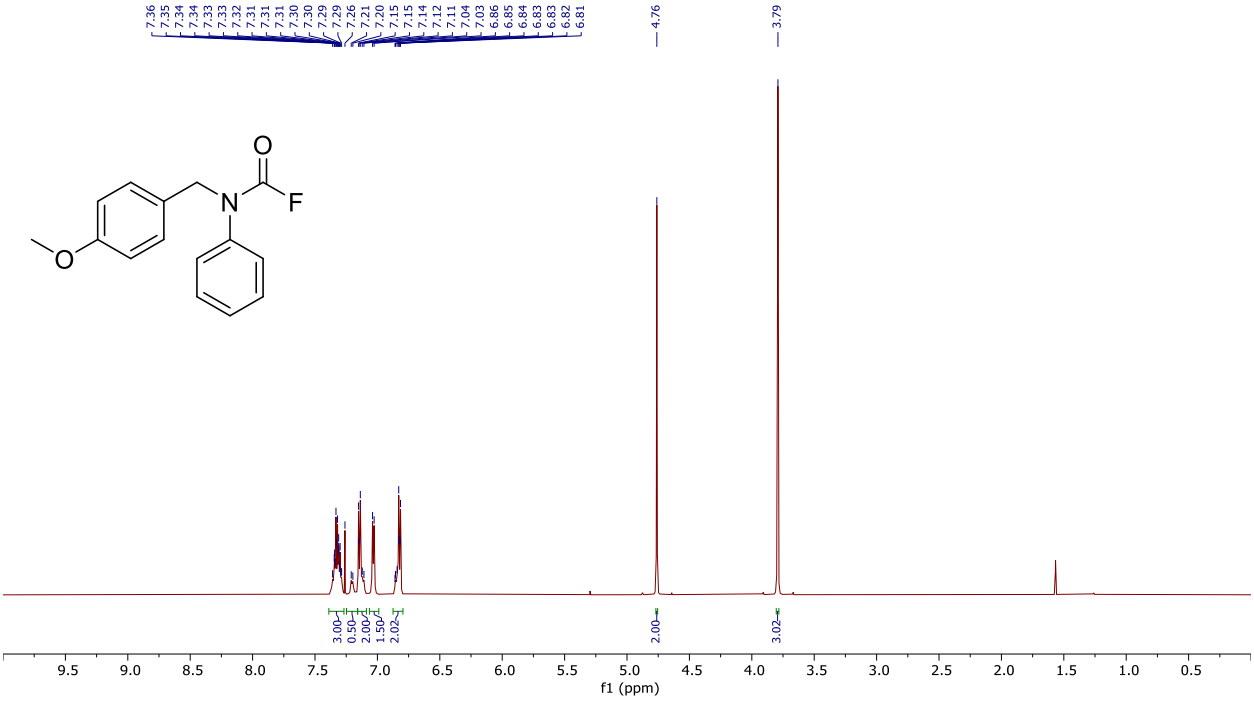

NMR Spectrum $CDCl_3$ (151 MHz)

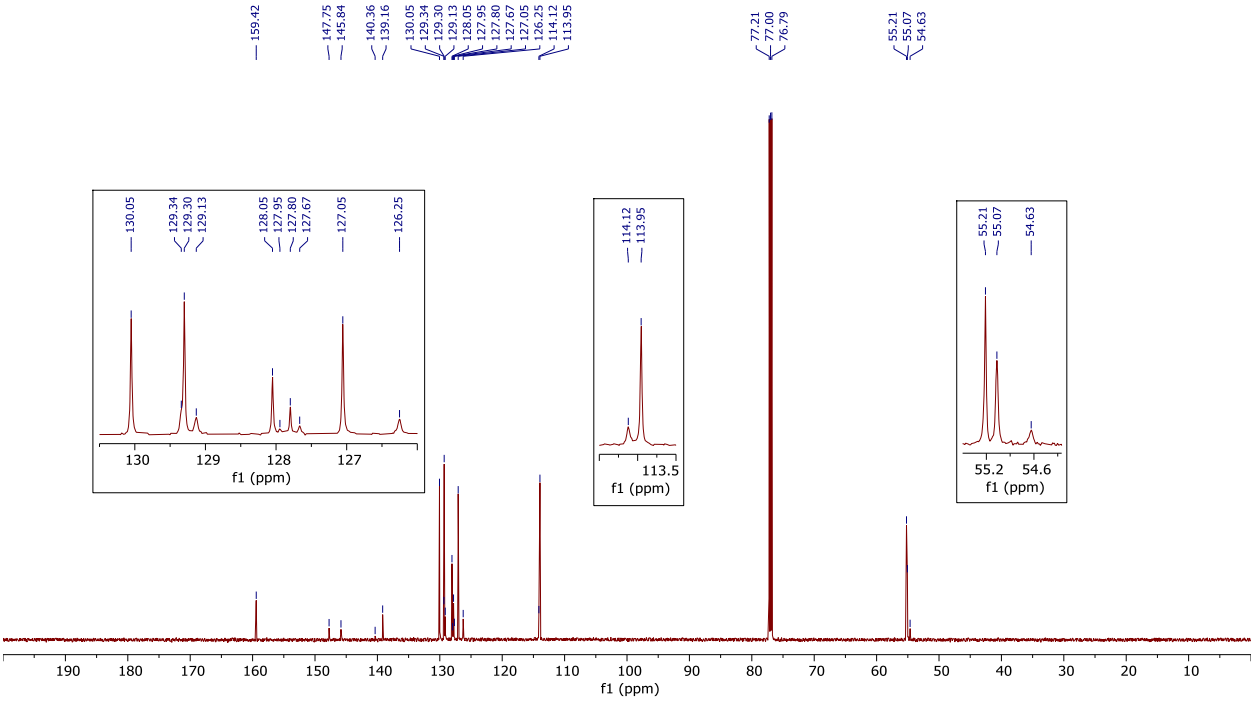

^{19}F {^{1}H} NMR Spectrum $CDCl_3$ (282 MHz)

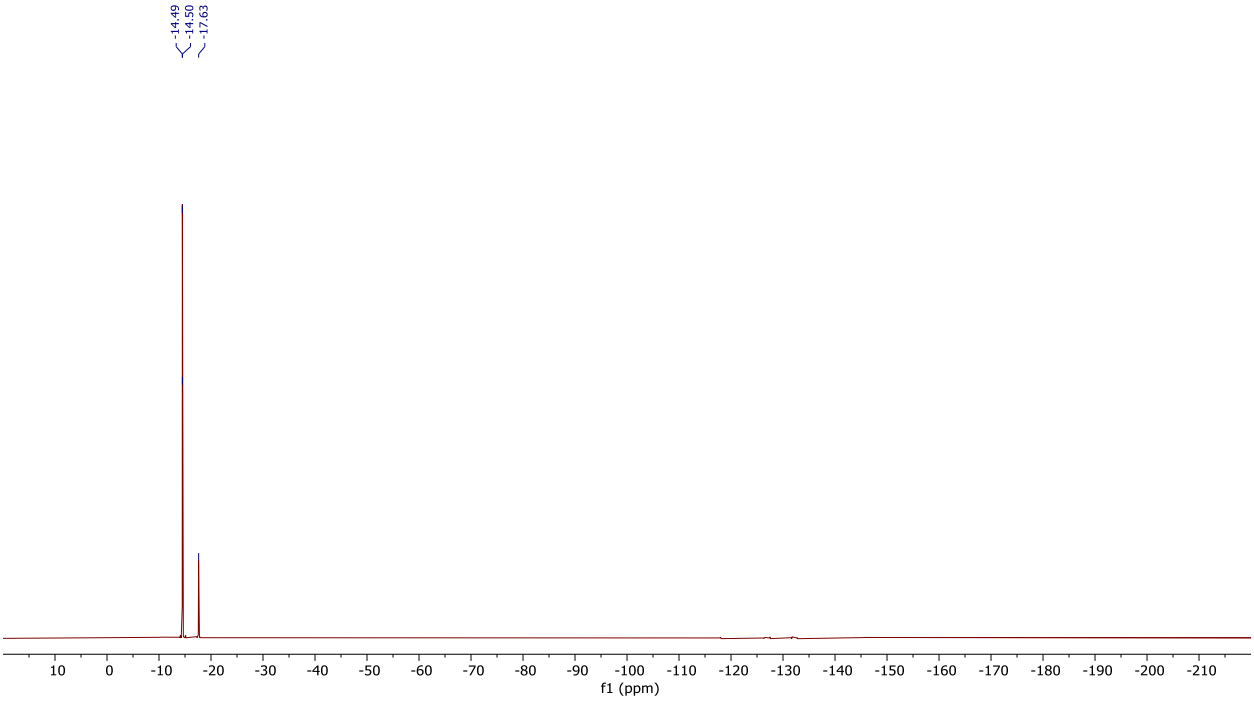

N-(1,3-benzodioxol-5-ylmethyl)-*N*-phenyl-carbamoyl fluoride, (2.2m)

^{1}H NMR Spectrum $CDCl_3$ (600 MHz)

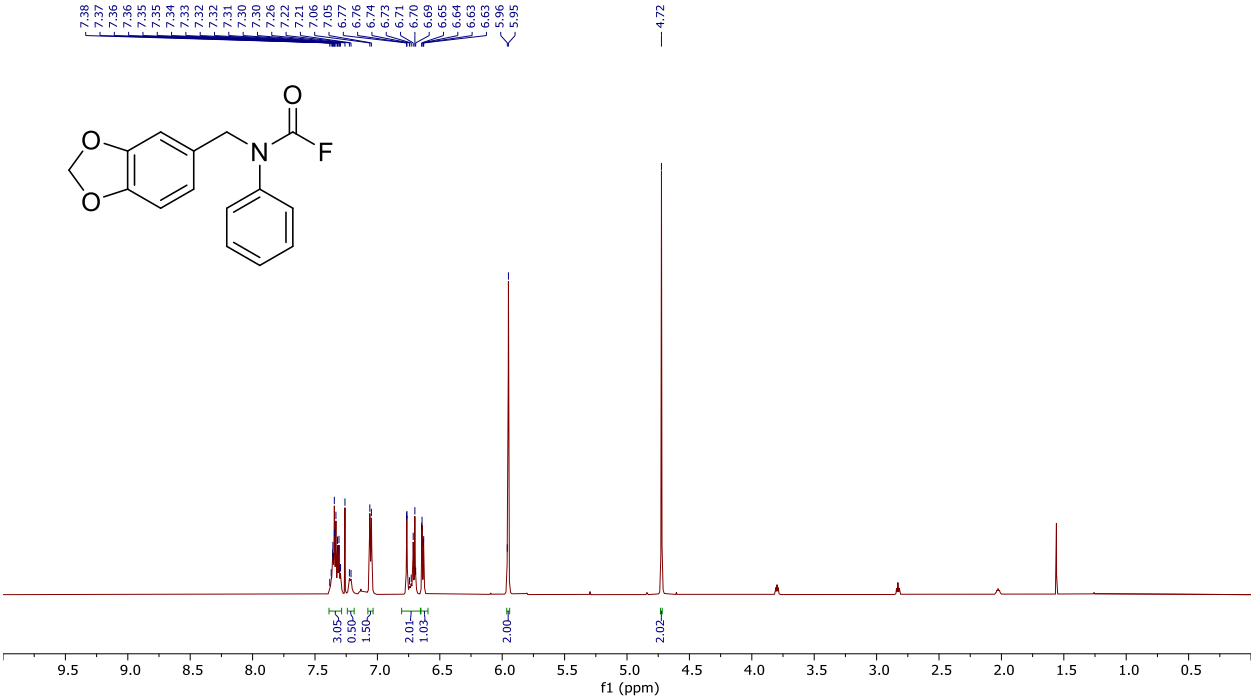

^{13}C NMR Spectrum $CDCl_3$ (151 MHz)

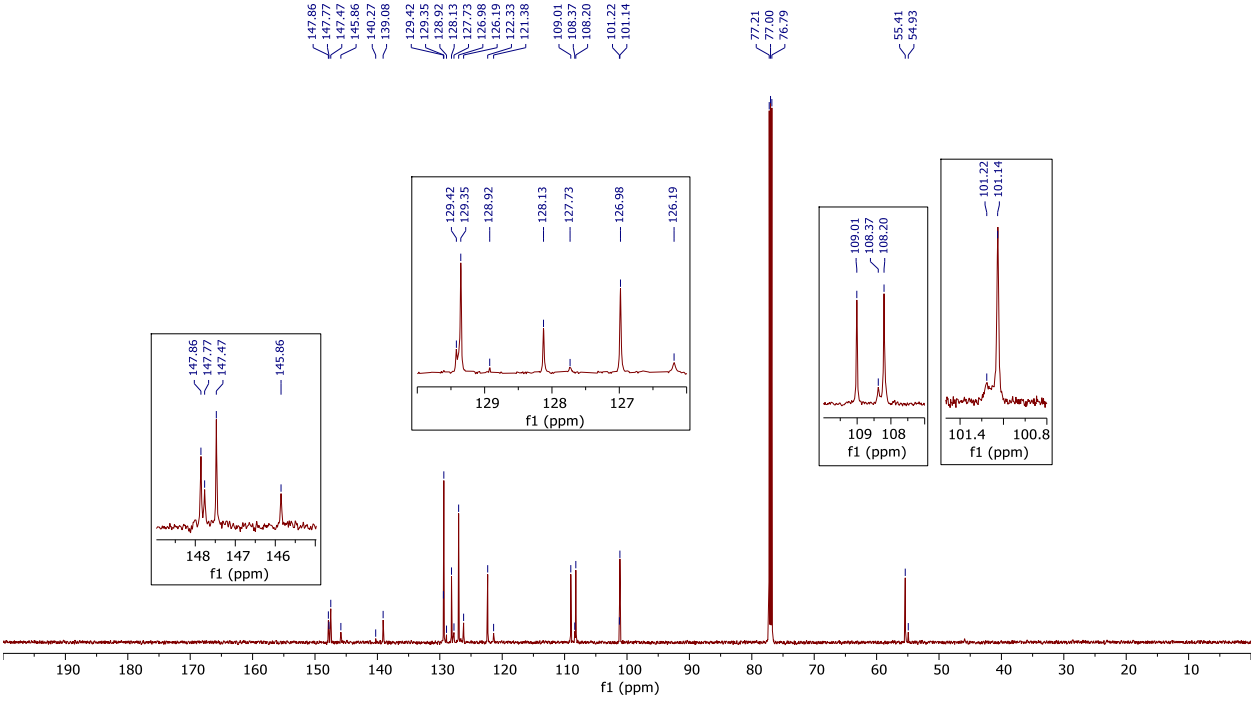

^{19}F {^{1}H} NMR Spectrum $CDCl_3$ (282 MHz)

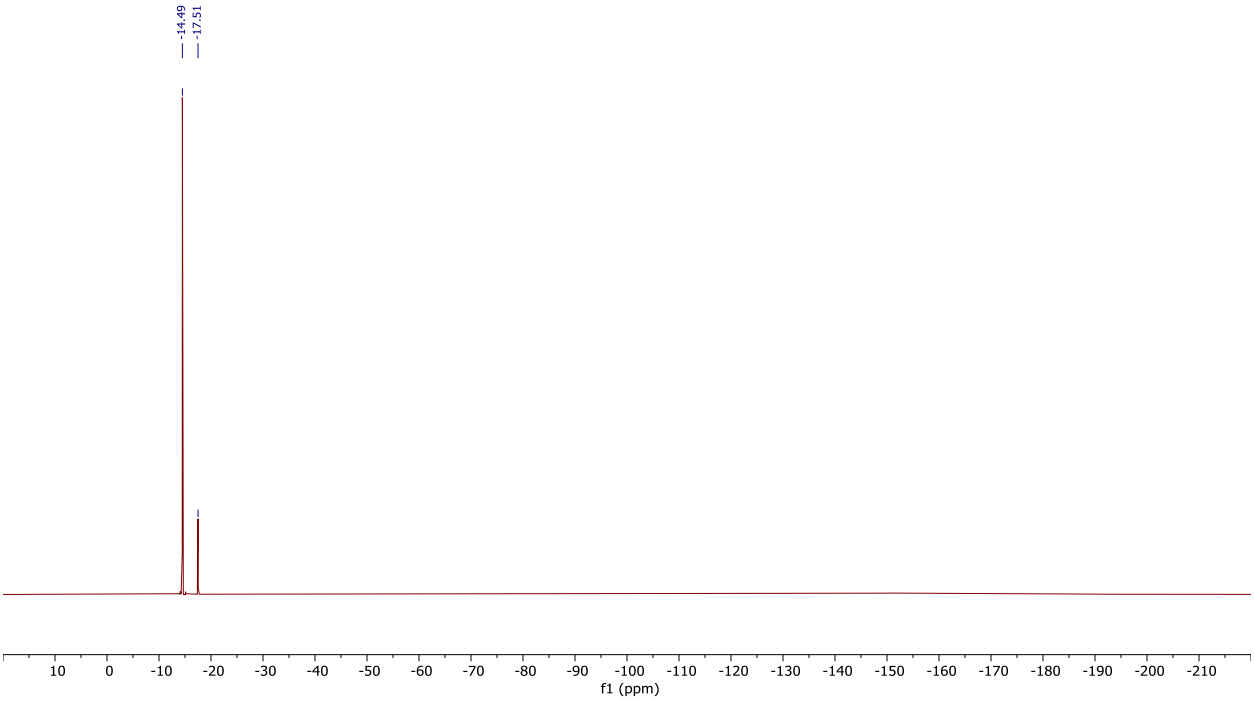

N-methyl-*N*-phenyl-carbamoyl fluoride, (2.2r)

^{1}H NMR Spectrum $CDCl_3$ (600 MHz)

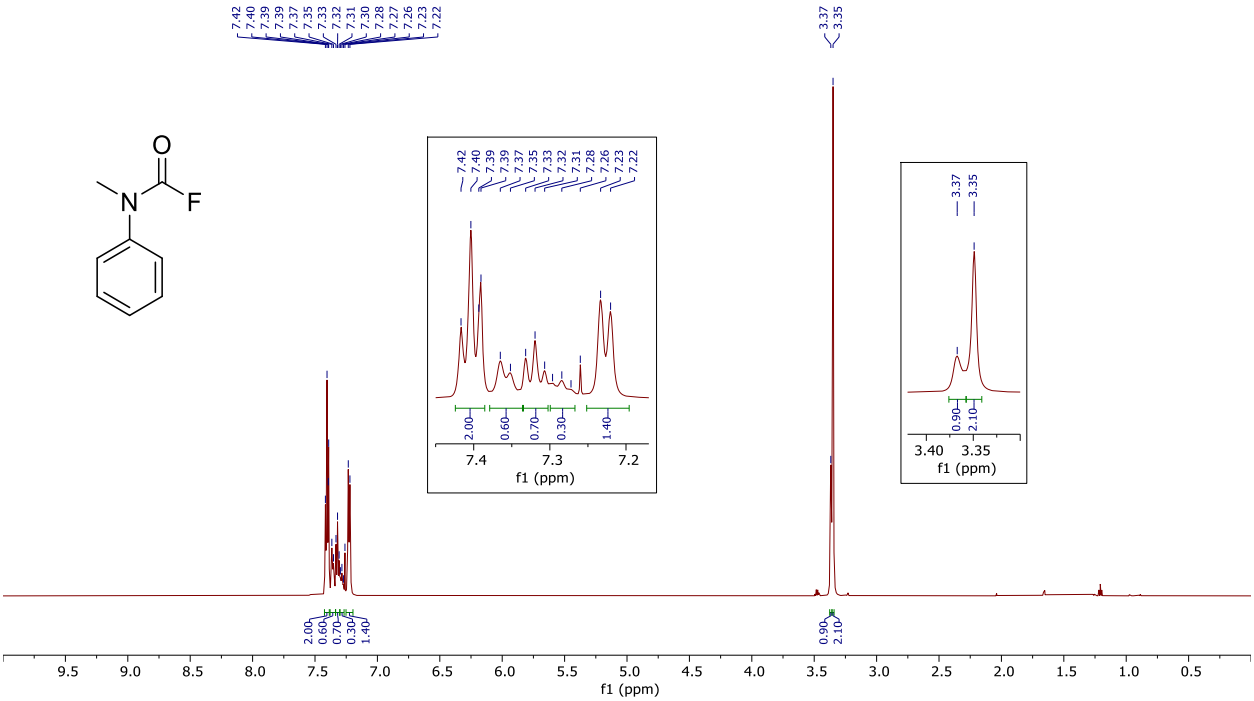

^{13}C NMR Spectrum $CDCl_3$ (151 MHz)

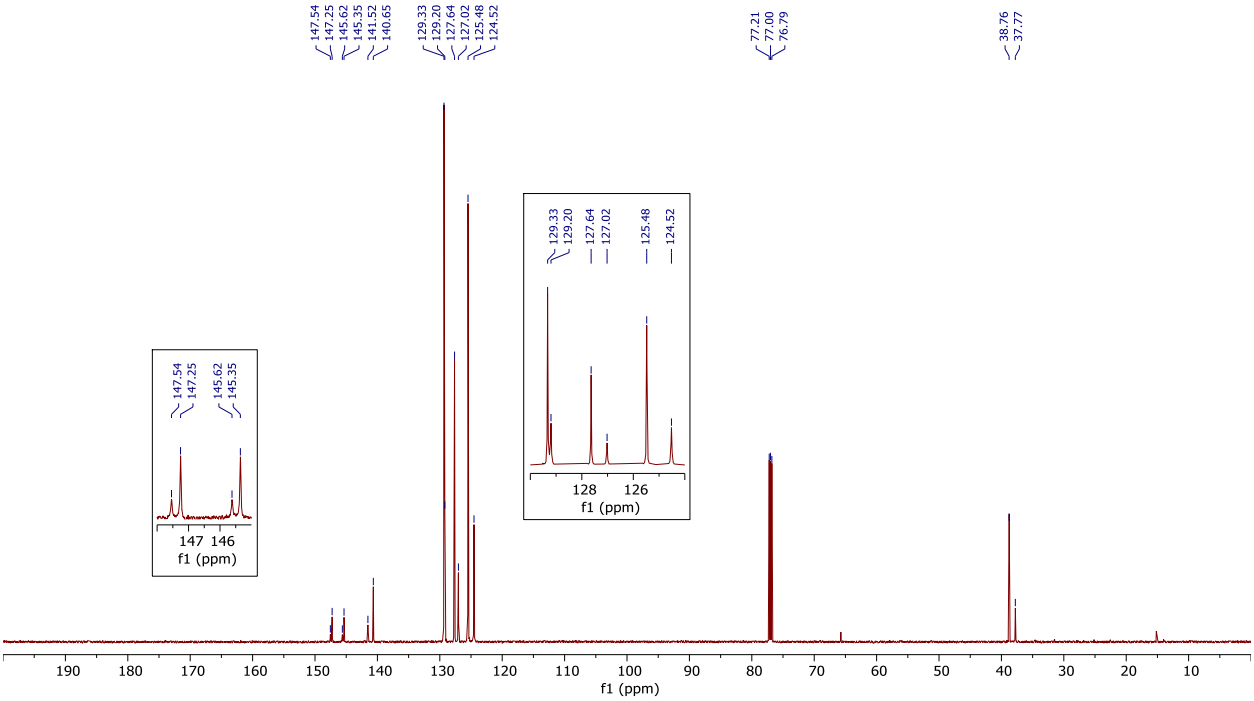

^{19}F {^{1}H} NMR Spectrum $CDCl_3$ (282 MHz)

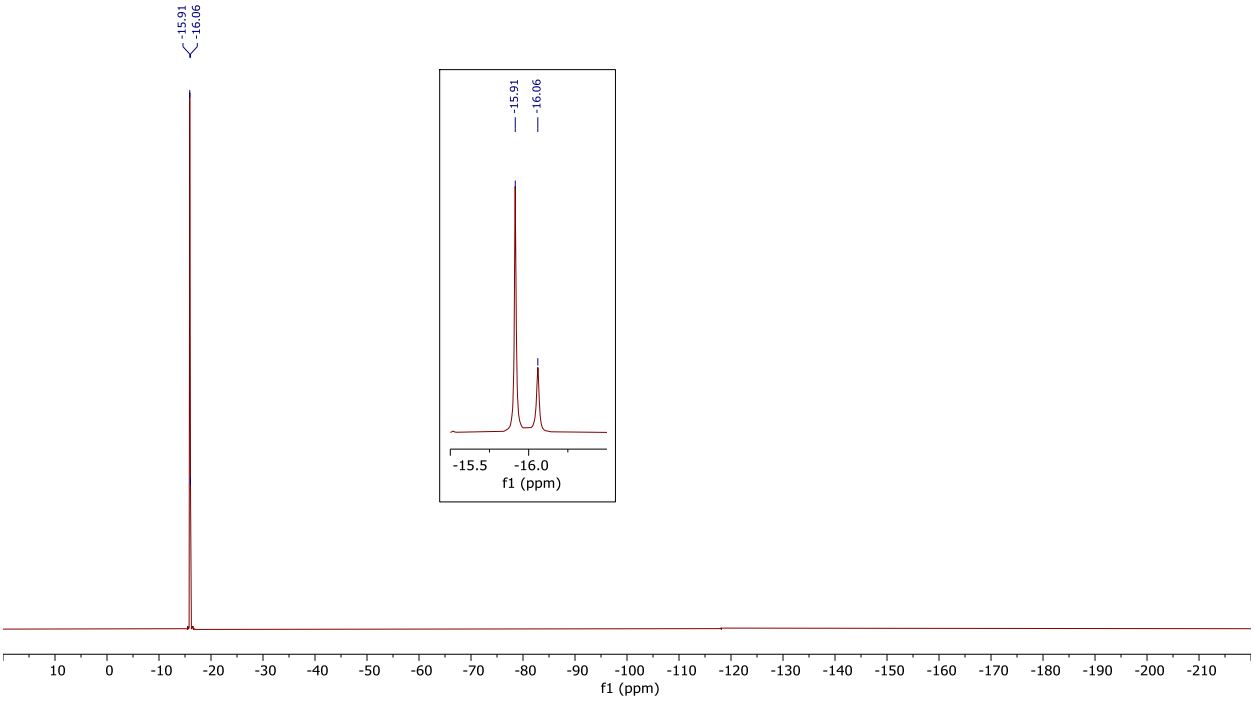

N-benzyl-N-tert-butyl-carbamoyl fluoride, (2.2p)

^{1}H NMR Spectrum $CDCl_3$ (600 MHz)

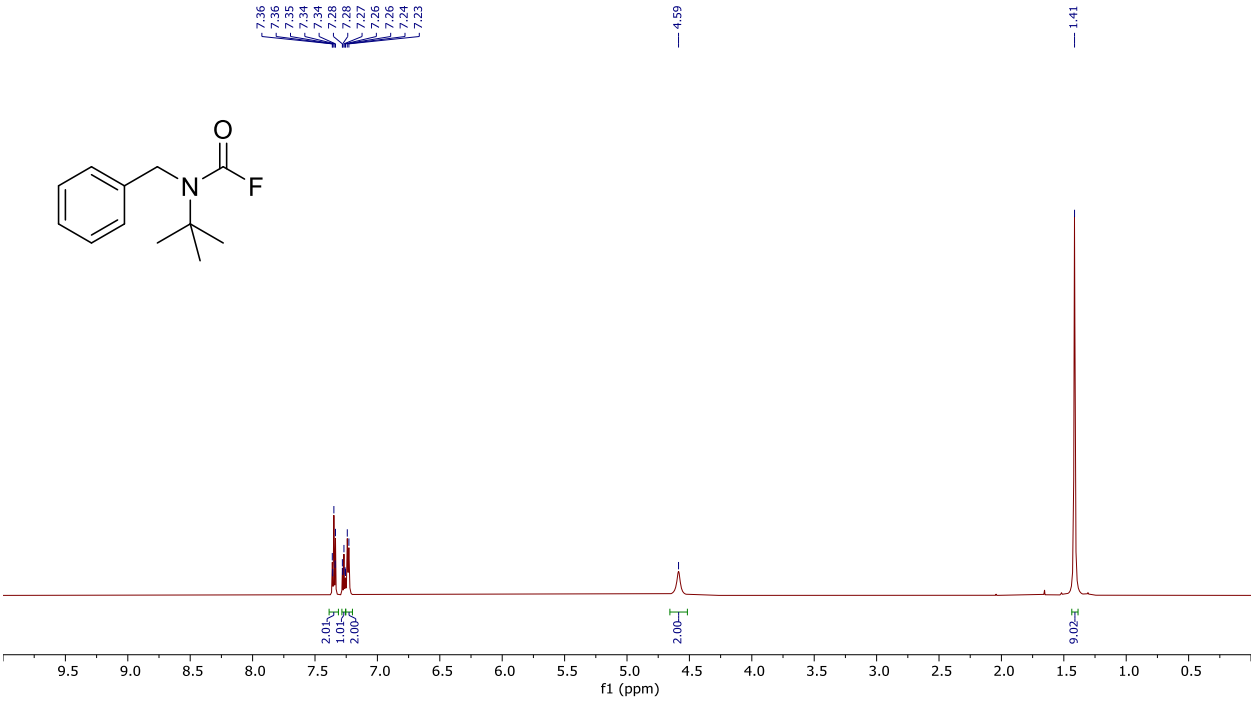

^{13}C NMR Spectrum $CDCl_3$ (151 MHz)

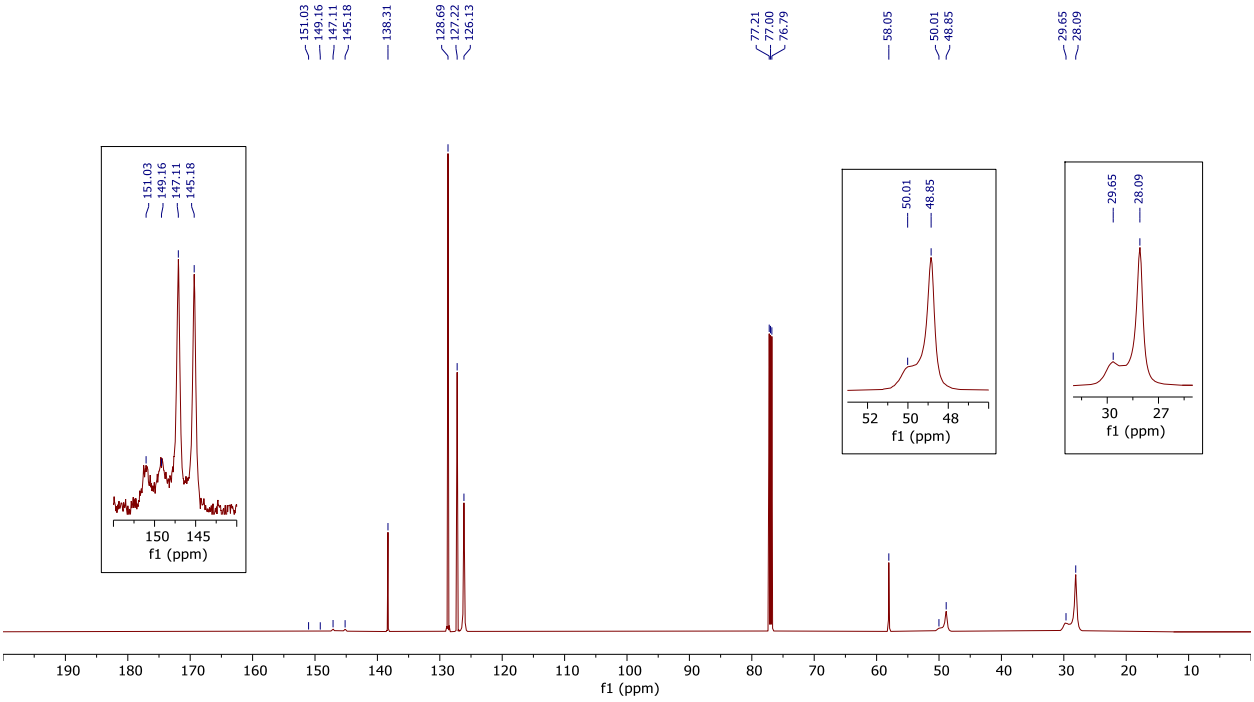

^{19}F {^{1}H} NMR Spectrum $CDCl_3$ (282 MHz)

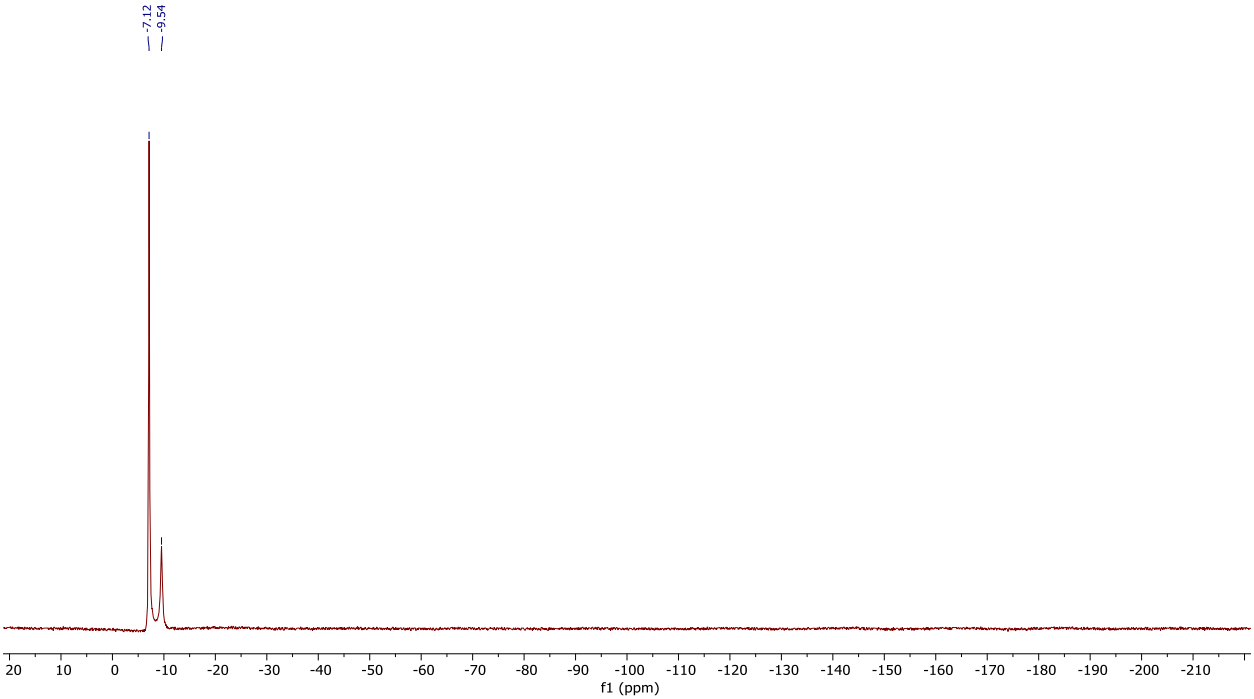

N,N-dibenzylcarbamoyl fluoride, (2.2q)

^{1}H NMR Spectrum $CDCl_3$ (600 MHz)

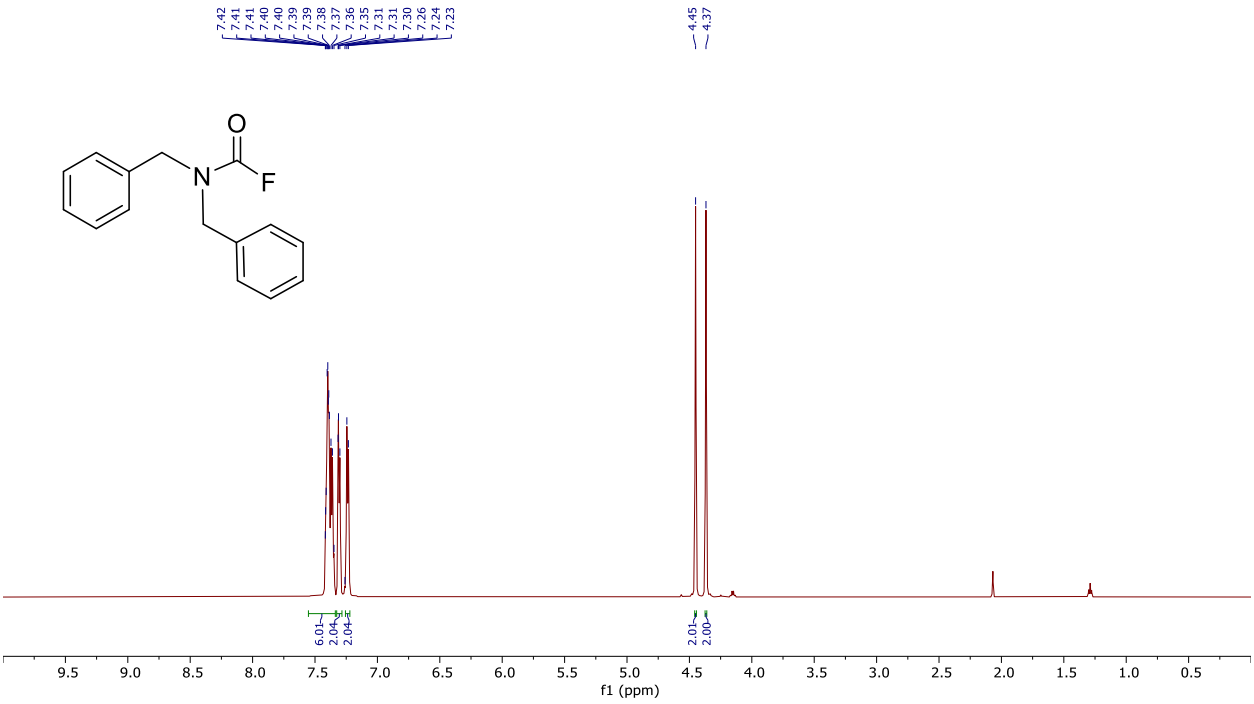

^{13}C NMR Spectrum $CDCl_3$ (150 MHz)

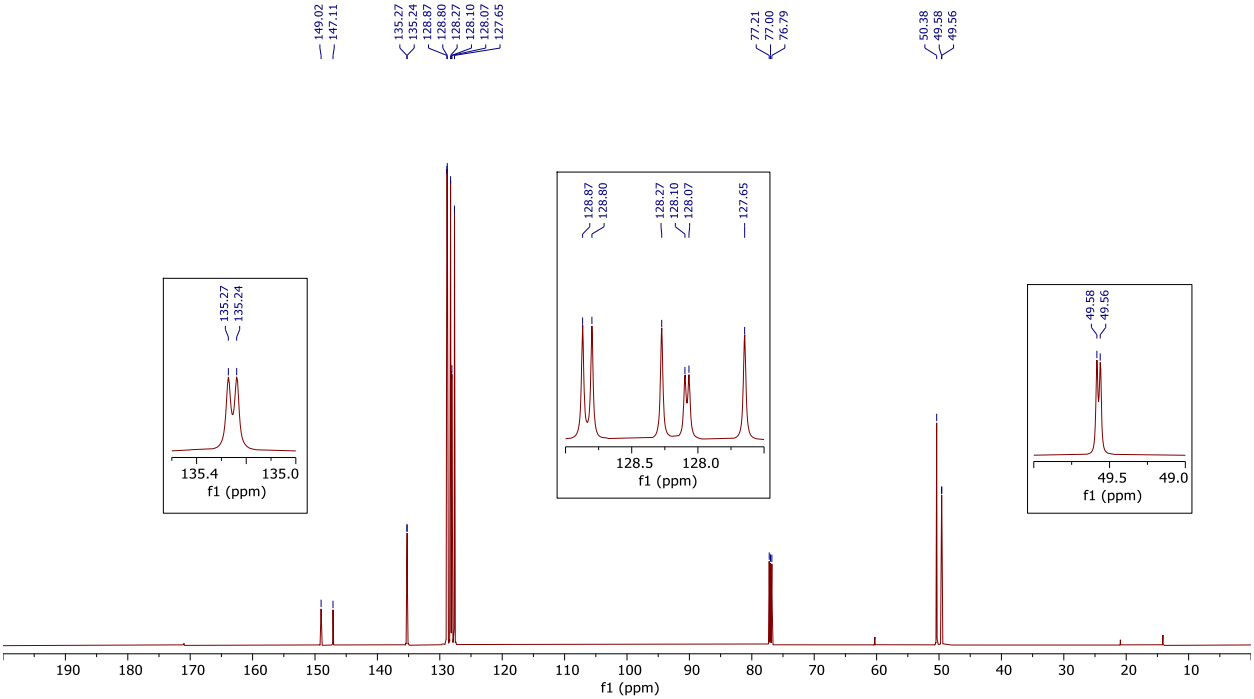

^{19}F {^{1}H} NMR Spectrum $CDCl_3$ (282 MHz)

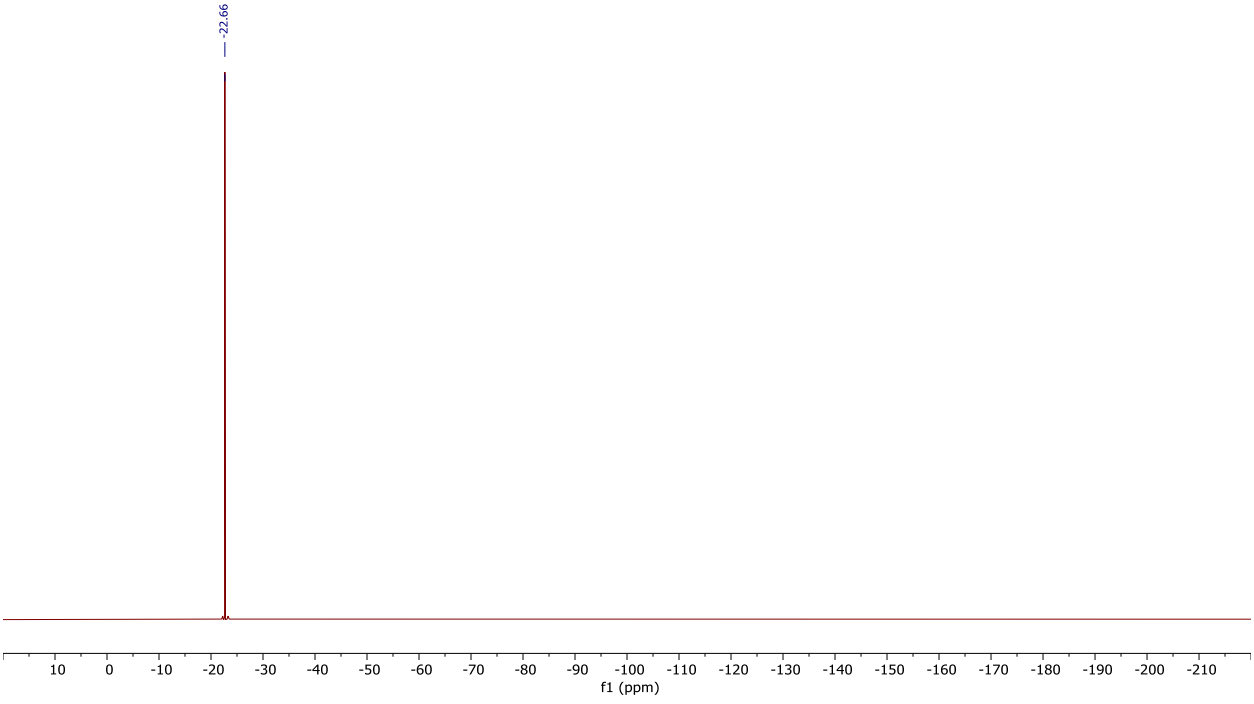

N-[(4-acetamidophenyl)methyl]-*N*-phenyl-carbamoyl fluoride, (2.2h)

^{1}H NMR Spectrum $CDCl_3$ (600 MHz)

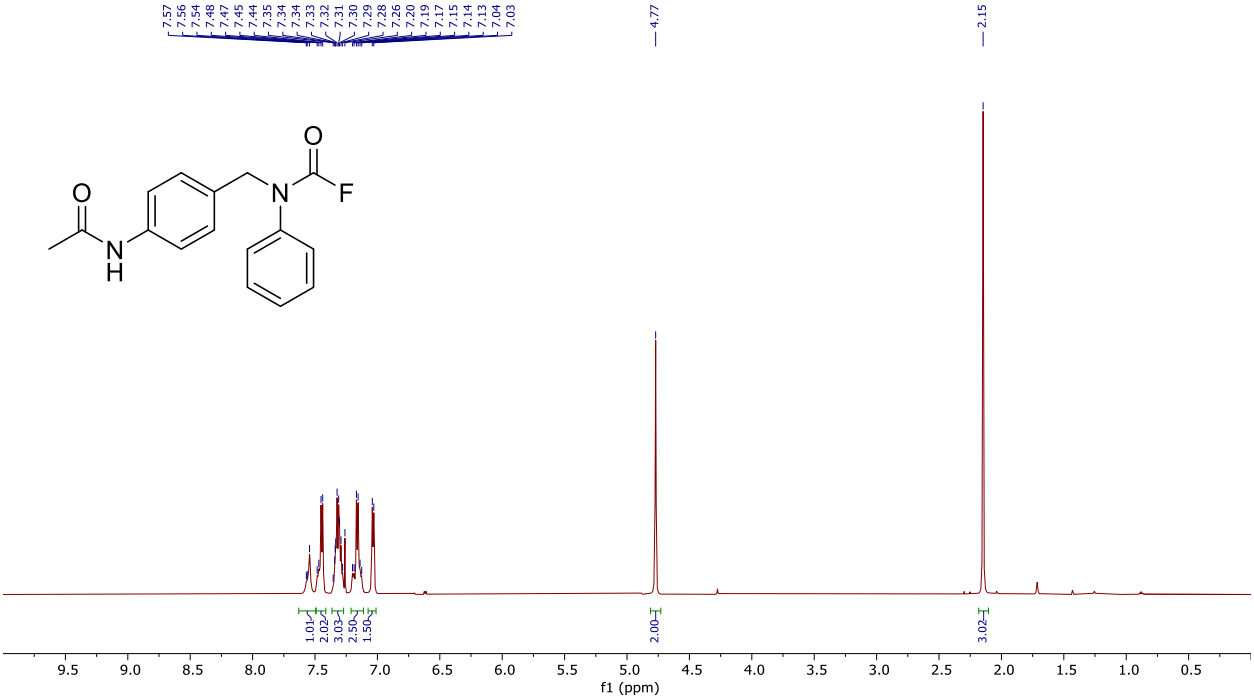

^{13}C NMR Spectrum $CDCl_3$ (151 MHz)

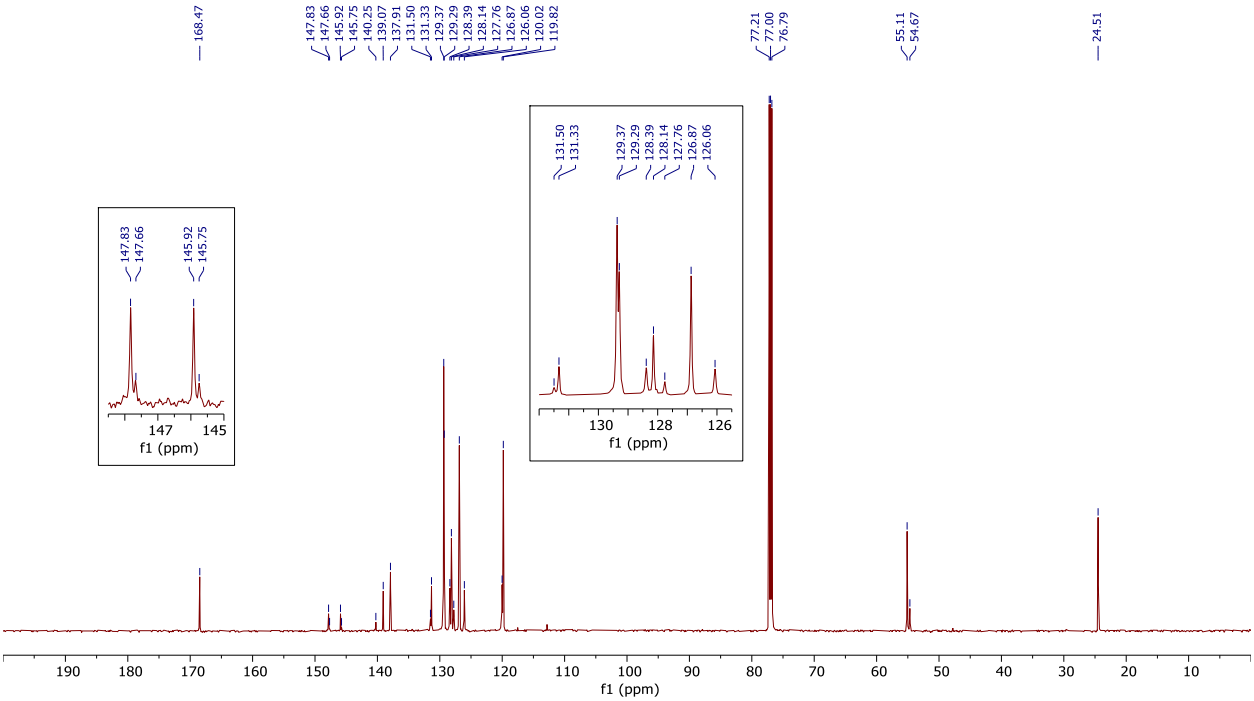

^{19}F {^{1}H} NMR Spectrum $CDCl_3$ (282 MHz)

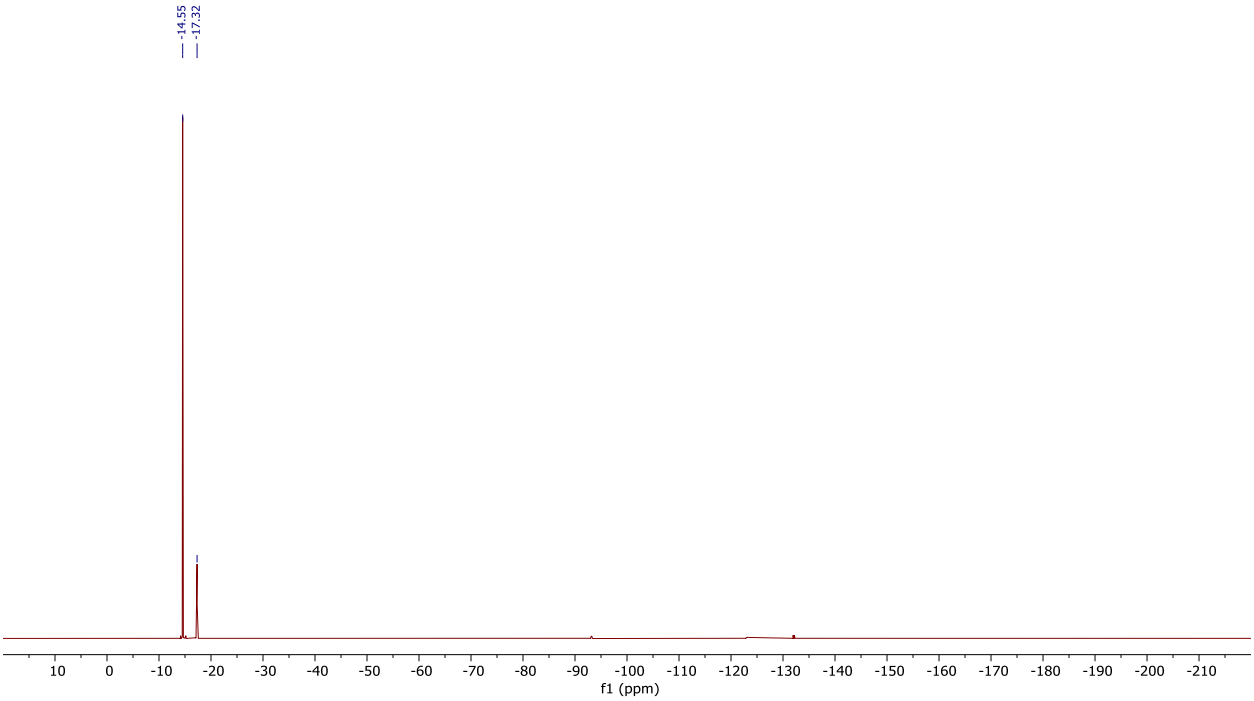

indoline-1-carbonyl fluoride, (2.2x)

^{1}H NMR Spectrum $CDCl_3$ (600 MHz)

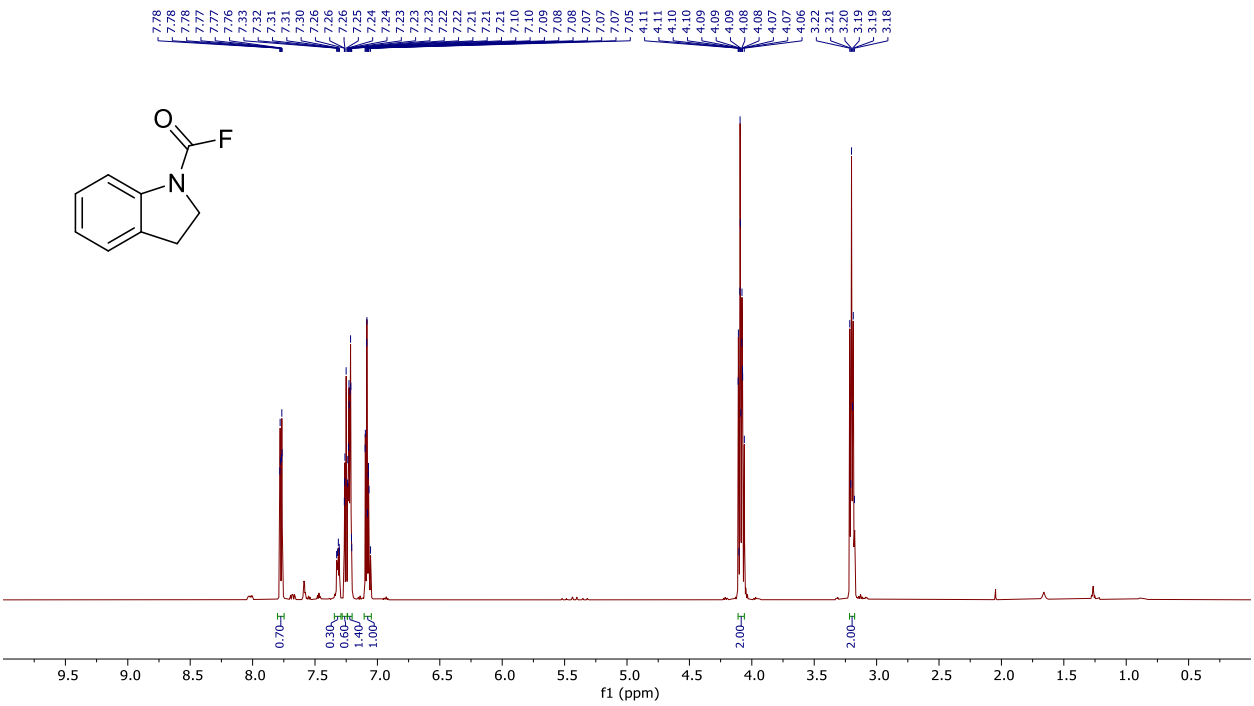

^{13}C NMR Spectrum $CDCl_3$ (151 MHz)

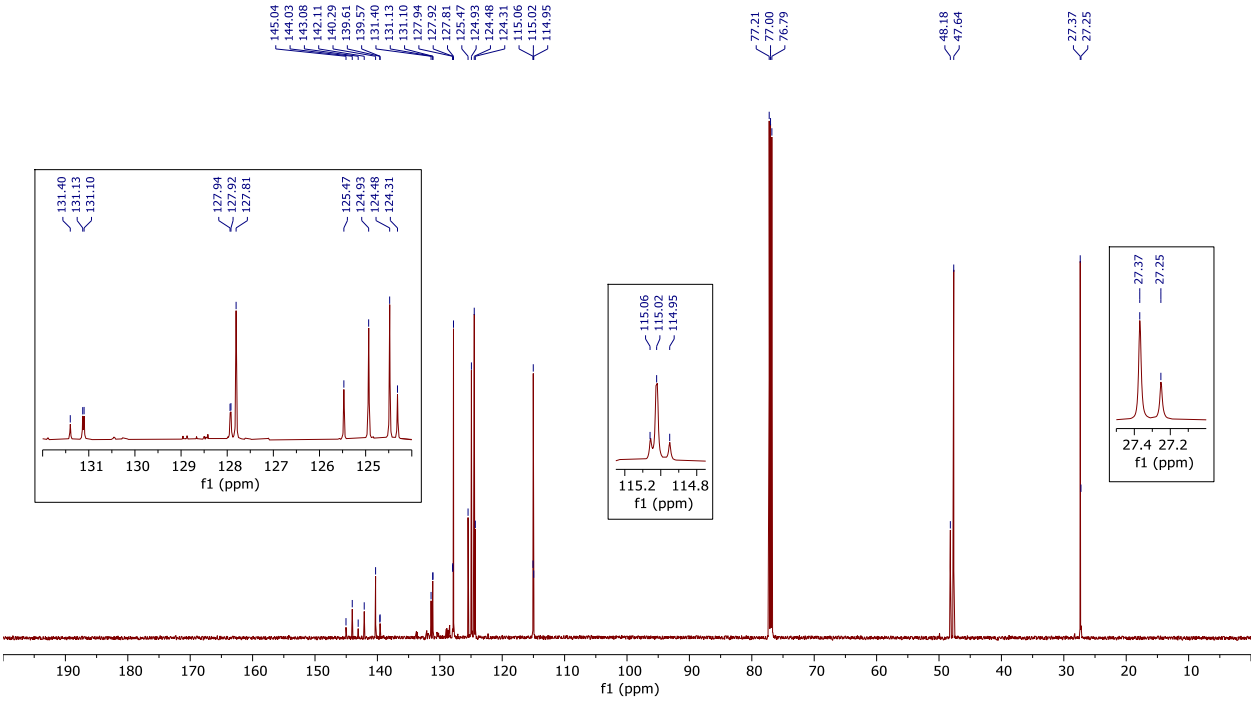

^{19}F {^{1}H} NMR Spectrum $CDCl_3$ (282 MHz)

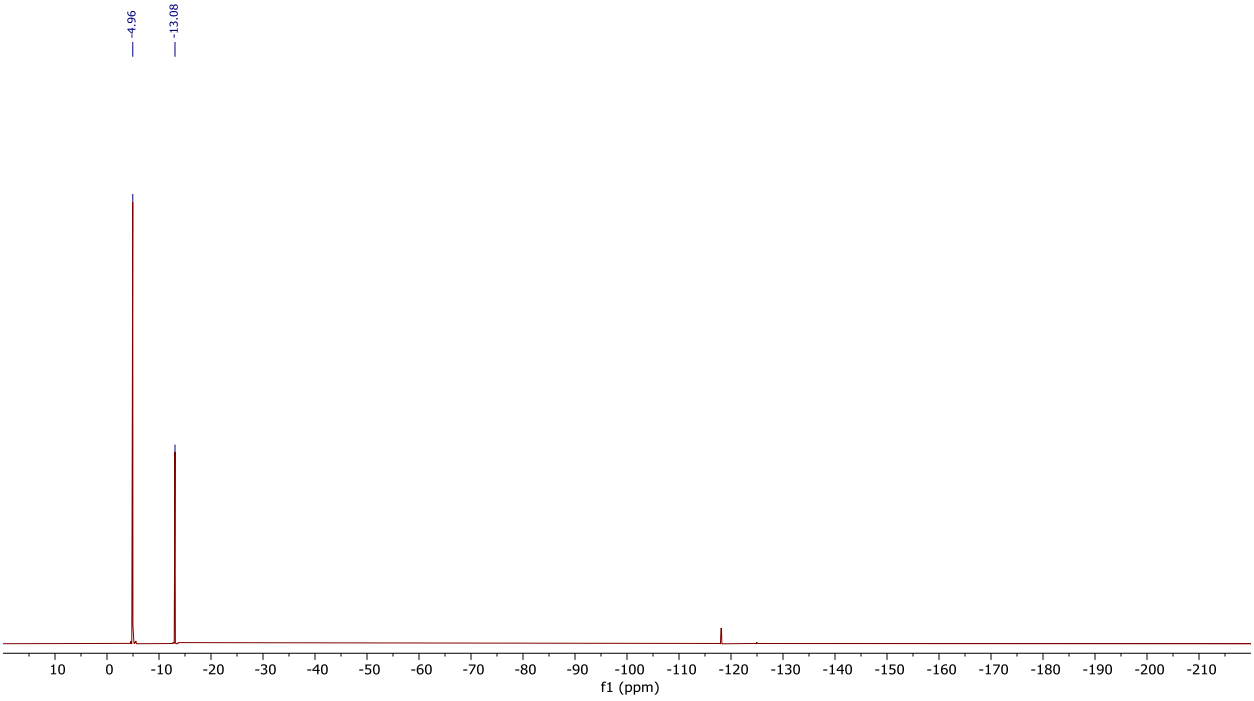

3,4-dihydro-2H-quinoline-1-carbonyl fluoride, (2.2u)

^{1}H NMR Spectrum $CDCl_3$ (600 MHz)

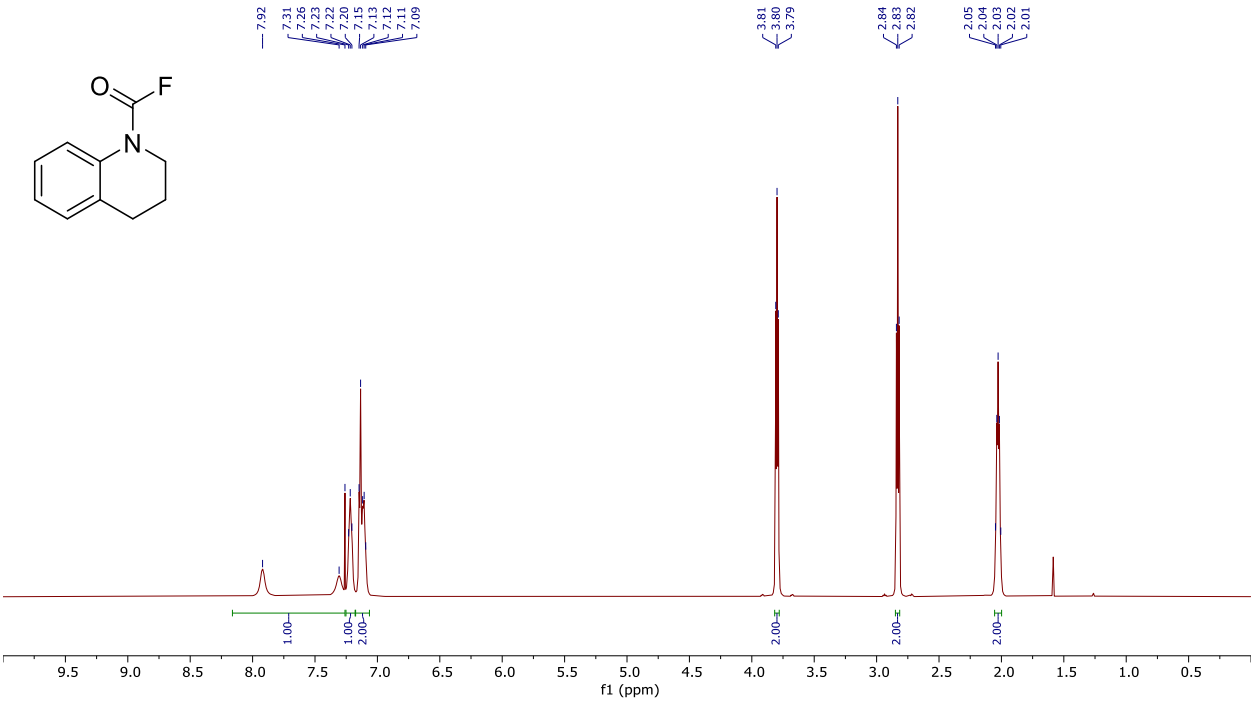

^{13}C NMR Spectrum $CDCl_3$ (151 MHz)

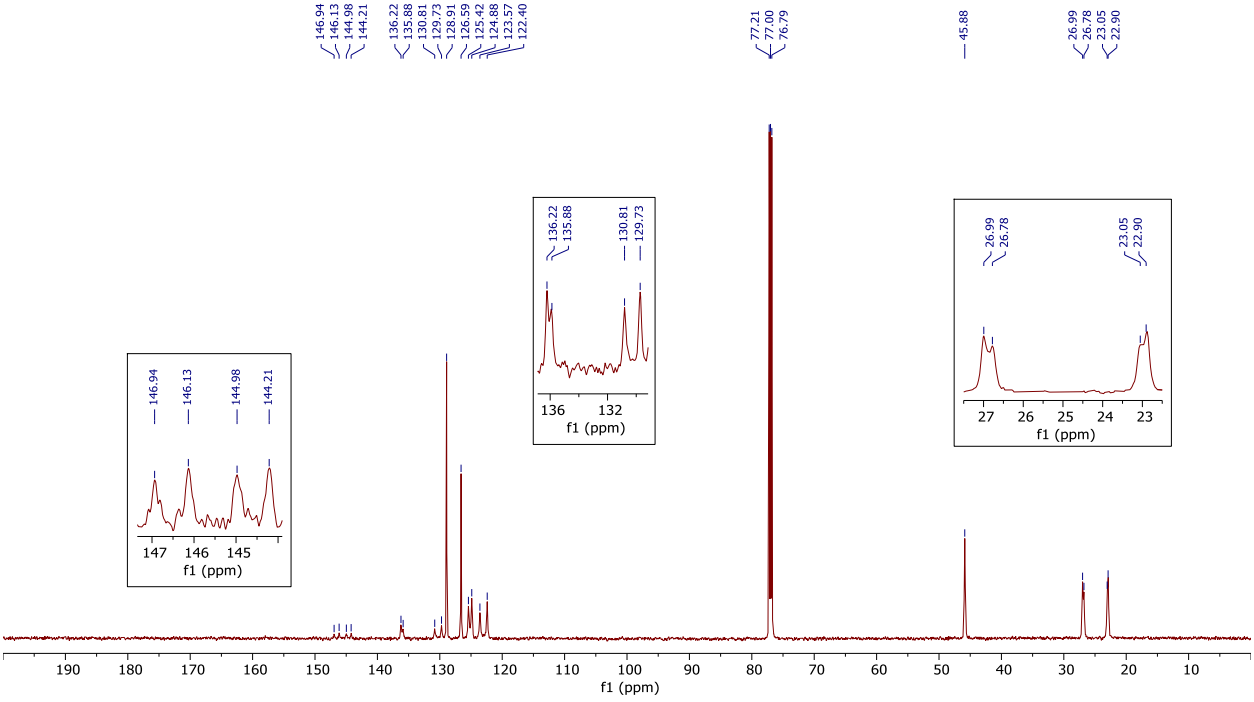

^{19}F {^{1}H} NMR Spectrum $CDCl_3$ (282 MHz)

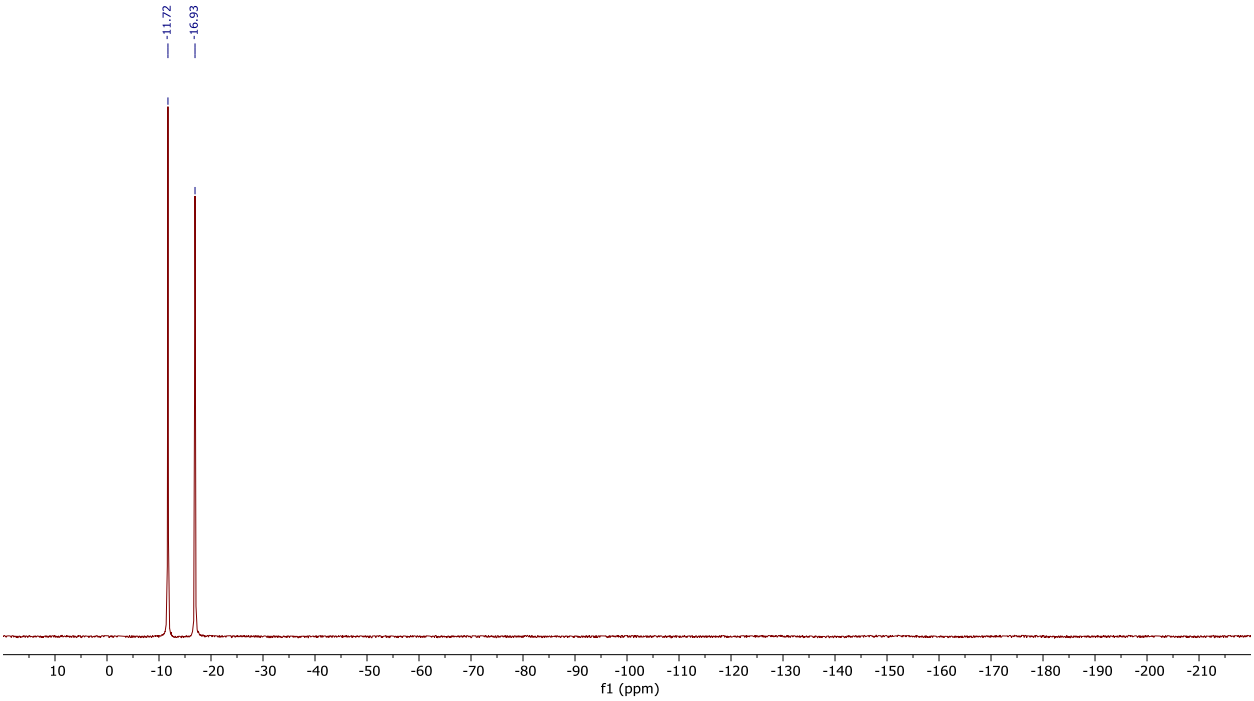

2-methyl-3,4-dihydro-2H-quinoline-1-carbonyl fluoride, (2.2v)

^{1}H NMR Spectrum $CDCl_3$ (600 MHz)

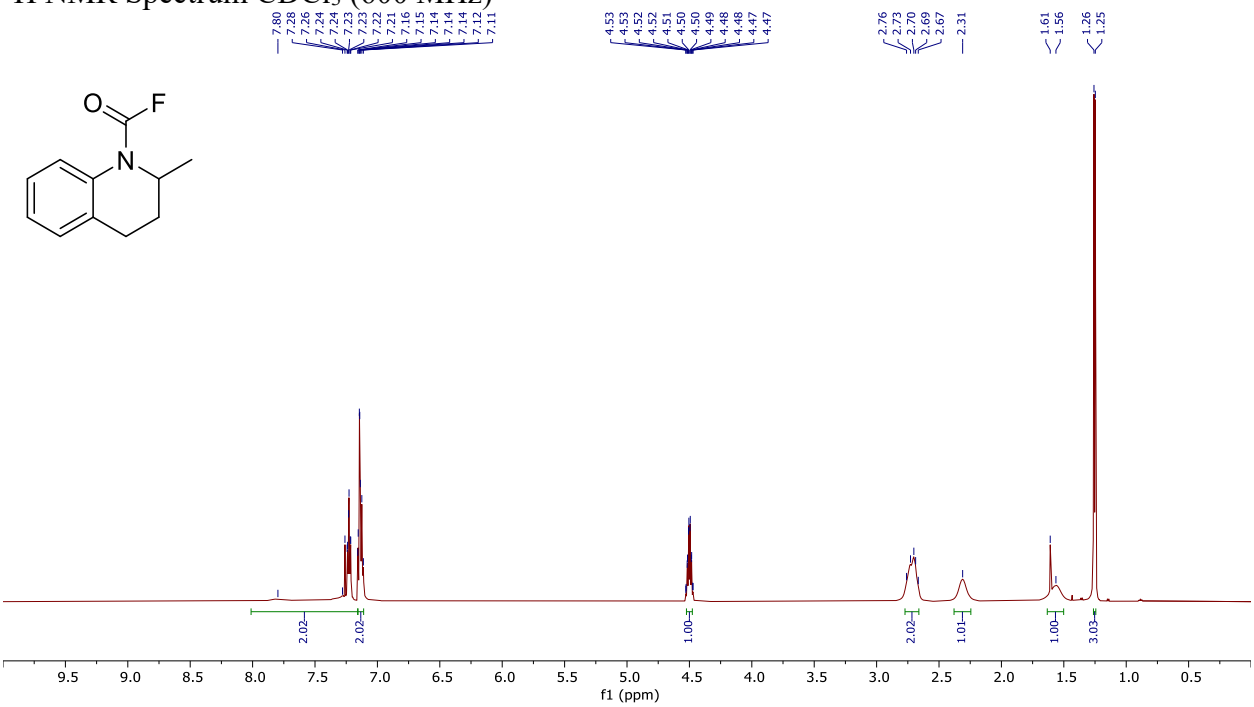

^{13}C NMR Spectrum $CDCl_3$ (151 MHz)

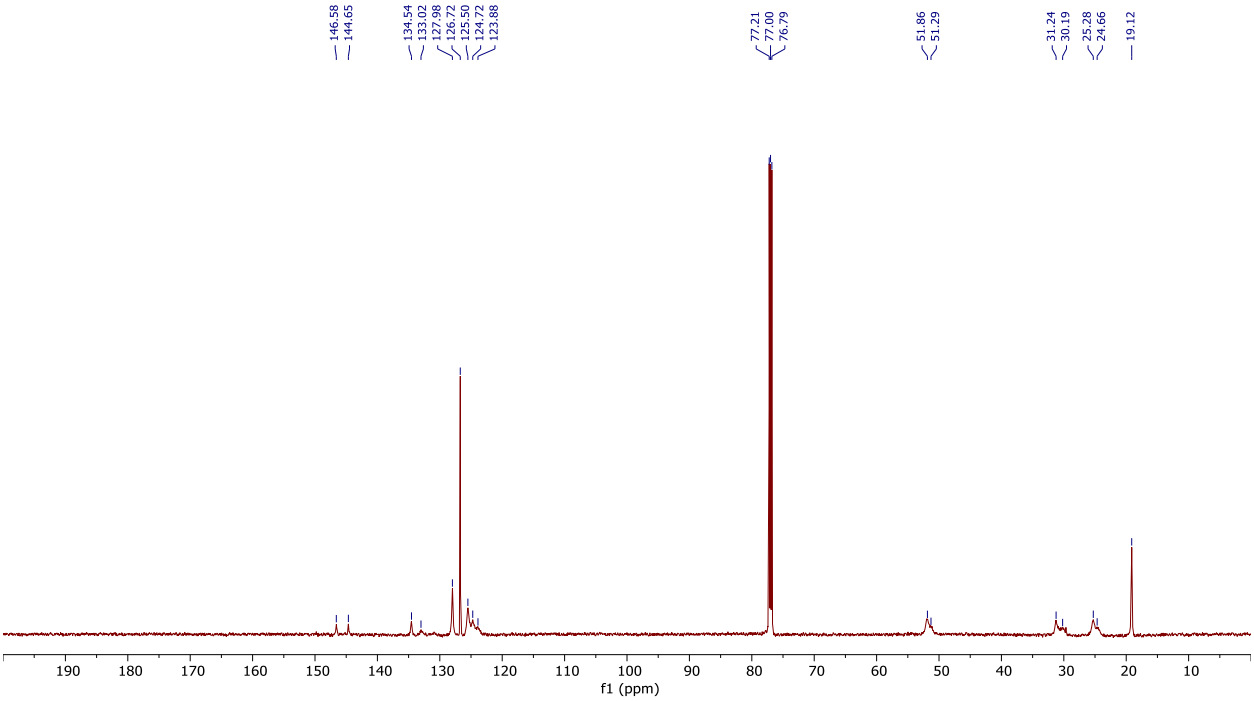

^{19}F {^{1}H} 3NMR Spectrum $CDCl_3$ (282 MHz)

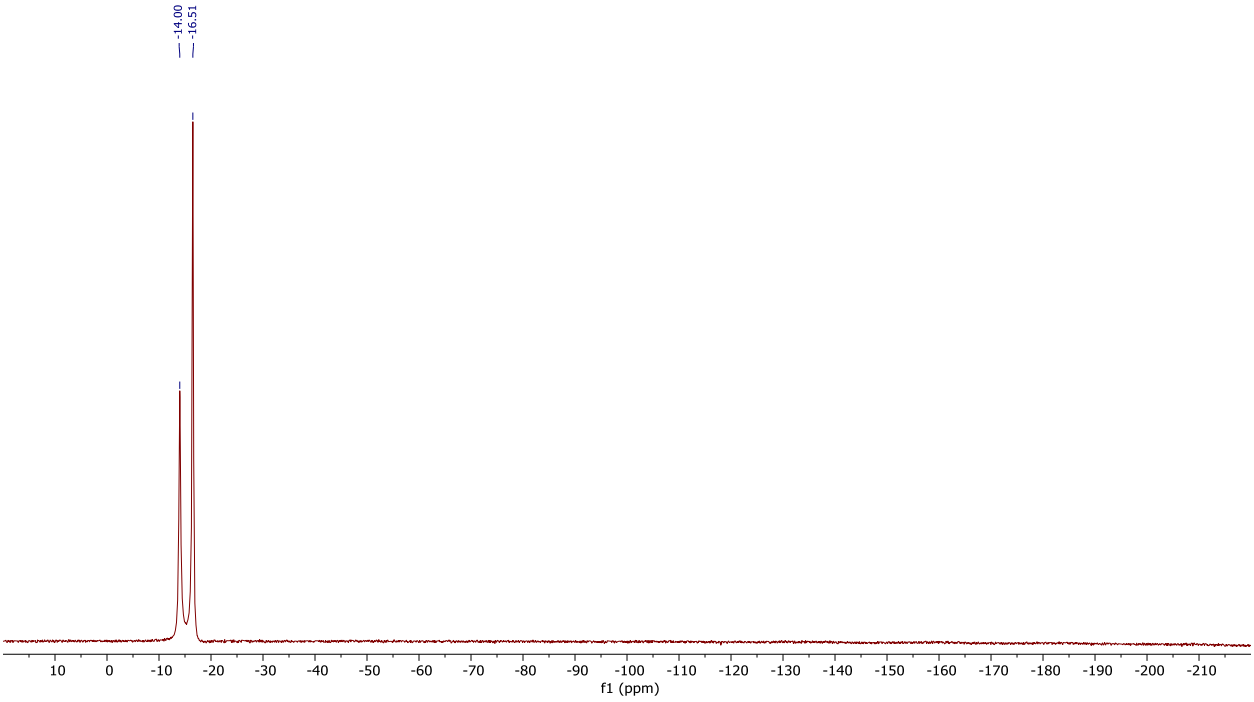

4-methyl-2-phenyl-piperazine-1-carbonyl fluoride, (2.2y)

^{1}H NMR Spectrum $CDCl_3$ (600 MHz)

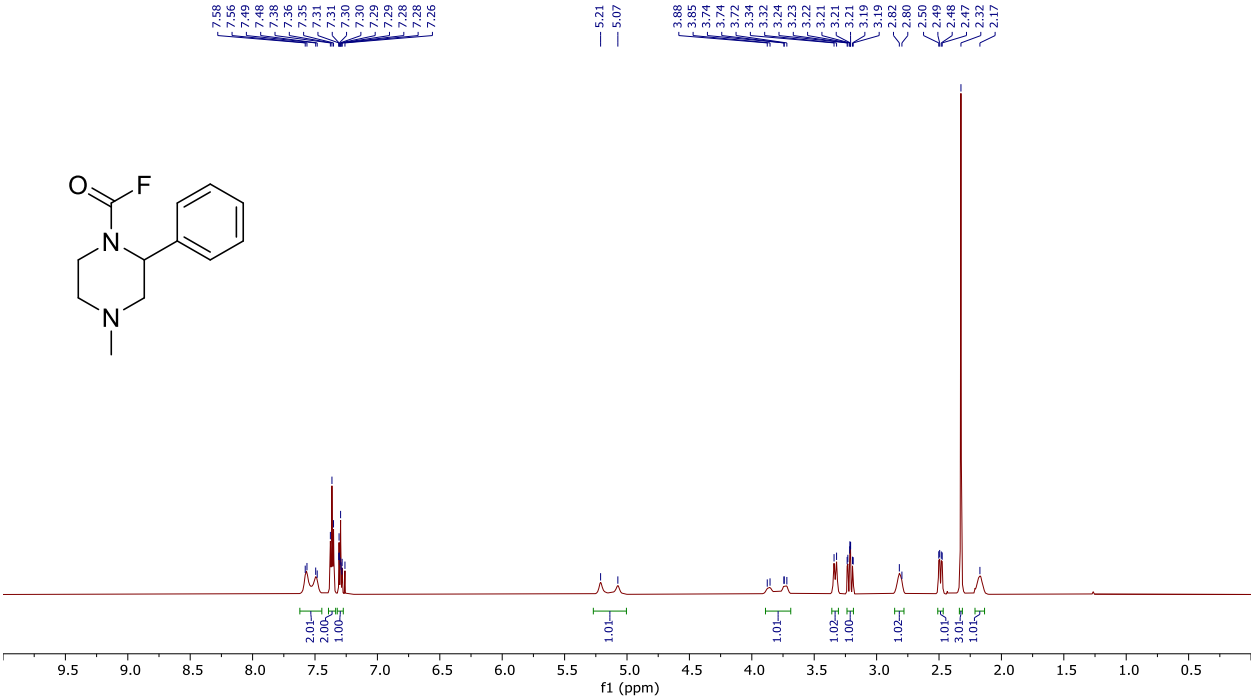

^{13}C NMR Spectrum $CDCl_3$ (151 MHz)

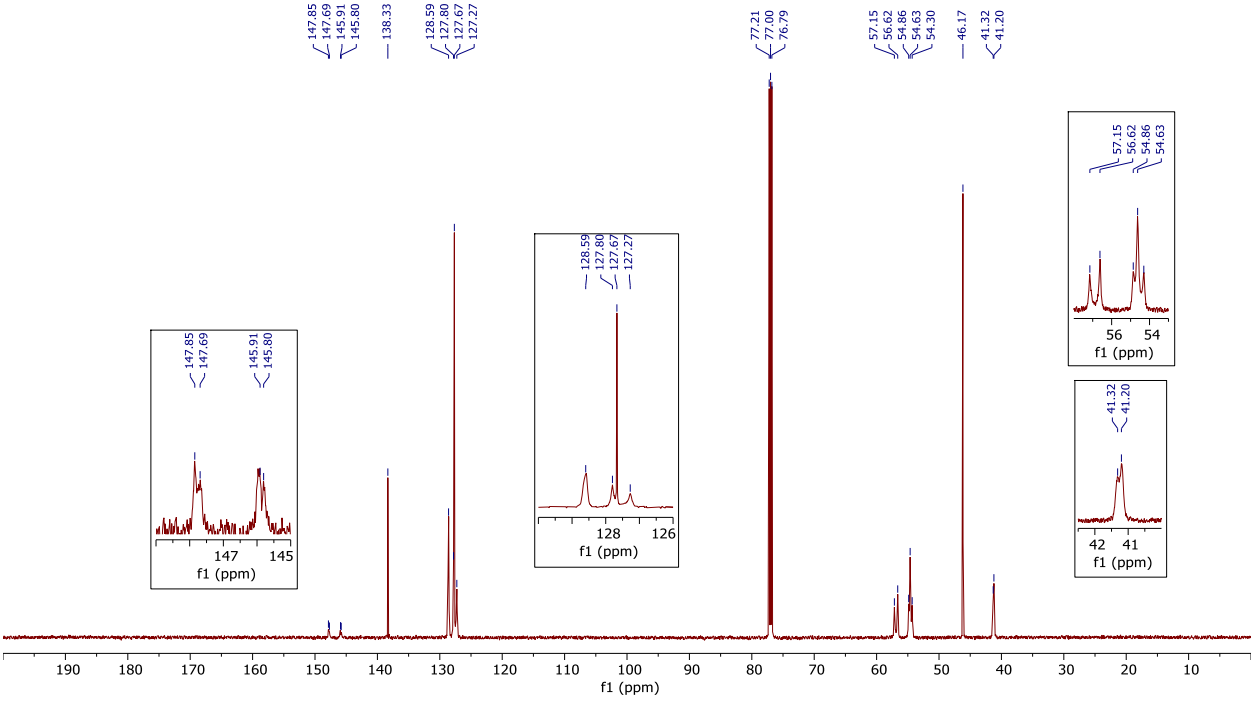

^{19}F {^{1}H} NMR Spectrum $CDCl_3$ (282 MHz)

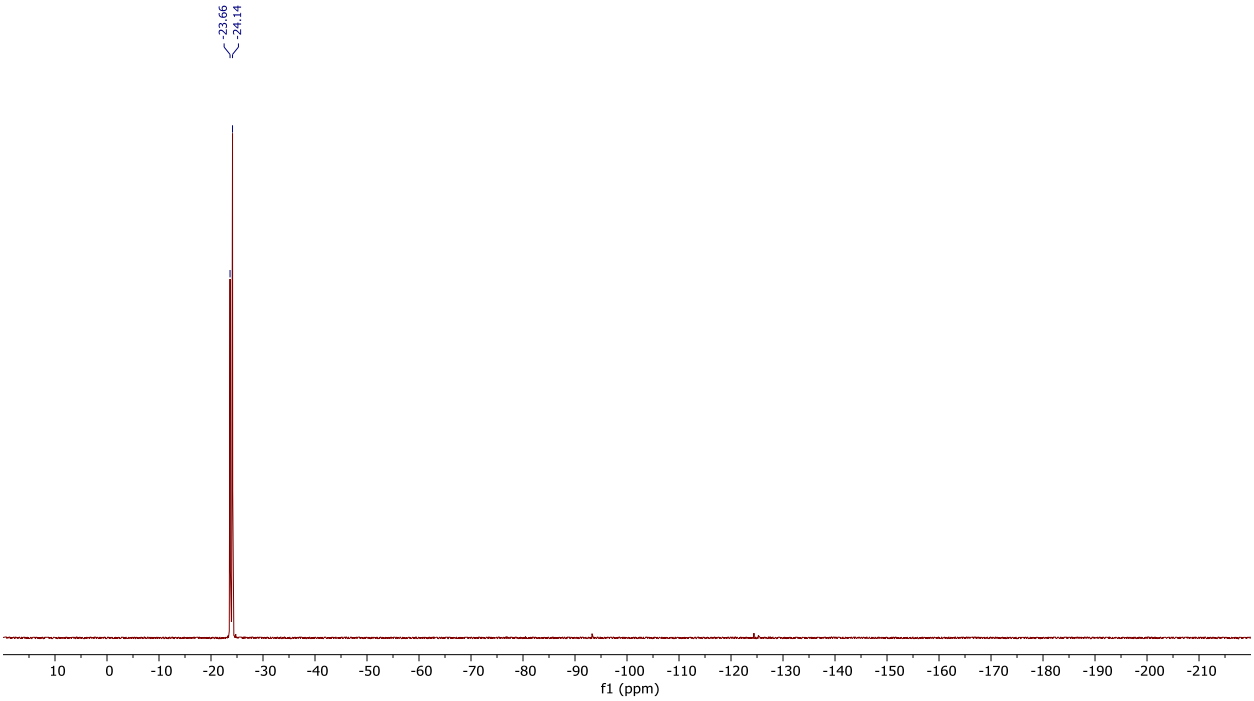

4-(furan-2-carbonyl)piperazine-1-carbonyl fluoride, (2.2aa)

^{1}H NMR Spectrum $CDCl_3$ (600 MHz)

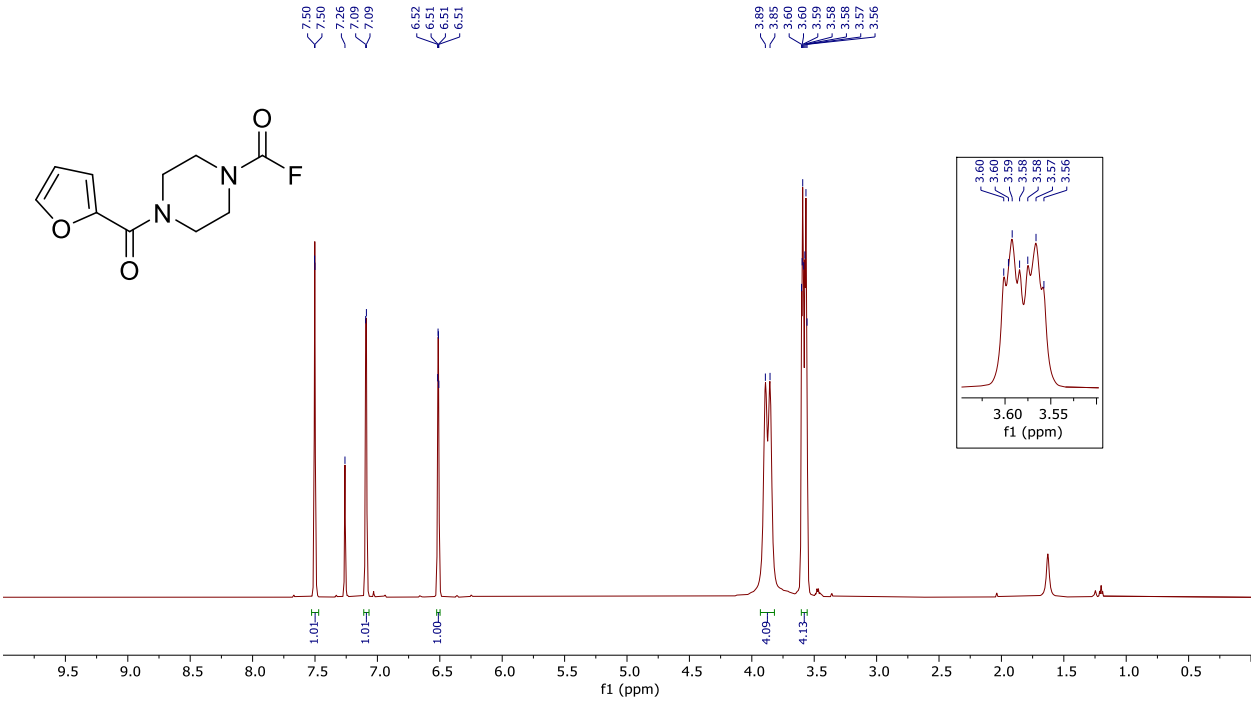

^{13}C NMR Spectrum $CDCl_3$ (151 MHz)

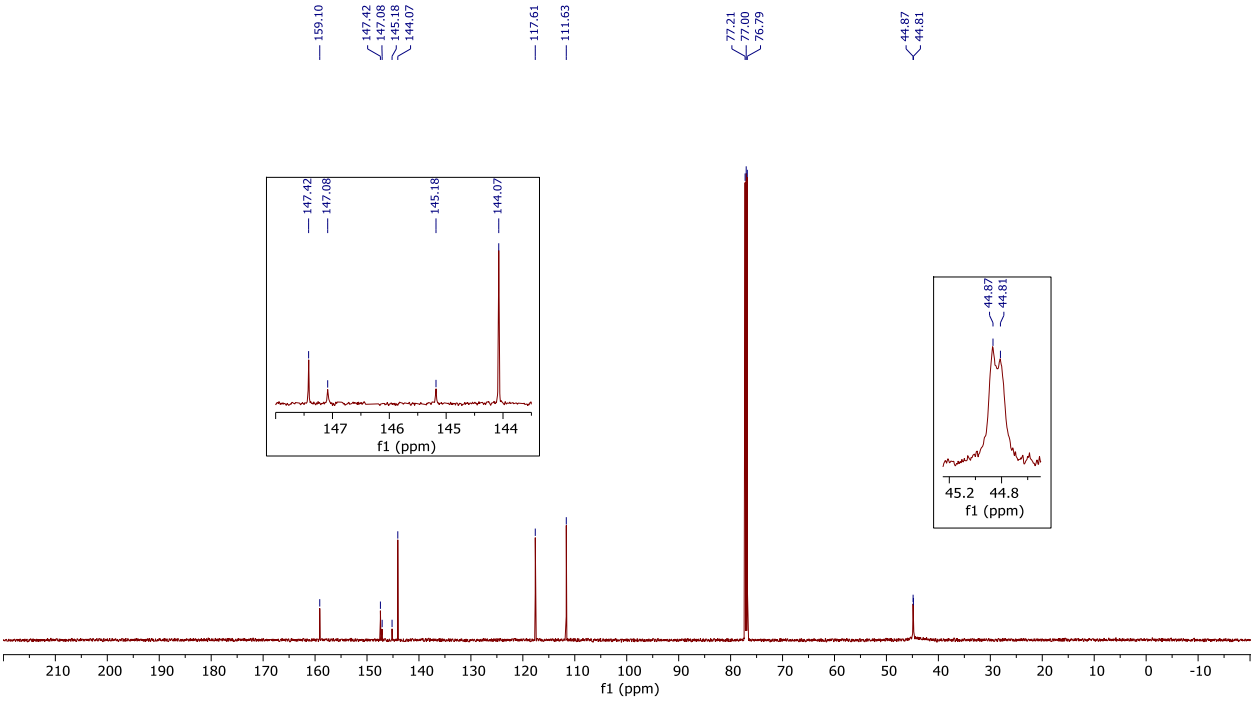

^{19}F {^{1}H} NMR Spectrum $CDCl_3$ (282 MHz)

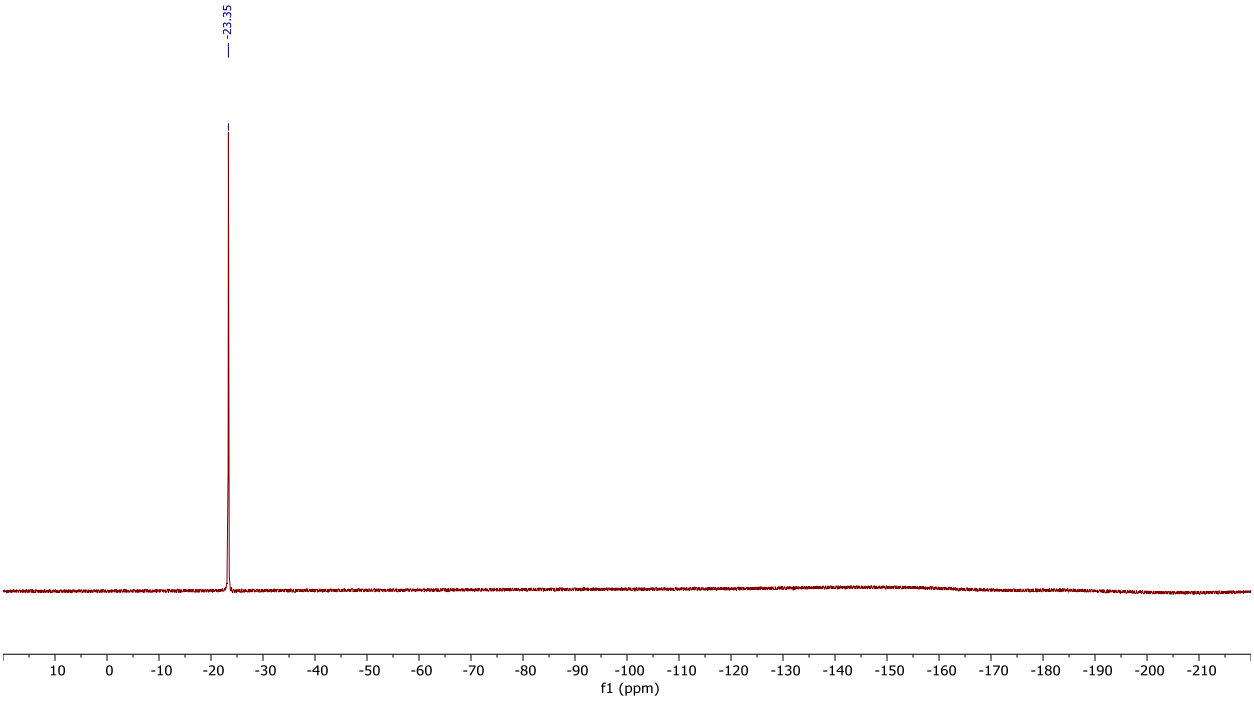

4-benzhydrylpiperazine-1-carbonyl fluoride, (2.2z)

^{1}H NMR Spectrum $CDCl_3$ (600 MHz)

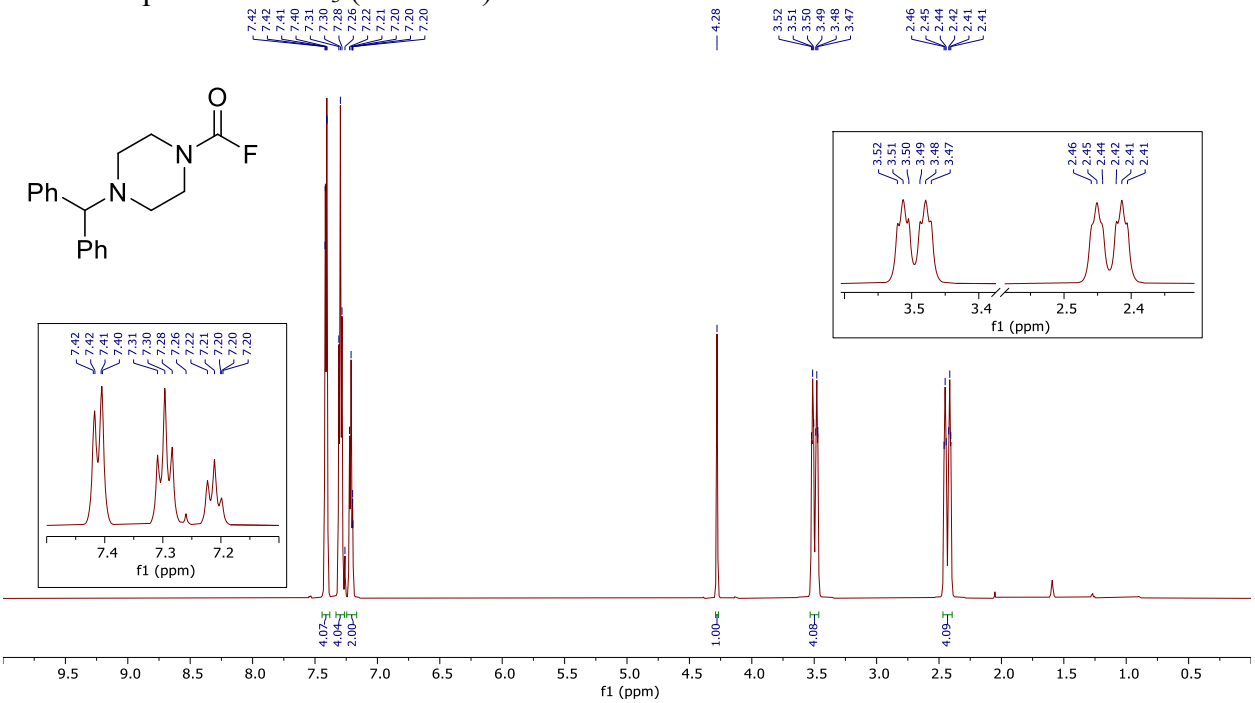

^{13}C NMR Spectrum $CDCl_3$ (151 MHz)

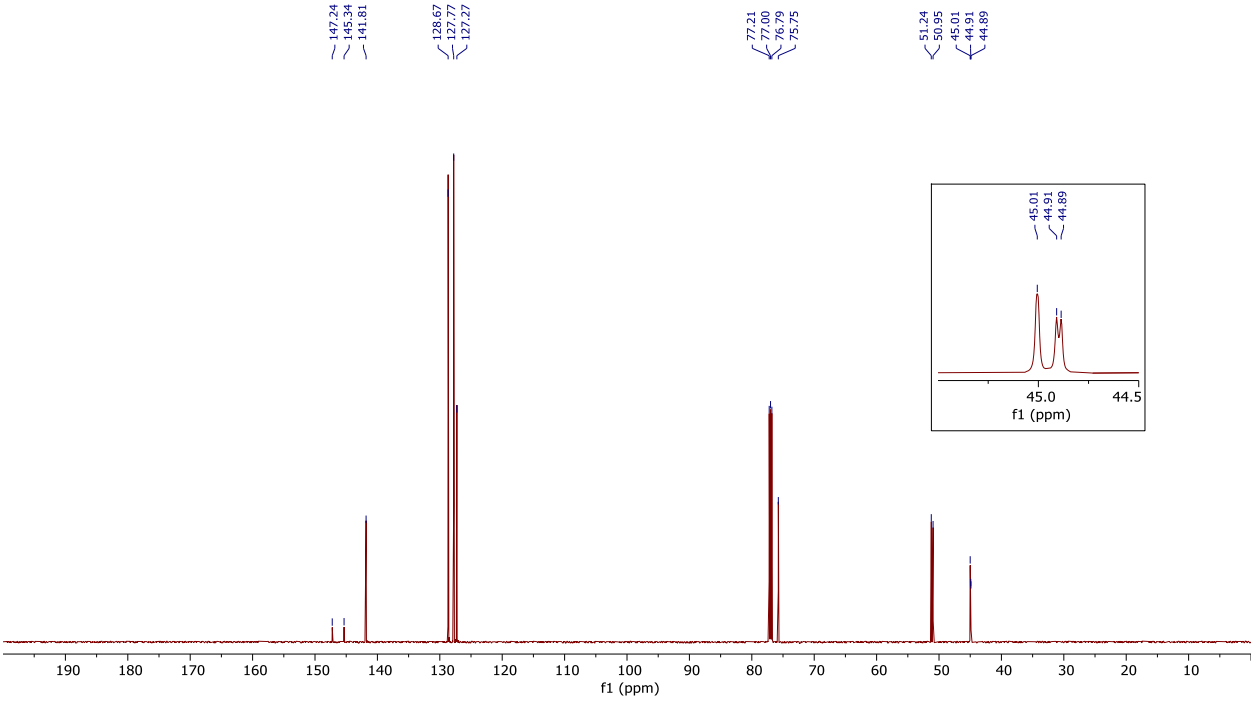

^{19}F {^{1}H} NMR Spectrum $CDCl_3$ (282 MHz)

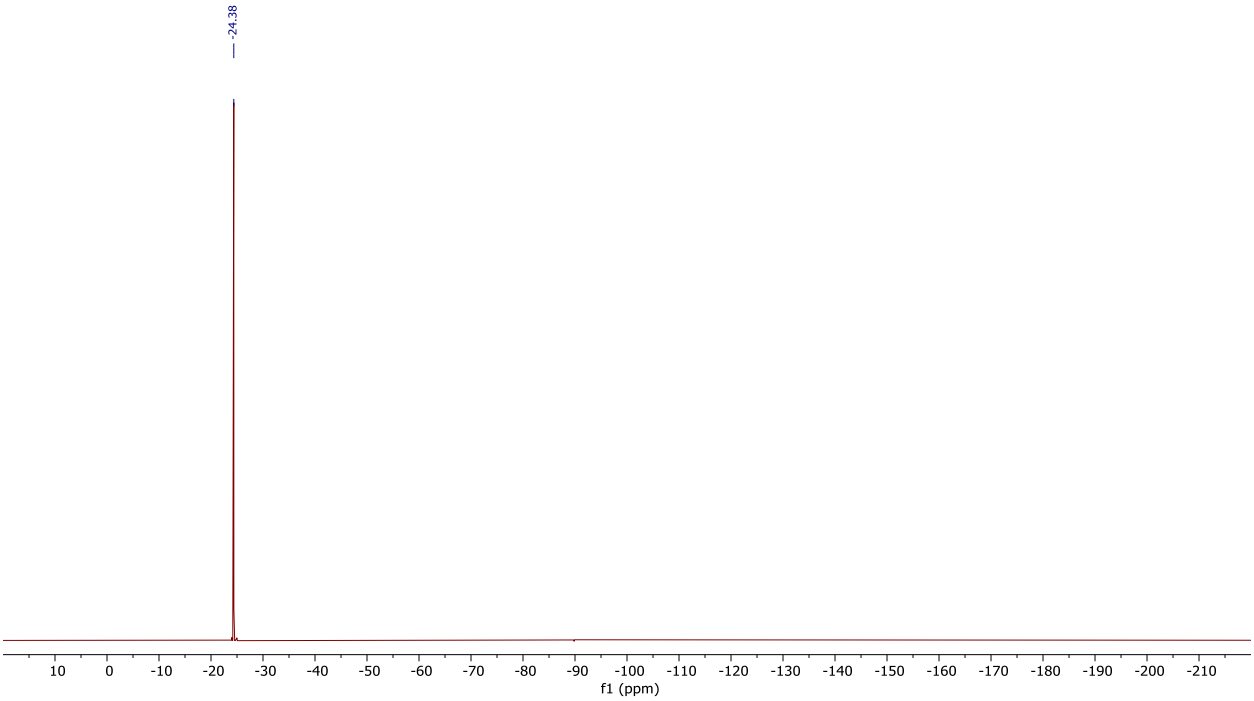

benzo[b][1]benzazepine-11-carbonyl fluoride, (2.2t)

^{1}H NMR Spectrum $CDCl_3$ (600 MHz)

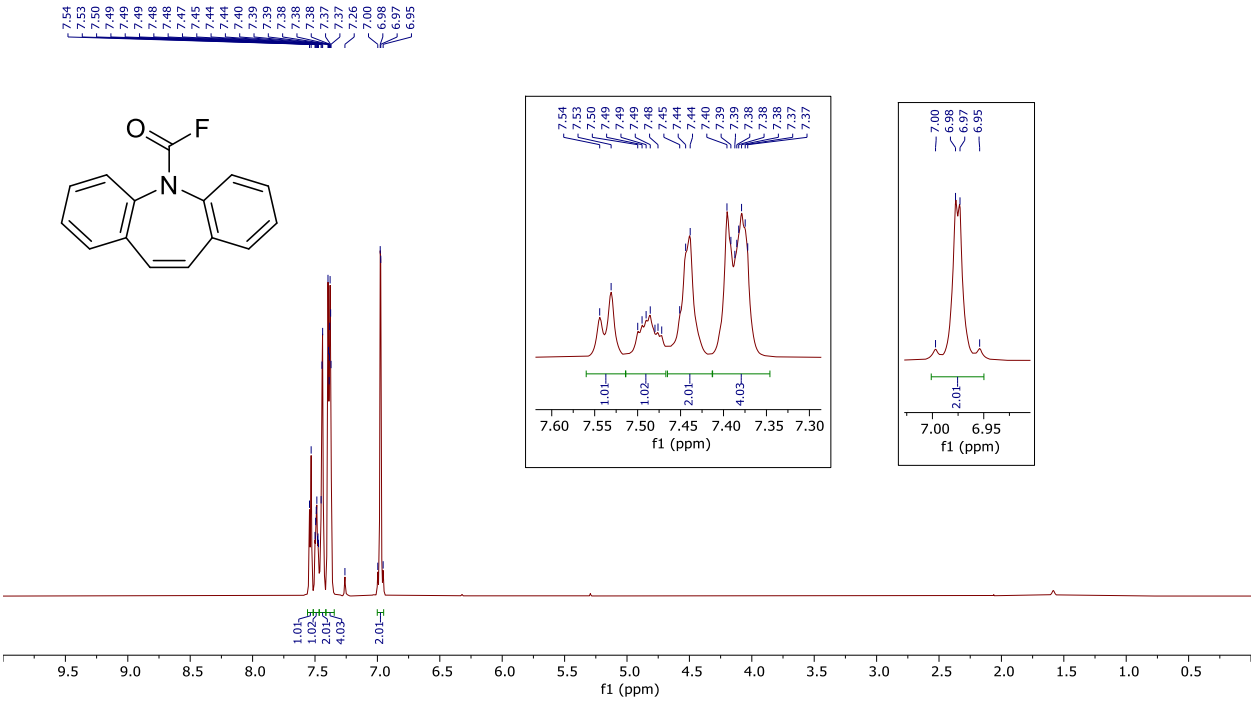

^{13}C NMR Spectrum $CDCl_3$ (151 MHz)

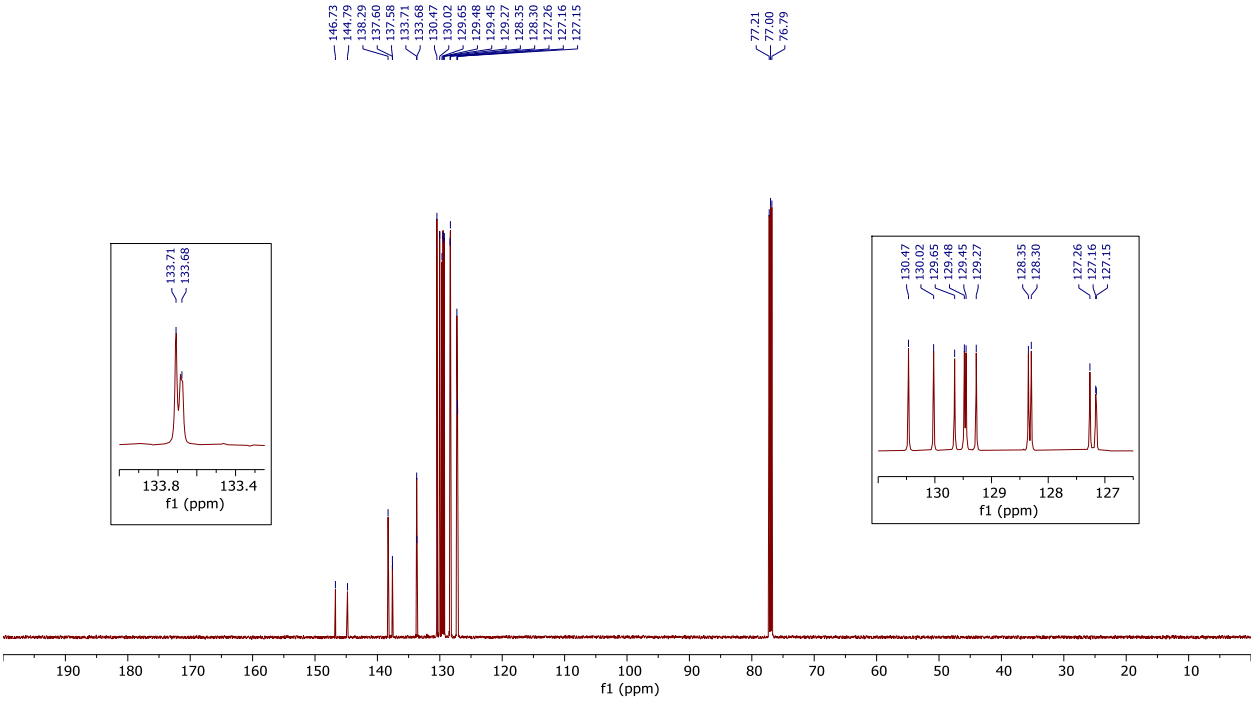

^{19}F {^{1}H} NMR Spectrum $CDCl_3$ (282 MHz)

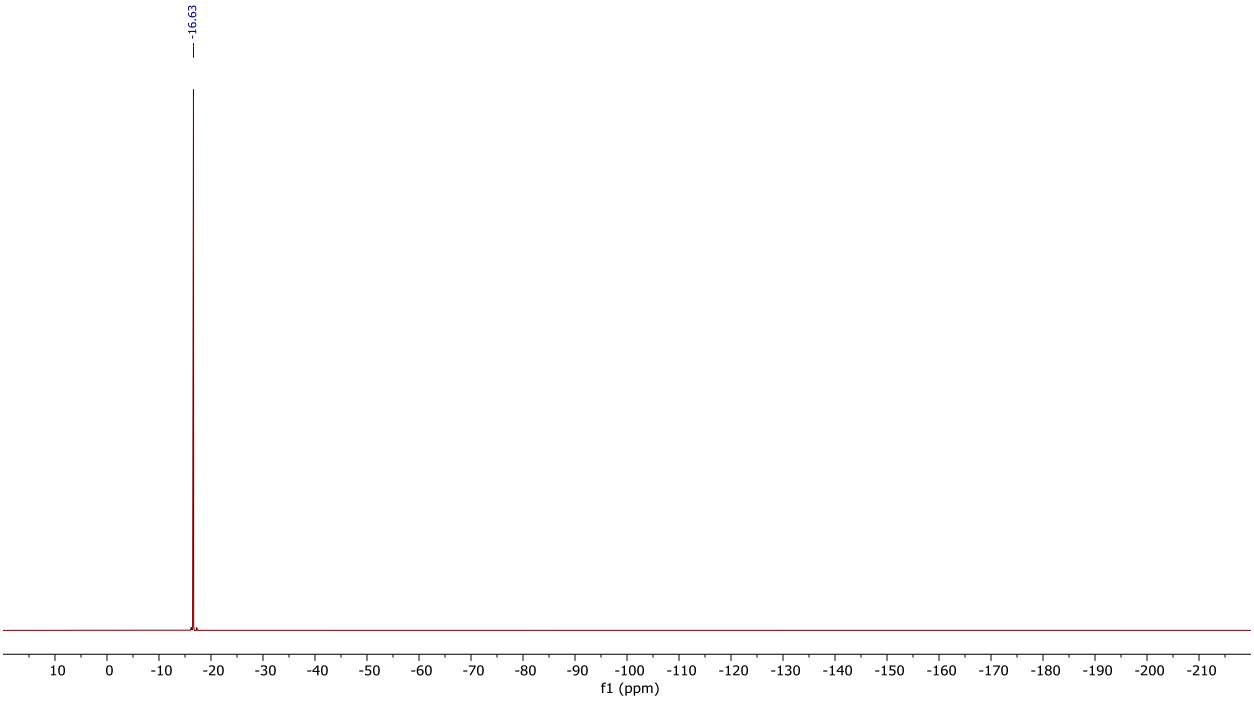

phenothiazine-10-carbonyl fluoride, (2.2ac)

^{1}H NMR Spectrum $CDCl_3$ (600 MHz)

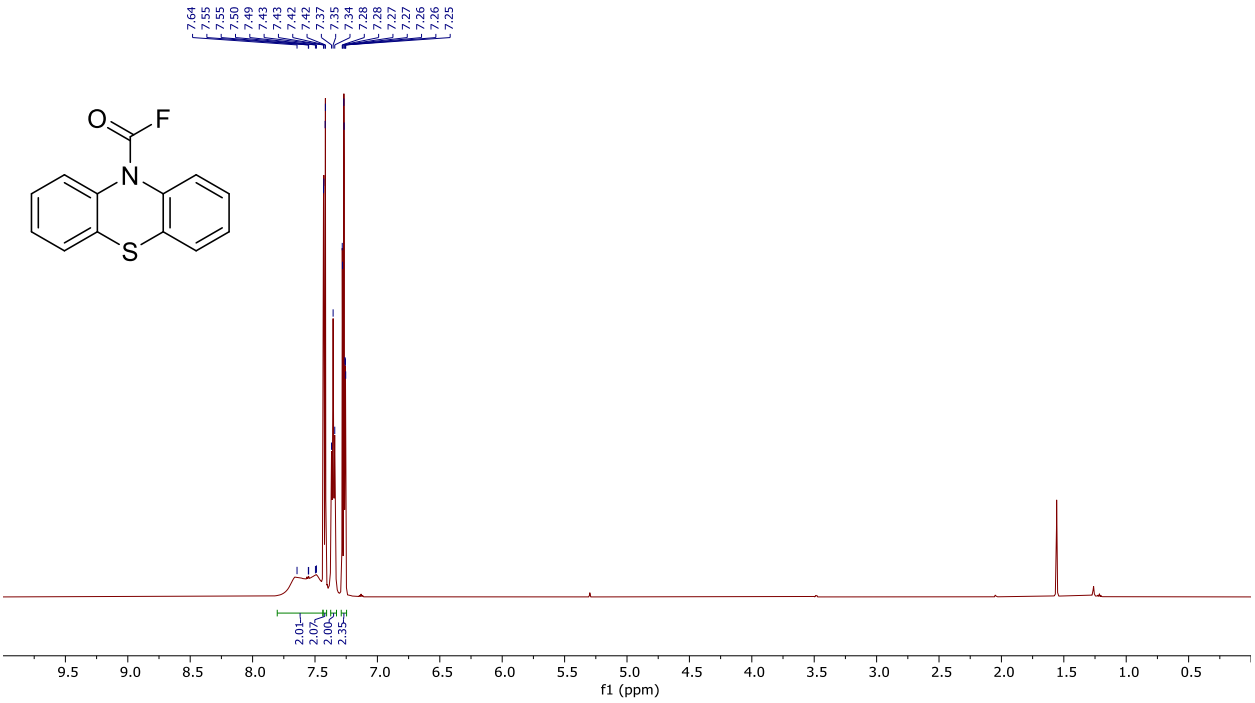

^{13}C NMR Spectrum $CDCl_3$ (151 MHz)

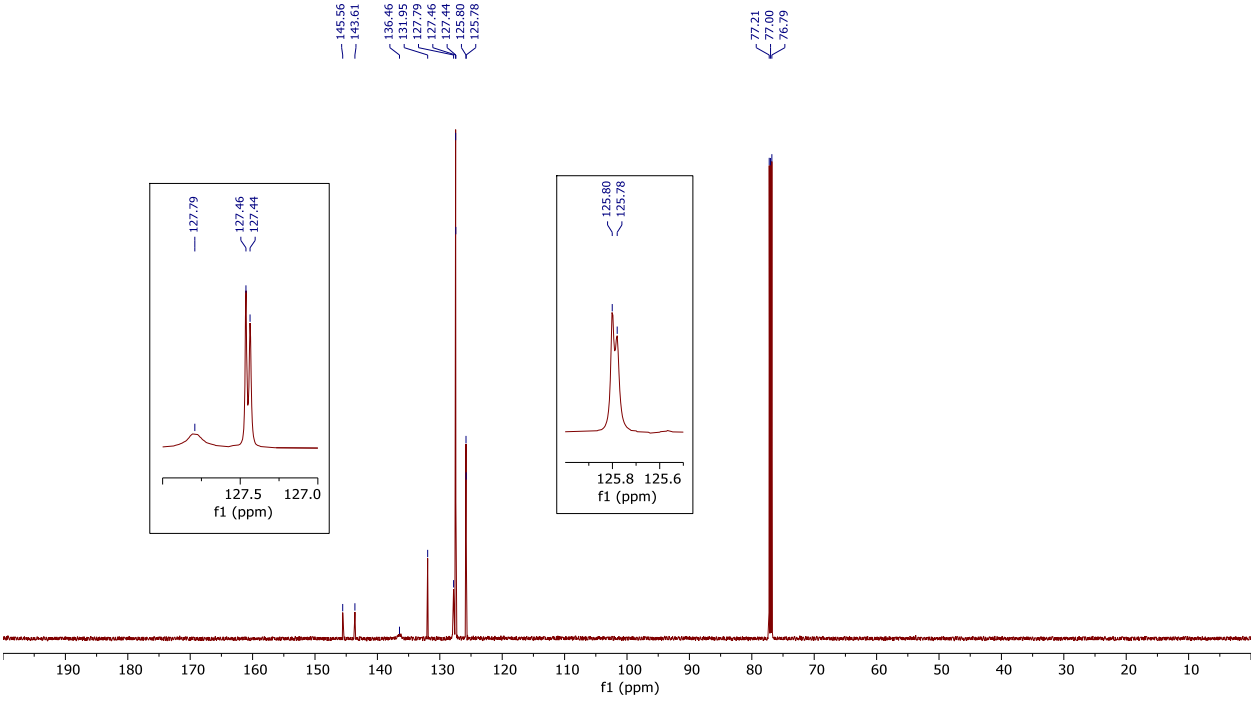

^{19}F {^{1}H} NMR Spectrum $CDCl_3$ (282 MHz)

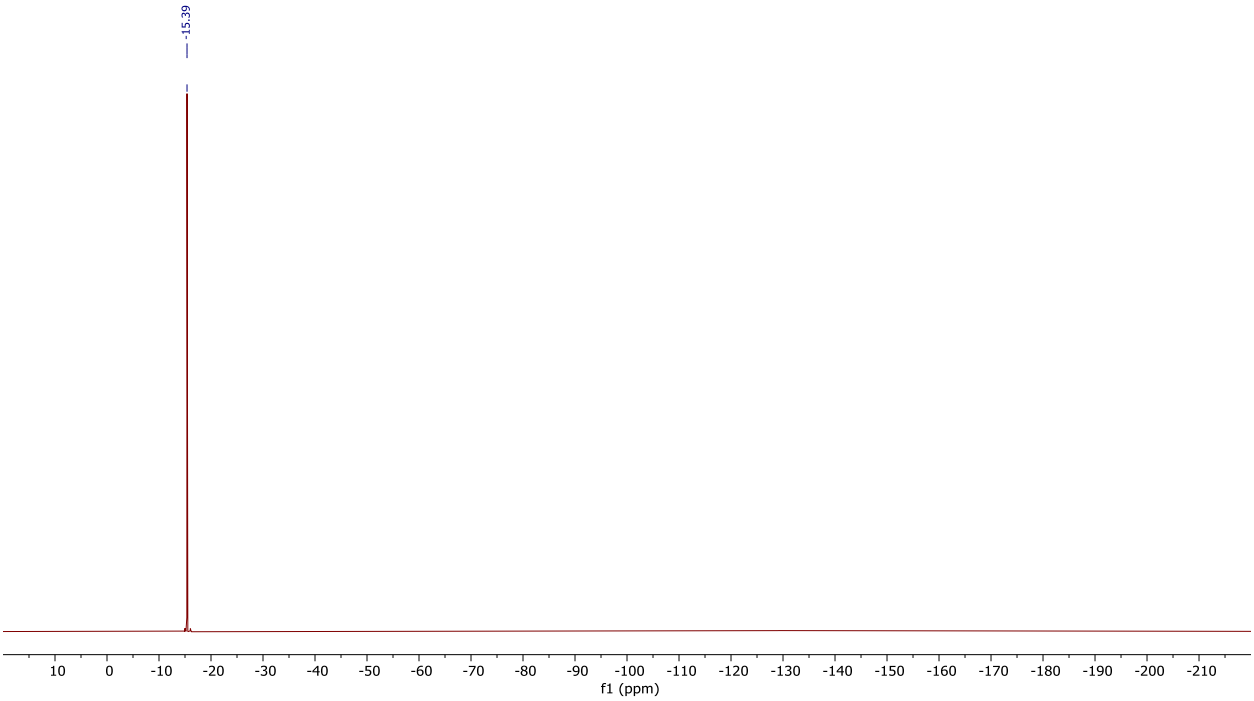

3-oxo-8-azabicyclo[3.2.1]octane-8-carbonyl fluoride, (2.2ab)

^{1}H NMR Spectrum $CDCl_3$ (600 MHz)

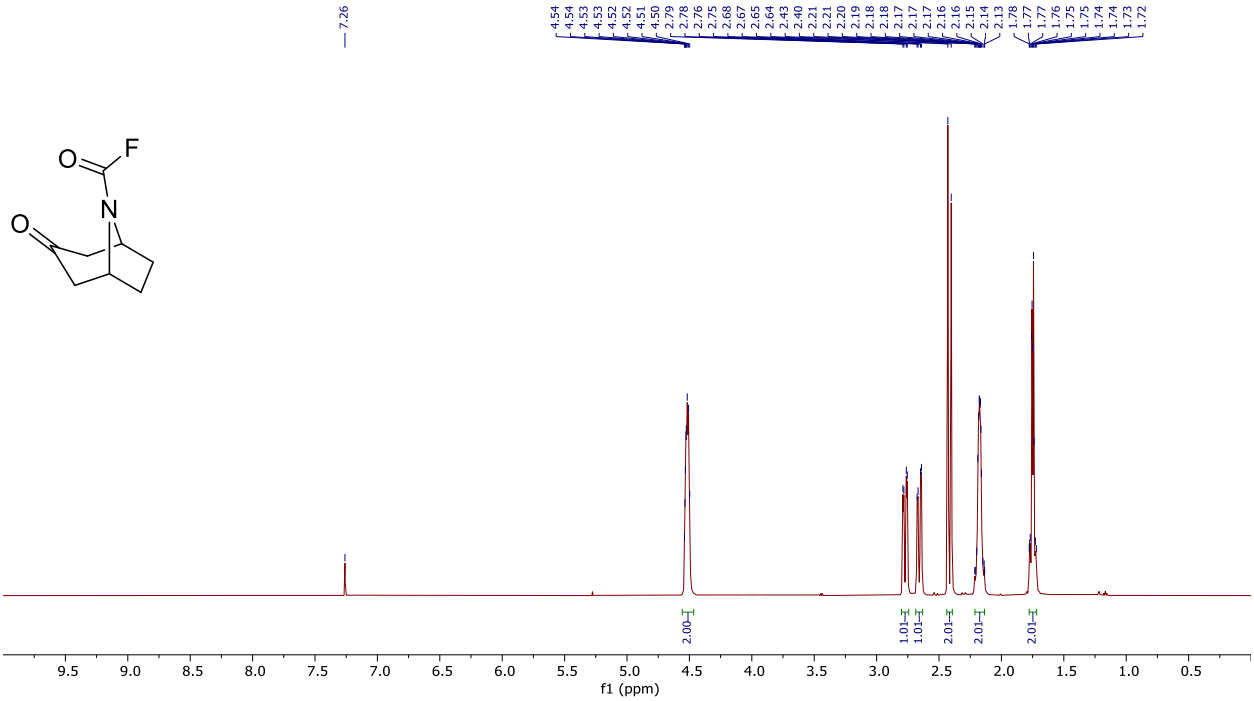

^{13}C NMR Spectrum $CDCl_3$ (151 MHz)

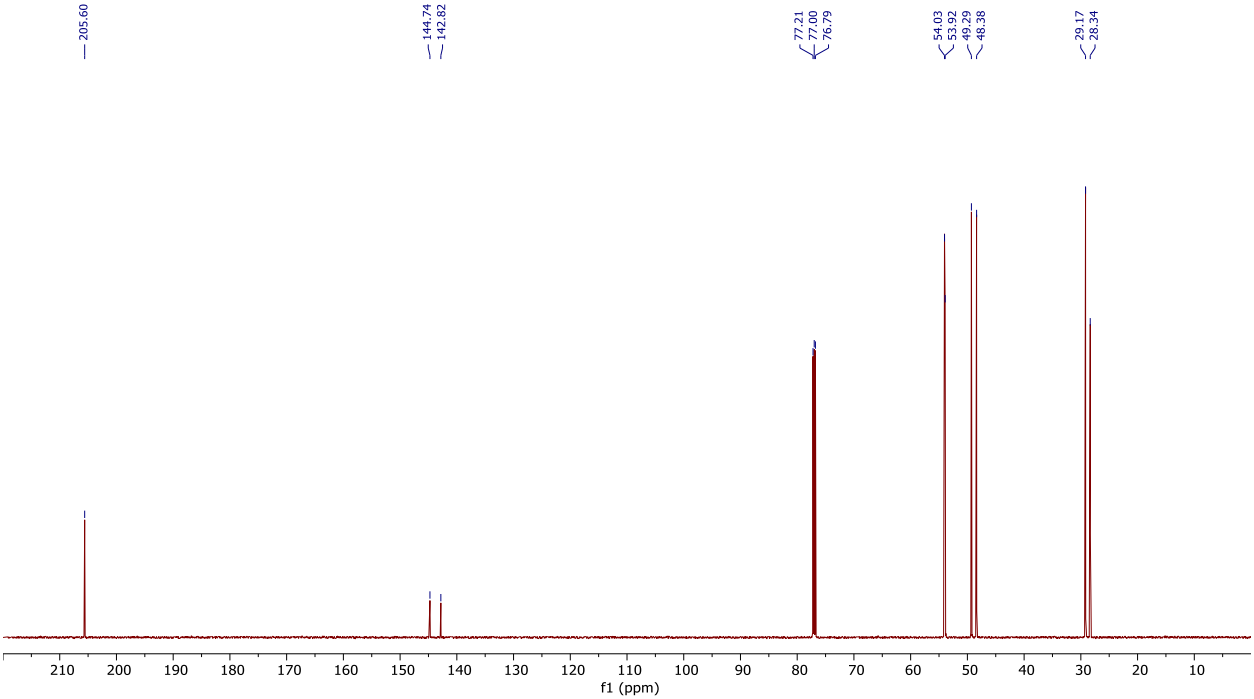

^{19}F {^{1}H} NMR Spectrum $CDCl_3$ (282 MHz)

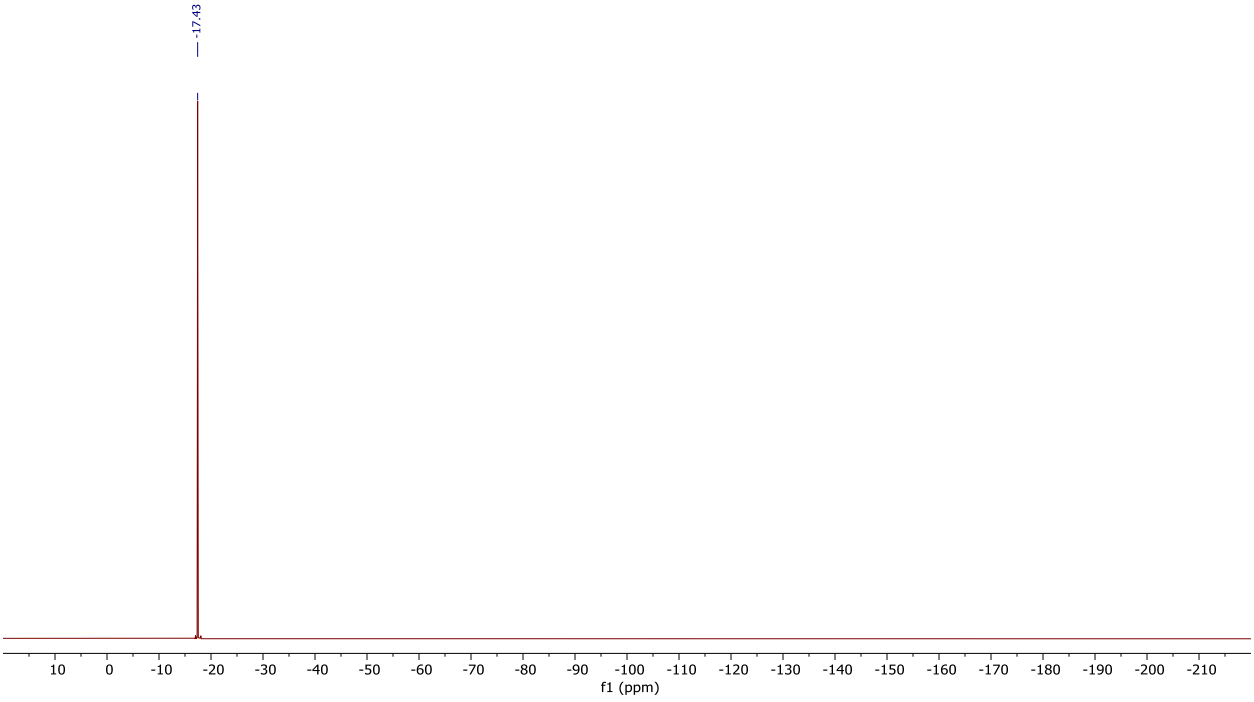

N-(3-methylbut-3-enyl)-*N*-phenyl-carbamoyl fluoride, (2.2l)

^{1}H NMR Spectrum $CDCl_3$ (600 MHz)

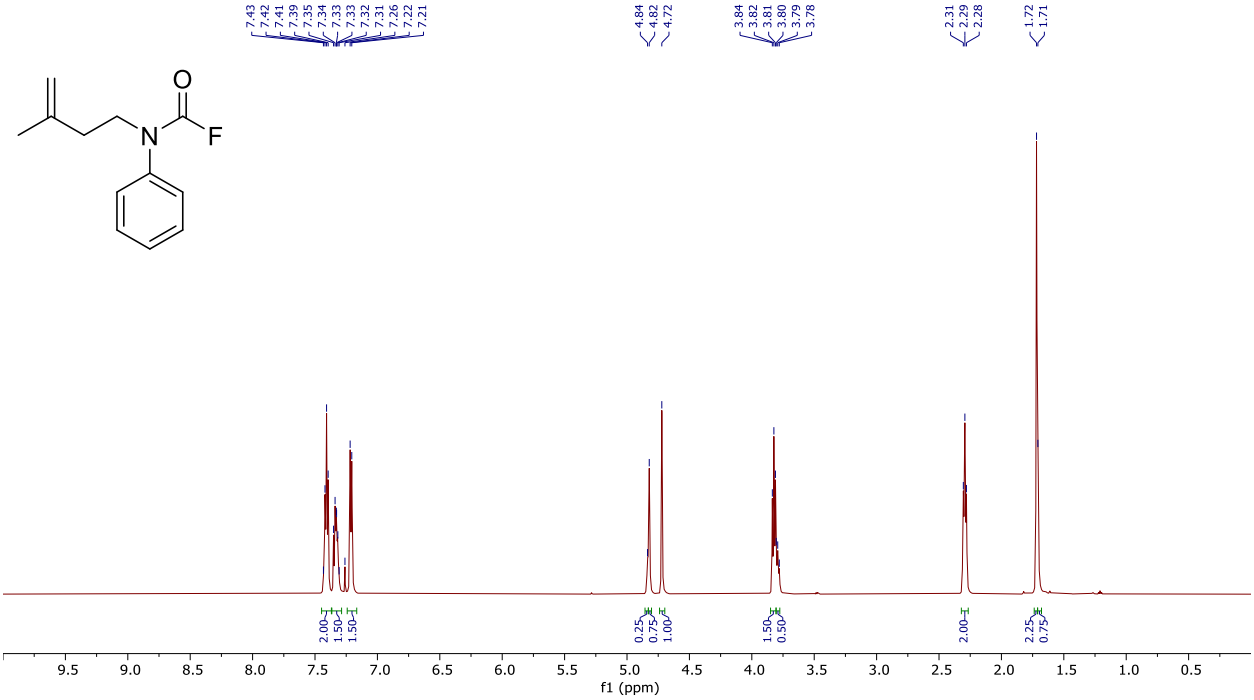

^{13}C NMR Spectrum $CDCl_3$ (151 MHz)

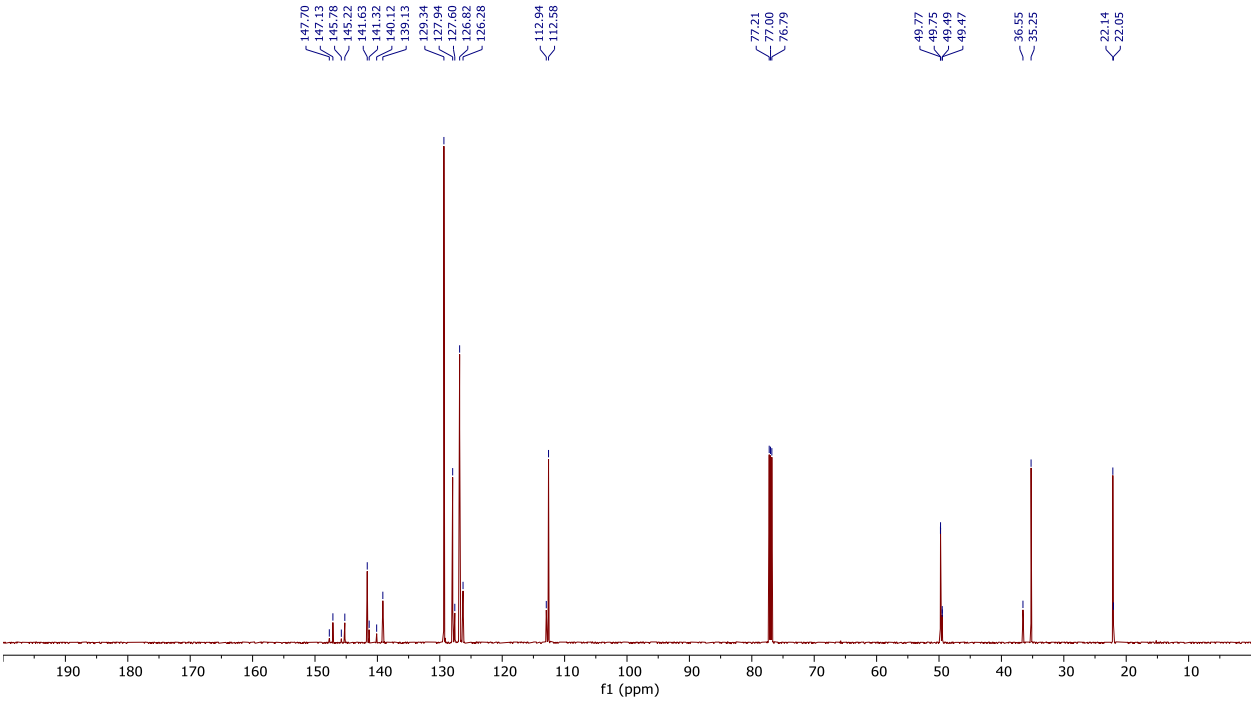

^{19}F {^{1}H} NMR Spectrum $CDCl_3$ (564 MHz)

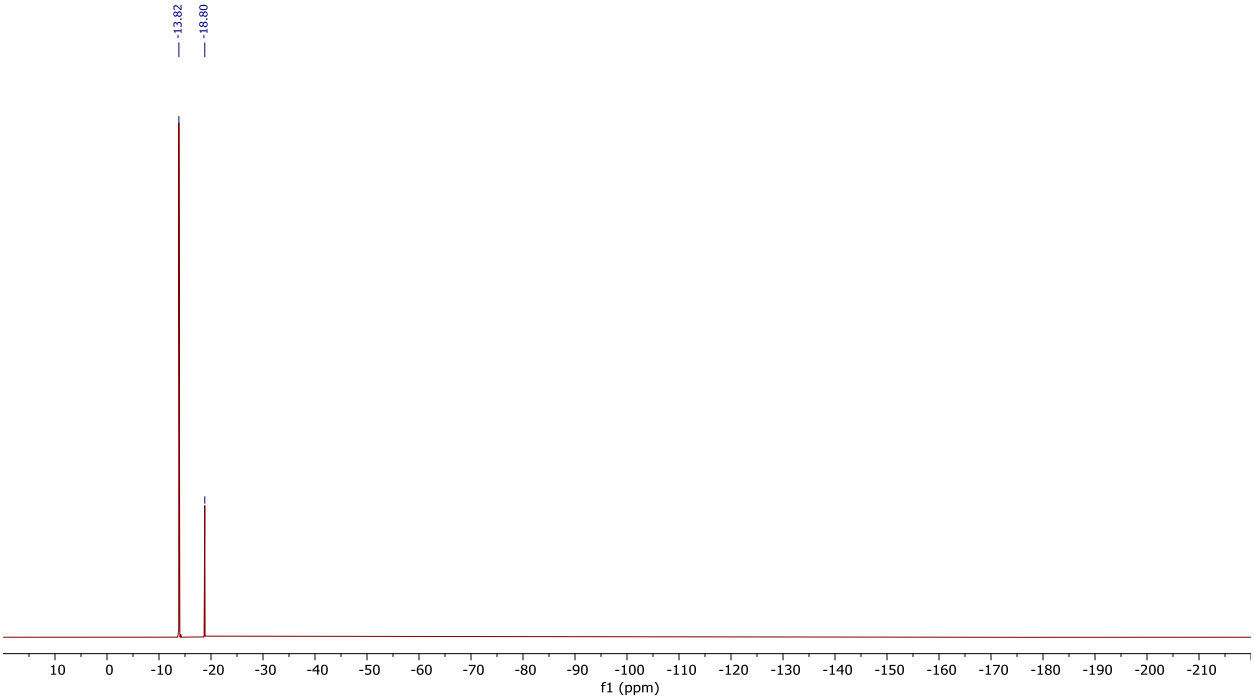

_N_-benzyl-_N_-(3-methylbut-3-enyl)carbamoyl fluoride, (2.2k)

^{1}H NMR Spectrum $CDCl_3$ (600 MHz)

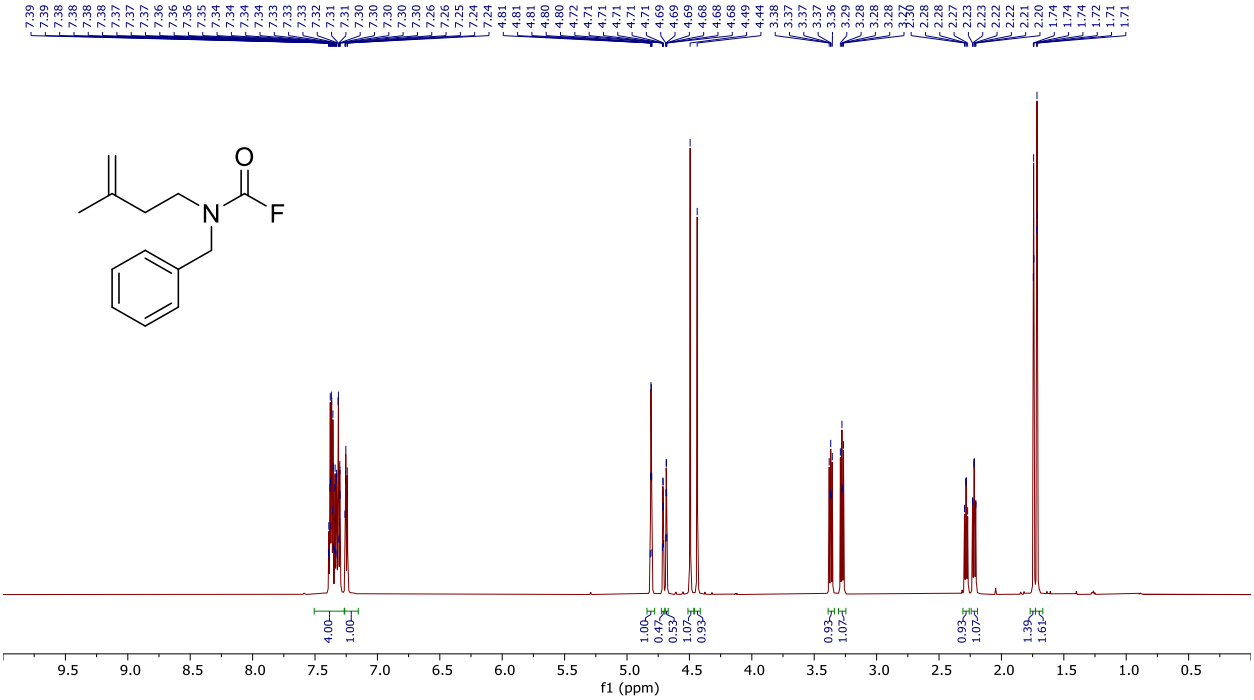

^{13}C NMR Spectrum $CDCl_3$ (151 MHz)

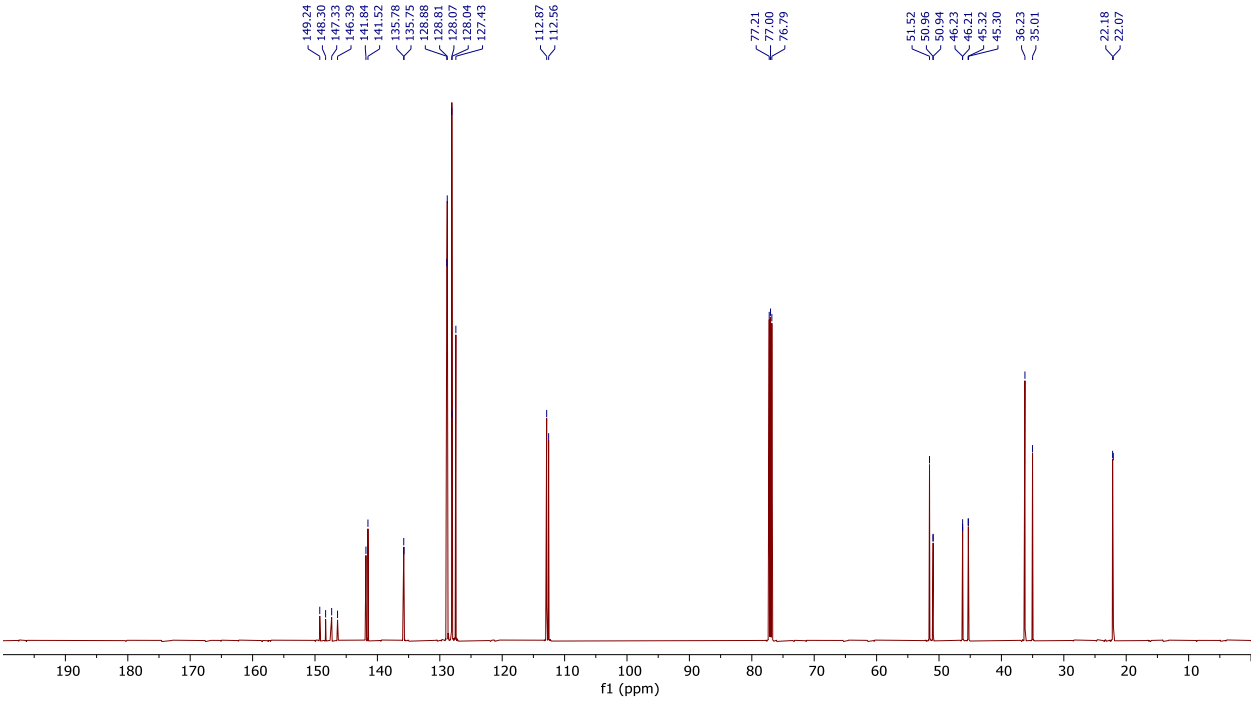

^{19}F {^{1}H} NMR Spectrum $CDCl_3$ (564 MHz)

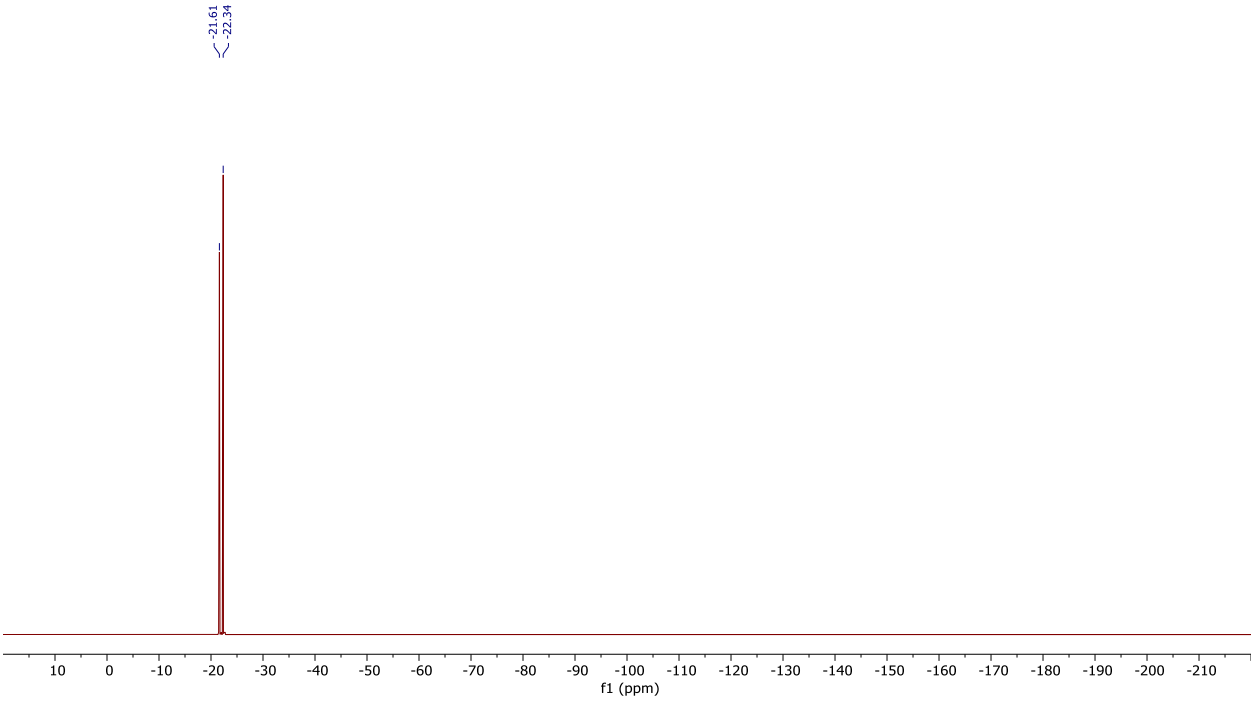

N-benzyl-*N*-(2-isopropenylphenyl)carbamoyl fluoride, (2.2s)

^{1}H NMR Spectrum $CDCl_3$ (600 MHz)

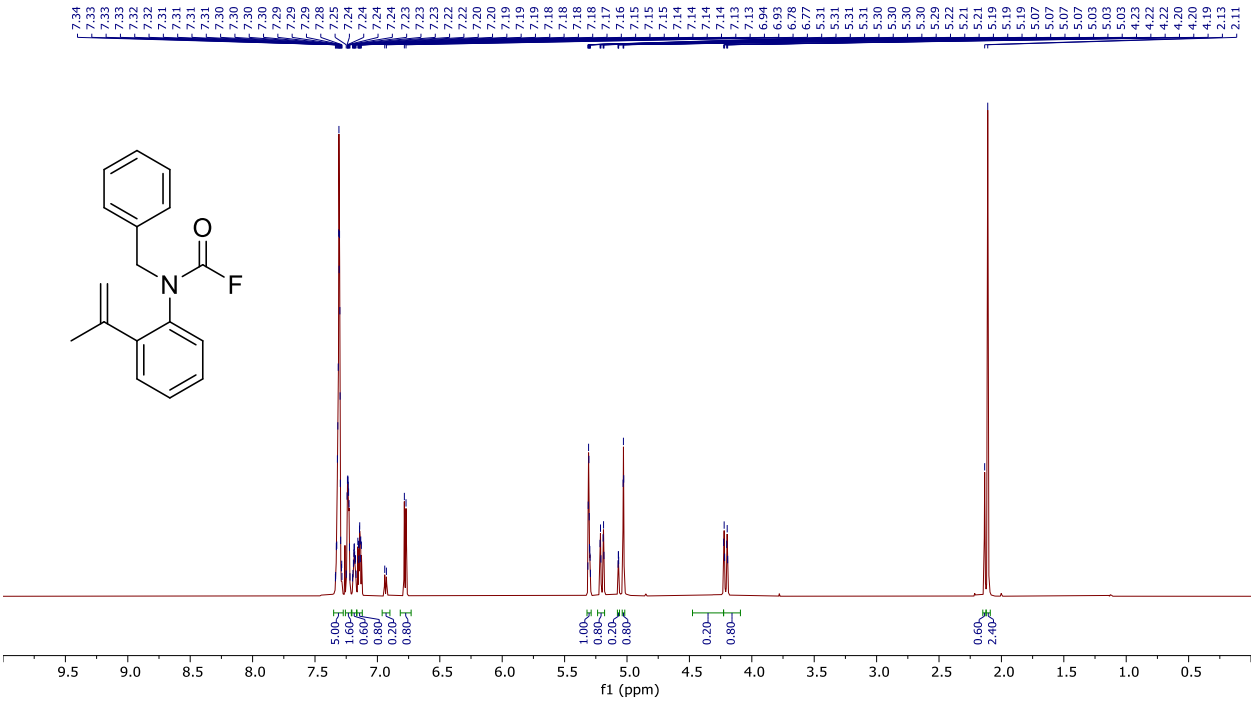

^{13}C NMR Spectrum $CDCl_3$ (151 MHz)

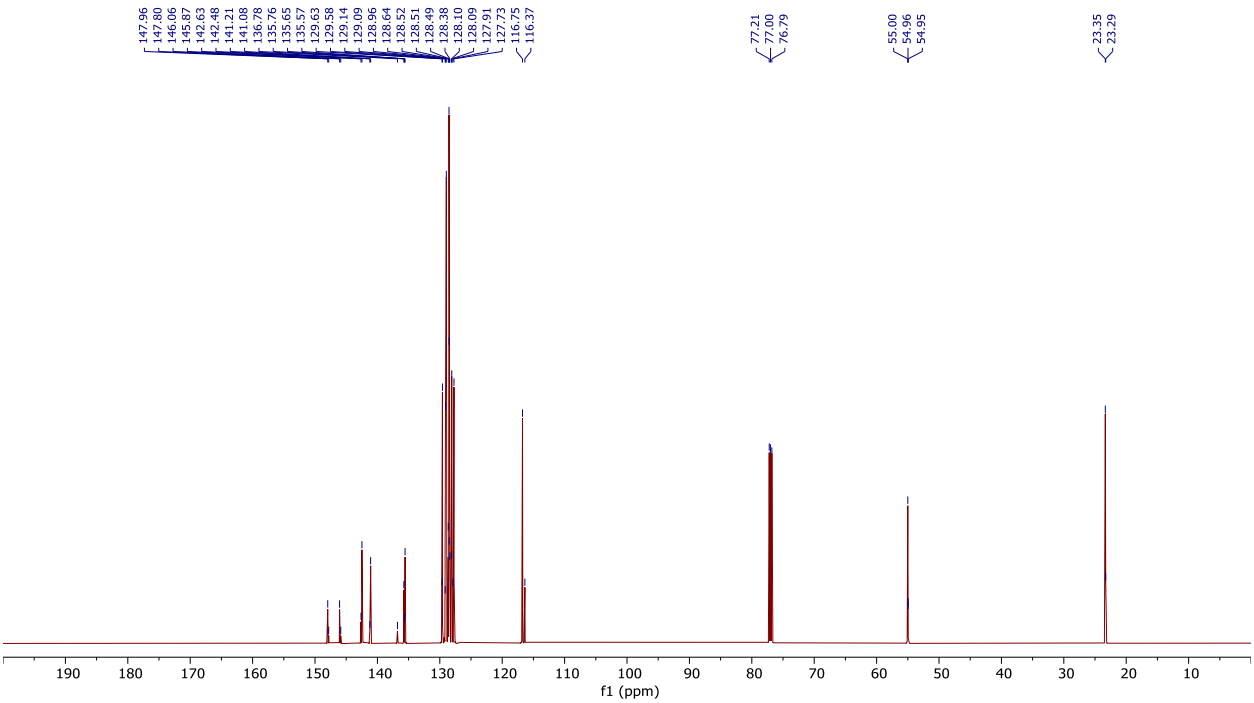

^{19}F {^{1}H} NMR Spectrum $CDCl_3$ (564 MHz)

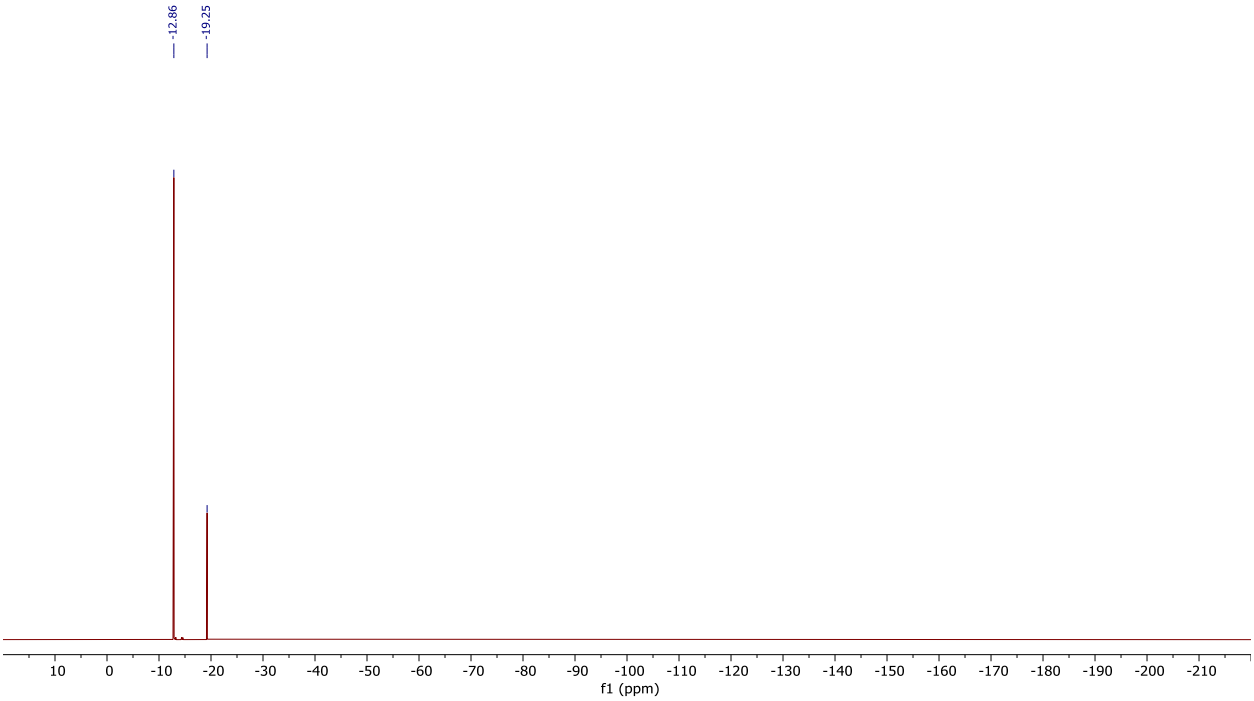

_N_-phenyl-_N_-[[5-[3-(trifluoromethyl)phenyl]-1,2,4-oxadiazol-3-yl]methyl]carbamoyl fluoride, (2.2ae)

^{1}H NMR Spectrum $CDCl_3$ (600 MHz)

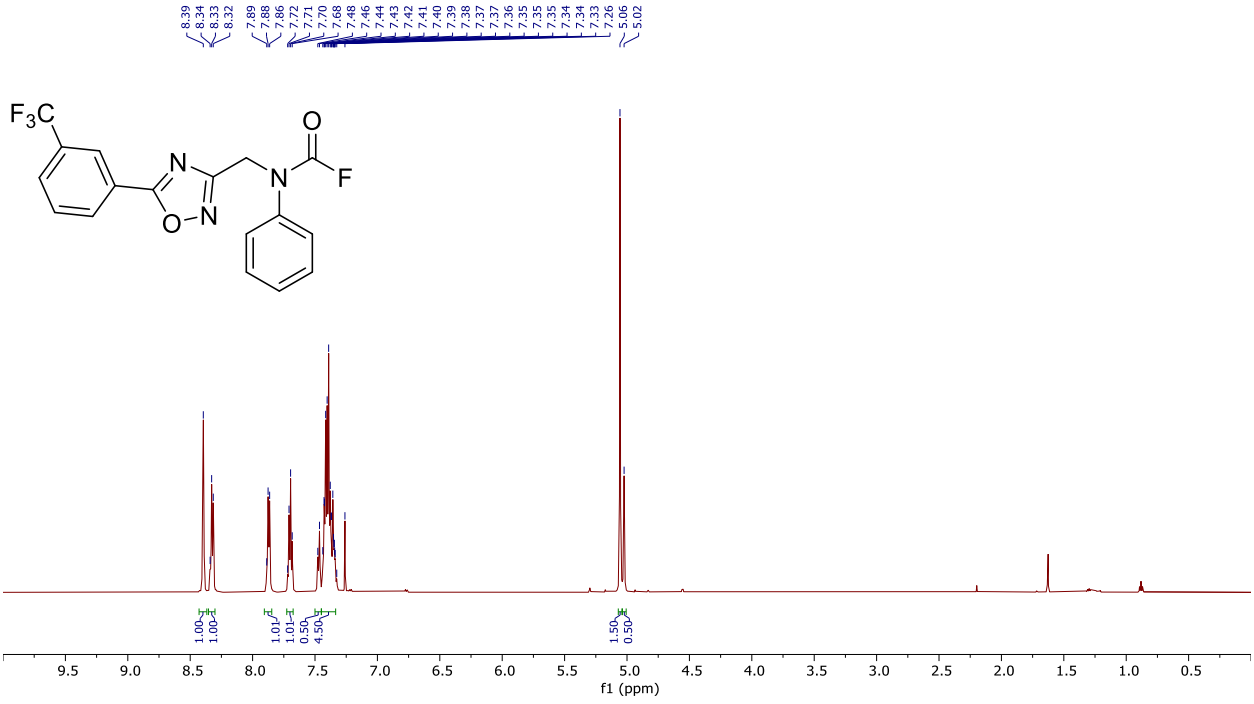

^{13}C NMR Spectrum $CDCl_3$ (151 MHz)

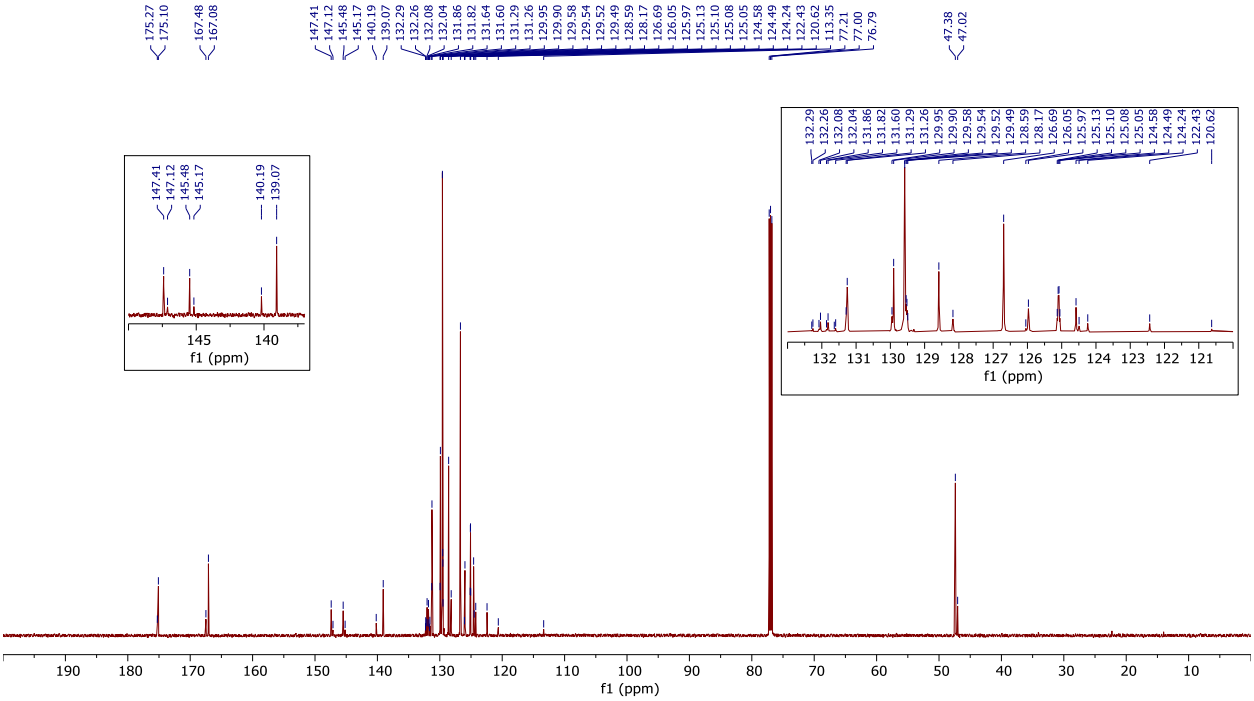

^{19}F {^{1}H} NMR Spectrum $CDCl_3$ (564 MHz)

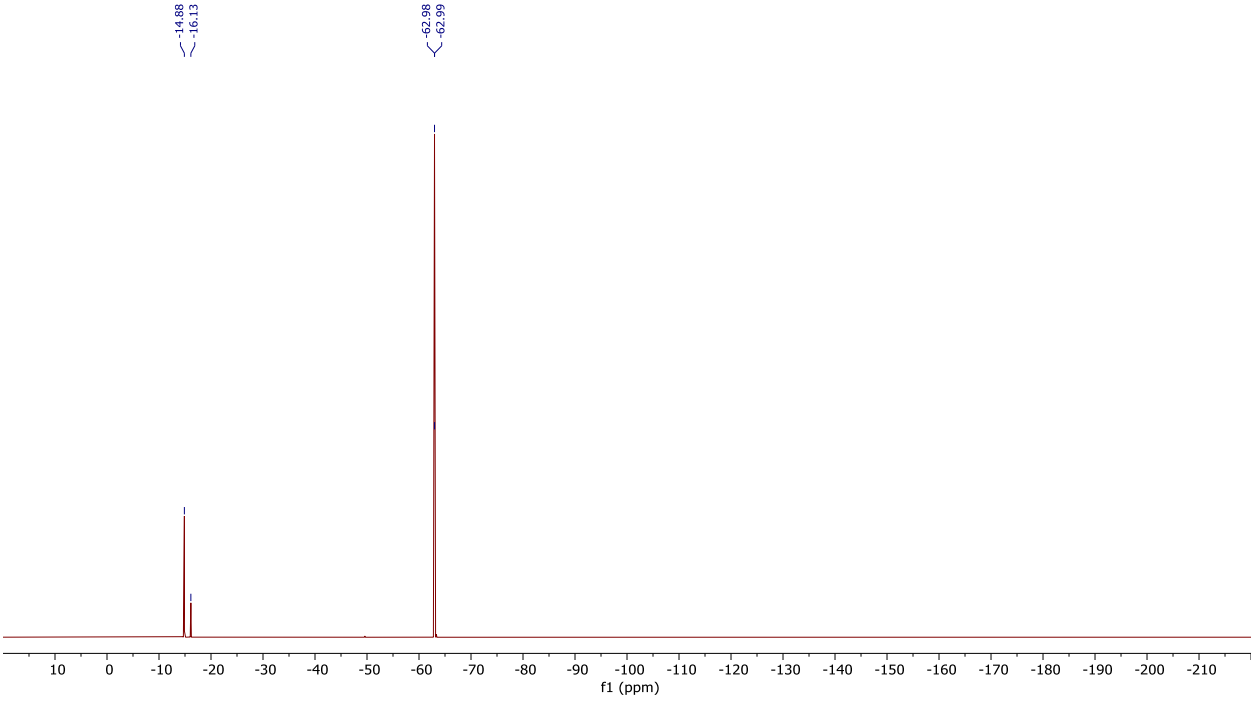

Chapter 3 NMR Spectra

Carbamoyl Pd–Cl, (3.10)

^{1}H NMR Spectrum $CDCl_3$ (400 MHz)

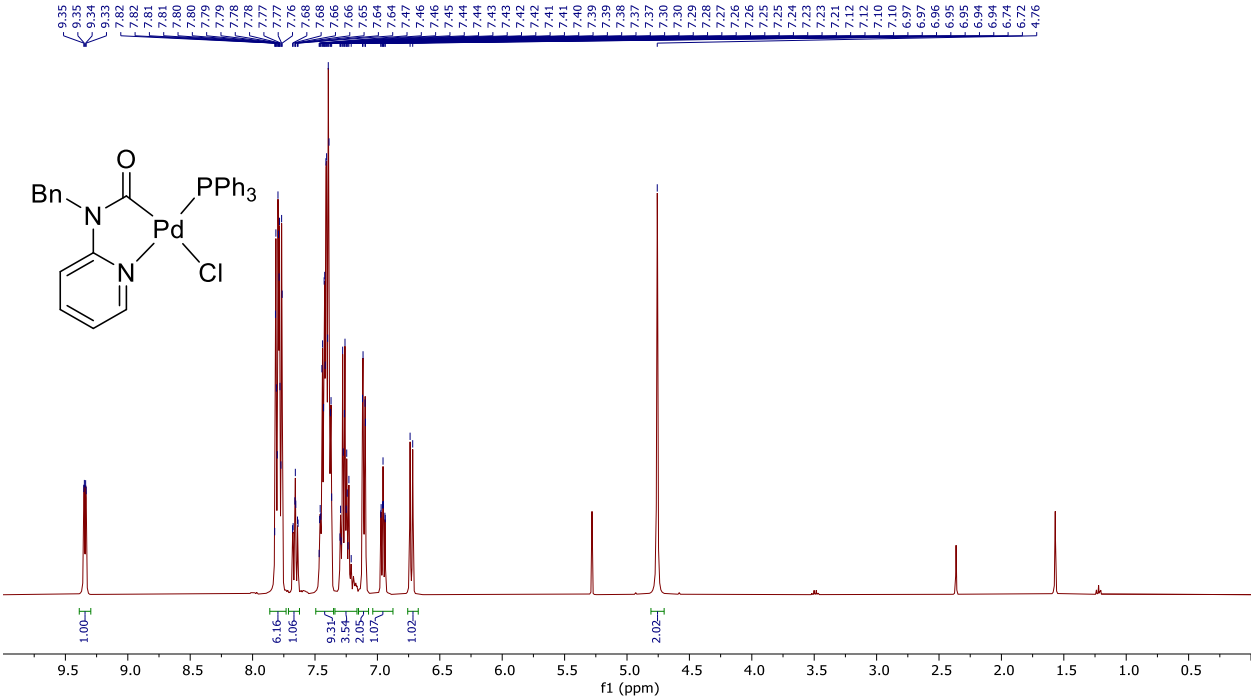

^{13}C NMR Spectrum $CDCl_3$ (101 MHz)

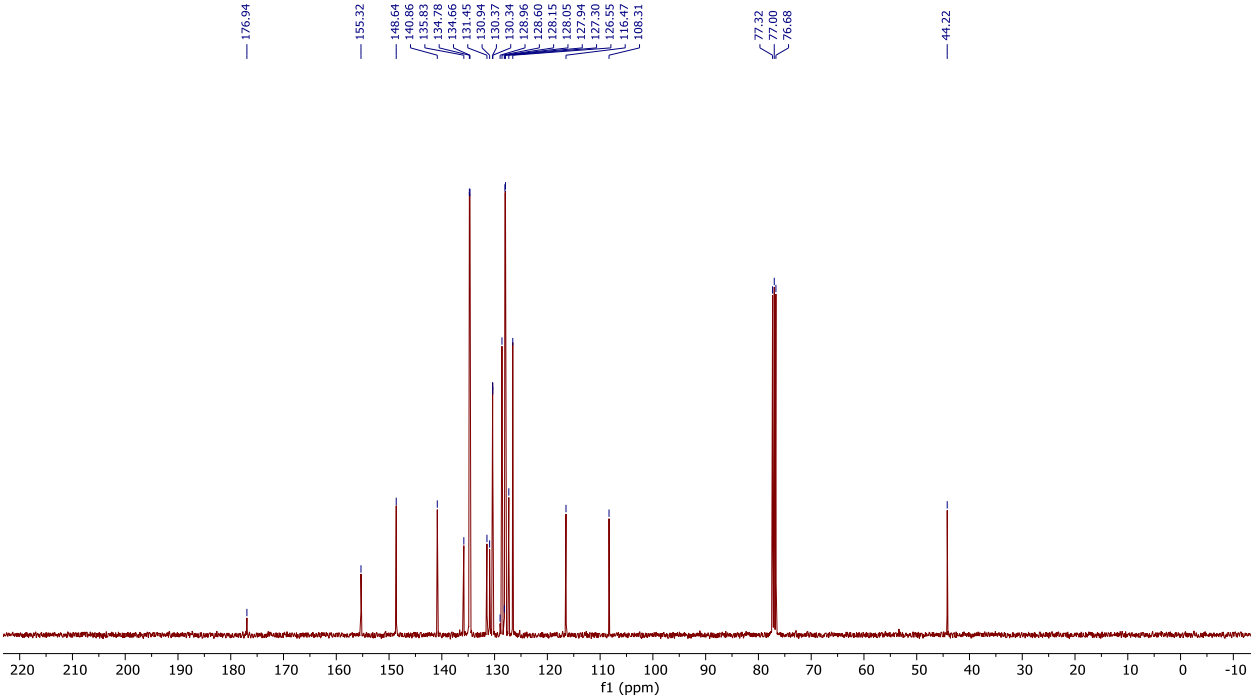

^{31}P {^{1}H} NMR Spectrum $CDCl_3$ (101 MHz)

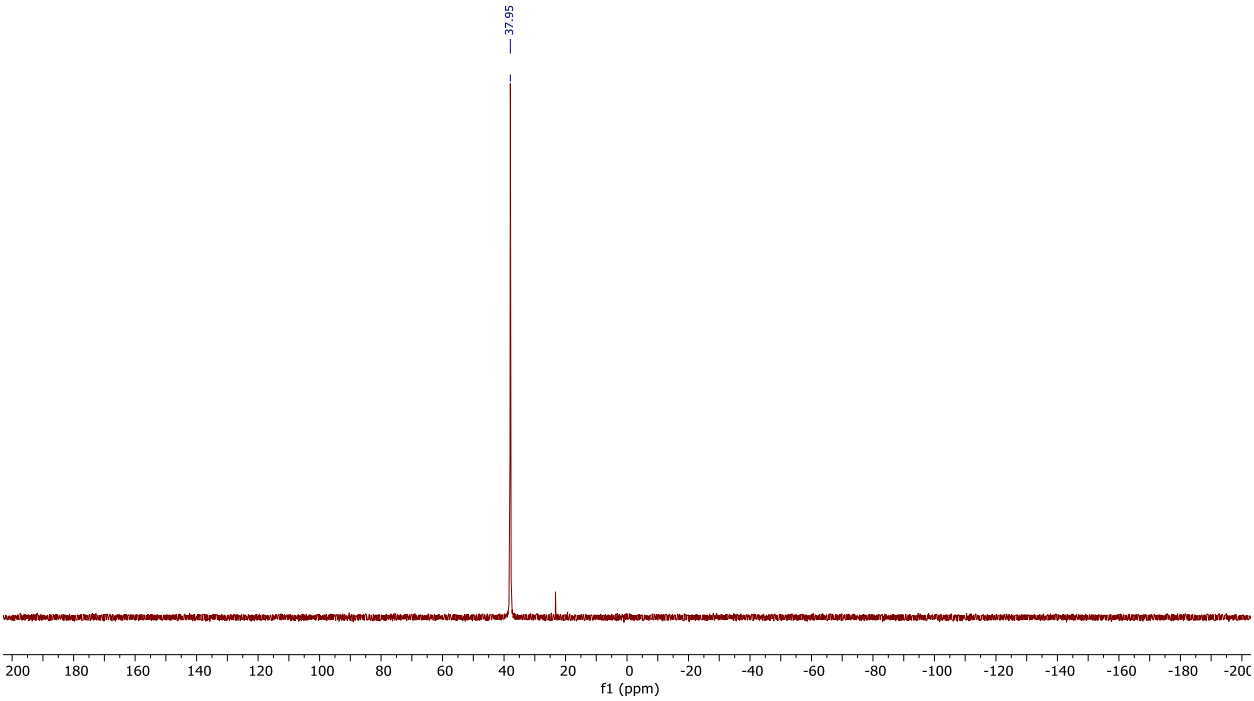

Carbamoyl Pd–I, (3.12)

^{1}H NMR Spectrum $CDCl_3$ (300 MHz)

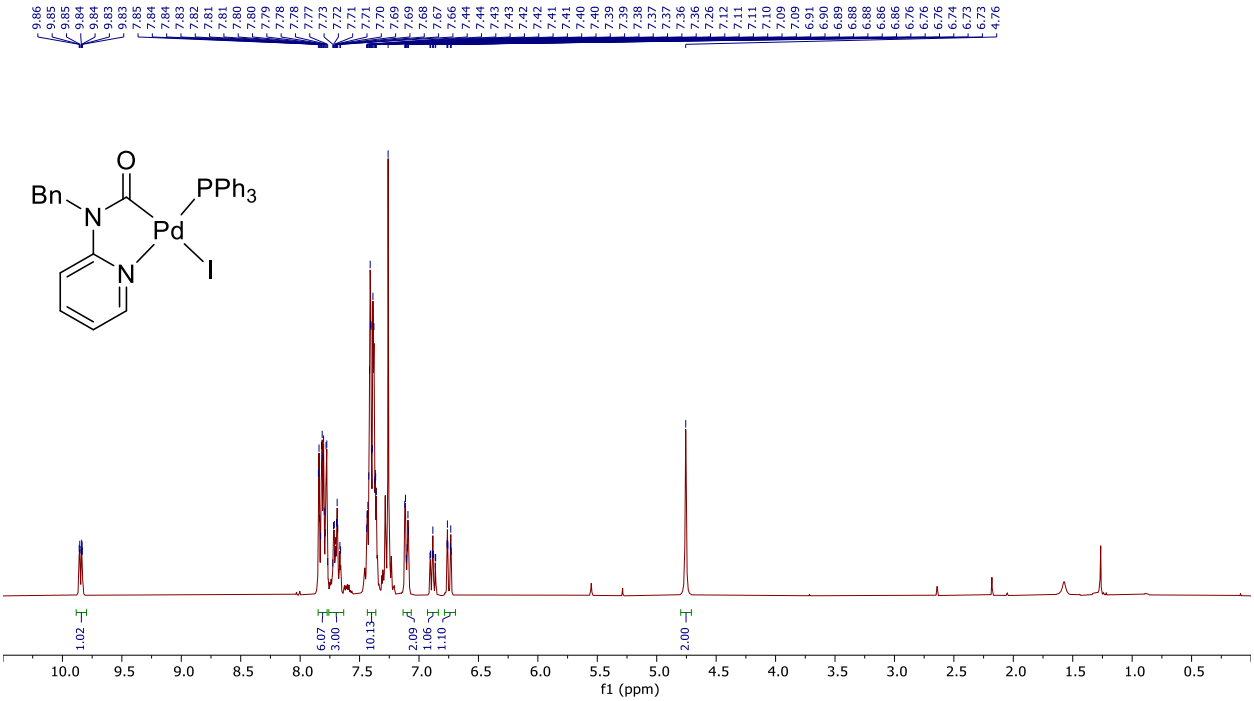

^{13}C NMR Spectrum $CDCl_3$ (75 MHz)

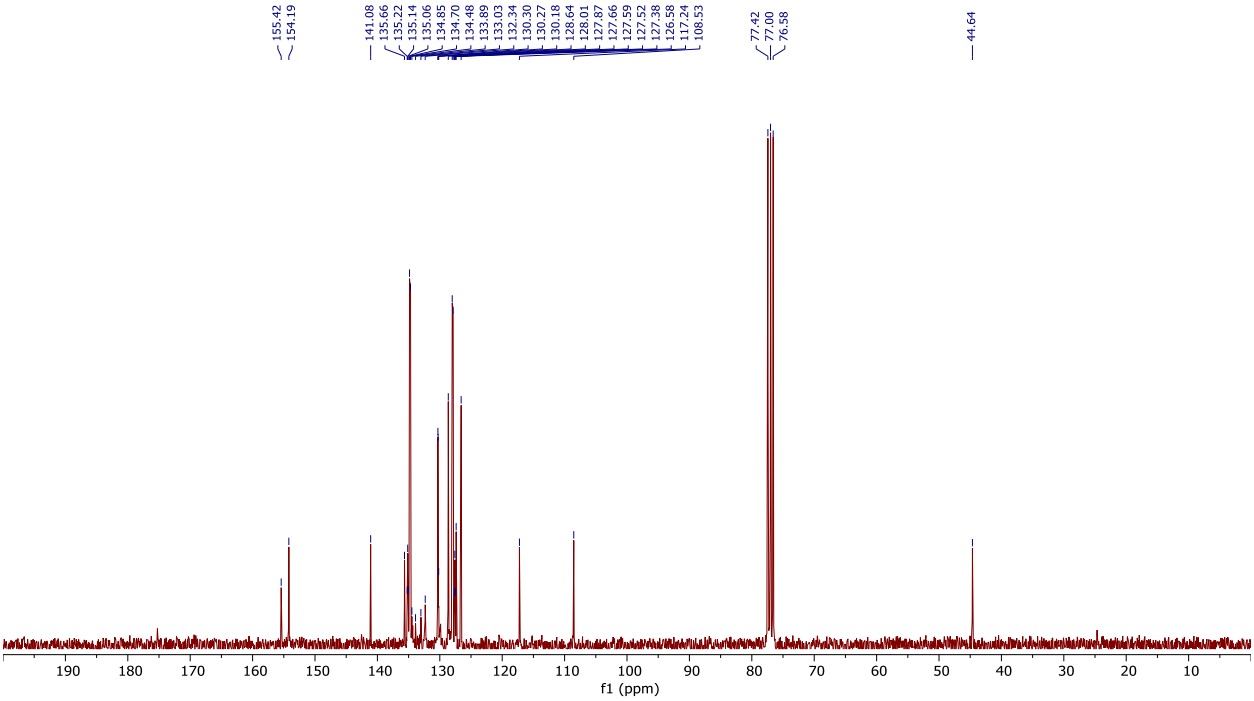

^{31}P {^{1}H} NMR Spectrum $CDCl_3$ (121 MHz)

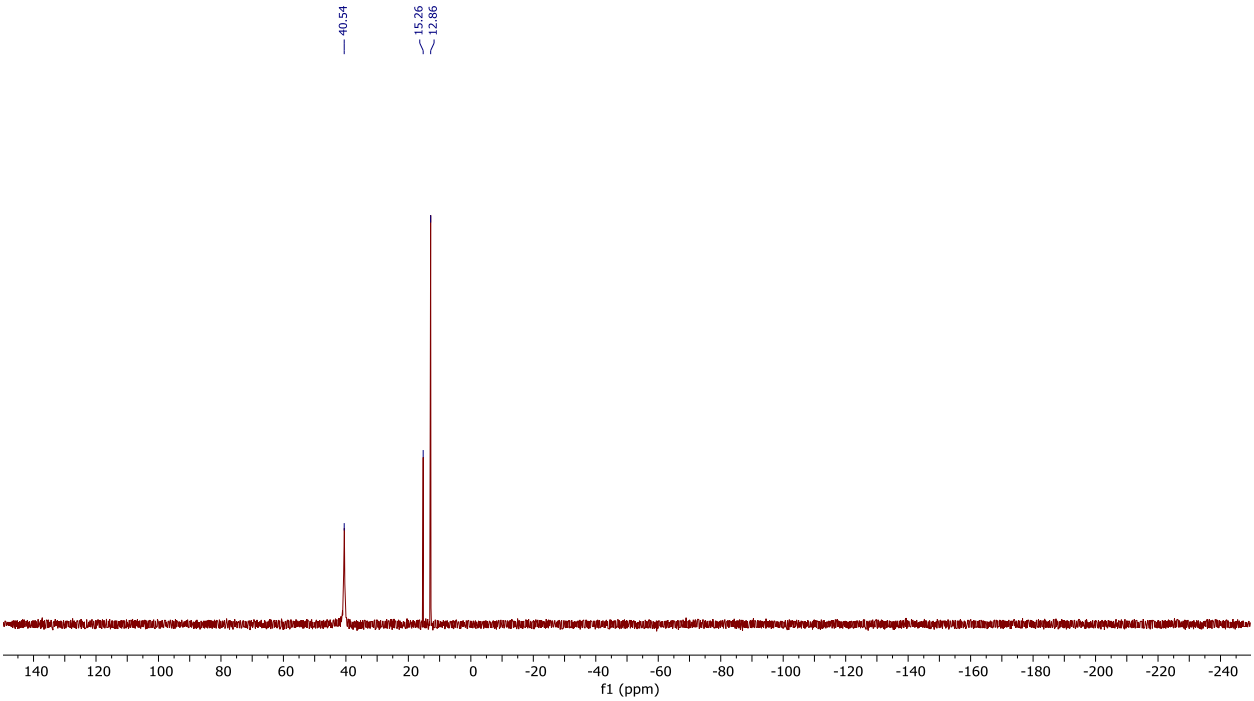

Carbamoyl Pd–F, (3.4)

^{1}H NMR Spectrum $CDCl_3$ (700 MHz)

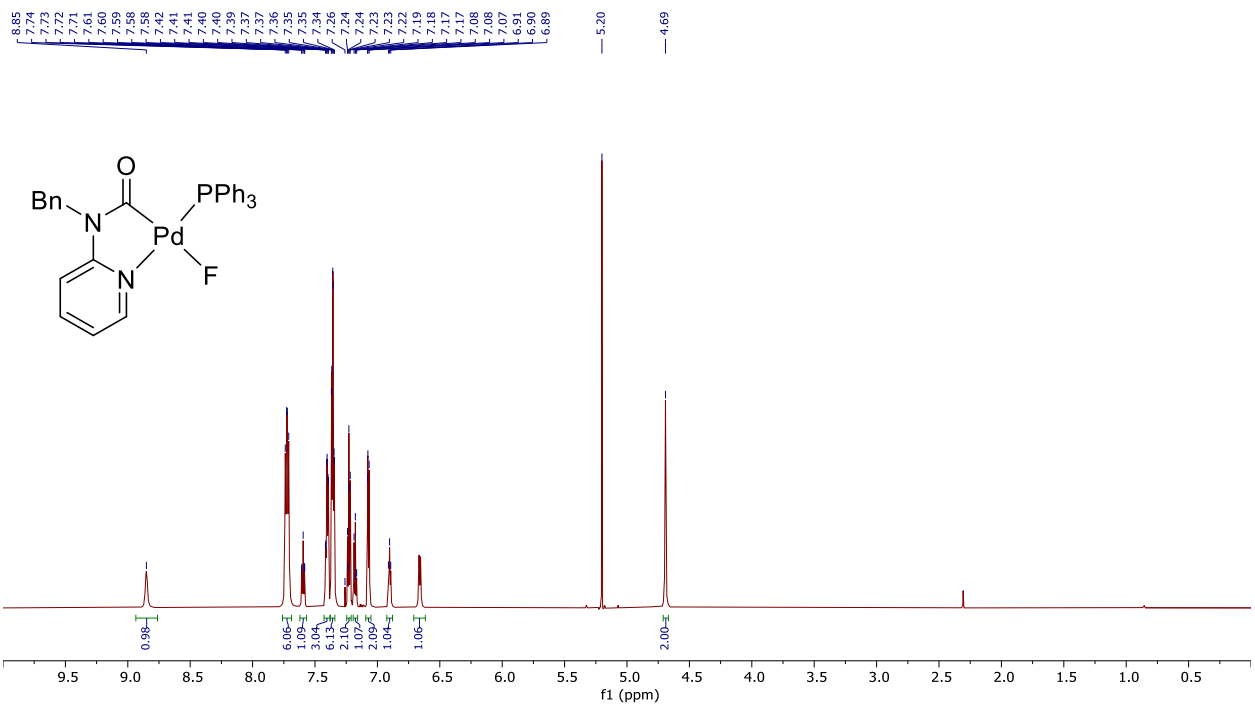

^{13}C NMR Spectrum $CDCl_3$ (176 MHz)

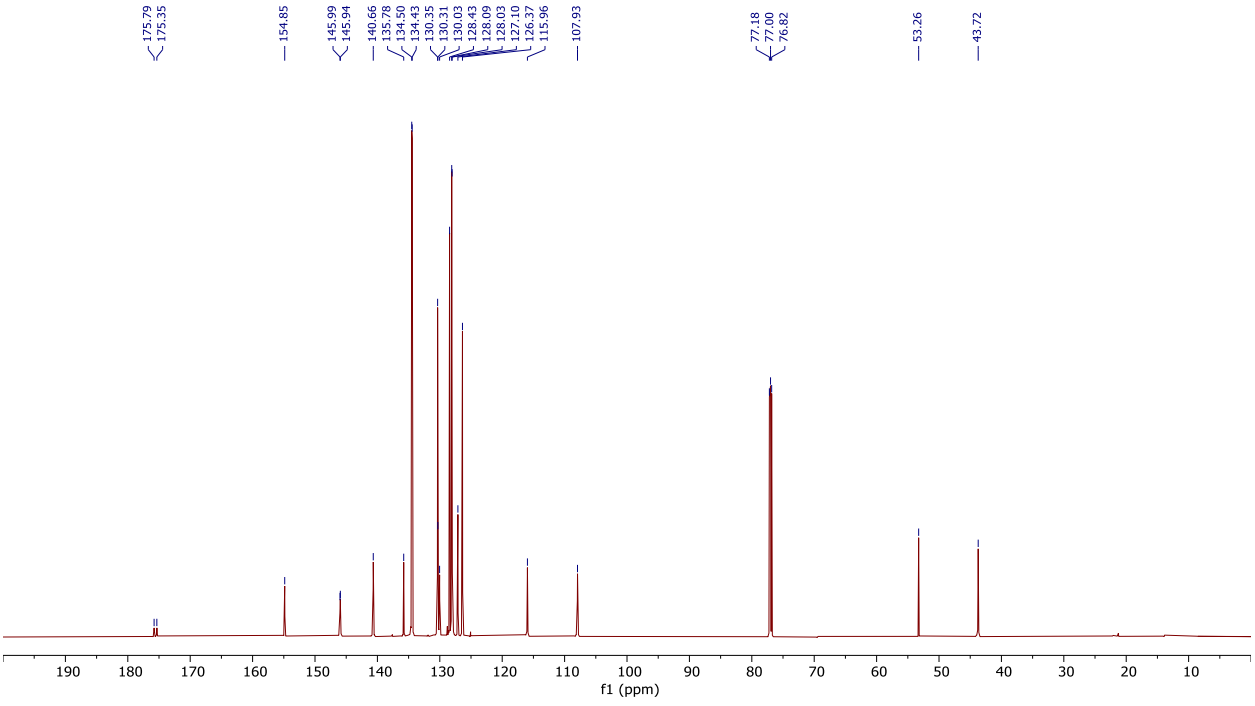

^{19}F {^{1}H} NMR Spectrum $CDCl_3$ (659 MHz)

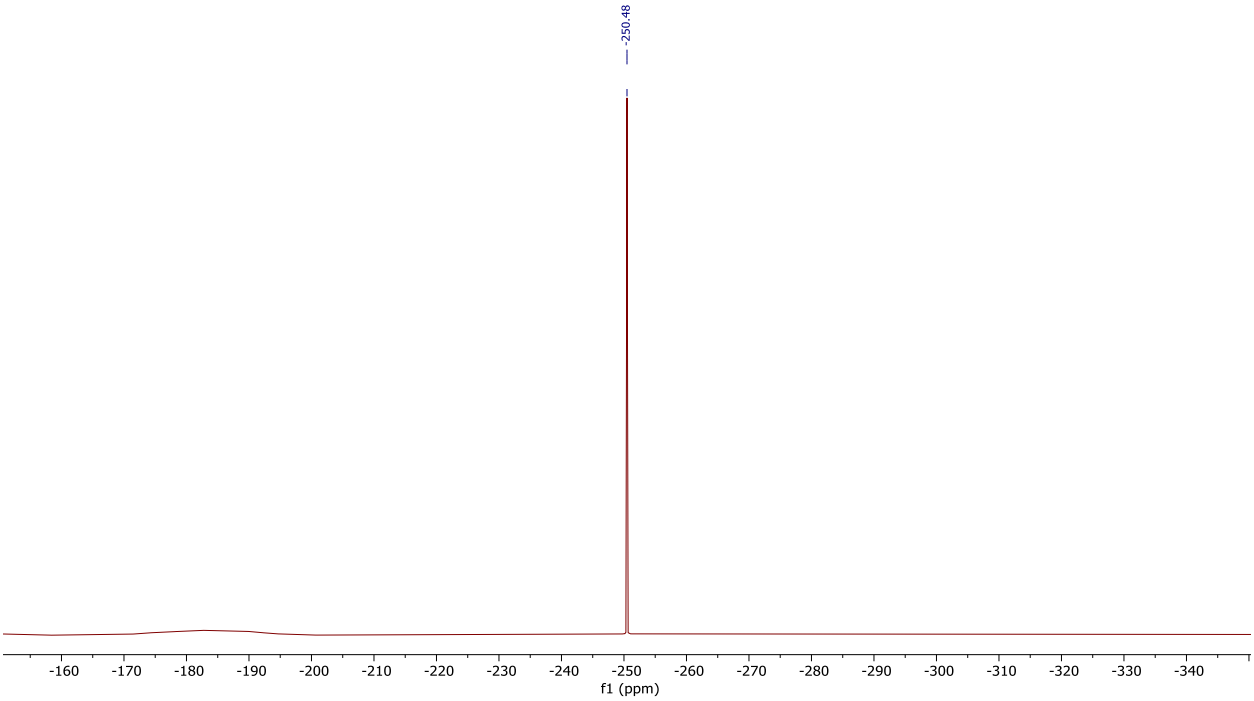

^{31}P {^{1}H} NMR Spectrum $CDCl_3$ (121 MHz)

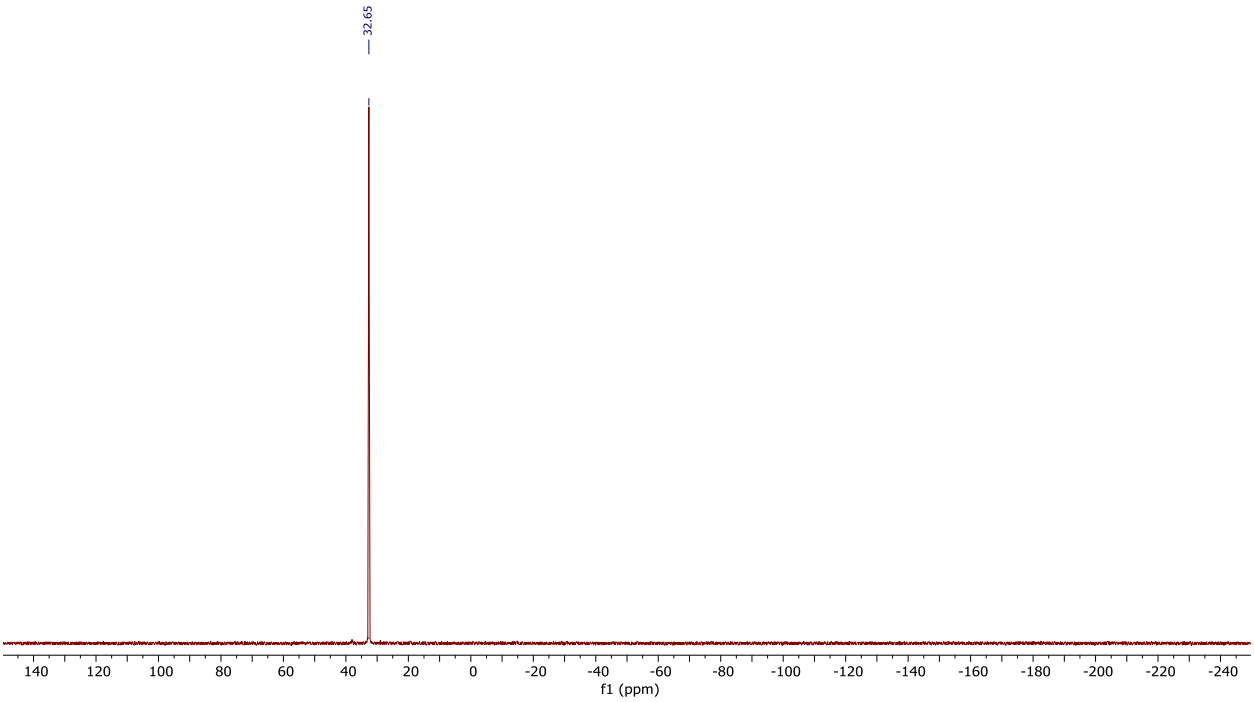

^{1}H-^{1}H COSY NMR Spectrum $CDCl_3$ (700 MHz)

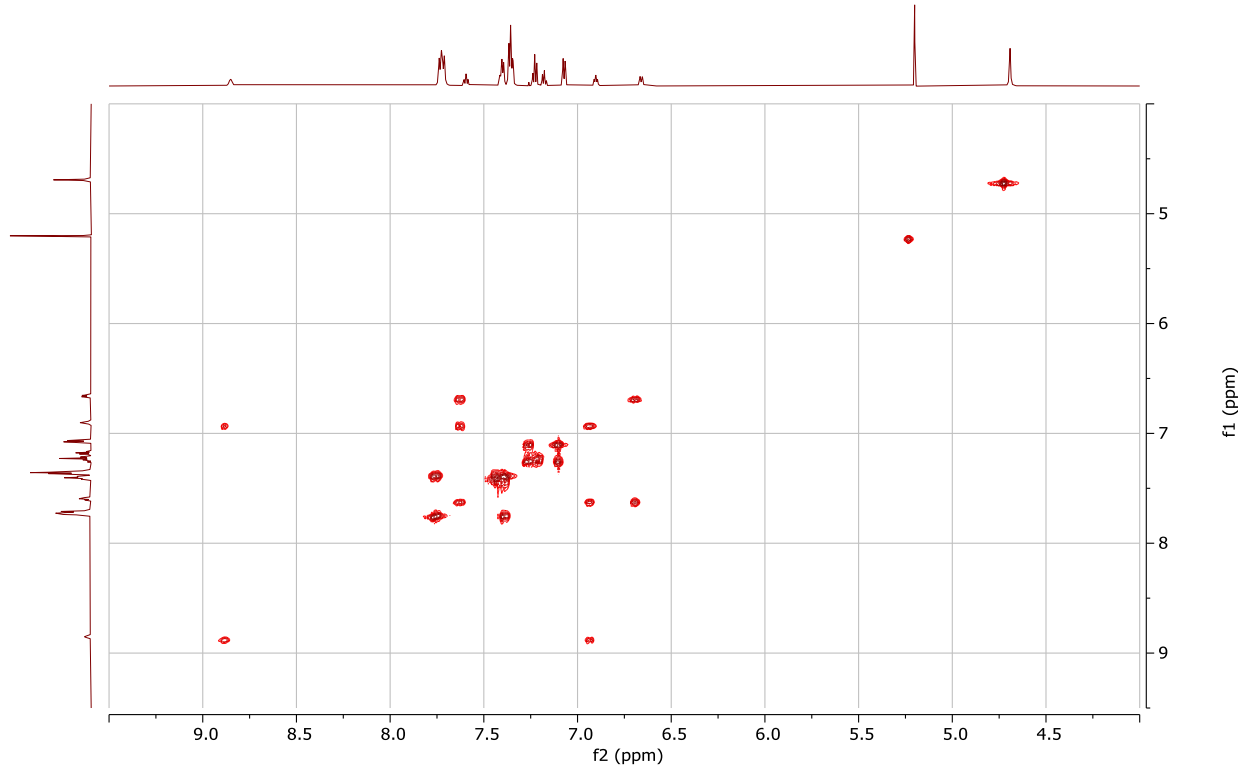

^{1}H-^{13}C HSQC NMR Spectrum $CDCl_3$ (700 MHz)

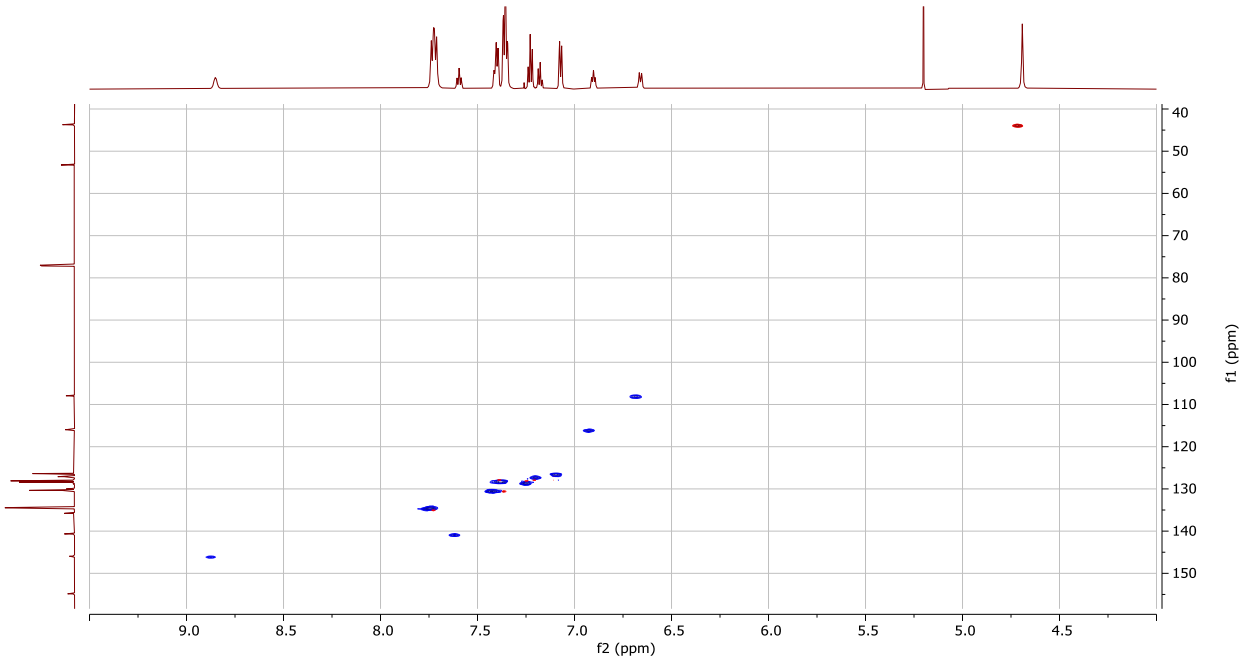

^{1}H-^{13}C HSQC NMR Spectrum $CDCl_3$ (700 MHz)

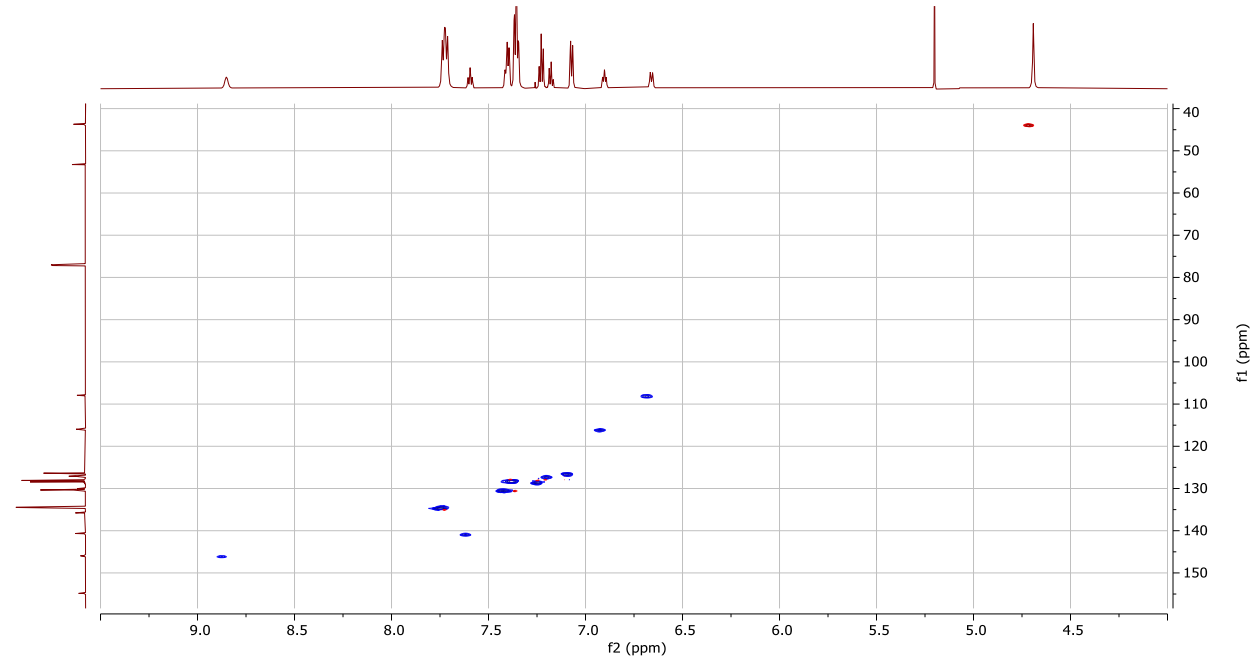

^{1}H-^{13}C HMBC NMR Spectrum $CDCl_3$ (700 MHz)

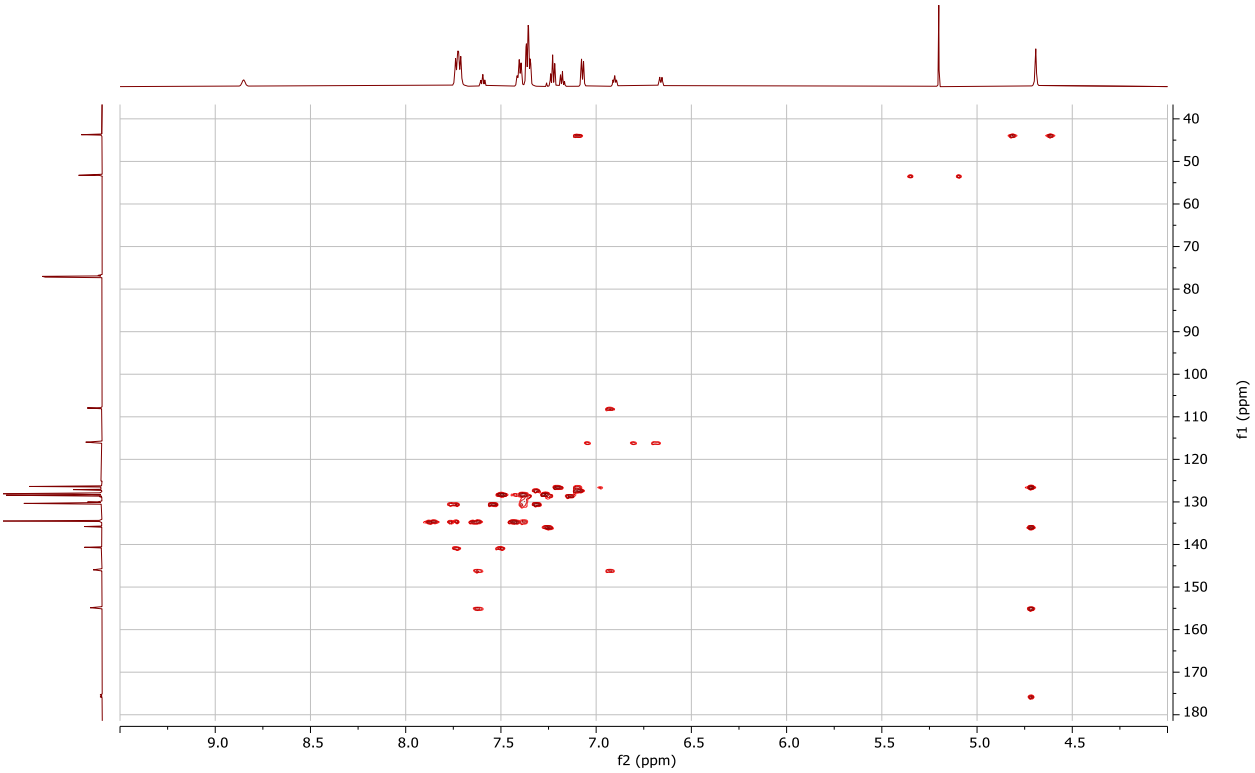

^{1}H-^{15}N HMBC NMR Spectrum $CDCl_3$ (700 MHz)

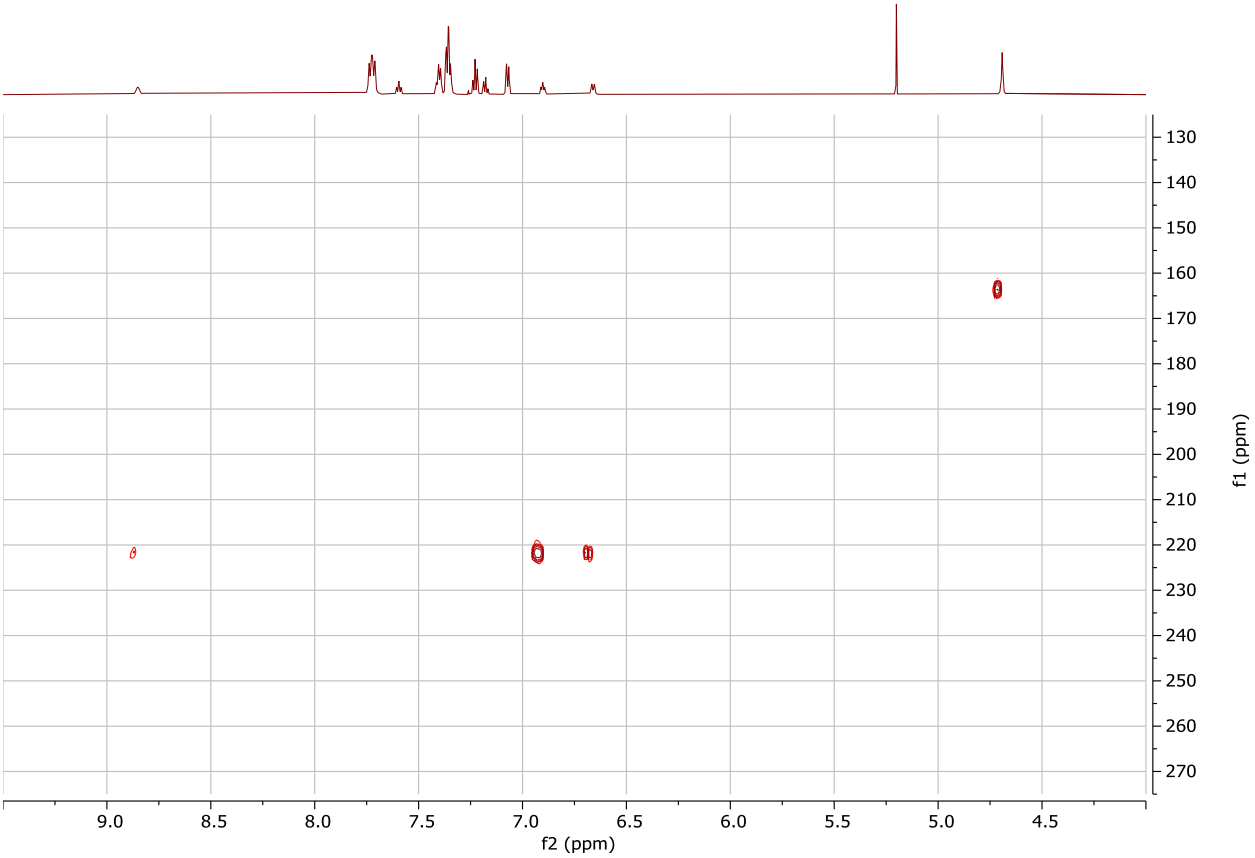

^{19}F-^{13}C HMBC NMR Spectrum $CDCl_3$ (659 MHz)

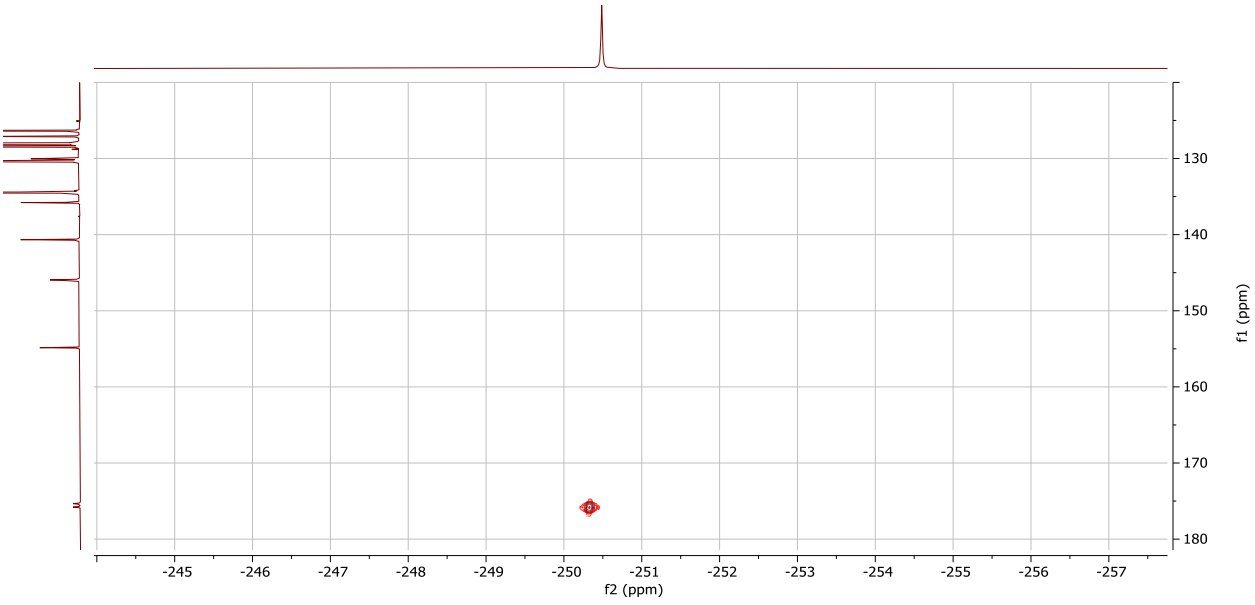

Chapter 4 NMR Spectra

N-benzyl-*N*,5-diphenyl-pentanamide

^{1}H NMR Spectrum $CDCl_3$ (600 MHz)

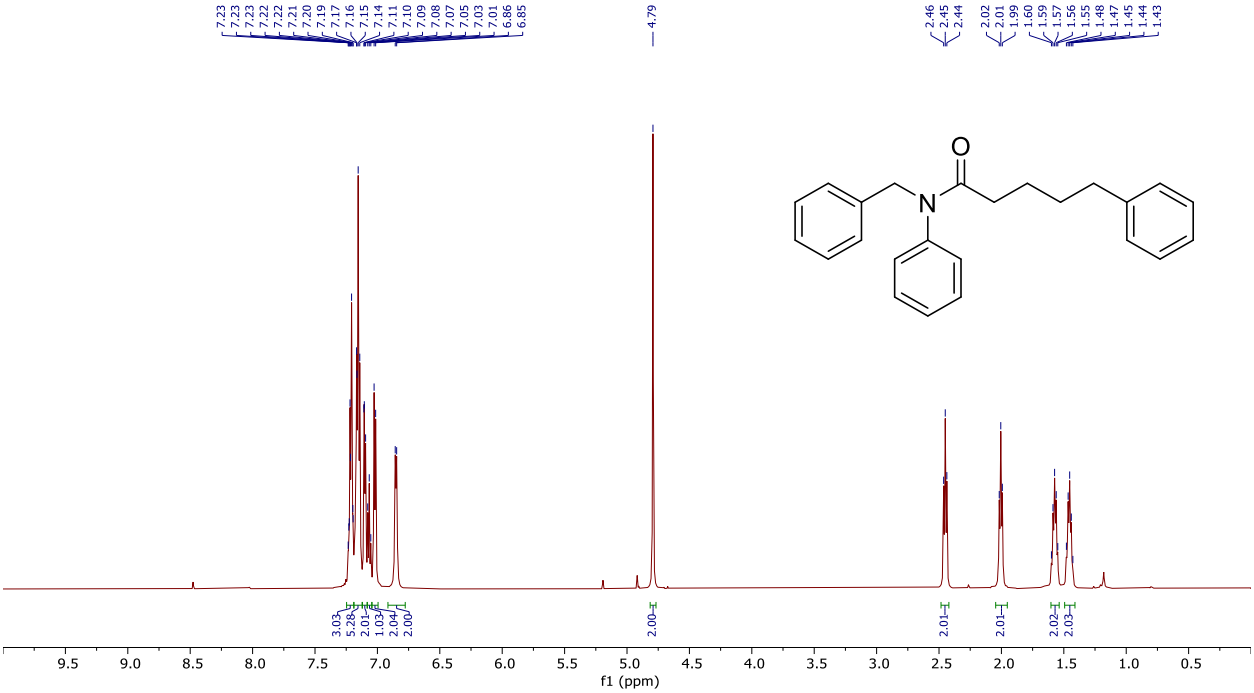

^{13}C NMR Spectrum $CDCl_3$ (151 MHz)

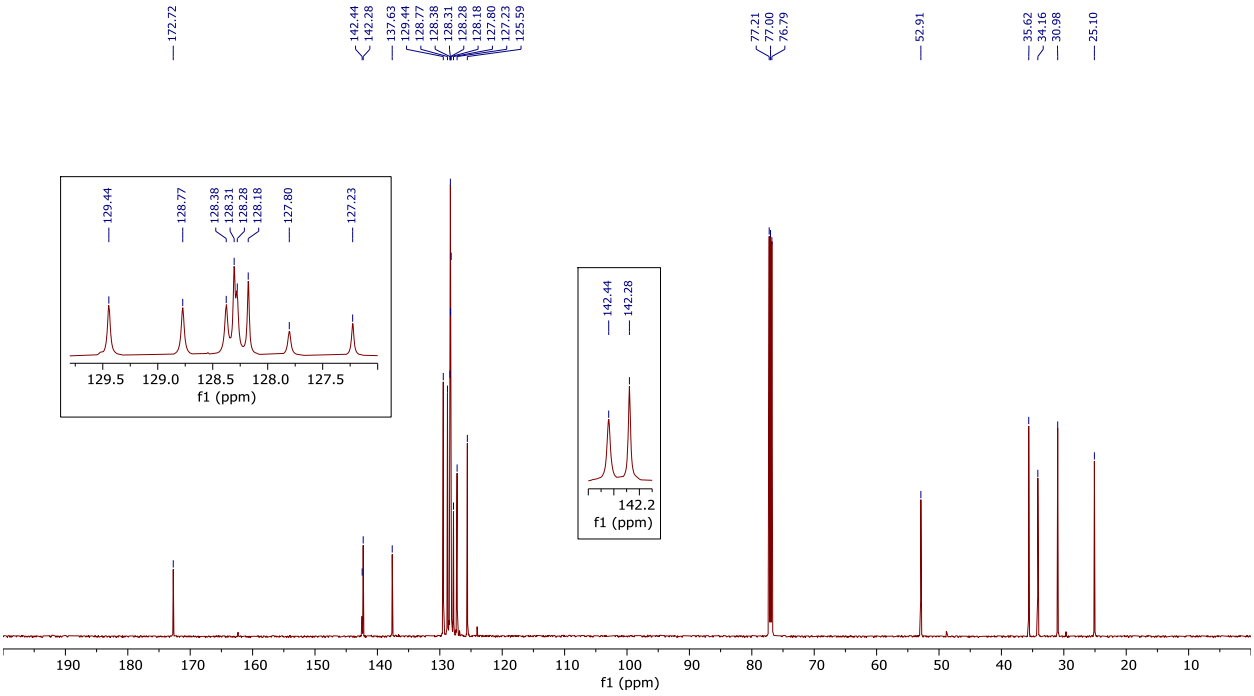

N-benzyl-4-(1-naphthyl)-*N*-phenyl-butanamide

^{1}H NMR Spectrum $CDCl_3$ (600 MHz)

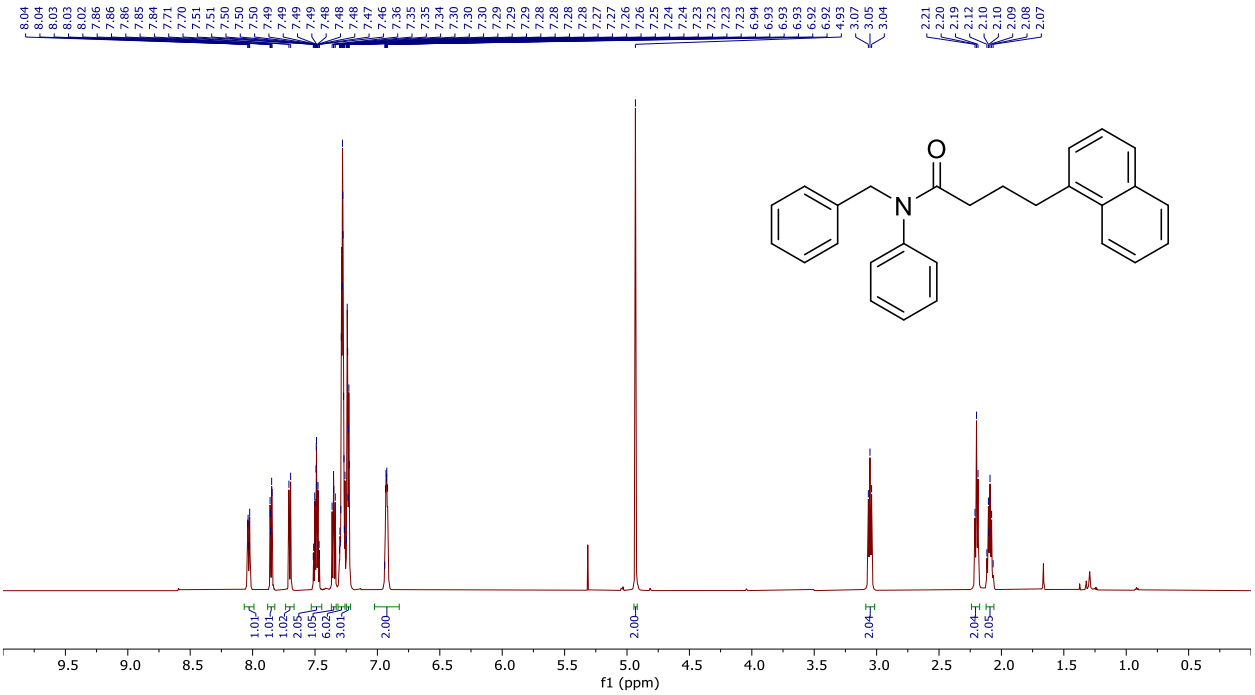

^{13}C NMR Spectrum $CDCl_3$ (151 MHz)

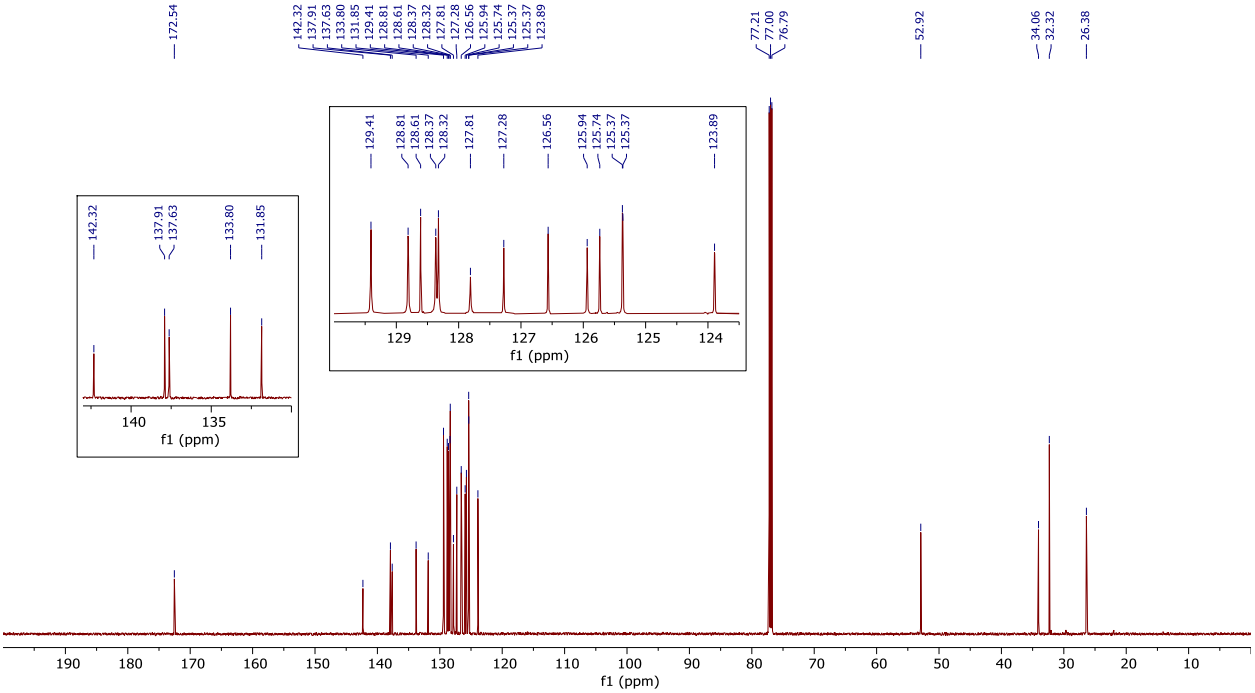

4-(1,3-benzodioxol-5-yloxy)-*N*-benzyl-*N*-phenyl-butanamide

^{1}H NMR Spectrum $CDCl_3$ (600 MHz)

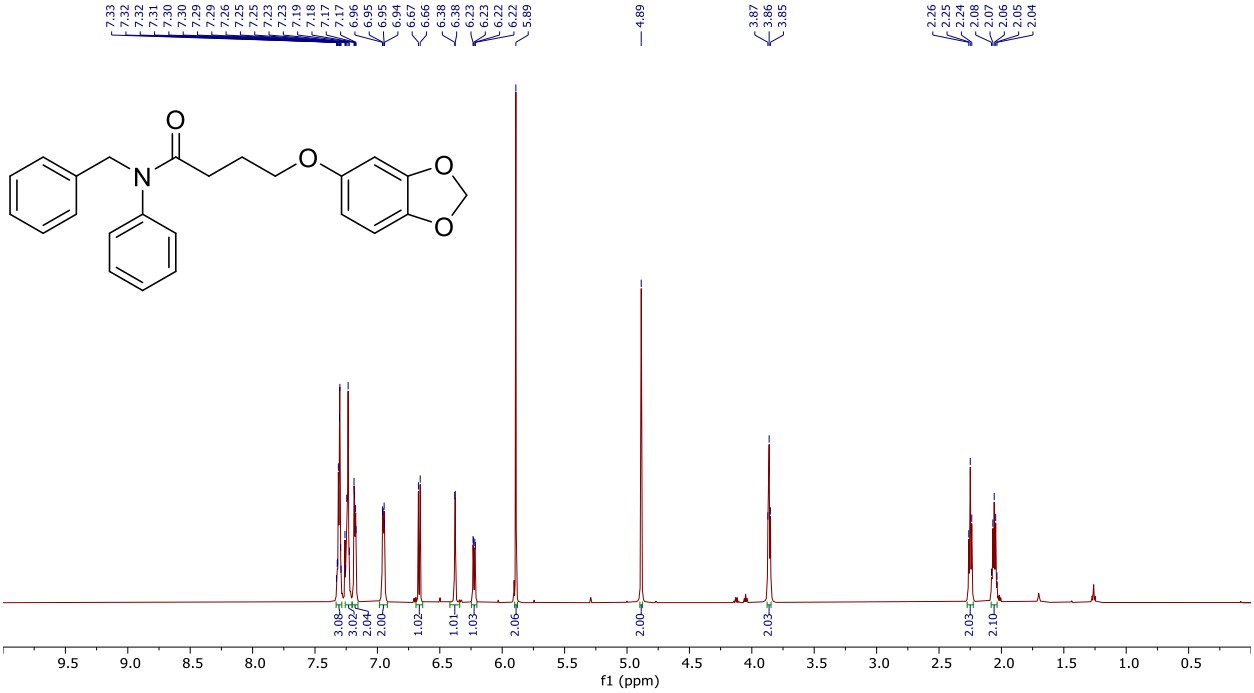

^{13}C NMR Spectrum $CDCl_3$ (151 MHz)

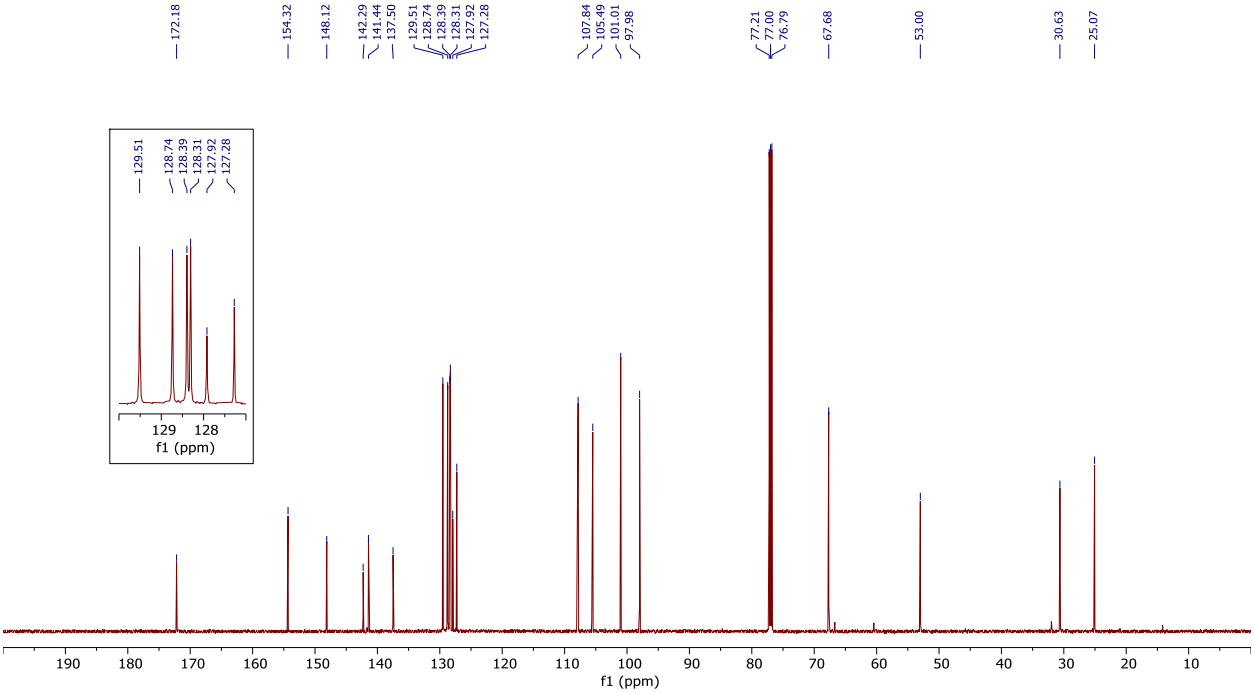

N-[(4-methoxyphenyl)methyl]-*N*,3-diphenyl-propanamide

^{1}H NMR Spectrum $CDCl_3$ (600 MHz)

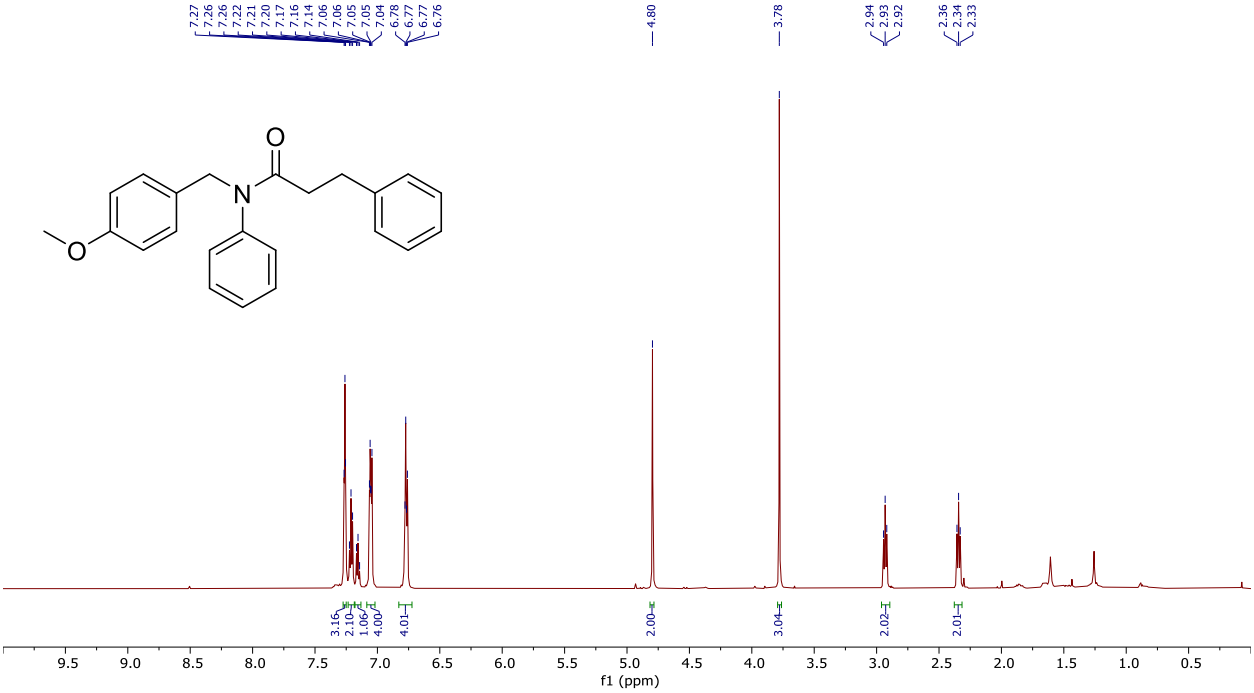

^{13}C NMR Spectrum $CDCl_3$ (151 MHz)

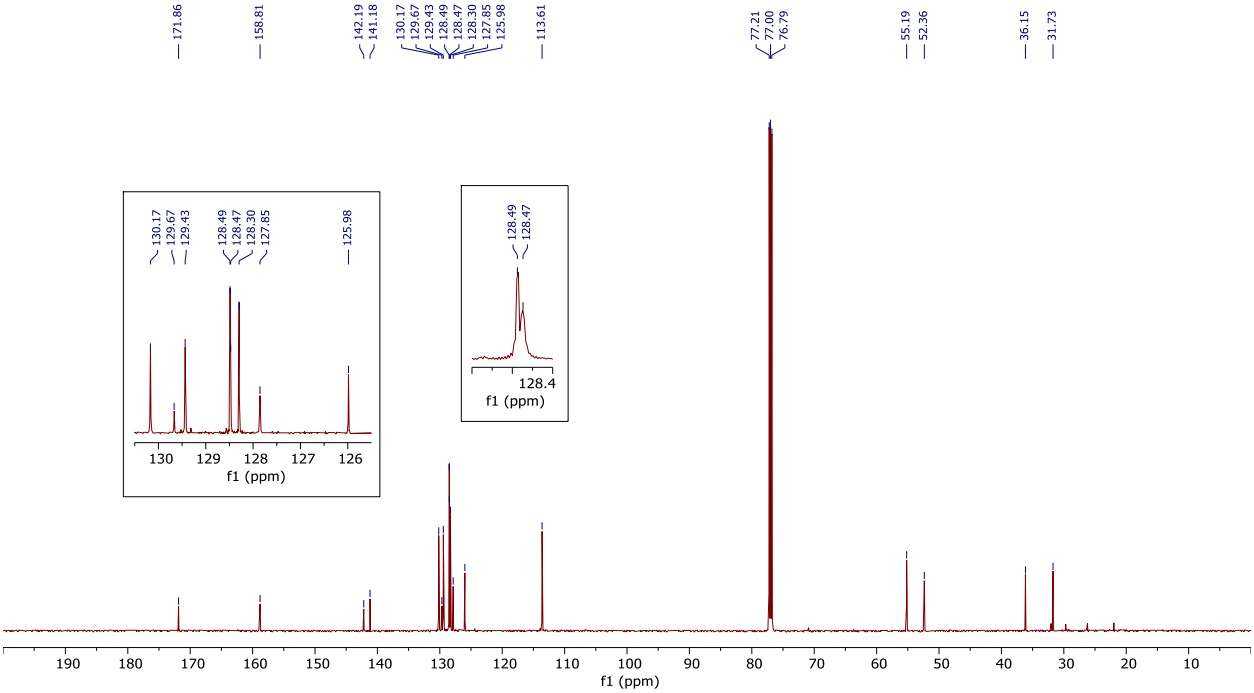

N-[(4-methoxyphenyl)methyl]-*N*-phenyl-3-(p-tolyl)propanamide

^{1}H NMR Spectrum $CDCl_3$ (600 MHz)

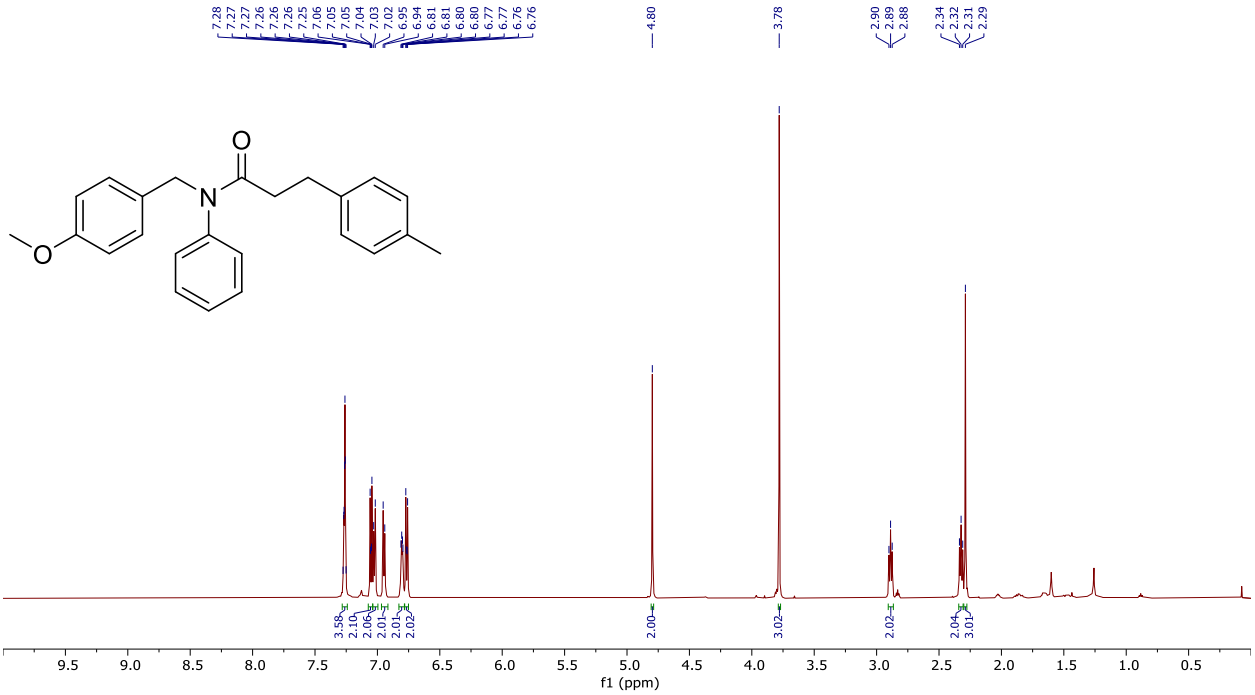

^{13}C NMR Spectrum $CDCl_3$ (151 MHz)

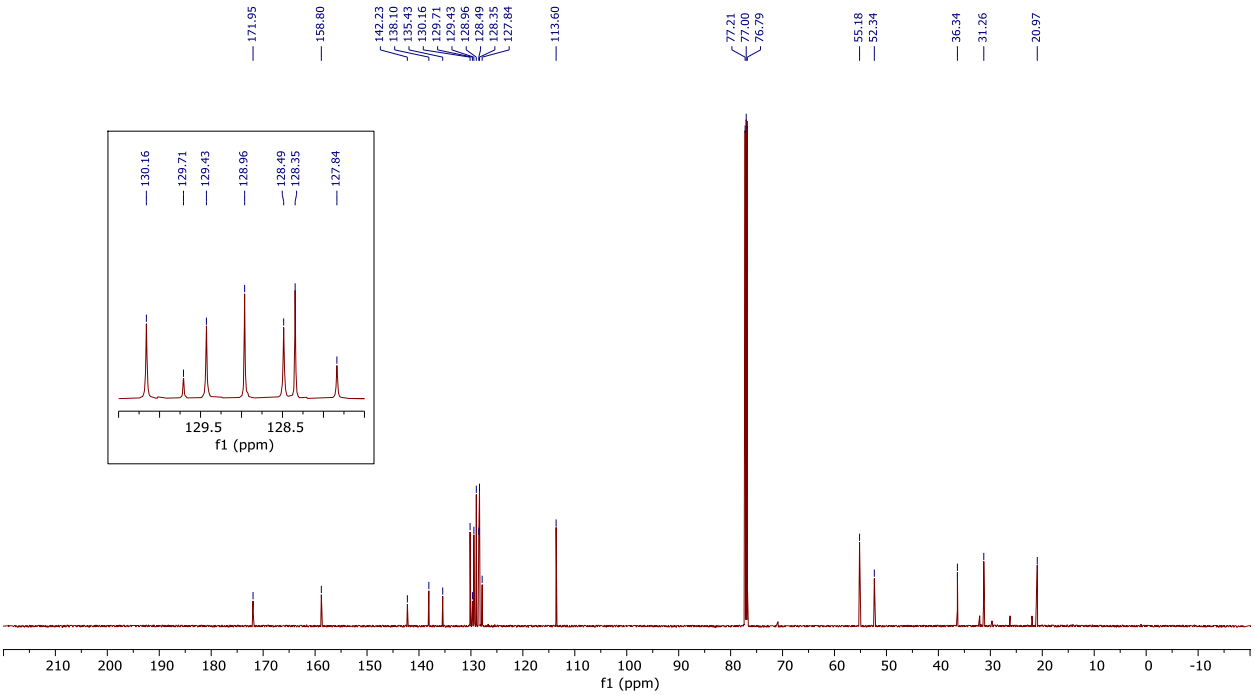

3-(4-methoxyphenyl)-*N*-[(4-methoxyphenyl)methyl]-*N*-phenyl-propanamide

^{1}H NMR Spectrum $CDCl_3$ (600 MHz)

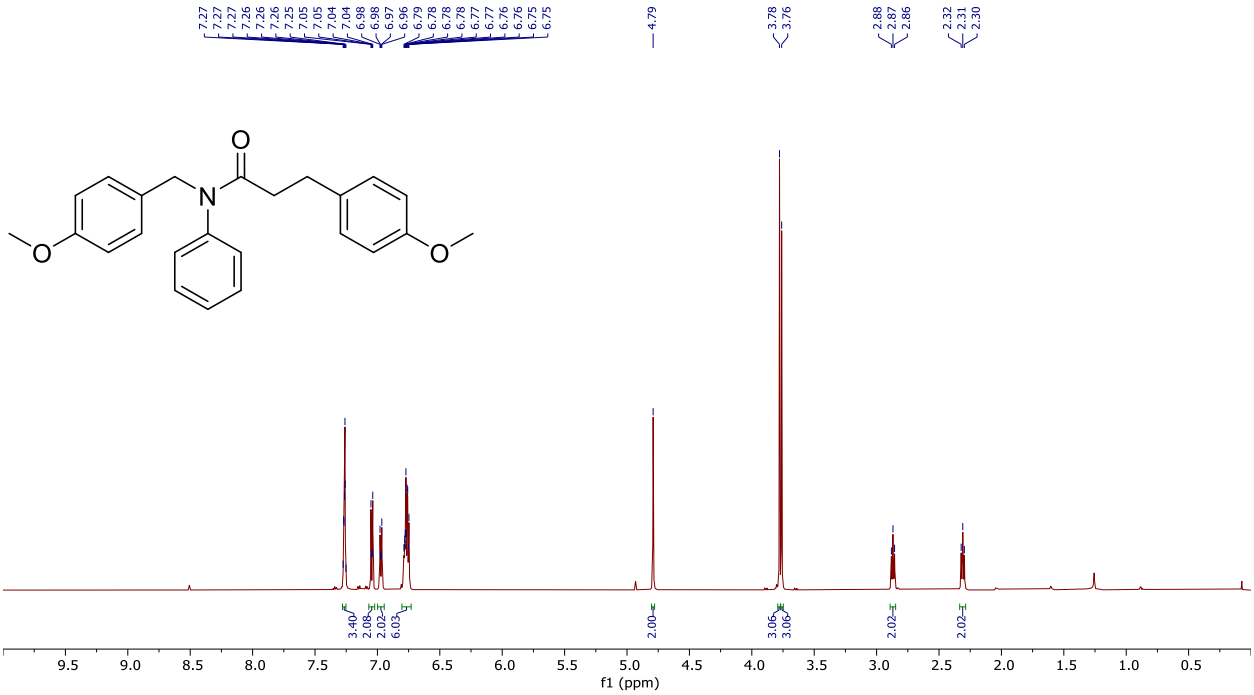

^{13}C NMR Spectrum $CDCl_3$ (151 MHz)

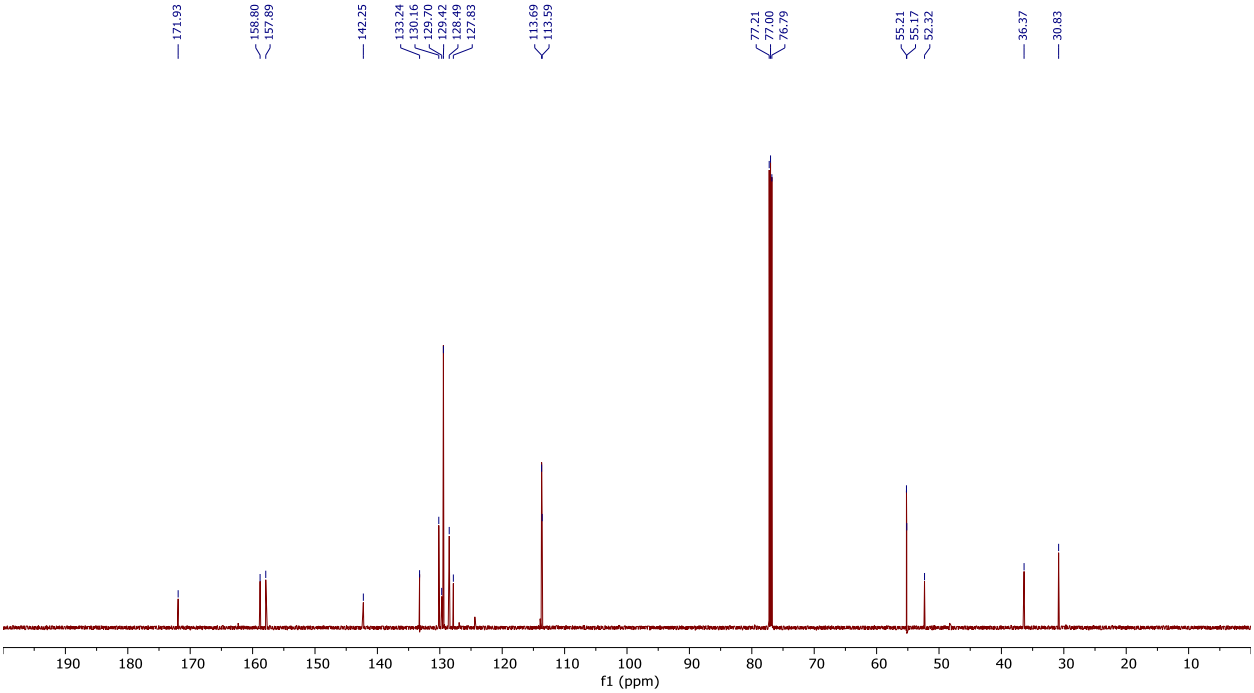

N-[(4-methoxyphenyl)methyl]-4-phenoxy-*N*-phenyl-butanamide

^{1}H NMR Spectrum $CDCl_3$ (600 MHz)

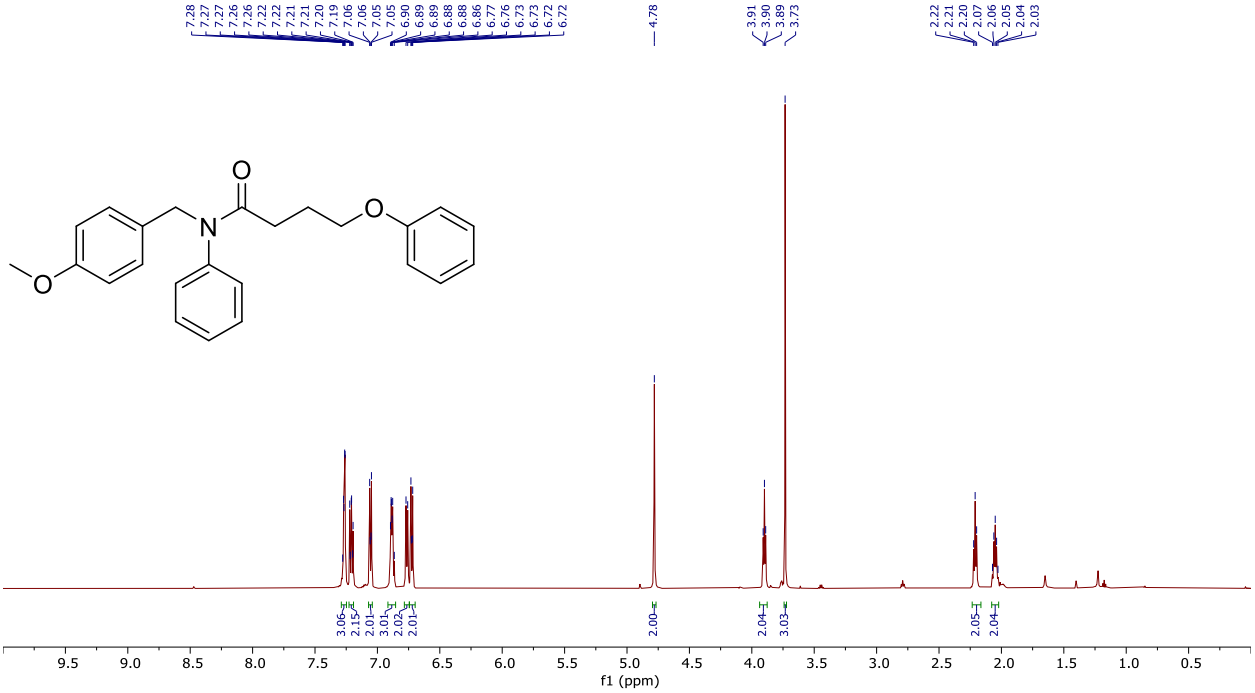

^{13}C NMR Spectrum $CDCl_3$ (151 MHz)

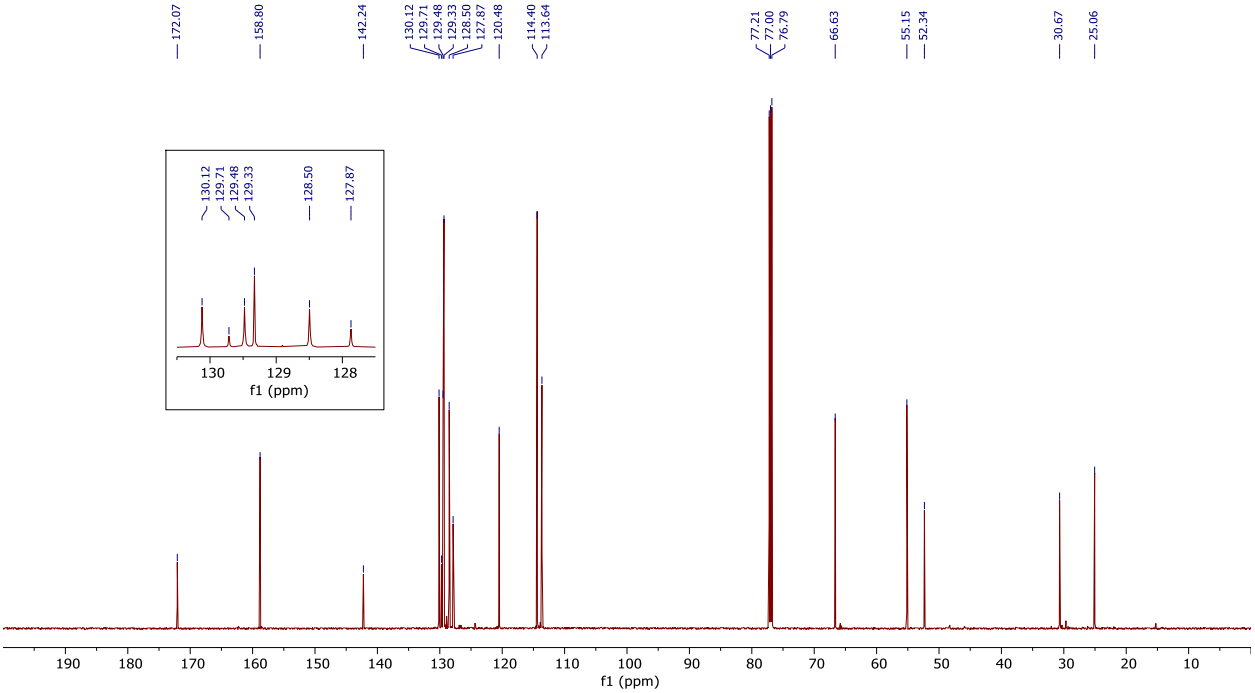

4-(4-methoxyphenoxy)-*N*-[(4-methoxyphenyl)methyl]-*N*-phenyl-butanamide

^{1}H NMR Spectrum $CDCl_3$ (600 MHz)

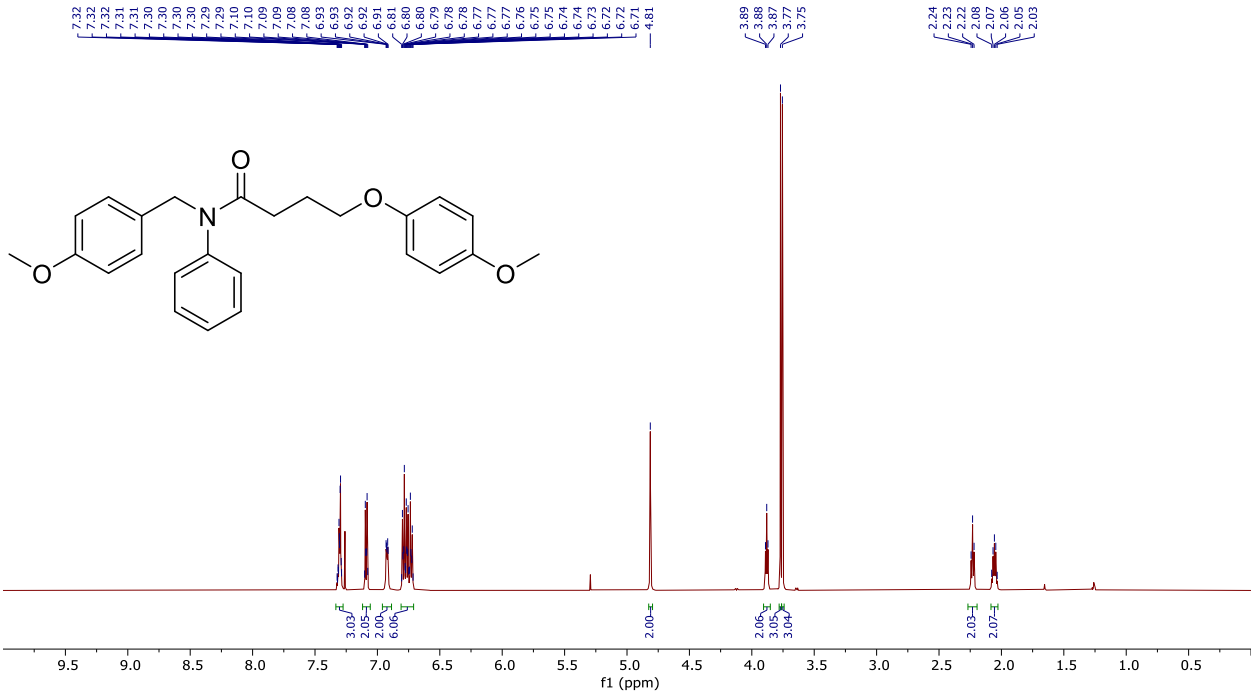

^{13}C NMR Spectrum $CDCl_3$ (151 MHz)

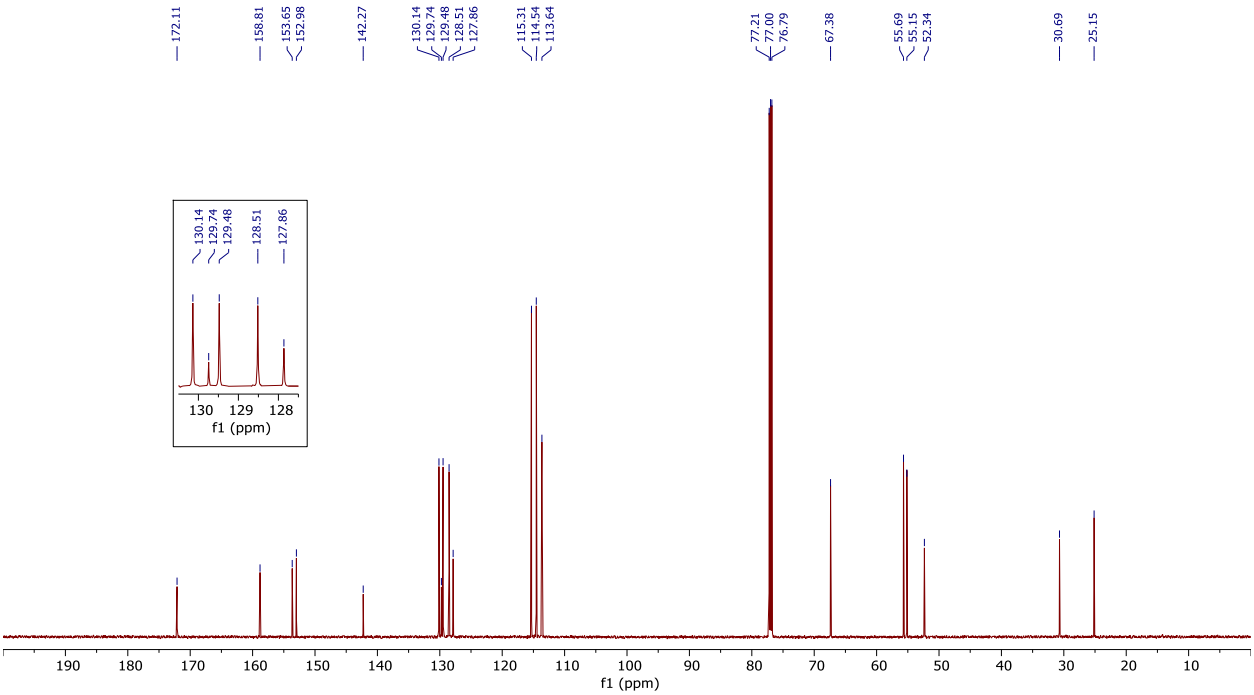

N-benzyl-4-(4-cyanophenoxy)-*N*-phenyl-butanamide

^{1}H NMR Spectrum $CDCl_3$ (600 MHz)

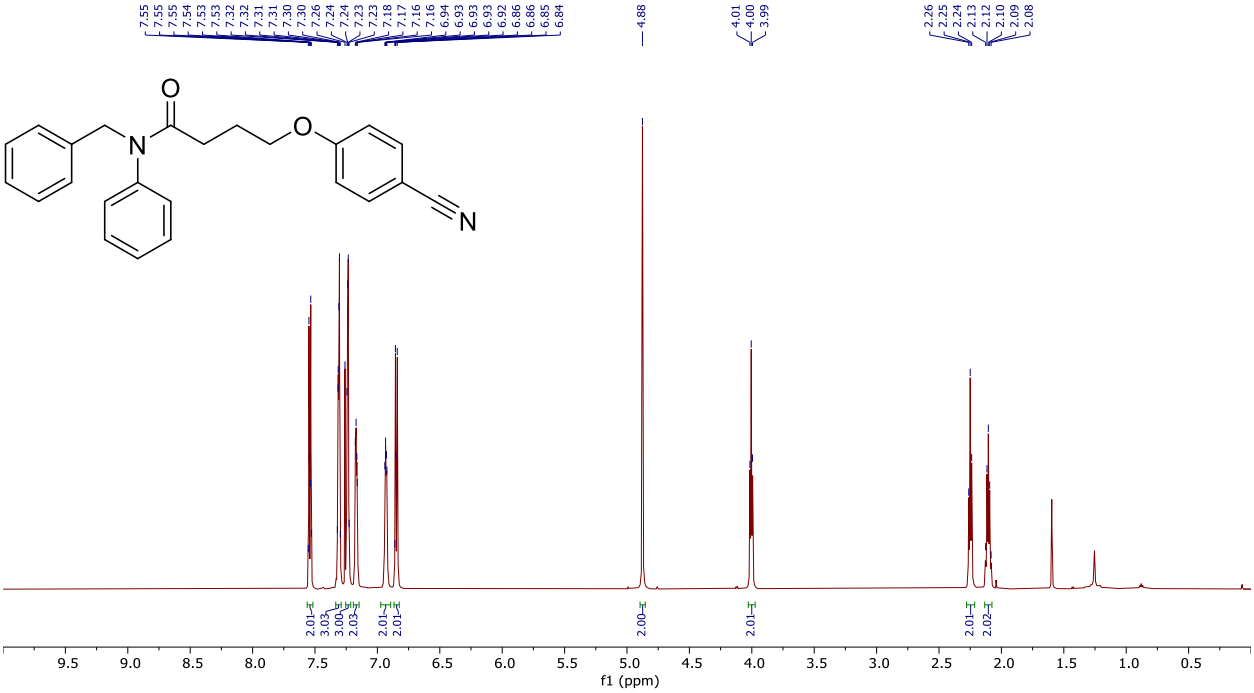

^{13}C NMR Spectrum $CDCl_3$ (151 MHz)

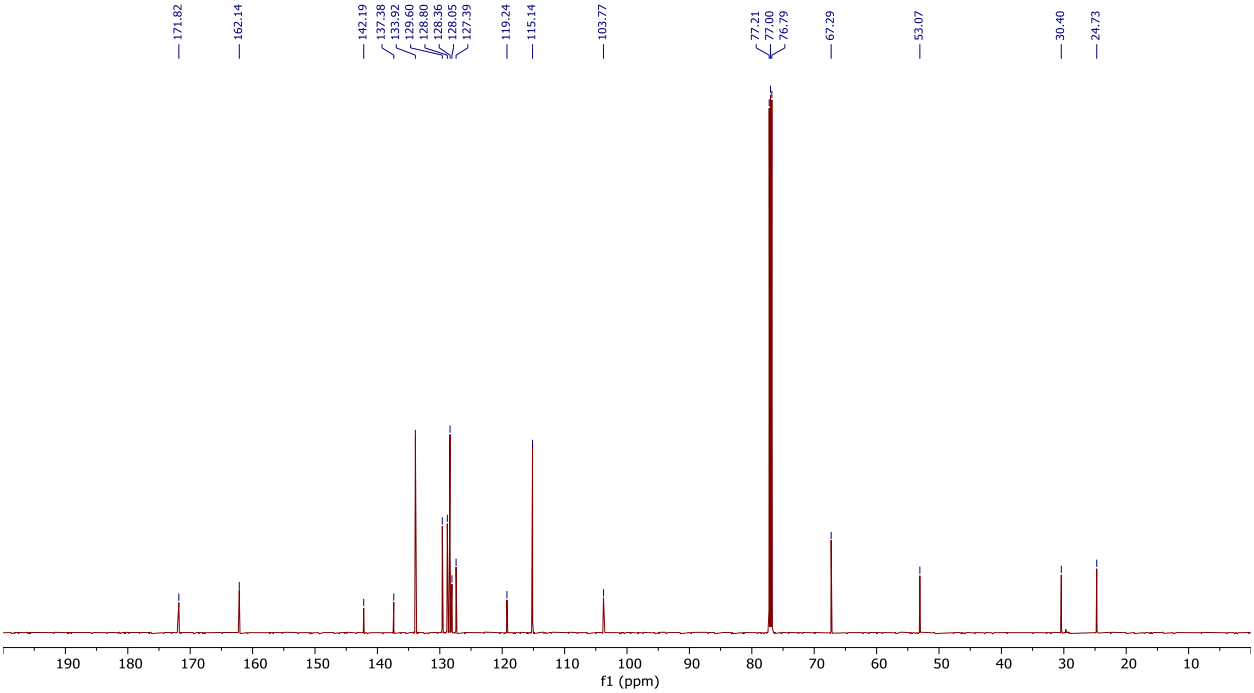

N-benzyl-*N*-phenyl-4-[3-(trifluoromethyl)phenoxy]butanamide

^{1}H NMR Spectrum $CDCl_3$ (600 MHz)

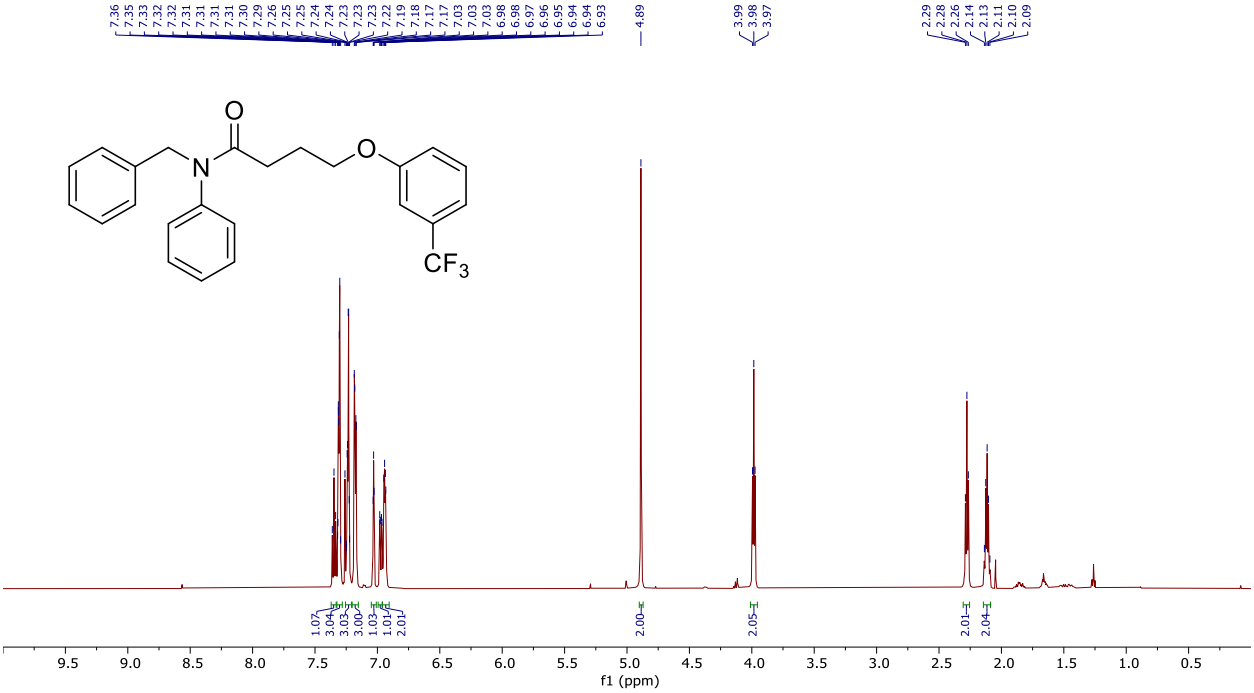

^{13}C NMR Spectrum $CDCl_3$ (151 MHz)

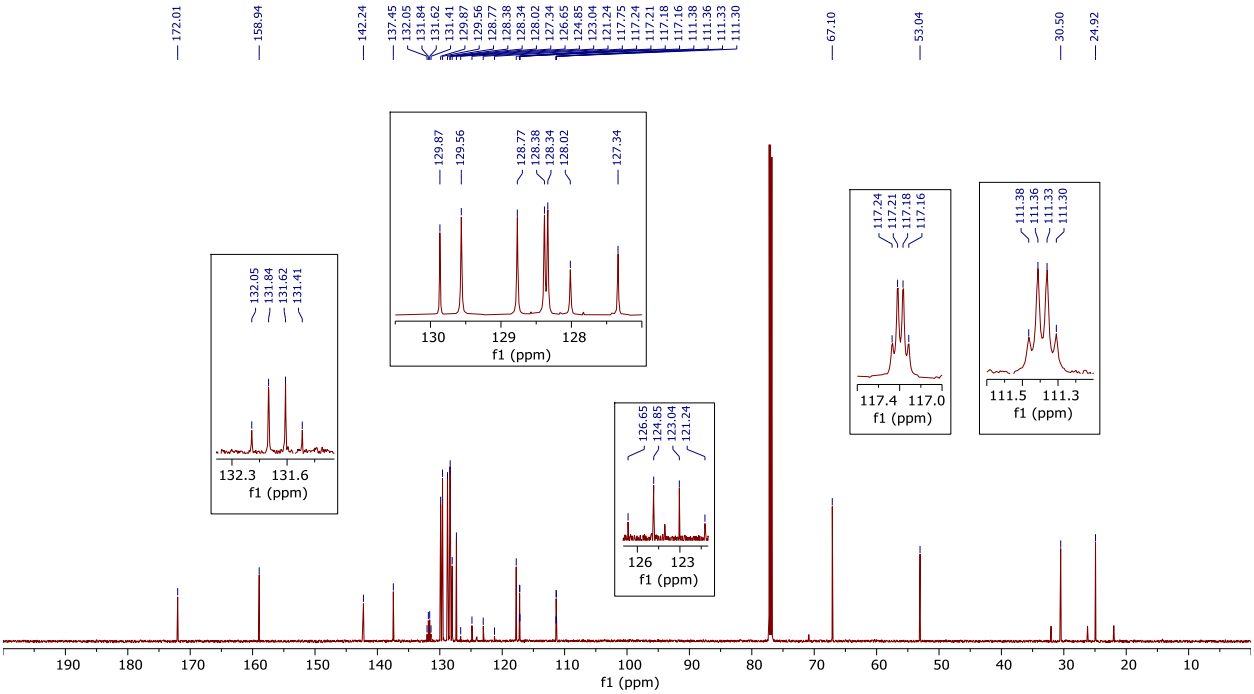

^{19}F NMR Spectrum $CDCl_3$ (282 MHz)

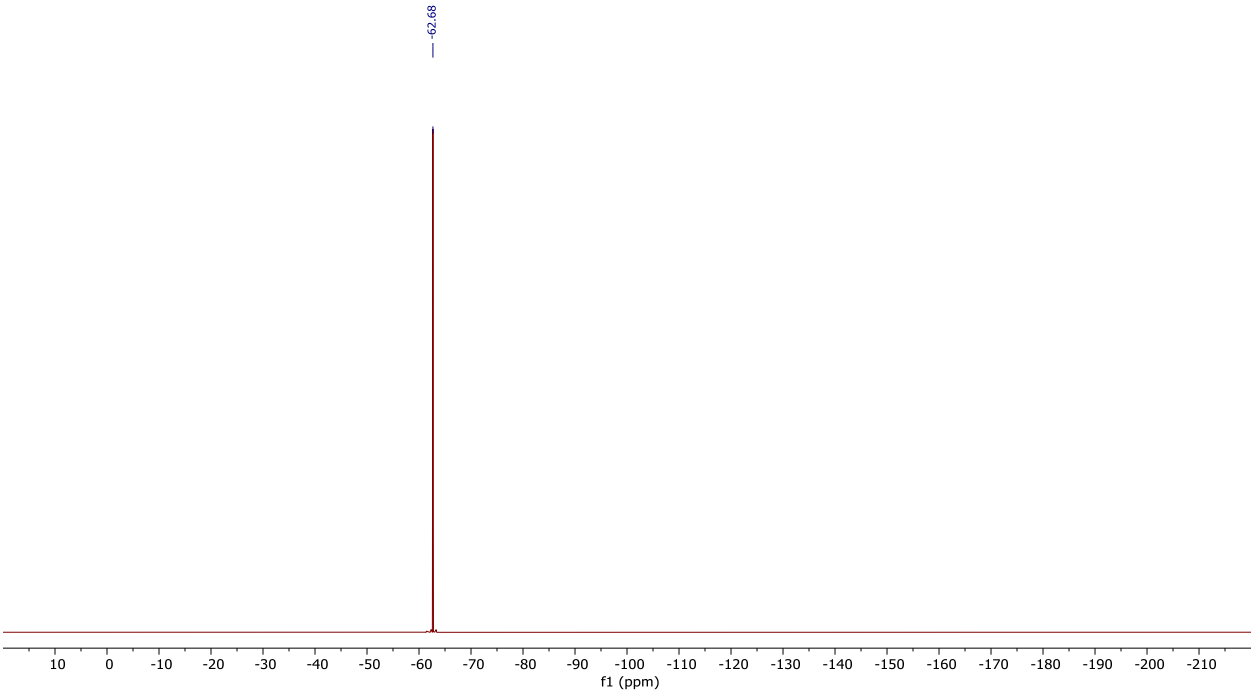

N-[(4-methoxyphenyl)methyl]-*N*,5-diphenyl-pentanamide

^{1}H NMR Spectrum $CDCl_3$ (600 MHz)

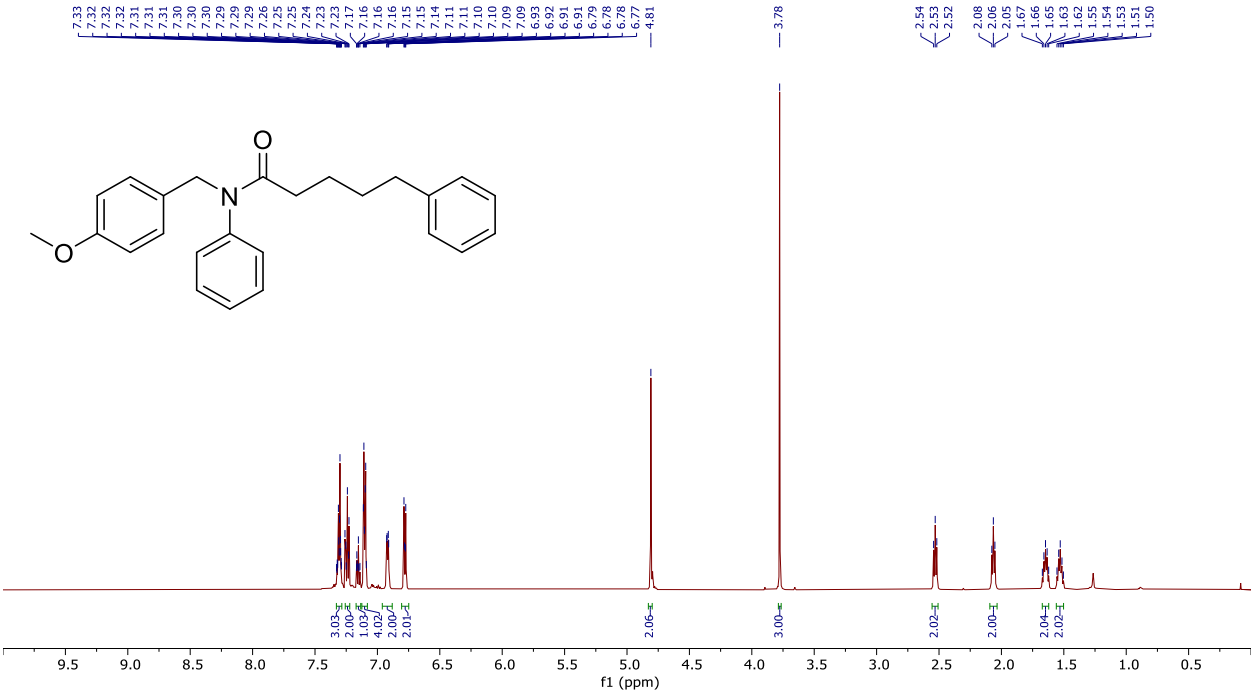

^{13}C NMR Spectrum $CDCl_3$ (151 MHz)

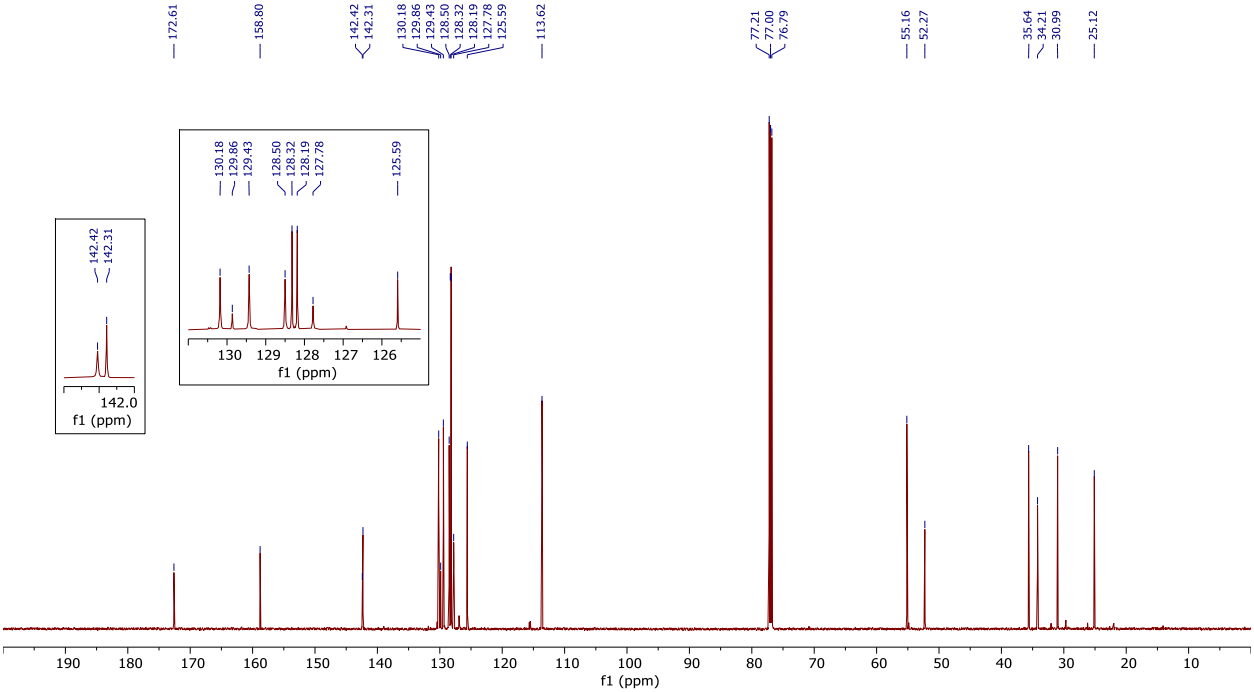

N-[[4-(dimethylamino)phenyl]methyl]-*N*,5-diphenyl-pentanamide

^{1}H NMR Spectrum $CDCl_3$ (300 MHz)

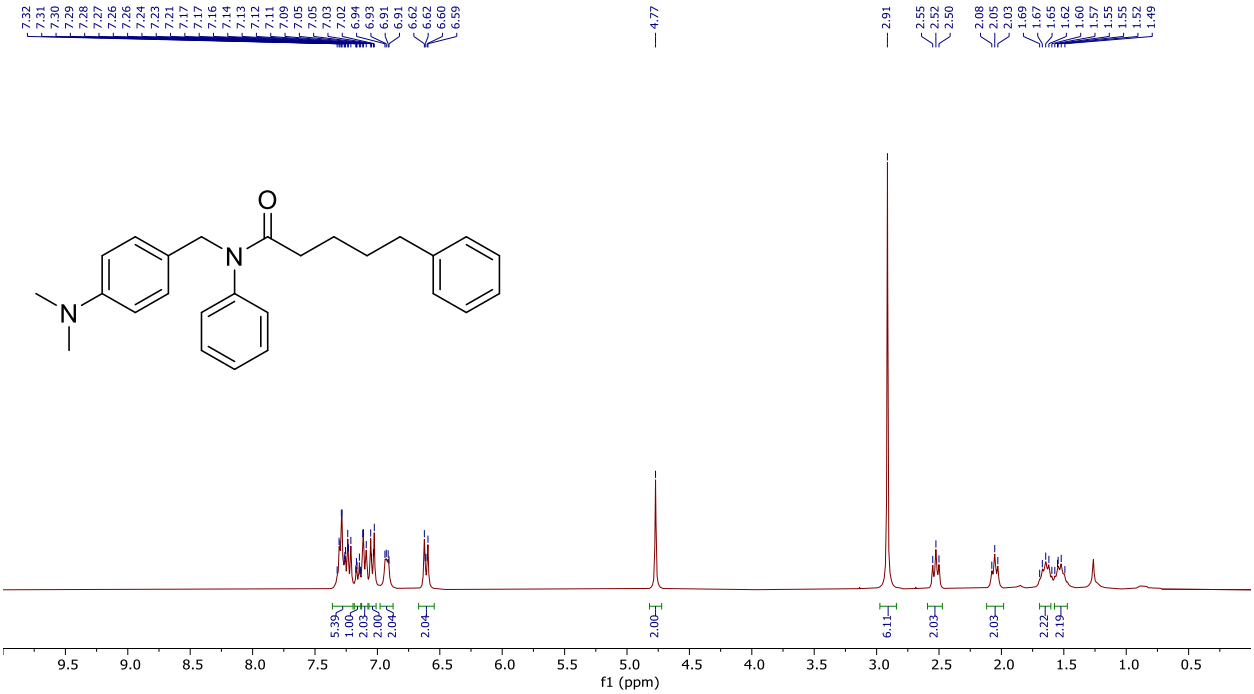

^{13}C NMR Spectrum $CDCl_3$ (75 MHz)

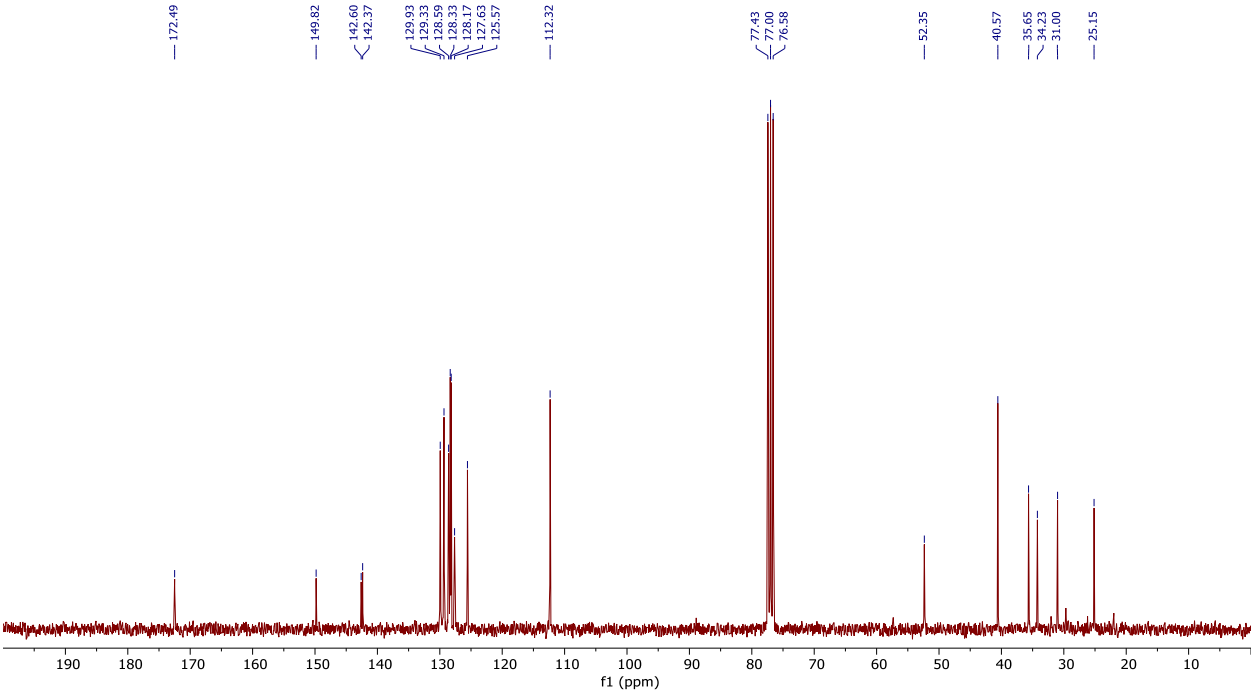

N-(1,3-benzodioxol-5-ylmethyl)-*N*,5-diphenyl-pentanamide

^{1}H NMR Spectrum $CDCl_3$ (600 MHz)

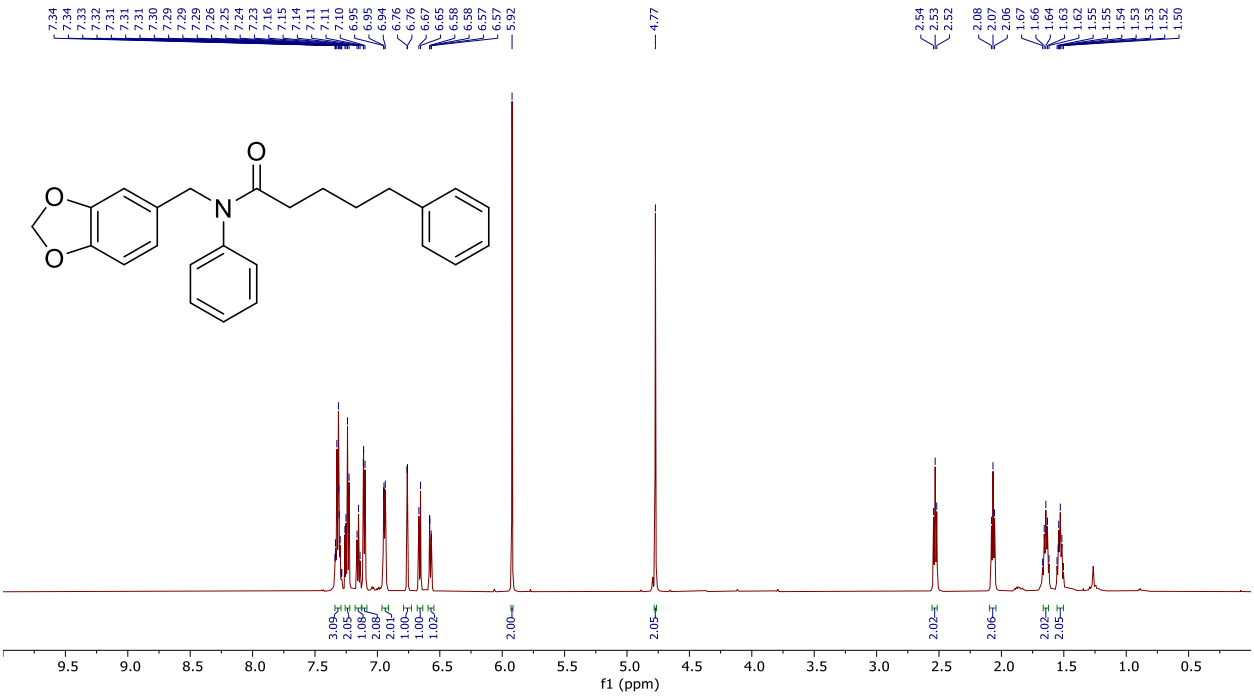

^{13}C NMR Spectrum $CDCl_3$ (151 MHz)

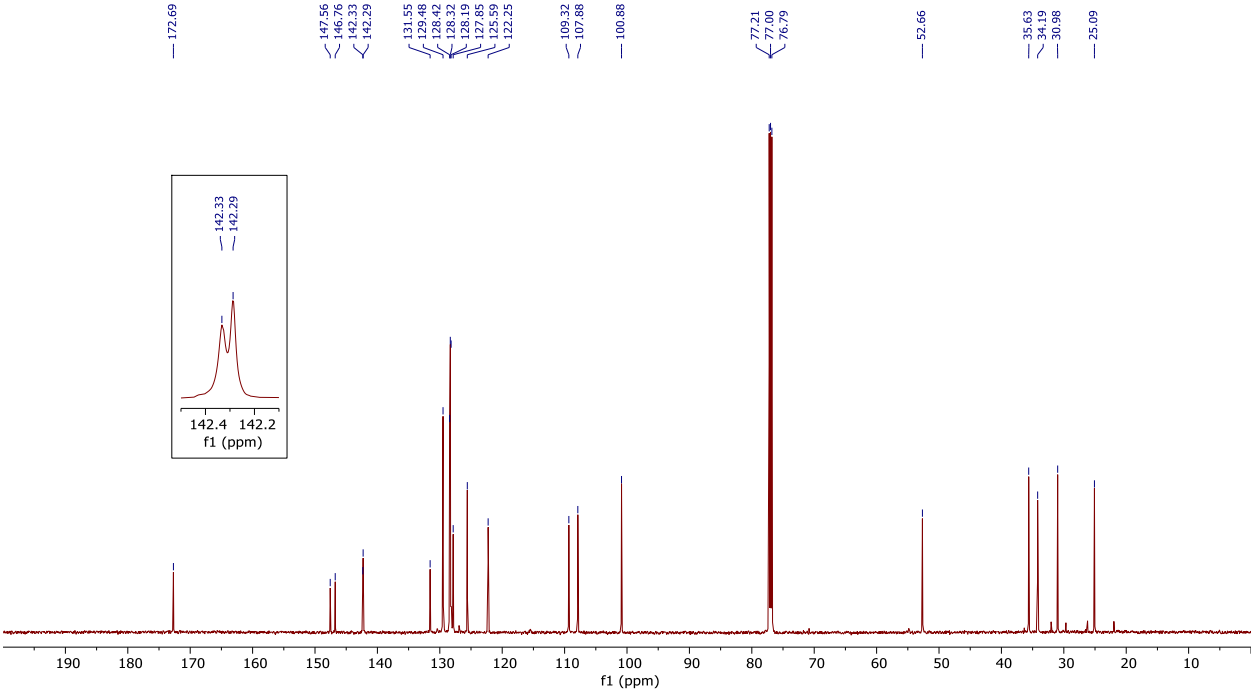

3-cyclohexyl-*N*-[(4-methoxyphenyl)methyl]-*N*-phenyl-propanamide

^{1}H NMR Spectrum $CDCl_3$ (600 MHz)

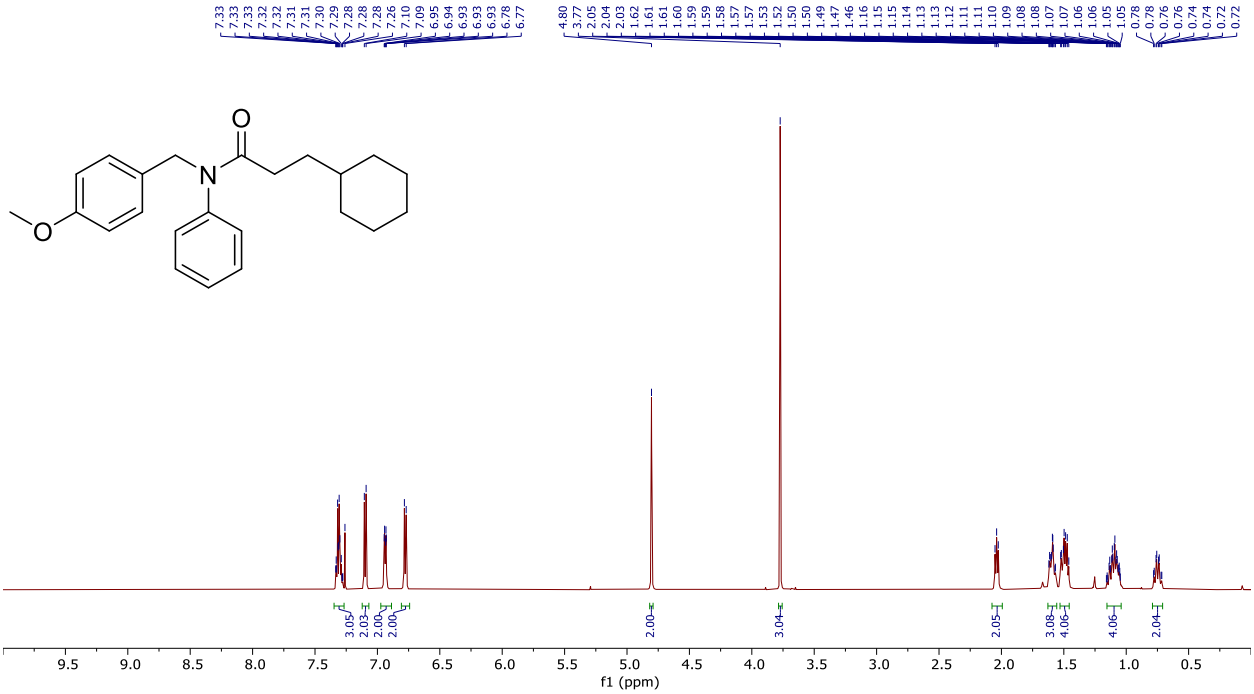

^{13}C NMR Spectrum $CDCl_3$ (151 MHz)

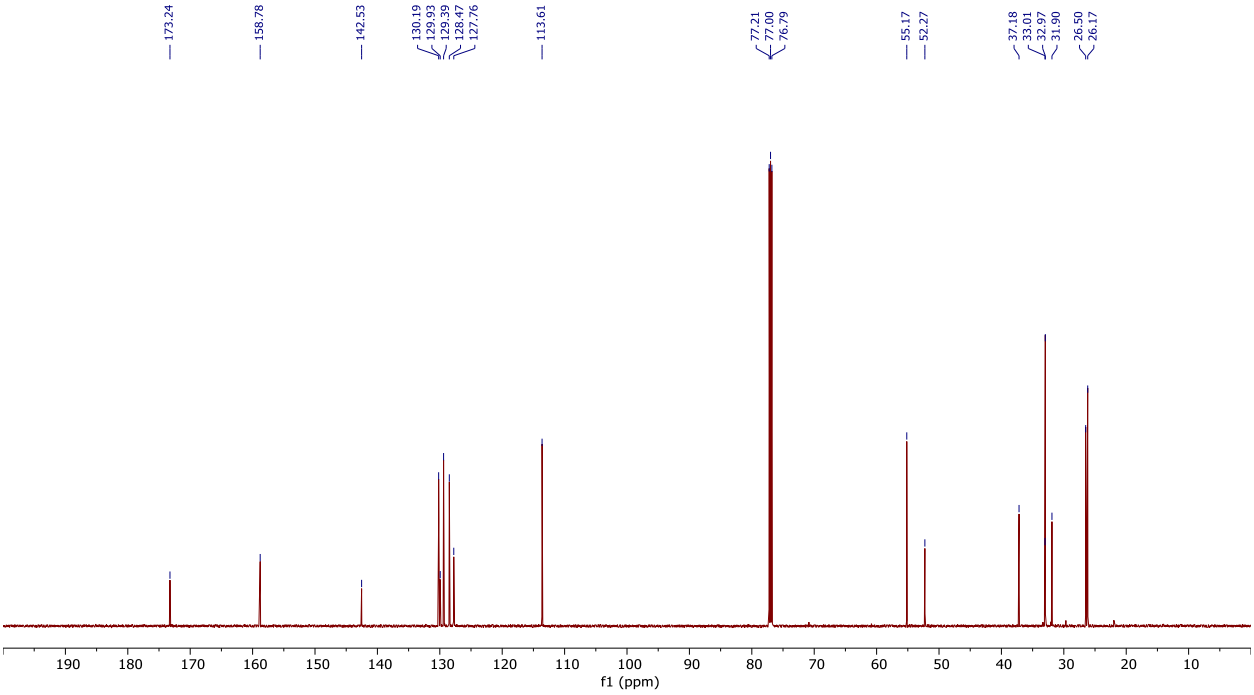

N-[(4-methoxyphenyl)methyl]-*N*-phenyl-4-trimethylsilyl-butanamide

^{1}H NMR Spectrum $CDCl_3$ (600 MHz)

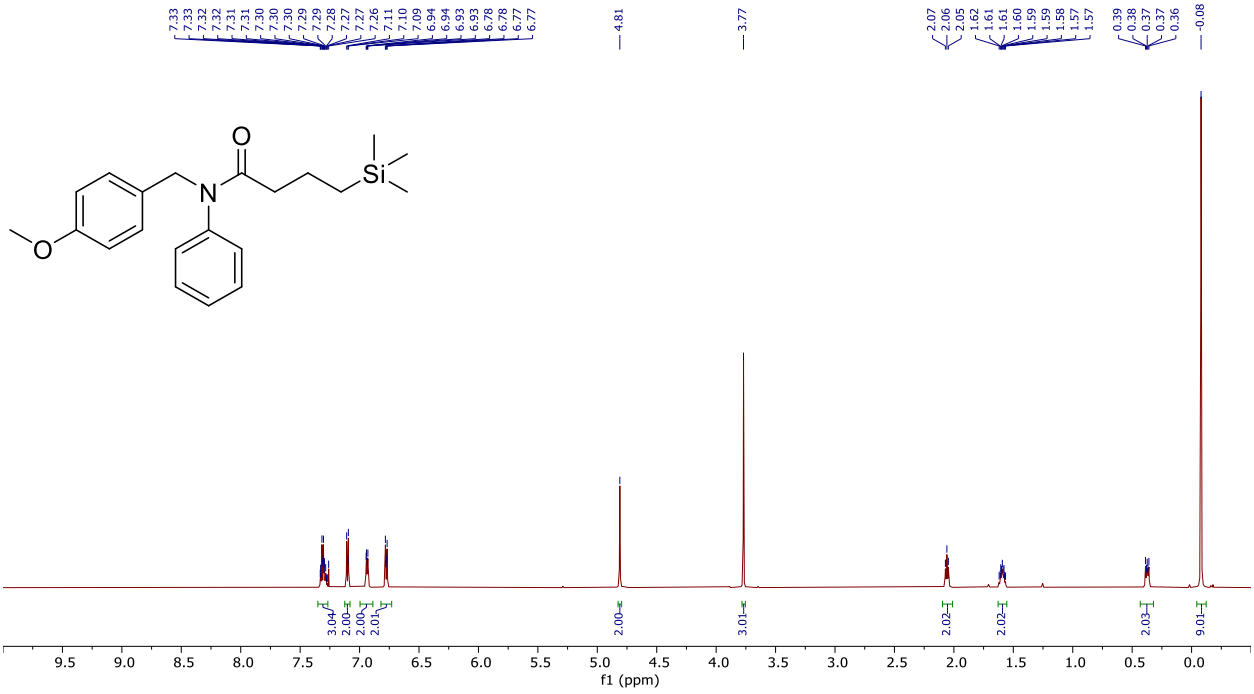

^{13}C NMR Spectrum $CDCl_3$ (151 MHz)

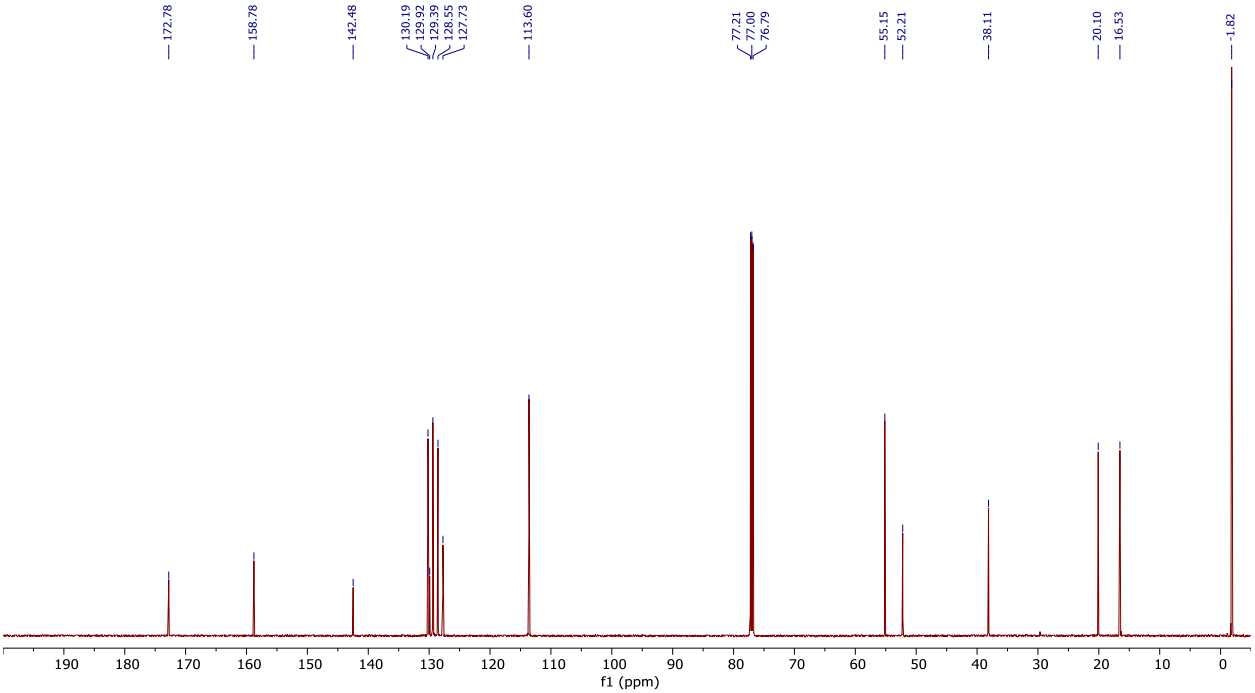

4-carbazol-9-yl-*N*-[(4-methoxyphenyl)methyl]-*N*-phenyl-butanamide

^{1}H NMR Spectrum $CDCl_3$ (600 MHz)

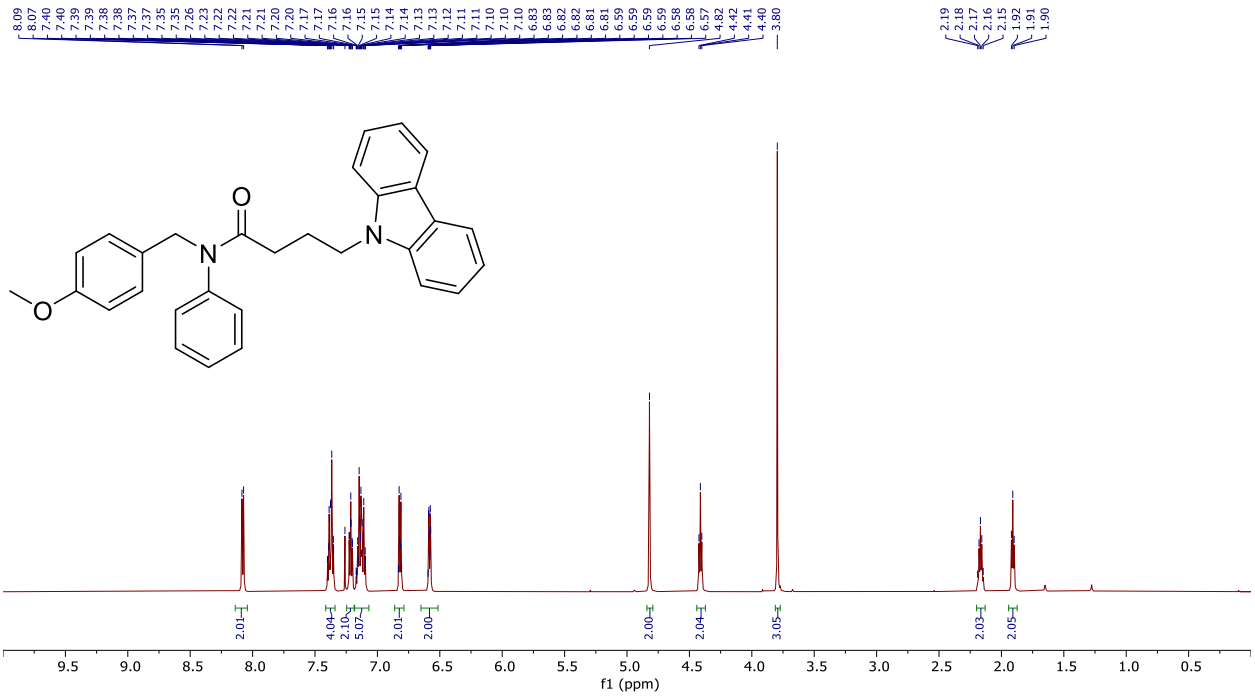

^{13}C NMR Spectrum $CDCl_3$ (151 MHz)

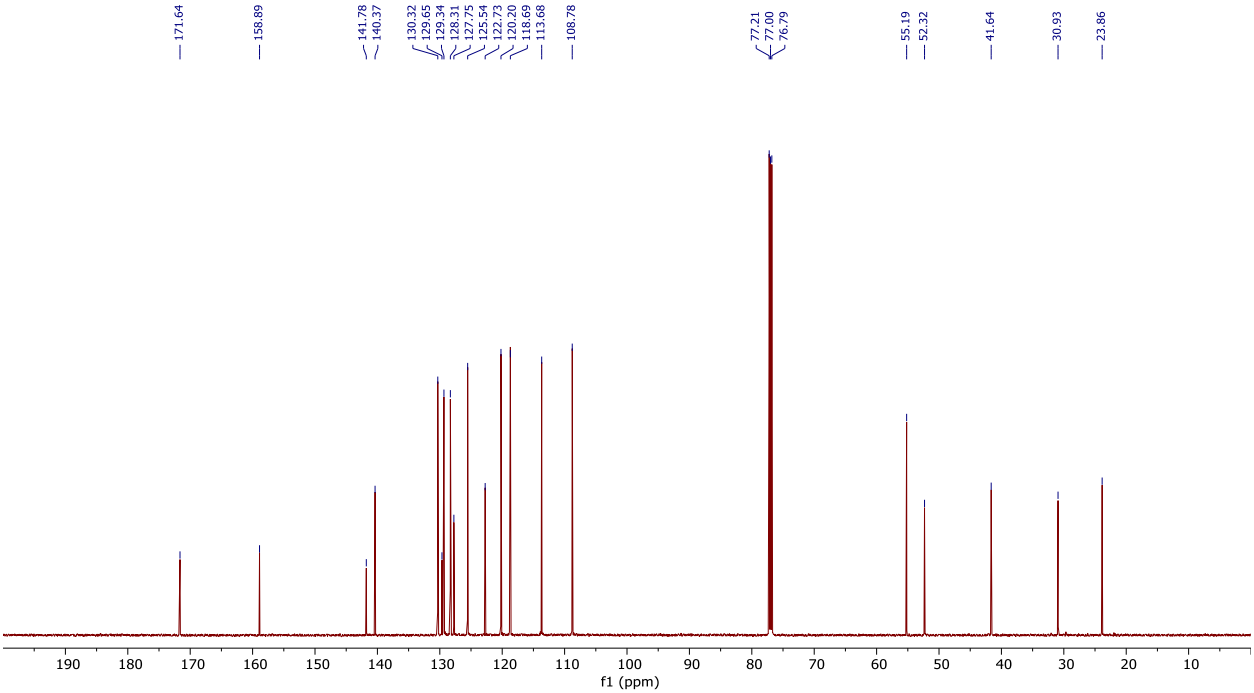

N-benzyl-3-ferrocenyl-*N*-phenyl-propanamide

^{1}H NMR Spectrum $CDCl_3$ (600 MHz)

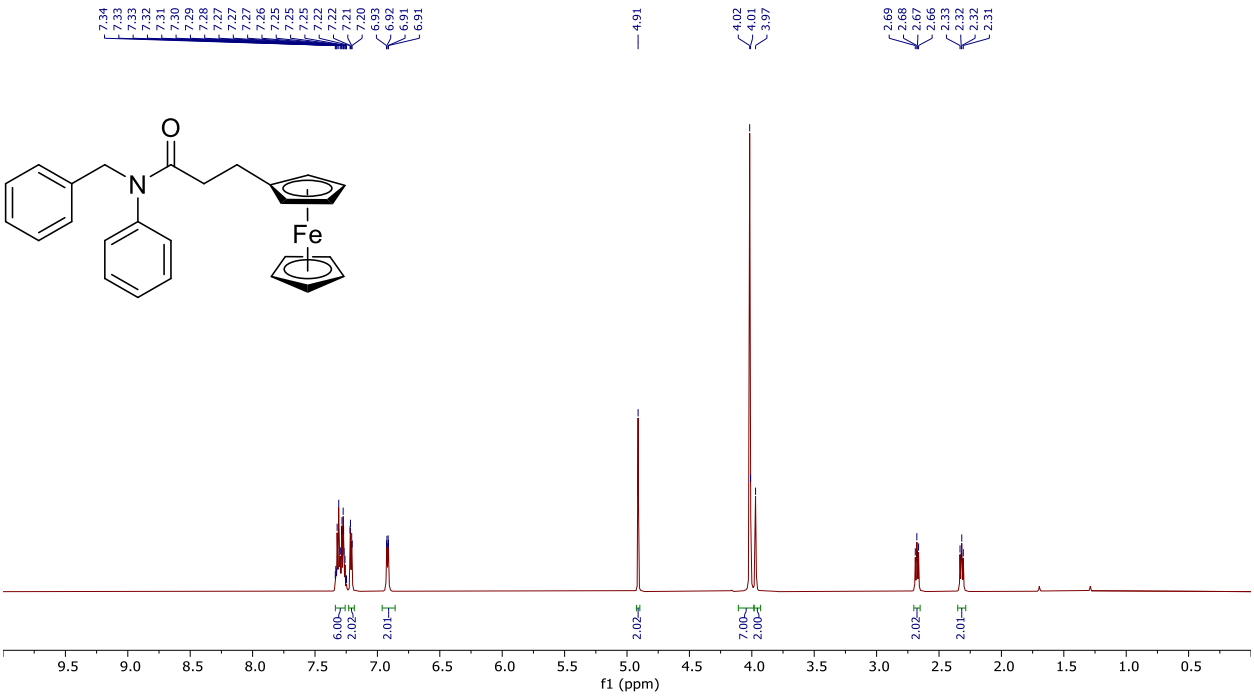

^{13}C NMR Spectrum $CDCl_3$ (151 MHz)

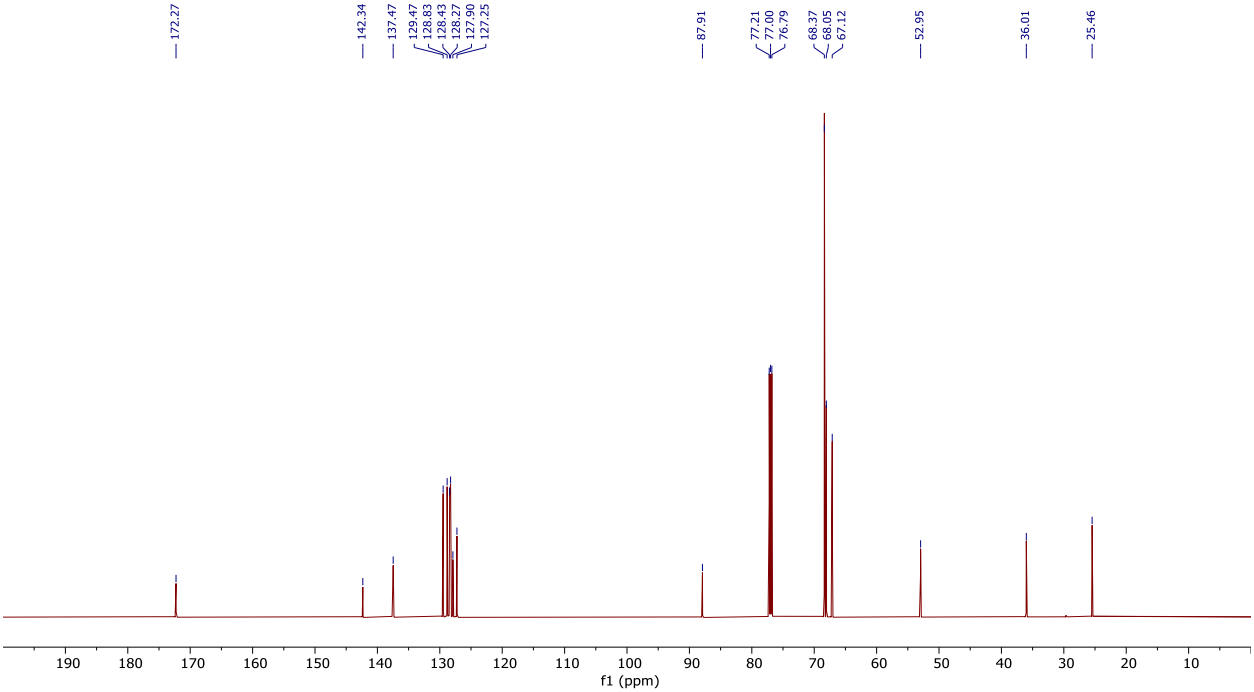

_N_-[(4-methoxyphenyl)methyl]-4-(1-methylpyrazol-3-yl)oxy-_N_-phenyl-butanamide

^{1}H NMR Spectrum $CDCl_3$ (600 MHz)

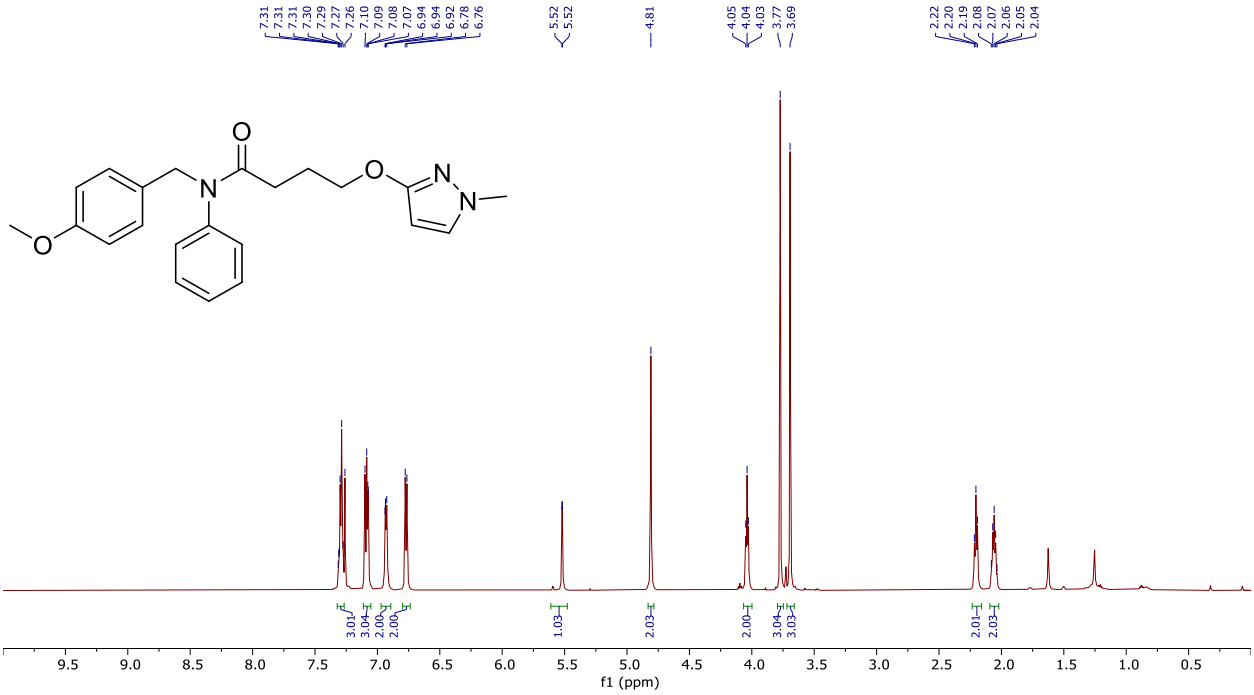

^{13}C NMR Spectrum $CDCl_3$ (151 MHz)

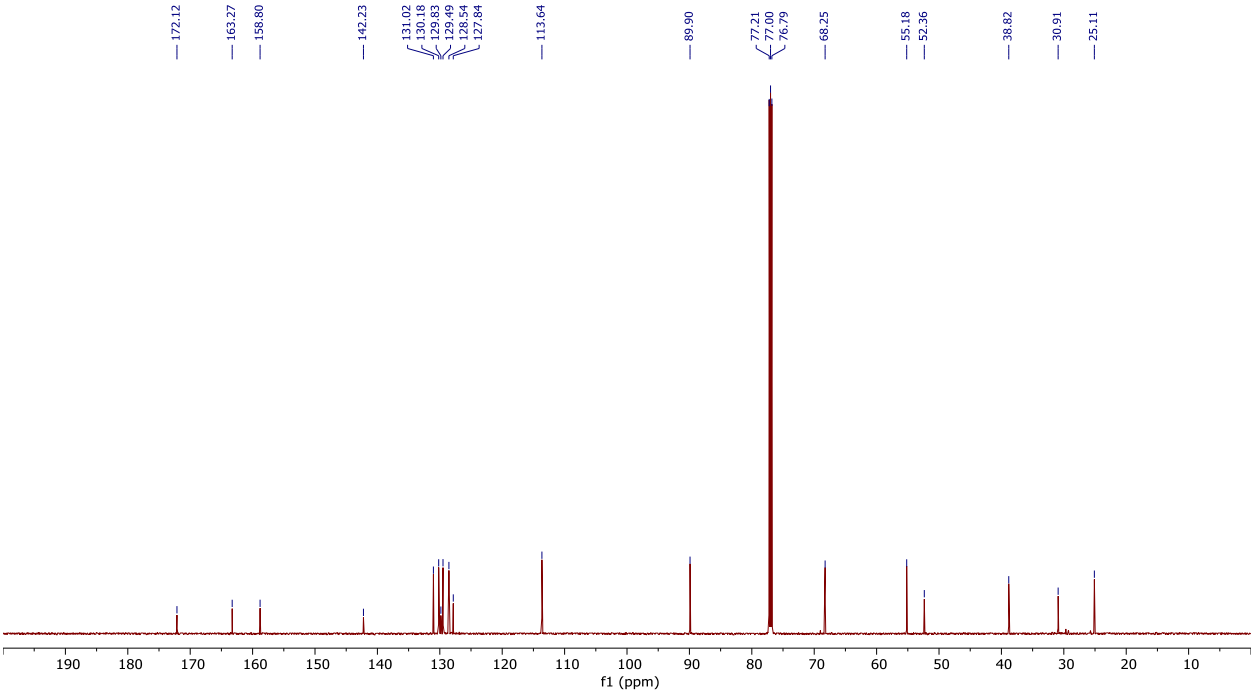

_N_-benzyl-4-(4-fluorophenoxy)-_N_-(4-fluorophenyl)butanamide

^{1}H NMR Spectrum $CDCl_3$ (600 MHz)

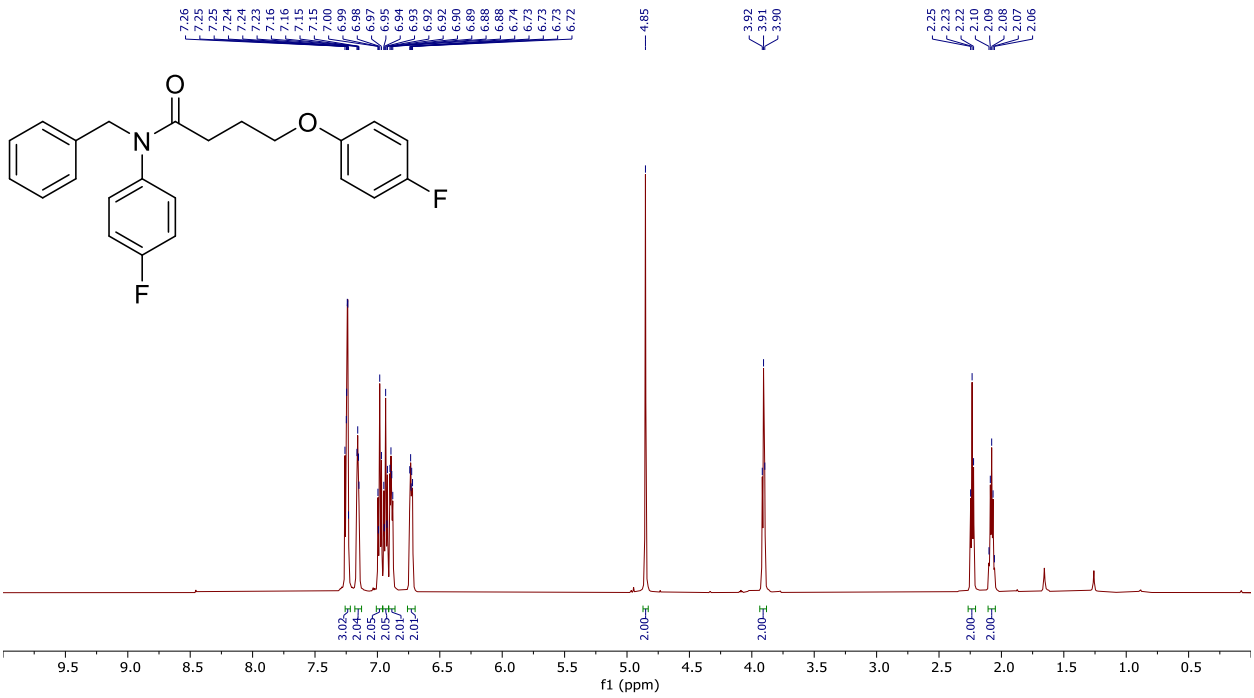

^{13}C NMR Spectrum $CDCl_3$ (151 MHz)

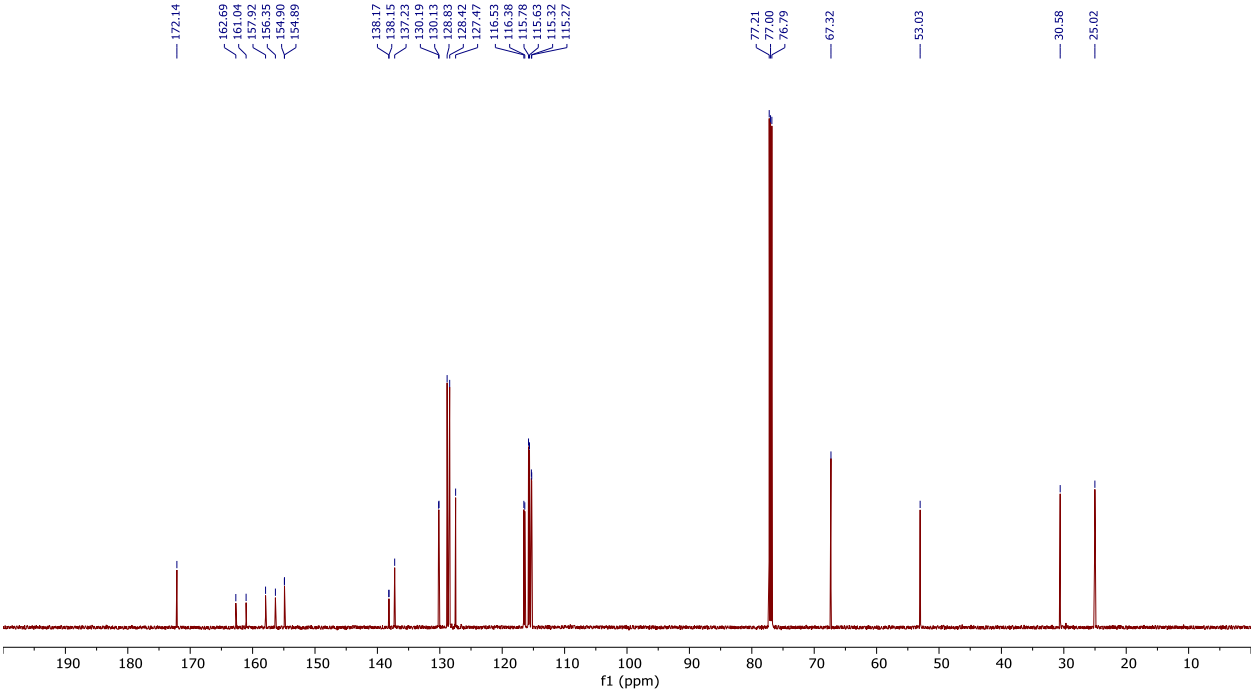

^{19}F NMR Spectrum $CDCl_3$ (282 MHz)

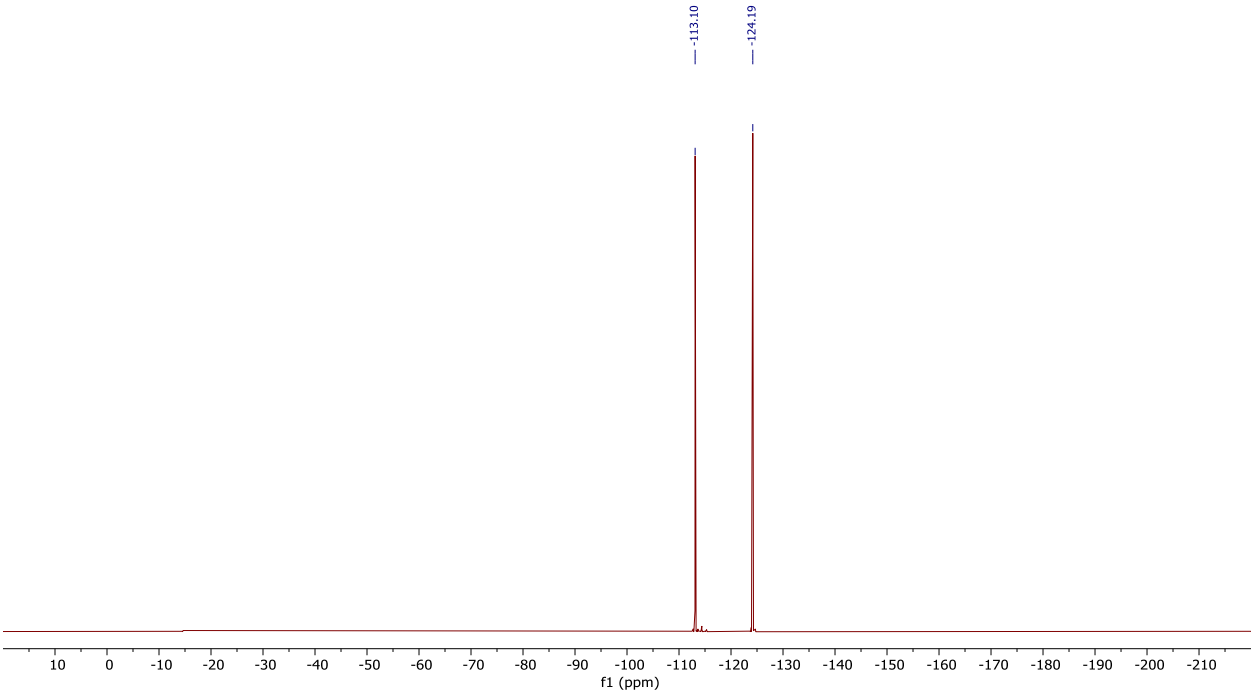

_N_-benzyl-4-(4-methoxyphenoxy)-_N_-phenyl-butanamide

^{1}H NMR Spectrum $CDCl_3$ (600 MHz)

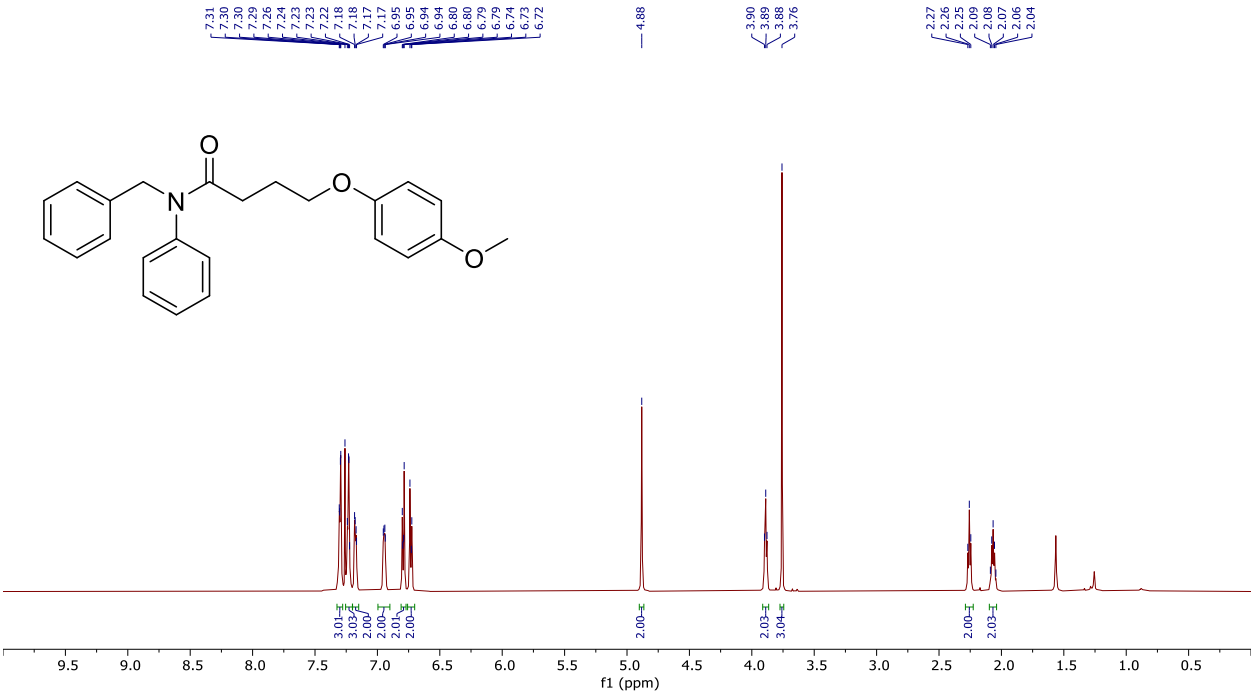

^{13}C NMR Spectrum $CDCl_3$ (151 MHz)

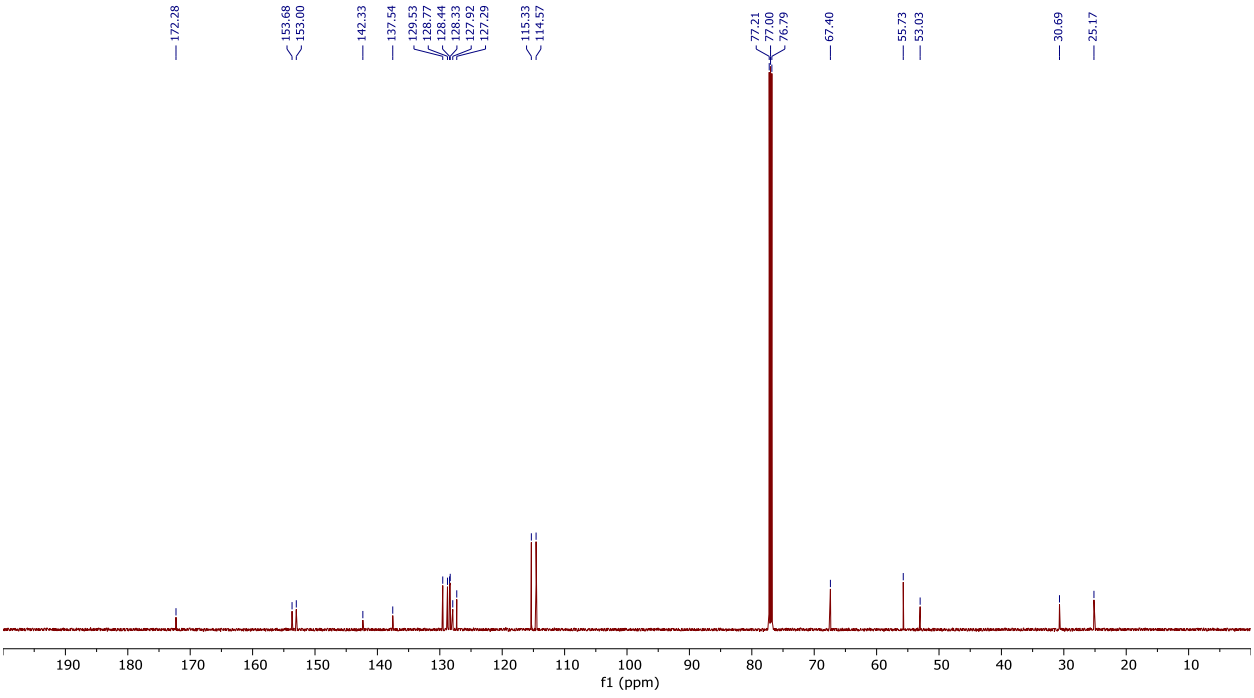

4-[tert-butyl(dimethyl)silyl]oxy-*N*-[(4-methoxyphenyl)methyl]-*N*-phenyl-butanamide

^{1}H NMR Spectrum $CDCl_3$ (600 MHz)

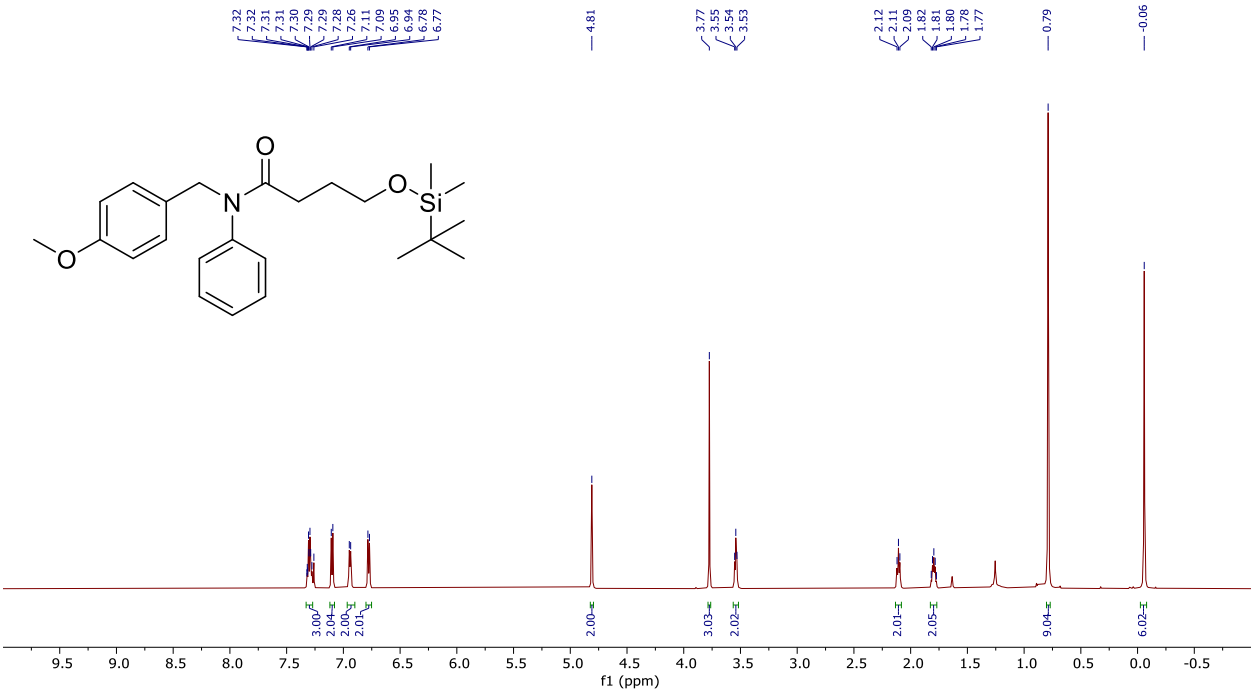

^{13}C NMR Spectrum $CDCl_3$ (151 MHz)

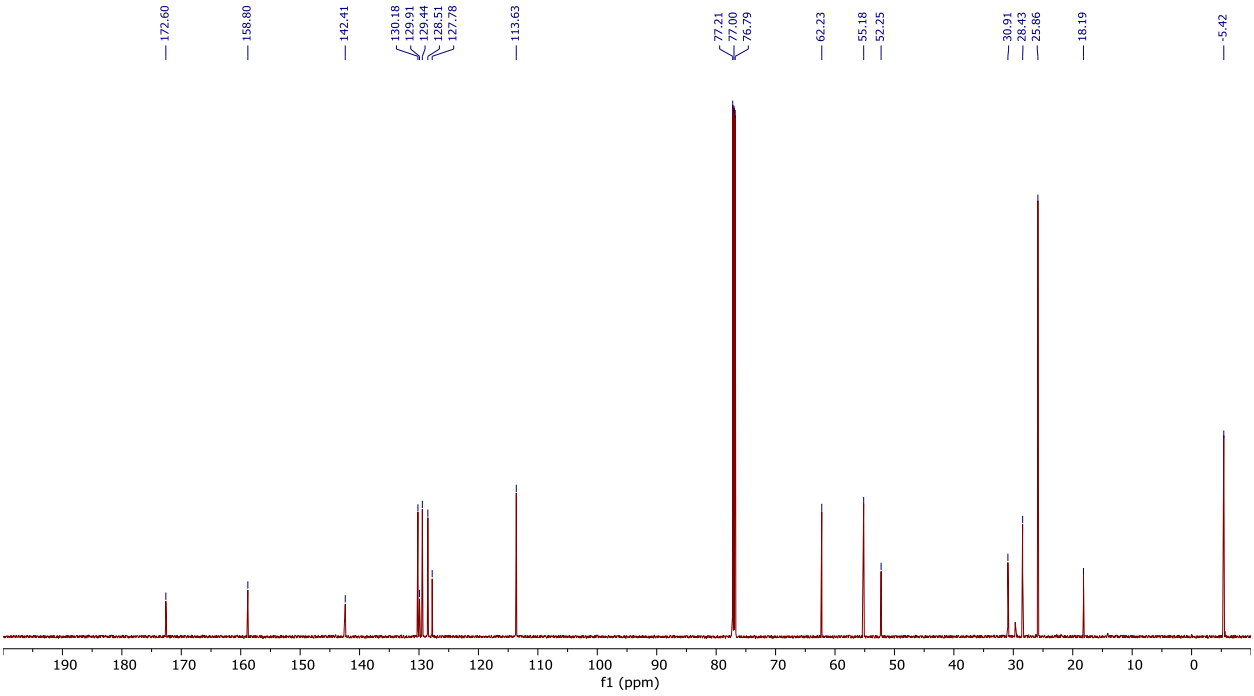

tert-butyl *N*-[4-[*N*-[(4-methoxyphenyl)methyl]anilino]-4-oxo-butyl]carbamate

^{1}H NMR Spectrum $CDCl_3$ (600 MHz)

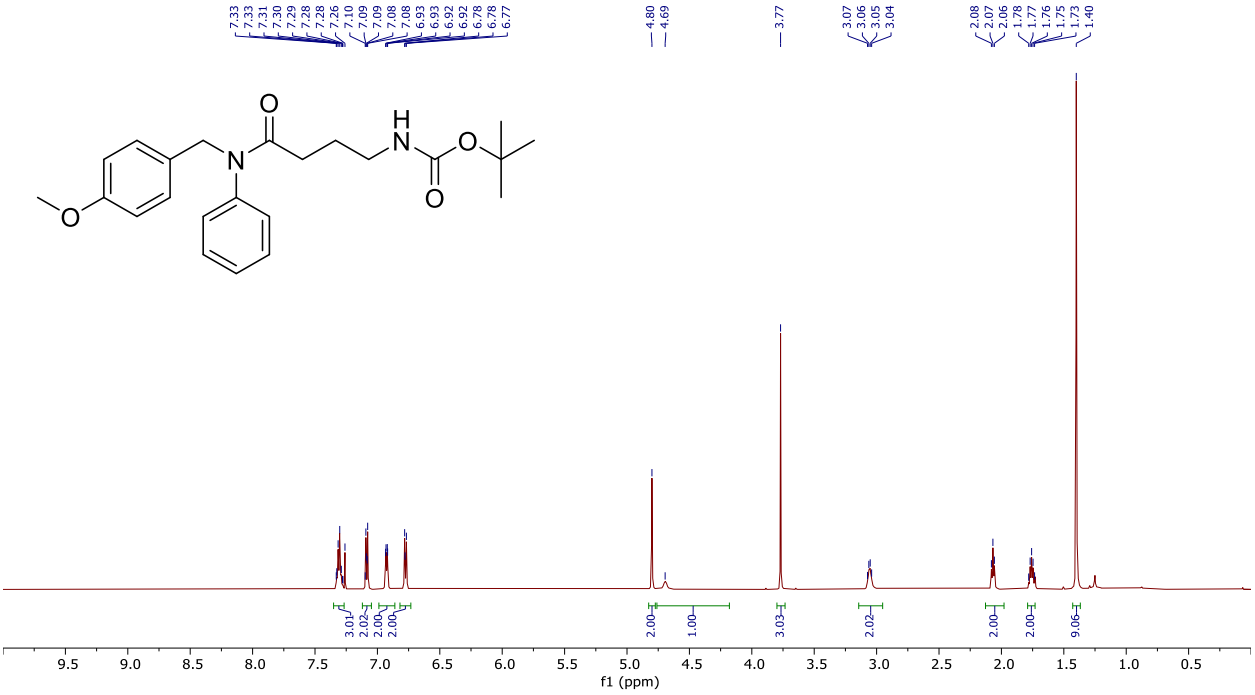

^{13}C NMR Spectrum $CDCl_3$ (151 MHz)

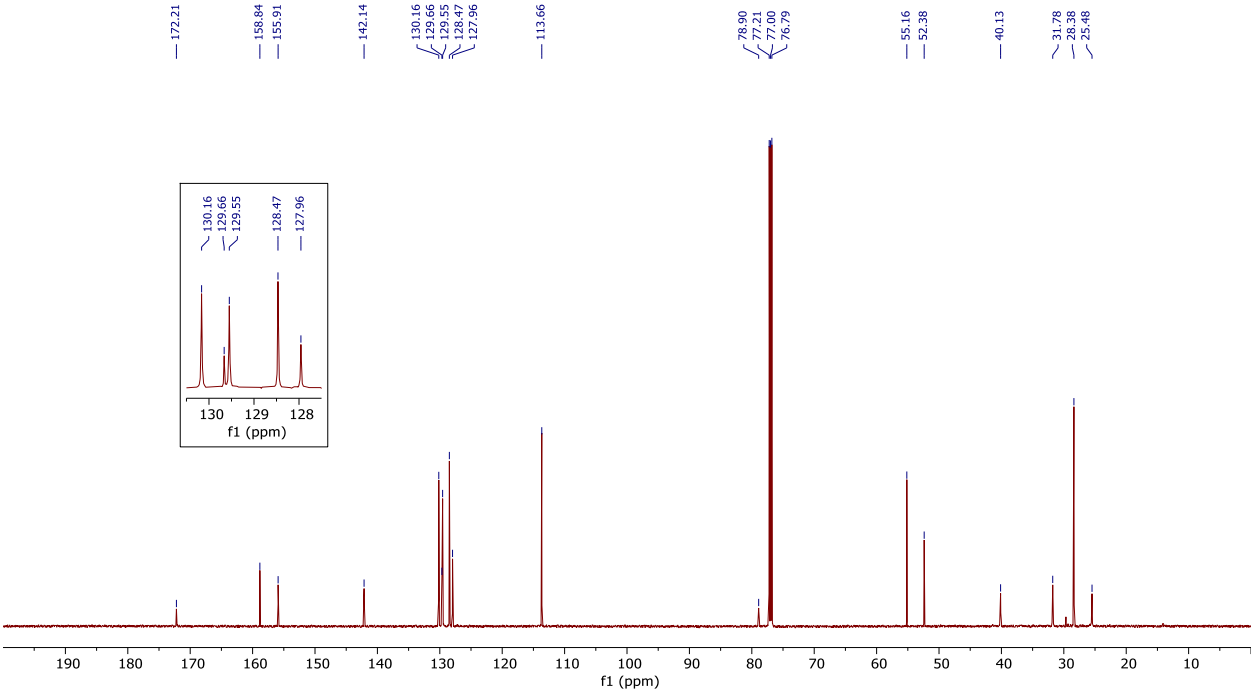

tert-butyl *N*-(4-indolin-1-yl-4-oxo-butyl)carbamate

^{1}H NMR Spectrum $CDCl_3$ (600 MHz)

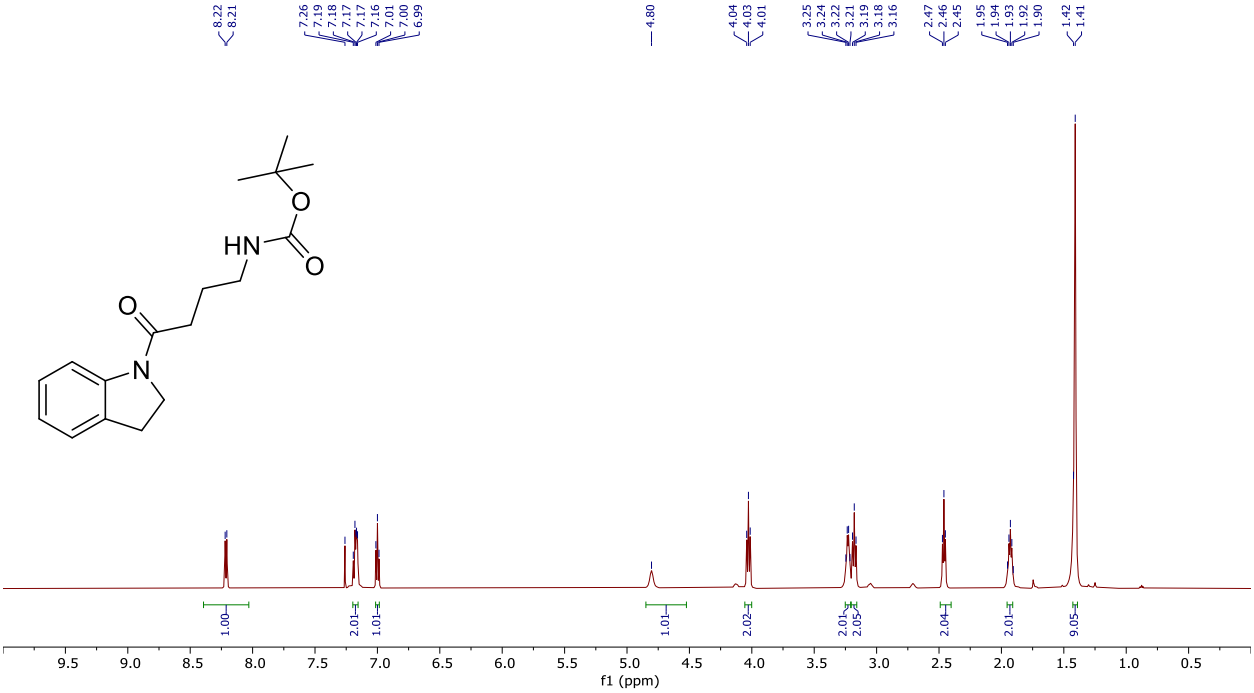

^{13}C NMR Spectrum $CDCl_3$ (151 MHz)

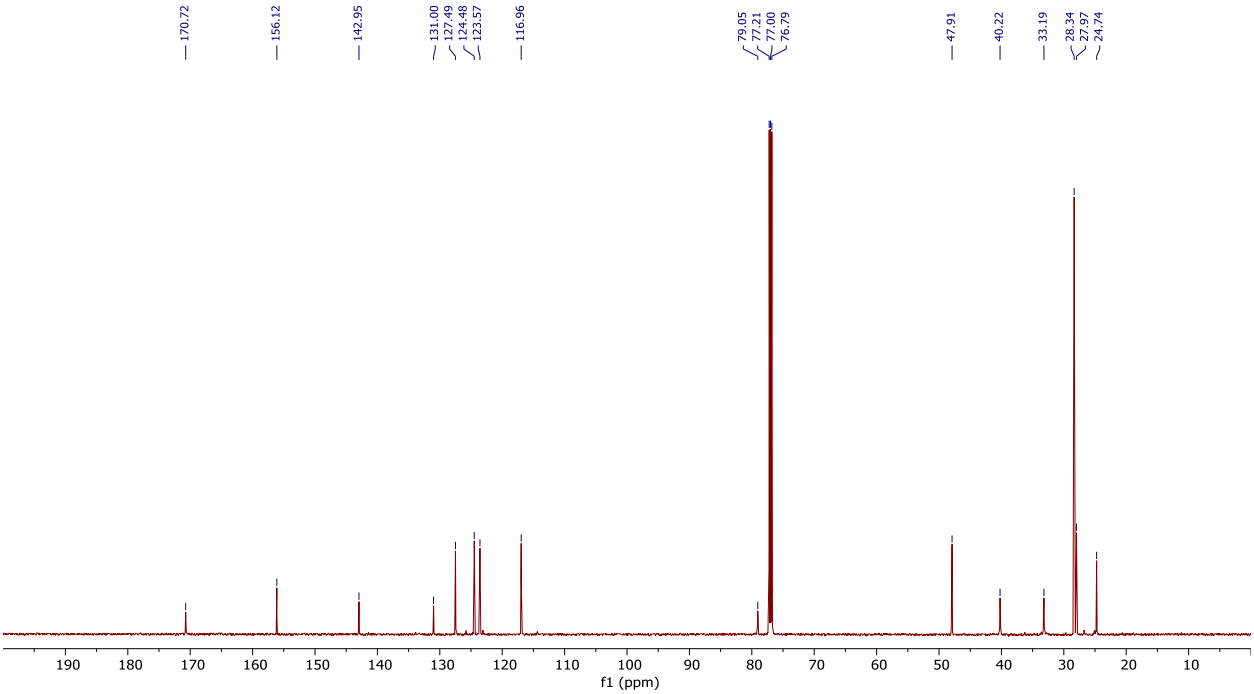

tert-butyl *N*-(4-benzo[b][1]benzazepin-11-yl-4-oxo-butyl)carbamate

^{1}H NMR Spectrum $CDCl_3$ (600 MHz)

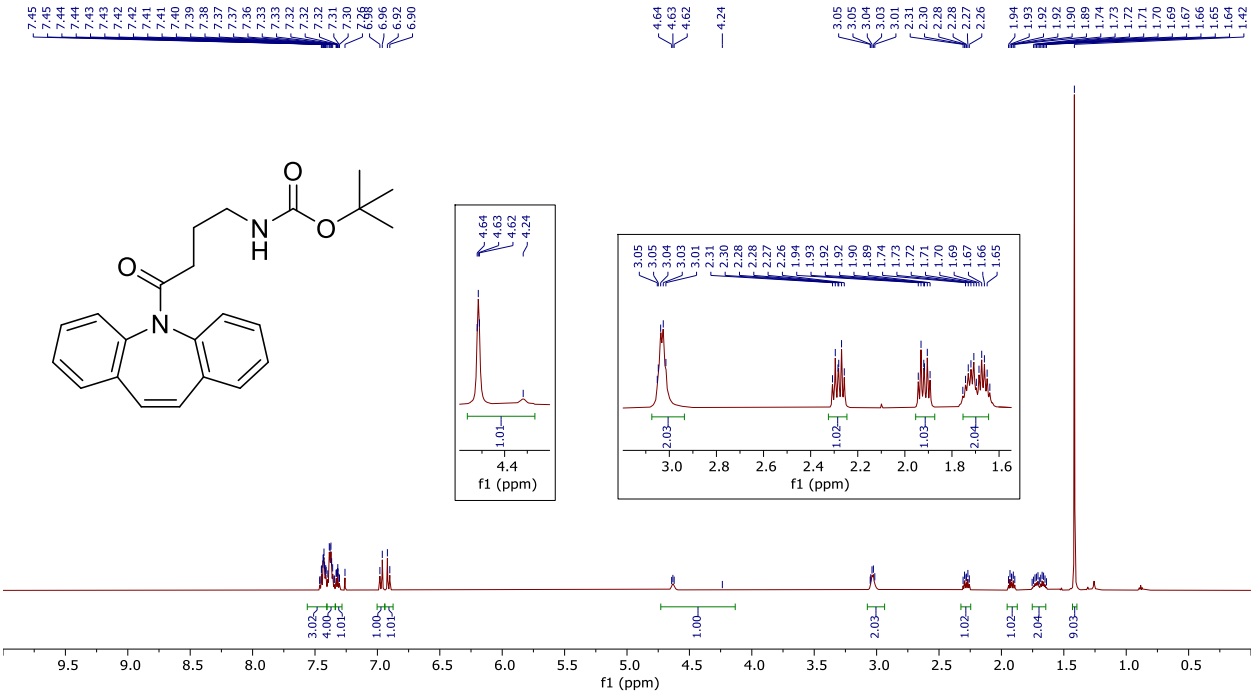

^{13}C NMR Spectrum $CDCl_3$ (151 MHz)

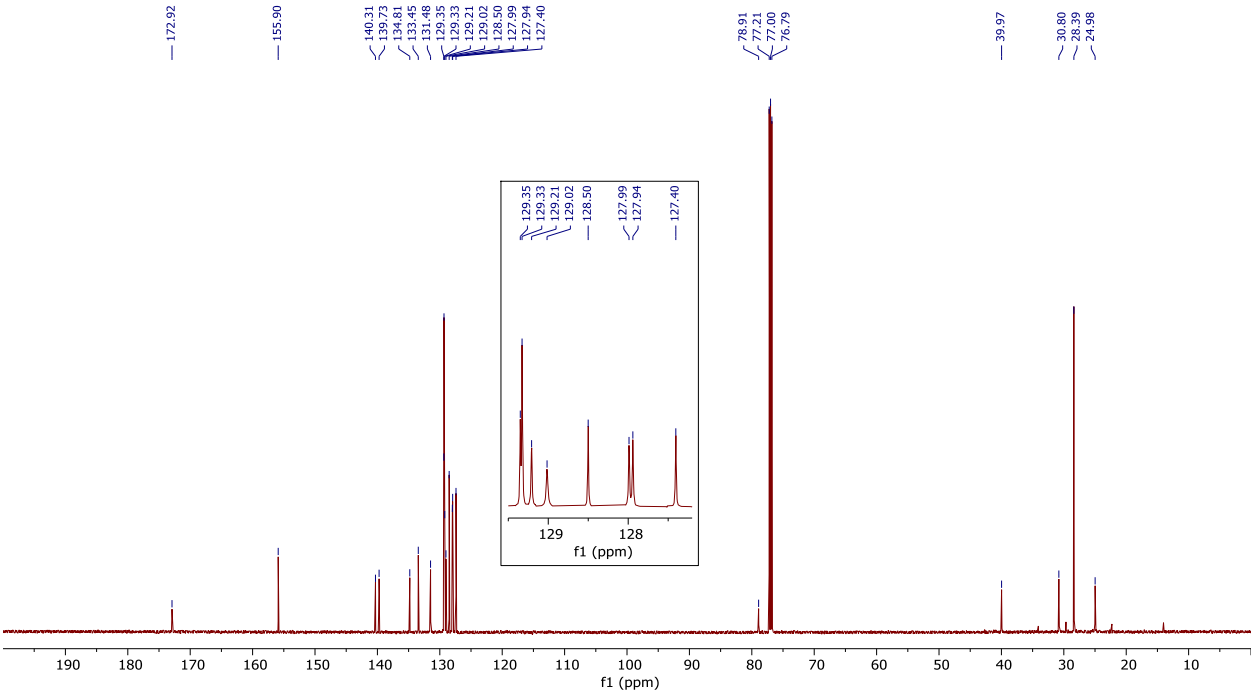

tert-butyl _N_-[4-[_N_-[(4-acetamidophenyl)methyl]anilino]-4-oxo-butyl]carbamate

^{1}H NMR Spectrum $CDCl_3$ (600 MHz)

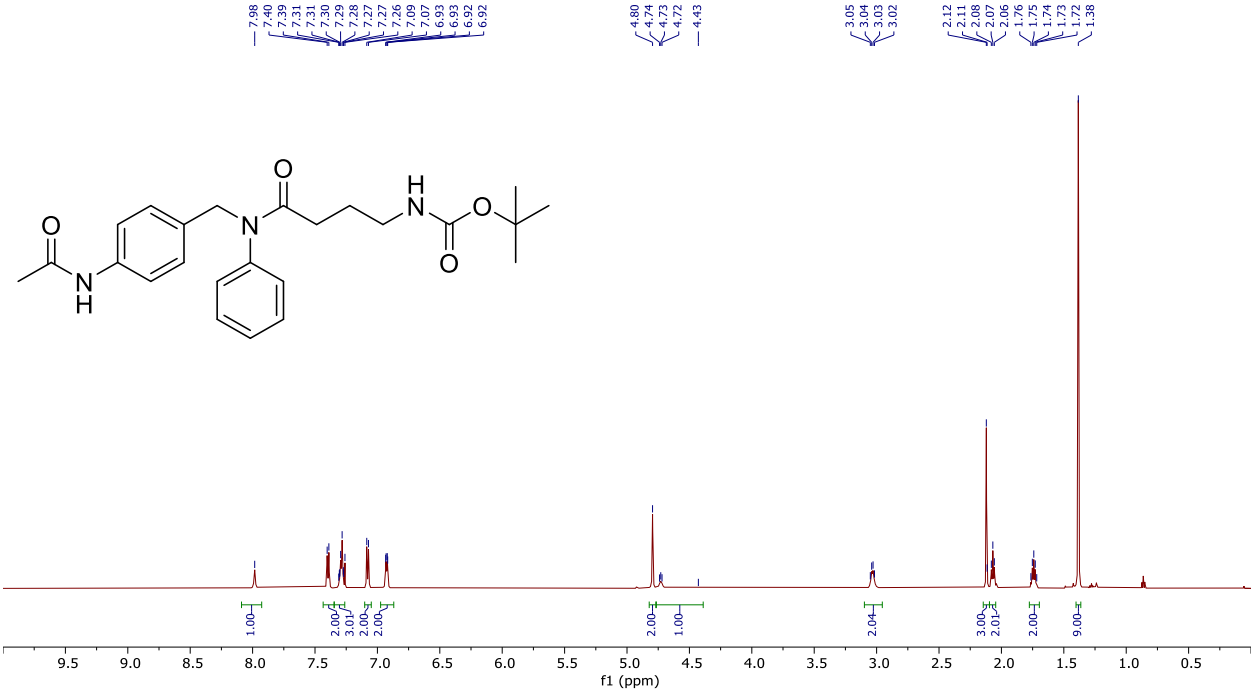

^{13}C NMR Spectrum $CDCl_3$ (151 MHz)

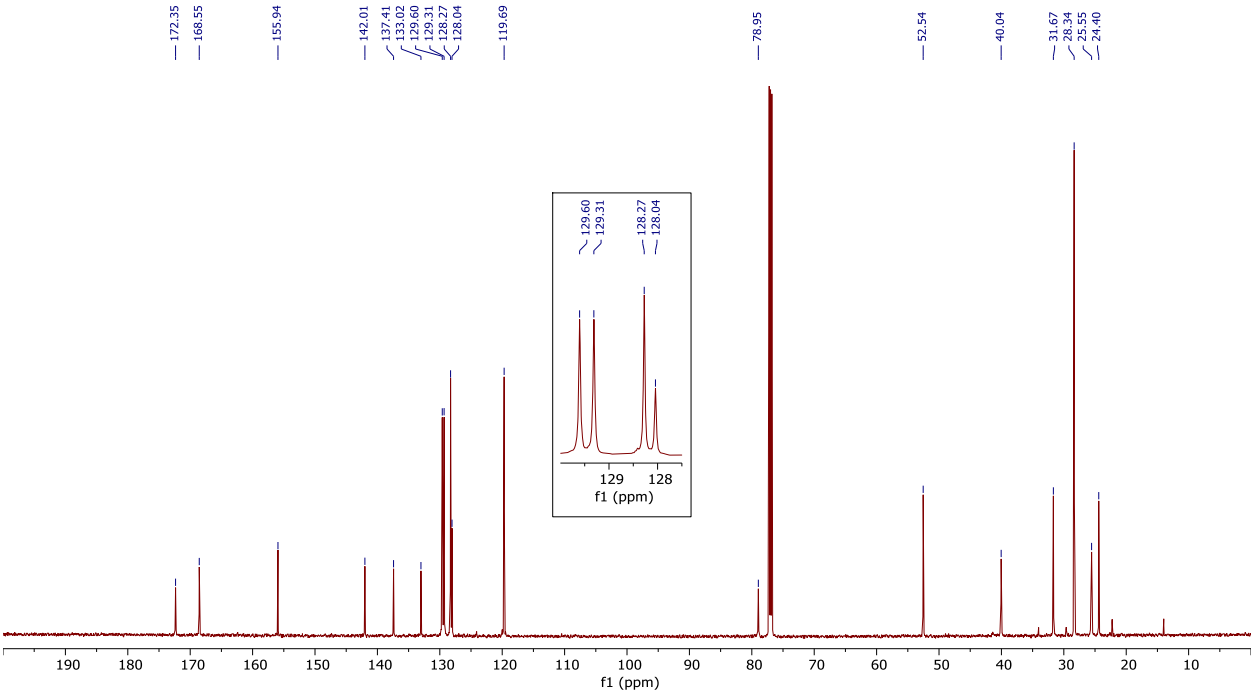

tert-butyl _N_-[4-[4-(furan-2-carbonyl)piperazin-1-yl]-4-oxo-butyl]carbamate

^{1}H NMR Spectrum $CDCl_3$ (600 MHz)

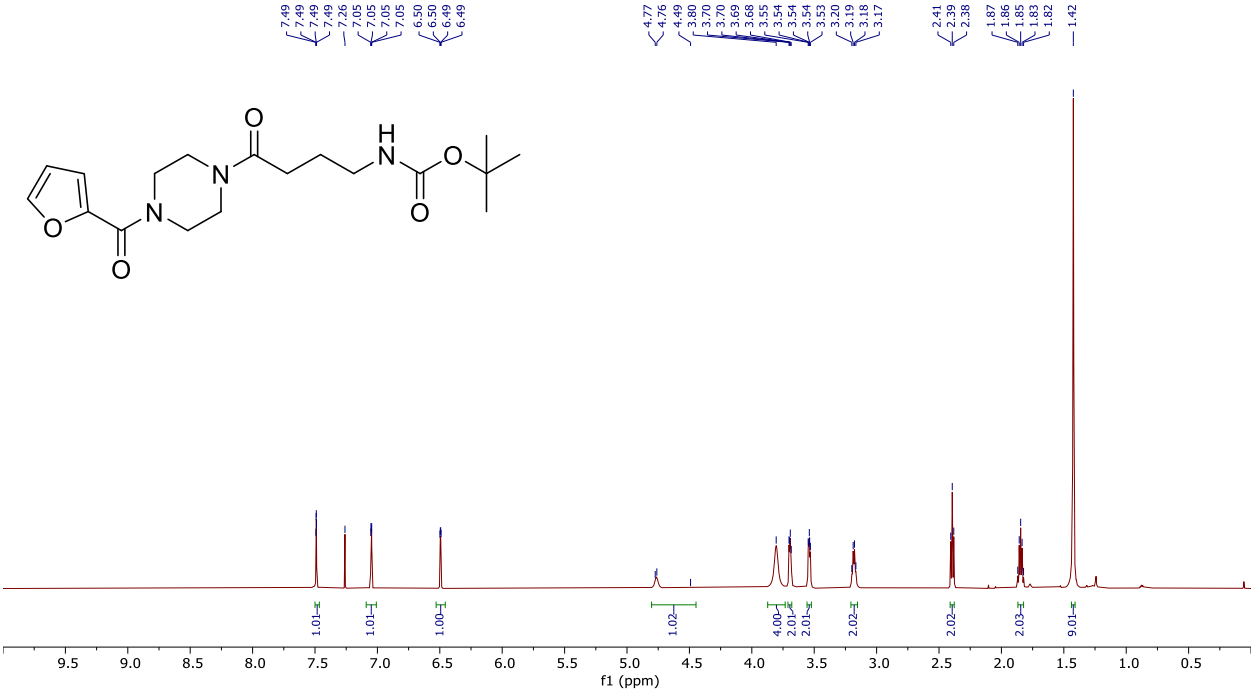

^{13}C NMR Spectrum $CDCl_3$ (151 MHz)

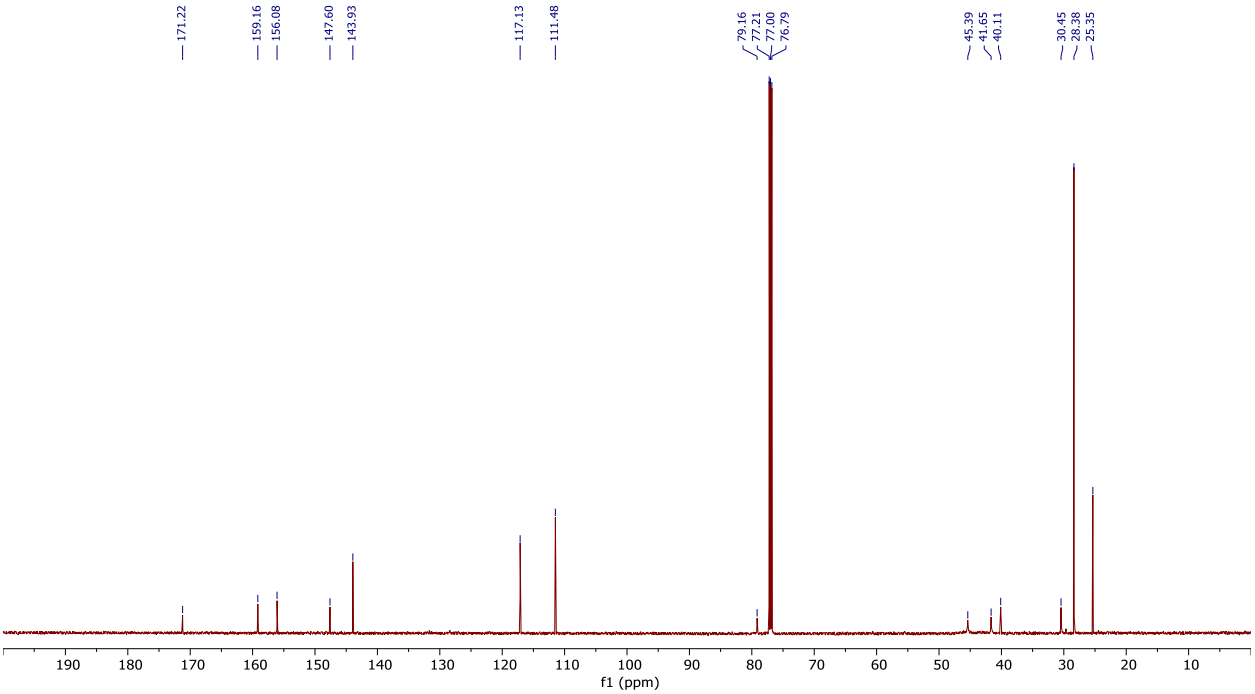

tert-butyl *N*-[4-(dibenzylamino)-4-oxo-butyl]carbamate

^{1}H NMR Spectrum $CDCl_3$ (600 MHz)

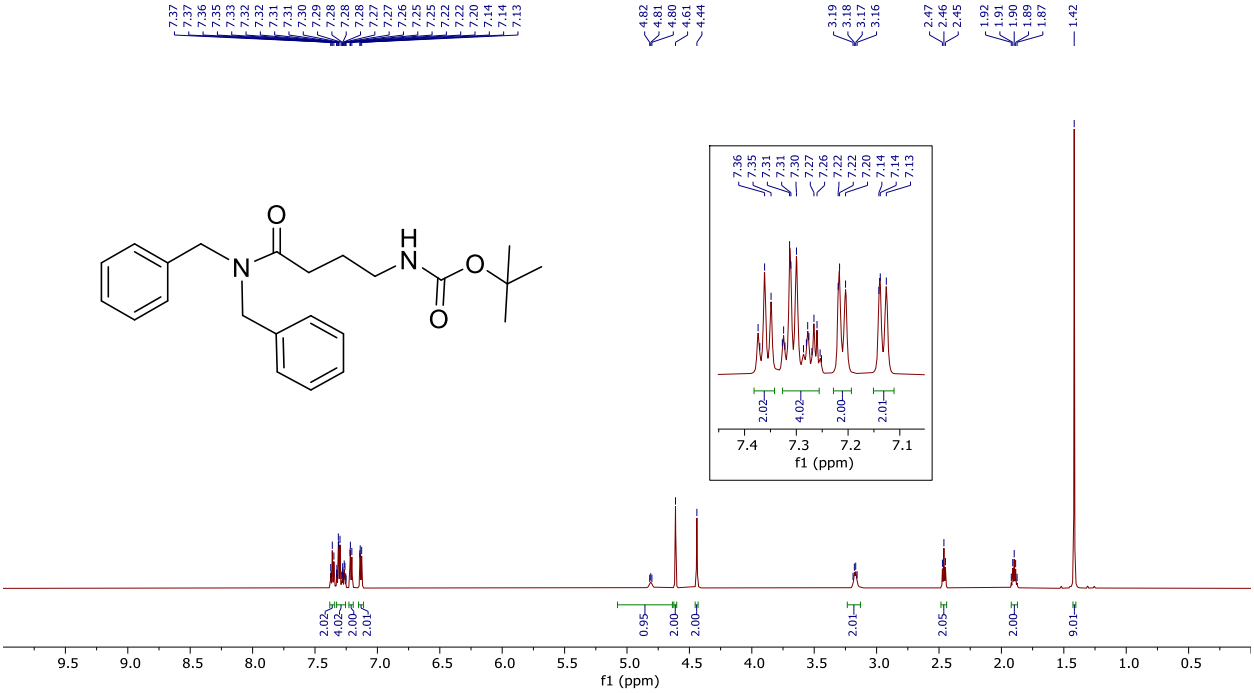

^{13}C NMR Spectrum $CDCl_3$ (151 MHz)

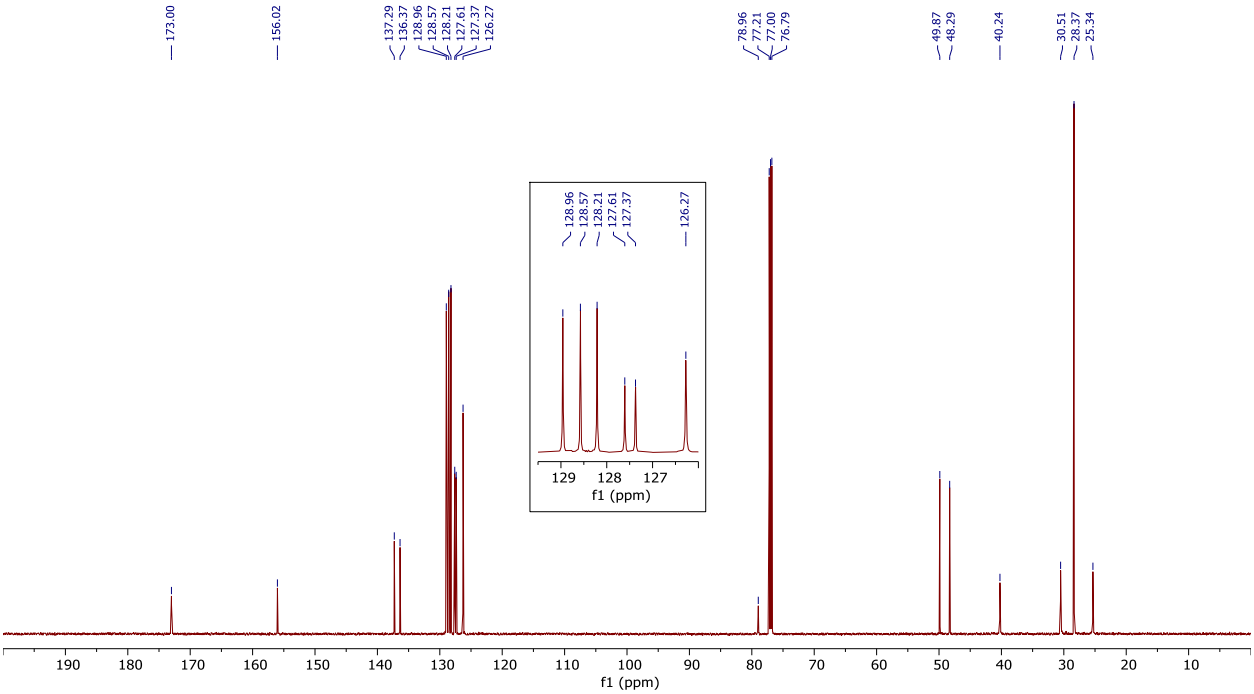

tert-butyl *N*-[4-(*N*-benzylanilino)-4-oxo-butyl]carbamate

^{1}H NMR Spectrum $CDCl_3$ (600 MHz)

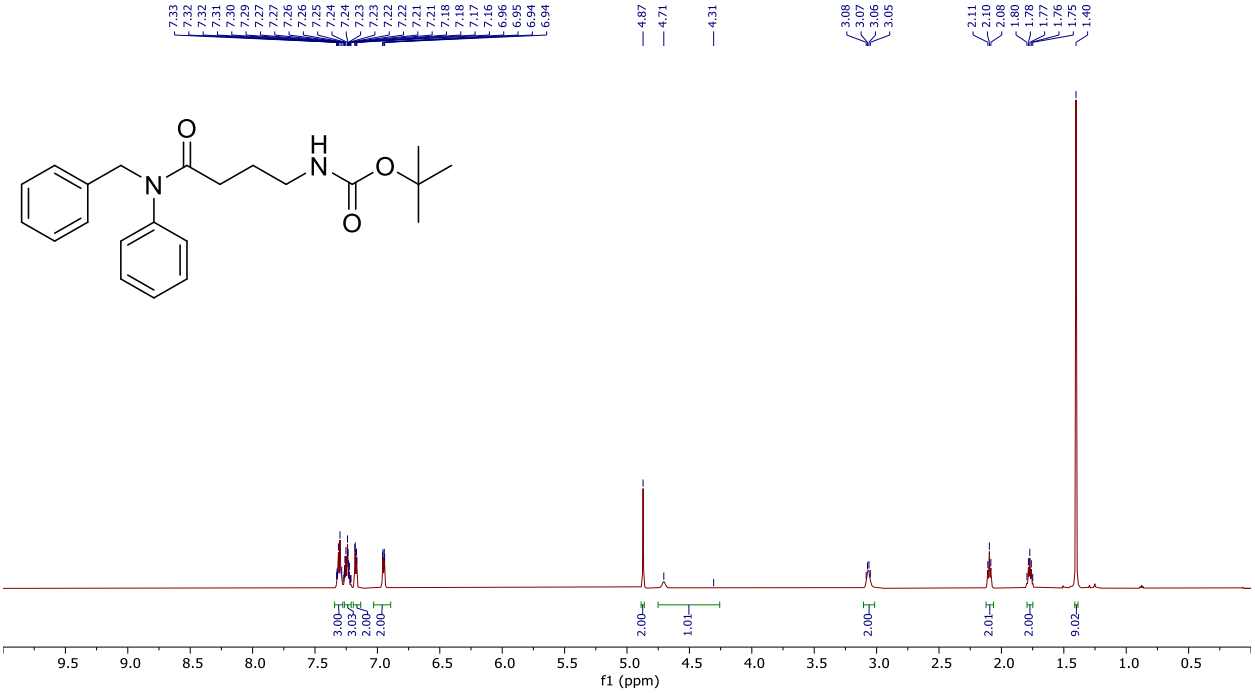

^{13}C NMR Spectrum $CDCl_3$ (151 MHz)

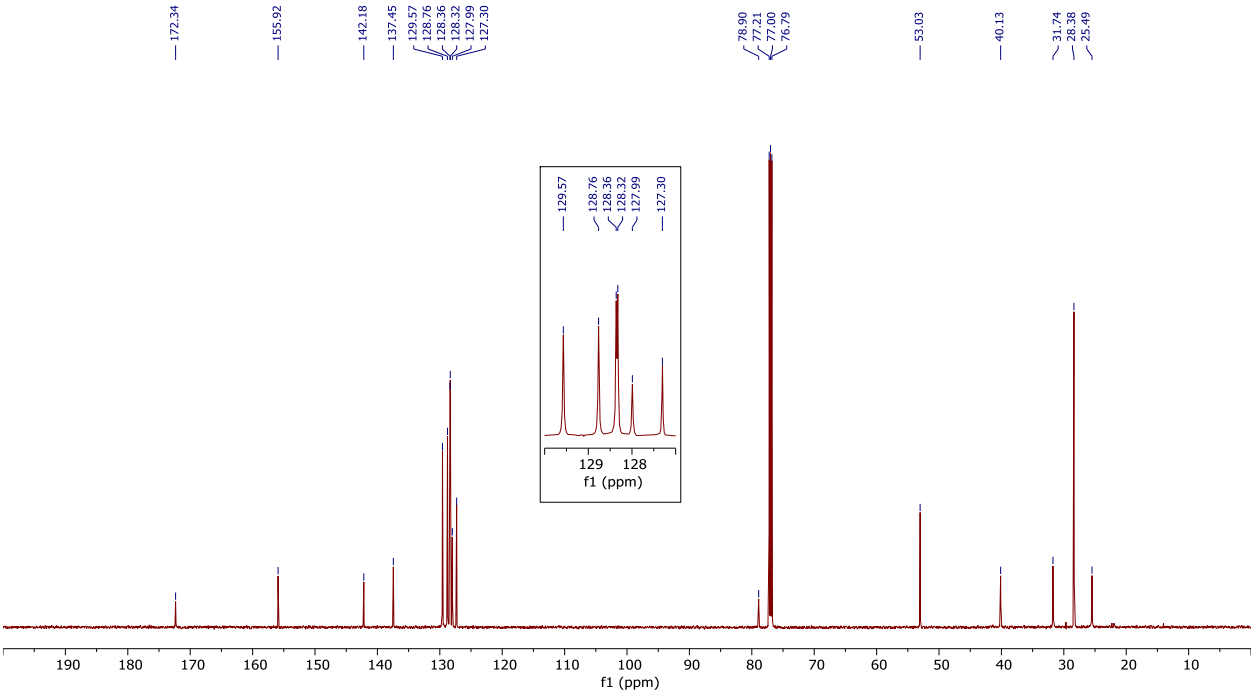

tert-butyl _N_-[4-[_N_-[(4-fluorophenyl)methyl]anilino]-4-oxo-butyl]carbamate

^{1}H NMR Spectrum $CDCl_3$ (600 MHz)

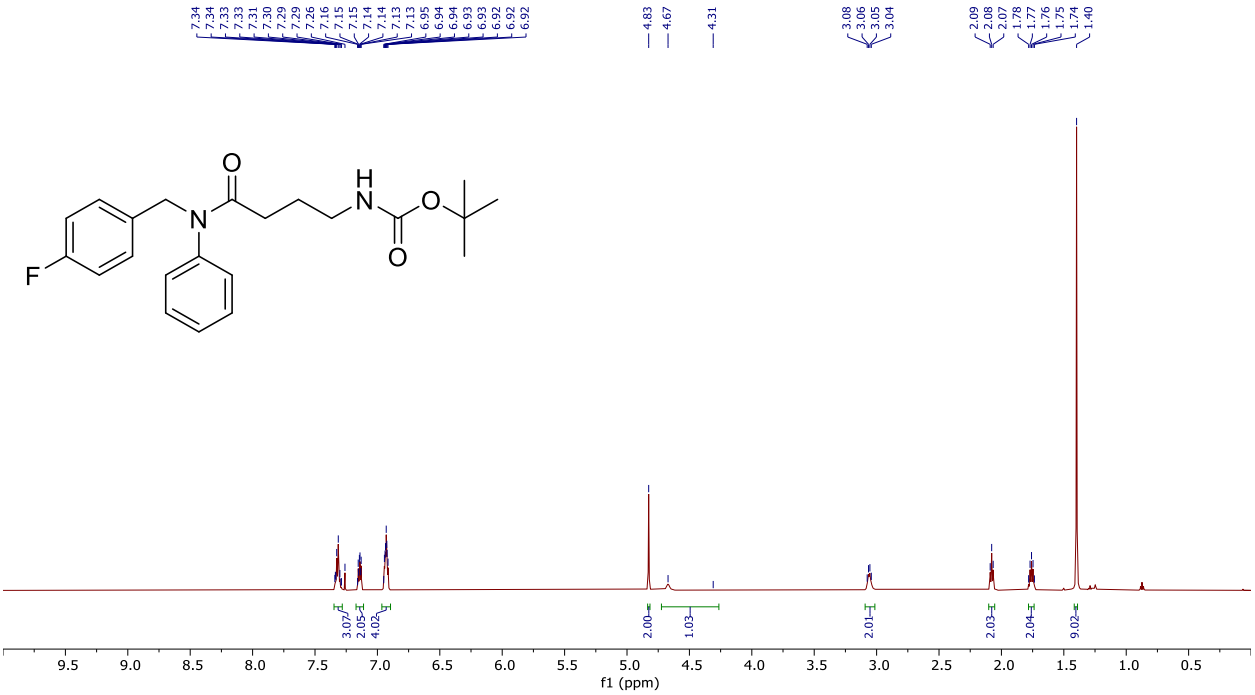

^{13}C NMR Spectrum $CDCl_3$ (151 MHz)

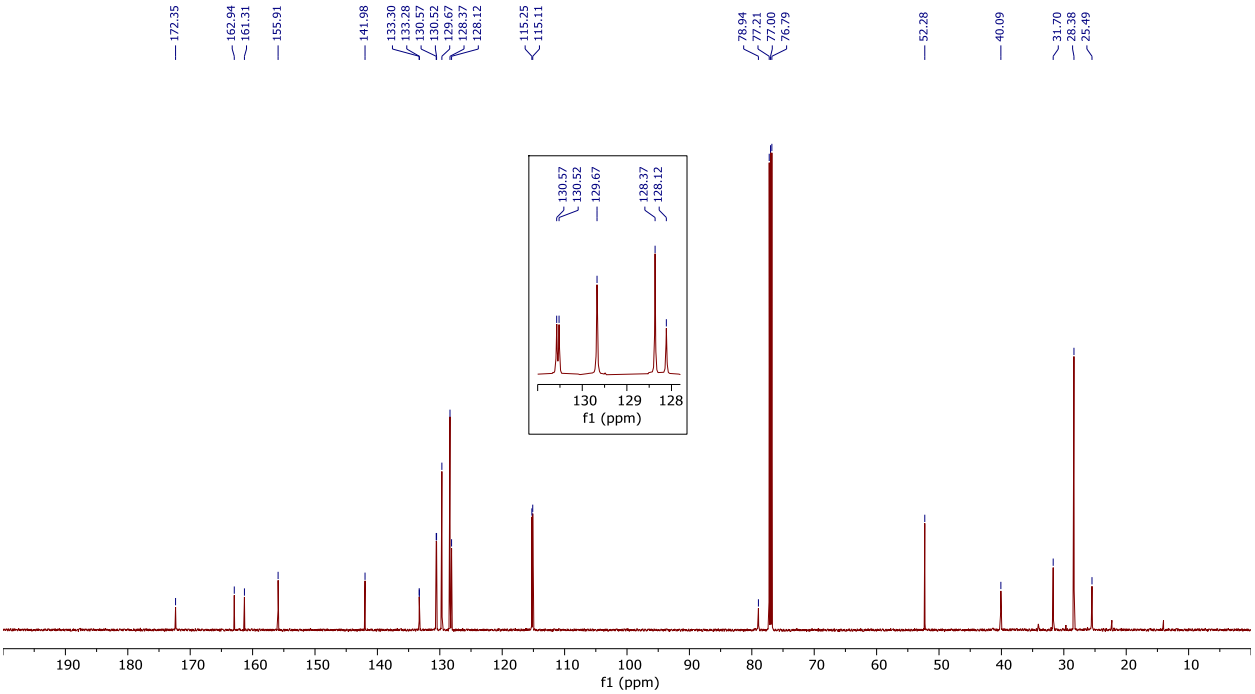

^{19}F NMR Spectrum $CDCl_3$ (282 MHz)

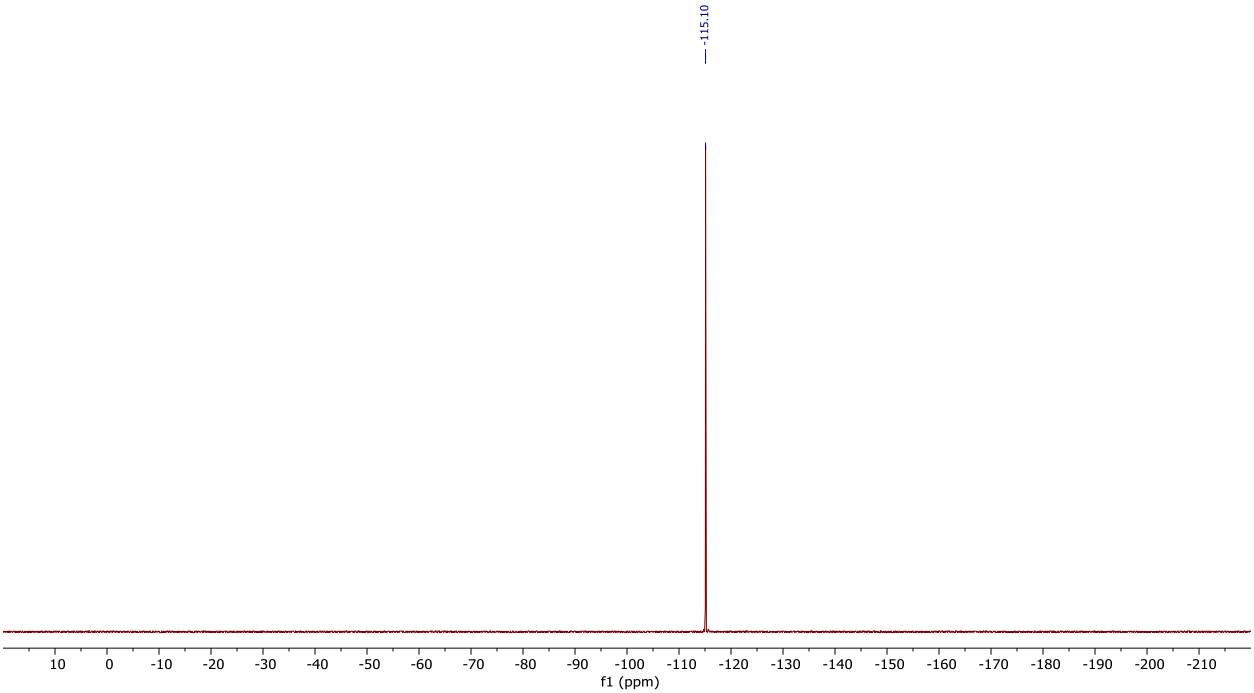

tert-butyl _N_-[4-[_N_-[[4-(dimethylamino)phenyl]methyl]anilino]-4-oxo-butyl]carbamate

^{1}H NMR Spectrum $CDCl_3$ (600 MHz)

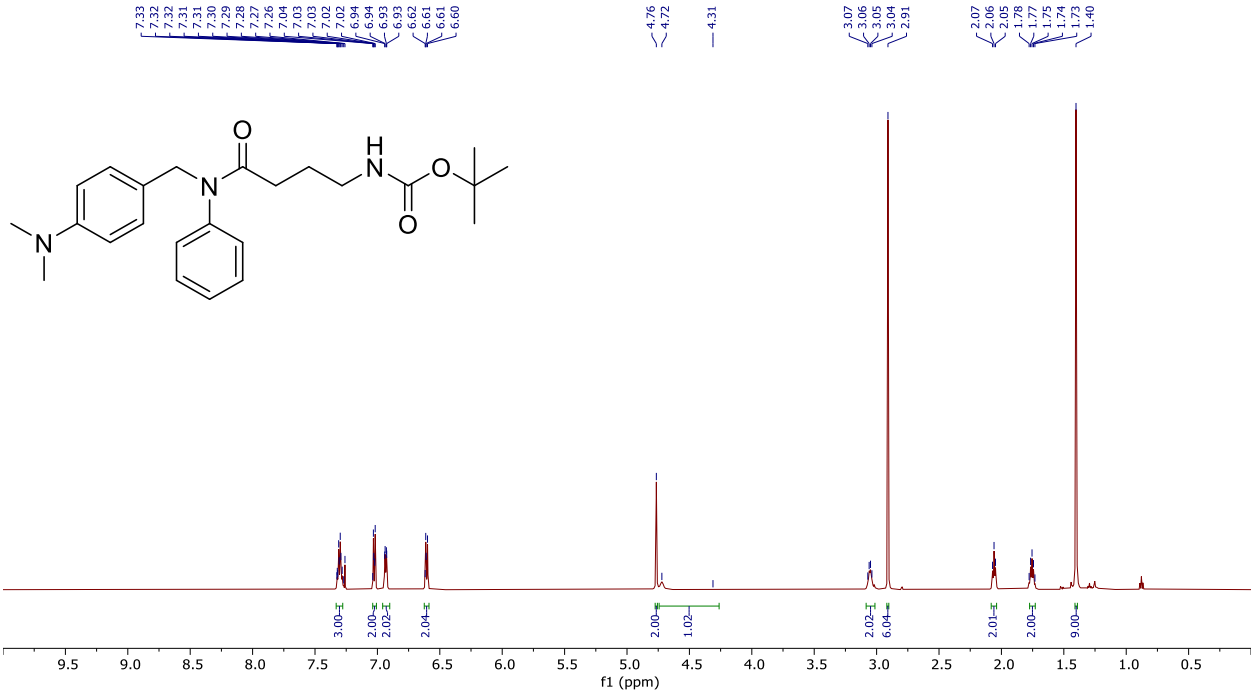

^{13}C NMR Spectrum $CDCl_3$ (151 MHz)

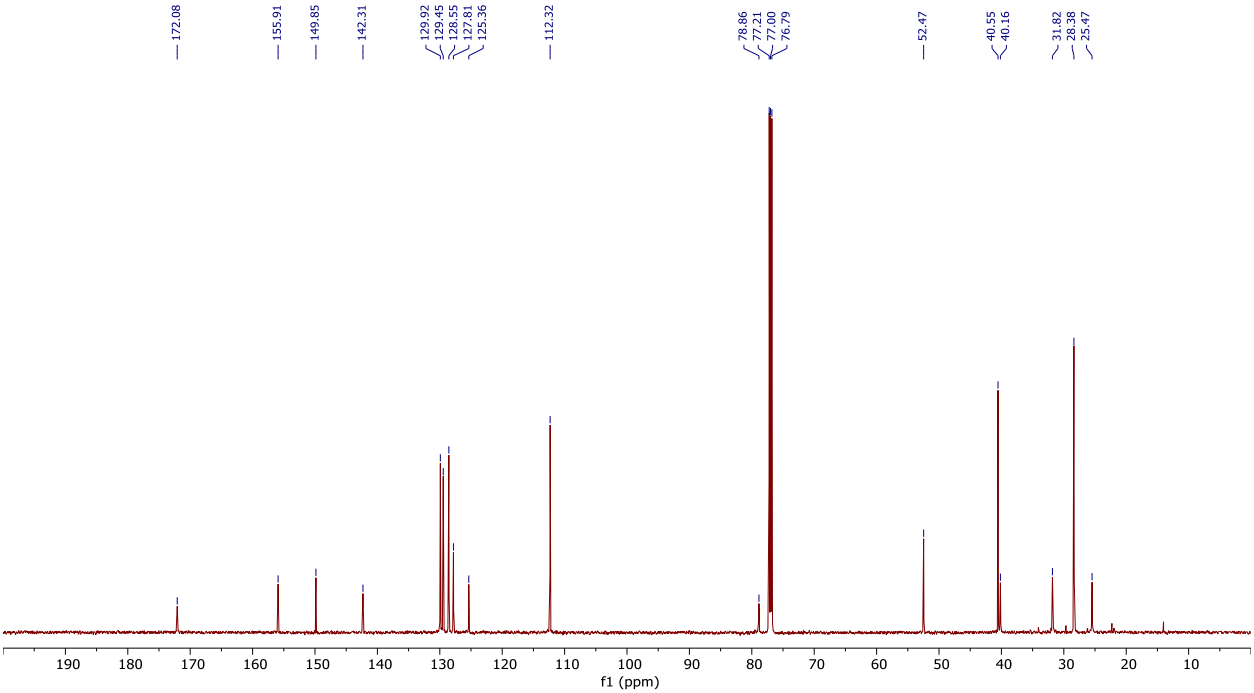

tert-butyl *N*-[4-[*N*-(1,3-benzodioxol-5-ylmethyl)anilino]-4-oxo-butyl]carbamate

^{1}H NMR Spectrum $CDCl_3$ (600 MHz)

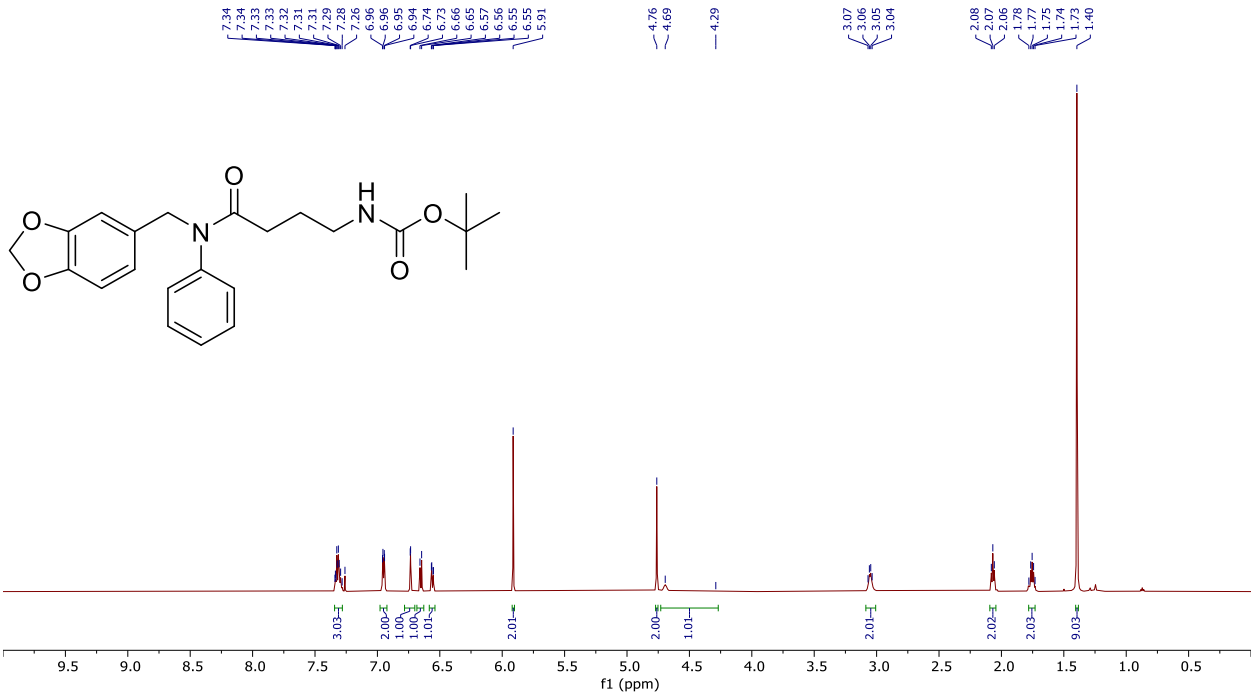

^{13}C NMR Spectrum $CDCl_3$ (151 MHz)

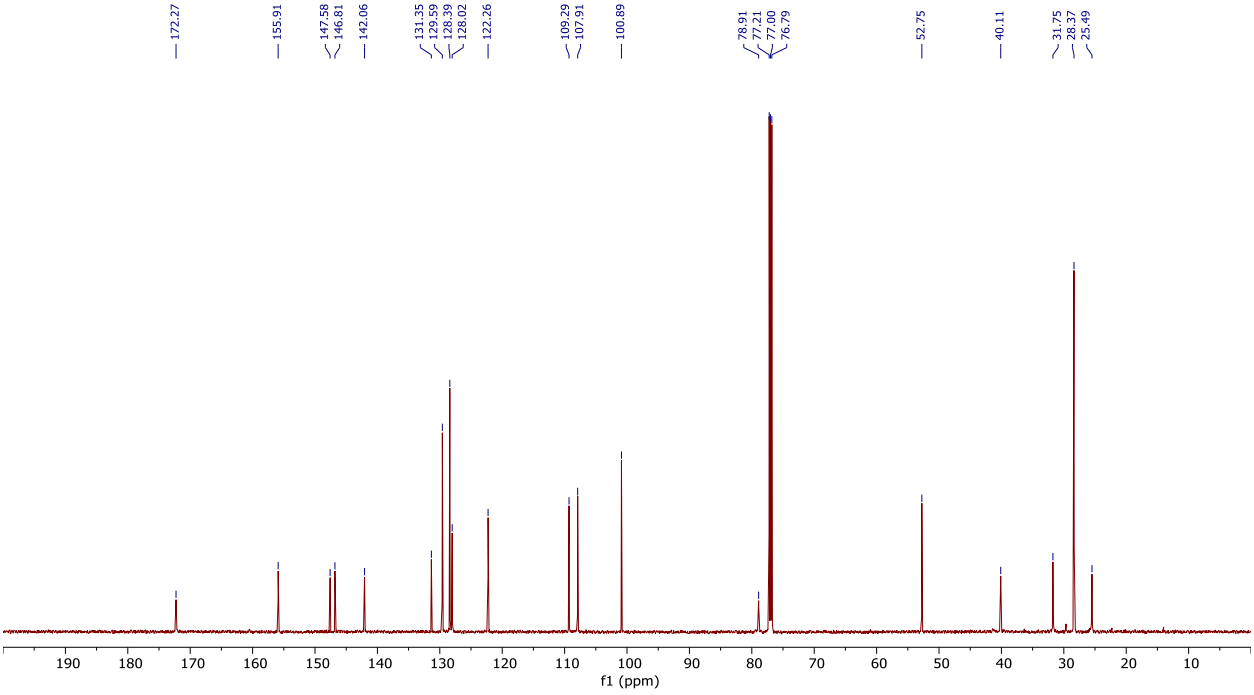

tert-butyl *N*-[4-(*N*-benzyl-4-methoxy-anilino)-4-oxo-butyl]carbamate

^{1}H NMR Spectrum $CDCl_3$ (600 MHz)

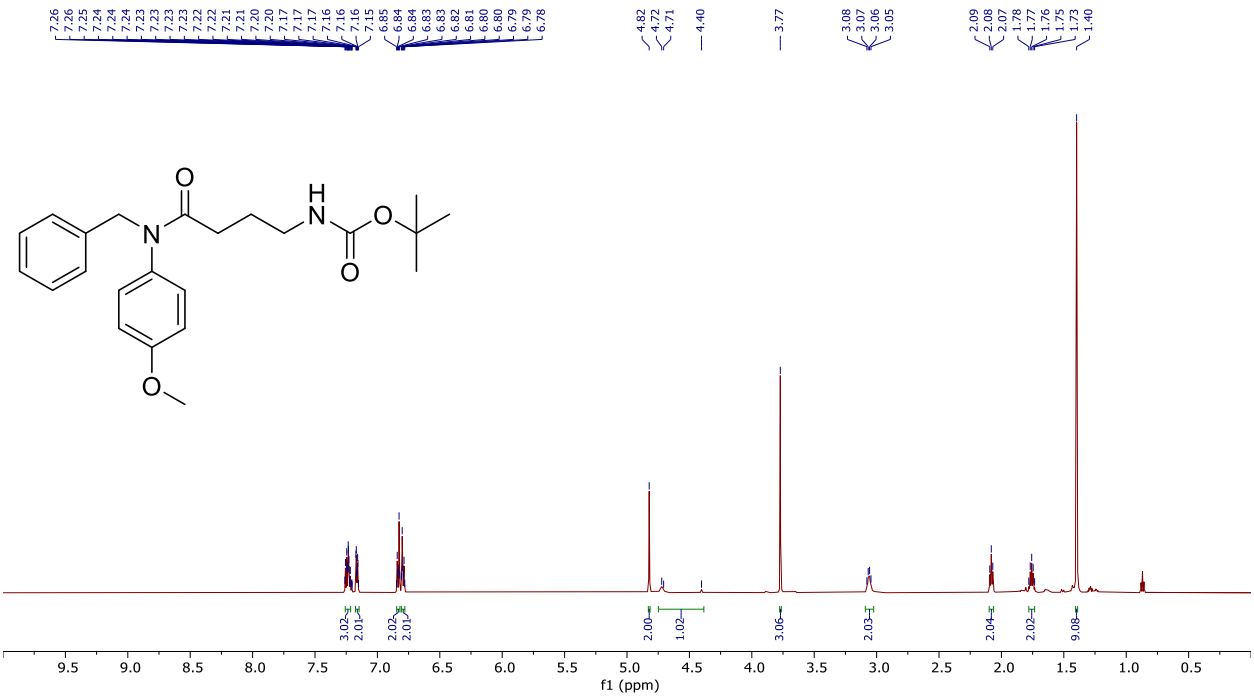

^{13}C NMR Spectrum $CDCl_3$ (151 MHz)

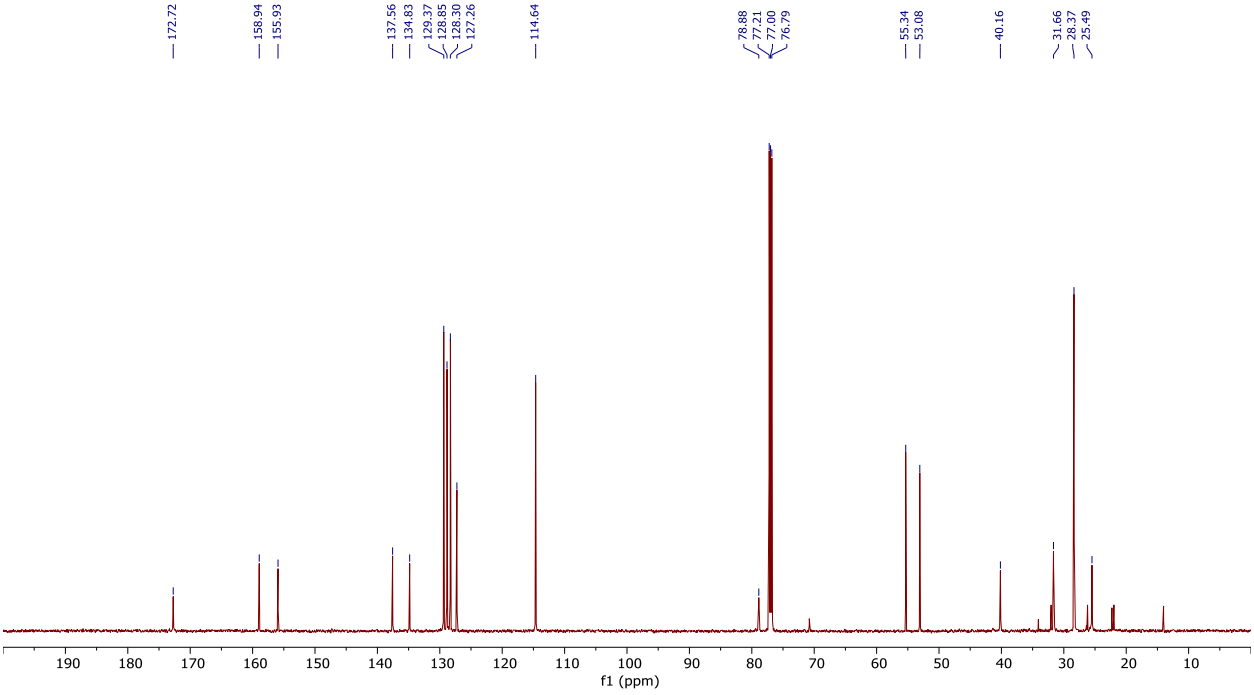

tert-butyl *N*-[4-(*N*-benzyl-2,4-dimethyl-anilino)-4-oxo-butyl]carbamate

^{1}H NMR Spectrum $CDCl_3$ (600 MHz)

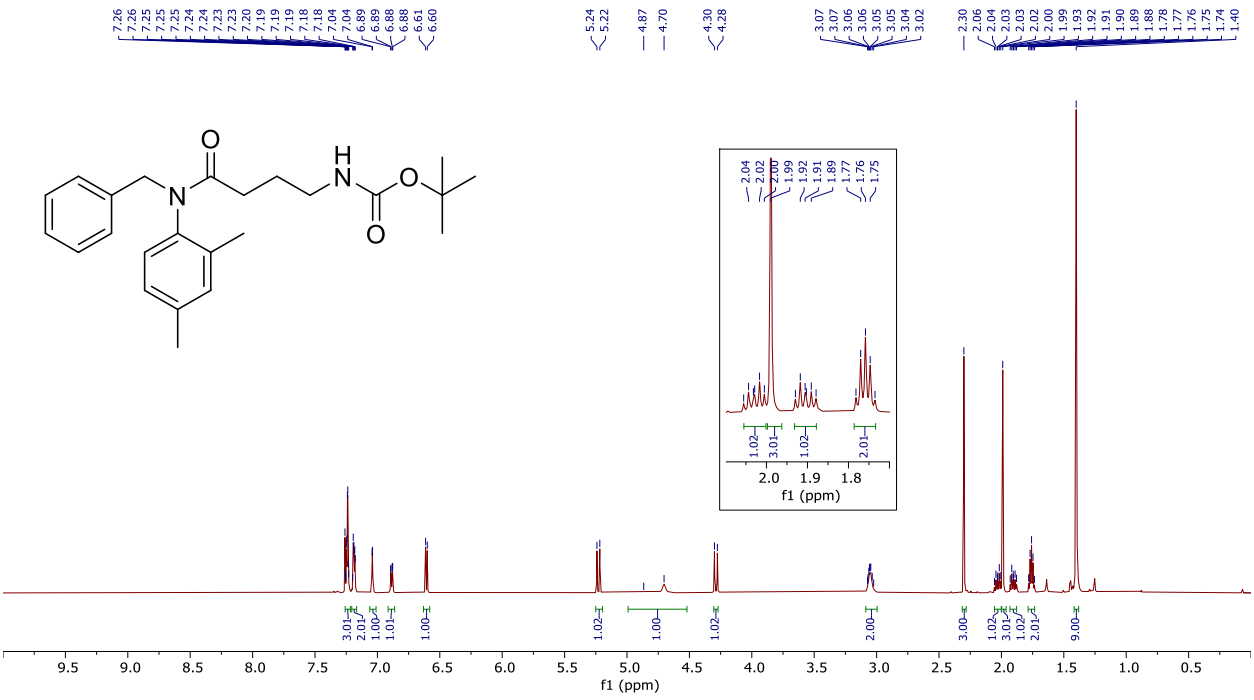

^{13}C NMR Spectrum $CDCl_3$ (151 MHz)

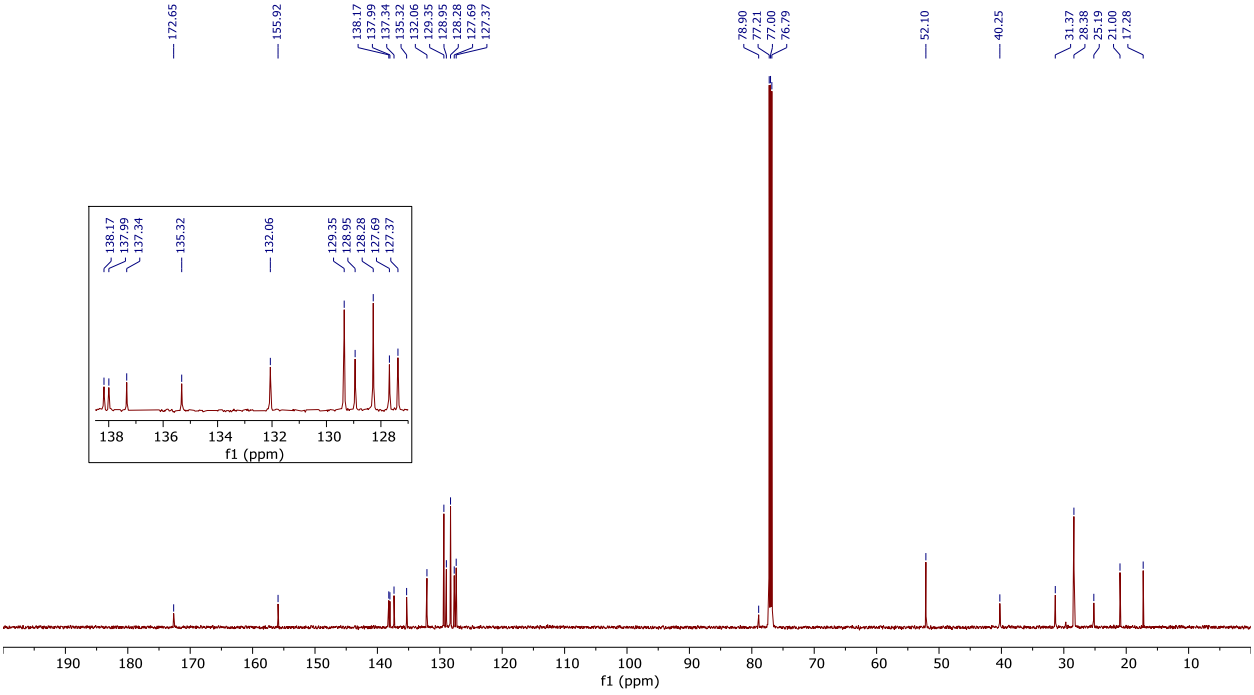

tert-butyl _N_-[4-[_N_-benzyl-4-(trifluoromethyl)anilino]-4-oxo-butyl]carbamate

^{1}H NMR Spectrum $CDCl_3$ (600 MHz)

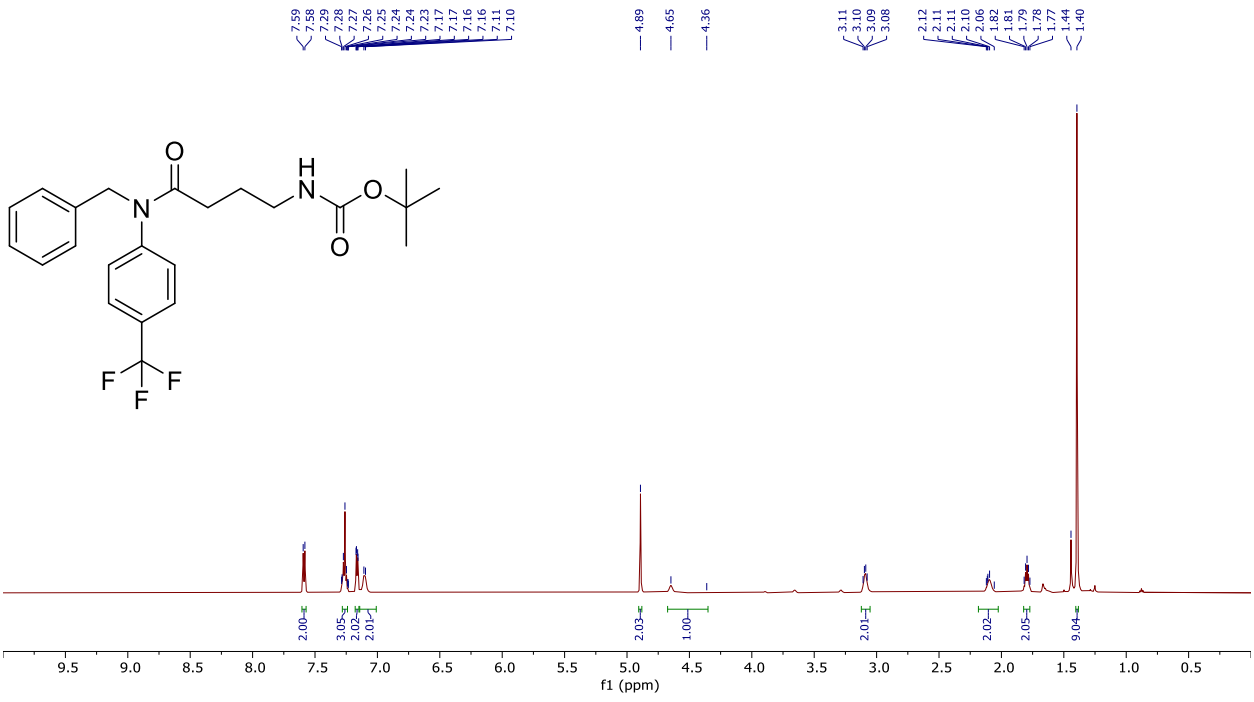

^{13}C NMR Spectrum $CDCl_3$ (151 MHz)

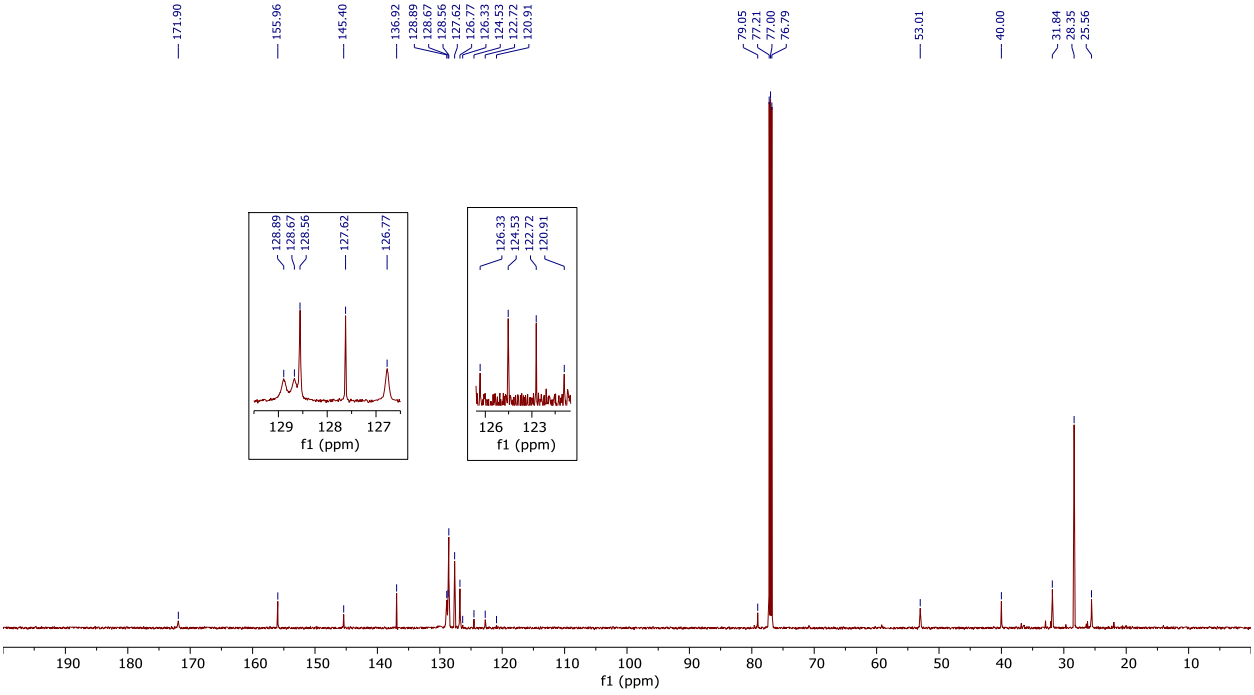

^{19}F NMR Spectrum $CDCl_3$ (282 MHz)

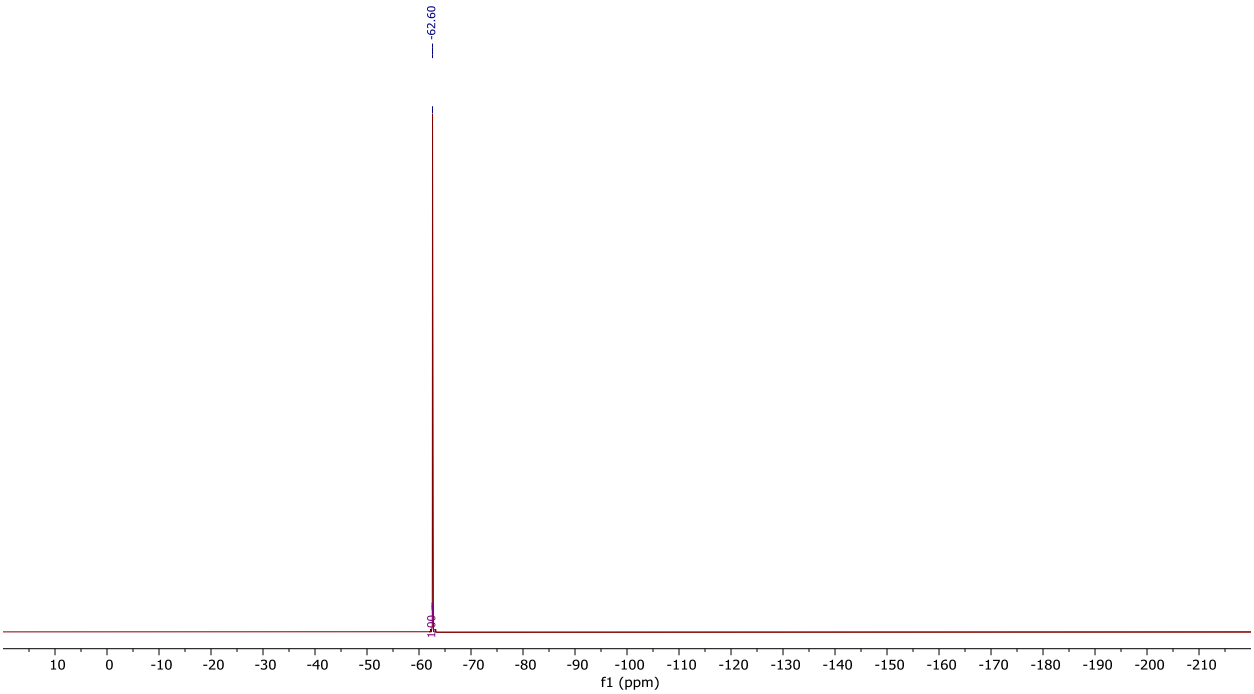

tert-butyl _N_-[4-[benzyl(_tert_-butyl)amino]-4-oxo-butyl]carbamate

^{1}H NMR Spectrum $CDCl_3$ (600 MHz)

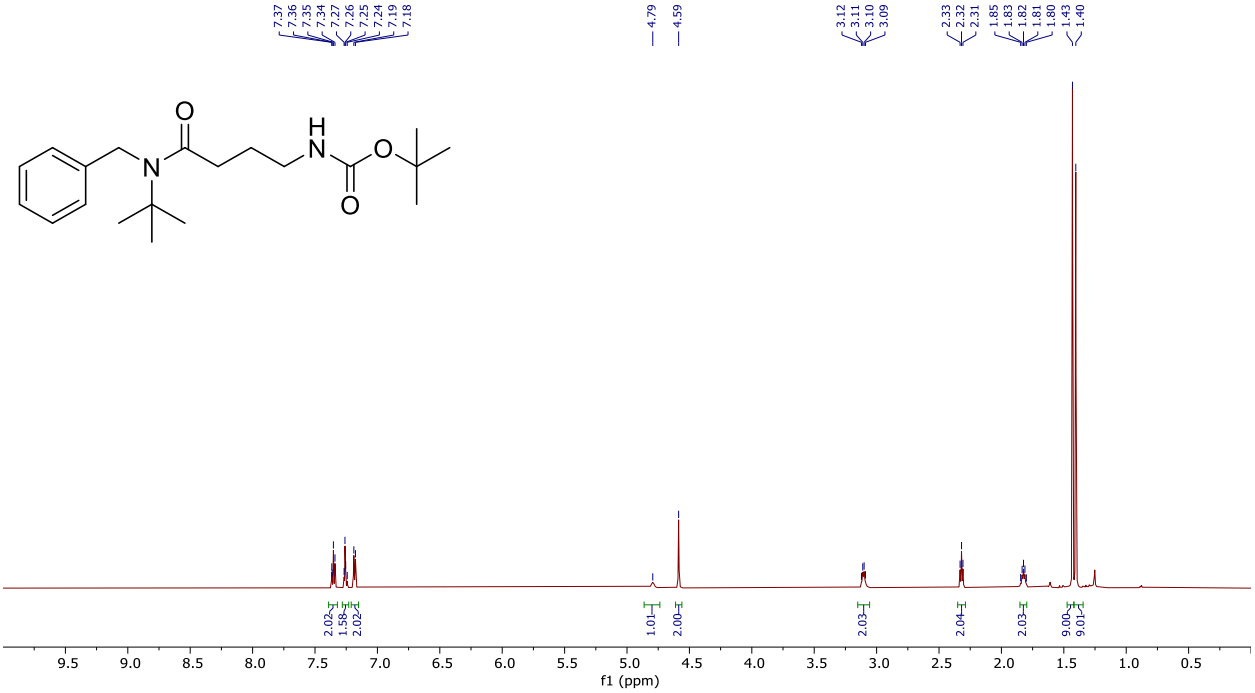

^{13}C NMR Spectrum $CDCl_3$ (151 MHz)

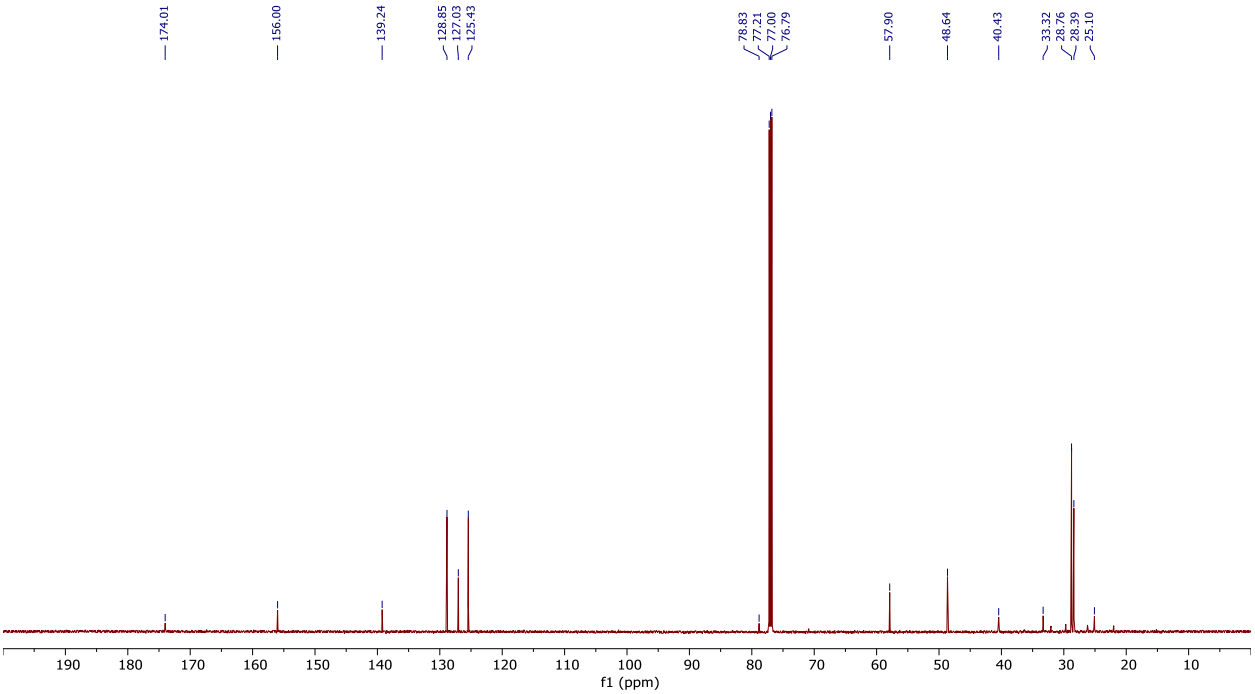

tert-butyl *N*-[4-(*N*-methylanilino)-4-oxo-butyl]carbamate

^{1}H NMR Spectrum $CDCl_3$ (600 MHz)

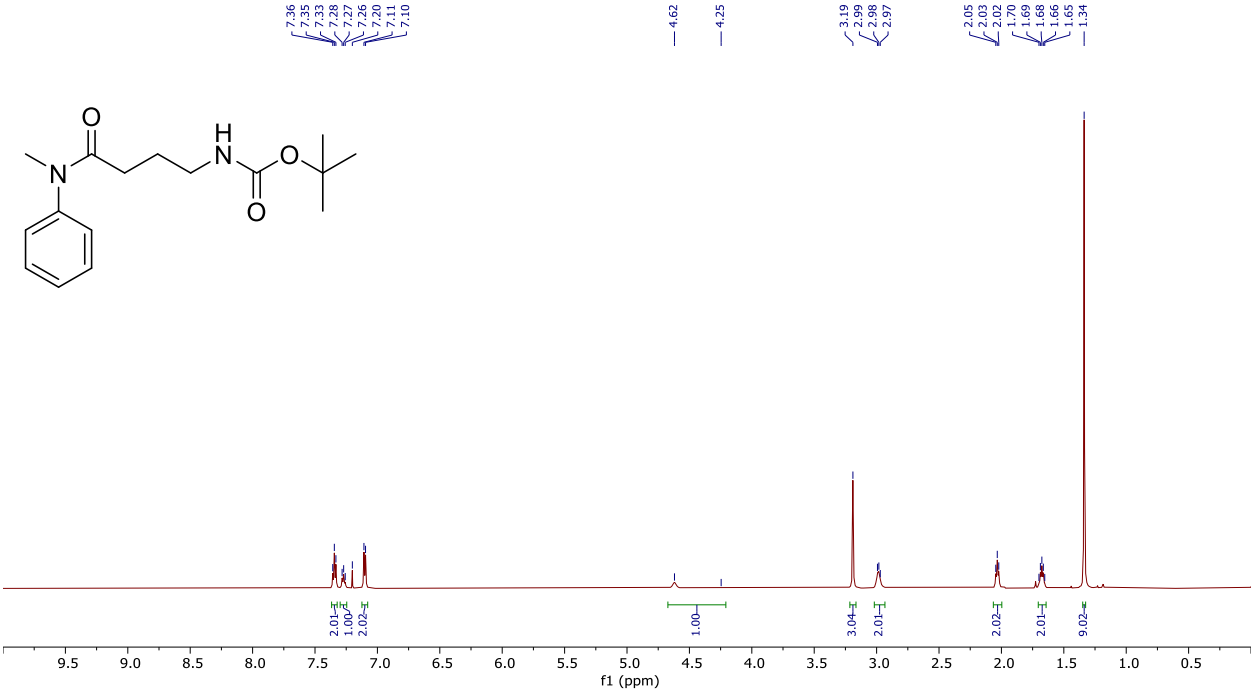

^{13}C NMR Spectrum $CDCl_3$ (151 MHz)

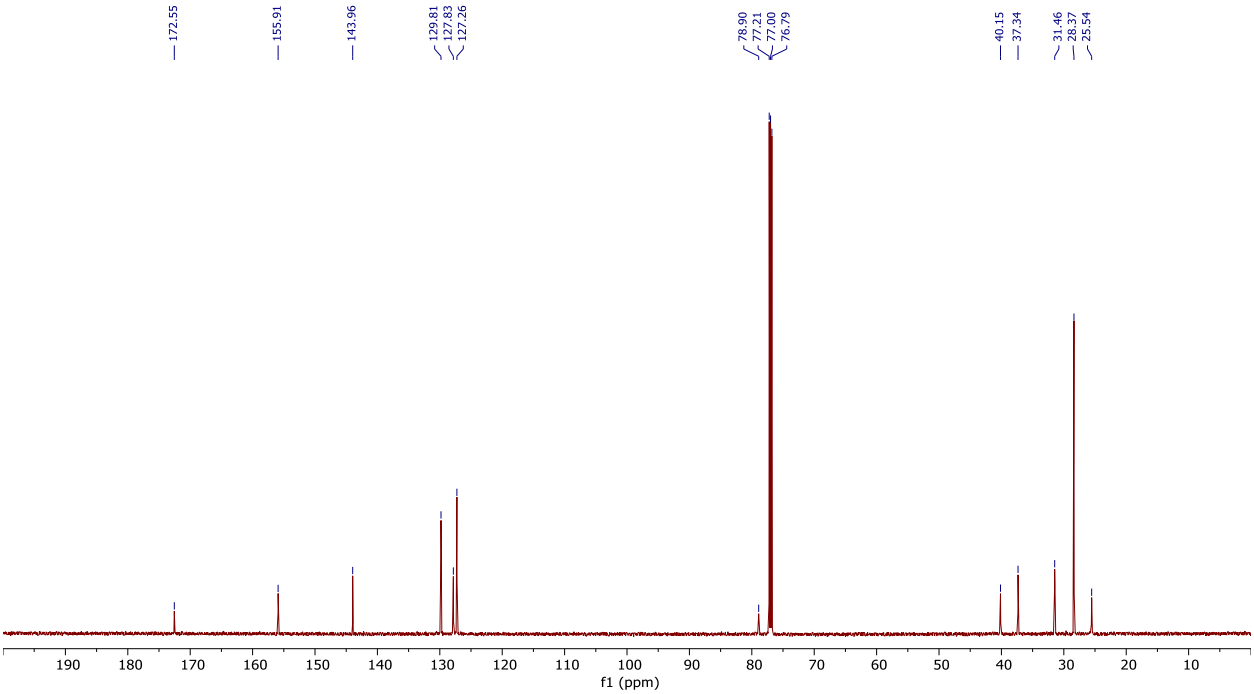

tert-butyl _N_-[4-(3,4-dihydro-_2H_-quinolin-1-yl)-4-oxo-butyl]carbamate

^{1}H NMR Spectrum $CDCl_3$ (600 MHz)

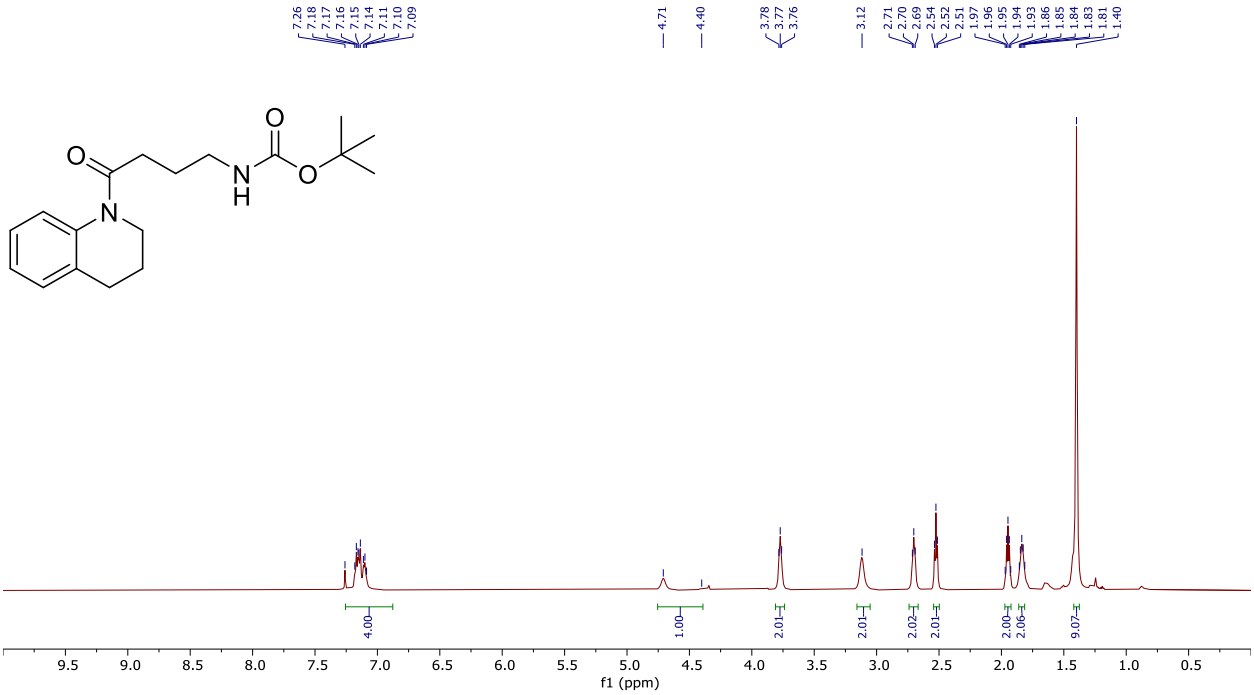

^{13}C NMR Spectrum $CDCl_3$ (151 MHz)

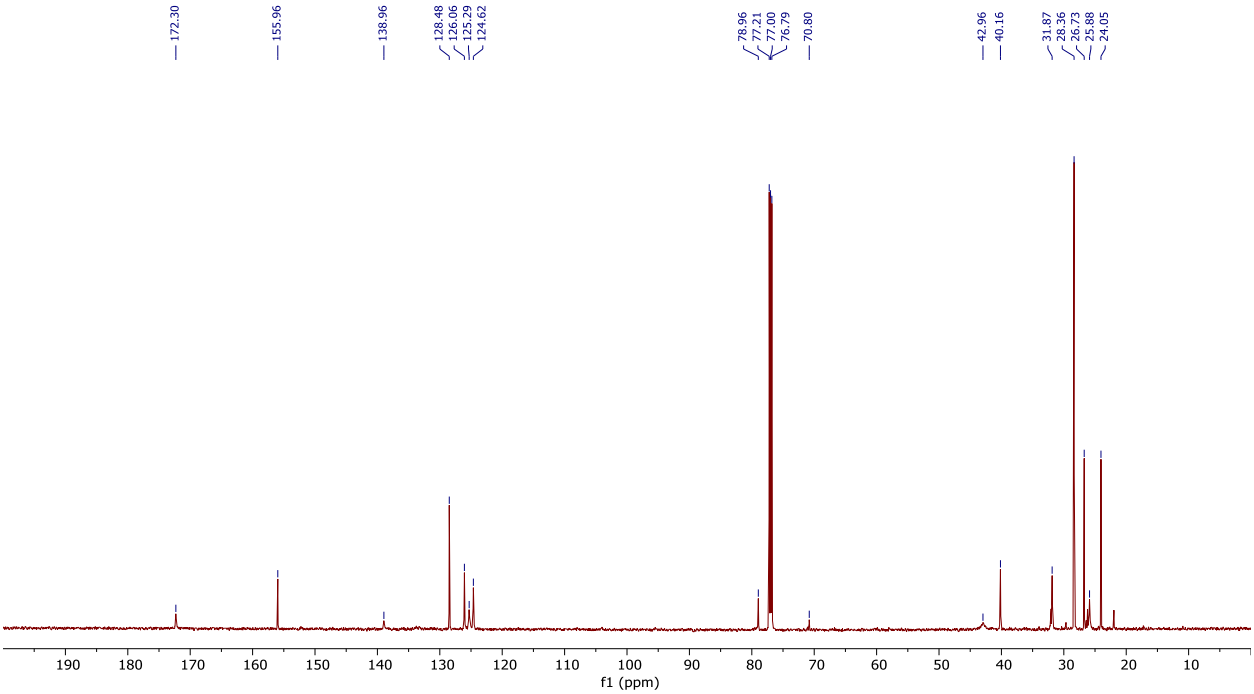

tert-butyl _N_-[4-(2-methyl-3,4-dihydro-_2H_-quinolin-1-yl)-4-oxo-butyl]carbamate

^{1}H NMR Spectrum $CDCl_3$, **55°C** (600 MHz)

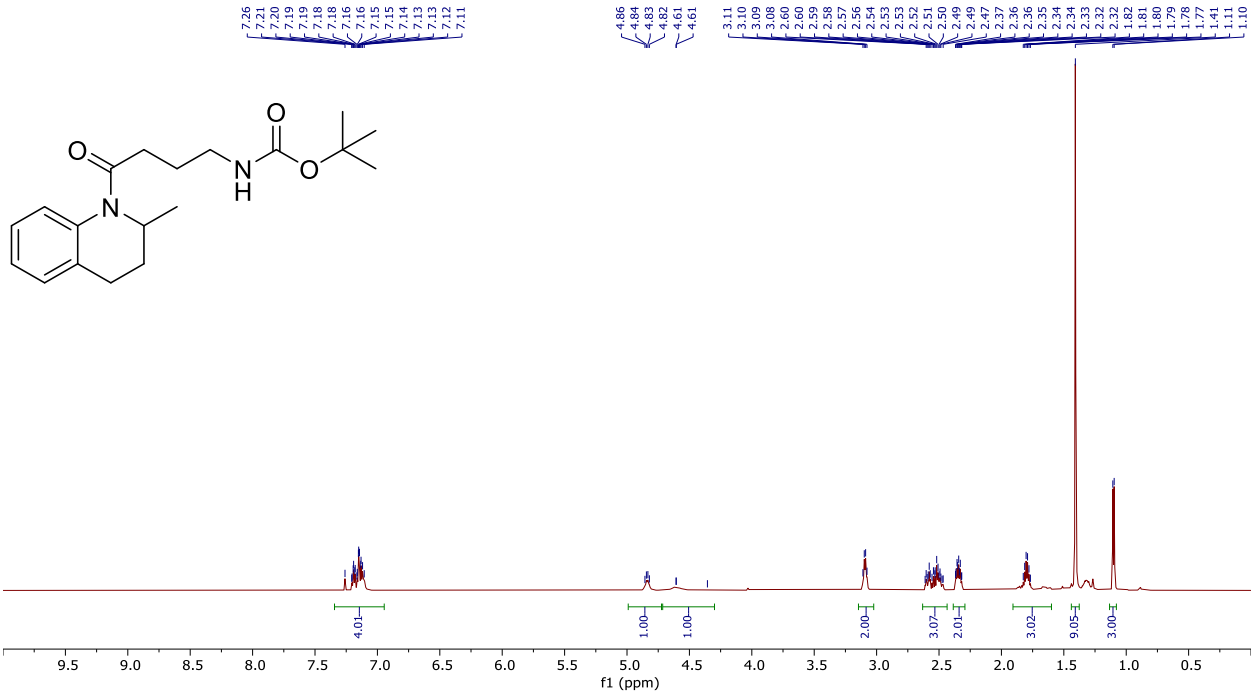

^{13}C NMR Spectrum $CDCl_3$, **55°C** (151 MHz)

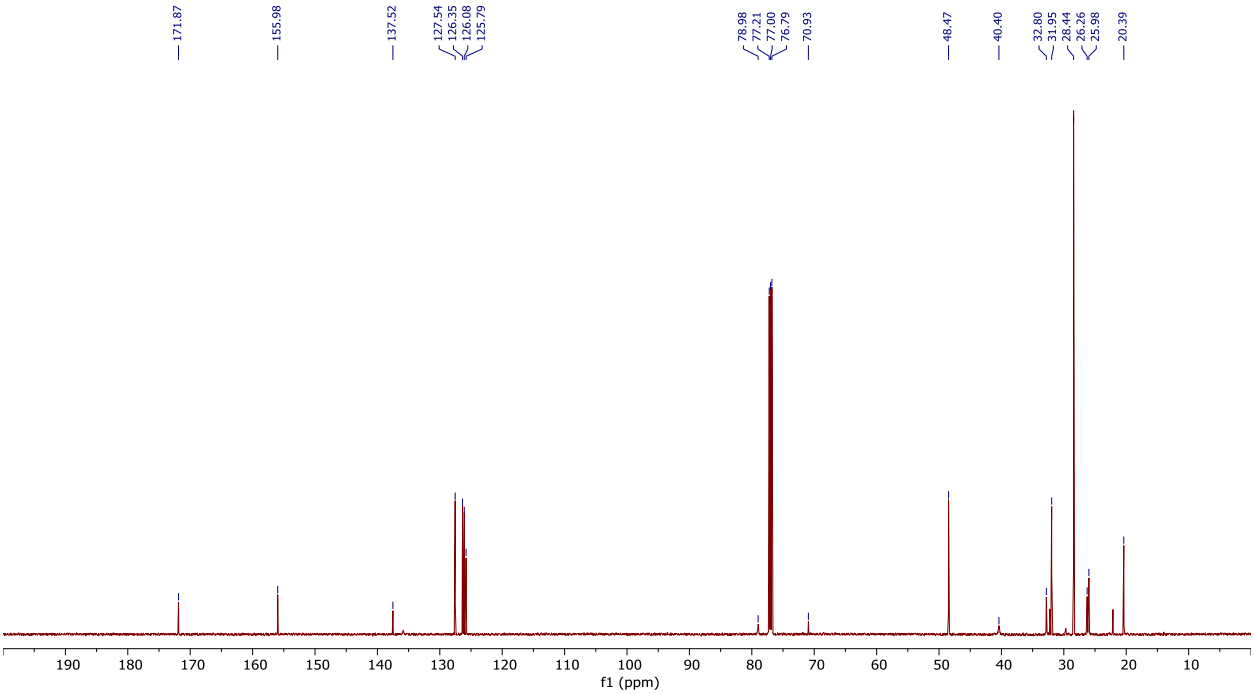

tert-butyl *N*-[4-oxo-4-(*N*-phenylanilino)butyl]carbamate

^{1}H NMR Spectrum $CDCl_3$ (600 MHz)

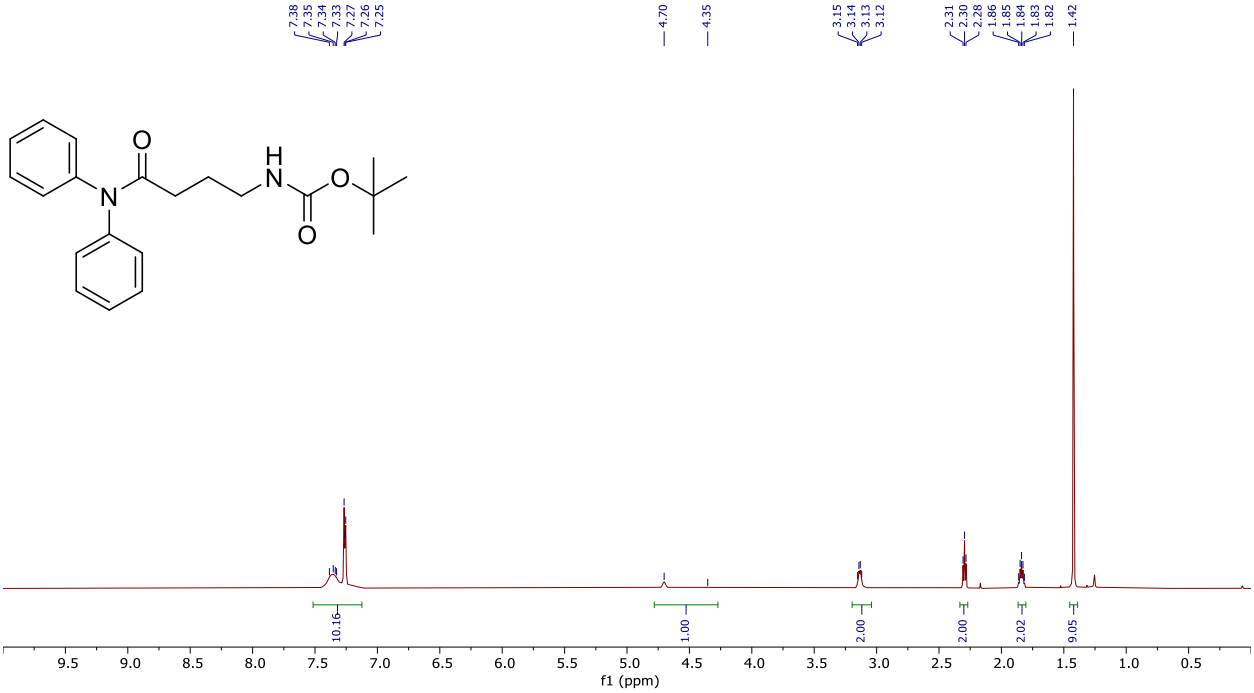

^{13}C NMR Spectrum $CDCl_3$ (151 MHz)

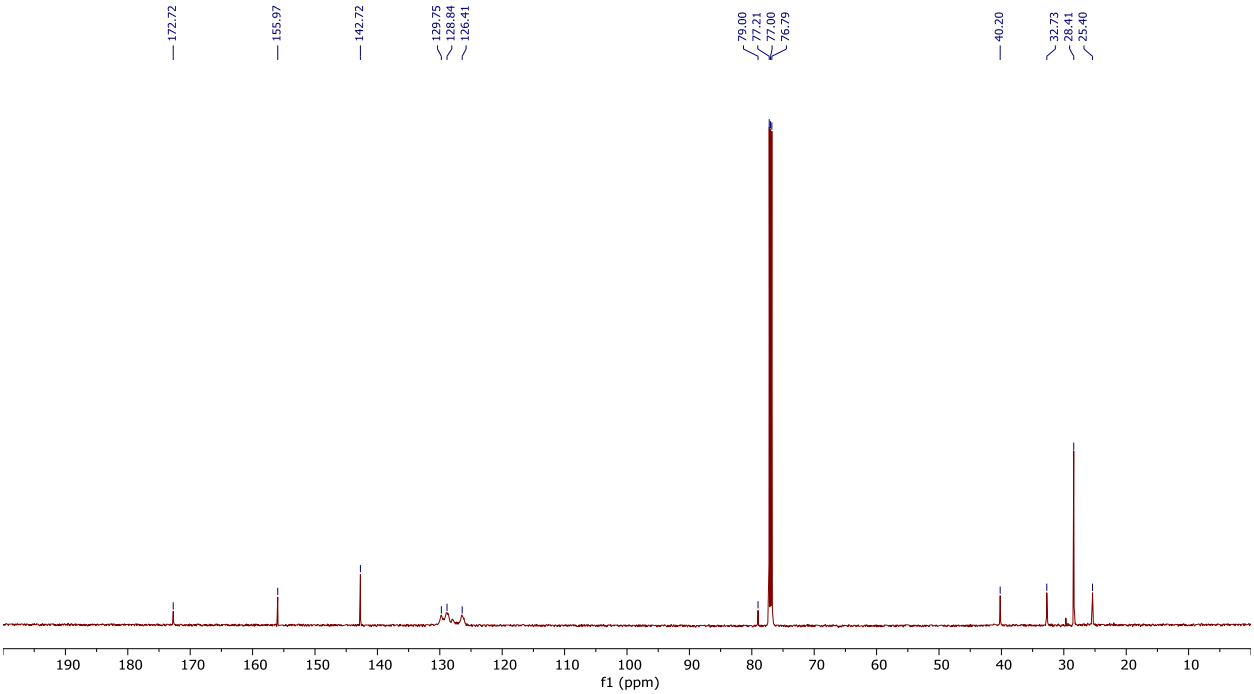

tert-butyl _N_-[4-(4-methyl-2-phenyl-piperazin-1-yl)-4-oxo-butyl]carbamate

^{1}H NMR Spectrum $CDCl_3$, **55°C** (600 MHz)

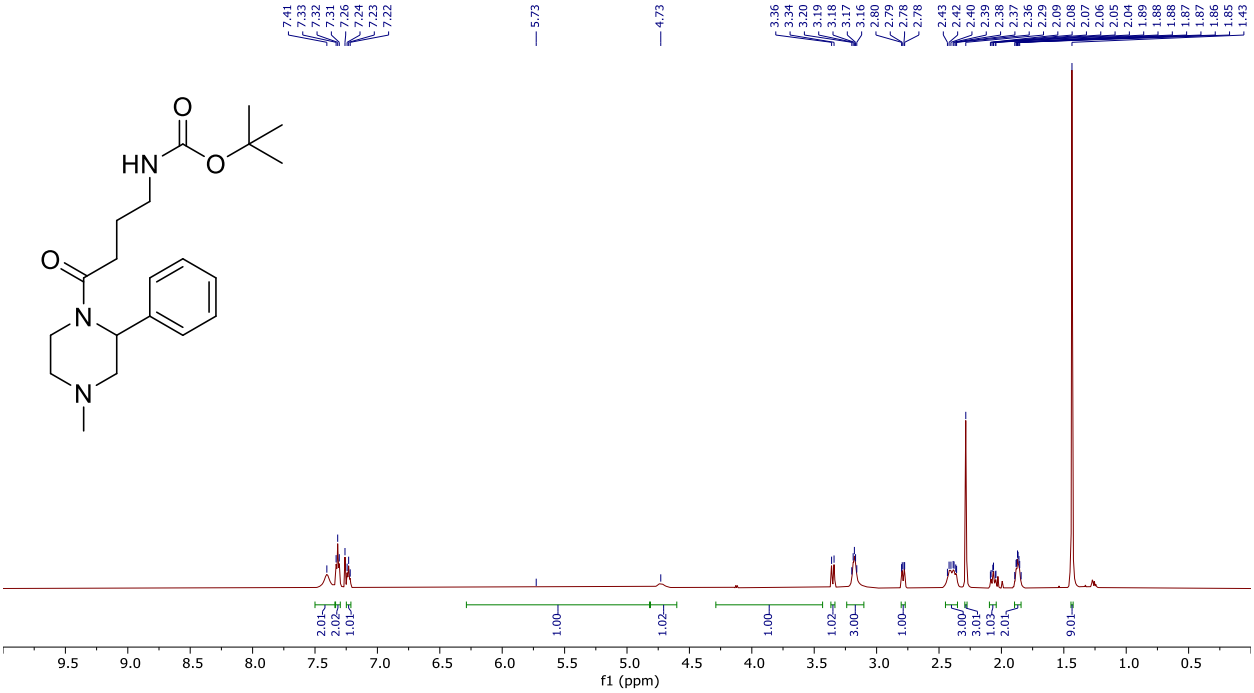

^{13}C NMR Spectrum $CDCl_3$, **55°C** (151 MHz)

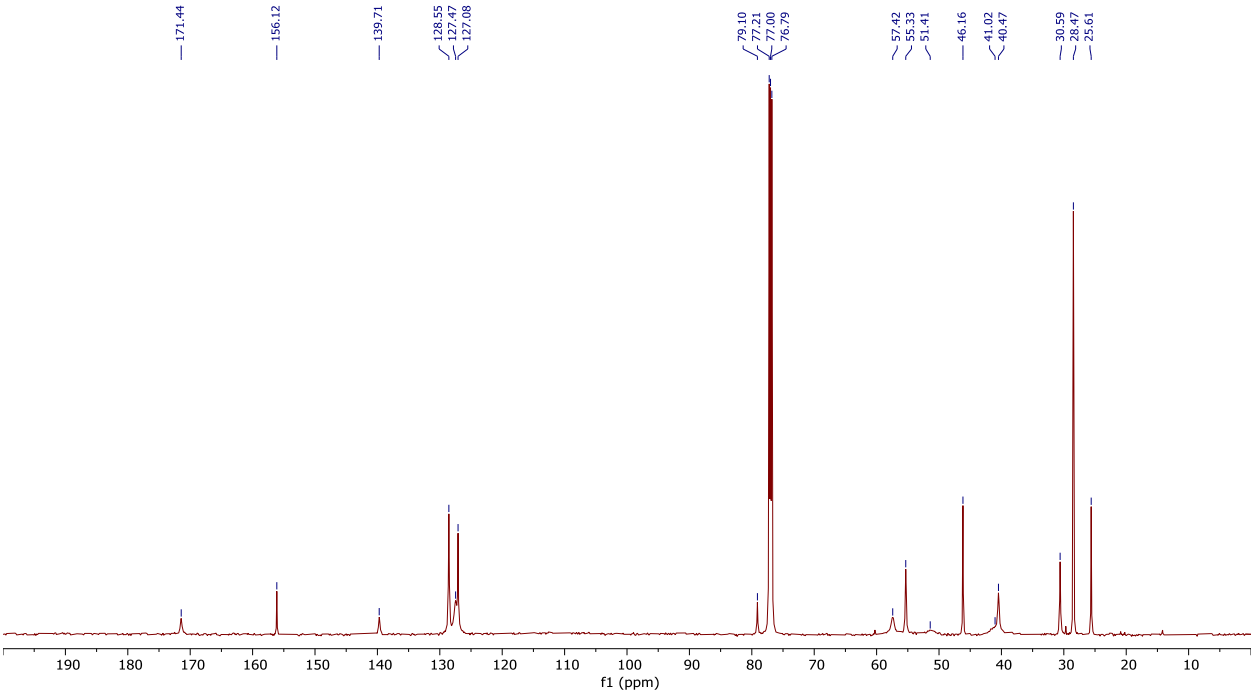

tert-butyl *N*-[4-(4-benzhydrylpiperazin-1-yl)-4-oxo-butyl]carbamate

^{1}H NMR Spectrum $CDCl_3$, **55°C** (600 MHz)

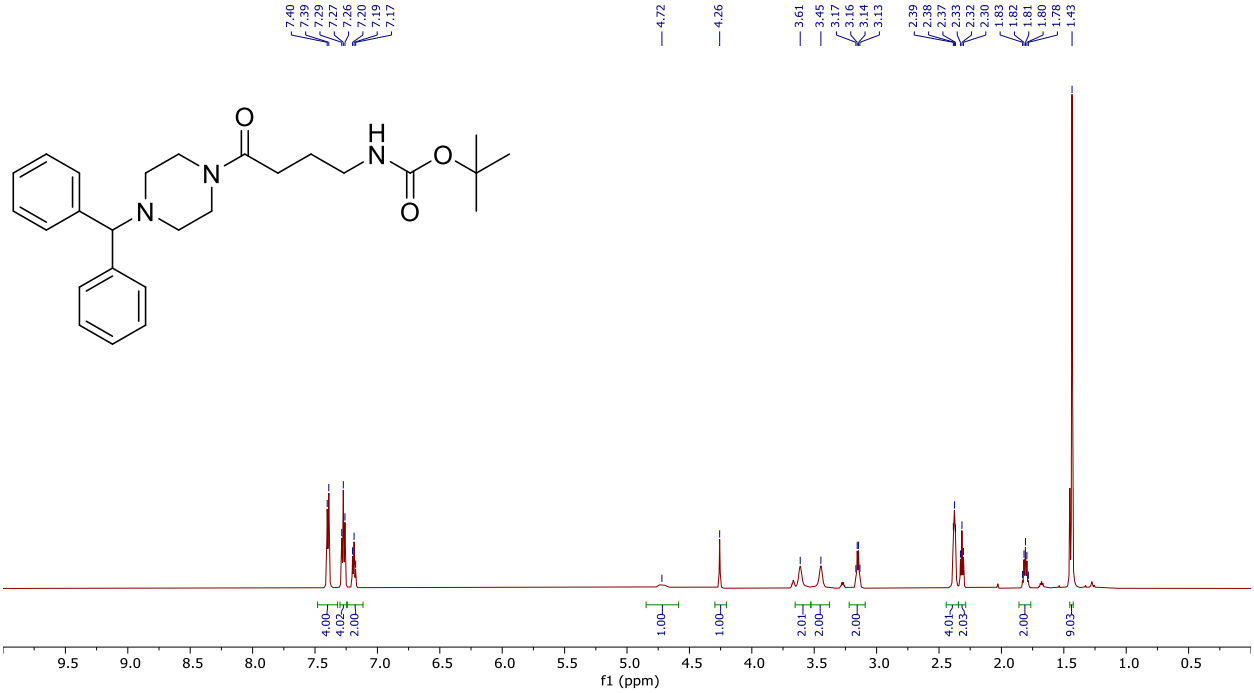

^{13}C NMR Spectrum $CDCl_3$, **55°C** (151 MHz)

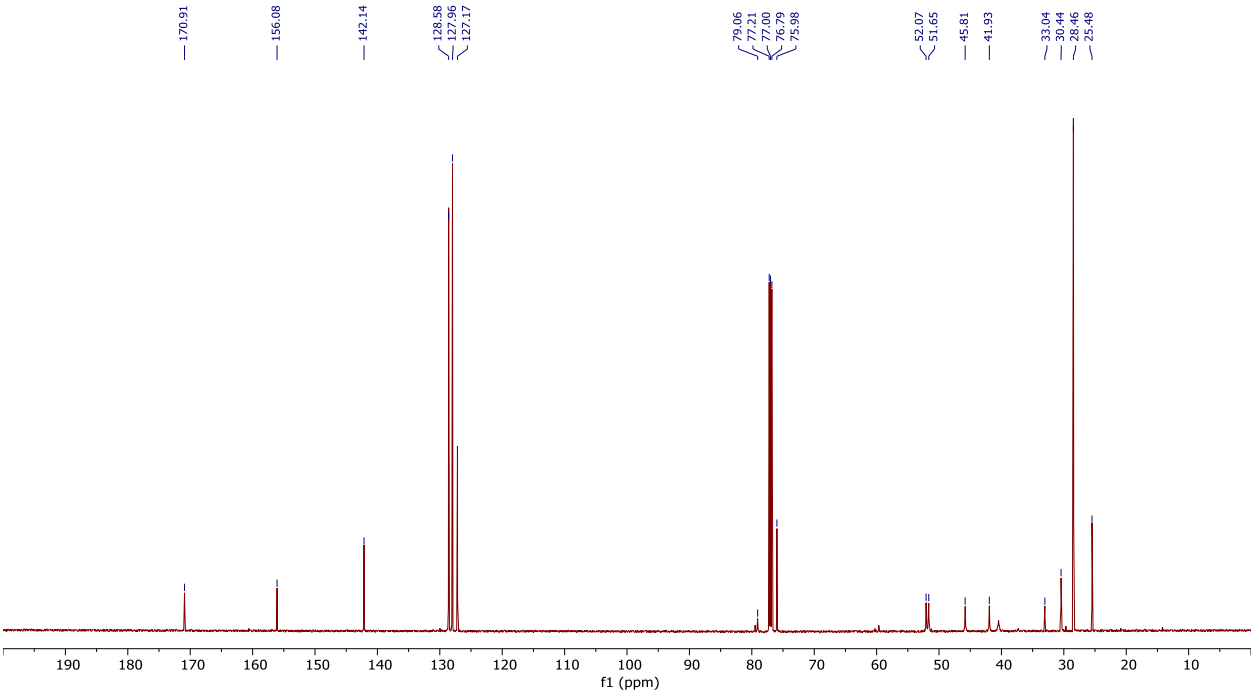

tert-butyl _N_-(4-oxo-4-phenothiazin-10-yl-butyl)carbamate

^{1}H NMR Spectrum $CDCl_3$ (600 MHz)

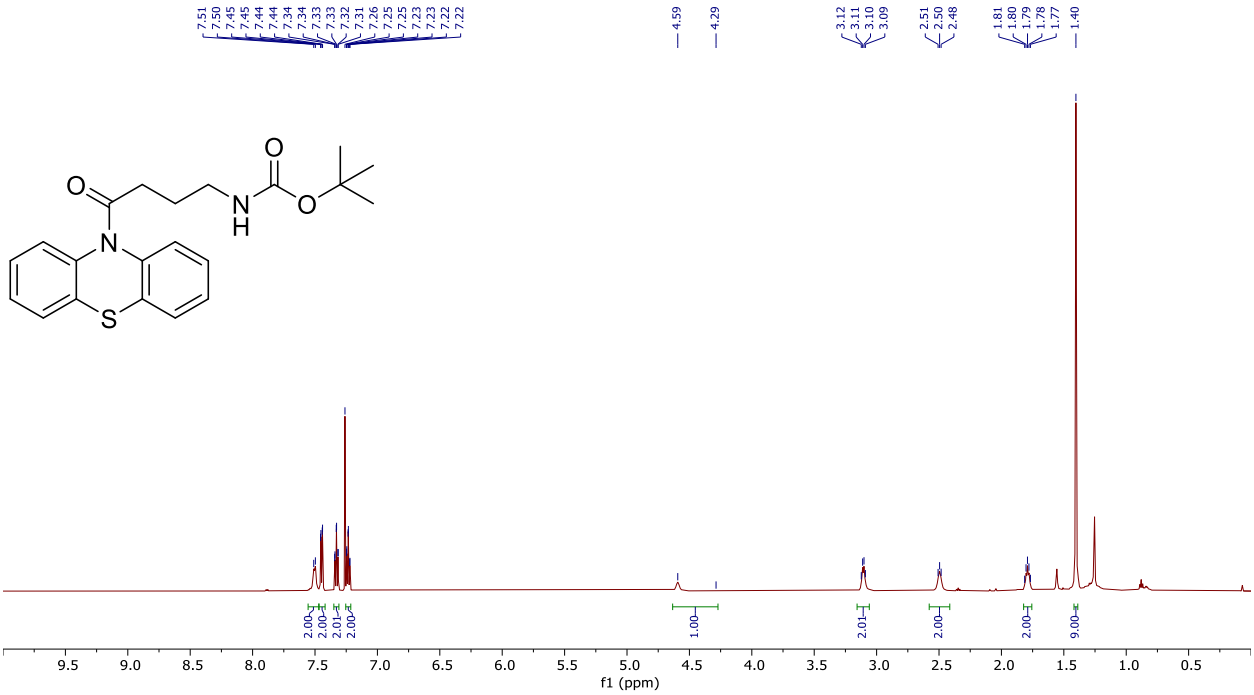

^{13}C NMR Spectrum $CDCl_3$ (151 MHz)

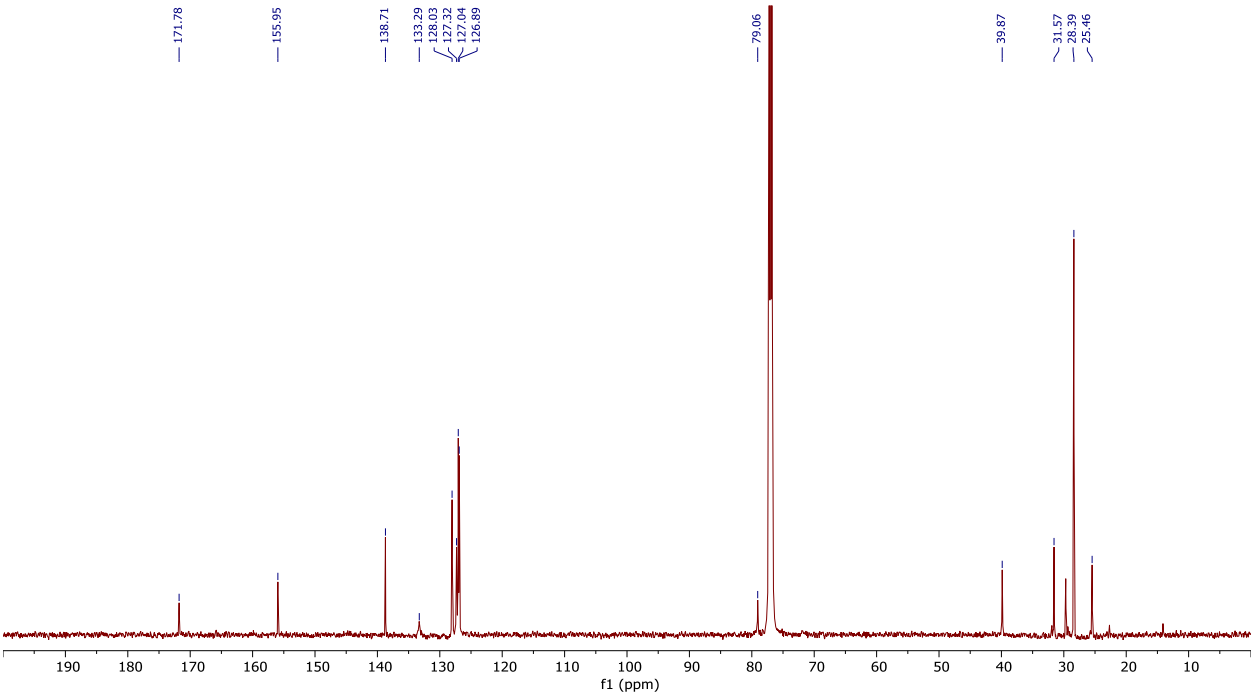

tert-butyl *N*-[4-(*N*-benzyl-4-fluoro-anilino)-4-oxo-butyl]carbamate

^{1}H NMR Spectrum $CDCl_3$ (600 MHz)

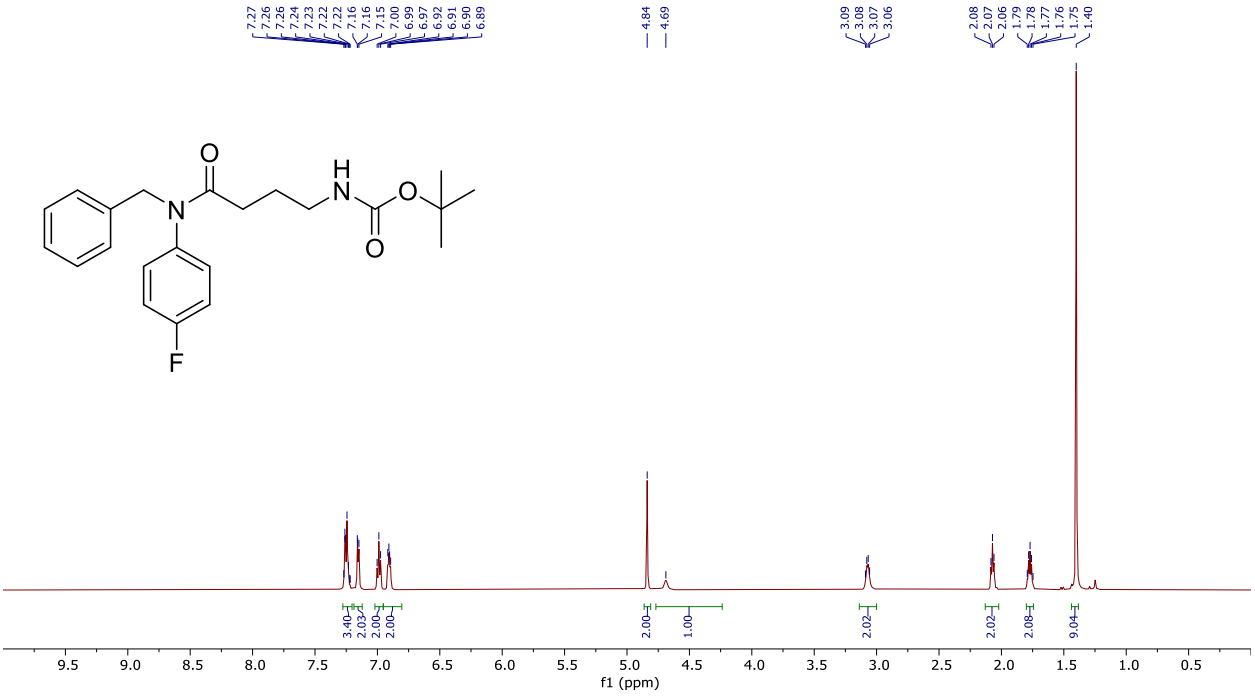

^{13}C NMR Spectrum $CDCl_3$ (151 MHz)

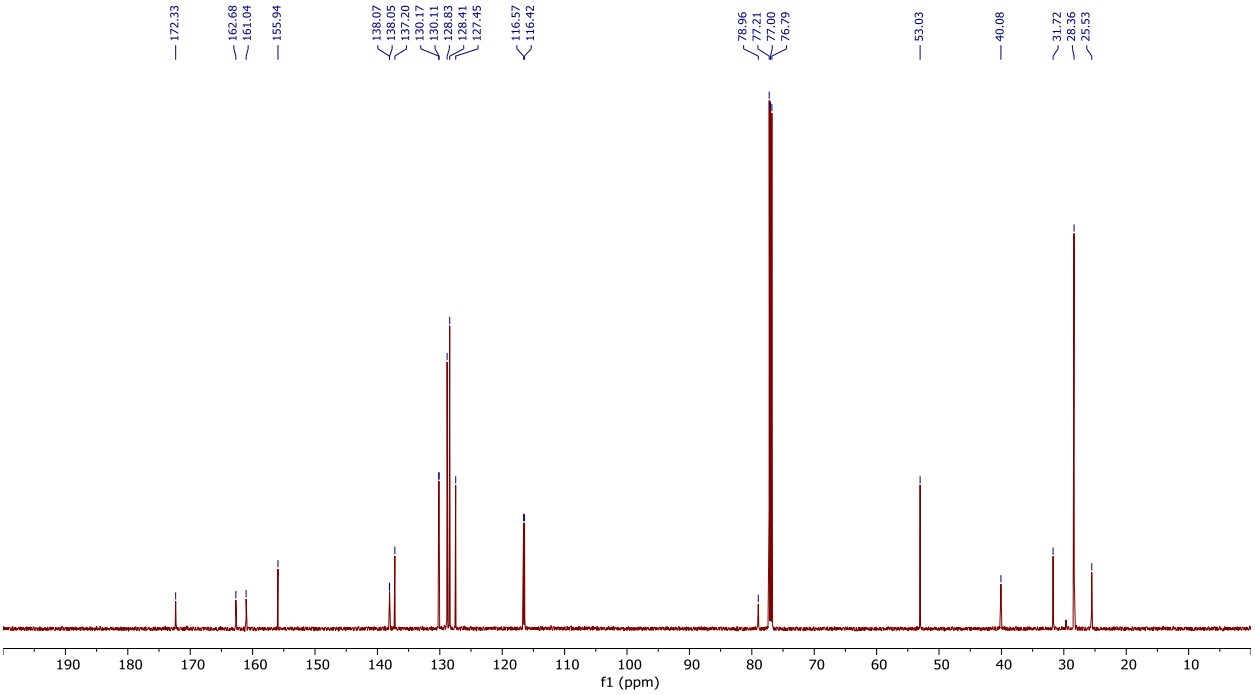

^{19}F NMR Spectrum $CDCl_3$ (282 MHz)

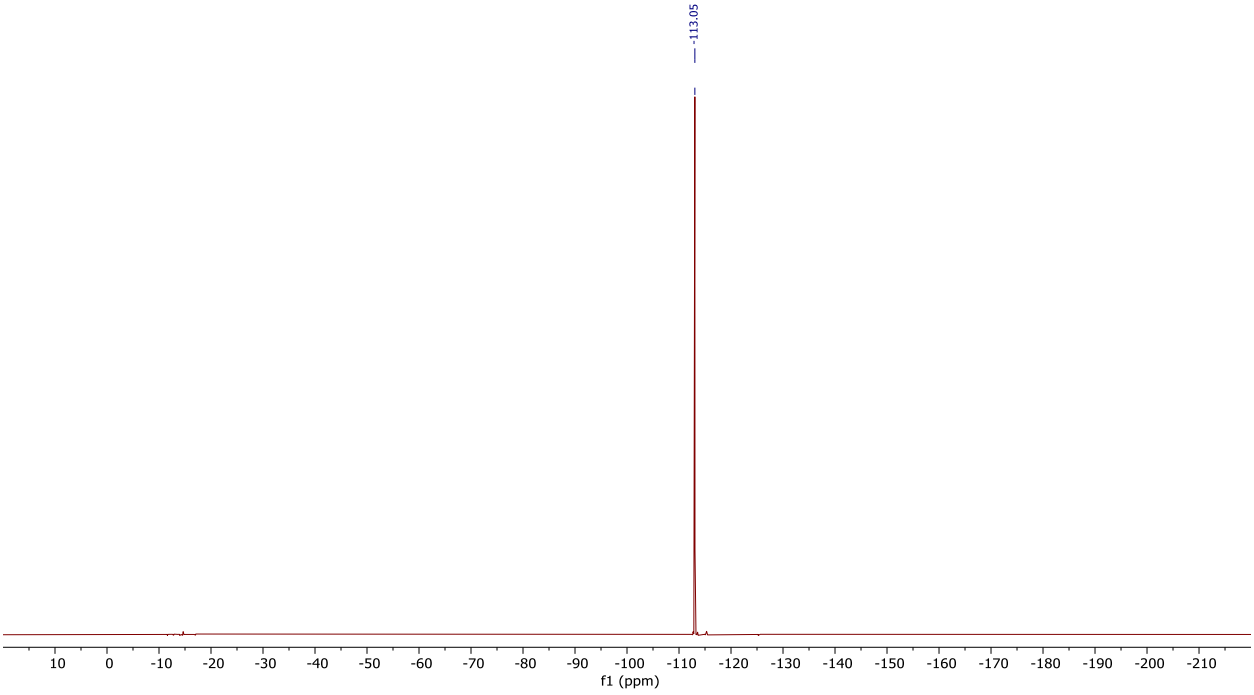

tert-butyl *N*-[4-[benzyl(2-pyridyl)amino]-4-oxo-butyl]carbamate

^{1}H NMR Spectrum $CDCl_3$ (600 MHz)

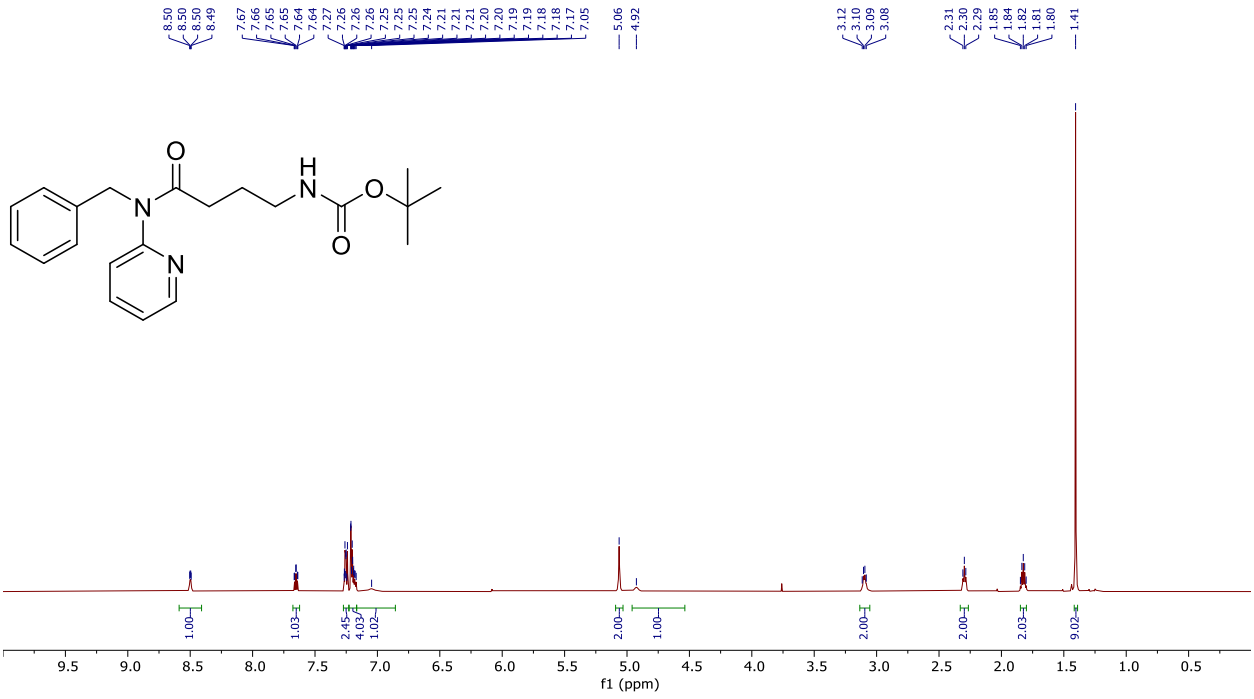

^{13}C NMR Spectrum $CDCl_3$ (151 MHz)

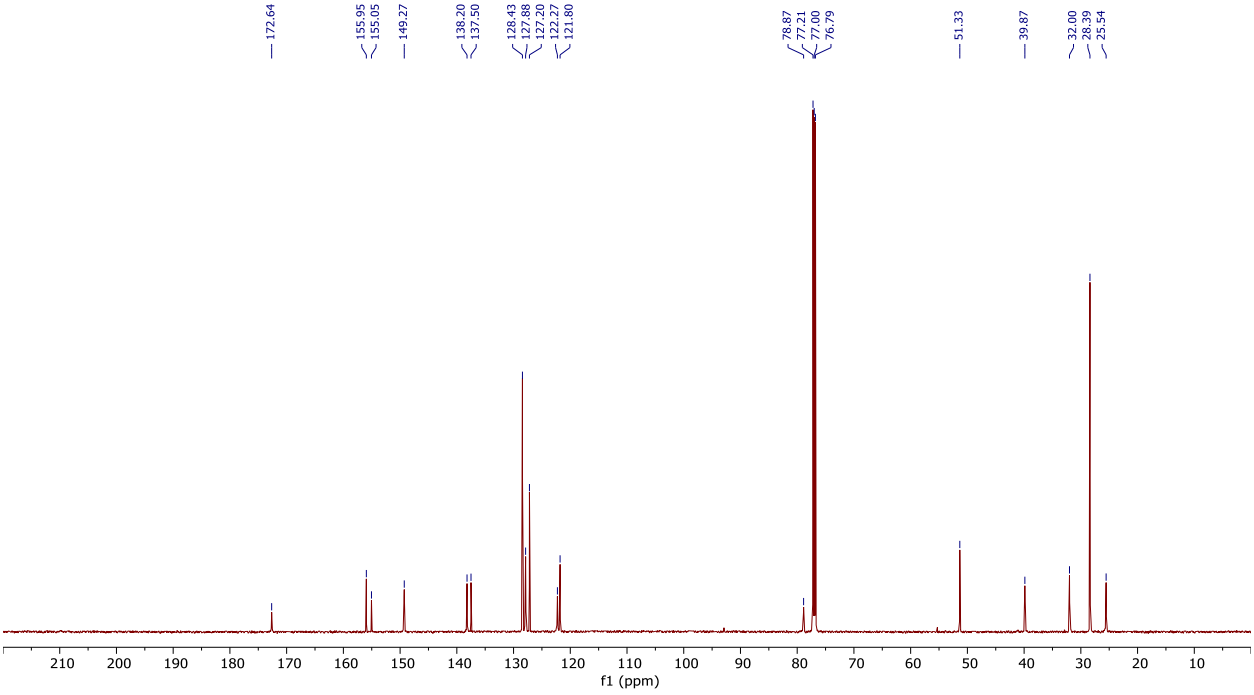

tert-butyl _N_-[4-[_N_-(3-methylbut-3-enyl)anilino]-4-oxo-butyl]carbamate

^{1}H NMR Spectrum $CDCl_3$ (600 MHz)

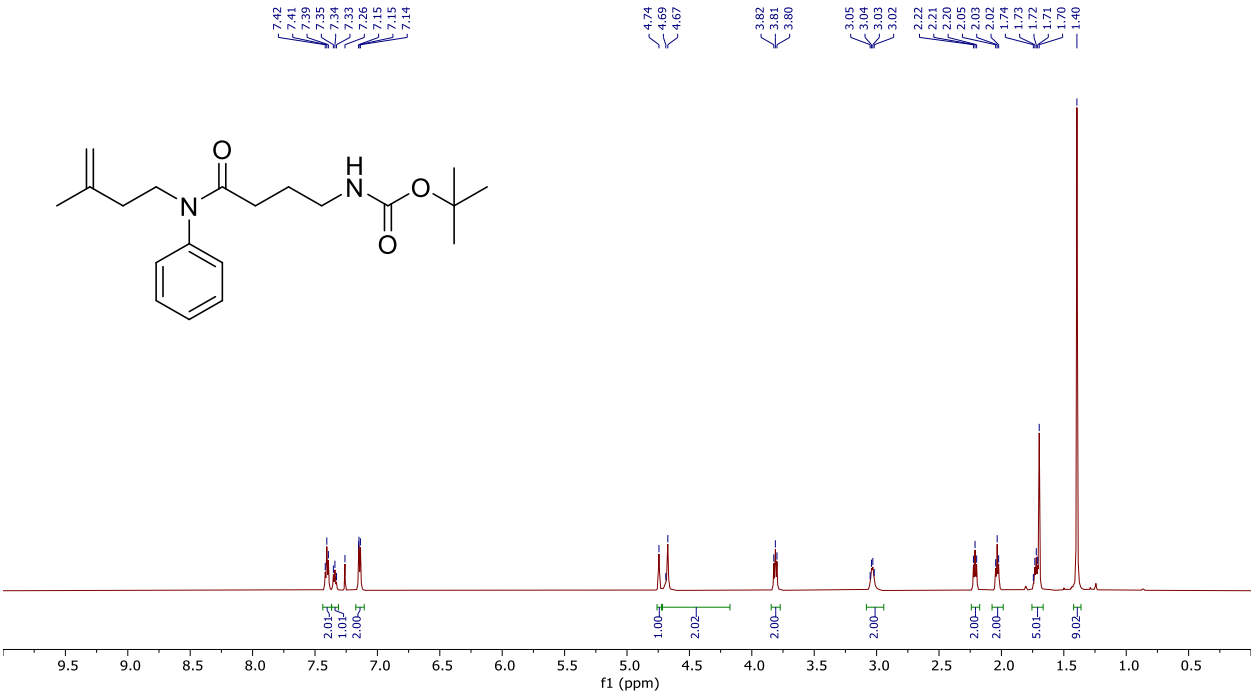

^{13}C NMR Spectrum $CDCl_3$ (151 MHz)

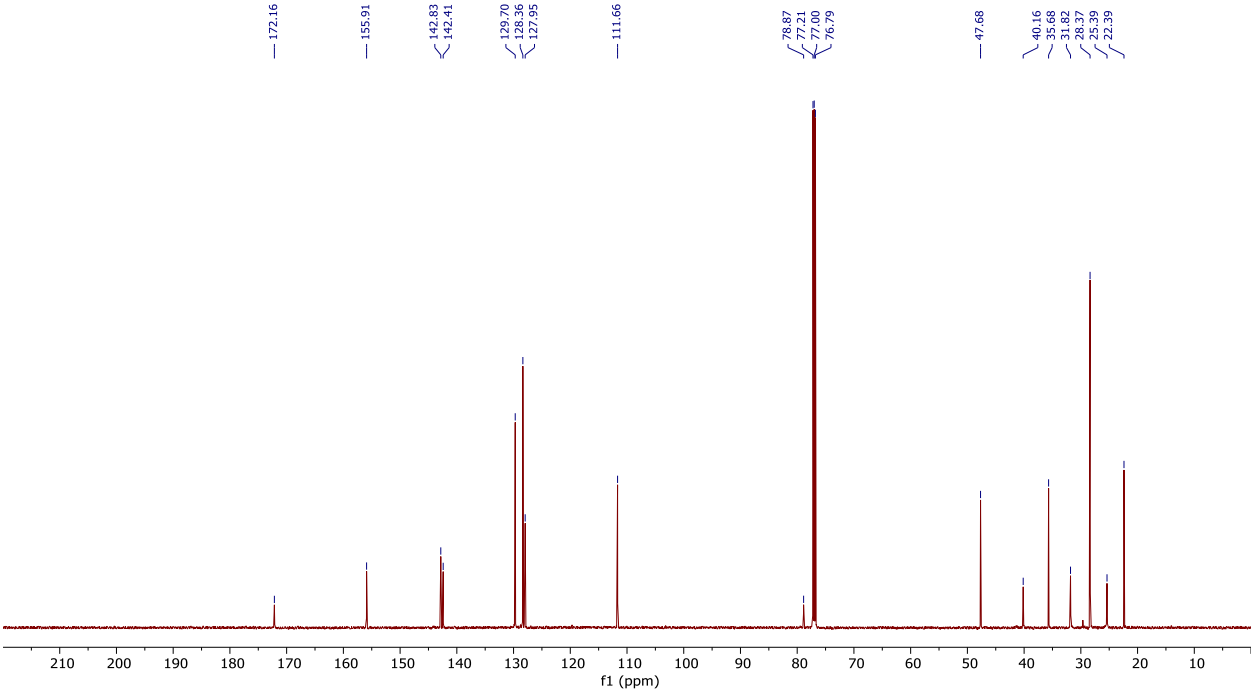

tert-butyl *N*-[4-[benzyl(3-methylbut-3-enyl)amino]-4-oxo-butyl]carbamate

^{1}H NMR Spectrum $CDCl_3$ (600 MHz)

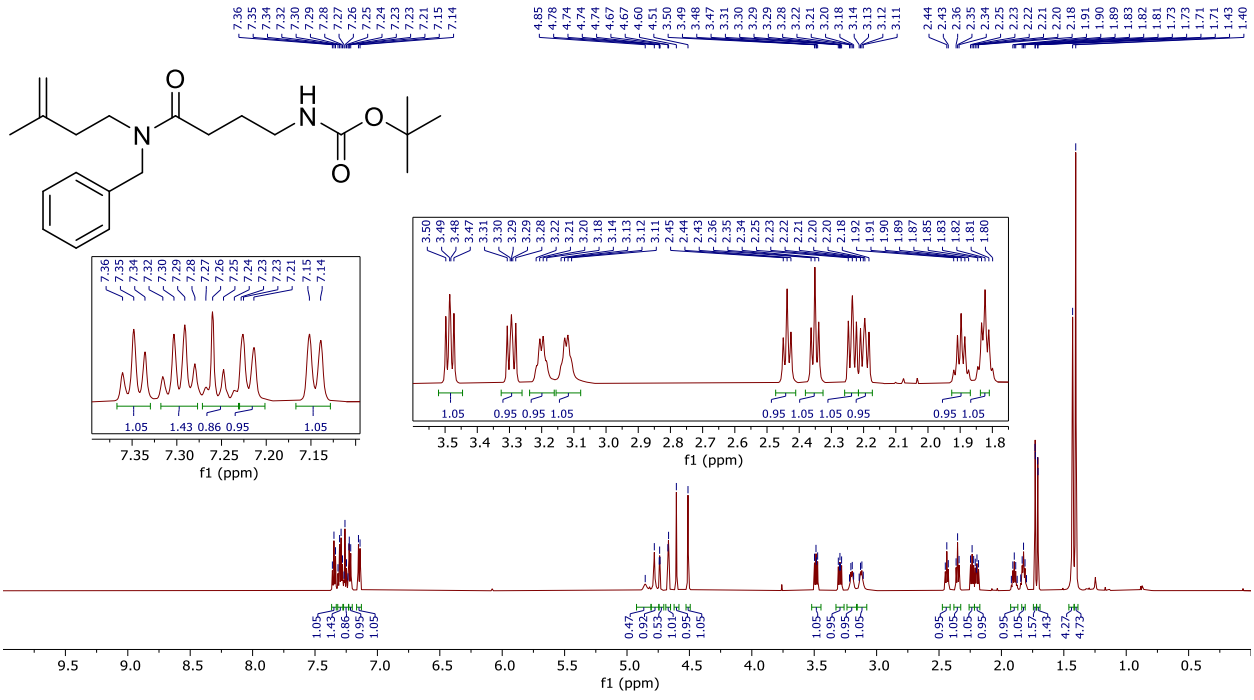

^{13}C NMR Spectrum $CDCl_3$ (151 MHz)

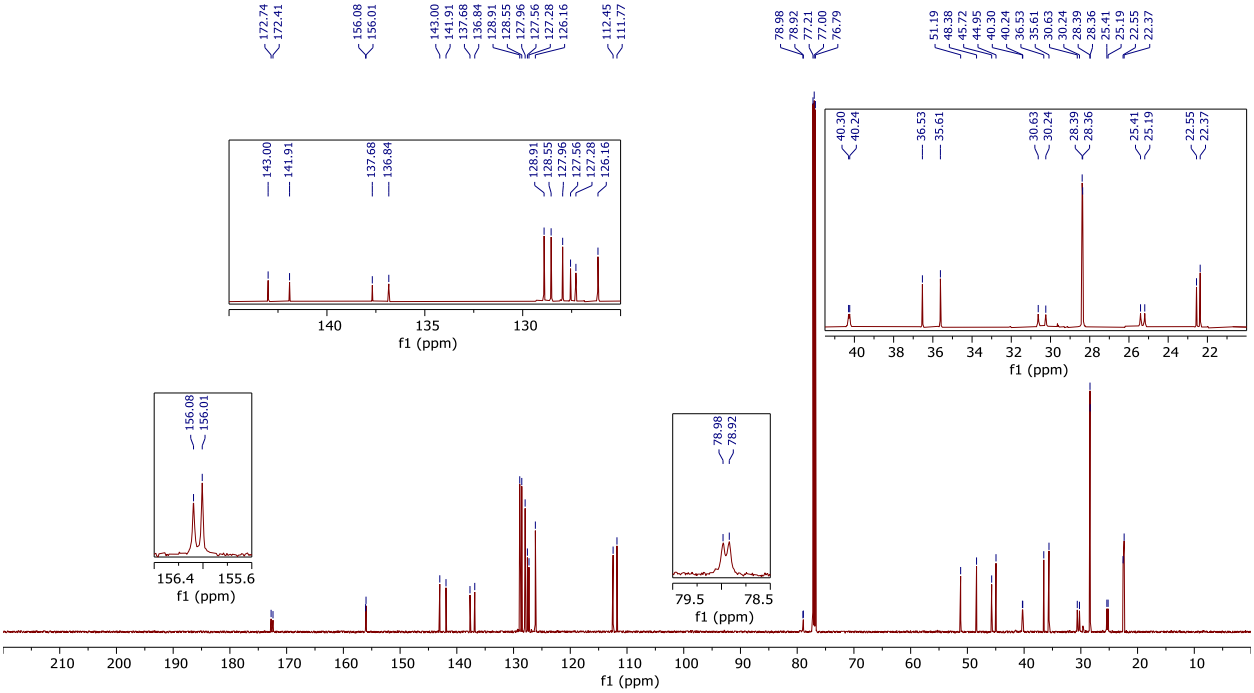

tert-butyl *N*-[3-[4-(anilinomethyl)phenyl]propyl]carbamate

^{1}H NMR Spectrum $CDCl_3$ (300 MHz)

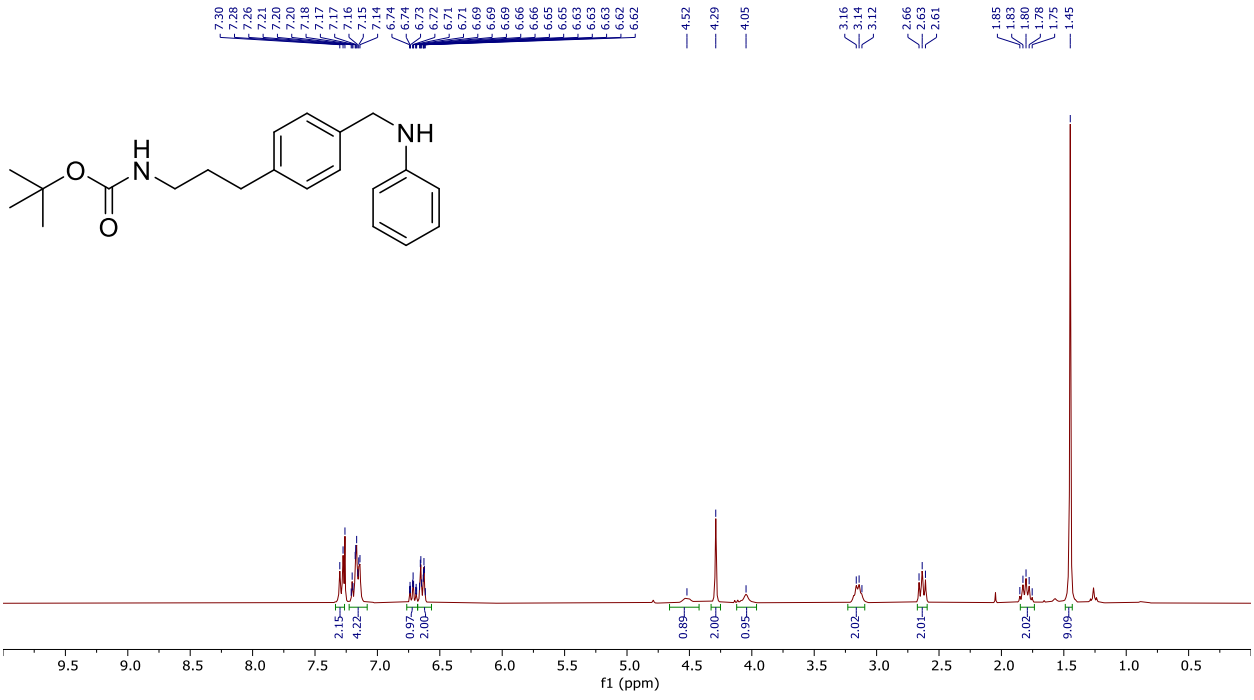

***tert*-butyl *N*-[3-[4-[(*N*-fluorocarbonylanilino)methyl]phenyl]propyl]carbamate**

^{1}H NMR Spectrum $CDCl_3$ (300 MHz)

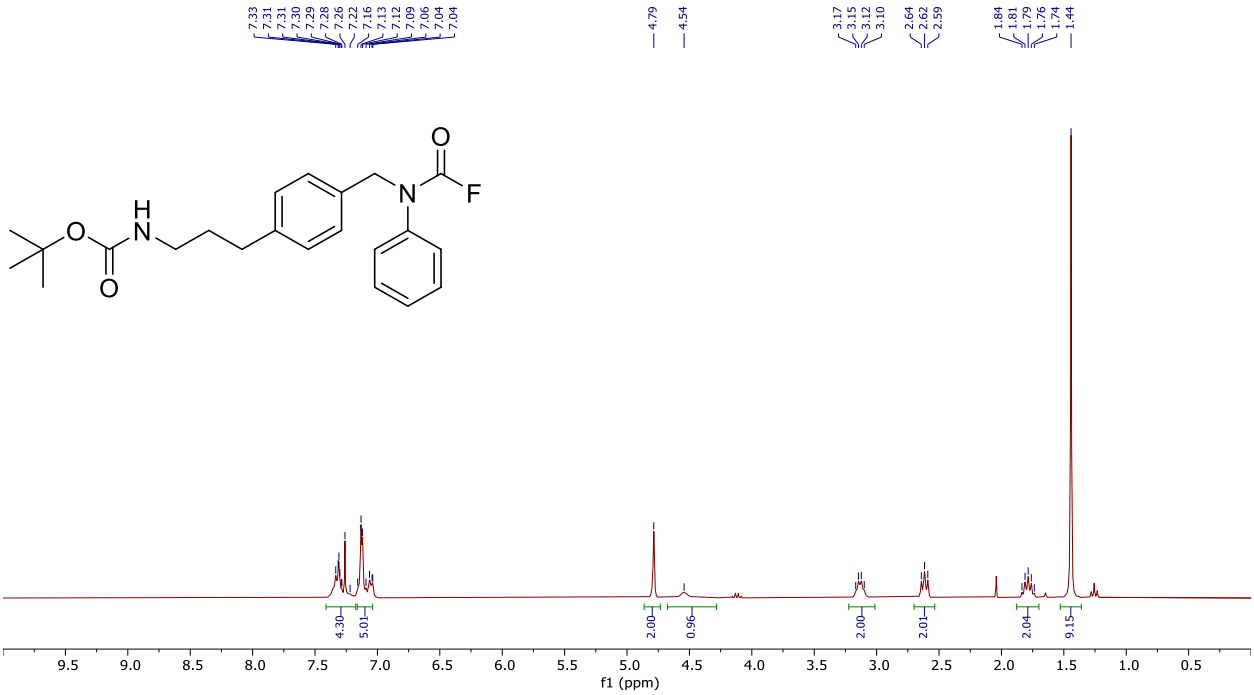

^{19}F NMR Spectrum $CDCl_3$ (282 MHz)

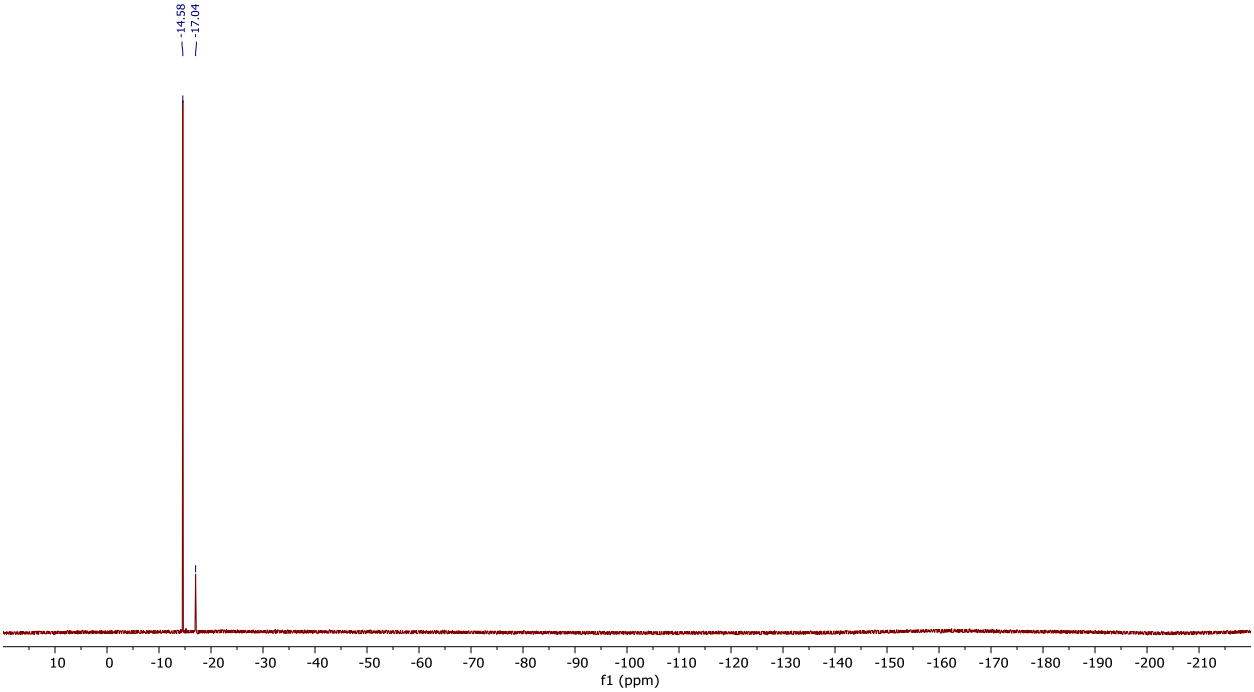

***tert*-butyl *N*-[3-[4-[[*N*-[4-(tert-butoxycarbonylamino)butanoyl]anilino]methyl]phenyl]propyl] carbamate**

^{1}H NMR Spectrum $CDCl_3$ (300 MHz)

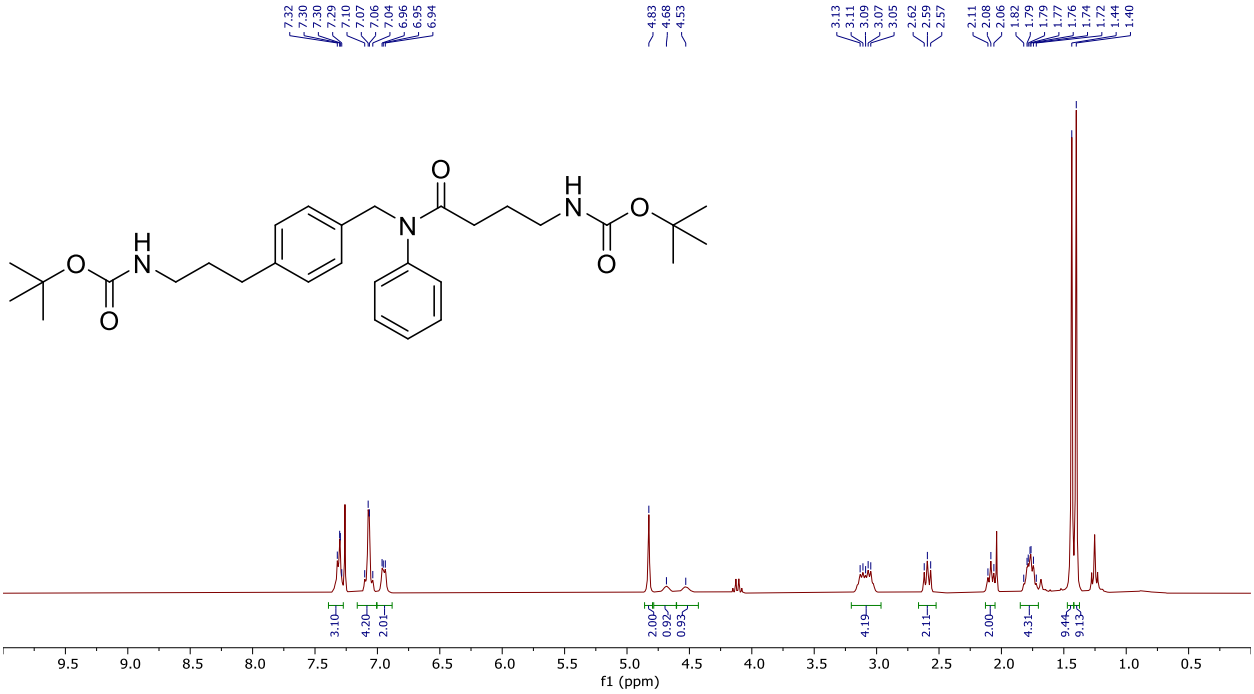

$[(PCy_3)_2Ni]_2N_2$

^{1}H NMR Spectrum C_6D_6 (400 MHz)

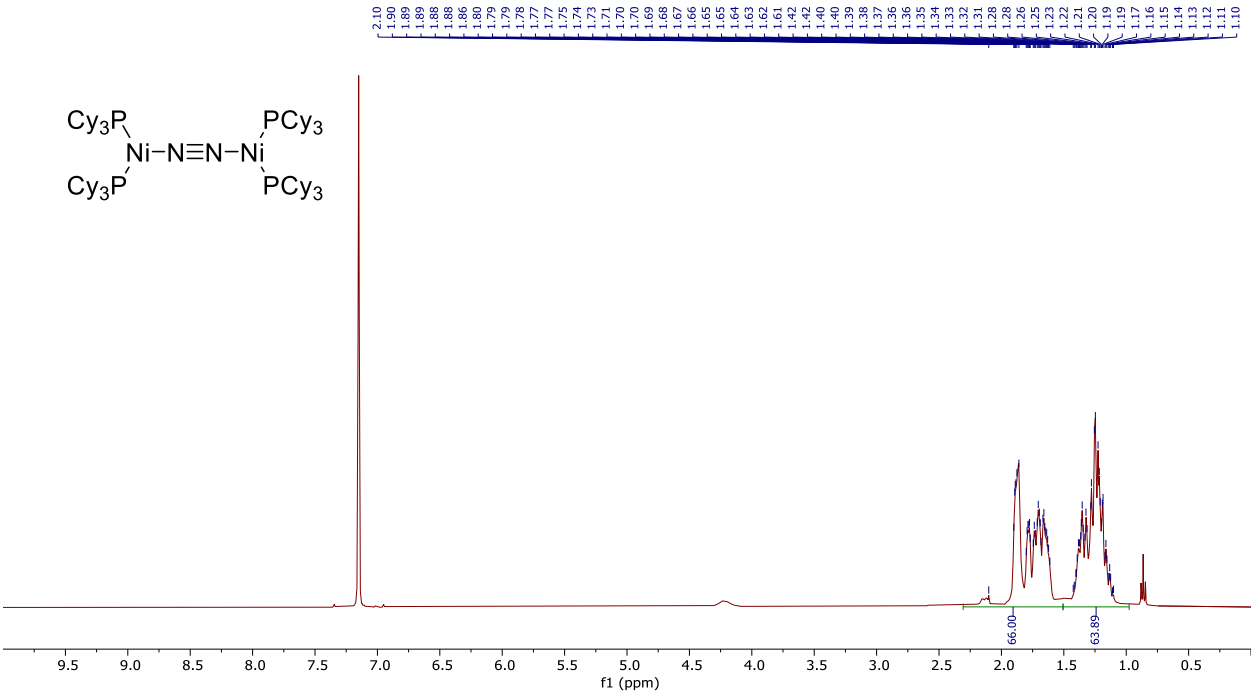

^{13}C NMR Spectrum C_6D_6 (101 MHz)

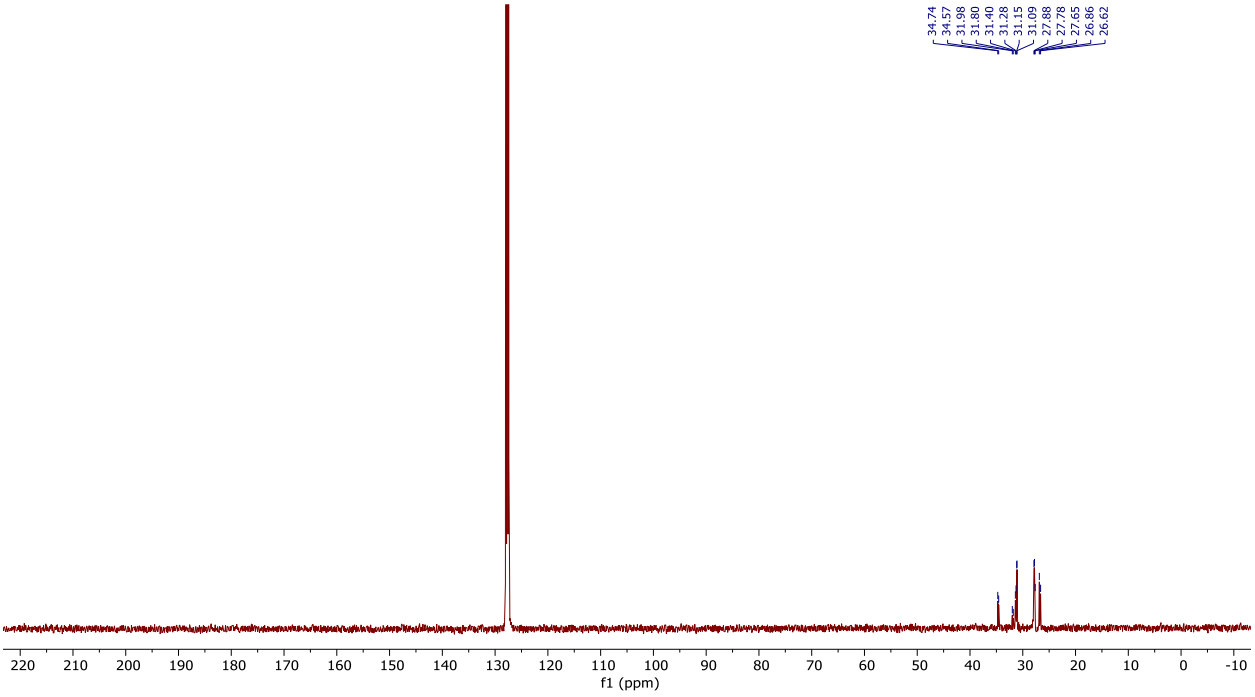

^{31}P {^{1}H} NMR Spectrum C_6D_6 (162 MHz)

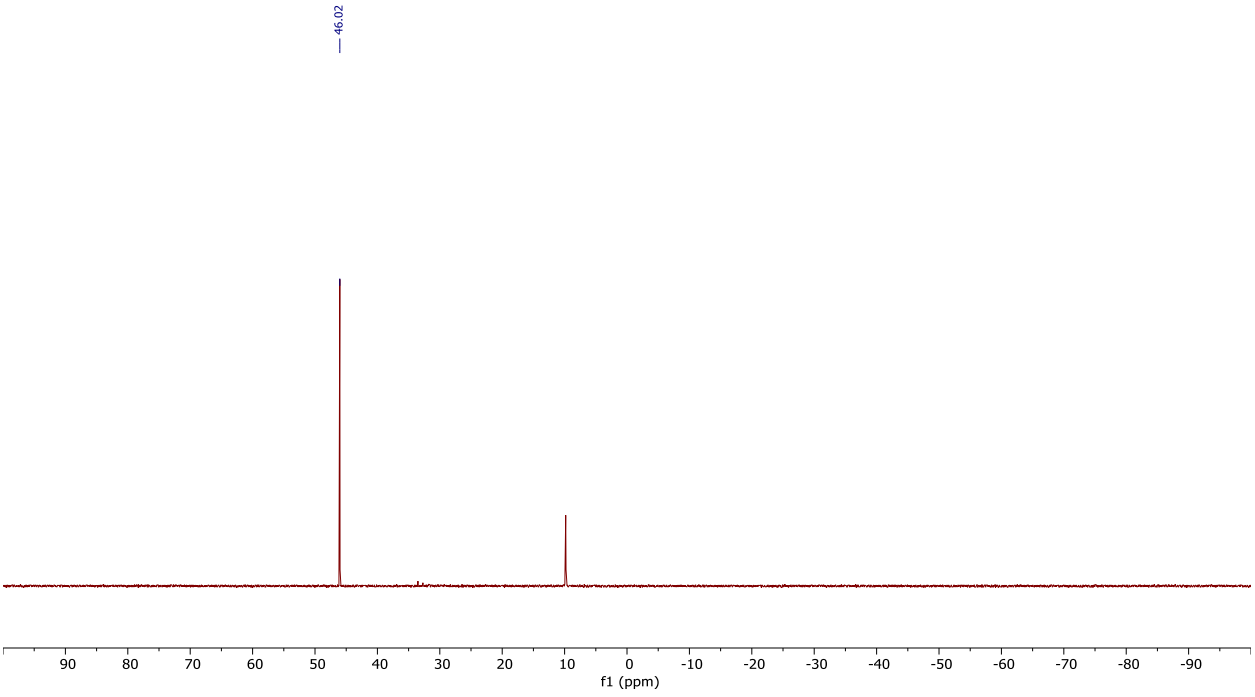

N-benzyl-N-(pyridin-2-yl)carbamoyl-tricyclohexyl Nickel (II) fluoride

^{1}H NMR Spectrum $CDCl_3$ (300 MHz)

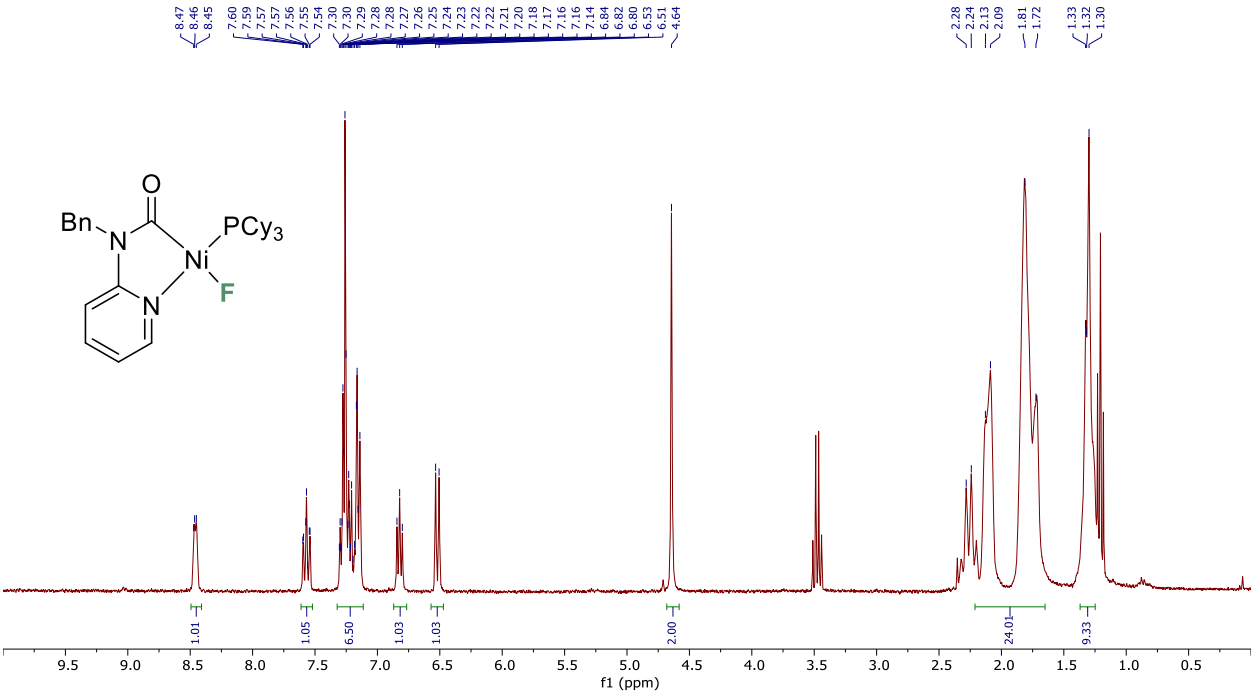

^{19}F {^{1}H) NMR Spectrum $CDCl_3$ (282 MHz)

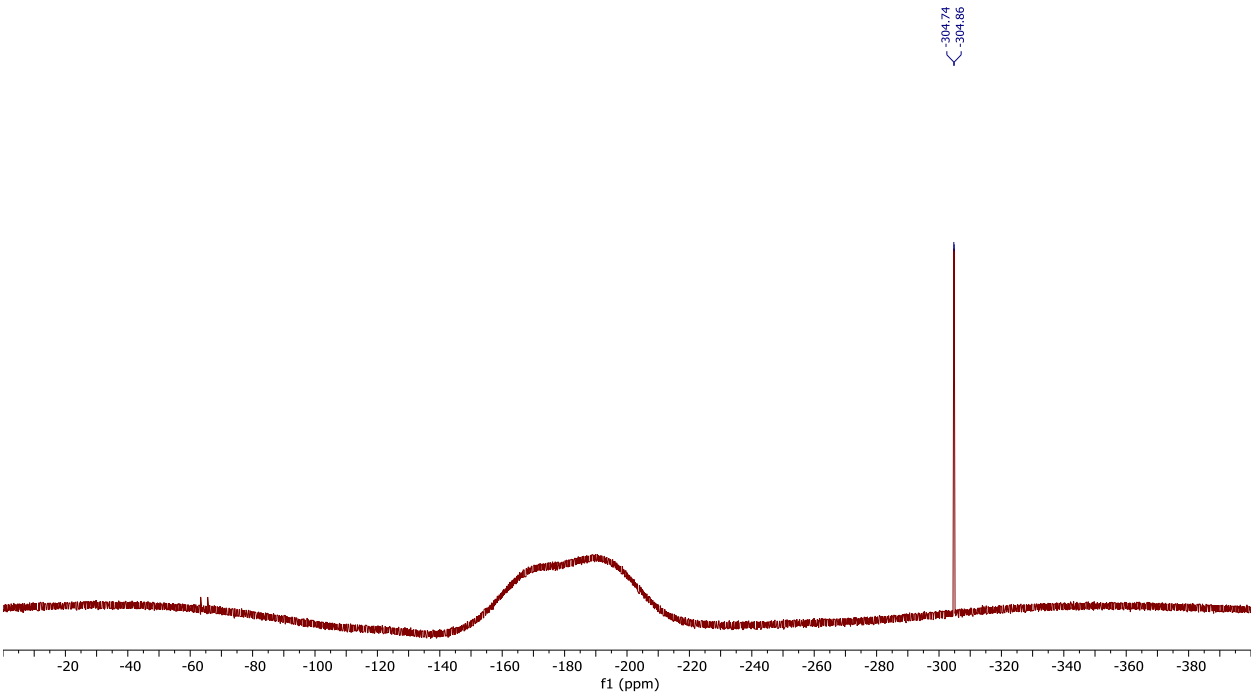

^{31}P {^{1}H} NMR Spectrum $CDCl_3$ (121 MHz)

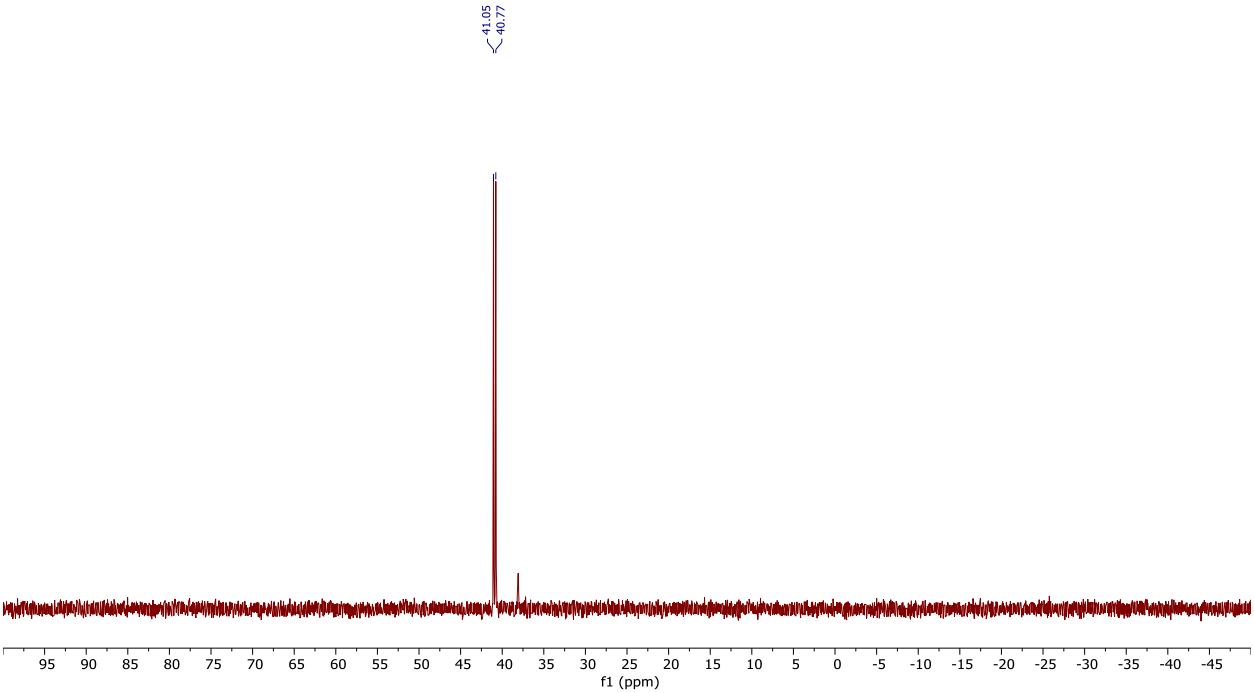

Indoline-1-carbamoyl-bis(tricyclohexyl) Nickel (II) fluoride

^{1}H NMR Spectrum $CDCl_3$ (300 MHz)

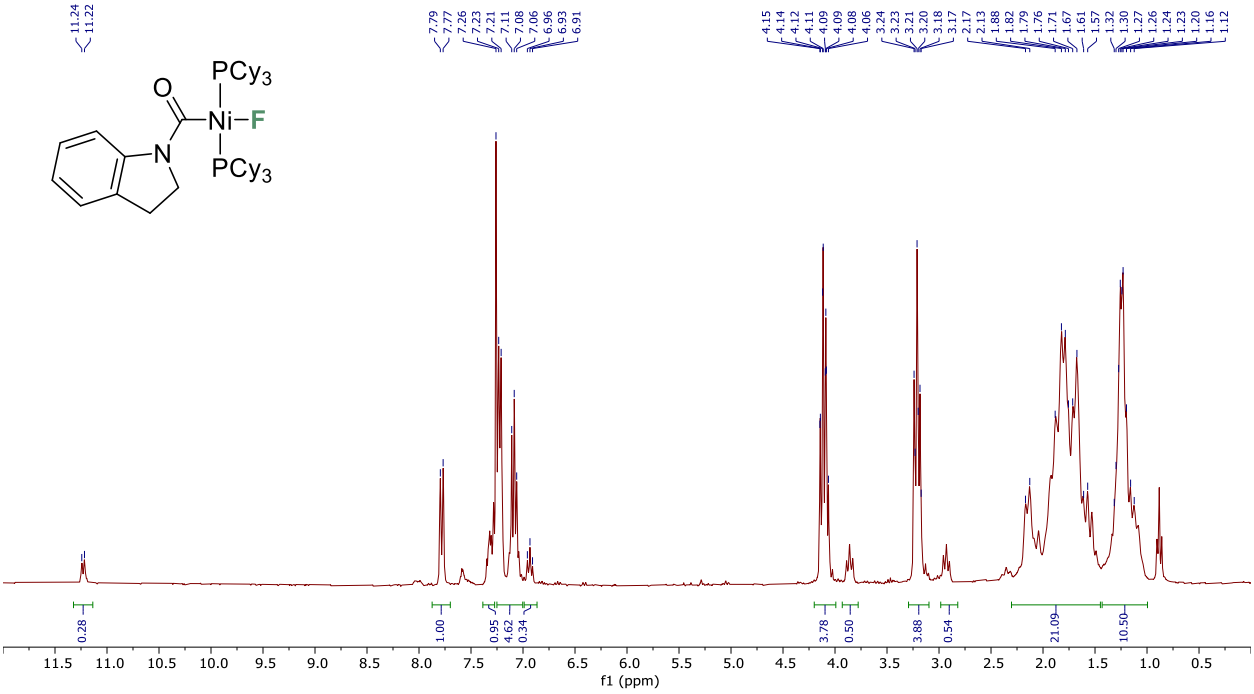

^{19}F {^{1}H) NMR Spectrum $CDCl_3$ (282 MHz)

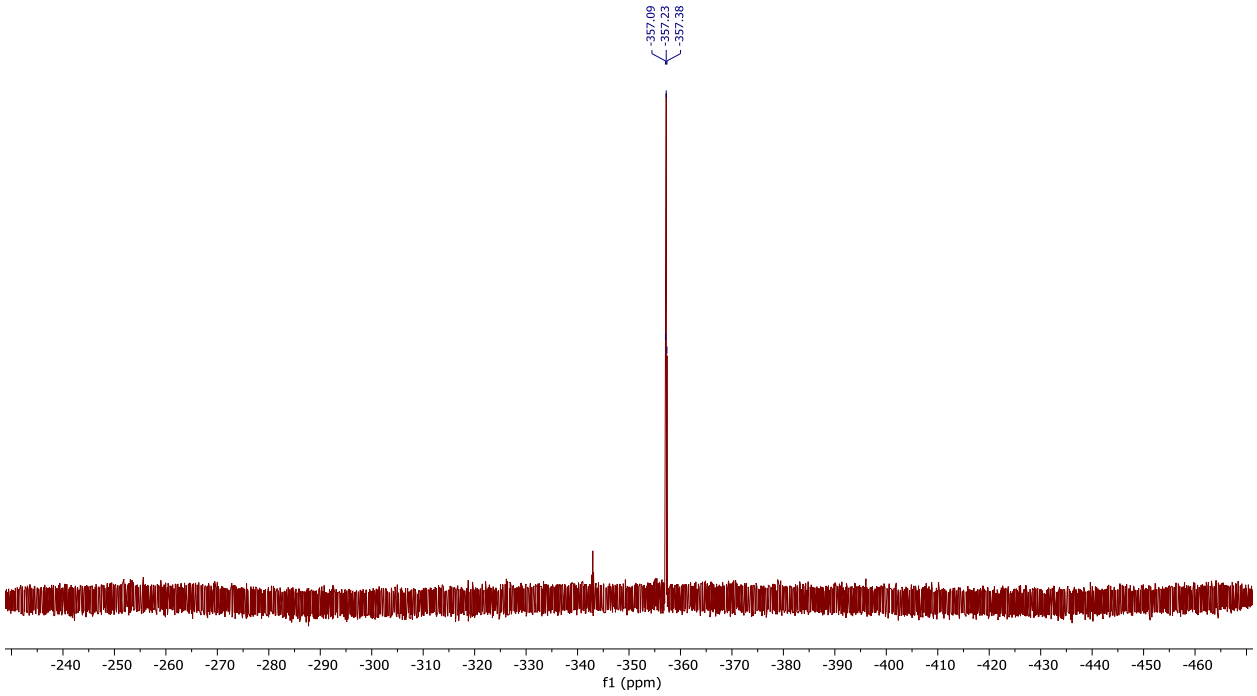

^{31}P {^{1}H} NMR Spectrum $CDCl_3$ (121 MHz)

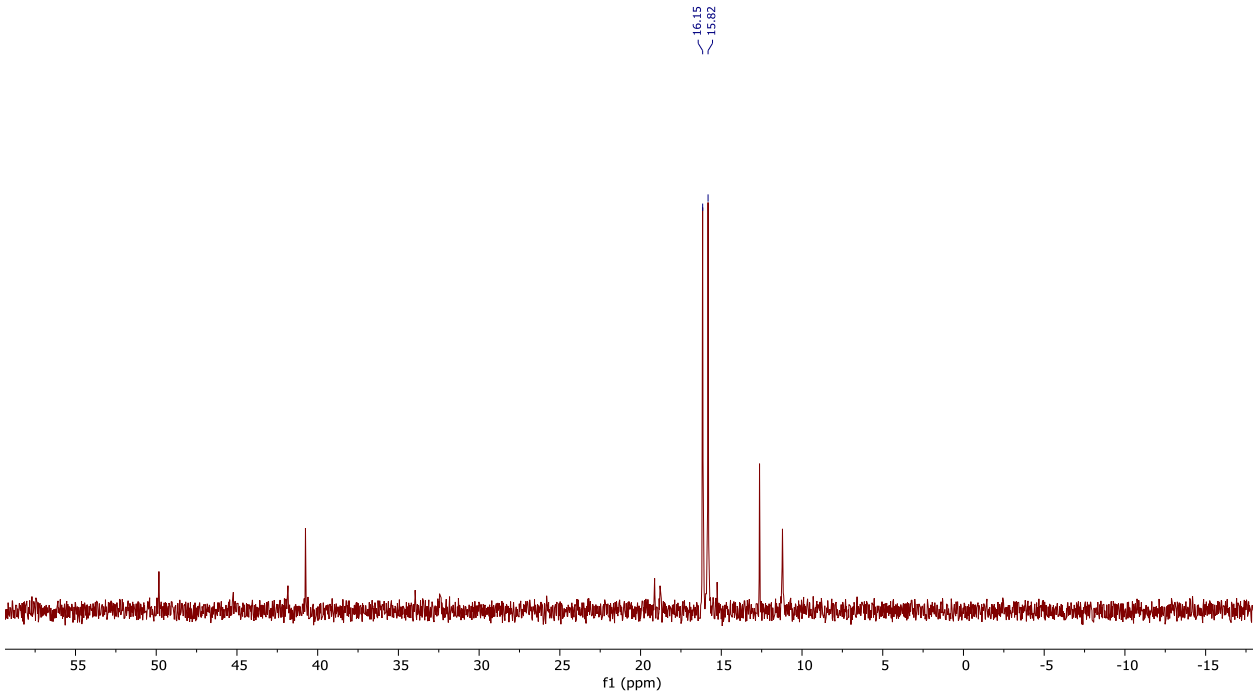

N-benzyl-N-(pyridin-2-yl)carbamoyl-[1,1′-Bis(diphenylphosphino) ferrocene] Nickel (II) fluoride

^{1}H NMR Spectrum C_6D_6 (300 MHz)

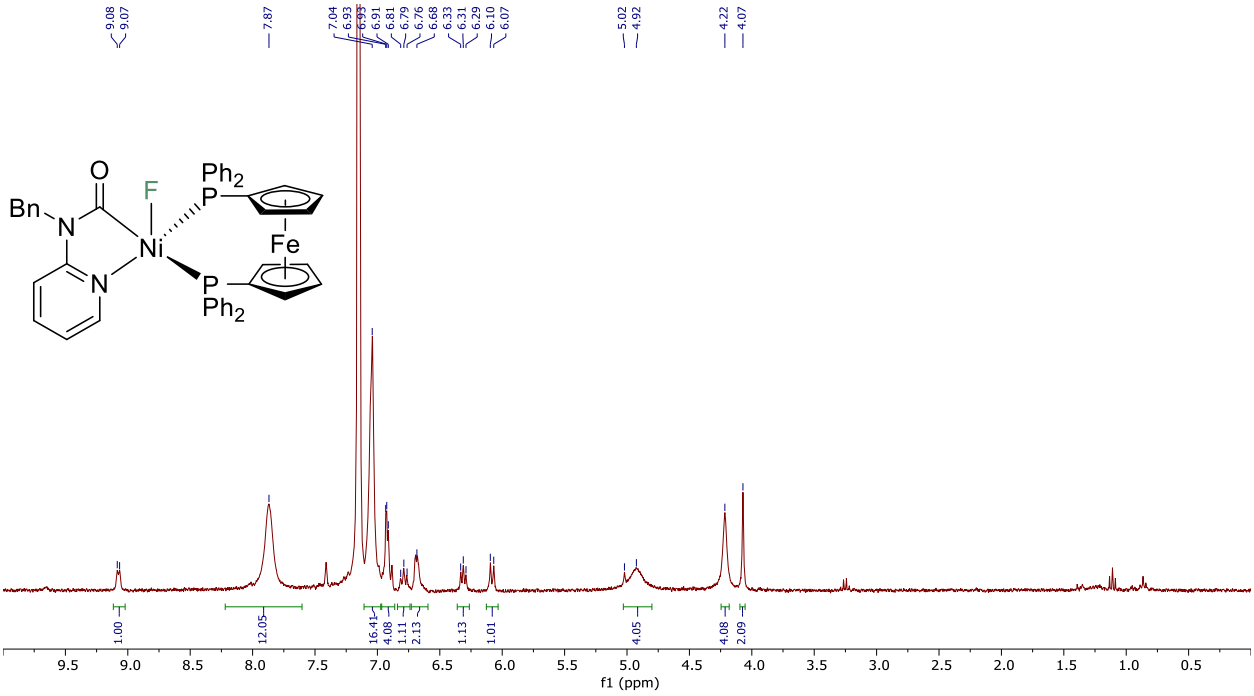

^{19}F {^{1}H) NMR Spectrum C_6D_6 (282 MHz)

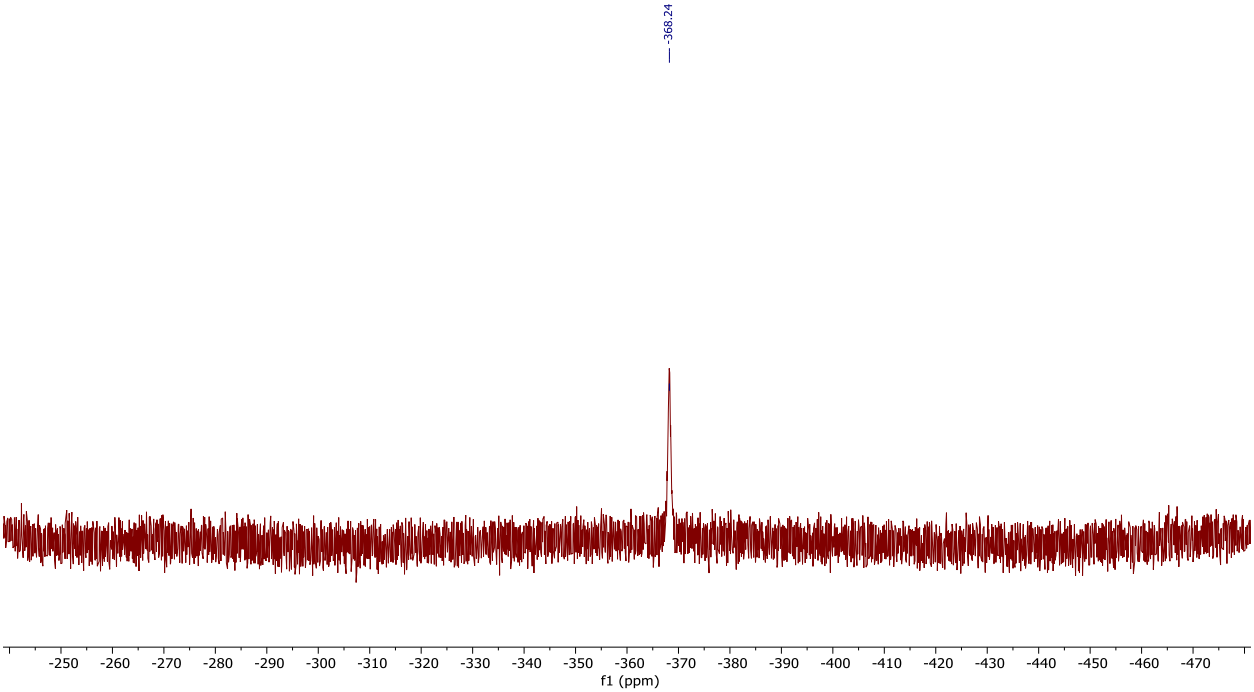

^{31}P {^{1}H} NMR Spectrum C_6D_6 (121 MHz)

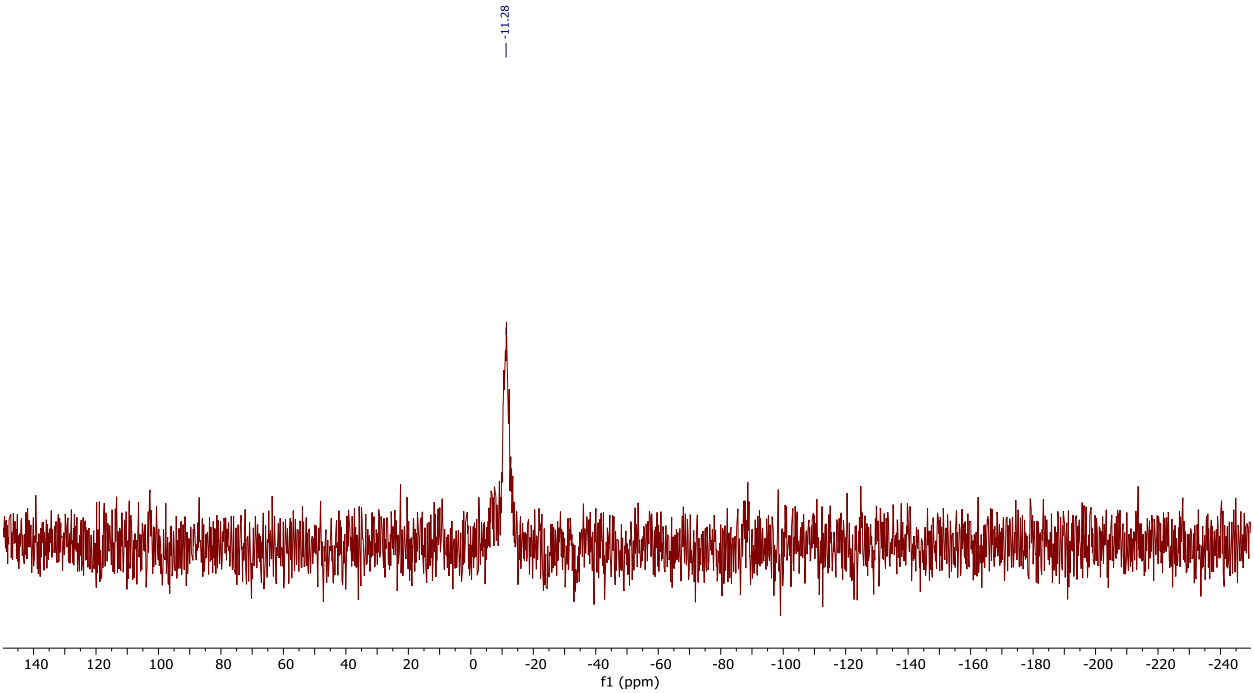

2-(9-borabicyclo[3.3.1]nonan-9-yl)ethylferrocene

^{1}H NMR Spectrum C_6D_6 (600 MHz)

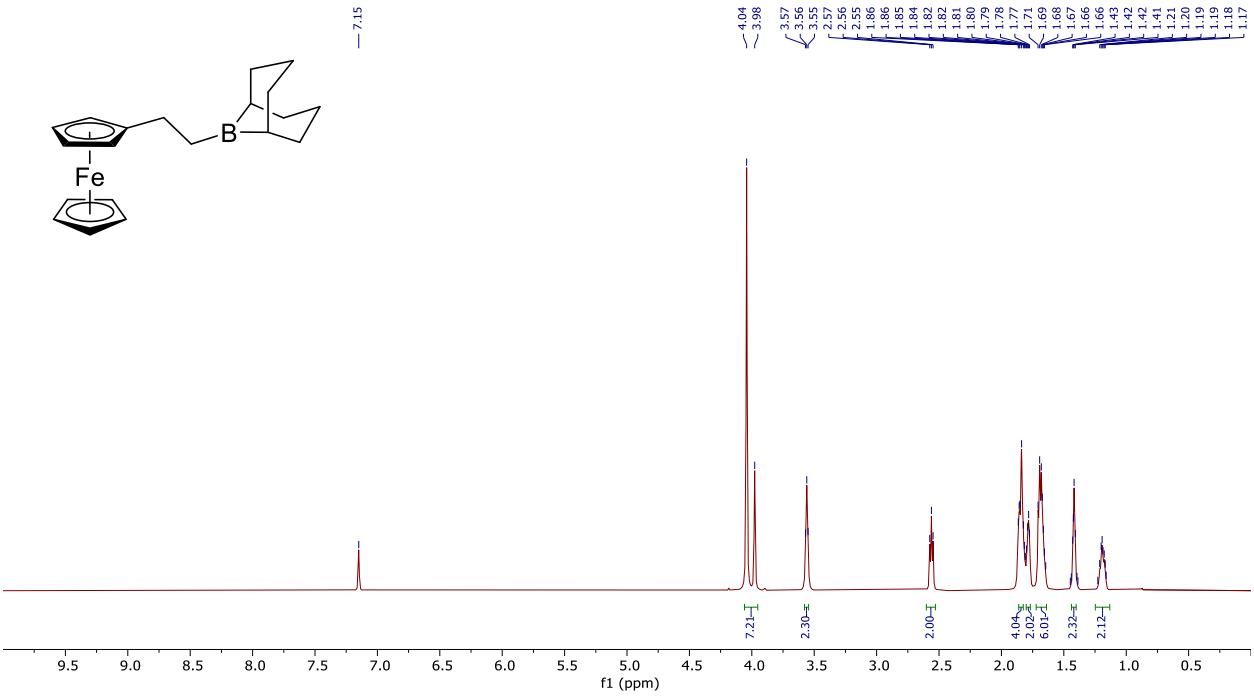

^{11}B {^{1}H) NMR Spectrum C_6D_6 (192 MHz)

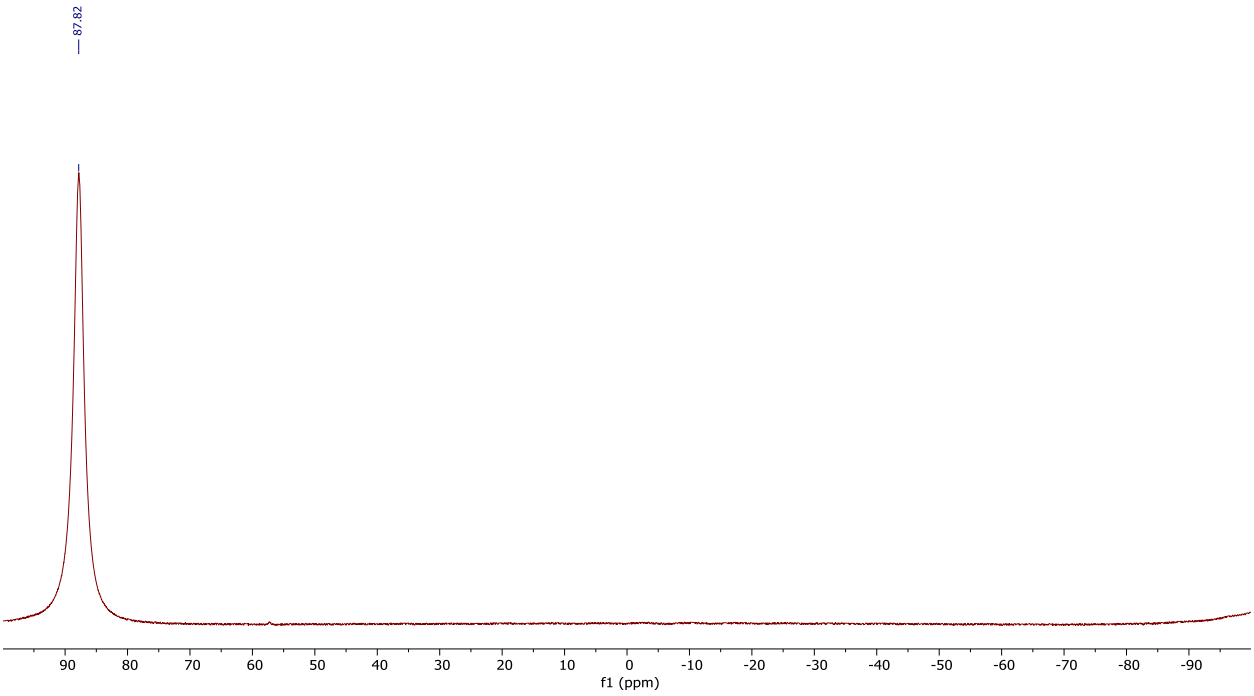

^{13}C NMR Spectrum C_6D_6 (151 MHz)

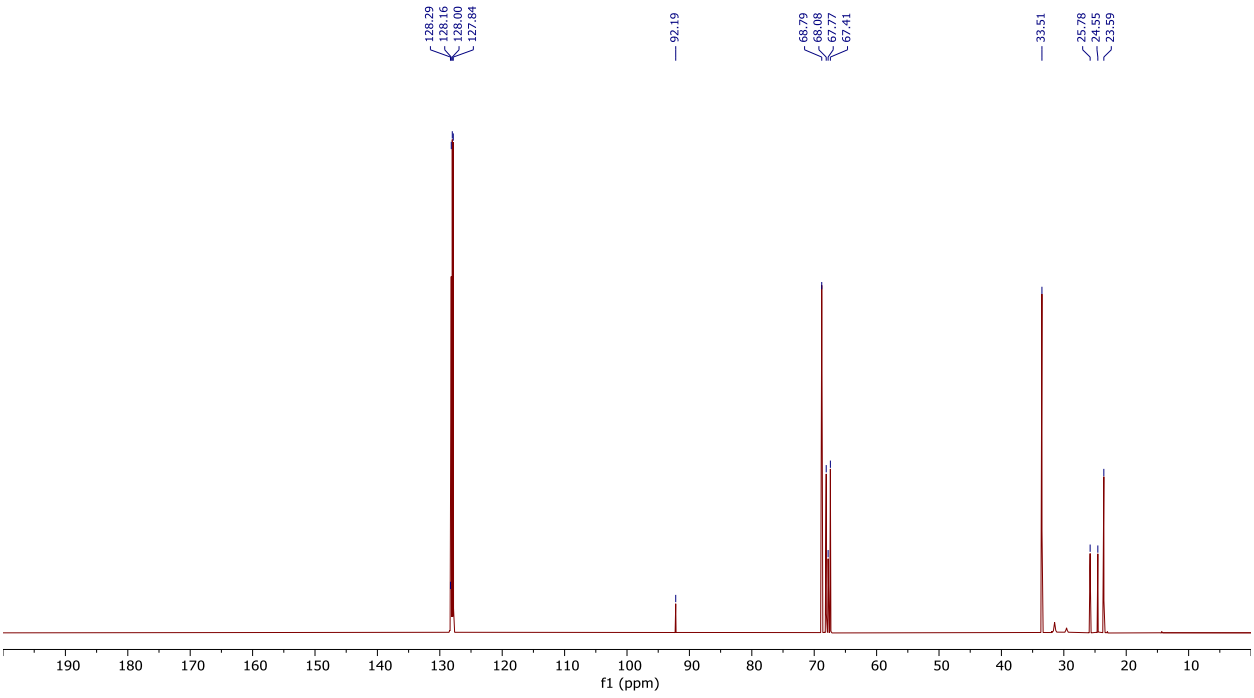

3-(9-borabicyclo[3.3.1]nonan-9-yl)propyl-trimethyl-silane

^{1}H NMR Spectrum C_6D_6 (600 MHz)

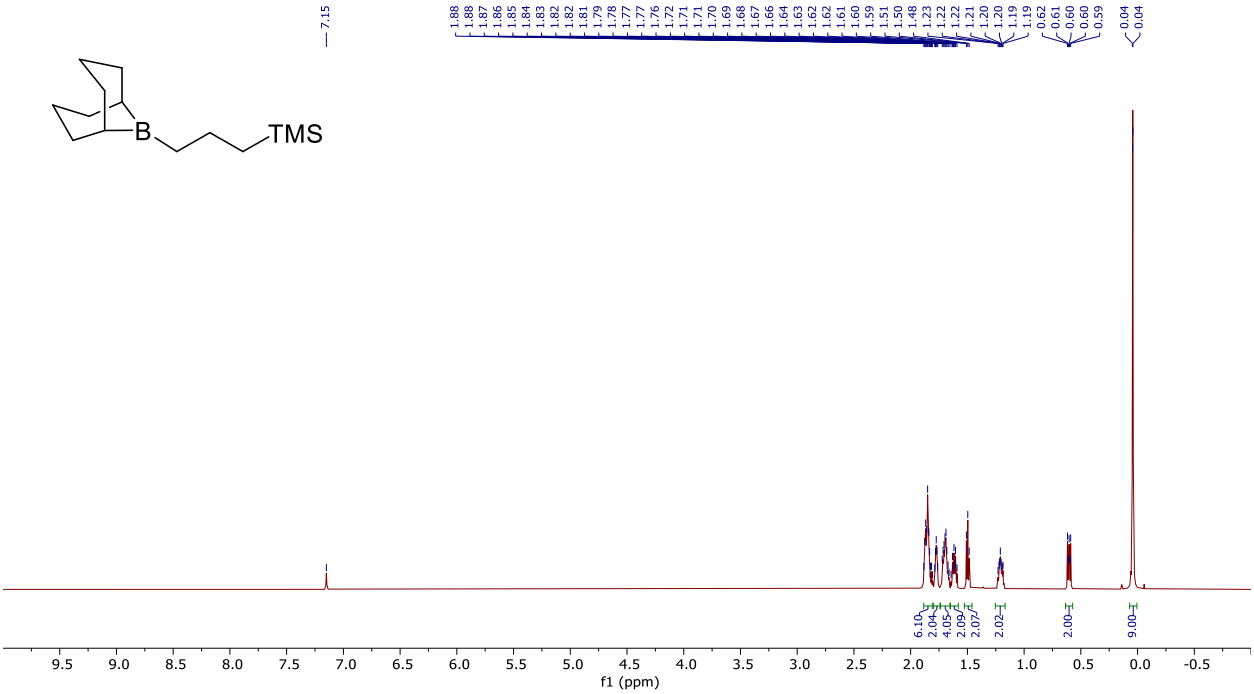

^{11}B {^{1}H) NMR Spectrum C_6D_6 (192 MHz)

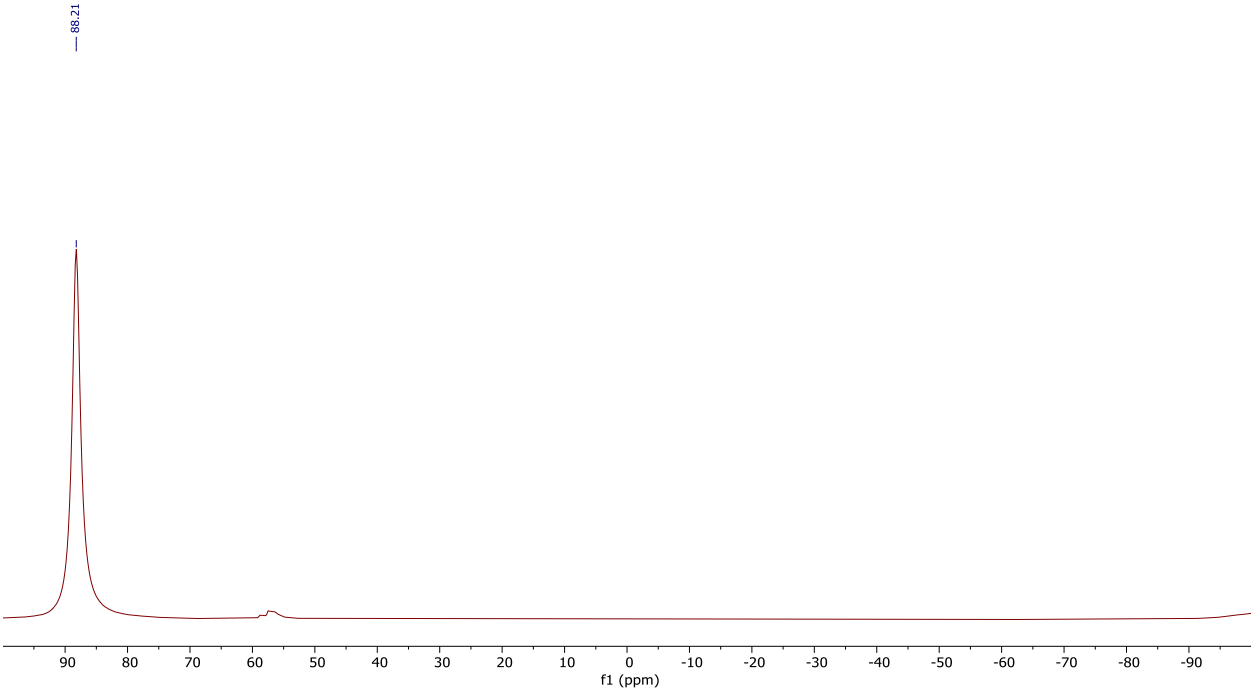

^{13}C NMR Spectrum C_6D_6 (151 MHz)

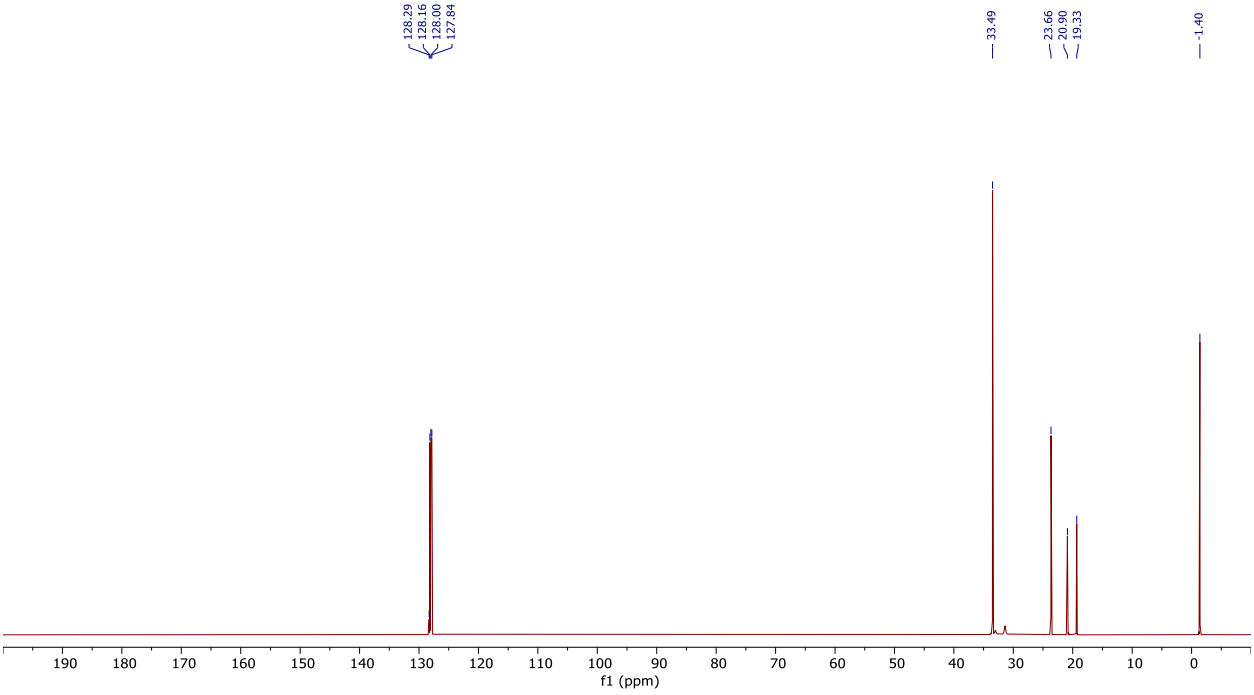

tert-butyl _N_-[3-(9-borabicyclo[3.3.1]nonan-9-yl)propyl]carbamate

^{1}H NMR Spectrum C_6D_6 (600 MHz)

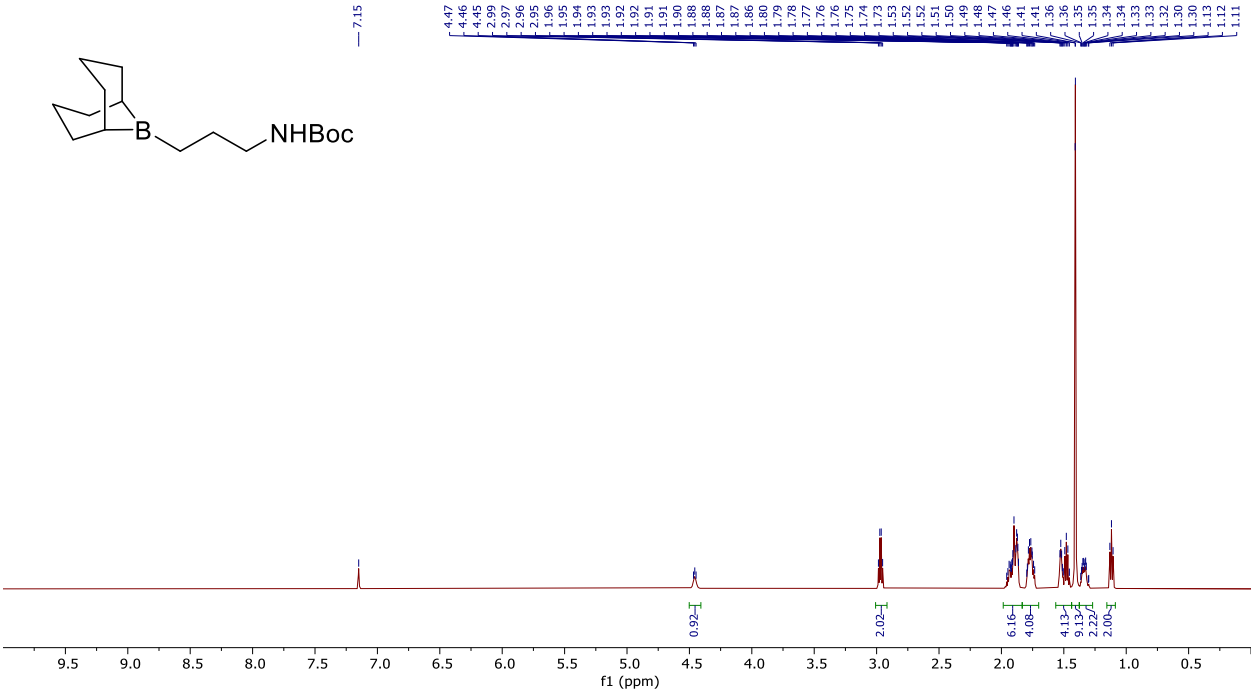

^{11}B {^{1}H) NMR Spectrum C_6D_6 (192 MHz)

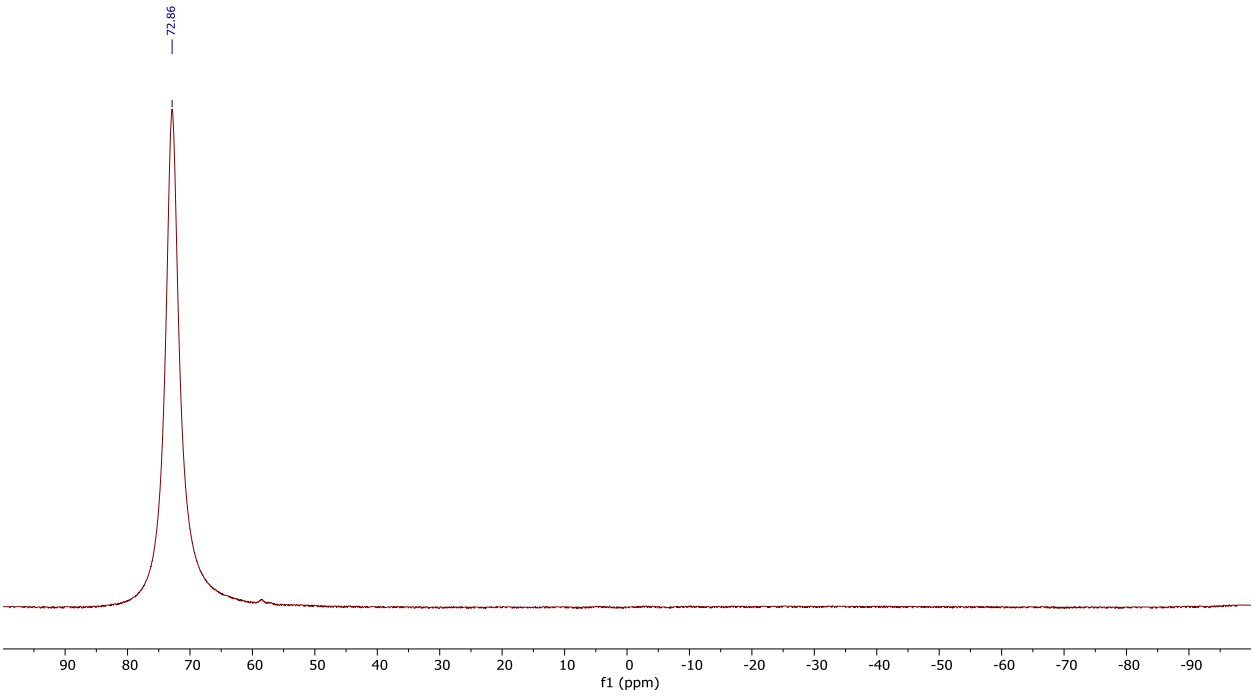

^{13}C NMR Spectrum C_6D_6 (151 MHz)

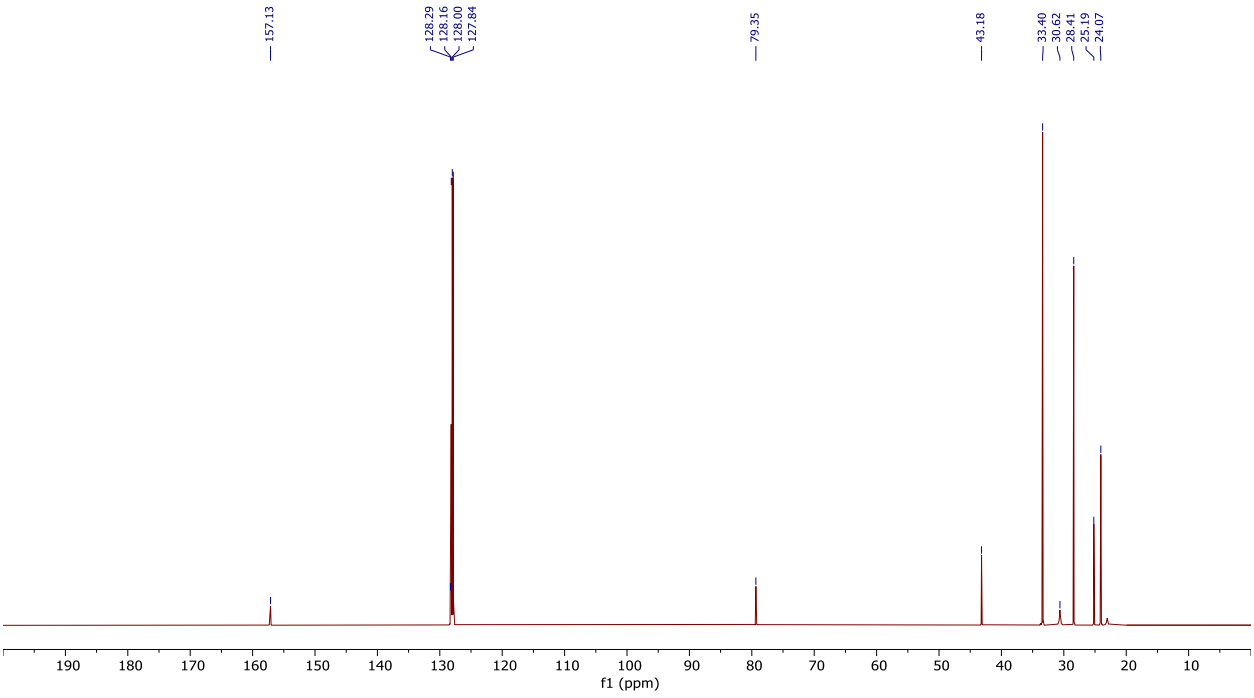

Sodium 2-(9-hydroxy-9-boranuidabicyclo[3.3.1]nonan-9-yl)ethylferrocene

^{11}B {^{1}H) NMR Spectrum C_6D_6 (192 MHz)

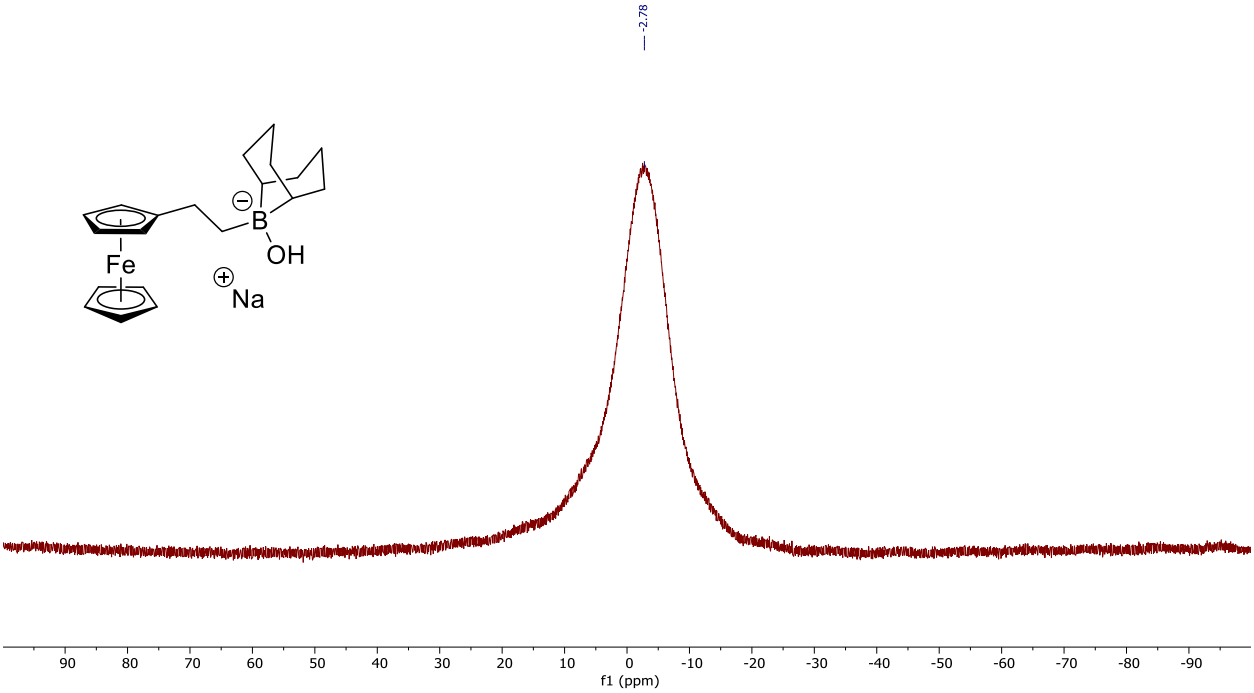

Sodium 3-(9-hydroxy-9-boranuidabicyclo[3.3.1]nonan-9-yl)propyl-trimethyl-silane

^{1}H NMR Spectrum C_6D_6 (600 MHz)

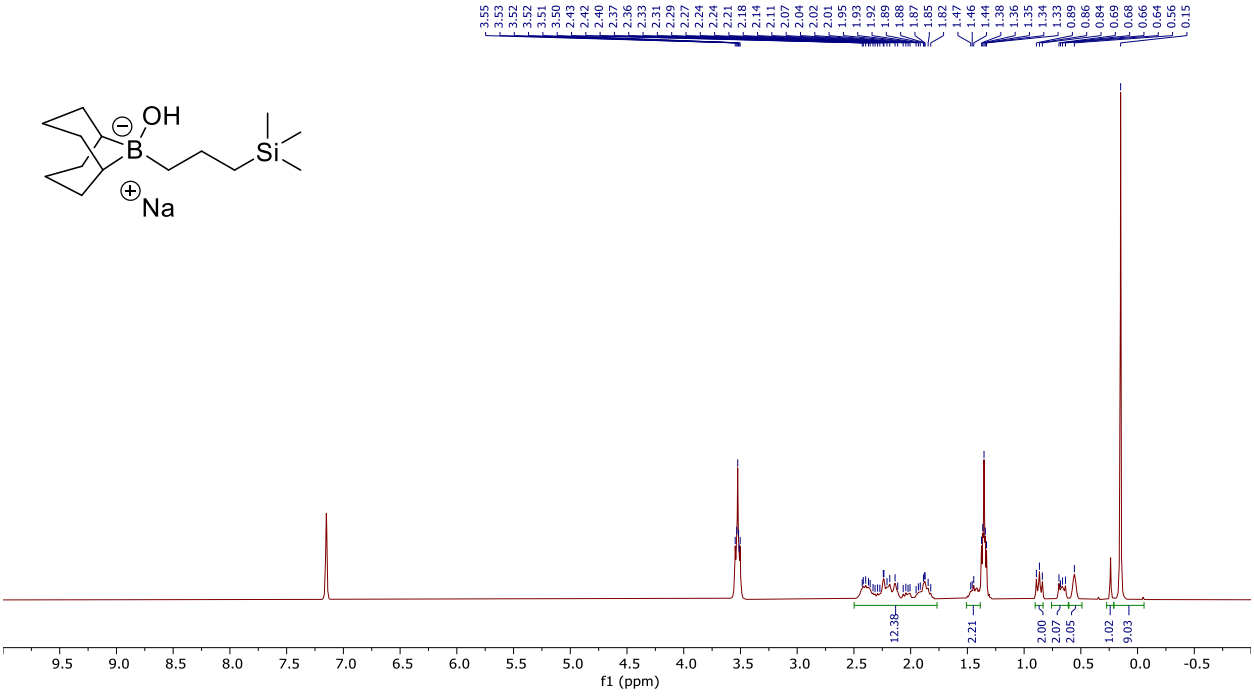

^{11}B {^{1}H) NMR Spectrum C_6D_6 (192 MHz)

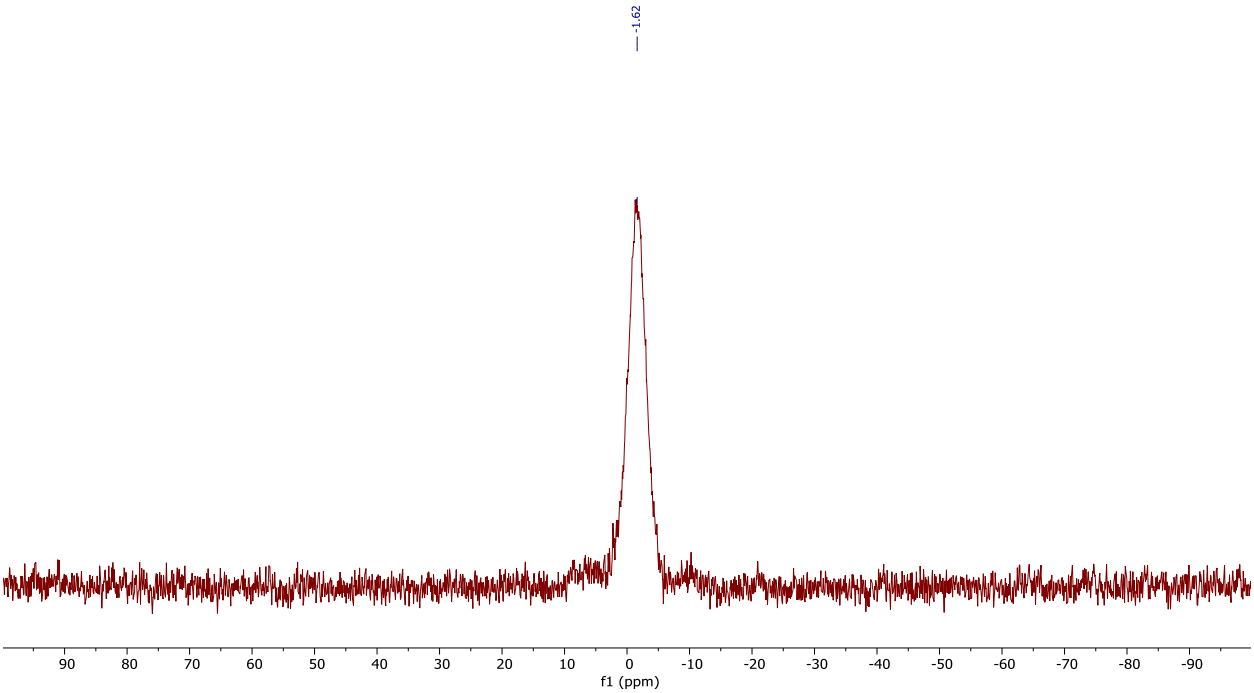

^{13}C NMR Spectrum C_6D_6 (151 MHz)

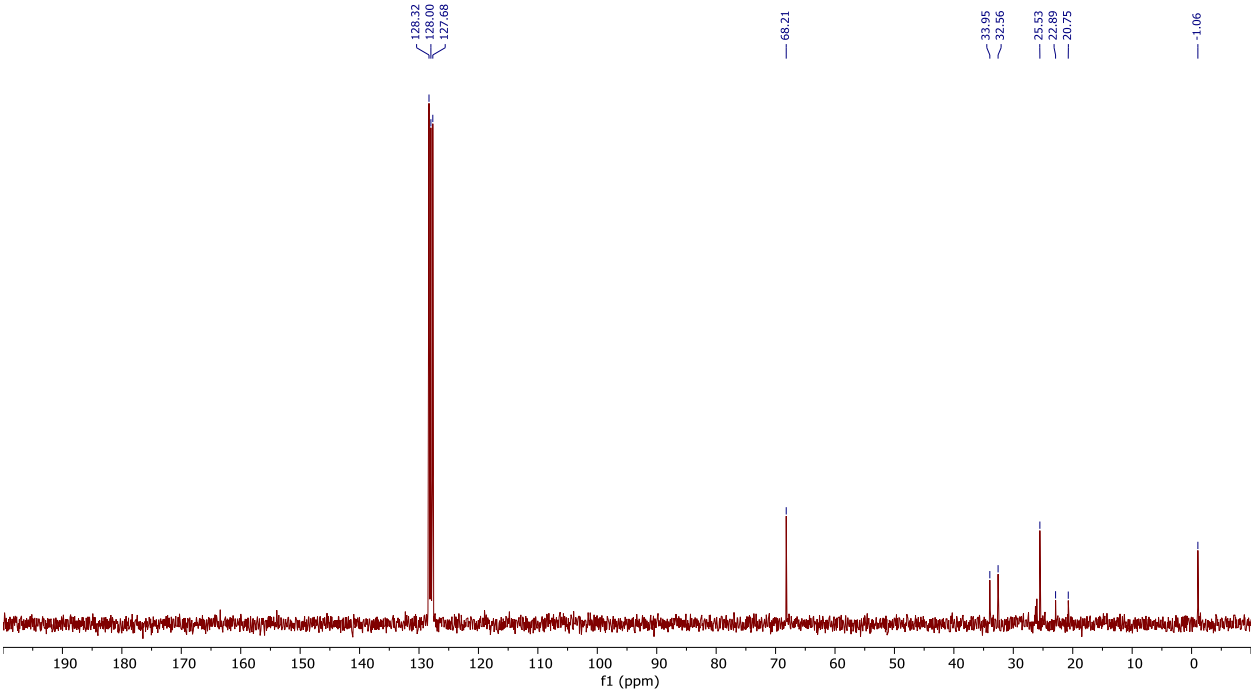

Sodium tert-butyl N-[3-(9-hydroxy-9-boranuidabicyclo[3.3.1]nonan-9-yl)propyl]carbamate

^{1}H NMR Spectrum C_6D_6 (600 MHz)

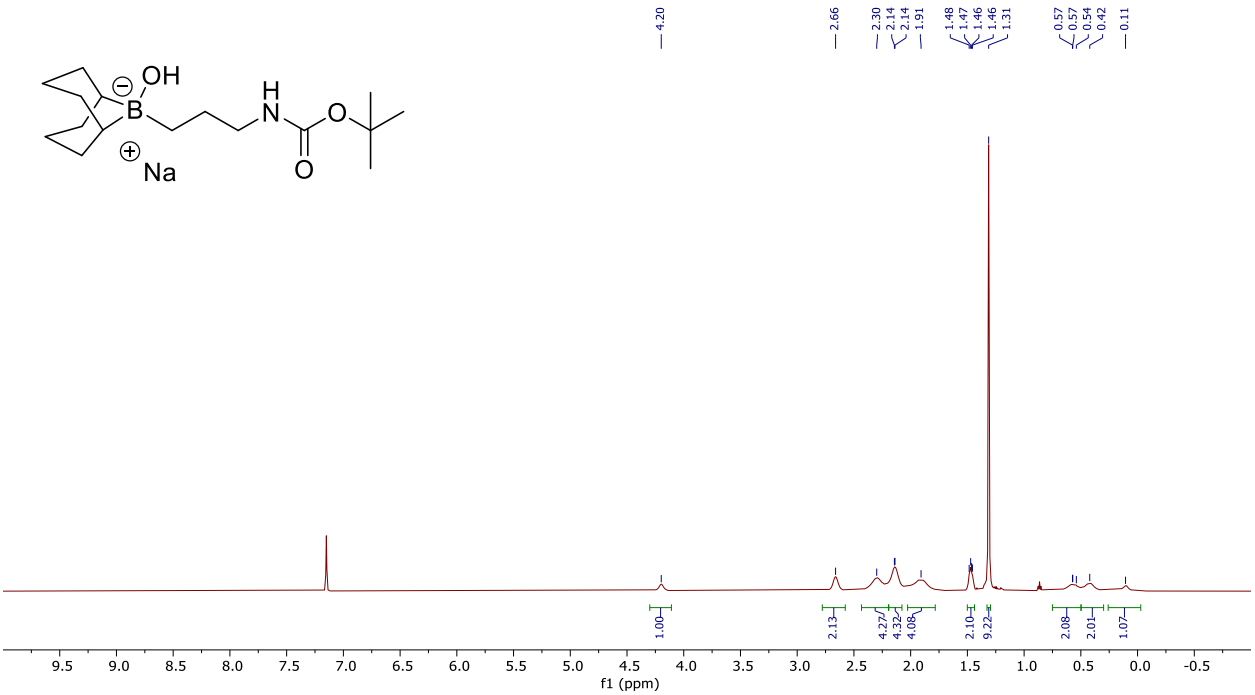

^{11}B {^{1}H) NMR Spectrum C_6D_6 (192 MHz)

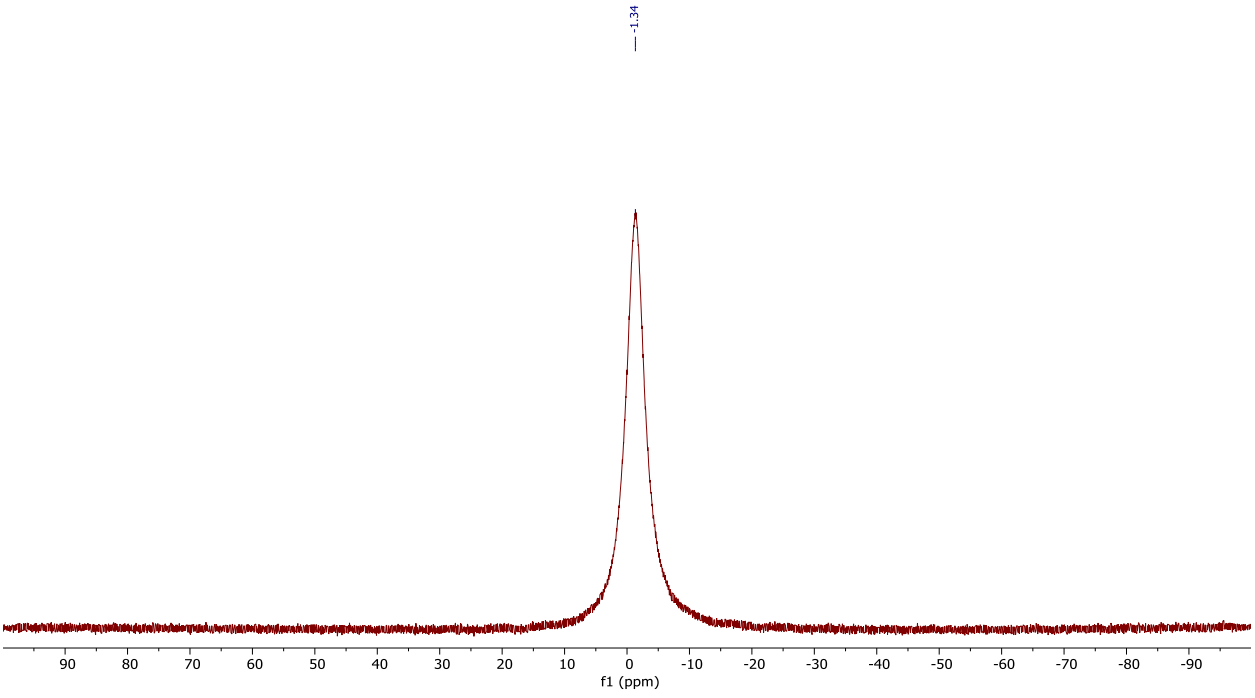

^{13}C NMR Spectrum C_6D_6 (151 MHz)

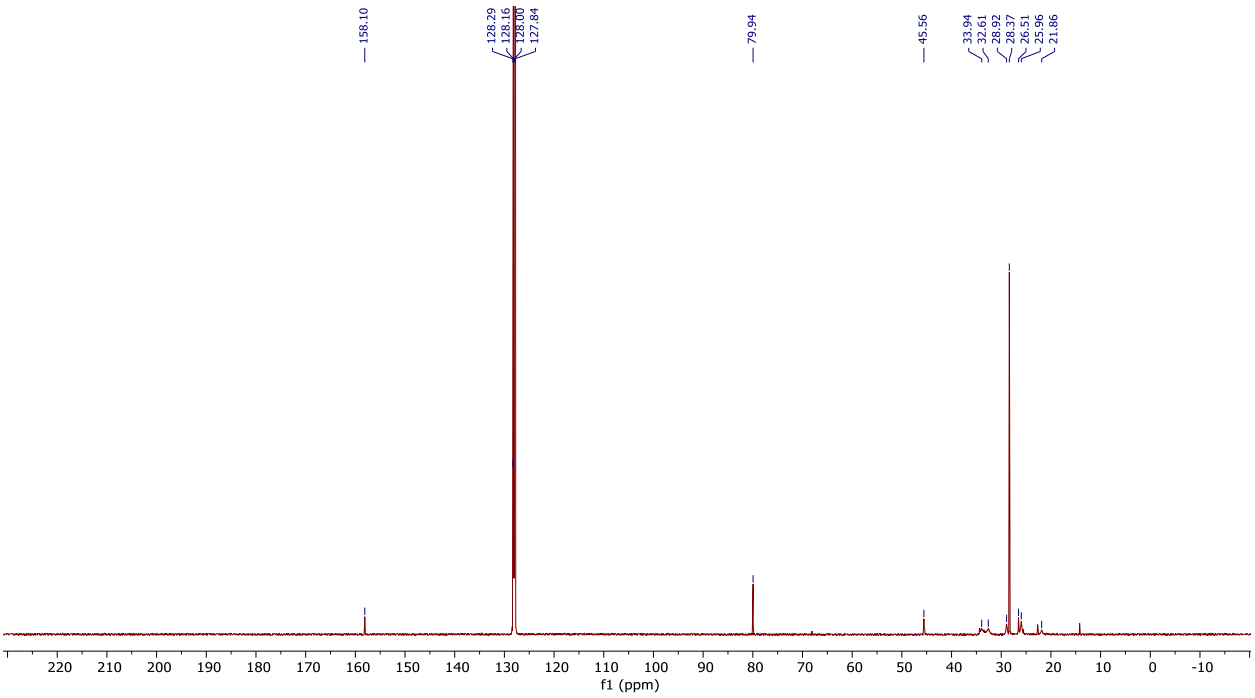

Complete List of References

Chapter 1

(1) Pitzer, J.; Steiner, K. Amides in Nature and Biocatalysis. *J. Biotechnol.* **2016**, *235*, 32–46. https://doi.org/10.1016/j.jbiotec.2016.03.023.

(2) Seavill, P. W.; Wilden, J. D. The Preparation and Applications of Amides Using Electrosynthesis. *Green Chem.* **2020**, *22* (22), 7737–7759. https://doi.org/10.1039/d0gc02976a.

(3) Rajamanickam, K. R.; Rajan, R. P. S.; Pootheri, N.; Lee, C.-F.; Lee, S. Recent Advances in Transition Metal-Free Strategies for the Transformation of Amides into Carbonyl Compounds. *Eur. J. Org. Chem.* **2025**, *28* (23), e202500210. https://doi.org/10.1002/ejoc.202500210.

(4) Kaiser, D.; Bauer, A.; Lemmerer, M.; Maulide, N. Amide Activation: An Emerging Tool for Chemoselective Synthesis. *Chem. Soc. Rev.* **2018**, *47* (21), 7899–7925. https://doi.org/10.1039/c8cs00335a.

(5) de Figueiredo, R. M.; Suppo, J.-S.; Campagne, J.-M. Nonclassical Routes for Amide Bond Formation. *Chem. Rev.* **2016**, *116* (19), 12029–12122. https://doi.org/10.1021/acs.chemrev.6b00237.

(6) Pattabiraman, V. R.; Bode, J. W. Rethinking Amide Bond Synthesis. *Nature* **2011**, *480* (7378), 471–479. https://doi.org/10.1038/nature10702.

(7) Ojeda-Porras, A.; Gamba-Sánchez, D. Recent Developments in Amide Synthesis Using Nonactivated Starting Materials. *J. Org. Chem.* **2016**, *81* (23), 11548–11555. https://doi.org/10.1021/acs.joc.6b02358.

(8) Allen, C. L.; Williams, J. M. J. Metal-Catalysed Approaches to Amide Bond Formation. *Chem. Soc. Rev.* **2011**, *40* (7), 3405–3415. https://doi.org/10.1039/c0cs00196a.

(9) Mujika, J. I.; Matxain, J. M.; Eriksson, L. A.; Lopez, X. Resonance Structures of the Amide Bond: The Advantages of Planarity. *Chem. – Eur. J.* **2006**, *12* (27), 7215–7224. https://doi.org/10.1002/chem.200600052.

(10) Serrano, E.; Martin, R. Forging Amides Through Metal-Catalyzed C–C Coupling with Isocyanates. *Eur. J. Org. Chem.* **2018**, *2018* (24), 3051–3064. https://doi.org/10.1002/ejoc.201800175.

(11) Charville, H.; Jackson, D.; Hodges, G.; Whiting, A. The Thermal and Boron-Catalysed Direct Amide Formation Reactions: Mechanistically Understudied yet Important Processes. *Chem. Commun.* **2010**, *46* (11), 1813–1823. https://doi.org/10.1039/b923093a.

(12) Palmer, R. J. Polyamides, Plastics. In *Encyclopedia of Polymer Science and Technology*; John Wiley & Sons, Ltd, 2001. https://doi.org/10.1002/0471440264.pst251.

(13) Lundberg, H.; Tinnis, F.; Selander, N.; Adolfsson, H. Catalytic Amide Formation from Non-Activated Carboxylic Acids and Amines. *Chem. Soc. Rev.* **2014**, *43* (8), 2714–2742. https://doi.org/10.1039/c3cs60345h.

(14) Yoshida, T.; Irizawa, T.; Ogura, K.; Komido, T. Process for Producing Dimethylacetamide. CA2329241A1, October 28, 1999. https://patents.google.com/patent/CA2329241A1/en (accessed 2026-07-25).

(15) Fergusson, S. B.; Marchildon, E. K.; Mutel, A. T. Process for Making Nylon 6,6. US6472501B1, October 29, 2002. https://patents.google.com/patent/US6472501B1/en (accessed 2026-07-25).
(16) Magano, J. Large-Scale Amidations in Process Chemistry: Practical Considerations for Reagent Selection and Reaction Execution. *Org. Process Res. Dev.* **2022**, *26* (6), 1562–1689. https://doi.org/10.1021/acs.oprd.2c00005.
(17) Fujita, T.; Suto, M.; Ogura, K. Process for Production of Dimethylformamide. US4251460A, February 17, 1981. https://patents.google.com/patent/US4251460A/en (accessed 2026-07-25).
(18) Grafmans, H.; Maas, S.; Weck, A.; Rütter, H.; Schulz, M.; Roβ, K.-H. Method for the Production of N,N-Dimethylacetamide (DMAC). US8193390B2, June 5, 2012. https://patents.google.com/patent/US8193390B2/en (accessed 2026-07-25).
(19) Magano, J. Large-Scale Amidations in Process Chemistry: Practical Considerations for Reagent Selection and Reaction Execution. *Org. Process Res. Dev.* **2022**, *26* (6), 1562–1689. https://doi.org/10.1021/acs.oprd.2c00005.
(20) Dunetz, J. R.; Magano, J.; Weisenburger, G. A. Large-Scale Applications of Amide Coupling Reagents for the Synthesis of Pharmaceuticals. *Org. Process Res. Dev.* **2015**, *20* (2), 140–177. https://doi.org/10.1021/op500305s.
(21) Valeur, E.; Bradley, M. Amide Bond Formation: Beyond the Myth of Coupling Reagents. *Chem. Soc. Rev.* **2009**, *38* (2), 606–631. https://doi.org/10.1039/b701677h.
(22) Hansen, S. V. F.; Ulven, T. Oxalyl Chloride as a Practical Carbon Monoxide Source for Carbonylation Reactions. *Org. Lett.* **2015**, *17* (11), 2832–2835. https://doi.org/10.1021/acs.orglett.5b01252.
(23) Montalbetti, C. A. G. N.; Falque, V. Amide Bond Formation and Peptide Coupling. *Tetrahedron* **2005**, *61* (46), 10827–10852. https://doi.org/10.1016/j.tet.2005.08.031.
(24) Shi, M.; Ye, N.; Chen, W.; Wang, H.; Cheung, C.; Parmentier, M.; Gallou, F.; Wu, B. Simple Synthesis of Amides via Their Acid Chlorides in Aqueous TPGS-750-M. *Org. Process Res. Dev.* **2020**, *24* (8), 1543–1548. https://doi.org/10.1021/acs.oprd.0c00303.
(25) Sabatini, M. T.; Boulton, L. T.; Sneddon, H. F.; Sheppard, T. D. A Green Chemistry Perspective on Catalytic Amide Bond Formation. *Nat. Catal.* **2019**, *2* (1), 10–17. https://doi.org/10.1038/s41929-018-0211-5.
(26) Liu, L.; Gu, Y.-C.; Zhang, C.-P. Recent Advances in the Synthesis and Transformation of Carbamoyl Fluorides, Fluoroformates, and Their Analogues. *Chem. Rec.* **2023**, *23* (9), e202300071. https://doi.org/10.1002/tcr.202300071.
(27) Jabbarpoor, M.; Le, C. M. Carbamoyl Fluorides: A Platform to Interrogate Fluoride-Enabled Reactivity. *Synthesis* **2025**, *57* (16), 2399–2410. https://doi.org/10.1055/a-2557-7635.
(28) Jäger, P.; Rentzea, C. N.; Kieczka, H. Carbamates and Carbamoyl Chlorides. In *Ullmann's Encyclopedia of Industrial Chemistry*; John Wiley & Sons, Ltd, 2000. https://doi.org/10.1002/14356007.a05_051.
(29) Shrestha, M.; Wu, X.; Huang, W.; Qu, J.; Chen, Y. Recent Advances in Transition Metal-Catalyzed Reactions of Carbamoyl Chlorides. *Org. Chem. Front.* **2021**, *8* (14), 4024–4045. https://doi.org/10.1039/d0qo01648a.
(30) Bonnefoy, C.; Chefdeville, E.; Tourvieille, C.; Panossian, A.; Hanquet, G.; Leroux, F.; Toulgoat, F.; Billard, T. Study of Carbamoyl Fluoride: Synthesis, Properties and Applications. *Chem. – Eur. J.* **2022**, *28* (43), e202201589. https://doi.org/10.1002/chem.202201589.

(31) Varjosaari, S. E.; Suating, P.; Adler, M. J. One-Pot Synthesis of O-Aryl Carbamates. *Synthesis* **2016**, *48* (01), 43–47. https://doi.org/10.1055/s-0035-1560726.
(32) Ganiu, M. O.; Nepal, B.; Van Houten, J. P.; Kartika, R. A Decade Review of Triphosgene and Its Applications in Organic Reactions. *Tetrahedron* **2020**, *76* (47), 131553. https://doi.org/10.1016/j.tet.2020.131553.
(33) Eckert, H.; Forster, B. Triphosgene, a Crystalline Phosgene Substitute. *Angew. Chem. Int. Ed. Engl.* **1987**. https://doi.org/10.1002/anie.198708941.
(34) Eckert, H.; Auerweck, J. Solvent-Free and Safe Process for the Quantitative Production of Phosgene from Triphosgene by Deactivated Imino-Based Catalysts. *Org. Process Res. Dev.* **2010**, *14* (6), 1501–1505. https://doi.org/10.1021/op100239n.
(35) Semler, G.; Schaeffer, G. Process for the Preparation of Carbamoyl Chlorides Derived from Secondary Amines. US4770820A, September 13, 1988. https://patents.google.com/patent/US4770820A/en (accessed 2026-07-26).
(36) D'Souza, M. J.; Kevill, D. N. Mechanistic Studies of the Solvolyses of Carbamoyl Chlorides and Related Reactions. *Int. J. Mol. Sci.* **2016**, *17* (1), 111. https://doi.org/10.3390/ijms17010111.
(37) Stare, M.; Laniewski, K.; Westermark, A.; Sjögren, M.; Tian, W. Investigation on the Formation and Hydrolysis of N,N-Dimethylcarbamoyl Chloride (DMCC) in Vilsmeier Reactions Using GC/MS as the Analytical Detection Method. *Org. Process Res. Dev.* **2009**, *13* (5), 857–862. https://doi.org/10.1021/op900018f.
(38) Rodis, N. P.; Digenis, G. A. Synthesis and In-Vitro Evaluation of Novel Low Molecular Weight Thiocarbamates as Inhibitors of Human Leukocyte Elastase. *J. Enzym. Inhib.* **2001**, *16* (2), 95–105. https://doi.org/10.1080/14756360109162359.
(39) Wang, G. T.; Chen, Y.; Wang, S.; Sciotti, R.; Sowin, T. Solid Phase Synthesis of Ureas of Secondary Amines via Carbamoyl Chloride. *Tetrahedron Lett.* **1997**, *38* (11), 1895–1898. https://doi.org/10.1016/S0040-4039(97)00245-1.
(40) Lemoucheux, L.; Rouden, J.; Ibazizene, M.; Sobrio, F.; Lasne, M.-C. Debenzylation of Tertiary Amines Using Phosgene or Triphosgene: An Efficient and Rapid Procedure for the Preparation of Carbamoyl Chlorides and Unsymmetrical Ureas. Application in Carbon-11 Chemistry. *J. Org. Chem.* **2003**, *68* (19), 7289–7297. https://doi.org/10.1021/jo0346297.
(41) Wu, S.; Chen, G.; Zhang, Q.; Wang, G.; Chen, Q.-H. 3-O-Carbamoyl-5,7,20-O-Trimethylsilybins: Synthesis and Preliminary Antiproliferative Evaluation. *Molecules* **2021**, *26* (21), 6421. https://doi.org/10.3390/molecules26216421.
(42) Brimble, M. A.; Bryant, C. J. Synthesis and Assignment of the Absolute Configuration of the Anti-Helicobacter Pylori Agents CJ-12,954 and CJ-13,014. *Org. Biomol. Chem.* **2007**, *5* (17), 2858–2866. https://doi.org/10.1039/b709932k.
(43) Gayke, M.; Hirapara, N.; Narode, H.; Bhosle, S. D.; Bhosale, R. S.; Yadav, J. S. Zinc Chloride-Catalyzed Synthesis of Carbamates: An Application for the Synthesis of the Anti-Alzheimer's Drug Rivastigmine. *ACS Omega* **2022**, *7* (40), 36017–36027. https://doi.org/10.1021/acsomega.2c05350.
(44) Mandava, V. N. B. R.; Vajrala, V. R.; Varanasi, G.; Adla, V. K.; Jambula, M. R.; Reddy, V. R. K. Preparation of Rivastigmine and Its Salts. US8013181B2, September 6, 2011. https://patents.google.com/patent/US8013181B2/en (accessed 2026-07-26).
(45) Cuevas, J.-C.; Patil, P.; Snieckus, V. A′,A′-Disilylated Tertiary Benzamides as Dual Ortho- and A′-Carbanion Synthons: Amide Peterson Olefination Routes to N-Benzoyl Enamines,

Isoquinolines, and Dibenzazocines. *Tetrahedron Lett.* **1989**, *30* (43), 5841–5844. https://doi.org/10.1016/S0040-4039(01)93485-9.
(46) Snieckus, V. Directed Ortho Metalation. Tertiary Amide and O-Carbamate Directors in Synthetic Strategies for Polysubstituted Aromatics. *Chem. Rev.* **2002**, *90* (6), 879–933. https://doi.org/10.1021/cr00104a001.
(47) Mills, R. J.; Taylor, N. J.; Snieckus, V. Directed Ortho Metalation of N,N-Diethylbenzamides. Silicon Protection of Ortho Sites and the o-Methyl Group. *J. Org. Chem.* **2002**, *54* (18), 4372–4385. https://doi.org/10.1021/jo00279a028.
(48) Comins, D. L.; Hong, H. Chiral Dihydropyridones as Synthetic Intermediates. Asymmetric Synthesis of (+)-Elaeokanine A and (+)-Elaeokanine C. *J. Am. Chem. Soc.* **2002**, *113* (17), 6672–6673. https://doi.org/10.1021/ja00017a047.
(49) Pichette Drapeau, M.; Tlili, A. Modern Synthesis of Carbamoyl Fluorides. *Tetrahedron Lett.* **2020**, *61* (47), 152539. https://doi.org/10.1016/j.tetlet.2020.152539.
(50) Onida, K.; Tlili, A. Direct Synthesis of Carbamoyl Fluorides by CO2 Deoxyfluorination. *Angew. Chem. Int. Ed.* **2019**, *58* (36), 12545–12548. https://doi.org/10.1002/anie.201907354.
(51) Bonnefoy, C.; Chefdeville, E.; Tourvieille, C.; Panossian, A.; Hanquet, G.; Leroux, F.; Toulgoat, F.; Billard, T. Study of Carbamoyl Fluoride: Synthesis, Properties and Applications. *Chem. – Eur. J.* **2022**, *28* (43), e202201589. https://doi.org/10.1002/chem.202201589.
(52) Cadwallader, D.; Tiburcio, T. R.; Cieszynski, G. A.; Le, C. M. Synthesis of Carbamoyl Fluorides Using a Difluorophosgene Surrogate Derived from Difluorocarbene and Pyridine N-Oxides. *J. Org. Chem.* **2022**, *87* (17), 11457–11468. https://doi.org/10.1021/acs.joc.2c01017.
(53) Hatch, C. E., III. Synthesis of N,N-Dialkylaminosulfenylcarbamate Insecticides via Carbamoyl Fluorides. *J. Org. Chem.* **2002**, *43* (20), 3953–3957. https://doi.org/10.1021/jo00414a033.
(54) Cadwallader, D.; Shevchuk, D.; Tiburcio, T. R.; Le, C. M. Fluoride-Catalyzed Cross-Coupling of Carbamoyl Fluorides and Alkynylsilanes. *Org. Lett.* **2023**, *25* (40), 7369–7373. https://doi.org/10.1021/acs.orglett.3c02871.
(55) McKnight, E. A.; Arora, R.; Pradhan, E.; Fujisato, Y. H.; Ajayi, A. J.; Lautens, M.; Zeng, T.; Le, C. M. BF3-Catalyzed Intramolecular Fluorocarbamoylation of Alkynes via Halide Recycling. *J. Am. Chem. Soc.* **2023**, *145* (20), 11012–11018. https://doi.org/10.1021/jacs.3c03982.
(56) Metzger, H. P.; Wilson, I. B. Evidence for an Electrophilic Mechanism in Catalysis by Hydrolytic Enzymes*. *Biochemistry* **2002**, *3* (7), 926–931. https://doi.org/10.1021/bi00895a013.
(57) Augustinsson, K. B.; Casida, J. E. Enzymic Hydrolysis of N:N-Dimethylcarbamoyl Fluoride. *Biochem. Pharmacol.* **1959**, *3* (1), 60–67. https://doi.org/10.1016/0006-2952(59)90009-7.
(58) Randall, G.; Meden, A.; Rutledge, M. T.; Prestreši, L.; Rambaher, M. H.; Chen, S.; Zdovc, I.; Gobec, S.; Knez, D.; Fellner, M. Carbamoyl Fluorides as Serine Hydrolase Inhibitors: A Case Study on FphI from *Staphylococcus Aureus*. *Bioorganic Chem.* **2026**, *176*, 109834. https://doi.org/10.1016/j.bioorg.2026.109834.
(59) Miyaura, Norio.; Suzuki, Akira. Palladium-Catalyzed Cross-Coupling Reactions of Organoboron Compounds. *Chem. Rev.* **2002**, *95* (7), 2457–2483. https://doi.org/10.1021/cr00039a007.

(60) Lennox, A. J. J.; Lloyd-Jones, G. C. Selection of Boron Reagents for Suzuki–Miyaura Coupling. *Chem. Soc. Rev.* **2014**, *43* (1), 412–443. https://doi.org/10.1039/c3cs60197h.
(61) Roughley, S. D.; Jordan, A. M. The Medicinal Chemist's Toolbox: An Analysis of Reactions Used in the Pursuit of Drug Candidates. *J. Med. Chem.* **2011**, *54* (10), 3451–3479. https://doi.org/10.1021/jm200187y.
(62) Brown, D. G.; Boström, J. Analysis of Past and Present Synthetic Methodologies on Medicinal Chemistry: Where Have All the New Reactions Gone?: Miniperspective. *J. Med. Chem.* **2015**, *59* (10), 4443–4458. https://doi.org/10.1021/acs.jmedchem.5b01409.
(63) Schneider, N.; Lowe, D. M.; Sayle, R. A.; Tarselli, M. A.; Landrum, G. A. Big Data from Pharmaceutical Patents: A Computational Analysis of Medicinal Chemists' Bread and Butter. *J. Med. Chem.* **2016**, *59* (9), 4385–4402. https://doi.org/10.1021/acs.jmedchem.6b00153.
(64) Duan, Y.-Z.; Deng, M.-Z. Palladium-Catalyzed Cross-Coupling Reaction of Arylboronic Acids with Chloroformate or Carbamoyl Chloride. *Synlett* **2005**, *2005* (02), 355–357. https://doi.org/10.1055/s-2004-837211.
(65) Magano, J.; Dunetz, J. R. Large-Scale Applications of Transition Metal-Catalyzed Couplings for the Synthesis of Pharmaceuticals. *Chem. Rev.* **2011**, *111* (3), 2177–2250. https://doi.org/10.1021/cr100346g.
(66) Blangetti, M.; Rosso, H.; Prandi, C.; Deagostino, A.; Venturello, P. Suzuki-Miyaura Cross-Coupling in Acylation Reactions, Scope and Recent Developments. *Molecules* **2013**, *18* (1), 1188–1213. https://doi.org/10.3390/molecules18011188.
(67) Krishnamoorthy, R.; Lam, S. Q.; Manley, C. M.; Herr, R. J. Palladium-Catalyzed Preparation of Weinreb Amides from Boronic Acids and N-Methyl-N-Methoxycarbamoyl Chloride. *J. Org. Chem.* **2010**, *75* (4), 1251–1258. https://doi.org/10.1021/jo902647h.
(68) Yasui, Y.; Tsuchida, S.; Miyabe, H.; Takemoto, Y. One-Pot Amidation of Olefins through Pd-Catalyzed Coupling of Alkylboranes and Carbamoyl Chlorides. *J. Org. Chem.* **2007**, *72* (15), 5898–5900. https://doi.org/10.1021/jo070724u.
(69) Christian, A. H.; Müller, P.; Monfette, S. Nickel Hydroxo Complexes as Intermediates in Nickel-Catalyzed Suzuki–Miyaura Cross-Coupling. *Organometallics* **2014**, *33* (9), 2134–2137. https://doi.org/10.1021/om5001327.
(70) Carrow, B. P.; Hartwig, J. F. Distinguishing Between Pathways for Transmetalation in Suzuki−Miyaura Reactions. *J. Am. Chem. Soc.* **2011**, *133* (7), 2116–2119. https://doi.org/10.1021/ja1108326.
(71) Payard, P.-A.; Perego, L. A.; Ciofini, I.; Grimaud, L. Taming Nickel-Catalyzed Suzuki-Miyaura Coupling: A Mechanistic Focus on Boron-to-Nickel Transmetalation. *ACS Catal.* **2018**, *8* (6), 4812–4823. https://doi.org/10.1021/acscatal.8b00933.
(72) Shrestha, M.; Wu, X.; Huang, W.; Qu, J.; Chen, Y. Recent Advances in Transition Metal-Catalyzed Reactions of Carbamoyl Chlorides. *Org. Chem. Front.* **2021**, *8* (14), 4024–4045. https://doi.org/10.1039/d0qo01648a.
(73) Le, C. M.; Sperger, T.; Fu, R.; Hou, X.; Lim, Y. H.; Schoenebeck, F.; Lautens, M. Stereoselective Synthesis of Methylene Oxindoles via Palladium(II)-Catalyzed Intramolecular Cross-Coupling of Carbamoyl Chlorides. *J. Am. Chem. Soc.* **2016**, *138* (43), 14441–14448. https://doi.org/10.1021/jacs.6b08925.
(74) Sperger, T.; Le, C. M.; Lautens, M.; Schoenebeck, F. Mechanistic Insights on the Pd-Catalyzed Addition of C–X Bonds across Alkynes – a Combined Experimental and Computational Study. *Chem. Sci.* **2017**, *8* (4), 2914–2922. https://doi.org/10.1039/c6sc05001h.

(75) Le, C. M.; Hou, X.; Sperger, T.; Schoenebeck, F.; Lautens, M. An Exclusively Trans-Selective Chlorocarbamoylation of Alkynes Enabled by a Palladium/Phosphaadamantane Catalyst. *Angew. Chem. Int. Ed.* **2015**, *54* (52), 15897–15900. https://doi.org/10.1002/anie.201507883.
(76) Balas, L.; Jousseaume, B.; Shin, H.; Verlhac, J. B.; Wallian, F. Palladium-Catalyzed Carbamoylation and Alkoxycarbonylation of Vinyl- and Arylorganotins: An Easy Entry into Vinyl or Aryl Amides and Esters. *Organometallics* **2002**, *10* (1), 366–368. https://doi.org/10.1021/om00047a077.
(77) Lemoucheux, L.; Rouden, J.; Lasne, M.-C. Cross-Coupling Reactions of Carbamoyl Chlorides and Grignard Reagents: A New Rapid Synthesis of Tertiary Amides. *Tetrahedron Lett.* **2000**, *41* (51), 9997–10001. https://doi.org/10.1016/S0040-4039(00)01783-4.
(78) Lysén, M.; Kelleher, S.; Begtrup, M.; Kristensen, J. L. Synthesis of Tertiary Benzamides via Pd-Catalyzed Coupling of Arylboronic Esters and Carbamoyl Chlorides. *J. Org. Chem.* **2005**, *70* (13), 5342–5343. https://doi.org/10.1021/jo050459h.
(79) He, F.; Hou, L.; Wu, X.; Ding, H.; Qu, J.; Chen, Y. Enantioselective Synthesis of α-Alkenylated γ-Lactam Enabled by Ni-Catalyzed 1,4-Arylcarbamoylation of 1,3-Dienes. *CCS Chem.* **2022**, *5* (2), 341–349. https://doi.org/10.31635/ccschem.022.202202010.
(80) Nielsen, C. D.-T.; Zivkovic, F. G.; Schoenebeck, F. Synthesis of N-CF3 Alkynamides and Derivatives Enabled by Ni-Catalyzed Alkynylation of N-CF3 Carbamoyl Fluorides. *J. Am. Chem. Soc.* **2021**, *143* (33), 13029–13033. https://doi.org/10.1021/jacs.1c07780.
(81) Li, Y.; Zhang, F.-P.; Wang, R.-H.; Qi, S.-L.; Luan, Y.-X.; Ye, M. Carbamoyl Fluoride-Enabled Enantioselective Ni-Catalyzed Carbocarbamoylation of Unactivated Alkenes. *J. Am. Chem. Soc.* **2020**, *142* (47), 19844–19849. https://doi.org/10.1021/jacs.0c09949.
(82) Han, L.; Boshevski, V.; Yang, Y.; Louvel, D.; Colombo, M.; Tran, G.; Lacôte, E.; Amgoune, A.; Tlili, A. Enabling Nickel-Catalyzed Suzuki–Miyaura Cross-Coupling of Carbamoyl Fluorides: Mechanism and Scope. *Chem. Eur. J.* **2025**, *3* (5), e202500213. https://doi.org/10.1002/ceur.202500213.

Chapter 2

(1) Cadwallader, D.; Tiburcio, T. R.; Cieszynski, G. A.; Le, C. M. Synthesis of Carbamoyl Fluorides Using a Difluorophosgene Surrogate Derived from Difluorocarbene and Pyridine N-Oxides. *J. Org. Chem.* **2022**, *87* (17), 11457–11468. https://doi.org/10.1021/acs.joc.2c01017.

(2) Semler, G.; Schaeffer, G. Process for the Preparation of Carbamoyl Chlorides Derived from Secondary Amines. US4770820A, September 13, 1988. https://patents.google.com/patent/US4770820A/en (accessed 2026-07-29).

(3) Cotarca, L.; Geller, T.; Répási, J. Bis(Trichloromethyl)Carbonate (BTC, Triphosgene): A Safer Alternative to Phosgene? *Org. Process Res. Dev.* **2017**, *21* (9), 1439–1446. https://doi.org/10.1021/acs.oprd.7b00220.

(4) Liu, L.; Gu, Y.-C.; Zhang, C.-P. Recent Advances in the Synthesis and Transformation of Carbamoyl Fluorides, Fluoroformates, and Their Analogues. *Chem. Rec.* **2023**, *23* (9), e202300071. https://doi.org/10.1002/tcr.202300071.

(5) Jabbarpoor, M.; Le, C. M. Carbamoyl Fluorides: A Platform to Interrogate Fluoride-Enabled Reactivity. *Synthesis* **2025**, *57* (16), 2399–2410. https://doi.org/10.1055/a-2557-7635.

(6) Lin, J.-H.; Xiao, J.-C. Fluorinated Ylides/Carbenes and Related Intermediates from Phosphonium/Sulfonium Salts. *Acc. Chem. Res.* **2020**, *53* (8), 1498–1510. https://doi.org/10.1021/acs.accounts.0c00244.

(7) Zhao, R.; Furman, T. R.; Roth, M. MSD's Process Safety Scale-Up Methodology for Pilot Plant Scale and Beyond. *Org. Process Res. Dev.* **2021**, *25* (11), 2566–2577. https://doi.org/10.1021/acs.oprd.1c00360.

(8) Armstrong, B. M.; Behre, T.; Turnbull, B. W. H.; Bishara, D.; Hartmanshenn, C.; McCarthy, E.; Whittington, M.; Ji, Y.; Jenks, A.; Desmond, R.; Muzzio, D. J.; Corry, J.; Zhao, R.; Kuhl, N.; Chung, C. K. Integrating Process Development and Safety Analysis for Scale-Up of a Diborane-Generating Reduction Reaction. *Org. Process Res. Dev.* **2023**, *27* (4), 763–774. https://doi.org/10.1021/acs.oprd.3c00018.

(9) Constable, D. J. C.; Jimenez-Gonzalez, C.; Henderson, R. K. Perspective on Solvent Use in the Pharmaceutical Industry. *Org. Process Res. Dev.* **2006**, *11* (1), 133–137. https://doi.org/10.1021/op060170h.

(10) Selekman, J. A.; Tran, K.; Xu, Z.; Dummeldinger, M.; Kiau, S.; Nolfo, J.; Janey, J. High-Throughput Extractions: A New Paradigm for Workup Optimization in Pharmaceutical Process Development. *Org. Process Res. Dev.* **2016**, *20* (10), 1728–1737. https://doi.org/10.1021/acs.oprd.6b00225.

(11) Allwein, S. P.; Roemmele, R. C.; Haley, J. J., Jr.; Mowrey, D. R.; Petrillo, D. E.; Reif, J. J.; Gingrich, D. E.; Bakale, R. P. Development and Scale-Up of an Optimized Route to the ALK Inhibitor CEP-28122. *Org. Process Res. Dev.* **2011**, *16* (1), 148–155. https://doi.org/10.1021/op200313v.

(12) Tran, D. N.; Zhdanko, A.; Barroso, S.; Nieste, P.; Rahmani, R.; Holan, J.; Hoefnagels, R.; Reniers, P.; Vermoortele, F.; Duguid, S.; Cazanave, L.; Figlus, M.; Muir, C.; Elliott, A.; Zhao, P.; Paden, W.; Diaz, C. H.; Bell, S. J.; Hashimoto, A.; Phadke, A.; Wiles, J. A.; Vogels, I.; Farina, V. Development of a Commercial Process for Odalasvir. *Org. Process Res. Dev.* **2021**, *26* (3), 832–848. https://doi.org/10.1021/acs.oprd.1c00237.

(13) Committee on Acute Exposure Guideline Levels; Committee on Toxicology; Board on Enviromental Studies and Toxicology; Devision on Earth and Life Studies. *Acute Exposure*

Guideline Levels for Selected Airborne Chemicals: Volume 18; National Academics Press, 2014.

(14) Kumar, R.; Kumar, S.; Pandey, M. K.; Kashid, V. S.; Radhakrishna, L.; Balakrishna, M. S. Synthesis of Phosphine Chalcogenides Under Solvent-Free Conditions Using a Rotary Ball Mill. *Eur. J. Inorg. Chem.* **2018**, *2018* (8), 1028–1037. https://doi.org/10.1002/ejic.201701414.

(15) Gupta, O. D.; Shreeve, J. M. Carbonyl Difluoride: A Versatile Fluorinating Reagent. *J. Chem. Soc. Chem. Commun.* **1984**, *20* (7), 416–417. https://doi.org/10.1039/C39840000416.

(16) Xiang, J.-C.; Gao, Q.-H.; Wu, A.-X. The Applications of DMSO. In *Solvents as Reagents in Organic Synthesis*; John Wiley & Sons, Ltd, 2017; pp 315–353. https://doi.org/10.1002/9783527805624.ch7.

(17) Jabbarpoor, M.; LeBlanc, J.; Chen, Z.; Cadwallader, D.; Le, C. M. Pd-Catalyzed Suzuki-Type Cross-Coupling of 2-Pyridyl Carbamoyl Fluorides. *Chem. Commun.* **2024**, *60* (66), 8700–8703. https://doi.org/10.1039/D4CC02431A.

(18) Tang, H.-J.; Shi, X.-M.; Zhu, X.-Y.; Wang, C.-Q.; Feng, C. Oxidation of Difluorocarbene by Pyridine N-Oxide and Ensuing Access to Carbamoyl Fluorides†. *Chin. J. Chem.* **2023**, *41* (22), 2981–2987. https://doi.org/10.1002/cjoc.202300316.

(19) Song, H.-X.; Han, Z.-Z.; Zhang, C.-P. Concise and Additive-Free Click Reactions between Amines and CF3SO3CF3. *Chem. – Eur. J.* **2019**, *25* (46), 10907–10912. https://doi.org/10.1002/chem.201901865.

(20) Alder, C. M.; Hayler, J. D.; Henderson, R. K.; Redman, A. M.; Shukla, L.; Shuster, L. E.; Sneddon, H. F. Updating and Further Expanding GSK's Solvent Sustainability Guide. *Green Chem.* **2016**, 18 (13), 3879–3890. https://doi.org/10.1039/c6gc00611f

(21) Pauluhn, J. Acute Nose-Only Exposure of Rats to Phosgene. Part I: Concentration × Time Dependence of LC50s, Nonlethal-Threshold Concentrations, and Analysis of Breathing Patterns. *Inhalation Toxicology* **2006**, 18 (6), 423–435.

Chapter 3

(1) Devi, E. S.; Alanthadka, A.; Tamilselvi, A.; Nagarajan, S.; Sridharan, V.; Maheswari, C. U. Metal-Free Oxidative Amidation of Aldehydes with Aminopyridines Employing Aqueous Hydrogen Peroxide. *Org. Biomol. Chem.* **2016**, *14* (35), 8228–8231. https://doi.org/10.1039/C6OB01454B.

(2) Abramovitch, R. A.; Singer, G. M. Direct Acylamination of Pyridine 1-Oxides. *J. Org. Chem.* **1974**, *39* (13), 1795–1802. https://doi.org/10.1021/jo00927a001.

(3) Kathiravan, S.; Ghosh, S.; Hogarth, G.; A. Nicholls, I. Copper Catalysed Amidation of Aryl Halides through Chelation Assistance. *Chem. Commun.* **2015**, *51* (23), 4834–4837. https://doi.org/10.1039/C4CC09940K.

(4) Więckowska, A.; Fransson, R.; Odell, L. R.; Larhed, M. Microwave-Assisted Synthesis of Weinreb and MAP Aryl Amides via Pd-Catalyzed Heck Aminocarbonylation Using Mo(CO)6 or W(CO)6. *J. Org. Chem.* **2011**, *76* (3), 978–981. https://doi.org/10.1021/jo102151u.

(5) Shrestha, M.; Wu, X.; Huang, W.; Qu, J.; Chen, Y. Recent Advances in Transition Metal-Catalyzed Reactions of Carbamoyl Chlorides. *Org. Chem. Front.* **2021**, *8* (14), 4024–4045. https://doi.org/10.1039/D0QO01648A.

(6) Brown, D. G.; Boström, J. Analysis of Past and Present Synthetic Methodologies on Medicinal Chemistry: Where Have All the New Reactions Gone? *J. Med. Chem.* **2016**, *59* (10), 4443–4458. https://doi.org/10.1021/acs.jmedchem.5b01409.

(7) McKnight, E. A.; Arora, R.; Pradhan, E.; Fujisato, Y. H.; Ajayi, A. J.; Lautens, M.; Zeng, T.; Le, C. M. BF3-Catalyzed Intramolecular Fluorocarbamoylation of Alkynes via Halide Recycling. ChemRxiv April 19, 2023. https://doi.org/10.26434/chemrxiv-2022-464nx-v2.

(8) Li, Y.; Zhang, F.-P.; Wang, R.-H.; Qi, S.-L.; Luan, Y.-X.; Ye, M. Carbamoyl Fluoride-Enabled Enantioselective Ni-Catalyzed Carbocarbamoylation of Unactivated Alkenes. *J. Am. Chem. Soc.* **2020**, *142* (47), 19844–19849. https://doi.org/10.1021/jacs.0c09949.

(9) Yasui, Y.; Tsuchida, S.; Miyabe, H.; Takemoto, Y. One-Pot Amidation of Olefins through Pd-Catalyzed Coupling of Alkylboranes and Carbamoyl Chlorides. *J. Org. Chem.* **2007**, *72* (15), 5898–5900. https://doi.org/10.1021/jo070724u.

(10) Le, C. M.; Sperger, T.; Fu, R.; Hou, X.; Lim, Y. H.; Schoenebeck, F.; Lautens, M. Stereoselective Synthesis of Methylene Oxindoles via Palladium(II)-Catalyzed Intramolecular Cross-Coupling of Carbamoyl Chlorides. *J. Am. Chem. Soc.* **2016**, *138* (43), 14441–14448. https://doi.org/10.1021/jacs.6b08925.

(11) Sperger, T.; Le, C. M.; Lautens, M.; Schoenebeck, F. Mechanistic Insights on the Pd-Catalyzed Addition of C–X Bonds across Alkynes – a Combined Experimental and Computational Study. *Chem. Sci.* **2017**, *8* (4), 2914–2922. https://doi.org/10.1039/C6SC05001H.

(12) Le, C. M.; Hou, X.; Sperger, T.; Schoenebeck, F.; Lautens, M. An Exclusively Trans-Selective Chlorocarbamoylation of Alkynes Enabled by a Palladium/Phosphaadamantane Catalyst. *Angew. Chem. Int. Ed.* **2015**, *54* (52), 15897–15900. https://doi.org/10.1002/anie.201507883.

(13) Acosta-Guzmán, P.; Ojeda-Porras, A.; Gamba-Sánchez, D. Contemporary Approaches for Amide Bond Formation. *Adv. Synth. Catal.* **2023**, *365* (24), 4359–4391. https://doi.org/10.1002/adsc.202301018.

(14) Imaizumi, T.; Otsubo, S.; Komai, M.; Takada, H.; Maemoto, M.; Kobayashi, A.; Otsubo, N. The Design, Synthesis and Evaluation of 2-Aminobenzoxazole Analogues as Potent and

Orally Efficacious ChemR23 Inhibitors. *Bioorg. Med. Chem.* **2020**, *28* (17), 115622. https://doi.org/10.1016/j.bmc.2020.115622.
(15) Duan, Y.-Z.; Deng, M.-Z. Palladium-Catalyzed Cross-Coupling Reaction of Arylboronic Acids with Chloroformate or Carbamoyl Chloride. *Synlett* **2005**, *2005* (02), 355–357. https://doi.org/10.1055/s-2004-837211.
(16) Nielsen, C. D.-T.; Zivkovic, F. G.; Schoenebeck, F. Synthesis of N-CF3 Alkynamides and Derivatives Enabled by Ni-Catalyzed Alkynylation of N-CF3 Carbamoyl Fluorides. *J. Am. Chem. Soc.* **2021**, *143* (33), 13029–13033. https://doi.org/10.1021/jacs.1c07780.
(17) He, F.; Hou, L.; Wu, X.; Ding, H.; Qu, J.; Chen, Y. Enantioselective Synthesis of α-Alkenylated γ-Lactam Enabled by Ni-Catalyzed 1,4-Arylcarbamoylation of 1,3-Dienes. *CCS Chem.* **2022**, *5* (2), 341–349. https://doi.org/10.31635/ccschem.022.202202010.
(18) Sambiagio, C.; Schönbauer, D.; Blieck, R.; Dao-Huy, T.; Pototschnig, G.; Schaaf, P.; Wiesinger, T.; Zia, M. F.; Wencel-Delord, J.; Besset, T.; Maes, B. U. W.; Schnürch, M. A Comprehensive Overview of Directing Groups Applied in Metal-Catalysed C–H Functionalisation Chemistry. *Chem. Soc. Rev.* **2018**, *47* (17), 6603–6743. https://doi.org/10.1039/C8CS00201K.
(19) Ahrens, T.; Kohlmann, J.; Ahrens, M.; Braun, T. Functionalization of Fluorinated Molecules by Transition-Metal-Mediated C–F Bond Activation To Access Fluorinated Building Blocks. *Chem. Rev.* **2015**, *115* (2), 931–972. https://doi.org/10.1021/cr500257c.
(20) Das, A.; Chatani, N. The Directing Group: A Tool for Efficient and Selective C–F Bond Activation. *ACS Catal.* **2021**, *11* (21), 12915–12930. https://doi.org/10.1021/acscatal.1c03896.
(21) Yu, D.; Lu, L.; Shen, Q. Palladium-Catalyzed Coupling of Polyfluorinated Arenes with Heteroarenes via C–F/C–H Activation. *Org. Lett.* **2013**, *15* (4), 940–943. https://doi.org/10.1021/ol303567t.
(22) Suggs, J. W. Isolation of a Stable Acylrhodium(III) Hydride Intermediate Formed during Aldehyde Decarbonylation. Hydroacylation. *J. Am. Chem. Soc.* **1978**, *100* (2), 640–641. https://doi.org/10.1021/ja00470a054.
(23) Grushin, V. V. Mixed Phosphine−Phosphine Oxide Ligands. *Chem. Rev.* **2004**, *104* (3), 1629–1662. https://doi.org/10.1021/cr030026j.
(24) Grushin, V. V. Synthesis of Hemilabile Phosphine−Phosphine Oxide Ligands via the Highly Selective Pd-Catalyzed Mono-Oxidation of Bidentate Phosphines: Scope, Limitations, and Mechanism. *Organometallics* **2001**, *20* (18), 3950–3961. https://doi.org/10.1021/om010454k.
(25) Yang, S.; Deng, M.; Daley, R. A.; Darù, A.; Wolf, W. J.; George, D. T.; Ma, S.; Werley, B. K.; Samolova, E.; Bailey, J. B.; Gembicky, M.; Marshall, J.; Wisniewski, S. R.; Blackmond, D. G.; Engle, K. M. Palladium Bisphosphine Monoxide Complexes: Synthesis, Scope, Mechanism, and Catalytic Relevance. *J. Am. Chem. Soc.* **2025**, *147* (1), 409–425. https://doi.org/10.1021/jacs.4c10718.
(26) Marshall, W. J.; Grushin, V. V. Palladium(II) and Palladium(0) Complexes of BINAP(O) (2-(Diphenylphosphino)-2‘-(Diphenylphosphinyl)-1,1‘-Binaphthyl). *Organometallics* **2003**, *22* (3), 555–562. https://doi.org/10.1021/om020838q.
(27) Gowrisankar, S.; Neumann, H.; Gördes, D.; Thurow, K.; Jiao, H.; Beller, M. A Convenient and Selective Palladium-Catalyzed Aerobic Oxidation of Alcohols. *Chem. – Eur. J.* **2013**, *19* (47), 15979–15984. https://doi.org/10.1002/chem.201302526.

(28) Denmark, S. E.; Smith, R. C.; Tymonko, S. A. Phosphine Oxides as Stabilizing Ligands for the Palladium-Catalyzed Cross-Coupling of Potassium Aryldimethylsilanolates. *Tetrahedron* **2007**, *63* (26), 5730–5738. https://doi.org/10.1016/j.tet.2007.02.017.
(29) Altan, O. A Rare Example of the in Situ Formation of Palladium Nanoparticles: The Emergence of Catalytically Active Palladium Nanoparticles from Pd (II) Phosphine Complexes in the Suzuki–Miyaura Coupling Reaction. *Appl. Organomet. Chem.* **2022**, *36* (6), e6690. https://doi.org/10.1002/aoc.6690.
(30) Molnár, Á. Efficient, Selective, and Recyclable Palladium Catalysts in Carbon−Carbon Coupling Reactions. *Chem. Rev.* **2011**, *111* (3), 2251–2320. https://doi.org/10.1021/cr100355b.
(31) Chagunda, I. C.; Fisher, T.; Schierling, M.; McIndoe, J. S. Poisonous Truth about the Mercury Drop Test: The Effect of Elemental Mercury on Pd(0) and Pd(II)ArX Intermediates. *Organometallics* **2023**, *42* (19), 2938–2945. https://doi.org/10.1021/acs.organomet.3c00340.
(32) Lennox, A. J. J.; Lloyd-Jones, G. C. Selection of Boron Reagents for Suzuki–Miyaura Coupling. *Chem. Soc. Rev.* **2014**, *43* (1), 412–443. https://doi.org/10.1039/c3cs60197h.
(33) Tokunaga, Y.; Ueno, H.; Shimomura, Y.; Seo, T. Formation of Boroxine: Its Stability and Thermodynamic Parameters in Solution. *HETEROCYCLES* **2002**. https://doi.org/10.3987/com-02-9464.
(34) Tokunaga, Y. Boroxine Chemistry: From Fundamental Studies to Applications in Supramolecular and Synthetic Organic Chemistry. *HETEROCYCLES* **2013**. https://doi.org/10.3987/rev-13-767.
(35) Li, C.; Sotorrios, L.; Boaler, P. J.; Olikauskas, V.; Amico, M.; García-Domínguez, A.; Leach, A. G.; Lloyd-Jones, G. C. The Boroxine–Boronic Acid Equilibrium. *J. Am. Chem. Soc.* **2025**, *147* (42), 38237–38253. https://doi.org/10.1021/jacs.5c10835.
(36) Roşca, S.; Olaru, M.; Raţ, C. I. (2,4,6-Trimethylphenyl)Boronic Acid–Triphenylphosphine Oxide (1/1). *Acta Crystallogr. Sect. E Struct. Rep. Online* **2012**, *68* (1), o31–o31. https://doi.org/10.1107/S1600536811051609.
(37) Guadalupe Vasquez-Ríos, M.; Campillo-Alvarado, G.; MacGillivray, L. R. Mechanochemical Mediated Coexistence of B←N Coordination and Hydrogen Bonding. *Angew. Chem. Int. Ed.* **2023**, *62* (35), e202308350. https://doi.org/10.1002/anie.202308350.
(38) Georgiou, I.; Kervyn, S.; Rossignon, A.; De Leo, F.; Wouters, J.; Bruylants, G.; Bonifazi, D. Versatile Self-Adapting Boronic Acids for H-Bond Recognition: From Discrete to Polymeric Supramolecules. *J. Am. Chem. Soc.* **2017**, *139* (7), 2710–2727. https://doi.org/10.1021/jacs.6b11362.
(39) Begimova, G.; Tupikina, E. Yu.; Yu, V. K.; Denisov, G. S.; Bodensteiner, M.; Shenderovich, I. G. Effect of Hydrogen Bonding to Water on the 31P Chemical Shift Tensor of Phenyl- and Trialkylphosphine Oxides and α-Amino Phosphonates. *J. Phys. Chem. C* **2016**, *120* (16), 8717–8729. https://doi.org/10.1021/acs.jpcc.6b01140.
(40) Ng, S. W. A Second Monoclinic Modification of Triphenylphosphine Oxide Hemihydrate. *Acta Crystallogr. Sect. E Struct. Rep. Online* **2009**, *65* (6), o1431–o1431. https://doi.org/10.1107/S1600536809019254.
(41) De Graaf, Wim.; Boersma, Jaap.; Smeets, W. J. J.; Spek, A. L.; Van Koten, Gerard. Dimethyl(N,N,N',N'-Tetramethylethanediamine)Palladium(II) and Dimethyl[1,2-Bis(Dimethylphosphino)Ethane]Palladium(II): Syntheses, x-Ray Crystal Structures, and Thermolysis, Oxidative-Addition and Ligand-Exchange Reactions. *Organometallics* **1989**, *8* (12), 2907–2917. https://doi.org/10.1021/om00114a028.

(42) King, R. P.; Buchwald, S. L. Synthesis of (MeCN)2Pd(CF3)OTs, a General Precursor to Palladium(II) Trifluoromethyl Complexes LPd(CF3)X. *Organometallics* **2019**, *38* (19), 3490–3493. https://doi.org/10.1021/acs.organomet.9b00516.

Chapter 4

(1) Nielsen, C. D.-T.; Zivkovic, F. G.; Schoenebeck, F. Synthesis of N-CF3 Alkynamides and Derivatives Enabled by Ni-Catalyzed Alkynylation of N-CF3 Carbamoyl Fluorides. *J. Am. Chem. Soc.* **2021**, *143* (33), 13029–13033. https://doi.org/10.1021/jacs.1c07780.

(2) Jabbarpoor, M.; LeBlanc, J.; Chen, Z.; Cadwallader, D.; Le, C. M. Pd-Catalyzed Suzuki-Type Cross-Coupling of 2-Pyridyl Carbamoyl Fluorides. *Chem. Commun.* **2024**, *60* (66), 8700–8703. https://doi.org/10.1039/D4CC02431A.

(3) Yasui, Y.; Tsuchida, S.; Miyabe, H.; Takemoto, Y. One-Pot Amidation of Olefins through Pd-Catalyzed Coupling of Alkylboranes and Carbamoyl Chlorides. *J. Org. Chem.* **2007**, *72* (15), 5898–5900. https://doi.org/10.1021/jo070724u.

(4) Pearson, R. G. Hard and Soft Acids and Bases, HSAB, Part 1: Fundamental Principles. *J. Chem. Educ.* **1968**, *45* (9), 581. https://doi.org/10.1021/ed045p581.

(5) Pearson, R. G. Hard and Soft Acids and Bases. *J. Am. Chem. Soc.* **1963**, *85* (22), 3533–3539. https://doi.org/10.1021/ja00905a001.

(6) Moloto, B. P.; Vermeeren, P.; Dalla Tiezza, M.; Esterhuysen, C.; Bickelhaupt, F. M.; Hamlin, T. A. Palladium-Catalyzed Activation of Carbon–Halogen Bonds: Electrostatics-Controlled Reactivity. *Eur. J. Org. Chem.* **2022**, *2022* (26), e202200722. https://doi.org/10.1002/ejoc.202200722.

(7) Rio, J.; Liang, H.; Perrin, M.-E.; Perego, L.; Grimaud, L.; Payard, P.-A. We Already Know Everything about Oxidative Addition to Pd(0) - Do We? *ACS Catal.* **2023**, *13* (17), 11399–11421. https://doi.org/10.1021/acscatal.3c01943.

(8) Anjali, B. A.; Suresh, C. H. Interpreting Oxidative Addition of Ph–X (X = CH3, F, Cl, and Br) to Monoligated Pd(0) Catalysts Using Molecular Electrostatic Potential. *ACS Omega* **2017**, *2* (8), 4196–4206. https://doi.org/10.1021/acsomega.7b00745.

(9) Amii, H.; Uneyama, K. C−F Bond Activation in Organic Synthesis. *Chem. Rev.* **2009**, *109* (5), 2119–2183. https://doi.org/10.1021/cr800388c.

(10) Ariafard, A.; Lin, Z. Understanding the Relative Easiness of Oxidative Addition of Aryl and Alkyl Halides to Palladium(0). *Organometallics* **2006**, *25* (16), 4030–4033. https://doi.org/10.1021/om060236x.

(11) Chernyshev, V. M.; Ananikov, V. P. Nickel and Palladium Catalysis: Stronger Demand than Ever. *ACS Catal.* **2022**, *12* (2), 1180–1200. https://doi.org/10.1021/acscatal.1c04705.

(12) Lin; Liu, L.; Fu, Y.; Luo, S.-W.; Chen, Q.; Guo, Q.-X. Comparing Nickel- and Palladium-Catalyzed Heck Reactions. *Organometallics* **2004**, *23* (9), 2114–2123. https://doi.org/10.1021/om034067h.

(13) Cooper, A. K.; Burton, P. M.; Nelson, D. J. Nickel versus Palladium in Cross-Coupling Catalysis: On the Role of Substrate Coordination to Zerovalent Metal Complexes. *Synthesis* **2020**, *52* (04), 565–573. https://doi.org/10.1055/s-0039-1690045.

(14) Jasim, N. A.; Perutz, R. N.; Whitwood, A. C.; Braun, T.; Izundu, J.; Neumann, B.; Rothfeld, S.; Stammler, H.-G. Contrasting Reactivity of Fluoropyridines at Palladium and Platinum: C−F Oxidative Addition at Palladium, P−C and C−F Activation at Platinum. *Organometallics* **2004**, *23* (26), 6140–6149. https://doi.org/10.1021/om049448p.

(15) Mastrorilli, P.; Moro, G.; Nobile, C. F.; Latronico, M. New Nickel(O) Complexes with Bulky Diphosphine Ligands. *Inorganica Chim. Acta* **1992**, *192* (2), 183–187. https://doi.org/10.1016/S0020-1693(00)80757-4.

(16) Chung, T. C.; Janvikul, W.; Lu, H. L. A Novel "Stable" Radical Initiator Based on the Oxidation Adducts of Alkyl-9-BBN. *J. Am. Chem. Soc.* **1996**, *118* (3), 705–706. https://doi.org/10.1021/ja9527737.
(17) Ollivier, C.; Renaud, P. Organoboranes as a Source of Radicals. *Chem. Rev.* **2001**, *101* (11), 3415–3434. https://doi.org/10.1021/cr010001p.
(18) Chang, L.; An, Q.; Duan, L.; Feng, K.; Zuo, Z. Alkoxy Radicals See the Light: New Paradigms of Photochemical Synthesis. *Chem. Rev.* **2022**, *122* (2), 2429–2486. https://doi.org/10.1021/acs.chemrev.1c00256.
(19) Gehani, A. A. M. A. E.; A. Maashi, H.; Harnedy, J.; C. Morrill, L. Electrochemical Generation and Utilization of Alkoxy Radicals. *Chem. Commun.* **2023**, *59* (25), 3655–3664. https://doi.org/10.1039/D3CC00302G.
(20) Banoun, C.; Bourdreux, F.; Magnier, E.; Dagousset, G. Intermolecular C–O Bond Formation with Alkoxyl Radicals: Photoredox-Catalyzed α-Alkoxylation of Carbonyl Compounds. *Org. Lett.* **2021**, *23* (22), 8926–8930. https://doi.org/10.1021/acs.orglett.1c03444.
(21) He, X.; Zhao, Y.; Zhang, Z.; Shen, X. Tuning the Reactivity of Alkoxyl Radicals from Cyclization to 1,2-Silyl Transfer: Stereoselective Synthesis of β-Substituted Cycloalcohols. *Org. Lett.* **2022**, *24* (10), 1991–1995. https://doi.org/10.1021/acs.orglett.2c00428.
(22) Yang, Z.; Niu, Y.; He, X.; Chen, S.; Liu, S.; Li, Z.; Chen, X.; Zhang, Y.; Lan, Y.; Shen, X. Tuning the Reactivity of Alkoxyl Radicals from 1,5-Hydrogen Atom Transfer to 1,2-Silyl Transfer. *Nat. Commun.* **2021**, *12* (1), 2131. https://doi.org/10.1038/s41467-021-22382-y.
(23) Köster, R.; Seidel, G.; Wrackmeyer, B. Alkalimetall-Trialkylhydroxyborate Und (Alkalimetalloxy)Dialkylborane[1]. *Chem. Ber.* **1992**, *125* (3), 617–625. https://doi.org/10.1002/cber.19921250313.
(24) Bhagat, K. K.; Cheke, R. S.; Gavali, V. D.; Kharkar, P. S.; Arote, N. D. A Brief Review on Metal-Curcumin Complexes: Synthesis Approaches and Their Pharmaceutical Applications. *Discov. Chem.* **2025**, *2* (1), 119. https://doi.org/10.1007/s44371-025-00174-3.
(25) Amaya, T.; Maegawa, Y.; Masuda, T.; Osafune, Y.; Hirao, T. Selective Intermolecular Oxidative Cross-Coupling of Enolates. *J. Am. Chem. Soc.* **2015**, *137* (32), 10072–10075. https://doi.org/10.1021/jacs.5b05058.
(26) Yalpani, M.; Boese, R.; Seevogel, K.; Köuster, R. Monomeric and Dimeric Acyloxydialkylboranes. *J. Chem. Soc. Dalton Trans.* **1993**, No. 1, 47–50. https://doi.org/10.1039/DT9930000047.
(27) Bubnov, Yu. N.; Zheludeva, V. I.; Ignatenko, A. V. Synthesis of 1-Substituted 1-Vinylcycloalkanes by Allylboration of Carbonyl Compounds and Ethoxyacetylene with Diorganylborylethylidenecyclopentane and a Diorganylborylethylidenecyclohexane. *Bull. Acad. Sci. USSR Div. Chem. Sci.* **1989**, *38* (2), 366–372. https://doi.org/10.1007/BF00953631.
(28) Kliegel, W.; Nanninga, D. Borchelate von Salicylaldehydnitronen. *J. Organomet. Chem.* **1983**, *243* (4), 373–385. https://doi.org/10.1016/S0022-328X(00)98570-X.
(29) Hojoh, K.; Shido, Y.; Ohmiya, H.; Sawamura, M. Construction of Quaternary Stereogenic Carbon Centers through Copper-Catalyzed Enantioselective Allylic Cross-Coupling with Alkylboranes. *Angew. Chem. Int. Ed.* **2014**, *53* (19), 4954–4958. https://doi.org/10.1002/anie.201402386.
(30) Schäfer, F.; Lamm, J.-H.; Neumann, B.; Stammler, H.-G.; Mitzel, N. W. Silicon-Bridged Bi- and Tridentate Lewis Acidic Host Systems. *Eur. J. Inorg. Chem.* **2021**, *2021* (32), 3265–3271. https://doi.org/10.1002/ejic.202100497.

(31) Eisenberger, P.; Bestvater, B. P.; Keske, E. C.; Crudden, C. M. Hydrogenations at Room Temperature and Atmospheric Pressure with Mesoionic Carbene-Stabilized Borenium Catalysts. *Angew. Chem. Int. Ed.* **2015**, *54* (8), 2467–2471. https://doi.org/10.1002/anie.201409250.
(32) Bubnov, Yu. N.; Zheludeva, V. I.; Ignatenko, A. V. Synthesis of 1-Substituted 1-Vinylcycloalkanes by Allylboration of Carbonyl Compounds and Ethoxyacetylene with Diorganylborylethylidenecyclopentane and a Diorganylborylethylidenecyclohexane. *Bull. Acad. Sci. USSR Div. Chem. Sci.* **1989**, *38* (2), 366–372. https://doi.org/10.1007/BF00953631.
(33) W. Kramer, G.; C. Brown, H. Organoboranes: XIX. The Preparation and Some Unusual Chemistry of b-Allyl Derivatives of 9-Borabicyclo[3.3.1]Nonane. *J. Organomet. Chem.* **1977**, *132* (1), 9–27. https://doi.org/10.1016/S0022-328X(00)92510-5.
(34) Curran, D. P.; Moura-Letts, G.; Pohlman, M. Solution-Phase Mixture Synthesis with Fluorous Tagging En Route: Total Synthesis of an Eight-Member Stereoisomer Library of Passifloricins. *Angew. Chem. Int. Ed.* **2006**, *45* (15), 2423–2426. https://doi.org/10.1002/anie.200600041.
(35) O'Keefe, B. M.; Mans, D. M.; Kaelin, D. E. J.; Martin, S. F. Total Synthesis of Isokidamycin. *J. Am. Chem. Soc.* **2010**, *132* (44), 15528–15530. https://doi.org/10.1021/ja107926f.
(36) Benaissa, I.; Rialland, B.; Bennaamane, S.; Espada, M. F.; Saffon-Merceron, N.; Fustier-Boutignon, M.; Clot, E.; Mézailles, N. N2 Functionalization via Molybdenum-Nitride Complex: Stepwise BH Bond Additions. *Angew. Chem. Int. Ed.* **2024**, *63* (29), e202402586. https://doi.org/10.1002/anie.202402586.
(37) Köuster, R.; Seidel, G.; Schüuβler, W.; Wrackmeyer, B. Die Ersten Organobor-Tellur-Verbindungen[1]. *Chem. Ber.* **1995**. https://doi.org/10.1002/cber.19951280113.
(38) Soderquist, J. A.; Najafi, M. R. Selective Oxidation of Organoboranes with Anhydrous Trimethylamine N-Oxide. *J. Org. Chem.* **1986**, *51* (8), 1330–1336. https://doi.org/10.1021/jo00358a032.
(39) Matos, K.; Soderquist, J. A. Alkylboranes in the Suzuki−Miyaura Coupling: Stereochemical and Mechanistic Studies. *J. Org. Chem.* **1998**, *63* (3), 461–470. https://doi.org/10.1021/jo971681s.
(40) *Synthesis of Functionalized [3], [4], [5] and [6]Dendralenes through Palladium-Catalyzed Cross-Couplings of Substituted Allenoates - Lippincott - 2017 - Angewandte Chemie International Edition - Wiley Online Library*. https://onlinelibrary.wiley.com/doi/10.1002/anie.201609636 (accessed 2026-06-29).
(41) Jiang, Y.; Kwan, E. E.; Ping, Y.; Liu, R. Y. Synthesis of Diaryl Ethers by Formal Oxygen Insertion Between Suzuki–Miyaura Coupling Partners. *ACS Catal.* **2025**, *15* (15), 13588–13594. https://doi.org/10.1021/acscatal.5c03249.
(42) Zhu, C.; Wang, R.; Falck, J. R. Mild and Rapid Hydroxylation of Aryl/Heteroaryl Boronic Acids and Boronate Esters with N-Oxides. *Org. Lett.* **2012**, *14* (13), 3494–3497. https://doi.org/10.1021/ol301463c.
(43) Diccianni, J.; Lin, Q.; Diao, T. Mechanisms of Nickel-Catalyzed Coupling Reactions and Applications in Alkene Functionalization. *Acc. Chem. Res.* **2020**, *53* (4), 906–919. https://doi.org/10.1021/acs.accounts.0c00032.
(44) Diccianni, J. B.; Diao, T. Mechanisms of Nickel-Catalyzed Cross-Coupling Reactions. *Trends Chem.* **2019**, *1* (9), 830–844. https://doi.org/10.1016/j.trechm.2019.08.004.

(45) Mohadjer Beromi, M.; Nova, A.; Balcells, D.; Brasacchio, A. M.; Brudvig, G. W.; Guard, L. M.; Hazari, N.; Vinyard, D. J. Mechanistic Study of an Improved Ni Precatalyst for Suzuki–Miyaura Reactions of Aryl Sulfamates: Understanding the Role of Ni(I) Species. *J. Am. Chem. Soc.* **2016**, *139* (2), 922–936. https://doi.org/10.1021/jacs.6b11412.
(46) Christian, A. H.; Müller, P.; Monfette, S. Nickel Hydroxo Complexes as Intermediates in Nickel-Catalyzed Suzuki–Miyaura Cross-Coupling. *Organometallics* **2014**, *33* (9), 2134–2137. https://doi.org/10.1021/om5001327.
(47) Singh, S.; Sunoj, R. B. Mechanism and Origin of Enantioselectivity in Nickel-Catalyzed Alkyl–Alkyl Suzuki Coupling Reaction. *J. Phys. Chem. A* **2019**, *123* (31), 6701–6710. https://doi.org/10.1021/acs.jpca.9b04284.
(48) Mohadjer Beromi, M.; Banerjee, G.; Brudvig, G. W.; Hazari, N.; Mercado, B. Q. Nickel(I) Aryl Species: Synthesis, Properties, and Catalytic Activity. *ACS Catal.* **2018**, *8* (3), 2526–2533. https://doi.org/10.1021/acscatal.8b00546.
(49) Matsubara, K.; Fukahori, Y.; Inatomi, T.; Tazaki, S.; Yamada, Y.; Koga, Y.; Kanegawa, S.; Nakamura, T. Monomeric Three-Coordinate N-Heterocyclic Carbene Nickel(I) Complexes: Synthesis, Structures, and Catalytic Applications in Cross-Coupling Reactions. *Organometallics* **2016**, *35* (19), 3281–3287. https://doi.org/10.1021/acs.organomet.6b00419.
(50) Li, Z.; Jiang, Y.-Y.; Fu, Y. Theoretical Study on the Mechanism of Ni-Catalyzed Alkyl–Alkyl Suzuki Cross-Coupling. *Chem. Eur. J.* **2012**, *18* (14), 4345–4357. https://doi.org/10.1002/chem.201103882.
(51) West, M. J.; Watson, A. J. B. Ni vs. Pd in Suzuki–Miyaura Sp2–Sp2 Cross-Coupling: A Head-to-Head Study in a Comparable Precatalyst/Ligand System. *Org. Biomol. Chem.* **2019**, *17* (20), 5055–5059. https://doi.org/10.1039/c9ob00561g.
(52) Bena, A. R.; Pieber, B. Advances in NiI/NiIII-Catalyzed C(Sp2)–Heteroatom Cross-Couplings. *ACS Catal.* **2026**, *16* (2), 866–881. https://doi.org/10.1021/acscatal.5c07964.
(53) Fan, P.; Lan, Y.; Zhang, C.; Wang, C. Nickel/Photo-Cocatalyzed Asymmetric Acyl-Carbamoylation of Alkenes. *J. Am. Chem. Soc.* **2020**, *142* (5), 2180–2186. https://doi.org/10.1021/jacs.9b12554.
(54) Le, C. M.; Sperger, T.; Fu, R.; Hou, X.; Lim, Y. H.; Schoenebeck, F.; Lautens, M. Stereoselective Synthesis of Methylene Oxindoles via Palladium(II)-Catalyzed Intramolecular Cross-Coupling of Carbamoyl Chlorides. *J. Am. Chem. Soc.* **2016**, *138* (43), 14441–14448. https://doi.org/10.1021/jacs.6b08925.
(55) Pilloni, G.; Toffoletti, A.; Bandoli, G.; Longato, B. Homoleptic Complexes of Cobalt(0) and Nickel(0,I) with 1,1‘-Bis(Diphenylphosphino)Ferrocene (Dppf): Synthesis and Characterization. *Inorg. Chem.* **2006**, *45* (25), 10321–10328. https://doi.org/10.1021/ic061185z.
(56) Cleaves, P. A.; Ayres, A. J.; Vondung, L.; Stewart, J. C.; Cobb, P. J.; Wooles, A. J.; Liddle, S. T. Bridged and Unbridged Nickel–Nickel Bonds Supported by Cyclopentadienyl and Phosphine Ligand Sets. *Organometallics* **2020**, *39* (24), 4735–4746. https://doi.org/10.1021/acs.organomet.0c00708.
(57) Xu, W.; Li, M.; Qiao, L.; Xie, J. Recent Advances of Dinuclear Nickel- and Palladium-Complexes in Homogeneous Catalysis. *Chem. Commun.* **2020**, *56* (61), 8524–8536. https://doi.org/10.1039/d0cc02542a.
(58) Inatomi, T.; Koga, Y.; Matsubara, K. Dinuclear Nickel(I) and Palladium(I) Complexes for Highly Active Transformations of Organic Compounds. *Molecules* **2018**, *23* (1), 140. https://doi.org/10.3390/molecules23010140.

(59) Demadis, K. D.; Hartshorn, C. M.; Meyer, T. J. The Localized-to-Delocalized Transition in Mixed-Valence Chemistry. *Chem. Rev.* **2001**, *101* (9), 2655–2686. https://doi.org/10.1021/cr990413m.
(60) Robin, M. B.; Day, P. Mixed Valence Chemistry-A Survey and Classification. In *Advances in Inorganic Chemistry and Radiochemistry*; Emeléus, H. J., Sharpe, A. G., Eds.; Academic Press, 1968; Vol. 10, pp 247–422. https://doi.org/10.1016/S0065-2792(08)60179-X.
(61) Witzke, R. J.; Tilley, T. D. Synthesis and Reactivity of a Dimeric Ni(I) Methyl Complex. *Organometallics* **2022**, *41* (12), 1565–1571. https://doi.org/10.1021/acs.organomet.2c00188.
(62) Herrmann, W. A.; Krüger, C.; Goddard, R.; Bernal, I. Transition Metal Methylene Complexes: III. Methylene (CH2), a Carbonyl Analogous Ligand; Crystal Structure of μ-Methylenebis(Carbonyl-H5-Cyclopentadienylrhodium)(Rh—Rh. *J. Organomet. Chem.* **1977**, *140* (1), 73–89. https://doi.org/10.1016/S0022-328X(00)84398-3.
(63) Herrmann, W. A. The Methylene Bridge. *Adv. Organomet. Chem.* **1982**. https://doi.org/10.1016/S0065-3055(08)60522-5.
(64) Gao, Y.; Jennings, M. C.; Puddephatt, R. J. A Diruthenium μ-Methylene Complex. *Organometallics* **2001**, *20* (9), 1882–1888. https://doi.org/10.1021/om0010417.
(65) Wu, Y.; Shan, C.; Ying, J.; Su, J.; Zhu, J.; Liu, L. L.; Zhao, Y. Catalytic Hydroboration of Aldehydes, Ketones, Alkynes and Alkenes Initiated by NaOH. *Green Chem.* **2017**, *19* (17), 4169–4175. https://doi.org/10.1039/c7gc01632h.
(66) Malapit, C. A.; Bour, J. R.; Brigham, C. E.; Sanford, M. S. Base-Free Nickel-Catalysed Decarbonylative Suzuki–Miyaura Coupling of Acid Fluorides. *Nature* **2018**, *563* (7729), 100–104. https://doi.org/10.1038/s41586-018-0628-7.
(67) Ohashi, M.; Saijo, H.; Shibata, M.; Ogoshi, S. Palladium-Catalyzed Base-Free Suzuki–Miyaura Coupling Reactions of Fluorinated Alkenes and Arenes via a Palladium Fluoride Key Intermediate. *Eur. J. Org. Chem.* **2013**, *2013* (3), 443–447. https://doi.org/10.1002/ejoc.201201405.
(68) Köuster, R.; Seidel, G.; Schüuβler, W.; Wrackmeyer, B. Die Ersten Organobor-Tellur-Verbindungen[1]. *Chem. Ber.* **1995**, *128* (1), 87–89. https://doi.org/10.1002/cber.19951280113.
(69) Cypcar, A. D.; Kerr, T. A.; Yang, J. Y. Thermochemical Studies of Nickel Hydride Complexes with Cationic Ligands in Aqueous and Organic Solvents. *Organometallics* **2022**, *41* (18), 2605–2611. https://doi.org/10.1021/acs.organomet.2c00319.
(70) Connelly Robinson, S. J.; Zall, C. M.; Miller, D. L.; Linehan, J. C.; Appel, A. M. Solvent Influence on the Thermodynamics for Hydride Transfer from Bis(Diphosphine) Complexes of Nickel. *Dalton Trans.* **2016**, *45* (24), 10017–10023. https://doi.org/10.1039/c6dt00309e.
(71) Korch, K. M.; Watson, D. A. Cross-Coupling of Heteroatomic Electrophiles. *Chem. Rev.* **2019**, *119* (13), 8192–8228. https://doi.org/10.1021/acs.chemrev.8b00628.
(72) Knappke, C. E. I.; Grupe, S.; Gärtner, D.; Corpet, M.; Gosmini, C.; Jacobi von Wangelin, A. Reductive Cross-Coupling Reactions between Two Electrophiles. *Chem. – Eur. J.* **2014**, *20* (23), 6828–6842. https://doi.org/10.1002/chem.201402302.
(73) Diccianni, J. B.; Katigbak, J.; Hu, C.; Diao, T. Mechanistic Characterization of (Xantphos)Ni(I)-Mediated Alkyl Bromide Activation: Oxidative Addition, Electron Transfer, or Halogen-Atom Abstraction. *J. Am. Chem. Soc.* **2019**, *141* (4), 1788–1796. https://doi.org/10.1021/jacs.8b13499.
(74) Chakraborty, U.; Urban, F.; Mühldorf, B.; Rebreyend, C.; de Bruin, B.; van Velzen, N.; Harder, S.; Wolf, R. Accessing the CpArNi(I) Synthon: Reactions with N-Heterocyclic

Carbenes, TEMPO, Sulfur, and Selenium. *Organometallics* **2016**, *35* (11), 1624–1631. https://doi.org/10.1021/acs.organomet.6b00084.
(75) Rettenmeier, C.; Wadepohl, H.; Gade, L. H. Stereoselective Hydrodehalogenation via a Radical-Based Mechanism Involving T-Shaped Chiral Nickel(I) Pincer Complexes. *Chem. – Eur. J.* **2014**, *20* (31), 9657–9665. https://doi.org/10.1002/chem.201403243.
(76) Ma, Z.; Mahmudov, K. T.; Aliyeva, V. A.; Gurbanov, A. V.; Pombeiro, A. J. L. TEMPO in Metal Complex Catalysis. *Coord. Chem. Rev.* **2020**, *423*, 213482. https://doi.org/10.1016/j.ccr.2020.213482.
(77) Chaumeil, H.; Signorella, S.; Le Drian, C. Suzuki Cross-Coupling Reaction of Sterically Hindered Aryl Boronates with 3-Iodo-4-Methoxybenzoic Acid Methylester. Tetrahedron 2000, 56 (49), 9655–9662. https://doi.org/10.1016/S0040-4020(00)00928-5
(78) Matos, K.; Soderquist, J. A. Alkylboranes in the Suzuki−Miyaura Coupling: Stereochemical and Mechanistic Studies. J. Org. Chem. 1998, 63 (3), 461–470. https://doi.org/10.1021/jo971681s
(79) Sato, M.; Miyaura, N.; Suzuki, A. Cross-Coupling Reaction of Alkyl- or Arylboronic Acid Esters with Organic Halides Induced by Thallium(I) Salts and Palladium-Catalyst. Chem. Lett. 1989, 18 (8), 1405–1408. https://doi.org/10.1246/cl.1989.1405